POLITECHNIKA WARSZAWSKA

DYSCYPLINA NAUKOWA INŻYNIERIA MATERIAŁOWA
DZIEDZINA NAUK INŻYNIERYJNO-TECHNICZNYCH

Rozprawa doktorska

mgr Marta Dobrosielska

Nowe aspekty wykorzystania biogenicznej krzemionki jako napełniacza w kompozytach polimerowych

Promotorzy
Dr hab. Renata Dobrucka, prof. UEP
Dr hab. Robert Przekop, prof. UAM

WARSZAWA 2024

Niniejsze badania były finansowane z projektu „Zaawansowane biokompozyty dla Gospodarki jutra BIO-GNET" NP POIR.04.04.00-00-1792/18-00.
Projekt finansowany przez Fundację na rzecz Nauki Polskiej ze środków Europejskiego Funduszu Rozwoju Regionalnego w ramach Programu Operacyjnego Inteligentny Rozwój 2014-2020 (PO IR), Oś IV: Zwiększenie potencjału naukowo-badawczego, Działanie 4.4: Zwiększenie potencjału kadrowego sektora B+R, konkurs TEAM-NET.

Niniejsze badania realizowane były w części w Centrum Zaawansowanych Technologii UAM w Poznaniu.

Składam najserdeczniejsze wyrazy wdzięczności
Doktor habilitowanej **Renacie Dobruckiej**
za nieocenioną pomoc w realizacji badań,
za wsparcie w trudnych dla mnie momentach,
za zrozumienie.

Serdeczne podziękowania pragnę również złożyć
Doktorowi habilitowanemu **Robertowi Przekopowi**
za obdarzenie zaufaniem,
za nieocenioną pomoc od samego początku,
za poświęcony czas.

Streszczenie

Powszechnie znanym faktem jest, że właściwości kompozytu zależą od wielkości cząstek napełniacza. Ziemia okrzemkowa jest jednym z napełniaczy stosowanym w kompozytach polimerowych od dziesięcioleci, jednak do tej pory nie poświęcano wiele uwagi wpływowi wielkości pancerza na właściwości kompozytu. W niniejszej pracy podjęto próbę zweryfikowania relacji pomiędzy tą wielkością a właściwościami kompozytów polimerowych z tego typu napełniaczem. W tym celu opracowano technikę frakcjonowania ziemi okrzemkowej metodą hydrauliczną, czego efektem było wyodrębnienie frakcji okrzemek o określonym zakresie wielkości cząstek. Charakterystyka mikroskopowa oraz statystyczna pozwoliła na dobre zdefiniowanie struktury, rozmiarów oraz morfologii, pokazując duże zróżnicowanie - cząstki połamane, zaglomerowane oraz cechy wynikające z biologii wzrostu pancerzyka. W ten sposób przygotowany napełniacz pozwolił na uzyskanie kompozytów zawierających napełniacz o kontrolowanej wielkości i geometrii w zakresie od kilkudziesięciu nanometrów do kilkuset mikrometrów. Weryfikacja hipotezy badawczej odbyła się w oparciu o kompozyty termoplastyczne (polilaktyd, poliamid) i duroplastyczne (żywice epoksydowe) zawierające napełniacz w ilości do 70% obj. Przetwórstwo kompozytów prowadzono za pomocą metod tradycyjnych, takich jak: techniki ekstruzji i wtrysku w przypadku polimerów termoplastycznych, odlewanie w formach silikonowych w przypadku duroplastów. Zastosowano również nowoczesną technikę przetwórczą, druk 3D FDM. Zwrócono również uwagę na parametry reologiczne badanych systemów kompozytowych, które będą zależały od oddziaływań chemicznych, wielkości cząstek napełniacza oraz czynników pomocniczych takich jak woski naturalne czy syntetyczne. Zastosowano techniki mikroskopowe, badania mechaniczne, reologiczne, spektroskopowe, badania energii powierzchniowej czy analizę termiczną. Finalnie zwrócono również uwagę na praktyczne wykorzystanie opracowanego kompozytu, badając właściwości funkcjonalne i starzeniowe. Dopełnieniem weryfikacji koncepcji geometrycznego wpływu biokrzemionki było rozróżnienie tego efektów chemicznych oddziaływań powierzchni napełniacza z osnową polimerową. W tym celu zastosowano obróbkę chemiczną ziemi okrzemkowej za pomocą organofunkcyjnych silanów z grupami metylowymi, n-oktylowymi, epoksydowymi i aminowymi.

Słowa kluczowe: biokompozyty, ziemia okrzemkowa, frakcjonowanie, napełniacz mineralny, wielkość cząstek, polimery

Summary

It is a well-known fact that composite properties depend on the particle size of the filler. Diatomaceous earth has been one of the fillers used in polymer composites for decades, but until now little attention has been paid to the effect of armor size on composite properties. In the present study, an attempt was made to verify the relationship between this size and the properties of polymer composites with this type of filler. For this purpose, a technique for fractionating diatomaceous earth using a hydraulic method was developed, resulting in the separation of diatomite fractions with a certain range of particle sizes. Microscopic and statistical characterization allowed a good definition of the structure, size and morphology, showing a great diversity - broken particles, zaglomerated particles and features resulting from the biology of armor growth. Thus prepared, the filler allowed to obtain filler-containing composites with controlled size and geometry in the range of tens of nanometers to several hundred micrometers. The research hypothesis was verified using thermoplastic (polylactide, polyamide) and duroplastic (epoxy resins) composites containing filler up to 70% vol. Composite processing was carried out using traditional methods, such as extrusion and injection molding techniques for thermoplastic polymers, silicone mold casting for duroplastics. Modern techniques, such as 3D printing by FDM technique, were also used. Attention was also paid to the rheological parameters of the composite systems studied, which will also depend on chemical interactions, filler particle size and auxiliary factors such as natural or synthetic waxes. Microscopic, mechanical, rheological, spectroscopic, surface energy or thermal analysis techniques were used. Final attention was also paid to the practical use of the developed composite, studying functional and aging properties. The verification of the concept of the geometric effect of biosilica was completed by distinguishing this effect of chemical interactions of the filler surface with the polymer matrix. For this purpose, chemical treatment of diatomaceous earth with organofunctional silanes with methyl, n-octyl, epoxy and amine groups was applied.

Key words: biocomposites, diatomaceous earth, fractionation, mineral filler, particle size, polymers

Spis treści

Wykaz publikacji monotematycznych

W niniejszej rozprawie doktorskiej skupiono się na problemie badawczym, jakim jest zastosowanie amorficznej ziemi okrzemkowej jako napełniacza w kompozytach polimerowych. Prace badawcze obejmowały w pierwszej fazie zaprojektowanie i przeprowadzenie procesu rozdziału bionapełniacza na frakcje o szerokim spektrum wielkości cząstek. W fazie drugiej stosowano tak przygotowaną biokrzemionkę jako napełniacz kompozytów na osnowie polilaktydowej i poliamidowej. Przeprowadzono szeroki zakres badań począwszy od określenia struktury napełniacza, przez badania mechaniczne otrzymanych kompozytów, aż po badania starzeniowe w warunkach imitujących proces standardowej eksploatacji materiałów w środowisku.

Podstawę rozprawy stanowi cykl dziesięciu artykułów naukowych H1 – H10:

H1 ***Biogenic Composite Filaments Based on Polylactide and Diatomaceous Earth for 3D Printing***

Dobrosielska M., Przekop R.E., Sztorch B., Brząkalski D., Zgłobicka I., Łępicka M., Dobosz R., Kurzydłowski K.J., Materials 13, 20, 4632, 2020

iF = 3.748 M = 140

H2 ***A New Method of Diatomaceous Earth Fractionation—A Bio-Raw Material Source for Epoxy-Based Composites***

Dobrosielska M., Dobrucka R., Gloc M., Brząkalski D., Szymański M., Kurzydłowski K.J., Przekop R.E., Materials, 14, 1663, 2021

iF = 3.748 M = 140

H3 ***Methodological Aspects of Obtaining and Characterizing Composites Based on Biogenic Diatomaceous Silica and Epoxy Resin***

Dobrosielska M., Dobrucka R., Brząkalski D., Gloc M., Rębiś J., Głowacka J., Kurzydłowski K.J., Przekop R.E., Materials, 14, 4607, 2021

iF = 3.748 M = 140

H4 ***Influence of Diatomaceous Earth Particle Size on Mechanical Properties of PLA/Diatomaceous Earth Composites***

Dobrosielska M., Dobrucka R., Brząkalski D., Frydrych M., Kozera P., Wieczorek M., Jałbrzykowski M., Kurzydłowski K.J., Przekop R.E., Materials, 15, 3607, 2022

iF = 3.748 M = 140

H5 ***Biocomposites Based on Polyamide 11/Diatoms with Different Sized Frustules***

Dobrosielska M., Dobrucka R., Kozera P., Kozera R., Kołodziejczak M., Gabriel E., Głowacka J., Jałbrzykowski M., Kurzydłowski K.J., Przekop R.E.; Polymers, 14, 3153, 2022

iF = 4.967 M = 100

H6 ***Polyamide 11 Composites Reinforced with Diatomite Biofiller—Mechanical, Rheological and Crystallization Properties***

Dobrosielska M., Dobrucka R., Pajewska-Szmyt M., Brząkalski D., Kozera P., Martyła A., Gabriel E., Kurzydłowski K.J., Przekop R.E., Polymers, 15, 1563, 2023

iF = 4.967 M = 100

H7 ***Beeswax as a natural alternative to synthetic waxes for fabrication of PLA/Diatomaceous earth composites***

Dobrosielska M., Dobrucka R., Kozera P., Brząkalski D., Gabriel E., Głowacka J., Jałbrzykowski M., Kurzydłowski K.J., Przekop R.E., Scientific Reports, 12, 1161, 2023

iF = 4.996 M = 140

H8 ***Effect of Wax Additives and Silanization of Diatom Surfaces on Thermomechanical Properties of Polylactide Composites***

Dobrosielska M., Dobrucka R., Pajewska-Szmyt M., Kozera P., Gabriel E., Głowacka J., Brząkalski D., Kurzydłowski K.J., Przekop R.E., Polymers, 14, 5511, 2022

iF = 4.967 M = 100

H9 ***Effect of wax type on selected properties of biocomposites***

Dobrosielska M., Dobrucka R., Kurzydłowski K.J., Przekop R.E., Przemysł Chemiczny, 103, 7, 2024

iF = 4.996 M = 140

H10 ***The Influence of Environmental Factors on the Degradation of PLA/Diatomaceous Earth Composites***

Dobrosielska M., Dobrucka R., Brząkalski D., Pajewska-Szmyt M., Kurzydłowski K.J., Przekop R.E., Polymers, 16, 1450, 2024

iF = 4.967 M = 100

Wykaz stosowanych skrótów

APTES	3-aminopropylotrietoksysilan
DE	*Diatomaceous Earth*, ziemia okrzemkowa
DLS	*Dynamic Light Scattering*, metoda dynamicznego rozpraszania światła
DMTA	*Dynamic Mechanical Thermal Analysis*, badanie dynamicznych właściwości termomechanicznych
DSA	*Dynamic Contact Angle*, kąt zwilżania
DSC	*Differential Scanning Calorimetry*, skaningowa kalorymetria różnicowa
EP	*Epoxy Resin*, żywica epoksydowa
FDM	*Fused Deposition Modelling*
FT-IR	*Fourier-Transform Infrared Spectroscopy*, Spektroskopia w podczerwieni z transformacją Fouriera
iPP	izotaktyczny polipropylen
MFR	masowy wskaźnik szybkości płynięcia
MVR	objętościowy wskaźnik szybkości płynięcia
PA11	poliamid 11
PA6	poliamid 6
PEI	polieteroimid
PLA	polilaktyd
PP	polipropylen
PU	poliuretan
SBS	kauczuk styren-butadien-styren
SEM	*Scanning Electron Microscope*, skaningowy mikroskop elektronowy
SEM/EDS	skaningowa mikroskopia elektronowa z analizatorem EDS (metoda spektroskopii dyspersji energii)

TPU	termoplastyczny poliuretan
WCA	*Water Contact Angle*, kąt zwilżania powierzchni wodą
XRD	*X-Ray Diffraction*, Dyfrakcja Rentgenowska

CZĘŚĆ I

1. Wprowadzenie

Każdego roku setki milionów ton materiałów polimerowych w różnych postaciach jest przetwarzanych w wielu gałęziach przemysłu. Według danych Eurostatu w 2021 roku w całej Unii Europejskiej wyprodukowano ponad 16 mln ton odpadów pochodzących tylko z opakowań z tworzyw sztucznych. Jedynie około 40% z nich poddano recyklingowi. To oznacza, że niemal 10 mln ton zużytych opakowań mogło trafić do środowiska w niezmienionej, nieprzetworzonej formie. W tym zawierają się m.in. foliowe jednorazowe torebki, których średnie czas użycia przez konsumenta wynosi jedynie 12 minut. Polska znajduje się na 5. miejscu wśród producentów opakowań z tworzyw sztucznych w Unii Europejskiej. Pomimo rosnącej świadomości społeczeństwa na temat gospodarowania odpadami, w latach 2014-2021 następował ciągły wzrost zużytych opakowań z tworzyw sztucznych z niemal 30 kg/osobę rocznie do około 36 kg/osobę rocznie. Ocena cyklu życia (LCA - *Life Cycle Assessment*) każdego wytworzonego produktu, niezależnie od jego przeznaczenia, jest kluczowa w celu oszacowania śladu środowiskowego tego wyrobu [1]. W analizie brane są pod uwagę wszystkie dostępne dane i śledzone są wszystkie etapy życia takiego produktu, począwszy od pozyskiwania surowców i ich przetwarzanie, przez proces otrzymywania produktu, metody dystrybucji, czas i sposoby użycia produktu, aż po ostatni etap, jakim jest koniec okresu użytkowania i związane z nim sposoby przetwarzania bądź ponownego wykorzystania danego produktu. Tylko w 2015 roku tworzywa sztuczne, odpowiadały za 1.781 mld ton ekwiwalentu CO_2 w ciągu cyklu życia produktu, gdzie produkcja obejmowała średnio 1085 mln ton, konwersja 535 mln ton, a wycofanie z użycia 161 mln ton. Dane te przekładały się na ponad 3% globalnej emisji gazów cieplarnianych [2]. Z tego względu nadal kluczowy pozostaje zrównoważony rozwój (sustainable development) oraz rola gospodarki o obiegu zamkniętym, co, miejmy nadzieję, pozwoli w dłuższej perspektywie zapobiec całkowitej degradacji środowiska naturalnego czy nadmiernej eksploatacji złóż, a także pozwoli ograniczyć emisję gazów cieplarnianych do środowiska. W koncepcji gospodarki o obiegu zamkniętym w kontekście gospodarowania odpadami istotna jest zasada „5R".

Koncepcja „5R" składa się z pięciu zasad, które brzmią, zależnie od źródła:

- *refuse* (odmawiaj) - zrezygnuj z plastikowych opakowań, które nie są niezbędne,

- *reduce* (ogranicz) - nie kupuj, jeśli nie potrzebujesz,
- *reuse* (użyj ponownie) – napraw, przerób, zastosuj ponownie,
- *recycle* (segreguj) – poddaj recyklingowi, gromadź odpady selektywnie,
- *rot* (kompostuj) – przekształć w cenny kompost, np. w przydomowym ogródku.

Powyższe zasady są elastyczne, a więc można stosować niemal do każdego typu odpadów, zarówno produkowanych w warunkach domowych, jak i w wyniku działalności przemysłowej. Tworzywa sztuczne są niezwykle ważnym elementem obecnej cywilizacji. Dążenie do ich wyeliminowania z masowego użycia nie jest korzystne ze względu na możliwe zahamowanie postępu technologicznego. Potencjalnie dobrym rozwiązaniem wydaje się biodegradacja materiałów kompozytowych, która jednak cechuje się szeregiem błędnych założeń, m.in. kompostowanie tworzyw sztucznych nie tylko powoduje przenikanie do gleby cząstek tworzyw sztucznych lub innych związków chemicznych obecnych w kompozycie, które nie są wrażliwe na działanie czynników biodegradacji, ale też nie bierze pod uwagę zużycia energii i wody podczas produkcji tych materiałów kompozytowych, a więc całość procesu jest nieefektywna energetycznie. Ponadto podczas rozkładu takiego biomateriału następuje emisja CO_2, która ma istotny wpływ na wzrost gazów cieplarnianych w atmosferze. Biorąc pod uwagę powyższe, proces biodegradacji nie przynosi dodatkowych korzyści, energetycznych czy materiałowych, w łańcuchu życia produktu.

W niniejszym cyklu badawczym skupiono się na otrzymaniu nowego rodzaju biokompozytu opartego w pełni o surowce pochodzenia naturalnego, gdzie potencjalnie możliwe będzie zastosowanie zasad 5R – „recycle”, jednak głównym końcowym założeniem przeprowadzonych badań było stworzenie materiału zarówno możliwego do recyclingu, ale jednocześnie odpornego na czynniki środowiskowe, dzięki zastosowaniu różnorodnych modyfikacji chemicznych. Tak zaprojektowany materiał pozwala zarówno ograniczyć jego rolę w środowisku i zakończyć cykl życia etapem recyklingu, dzięki czemu wpisuje się w zasadę gospodarki o obiegu zamkniętym, jak również, w celu efektywnego wykorzystania jego potencjału, możliwym jest jego relatywnie długotrwałe użytkowanie, co pozwala na wydłużenie cyklu życia i zredukowanie śladu węglowego. Kierunek zastosowań miał

koncentrować się na użyciu osnowy termoplastycznej w połączeniu z ziemią okrzemkową jako materiału konstrukcyjnego, a nie powszechnie znanym polu aplikacji w branży opakowaniowej.

Wytworzone kompozyty składały się z amorficznej ziemi okrzemkowej jako napełniacza, która została pozyskana z odnawialnych źródeł naturalnych, a więc jej proces otrzymywania nie pozostawił negatywnego wpływu na środowisko. Proces frakcjonowania cząstek napełniacza zaprojektowano w taki sposób, aby był zarówno prosty, niewymagający dużych nakładów energii, ale przy tym efektywny i wydajny. Osnowę konstrukcyjnych materiałów kompozytowych stanowił, w zależności od wybranego zagadnienia badawczego, polilaktyd lub poliamid 11, które klasyfikuje się jako biopolimery. Podjęto również udane próby wytworzenia i scharakteryzowania wysokonapełnionego kompozytu żywica epoksydowa/ziemia okrzemkowa, gdzie maksymalnie 70% objętości układu stanowił bionapełniacz. Zrealizowane prace miały na celu w szczególności nowe spojrzenie na kwestię użycia ziemi okrzemkowej w zaawansowanych materiałach kompozytowych z uwzględnieniem zagadnień wielkości cząstek oraz jego wpływu na parametry przetwórcze, mechaniczne i starzeniowe takiego materiału.

2. Dotychczasowy stan wiedzy z zakresu przedmiotu

2.1. Ziemia okrzemkowa – charakterystyka i właściwości fizykochemiczne

Okrzemki (łac: *Bacillariophyceae*) stanowią najbardziej rozpowszechnioną grupę alg na świecie. Są jednym z najbardziej spektakularnych przykładów nanostrukturalnych materiałów pochodzenia biologicznego [3]. Każda skorupka okrzemek ma specyficzne dla danego gatunku, regularnie rozmieszczone cechy [4]. Posiadają one skomplikowane ściany komórkowe, które są zbudowane z pektyny wysyconej krzemionką SiO_2 [5-6]. Za ich brunatny kolor odpowiedzialne są barwniki asymilacyjne, tj. chlorofil a, chlorofil c, karotenoidy (głównie fukoksantyna). Okrzemki stanowią główny fitoplankton w ekosystemach wodnych i odpowiadają za około 20-25% wydzielania tlenu i wiązanie węgla na świecie [7]. Żyją samotnie lub tworzą kolonie, a główne miejsce ich występowania stanowią wilgotne obszary na całym świecie, gdzie z powodzeniem mogą przeprowadzać fotosyntezę. Występują w środowisku wodnym, zarówno w wodach słonych, jak i słodkich, ze względu na swoją różnorodność gatunkową, dzięki której dostosowują się do różnych warunków. Ich pancerzyki składają się w głównej mierze z biokrzemionki (SiO_2), a więc są również źródłem krzemu w środowisku. Dzięki swoim specyficznym właściwościom i budowie hierarchicznej, znajdują zastosowanie we wszelakich gałęziach przemysłu, m.in. w medycynie jako suplementy diety pozytywnie wpływające na funkcjonowanie przewodu pokarmowego czy kondycję kości, co jest związane z ich doskonałymi właściwościami adsorpcyjnymi. Mimo, wydawać by się mogło, niedostatecznie rozwiniętej powierzchni właściwej ziemia okrzemkowa również sprawdza się jako złoże filtracyjne zarówno w przemyśle spożywczym, jak i we wszelkiego rodzaju procesach wymagających oczyszczania substancji zarówno ciekłych, jak i gazowych z pozostałości poprocesowych, tj. związków organicznych takich jak rozpuszczalniki czy oleje. Ponadto niska gęstość okrzemek, spowodowana obecnością struktury porowatej, sprawia, że ziemia okrzemkowa stanowi doskonały napełniacz do otrzymywania wyrobów w przemyśle farbiarskim, papierniczym, motoryzacyjnym czy szeroko rozumianym przemyśle tworzyw sztucznych, gdzie pozwala obniżyć koszta produkcyjne. Nie tylko niska gęstość, ale także wpływ okrzemek na właściwości wytworzonych kompozytów jest kluczowy.

Okrzemki kopalne występują w postaci diatomitu lub ziemi okrzemkowej. Zawartość krzemionki w diatomicie waha się od 60% do 95%, reszta to zanieczyszczenia, takie jak węglany, tlenki żelaza, kwarc, iły lub substancje pochodzenia wulkanicznego [8-9]. Pełny skład pierwiastkowy okrzemki o zawartości biokrzemionki na poziomie 75% przedstawiono

na Rysunku 1. Jeden cm^3 diatomitu zawiera około 2.5 miliarda muszli okrzemek [10-11]. Głównie występują w wodach słodkich i słonych, w tym na dnie zbiorników wodnych, ale również mogą żyć na glebie, wilgotnych skałach czy śniegu lub lodzie. Okrzemki, w zależności od gatunku, mogą występować w formie przytwierdzonej do podłoża lub swobodnie unosić się w toni wodnej, gdzie wchodzą w skład fitoplanktonu [12]. Łatwość pozyskiwania dużych ilości ziemi okrzemkowej ze środowiska naturalnego otwiera możliwość wykorzystania jej w zastosowaniach przemysłowych. Ponieważ okrzemki wykazują zdolność do adsorpcji jonów metali ciężkich (niklu, ołowiu, cynku i tytanu) i uczestniczą w utlenianiu wody, są one wykorzystywane do uzdatniania wody [13-14]. Ponadto, ze względu na swoje unikalne właściwości, w tym możliwość filtracji gazów i ich absorpcji, bakteriobójczość czy doskonała izolacyjność, stanowią alternatywę dla powszechnie stosowanych napełniaczy syntetycznych dodawanych do polimerów termoplastycznych, duroplastycznych czy elastomerów. Ponadto jest również stosowana jako dodatek do materiałów opakowaniowych czy wypełnień dentystycznych, przy produkcji cementu, filtracji, nanotechnologii, chromatografii, a głównie jako adsorbent [15-17].

Rysunek 1. Skład pierwiastkowy ziemi okrzemkowej, na postawie **[H1]**.

Okrzemki zaliczane są do jednokomórkowych eukariotycznych organizmów o stopniu morfologiczno-rozwojowym według Paschera w formie kokalnej, co oznacza, że nie posiadają wici ani nibynóżek, a do poruszania się wykorzystują ruch ślizgowy. Ich gatunkową cechą charakterystyczną jest posiadanie dobrze wykształconej ściany komórkowej, nazywanej pancerzykiem, która składa się w głównej mierze z uwodnionej

krzemionki, co bezpośrednio wpływa na sztywność i odporność na pękanie. Budowa okrzemek również jest charakterystyczna, bo składają się z dwóch części – wieczka i denka, które stanowią odpowiednio część dolną i część wierzchnią (okrywę) (Rysunek 2), na powierzchni pancerzyka występują pory (Rysunek 3), a więc okrzemka cechuje się hierarchiczną strukturą porowatą, gdzie przeważa udział mezoporów. Okrywy są z kolei zbudowane z pasa obwodowego i tarczki szczytowej, gdzie pas obwodowy bierze udział w „suwakowym" mechanizmie tworzenia kolonii (Rysunek 4). Proces rozmnażania okrzemek polega na podziale komórkowym, gdzie dwa protoplasty potomne dzielą ze sobą pancerzyk, a następnie każdy z nich dobudowuje denko. Taki mechanizm tworzenia kolonii powoduje zmniejszenie jednej linii w populacji po kolejnych podziałach. W celu przeciwdziałania temu efektowi okrzemki wykształciły zdolność do tworzenia auksospory, która dzieli się na komórki o dużych rozmiarach, a dopiero w dalszych etapach powstają osobniki o rozmiarach charakterystycznych dla danego gatunku [18].

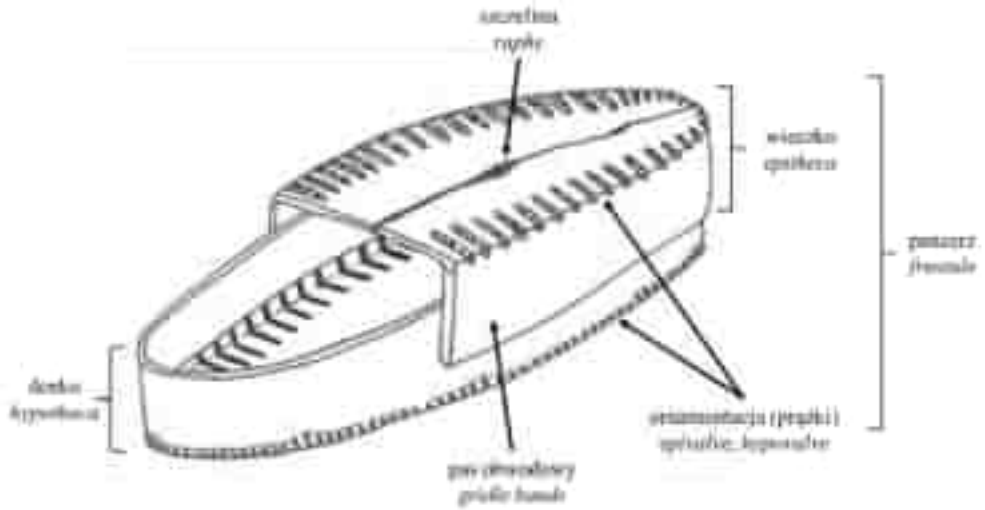

Rysunek 2. Budowa okrzemki. Opracowanie własne.

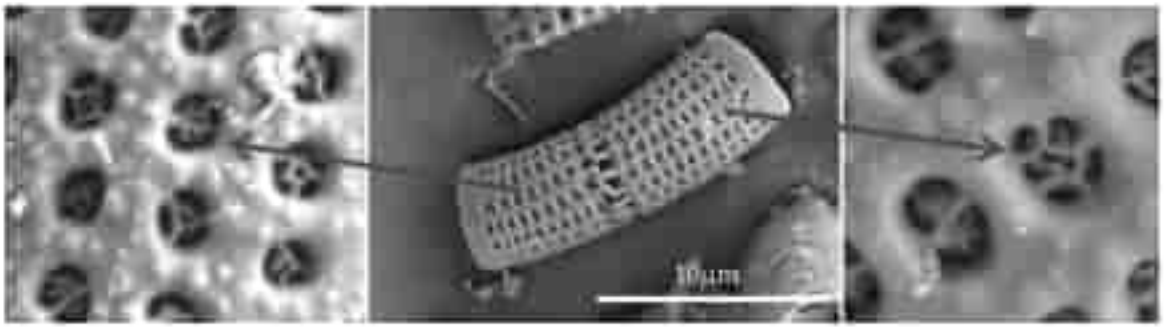

Rysunek 3. Pory zlokalizowane na powierzchni pancerzyka okrzemki, na podstawie **[H2]**.

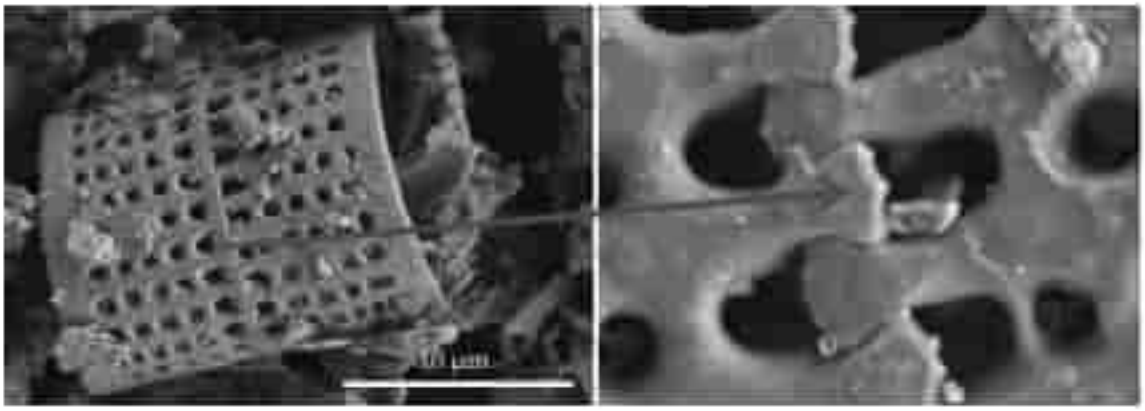

Rysunek 4. Mechanizm zamka – mechanizm tworzenia kolonii, na podstawie **[H2]**.

Kształty pancerzyków okrzemek są ściśle powiązane z ich gatunkiem, ale przeważnie posiadają pancerzyk o regularnych geometrycznych kształtach o wymiarach 5 μm - 0,5 mm [19]. Okrzemki jako ziemia okrzemkowa występują w różnej postaci, tj. ich pancerzyki mogą przyjmować formę pancerzyków połamanych, niepołamanych, a także jako struktury zaglomerowane, co zostało przedstawione na Rysunku 5. W toku niniejszych badań stwierdzono, iż rozmiary pancerzyków połamanych zawierają się w przedziale 0.5 – 3 μm, pancerzyków niepołamanych 3 – 40 μm, a struktur zaglomerowanych powyżej 40 μm. Poszczególne gatunki okrzemek są identyfikowane m.in. na podstawie ornamentacji krzemionkowych skorupek oraz kształtu samej okrzemki [20].

Rysunek 5. Zdjęcie SEM ziemi okrzemkowej; widoczne pancerzyki połamane, niepołamane i zaglomerowane. Na podstawie **[H1]**.

Wśród okrzemek można wyróżnić dwie grupy zróżnicowane między sobą ze względu na budowę komórki. Okrzemki centryczne (symetria promienista), Coscinodiscophyceae, cechują się posiadaniem komórek cylindrycznych, elipsoidalnych czy o kształcie dysku. Ornamentacja okrzemek, czyli sposób ułożenia perforacji w pancerzyku, ma również

charakter promienisty. Okrzemki pierzaste, czyli o symetrii dwubocznej, posiadają kształt zbliżony do prostopadłościanu, a nazwa ich grupy pochodzi od sposobu ornamentacji pancerzyka. Ponadto kolejną cechą charakterystyczną okrzemek pierzastych jest występowanie szczeliny w jednej bądź obu okrywach. Okrzemki bezszczelinowe noszą nazwę Fragilariophyceae, natomiast szczelinowe Bacillariophyceae. W przypadku okrzemek dwuszczelinowych zdolne są one do wykonywania zarówno ruchów ślizgowych, jak i obrotowych. W celu odróżnienia poszczególnych gatunków okrzemek wykorzystuje się ich charakterystyczne cechy, w tym cechy budowy komórki oraz rodzaj ornamentacji. Do najczęściej występujących okrzemek należą, m.in. Navicula tripunctata (gromada Bacillariophyta, rodzina Navicula), Chaetoceros (gromada Bacillariophyceae, rodzina Chaetocerotaceae), Pinnularia (gromada Bacillariophyceae, rodzina Pinnulariaceae, Bacillaria (gromada Bacillariophyceae, rodzina Bacillariaceae), Fragilariopsis kerguelensis (gromada Bacillariophycea, rodzina Bacillariaceae) [21].

2.2. Ziemia okrzemkowa w kompozytach termoplastycznych

Do polimerów, które wpisują się w idee gospodarki o obiegu zamkniętym należą, m.in. polilaktyd (PLA) czy poliamid 11 (PA11), które są biopolimerami pochodzącymi ze źródeł odnawialnych oraz mogą być poddawane recyklingowi, dzięki czemu ilość generowanych nieprzetwarzalnych odpadów na świecie mogłaby ulec zmniejszeniu. Właściwości fizykochemiczne tych polimerów, tj. ich wytrzymałość mechaniczna czy właściwości reologiczne z powodzeniem mogą być porównywalne, w pewnych warunkach, do właściwości polimerów tradycyjnych, biorąc pod uwagę ich ograniczony negatywny wpływ na środowisko.

Poprawa właściwości polimerów lub dostosowanie ich właściwości fizykochemicznych do potrzeb przemysłu czy konsumenta jest często uzyskiwana poprzez zastosowanie dodatków, np. napełniaczy naturalnych bądź syntetycznych. Tradycyjne napełniacze szeroko stosowane takie jak chociażby tlenki metali [22-23] czy cząstki metaliczne [24-26], mogą być zastępowane przez napełniacze naturalne, które nie tylko nadają tworzywom sztucznym podobne, a często lepsze właściwości fizykochemiczne, ale przede wszystkim ich szkodliwy wpływ na środowisko jest ograniczony. Do takich napełniaczy można zaliczyć ziemię okrzemkową, która jest nietoksyczna, pochodzi ze źródeł naturalnych, jest łatwa w obróbce przed wprowadzeniem do kompozytu, a koszty jej stosowania są na niskim poziomie. Zastosowanie ziemi okrzemkowej jako napełniacza kompozytów termoplastycznych w ostatnich latach znacząco wzrosło.

Do najczęściej stosowanych polimerów termoplastycznych należą, m.in. ABS (terpolimer akrylonitrylo-butadieno-styrenowy), PET (politereftalan etylenu), PE (polietylen), w tym LDPE (low density polyethylen) i HDPE (high density polyethylen), PP (polipropylen), PS (polistyren), PA (poliamid), PVC (polichlorek vinylu) czy PLA (polilaktyd), przy czym ostatni z nich pochodzi ze źródeł odnawialnych. Pozostałe wymienione polimery termoplastyczne często są ropopochodne, a przy tym ich wpływ na środowisko naturalne nie jest korzystny. Proces przetwórstwa polimerów termoplastycznych prowadzi się w stosunkowo niskich temperaturach, bo zależnie od tworzywa, w granicach 150-300°C. Mogą być one formowane szeroko dostępnymi i znanymi metodami przetwórczymi, w tym formowaniem wtryskowym, wytłaczaniem, czy za pomocą druku 3D (FDM), w zależności od typu polimeru. Proces otrzymywania kompozytów na bazie polimerów termoplastycznych zwykle jest prowadzony za pomocą stapiania w masie polimeru wraz z napełniaczem w granicach temperatury przetwórstwa danego polimeru. Ziemia

okrzemkowa, według doniesień literaturowych, wpływa zarówno na wzmocnienie kompozytu, tj. wytrzymałość mechaniczną oraz pozwala obniżyć gęstość wyrobu, stąd zastosowanie jej w formie napełniacza kompozytów termoplastycznych wydaje się być dobrym rozwiązaniem. W niniejszym rozdziale zostaną omówione kompozyty napełnione ziemią okrzemkową na osnowie polimerów termoplastycznych, ze szczególnym uwzględnieniem biopolimerów.

2.2.1. Kompozyty termoplastyczne - polilaktyd

Polilaktyd (PLA) zaliczany jest do biopolimerów ze względu na jego zdolność do biodegradacji oraz pozyskiwanie ze źródeł naturalnych, głównie poprzez fermentację mikrobiologiczną surowców skrobiowych [27]. Polilaktyd może występować w trzech odmianach stereochemicznych, tj. PLLA (poli(L-laktyd), PDLA (poli(D-laktyd) oraz PDLLA (poli(DL-laktyd). Dzięki swoim właściwościom może z powodzeniem zastępować szereg innych polimerów ropopochodnych. Może być przetwarzany na tych samych liniach produkcyjnych co tworzywo PET (formowanie z rozdmuchem, termoformowanie), a w przypadku polilaktydu o wyższym wskaźniku szybkości płynięcia może zastępować polistyren (formowanie wtryskowe) lub polipropylen (wytłaczanie włókien). PLA w określonych, kontrolowanych warunkach (temperatura min. 70°C, wilgotność min. 70%) może być poddawany kompostowaniu, gdzie ulega biodegradacji. Właściwości polilaktydu zależą od temperatury przetwarzania, od izomerów składowych, czasu wygrzewania oraz masy cząsteczkowej [28]. PLA cechuje się modułem Younga na poziomie około 3 GPa, wytrzymałością na rozciąganie pomiędzy 50 a 70 MPa i wydłużeniem przy zerwaniu ok. 4-7% oraz udarnością zbliżoną do 2,5 kJ/m^2. W porównaniu do innych polimerów, np. PS czy PET, PLA cechują lepsze właściwości mechaniczne, m.in. wytrzymałość na rozciąganie, jednakże, podobnie jak PS, PLA jest materiałem kruchym o niskiej udarności [29]. W zależności od składu izomerów składowych, polilaktyd cechuje się inną wytrzymałością na rozciąganie, np. polilaktyd o stosunku L,L/D,L 100/0 posiada wytrzymałość na rozciąganie na poziomie 64.8 MPa, natomiast w miarę wzrostu zawartości izomerów D,L wartości te ulegają obniżeniu do np. 51.7 MPa dla 80/20 L,L/D,L [30].

Ziemia okrzemkowa, potencjalnie, jest uważana za napełniacz powodujący wzmocnienie kompozytu w zakresie wytrzymałości mechanicznej, w tym wytrzymałości na rozciąganie, co zostało przedstawione m.in. w pracy Li T. [31], gdzie polilaktyd napełniono ziemią okrzemkową pochodzącą ze sztucznej hodowli w stężeniu od 2.5 do 10%

wag. Wykazano, że zarówno wytrzymałość mechaniczna, jak i twardość kompozytu mogą być zwiększone wtedy, kiedy zawartość ziemi okrzemkowej nie przekracza 5% wag. Zauważono również, że w przypadku wyższych napełnień wpływ na wytrzymałość mechaniczną ma tendencja napełniacza do aglomeracji, co osłabia efekt wzmocnienia. Sam proces wzmocnienia polilaktydu przez ziemię okrzemkową jest spowodowany przenikaniem polimeru przez pory napełniacza, co w konsekwencji tworzy wzajemnie przenikające się sieci. Li T. et. al. opublikowali również pracę [32], w której przeprowadzili ultraszybką degradację kompozytów PLA/DFs, gdzie pancerzyki okrzemek były ekstrahowane ze sztucznie hodowanych okrzemek w Morzu Południowochińskim. Do badań wybrano kompozyt o zawartości 5% napełniacza przebadany w poprzedniej pracy. Proces degradacji przeprowadzono w temperaturze ~30°C i ~60% wilgotności przez 12 tygodni w glebie pobranej ze środowiska naturalnego. Wykazano, że szybkość degradacji czystego polilaktydu w glebie jest bardzo niska, natomiast kompozyty PLA/DFs już po 4 tygodniach wykazały znaczne obniżenie właściwości mechanicznych, a po 12 tygodniach próbki rozpadły się, co uniemożliwiło wykonanie badań mechanicznych, co świadczy o znaczącym przyspieszeniu procesu degradacji czystego polilaktydu przez ziemię okrzemkową. Powierzchnia kompozytów PLA/DFs staje się szorstka, podczas gdy polilaktydu pozostaje praktycznie niezmieniona, a pory w kompozytach ulegają zwiększeniu aż do 50 μm po 8 tygodniach. Ponadto badania wykazały, że polilaktyd ulega powolnej degradacji powierzchniowej, co skutkuje jedynie niewielkimi zmianami w morfologii, właściwościach mechanicznych i porowatości, natomiast kompozyty degradują w całej objętości, co jest indukowane przez samą ziemię okrzemkową. Ziemia okrzemkowa, co wykazano, może wpływać na tworzenie się kryształów, które poprzez zwiększenie heterogeniczności w matrycy polimeru, skutkują propagacją pęknięć.

W kolejnej pracy podnoszącej zagadnienie modyfikacji polilaktydu ziemią okrzemkową autorzy [33] na podstawie wcześniej opublikowanych badań, podjęli próbę opracowania nowego typu membran nanowłóknistych (NFMs) składających się z polilaktydu i czynnika kontrolującego proces degradacji, czyli ziemi okrzemkowej o stężeniu 5% wag. Badania powstały w odpowiedzi na światowy problem zanieczyszczenia środowiska poprzez nieefektywną utylizację (lub praktycznie całkowity jej brak) maseczek ochronnych jednorazowych, wykorzystywanych podczas pandemii COVID-19. Opracowany filtr membranowy cechował się, dzięki zastosowaniu ziemi okrzemkowej jako napełniacza, wysoką szybkością degradacji (warunki naturalne, 42 dni). Ponadto ziemia okrzemkowa

również miała wpływ na poprawę wydajności filtracji poszczególnych substancji (PM, ponad 99%), co udało się osiągnąć dla membrany o grubości nawet jedynie 0.1 mm.

W pracy Agüero A. [34] również podjęto próbę opracowania kompozytu PLA/DE o zawartości 10% wag. napełniacza, jednak w tym przypadku wykorzystano również 3 różne kompatybilizatory, (3-glicydyloksypropylotrimetoksysilan (GLY), oligomer styrenowo-akrylowy na bazie żywicy epoksydowej (ESAO) oraz maleinizowany olej lniany (MLO), w celu poprawy oddziaływań polimer-wypełniacz. Po przeprowadzeniu silanizacji ziemi okrzemkowej za pomocą glicydoksypropylotrimetoksysilanu obserwowany był wzrost sztywności oraz twardości kompozytu, co skutkowało zmniejszeniem wytrzymałości na rozciąganie i udarności w porównaniu z referencyjnym kompozytem PLA/DE, gdzie zauważono, że cząstki napełniacza wykazują większą kompatybilność z matrycą polilaktydową, co umożliwia przenoszenie większych obciążeń wewnętrznych, a więc następuje poprawa udarności dla takich kompozytów. Dodatek ESAO oraz MLO skutkował znacznym wzrostem udarności w stosunku do PLA/DE, natomiast zauważono również, że dodatek samego MLO powoduje ponadto znaczne zwiększenie wydłużenia przy zerwaniu (prawie trzykrotny wzrost w stosunku do PLA/DE).

Jako kontynuacja badań Agüero A. [34] Gonzalez L. i inni [35] przeprowadzili modyfikację kompozytu PLA/DE za pomocą maleinizowanego oleju lnianego (MLO), ale stężenie diatomitu pozostało stałe (10% wag.), natomiast układ badano pod kątem wpływu różnego stężenia MLO na właściwości mechaniczne i fizykochemiczne. Do badań wykorzystano ziemię okrzemkową o wielkości cząstek 4 and 7 μm, trójkątnym kształcie pancerzyka i zaokrąglonych brzegach. Zaobserwowano wpływ samej ziemi okrzemkowej na zmianę parametrów termicznych polilaktydu, szczególnie na proces zimnej krystalizacji, gdzie po napełnieniu polilaktydu 10% wag. ziemi okrzemkowej proces zimnej krystalizacji następował przy temperaturze T_{cc} = 112◦C (PLA T_{cc} = 119◦C), co jest bezpośrednio związane z działaniem cząstek ziemi okrzemkowej, jako czynnika nukleującego, co sprzyja tworzeniu krystalitów. Ziemia okrzemkowa również poprawia stabilność termiczną polilaktydu – początek procesu degradacji (T_{onset}) w przypadku polilaktydu wynosił 264◦C, natomiast po dodaniu napełniacza zaobserwowano wzrost tej temperatury do 294,3◦C, co potwierdza, że dodatek niewielkich ilości materiałów nieorganicznych do matrycy polimerowej zapewnia zwiększoną stabilność termiczną [36]. Badając wpływ dodatku diatomitu na wytrzymałość mechaniczną kompozytów, zauważono również wzrost modułu Younga o niemal 50% w stosunku do czystego polilaktydu (900-1344 MPa), a przy tym jednoczesny spadek wydłużenia przy zerwaniu i wytrzymałości na rozciąganie,

co jest związane z występowaniem efektu punktowej koncentracji naprężeń, zwiększenia kruchości materiału przez charakter napełniacza, w konsekwencji szybszej propagacji pęknięcia, co bezpośrednio przekłada się również na wartości udarności kompozytów.

W pracy Cacciotii I. [37], oprócz diatomitu, do polilaktydu dodano również ekstrakt ze zmielonych ziaren kawy i wytworzono folie metodą *solvent casting technique*. Ziemia okrzemkowa została dodana w celu zapewnienia zarówno wzmocnienia mechanicznego, jak i fizycznej bariery dla przenikania tlenu, dzięki porowatej budowie cząstek okrzemek, co pozwoliło na obniżenie wartości parametru OTR (*Oxygen Transmission Rate*, wskaźnik przenikalności tlenu). Ponadto zauważono podobny efekt wzmocnienia polilaktydu, jaki był obserwowany w pozostałych przytoczonych pracach. Ziemia okrzemkowa pozytywnie wpłynęła na poprawę właściwości wytrzymałościowych kompozytów, w szczególności zaobserwowano wzrost modułu Younga o około 50% w stosunku do referencyjnego układu, co przekłada się na dobrą dyspersję napełniacza w osnowie polimerowej, co również zauważono za pomocą obserwacji SEM. Cząstki napełniacza, nawet po próbie rozciągania, wciąż pozostają dobrze zakotwiczone w matrycy polimeru, co oznacza, że nie są wyrywane/łamane podczas badania. Ponadto porowata struktura pancerzyków okrzemek pozwala na wnikanie łańcuchów polilaktydowych do ich wnętrza, co również znacząco poprawia oddziaływania napełniacz-osnowa.

W pracy [38] ziemia okrzemkowa została wykorzystana jako czynnik zapobiegający degradacji olejku rozmarynowego przy produkcji materiałów opakowaniowych na matrycy polilaktydowej. Wykazano, że cząsteczki olejku rozmarynowego poddane procesowi enkapsulacji, m.in. w ziemi okrzemkowej zachowują swoje właściwości podczas wytłaczania folii i nie ulegają termicznemu rozpadowi. Ponadto ziemia okrzemkowa, w zawartości powyżej 1% wag., wpływa na tworzenie defektów strukturalnych w wytłoczonej folii opakowaniowej. Natomiast w pracy [39] wskazano, że dodatek ziemi okrzemkowej do kompozytu PLA/PBAT (PBAT - kopolimer adypinianu butylenu i tereftalanu butylenu) zwiększał wydłużenie przy zerwaniu z 2.4% do 3.4% (1% wag. DE), ale jednocześnie obserwowano spadek tego parametru wraz ze wzrostem stężenia napełniacza (3.2% dla 3% wag. DE). Ponadto zauważono, że ziemia okrzemkowa pozytywnie wpływa na zdolność krystalizacji, jednocześnie wpływając na obniżenie parametrów termicznych kompozytów. W pracy Koranteng E. [40] również wykorzystano pochodną PBA, tj. PBAPU (prepolimer poliuretanowy na bazie estru adypinianu poli(butanodiolu)) jako modyfikator ziemi okrzemkowej stanowiącej napełniacz polilaktydu. Dzięki zastosowaniu modyfikacji uzyskano wyższą stabilność termiczną kompozytów (przy dodatku 20% wag. PBAPU), lepszą dyspersję

napełniacza w matrycy polimerowej oraz wyższą wytrzymałość na rozciąganie, która jednakże malała wraz ze wzrostem stężenia zarówno napełniacza krzemionkowego, jak i modyfikatora PBAPU (E_{PLA}=3.17 GPA, E_{PLA+DE}=7.25 GPA, $E_{PLA+DE+20\%wag.PBAPU}$=4.48 GPA). Ponadto uzyskano ponad dwukrotną poprawę parametrów w zakresie udarności dla kompozytu zawierającego 20% wag. PBAPU w stosunku do czystego polilaktydu.

Kalcynacja ziemi okrzemkowej (750°C) ma wpływ na zwiększenie powierzchni właściwej oraz średniej wielkości cząstek, co wykazano w pracy Łach M. [41], gdzie zauważono, że średni rozmiar cząstek wzrasta z 13.3 μm do 17.2 μm, co może być związane z aglomeracją cząstek DE podczas procesu kalcynacji. W niniejszej pracy ponadto wykorzystano trzy frakcje ziemi okrzemkowej o różnym rozmiarze cząstek, dzięki czemu wykazano, że w zależności od wielkości cząstek DE zmianom ulega, m.in. współczynnik przewodzenia ciepła, gdzie najwyższe wartości odnotowano dla diatomitu o frakcji 0.5-3 mm, a najniższe dla 0-0.063 mm. Wykazano również, że proces kalcynacji obniża współczynnik przewodzenia ciepła. Dodatek ziemi okrzemkowej do polilaktydu wpływa na poprawę właściwości akustycznych, tj. zdolności pochłaniania dźwięku, ze względu na unikalną porowatą strukturę DE. Wraz ze wzrostem porowatości poprawie ulegają zdolności do tłumienia dźwięku.

Polilaktyd jest najpowszechniejszym tworzywem termoplastycznym stosowanym w druku 3D techniką FDM, głównie ze względu na łatwość przetwarzania, niski skurcz termiczny podczas procesu drukowania [42] oraz brak emisji szkodliwych substancji chemicznych [43]. W tej technice polimer lub kompozyt termoplastyczny jest lokalnie podgrzewany w głowicy drukującej aż do jego stopienia, a następnie układany warstwowo zgodnie z zaprojektowanym cyfrowo modelem 3D fizycznej bryły. Na parametry, np. wytrzymałościowe gotowego wyrobu wpływa, m.in. grubość warstwy, szczeliny pomiędzy warstwami, gęstość materiału [44-45]. W celu poprawy właściwości polilaktydu stosuje się szereg napełniaczy, modyfikatorów. W pracy Zgłobicka I. [46], w celu modyfikacji właściwości polilaktydu, wytworzono kompozyt PLA/DE, o różnych typach osnowy polimerowej (2003D, 3001D, 3251D oraz 4043D (Ingeo Nature Work)), które cechują się m.in. różnicami we wskaźnikach szybkości płynięcia. Badania wykazały, że podobnie jak we wspomnianej wcześniej pracy Carrasco F. [36], polimer wnika w strukturę cząstek napełniacza i tym samym wpływa na zwiększone wiązanie matrycy polimerowej z napełniaczem, powodując wzmocnienie kompozytu, co przekłada się na wzrost sztywności. Wynika to również ze składu pierwiastkowego ziemi okrzemkowej (wysoka zawartość SiO_2, specyficzna budowa okrzemek, która powoduje wysoką odporność na ściskanie). Jednocześnie również w tej pracy

obserwowany jest spadek wytrzymałości na rozciąganie oraz wydłużenia przy zerwaniu, co jest charakterystyczne dla kompozytów termoplastycznych napełnionych ziemią okrzemkową. Jednoczenie obecność pancerzyków okrzemek w kompozycie, ze względu na to, iż są wypełnione powietrzem, skutkuje obniżeniem gęstości wyrobu, przy jednoczesnym zachowaniu właściwości mechanicznych.

Istotny z punktu widzenia wytrzymałości mechanicznej kompozytów, jest odpowiednie przygotowanie ziemi okrzemkowej przed modyfikacją polilaktydu. Jak przedstawiono wcześniej ziemia okrzemkowa wpływa bezpośrednio na zwiększoną szybkość degradacji kompozytu na bazie polilaktydu, a tym samym jest bardziej korzystna dla środowiska, pod kątem utylizacji odpadów, ale również jednocześnie wyższa wytrzymałość mechaniczna takiego kompozytu jest zachowana.

2.2.2. Kompozyty na matrycy poliamidowej i inne kompozyty termoplastyczne

Nie tylko polilaktyd, ale też inne polimery termoplastyczne są szeroko stosowane w różnych gałęziach przemysłu. W prawdzie stosowanie innych polimerów niesie za sobą inne problemy niż w przypadku polilaktydu, natomiast wspólny mianownik pozostaje ten sam – kwestia zanieczyszczenia środowiska materiałami nie pochodzącymi ze źródeł naturalnych. Z tego względu dodatek ziemi okrzemkowej nie tylko do biodegradowalnego polilaktydu zdaje się być dobrym rozwiązaniem z punktu widzenia ochrony środowiska.

W literaturze dostępne są doniesienia naukowe dotyczące napełniania PEI, SBS, PA, PP, PA11, PA6, PU czy TPU różnogatunkową ziemią okrzemkową czy też ziemią okrzemkową pochodzącą z recyklingu, co dodatkowo podwyższa istotny aspekt zagospodarowania odpadami. Kompozyt na bazie nylonu i recyklingowanej ziemi okrzemkowej wykazuje zwiększoną stabilność termiczną, natomiast wraz ze wzrostem stężenia napełniacza właściwości mechaniczne (udarność, wytrzymałość na rozciąganie) ulegały zmniejszeniu. Ponadto prosta metoda bezpośredniej impregnacji użyta do otrzymywania takiego kompozytu nie wymaga dużych nakładów. Wykorzystanie odpadów ziemi okrzemkowej z przemysłu browarniczego zmniejsza ilość generowanych w środowisku odpadów [47]. Ziemia okrzemkowa może być również wykorzystana jako napełniacz poliamidu 11 w kompozytach otrzymywanych za pomocą druku 3D metodą Selektywnego Spiekania Laserowego (SLS, *Selective Laser Sintering*). W pracy Andrusiv L. [48] dowiedziono, że wraz ze wzrostem zawartości ziemi okrzemkowej w kompozycie, składniki łączą się ze sobą, a krawędzie

pęknięć są bardziej czyste i równe, co oznacza, że poliamid 11 dobrze wiąże się z porowatym napełniaczem. Ponadto wytworzony kompozyt w miarę wzrostu stężenia ziemi okrzemkowej staje się mniej elastyczny i bardziej kruchy, natomiast zauważono, że wartości granicy plastyczności oraz modułu sprężystości wzrastają. Ziemia okrzemkowa jest również stosowana w połączeniu z innymi napełniaczami w celu jeszcze większej poprawy parametrów kompozytu. W pracy Cheng Z.-Z., [49] zbadano synergiczny wpływ połączenia diatomitu i haloizydu na właściwości mechaniczne kompozytu na osnowie PP i PA6. Zauważono, że napełniacz w stosunku 3:3 HNTs/DE ma znaczący wpływ na podwyższenie parametrów mechanicznych – wzrost wytrzymałości na rozciąganie o 16%, modułu Younga o 38% i o ponad 40% wytrzymałość na zginanie i udarność w porównaniu do czystego PP. Natomiast dla proporcji napełniaczy 5:1 wzrost w stosunku do czystego PA6 nastąpił o odpowiednio 46, 23, 43 i 45%. Wpływ ziemi okrzemkowej na właściwości polipropylenu (PP) zbadano również w pracach Liang J. Z. [50] i Chen Y. i Wang B. [51], gdzie zauważono, że ziemia okrzemkowa wpływa na właściwości reologiczne kompozytów, przy czym wraz ze wzrostem wielkości cząstek napełniacza wskaźnik MVR ulegał obniżeniu. Ziemia okrzemkowa może również działać jako katalizator w procesie termicznej degradacji polipropylenu, a ponadto bierze również udział w reakcji z produktami pirolizy poprzez utworzenie wiązań Si-O-C, co w konsekwencji prowadzi do powstania usieciowanej struktury i może promować wzrost grafenu podczas wysokotemperaturowego procesu grafityzacji. Dodatek ziemi okrzemkowej do izotaktycznego polipropylenu (iPP) prowadzi m.in. również do wzrostu wytrzymałości na rozciąganie, gdzie dodatek 5%, 10% i 15% wag. napełniacza prowadził do podwyższenia tego parametru o odpowiednio 6.2%, 8.4% i 12.0% w stosunku do czystego polipropylenu, a zarówno moduł Younga, jak i udarność takich kompozytów wzrastają wraz ze wzrostem stężenia ziemi okrzemkowej [52].

Kolejną grupą polimerów, w których zastosowano modyfikację za pomocą ziemi okrzemkowej są poliuretany. W pracy Kucińska-Lipka J. [53] podczas badania wpływu napełniacza na mobilność fragmentów makrocząsteczek polimeru oraz na modyfikację właściwości polimeru do druku 3D zauważono wpływ napełniacza w postaci ziemi okrzemkowej na sztywność polimerów termoplastycznych. Natomiast w pracy Mustafov S.D. [54] zauważono, że diatomit stosowany jako czynnik wzmacniający pianki poliuretanowe zwiększa ich powierzchnię i chropowatość, tym samym poprawia zdolność przyłączania się komórek w zastosowaniach medycznych. Podobny efekt zauważono w pracy Perera H.J. [55], gdzie ziemia okrzemkowa również odpowiedzialna była za zwiększenie chropowatości i porowatości kompozytu, a ponadto przyczyniła się do strukturyzacji powierzchni,

co zwiększyło kąt zwilżania kompozytu i poprawiło właściwości hydrofobowo-hydrofilowe. Ziemia okrzemkowa również wpływa na poprawę właściwości mechanicznej kompozytów na osnowie TPU, co zaobserwowano w pracy Kucuk F. [56], gdzie dodatek ziemi okrzemkowej, zwłaszcza w wyższym stężeniu, skutkował poprawą wytrzymałości na rozciąganie oraz twardości Shore'a, a także wzrostem temperatury zeszklenia czystego TPU, co jest związane z oddziaływaniami cząstek diatomitu z miękkimi segmentami struktury TPU. Natomiast wyższe stężenie napełniacza skutkuje wtórną aglomeracją cząstek w polimerze. W pracy Leskovac M. [57] zauważono również niską adhezję napełniacza diatomitowego do matrycy polimerowej PA, zwłaszcza w przypadku okrzemek o budowie cylindrycznej i o dużych rozmiarach. Natomiast w pracy Wu G. [58] zwrócono uwagę, m.in. że zastosowanie silanowych środków sprzęgających może wpływać na zwiększenie adhezji pomiędzy napełniaczem a matrycą polimerową i wpływać na zwiększenie właściwości mechanicznych kompozytu, w szczególności udarności. Ziemia okrzemkowa wykazuje również tendencje do sedymentacji, co zauważono w pracy Caccotti I. [59], gdzie matrycę polimerową stanowił polieteroamid (PEI). Niezależnie od stężenia napełniacza otrzymane w pracy układy cechowały się budową dwuwarstwową, gdzie jedną z warstw stanowiła zsedymentowana ziemia okrzemkowa, co negatywnie wpływało na wytrzymałość mechaniczną kompozytów, która była porównywalna do wytrzymałości na rozciąganie czystego polimeru. Cząstki okrzemek mogą być również z powodzeniem stosowane jako absorbenty m.in. środków przeciwoblodzeniowych, co powoduje, że kompozyt na bazie SBS i 30% wag. DE wykazuje właściwości przeciwoblodzeniowe, które zależne są od ilości środka w układzie [60]. Rozpuszczone środki przeciwoblodzeniowe przenikają do wnętrza kompozytu i są absorbowane w porach hydrofilowych okrzemek w wyniku interakcji pomiędzy DE, a hydrofilowym środkiem przeciwoblodzeniowym. Powierzchnia takiego kompozytu składa się z izolowanych wysp środków przeciwoblodzeniowych zlokalizowanych w przypowierzchniowych porach cząstek ziemi okrzemkowej. Dzięki porowatej strukturze okrzemek, kompozyt dłużej utrzymuje swoje właściwości przeciwoblodzeniowe, pomimo postępującego celowego niszczenia powierzchni, ponieważ odsłonięcie głębszych warstw w kompozycie pozwala na uwolnienie większych ilości środka zlokalizowanego w porach okrzemek głębiej położonych w kompozycie.

2.3. Ziemia okrzemkowa w kompozytach duroplastycznych i elastomerowych

Kolejną grupą kompozytów, do których modyfikacji wykorzystano ziemię okrzemkową są kompozyty duroplastyczne. W pracy Tasdemirci A. [61] zbadano wpływ okrzemek o cylindrycznych kształtach i wykazano, że ziemia okrzemkowa powoduje wzrost wytrzymałości mechanicznej nie tylko kompozytów termoplastycznych, co zostało opisane w poprzednio przytoczonych pracach, ale również duroplastycznych, gdzie 15% wag. ziemi okrzemkowej zwiększa zarówno moduł, jak i granicę plastyczności matrycy epoksydowej przy quasi-statycznych i wysokich prędkościach odkształcania bez znaczącego zmniejszenia odkształcenia przy zerwaniu. Z badań wynika, że potencjalnie ziemia okrzemkowa może być z powodzeniem stosowana jako materiał wzmacniający matrycę duroplastyczną. W grupie badawczej kontynuowano badania nad właściwościami ziemi okrzemkowej jako napełniacza kompozytów polimerowych w wyniku czego w 2013 roku opublikowano kolejną pracę podnoszącą to zagadnienie. Gültürk E.A., Güden M. i Tasdemirci A. [62] ponownie zbadali wpływ ziemi okrzemkowej, natomiast zastosowano napełniacz kalcynowany i porównawczo naturalny w różnych stężeniach. Zauważono m.in., że naturalna, niekalcynowana ziemia okrzemkowa wpływa na wyższa szybkość odkształcania kompozytów, natomiast dla kalcynowanej ziemi okrzemkowej efekt ten jest mniej widoczny. W 2016 roku ukazała praca Zeren D. [63], gdzie z badań wynika, że napełnienie żywicy epoksydowej około 6% wag. naturalnie występującą ziemią okrzemkową, uprzednio kalcynowaną w celu podniesienia stopnia krystaliczności, spowodowało wzrost wytrzymałości na ściskanie do 90 MPa, natomiast napełniacz bez kalcynacji wykazywał wzrost tego parametru od 60 do 79 MPa. Zauważono, że kalcynacja okrzemek w temperaturze powyżej 900°C powoduje zmianę struktury krystalicznej ziemi okrzemkowej ze struktury opalu do krystobalitu. Ponadto zauważono, że kalcynacja DE w 1000°C ma wpływ na wzrost granicy plastyczności żywicy epoksydowej o 50%, natomiast napełniacz kalcynowany poniżej tej temperatury powoduje wzrost o 25%, podczas gdy czysta niekalcynowana ziemia okrzemkowa jedynie o 16% w porównaniu do czystej żywicy epoksydowej. Natomiast kalcynacja napełniacza powyżej 1000°C ma również wpływ na ponad dwukrotne obniżenie jego powierzchni właściwej. Z badań wynika również, że podnosząc temperaturę kalcynacji ziemi okrzemkowej możliwe jest uzyskanie ziaren o większych rozmiarach, do około 500 nm w temperaturze 1200°C (wielkość ziaren po kalcynacji w 1000°C wynosiła mniej niż 100 nm).

Badania opublikowane przez Perera H.J. [64-65] w kolejnych latach, skupiły się na wytworzeniu hydrofobowego kompozytu ziemia okrzemkowa – żywica epoksydowa, gdzie jako czynnik zwiększający stopień hydrofobowości powierzchni zastosowano silanizację, zarówno fluorosilanem, jak i później silanem z grupami alkilowymi. W przypadku układów zawierających zmienną ilość fluorosilanu osiągnięto powierzchnię, której kąt zwilżania wyniósł ponad 160°, a więc osiągnięto wartości superhydrofobowej powierzchni. W przypadku zastosowania silanu o grupach alkilowych również możliwe było uzyskanie superhydrofobowej powierzchni o zbliżonych wartościach kąta zwilżania, natomiast zauważono, że najlepsze wyniki uzyskuje się dla 30% napełnienia kompozytu ziemią okrzemkową, gdzie powierzchnia jest wysycona cząstkami DE, a większa jej zawartość (powyżej 50%) obserwowany jest spadek kąta zwilżania, co jest związane ze zmniejszeniem chropowatości powierzchni. W pracy zaobserwowano również wpływ długości alkilowego łańcucha silanowego na właściwości hydrofobowo-hydrofilowe kompozytu. Alkilotrimetoksysilan, o wzorze sumarycznym $[CH_3(CH_2)_{n-1}(OCH_3)_3$, gdzie *n* wynosiło do 12 powodował wzrost hydrofobowości powierzchni, natomiast dla n=12 i powyżej 12 zaobserwowano plateau, a następnie spadek właściwości hydrofobowych.

Ziemia okrzemkowa posłużyła również do modyfikacji właściwości kompozytów hydrożelowych na bazie poliakrylamidu [66], gdzie udowodniono, że wraz ze wzrostem stężenia diatomitu wzrasta wytrzymałość na rozciąganie i wytrzymałość na ściskanie, odpowiednio z 23.6 kPa do 73.5 kPa dla najwyższego stężenia i 0.17 MPa do 2.26 MPa dla zawartości DE do 8 phr i jest to zawartość optymalna, gdyż większy dodatek powoduje tendencję spadkową. Zauważono również, że optymalna przeźroczystość kompozytu hydrożelowego występuje dla zawartości 4 phr diatomitu, a współczynnik pęcznienia gwałtownie spada wraz ze wzrostem stężenia DE, co można wyjaśnić tym, że zdolność absorpcji wody czystego hydrożelu jest większa niż dodanego diatomitu, a ziemia okrzemkowa działa jako dodatkowy czynnik sieciujący.

W 2021 roku powstały prace opisujące wpływ ziemi okrzemkowej na właściwości kompozytu duroplastycznego. Zespół Liu W. [67] zaproponował materiał składający się z ziemi okrzemkowej i żywicy fluorosilikonowej, który został zastosowany jako środek przeciwdziałający pleśni rozwijającej się na ścianach budynków mieszkalnych. Sprej DE/HLR-Si spowodował, że ściany uzyskały właściwości samoczyszczące i grzybobójcze, a właściwości hydrofobowe powierzchni utrzymywały się do około 380 dni po nałożeniu. Ponadto, dzięki obecności wiązań fluorowych, które zapobiegają fotodegradacji powierzchni, materiał wykazywał odporność na promieniowanie UV i po ekspozycji kompozytu przez

96 h nadal wykazywał właściwości superhydrofobowe, a kąt zwilżania był wyższy niż 155°. Ponadto ziemia okrzemkowa modyfikowana żywicą HLR-Si cechowała się większym rozmiarem cząstek niż czysta DE ze względu na wiązanie SiO_2 na ich powierzchni. W pracy Sun X. [68] przedstawiono wyniki badań dotyczące jednoetapowej syntezy superhydrofobowego kompozytu za bazie żywicy poliuretanowej (PU) i ziemi okrzemkowej modyfikowanej aminosilanem APTES, gdzie zauważono, że wraz ze wzrostem zawartości aminosilanu właściwości hydrofobowe ulegają delikatnemu obniżeniu, ale nadal kompozyt wykazuje właściwości superhydrofobowe (153-159° dla stężeń APTES odpowiednio 4-7%; kompozyt bez modyfikacji APTES – WCA 162° (30% DE)). Testy ścieralności wykazały, że zarówno niewielki dodatek silanu APTES, jak i silnie zakotwiczone cząstki ziemi okrzemkowej poprawiają odporność powłok na zużycie. Badane powłoki z powodzeniem mogą być nanoszone na różnego typu podłoża, m.in. płytki szklane, piaskowane płytki aluminiowe, płyty stalowe, płyty ze stopu aluminium, płyty żelazne, PET, gdzie wykazują zadowalającą odporność mechaniczną, a ponadto wykazuje odporność na większość powszechnie występujących zanieczyszczeń płynnych (zanieczyszczona woda, kawa, kwaśne napoje), kwasów, zasad czy roztworów, w tym roztworów różnych soli. W pracy Li X. [69] zaproponowano kompozyt na bazie ziemi okrzemkowej silanizowanej syntetyczną biopochodną eteru glicydowego. Zauważono, że napełniacz nie wykazuje tendencji do wtórnej aglomeracji w kompozycie i cechuje się dobrą dyspersją. Wykazano również, że po dodaniu diatomitu parametry termiczne i mechaniczne ulegają poprawie w zakresie temperatury początku degradacji, ale również w zakresie modułu elastyczności, gdzie dla czystej żywicy odnotowano wartość 1.8 GPa, a dla kompozytów zawierających DE, w zależności od jego stężenia, 4.1-4.4 GPa. Uzyskano również wzrost charakteru hydrofobowego powierzchni z 78.7° dla czystej żywicy do 88.9° dla kompozytu zawierającego 20% ziemi okrzemkowej. Wykazano, że kompozyty mogą być stosowane jako odnawialna i zrównoważona alternatywa dla kompozytów epoksydowych na bazie ropy naftowej.

W pracy [70] zbadano m.in. wpływ silanizowanej (APTES, PFOTS) ziemi okrzemkowej na właściwości hydrofobowo-hydrofilowe powierzchni kompozytów duroplastycznych otrzymanych metodą dip-coatingu i stwierdzono, że możliwe jest uzyskanie powierzchni o kącie zwilżania powyżej 135° w zależności od ilości nałożonych warstw żywicy epoksydowej modyfikowanej ziemią okrzemkową. Wartości superhydrofobowe uzyskały kompozyty jednowarstwowe DE-APTES-EPOXY oraz dwuwarstwowe DE-PFOTS-EPOXY i DE-PFOTS-APTES-EPOXY.

Ziemia okrzemkowa może być z powodzeniem stosowana w przypadku kompozytów na bazie żywic, jako czynnik wzmacniający, co wynika z wyżej przytoczonych prac, a ponadto możliwe jest również utworzenie kompozytu cechującego się powierzchnią o właściwościach superhydrofobowych. Jednocześnie metoda otrzymywania takich kompozytów jest istotna, gdyż zauważono, że w zależności od zastosowanej formy odlewniczej, możliwe jest uzyskanie kompozytu o innych właściwościach mechanicznych. Ziemia okrzemkowa jest również stosowana jako napełniacz kompozytów na bazie elastomerów, gdzie powoduje wzrost modułu sprężystości oraz zmniejsza odkształcenie przy zerwaniu. W pracy Lamastra F.R. [71] zaproponowano prostą i ekologiczną metodę modyfikacji ziemi okrzemkowej grupami silanolowymi w celu zwiększenia ich podatności na modyfikację dwufunkcyjnymi silanami zawierającymi grupy siarkowe do zastosowań w wyrobach gumowych. Wykazano, że dodatek silanizowanej ziemi okrzemkowej, w stosunku do czystego elastomeru, powoduje wzrost modułu sprężystości o około 50% oraz zmniejszenie odkształcenia przy zerwaniu o 30%. Ziemia okrzemkowa wykazuje dobrą interakcję pomiędzy matrycą polimeru oraz jest w niej dobrze zdyspergowana. Silanizowany diatomit natomiast wykazuje zdolność do wiązania z cząsteczkami elastomeru, co czyni go odpowiednim do zastosowania w wyrobach gumowych ze względu na efekt wzmacniający. W pracy Probic S.J. [72] zbadano przydatność ziemi okrzemkowej, jako czynnika zwiększającego adhezję pomiędzy stalą, a wyrobem gumowym, porównując ją z krzemionką. Wykazano, że rodzaj napełniacza nie tylko wpływa na charakterystykę sieciowania wyrobu, ale ma również istotny wpływ na właściwości mechaniczne; wytrzymałość na rozciąganie mieszanek z krzemionką jest stosunkowo wysoka (porównywalna z próbkami z udziałem ziemi okrzemkowej), ponadto ziemia okrzemkowa wpływa na zmniejszenie siły adhezji kompozytu, poprzez zmniejszenie mobilności łańcucha. W pracy Wang J. [73] zaproponowano kompozyty poliuretanowe (PU) z ziemią okrzemkową modyfikowaną APTES. Badania wykazały, że kompozyty wykazują poprawę właściwości mechanicznych (wydłużenie przy zerwaniu i wytrzymałość na rozciąganie wzrasta wraz ze wzrostem stężenia napełniacza, odpowiednio z 3.9 do 4.5 MPa i z 27.9 do 30.7 MPa), a także twardości Shore'A i właściwości termicznych w porównaniu z niemodyfikowanym elastomerem, co jest związane z silną interakcją cząstek modyfikowanej ziemi okrzemkowej i PU, z czego wynika, że ziemia okrzemkowa może wpływać na interakcje pomiędzy twardymi i miękkimi segmentami łańcucha polimerowego. W pracy Olewnik-Kruszkowska E. [74] zbadano wpływ m.in. biokrzemionki na właściwości kompozytów na bazie elastomeru, polidimetylosiloksanu, gdzie określono, że napełniacz wpływa znacząco na zwiększenie

właściwości dielektrycznych kompozytu, przy jednoczesnym braku negatywnego wpływu na właściwości mechaniczne, a wręcz odnotowano poprawę właściwości zarówno mechanicznych, jak i termicznych. Zauważono również przesunięcie stałej dielektrycznej w kierunku wyższych wartości w porównaniu z czystym elastomerem.

W pracy [75] ziemię okrzemkową wykorzystano jako napełniacz kompozytu na osnowie elastomerowej (NR- *natural rubber*), gdzie rozpatrywano dwie metody otrzymywania kompozytów, tj. jedno- i dwuetapową. Określono, że struktura niemodyfikowanej ziemi okrzemkowej może negatywnie wpływać na wiązanie z matrycą elastomerową, natomiast zastosowanie dodatku metakrylanu glicydylu (GMA) poprawia wiązania międzyfazowe, co skutkuje dalszą poprawą właściwości mechanicznych elastomerów poprzez interakcję chemiczną. Ponadto kompozyty modyfikowane GMA przygotowane metodą dwuetapową mają doskonałe właściwości mechaniczne i antypoślizgowe (wzrost wytrzymałości na rozciąganie i odporności na ścieranie o odpowiednio 37.8% i 11.7% w porównaniu z niemodyfikowanymi kompozytami). Natomiast w pracy [76] żywicę epoksydową napełniono 5, 10, 15 i 20% wag. niemodyfikowanej ziemi okrzemkowej oraz modyfikowanej polieteroimidem (PEI) i aminopropylotrietoksysilanem (APTES), gdzie stwierdzono, że dodatek modyfikowanej ziemi okrzemkowej poprawia właściwości mechanicznie i stabilność termiczną kompozytów w porównaniu z niemodyfikowaną ziemią okrzemkową (wzrost udarności o 36.8% dla 15% wag. napełniacza).

3. Cele badawcze

W niniejszej pracy założono, że wielkość cząstek napełniacza, jakim jest ziemia okrzemkowa, znacząco wpływa na właściwości zarówno mechaniczne, termiczne, jak i reologiczne kompozytów termoplastycznych i duroplastycznych. W związku z tym założono, że kontrola wielkości cząstek naturalnego napełniacza pozwoli na kontrolę właściwości wytworzonych kompozytów. W przypadku ziemi okrzemkowej zróżnicowanie wielkości cząstek może wynikać zarówno z procesów mechanicznego niszczenia struktury, jak również z faktu że jest to napełniacz biogeniczny i powstałe struktury mogą różnić się w zależności od fazy rozwoju mikroorganizmu. Założono również, że fizykochemia powierzchni napełniacza oddziałuje z osnową polimerową i ma wpływ na zmianę właściwości termomechanicznych takiego układu. Ponadto założono również, że niemożliwy jest efektywny rozdział cząstek poniżej 40 μm za pomocą standardowej metody przesiewania sitowego.

Celem badawczym było:

- opracowanie procesu frakcjonowania naturalnego napełniacza w prosty, wydajny sposób; założono, że proces rozdziału pozwoli ponadto na pełną kontrolę wielkości cząstek, a więc również na późniejszą kontrolę właściwości kompozytu,
- uzyskanie stabilnych, powtarzalnych parametrów geometrycznych napełniacza, co jest jednym z największych wyzwań i problemów technologicznych przy stosowaniu napełniaczy pochodzenia naturalnego,
- wytworzenie materiału pochodzenia naturalnego, który cechowałby się niepogorszonymi właściwościami w porównaniu do tradycyjnych układów kompozytowych,
- otrzymanie kompozytu, którego szybkości procesów starzenia będą możliwe do modyfikowania w zależności od zastosowanych modyfikatorów ziemi okrzemkowej.

4. Zakres prac eksperymentalnych i metodyka badawcza

Zaplanowano i zrealizowano szereg prac badawczych, których rezultaty zostały opublikowane w cyklu artykułów naukowych, stanowiących postawę niniejszej pracy. Pełny opis przeprowadzonych prac eksperymentalnych przedstawiono w pracach **[H1-H12]**. Poniżej krótko scharakteryzowano przeprowadzone badania oraz przedstawiono schemat otrzymywania biokompozytu (Rysunek 6.)

1) Zaplanowanie i opracowanie procesu hydraulicznego frakcjonowania amorficznej ziemi okrzemkowej o średnim rozmiarze cząstek 0.2 – 100 μm dostępnej handlowo. Opracowany proces pozwolił na efektywne oddzielenie cząstek połamanych, niepołamanych i zaglomerowanych przy jednoczesnej pełnej kontroli dystrybucji cząstek napełniacza za pomocą technik SEM i DLS.

2) Opracowanie metodologii odlewania kompozytów na bazie żywicy epoksydowej z różną zawartością frakcjonowanego napełniacza (biokrzemionka) 0 – 70 % obj.; porównanie dwóch technik przygotowania kompozytów duroplastycznych (odlewanie w formie silikonowej i w formie szklanej), scharakteryzowanie różnic we właściwościach mechanicznych, fizykochemicznych i powierzchni próbek otrzymywanych obiema metodami, m.in. ocena dyspersji napełniacza oraz wpływ rodzaju formy na dyspersję (SEM), porównanie właściwości termicznych (DSC).

3) Zbadanie wpływu niepełnego odgazowania mieszanek EP/DE na różne właściwości usieciowanych kompozytów – określenie wytrzymałości mechanicznej kompozytów (wytrzymałość na rozciąganie, zerwanie, udarność).

4) Określenie wpływu napełniacza mineralnego (biokrzemionka) na gęstość kompozytu EP/DE w porównaniu do referencyjnej żywicy epoksydowej oraz wpływu stężenia napełniacza na szereg właściwości kompozytu, ze szczególnym uwzględnieniem właściwości mechanicznych.

5) Ocena przydatności ziemi okrzemkowej jako napełniacza kompozytów termoplastycznych w kontekście druku 3D FDM i porównanie poszczególnych właściwości wytworzonych próbek tą metodą do szeroko stosowanej metody wtrysku.

6) Zbadanie wpływu wielkości cząstek frakcjonowanego napełniacza na właściwości kompozytów termoplastycznych na osnowie polilaktydowej z uwzględnieniem cząstek

o najmniejszych, największych oraz średnich rozmiarach. Porównanie właściwości otrzymanych kompozytów do próbek zawierających niefrakcjonowaną ziemię okrzemkową. Określenie w szczególności wpływu wielkości cząstek biokrzemionki na właściwości mechaniczne kompozytów (udarność) oraz właściwości reologiczne (MFR).

7) Modyfikacja drugiego typu termoplastycznego polimeru pochodzącego ze źródeł odnawialnych (poliamid 11) frakcjonowaną ziemią okrzemkową z uwzględnieniem jedynie większych cząstek napełniacza i ocena wpływu na właściwości kompozytu.

8) Badanie wytworzonych kompozytów, w szczególności termoplastycznych (PLA, PA11) narażonych na niekorzystnym warunki środowiskowe, tj. podwyższona wilgotność i temperatura i określenie zmian właściwości, w szczególności ocena właściwości hydrofobowo-hydrofilowych kompozytów.

9) Opracowanie metody silanizacji amorficznej ziemi okrzemkowej silanami różnego typu, tj. zawierających różne grupy funkcyjne i wprowadzenie ich zarówno do kompozytów polilaktydowych, jak i poliamidowych i porównanie wpływu procesu silanizacji na dyspersję napełniacza w osnowie polimeru, właściwości mechaniczne oraz reologiczne.

10) Porównanie właściwości kompozytów zawierających dwa typy wosków (naturalny, syntetyczny) w różnym stężeniu, ze szczególnym uwzględnieniem właściwości reologicznych. Zbadanie właściwości i ocena przydatności kompozytu cechującego się w pełni naturalnym składem chemicznym.

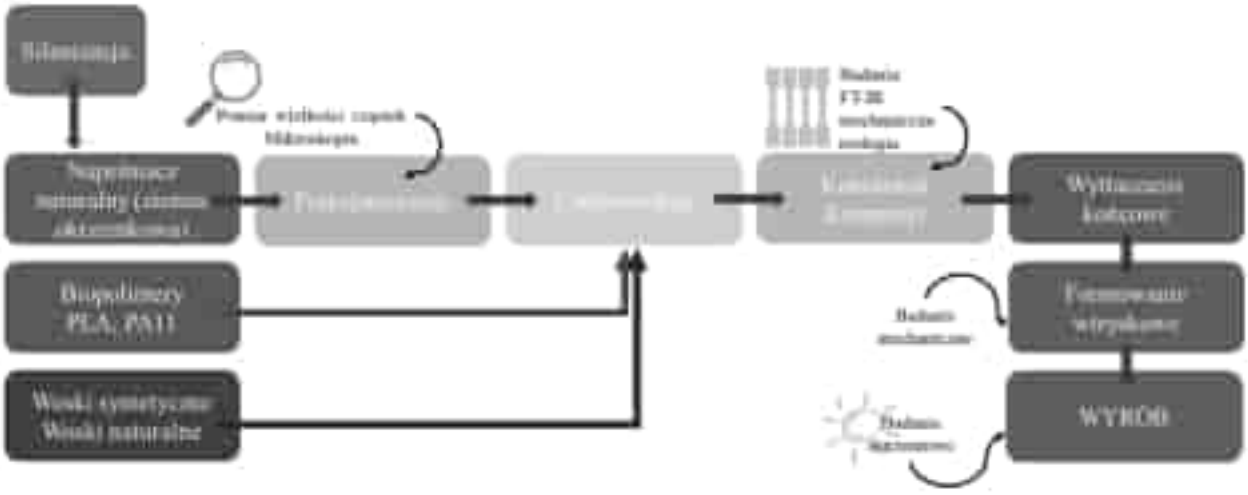

Rysunek 6. Koncepcja projektowania biokompozytu.

5. Opis najważniejszych rezultatów prac badawczych

Jak wspomniano w części literaturowej niniejszej rozprawy, ziemia okrzemkowa stosowana jako napełniacz szeregu polimerów termoplastycznych, duroplastycznych czy elastomerowych, a także m.in. żywic epoksydowych, znacząco wpływa na zmianę właściwości mechanicznych, termicznych, termomechanicznych, hydrofilowo-hydrofobowych, reologicznych i wielu innych. Dzięki swojej budowie posiada unikalne cechy, a różnorodność gatunkowa okrzemek jest niezwykle szeroka. W literaturze nieczęsto pojawiają się wzmianki na temat wielkości pancerzyków poszczególnych okrzemek, a wpływ wielkości cząstek na właściwości kompozytów napełnionych ziemią okrzemkową jest pomijany. Z tego względu w niniejszym cyklu prac badawczych, jako napełniacz kompozytów termoplastycznych i duroplastycznych, wybrano amorficzną ziemię okrzemkową, którą poddano frakcjonowaniu, co było pierwszym celem przeprowadzonych prac badawczych.

Przeprowadzone badania składały się na kilka głównych etapów:

1. Przygotowanie napełniacza -opracowanie metody frakcjonowania ziemi okrzemkowej, przeprowadzenie charakterystyki napełniacza.
2. Przygotowanie kompozytów na osnowie termoplastycznej (polilaktyd, PLA) modyfikowanych ziemią okrzemkową o różnej wielkości cząstek – metoda wytwarzania: druk 3D, formowanie wtryskowe.
3. Przygotowanie kompozytów na osnowie termoplastycznej (poliamid 11, PA11) modyfikowanych ziemią okrzemkową o różnej wielkości cząstek, z wyłączeniem cząstek o mniejszych rozmiarach – metoda wytwarzania: formowanie wtryskowe.
4. Przygotowanie kompozytów na osnowie termoplastycznej (polilaktyd, poliamid 11) modyfikowanych ziemią okrzemkową oraz różnymi typami wosków (naturalny, syntetyczny).
5. Przygotowanie kompozytów na osnowie duroplastycznej (żywica epoksydowa) modyfikowanych ziemią okrzemkową o różnej wielkości cząstek – metoda wytwarzania: odlewanie w formach szklanych, odlewanie w formach silikonowych.
6. Modyfikacja chemiczna ziemi okrzemkowej – silanizacja.

7. Przygotowanie kompozytów na osnowie termoplastycznej (polilaktyd, poliamid 11) napełnionych modyfikowaną chemicznie (silanizowaną) ziemią okrzemkową oraz, dla próbek na osnowie PLA, dodatkowo dwoma typami wosków (naturalny, syntetyczny).
8. Przeprowadzenie badań starzeniowych kompozytów wytworzonych metodą formowania wtryskowego na osnowie termoplastycznej (polilalaktyd).

Otrzymane próbki kompozytów zostały szeroko przebadane dostępnymi metodami instrumentalnymi, m.in. badania mechaniczne (wytrzymałość na rozciąganie, wytrzymałość na zginanie, udarność), badania reologiczne (pomiar wskaźnika szybkości płynięcia, pomiar lepkości), badania termiczne (DSC, TGA), badania termomechaniczne (DMTA), badania powierzchni (SEM, SEM/EDS, DSA). Badania prowadzono w części dla próbek kondycjonowanych w różnych warunkach środowiskowych, m.in. po kondycjonowaniu w warunkach pokojowych, po kondycjonowaniu w komorze klimatycznej (podwyższona temperatura, podwyższona wilgotność), po kondycjonowaniu w warunkach naturalnych z jednoczesnym monitorowaniem panujących warunków atmosferycznych.

Poniżej po krótce scharakteryzowano najważniejsze wnioski płynące z opublikowanych prac, z uwzględnieniem podziału na najważniejsze zagadnienia badawcze.

5.1. Frakcjonowanie ziemi okrzemkowej

W pierwszym etapie prac badawczych rozpoczęto próby frakcjonowania ziemi okrzemkowej, dostępnej komercyjnie, za pomocą zestawu sit o różnej wielkości oczek siatki (mesh). Rozdział prowadzono przy użyciu przesiewacza wibracyjnego. Uzyskano dwie, dobrze rozdzielone frakcje ziemi okrzemkowej, które wykorzystano w dalszych analizach oraz jako napełniacz polilaktydu do druku 3D FDM, co przestawiono w pracy **[H1]**. Kontrolę procesu rozdziału cząstek napełniacza prowadzono w oparciu o metodę dynamicznego rozpraszania światła (DLS), zarówno metodą na mokro (w zawiesinie wodnej), jak i na sucho. Tak zaprojektowany plan badawczy pozwolił na stwierdzenie różnic w zachowaniu napełniacza w różnych środowiskach i zauważono, że w zawiesinie wodnej następuje wtórna aglomeracja cząstek o większych rozmiarach (Rysunek 7), a więc można założyć, że problem ten będzie również obecny w matrycy polimerowej i będzie skutkował nierównomierną dyspersją napełniacza, a więc i wczesną propagacją pęknięcia kompozytu. Ponadto zauważono również, że w zależności od wielkości cząstek okrzemek występują różnice w wielkości porów oraz w wielkości powierzchni właściwej.

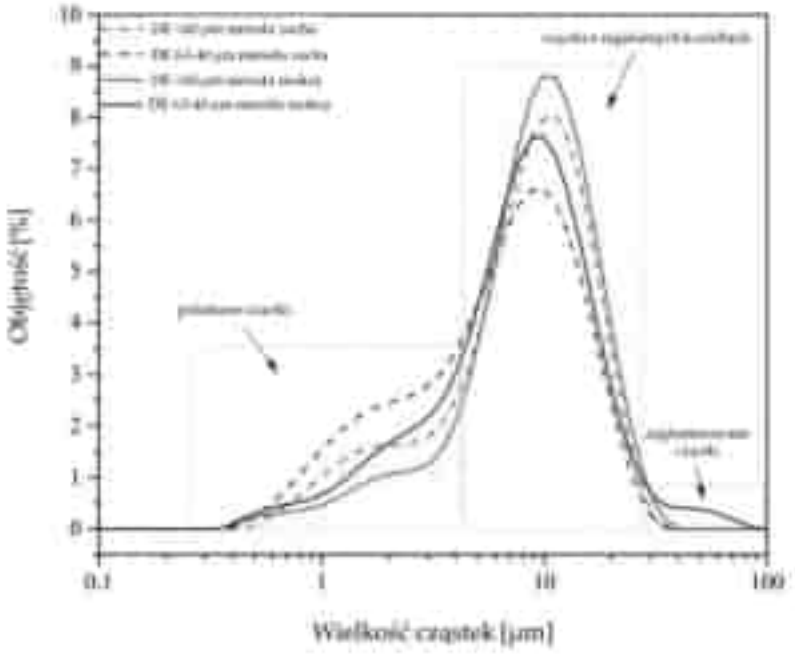

Rysunek 7. Pomiar wielkości cząstek frakcjonowanej ziemi okrzemkowej, metoda sucha oraz metoda mokra [H1].

Proces frakcjonowania ziemi okrzemkowej za pomocą zestawu sit i z wykorzystaniem metody przesiewania wibracyjnego nie był efektywny podczas stosowania na większą skalę, stąd podjęto decyzję o próbie usprawnienia metody rozdziału cząstek. W tym celu zaplanowano proces wykorzystujący zjawisko sedymentacji oraz prosty układ naczyń. W pracy **[H2]** napełniacz przygotowano ww. metodą, a kontrolę procesu prowadzono za pomocą metody dynamicznego rozpraszania światła (DLS) jak uprzednio oraz dodatkowo za pomocą skaningowej mikroskopii elektronowej (SEM). Metoda wykorzystująca zjawisko sedymentacji polegała na dozowaniu ustalonej ilości amorficznej ziemi okrzemkowej oraz wody demineralizowanej do naczynia pierwszego, następnie na mieszaniu mechanicznym powstałeś zawiesiny i pozostawieniu układu do sedymentacji na 3.5 h. Następnie ciecz znad osadu była przepompowywana za pomocą pompy wodnej do osobnego naczynia, a powstały osad pozostawiano do dalszych czynności. Osad uzupełniano wodą demineralizowaną do zadanej wcześniej objętości i proces powtarzano zarówno w przypadku uprzednio sporządzonej cieczy znad osadu, jak i w przypadku pozostałego po pierwszym etapie osadu. Sedymentację prowadzono przez różną ilość czasu, zależnie od sposobu otrzymania mieszaniny. Zaplanowaną metodę prowadzono kilkukrotnie aż do uzyskania 7 frakcji ziemi okrzemkowej o różnych wielkościach cząstek. Schemat procesu rozdziału cząstek ziemi okrzemkowej przedstawiono na Rysunku 8.

Rysunku 8. Schemat procesu frakcjonowania hydraulicznego ziemi okrzemkowej.

Podczas projektowania procesu rozdziału cząstek ziemi okrzemkowej założono, że cząstki o większych rozmiarach ulegają szybszej sedymentacji, a więc w frakcje powstałe z „Osadu 1" będą cechować się większym rozmiarem cząstek niż powstałe z „Cieczy znad osadu 1", co zostało potwierdzone za pomocą DLS oraz SEM. Końcowo uzyskano siedem frakcji o wielkości cząstek od 0.5 μm do aż ponad 1000 μm, gdzie największy udział procentowy stanowiła frakcja o średnio największym rozmiarze cząstek, tj. Frakcja 4. Jednakże poszczególne frakcje ziemi okrzemkowej zawierały niekiedy relatywnie duży udział cząstek o większych średnich rozmiarach cząstek, co oznacza, że proces nie został przeprowadzony w pełni i wymagał dalszych modyfikacji.

W dalszym etapie zadań badawczych proces frakcjonowania ziemi okrzemkowej został zmodyfikowany w taki sposób, aby poszczególne frakcje były płukane *n*-krotnie, zanim zostaną rozdzielone do dalszych etapów. Tak opracowana metoda rozdziału została przedstawiona w pracy **[H4]** oraz w zgłoszeniu patentowym [77]. Ponadto metoda opracowana w **[H4]** zakładała łączenie ze sobą osadów o niższej liczbie porządkowej w kierunku naczyń o wyższej liczbie porządkowej po przeprowadzeniu drugiego płukania. Schemat opracowanej metody frakcjonowania przedstawiono na Rysunku 9. Tak opracowana metoda pozwoliła na pełny rozdział poszczególnych frakcji ziemi okrzemkowej. Określono, że w miarę wzrostu czasu sedymentacji, uzyskano frakcje o najmniejszych rozmiarach, natomiast krótki czas sedymentacji pozwala na uzyskanie frakcji o największych rozmiarach cząstek. Jednocześnie, kontrola wielkości cząstek DLS na każdym etapie pozwoliła na zaplanowanie końcowego efektu, jakim jest oddzielenie cząstek połamanych od niepołamanych i zaglomerowanych i uzyskanie czystych frakcji ziemi okrzemkowej (Rysunek 10). Ponadto podczas przeprowadzania badań wydajności opracowanej metody

frakcjonowania określono, że część cząstek o najmniejszych rozmiarach jest porywana wraz z cieczą podczas procesu przepompowywania, stąd ubytek masy w stosunku do masy początkowej wynosił 4.85 %.

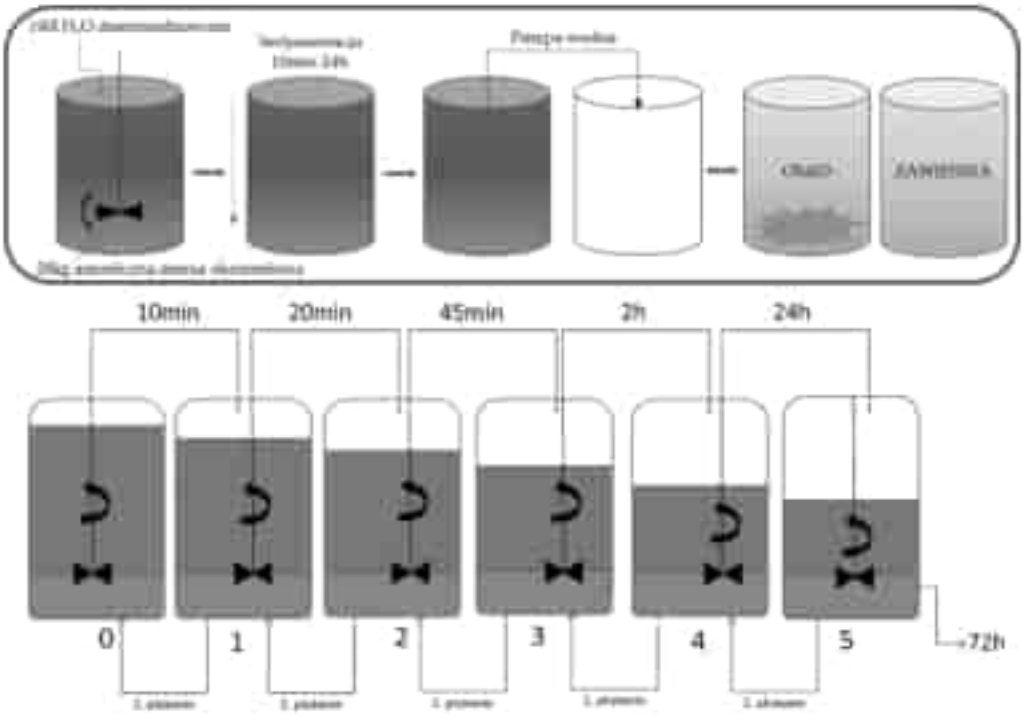

Rysunek 9. Schemat procesu frakcjonowania ziemi okrzemkowej na podstawie **[H4]**.

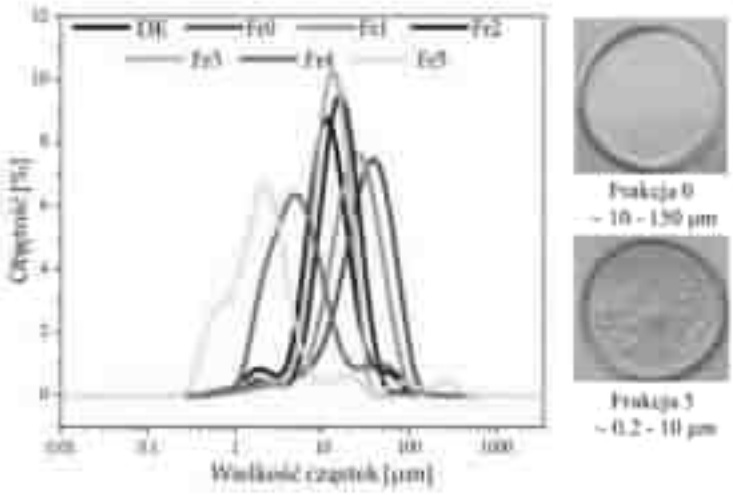

Rysunek 10. Wielkość cząstek poszczególnych frakcji ziemi okrzemkowej otrzymanych metodą frakcjonowania z wykorzystaniem zjawiska sedymentacji na podstawie **[H4]**.

Końcowo w zgłoszeniu patentowym [77] opracowana metoda rozdziału została zmodyfikowana o większą ilość płukań. Zaplanowano, że frakcje o niższej liczbie porządkowej zostaną płukane jednokrotnie, a te o wyższej liczbie porządkowej – dwukrotnie

oraz od 3 do 5-krotnie. W wyniku tak zaplanowanego procesu uzyskano końcowo cztery frakcje, które cechowały się stabilnością rozmiarową, podobnie jak w przypadku **[H4]**.

Przeprowadzono jeszcze jedną próbę modyfikacji metody frakcjonowania ziemi okrzemkowej, tym razem testowo w celu wyeliminowania frakcji o najmniejszym rozmiarze cząstek, co zostało opisane w pracy **[H5]**, gdzie dzięki zwiększeniu początkowej liczby płukań układu bazowego (amorficzna DE + woda demineralizowana – 10 płukań) uzyskano frakcje pozbawione cząstek o rozmiarach poniżej 3 μm, natomiast wyodrębniono frakcje o średnim rozmiarze ~5 i ~35 μm, przy czym w tym przypadku stosowano jeszcze prostszy układ naczyń, co zostało przedstawione schematycznie na Rysunku 11.

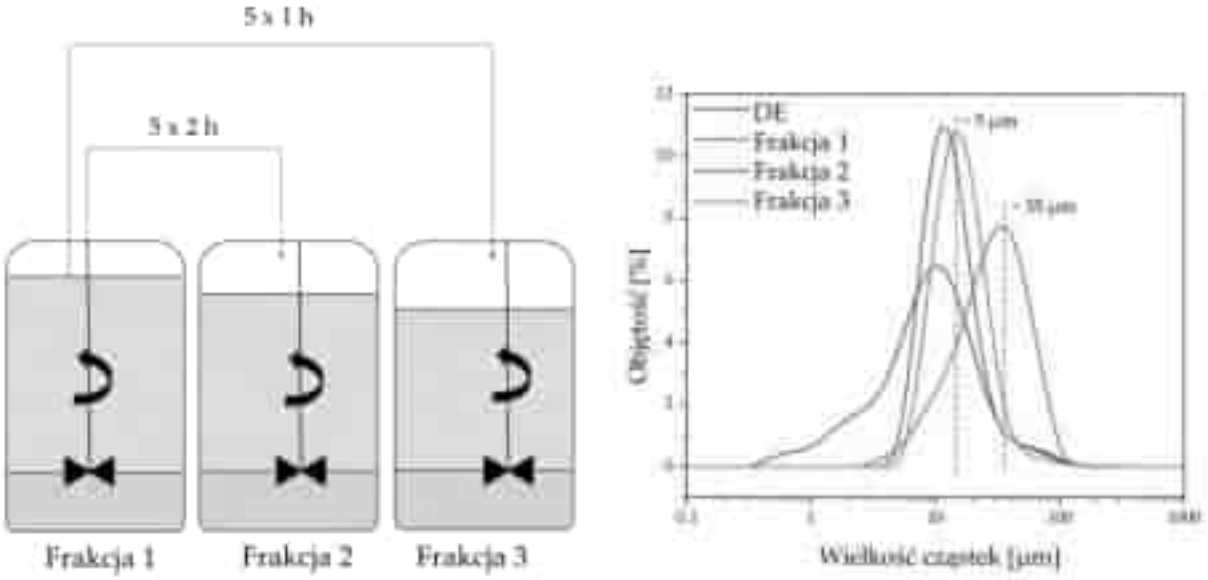

Rysunek 11. Proces frakcjonowania ziemi okrzemkowej zmodyfikowany o ilość płukań pierwszej frakcji **[H5]**.

Finalnie w wyniku zaplanowanych i przeprowadzonych prac zaproponowano efektywną metodę rozdziału cząstek napełniacza, która, jak przedstawiono powyżej, pozwoliła na uzyskanie pełnej kontroli nad wielkością cząstek ziemi okrzemkowej przy niewielkich nakładach energetycznych. W ten sposób zrealizowano pierwszy założony cel badawczy niniejszej pracy.

5.2. Wpływ ziemi okrzemkowej na właściwości układów kompozytowych

Zaplanowane prace badawcze, oprócz przygotowania napełniacza do dalszych etapów badań poprzez jego frakcjonowanie, obejmowały przede wszystkim zbadanie wpływu ziemi okrzemkowej na właściwości m.in. fizykochemiczne, mechaniczne, reologiczne układów

kompozytowych. W pierwszym etapie jako matrycę polimerową wybrano polilaktyd (PLA), a próbki do badań przygotowano m.in. metodą druku 3D FDM, co zostało przedstawione w pracy **[H1]**. Jako napełniacz stosowano ziemię okrzemkową o dwóch różnych frakcjach. W wyniku prowadzonych badań m.in. za pomocą obrazowania skaningowym mikroskopem elektronowym (SEM) określono, że ziemia okrzemkowa w postaci poszczególnych pancerzyków łączy się z uplastycznionym polimerem w sposób efektywny. Dzięki regularnym otworom obecnym w pancerzykach, które mogą być traktowane jako pory, polimer wnika do wnętrza okrzemki, dzięki czemu takie połączenie jest bardziej trwałe. Ponadto określono, że na powierzchni układów zawierających frakcje o większych rozmiarach cząstek występują centra hydrofilowe powstałe w wyniku wtórnej aglomeracji cząstek, co stanowi potwierdzenie wcześniejszej tezy opisanej w punkcie 5.1. Układy o cząstkach poniżej 40 μm cechowały się wartościami kąta zwilżania powierzchni na poziomie ~105° w zależności od stężenia napełniacza, natomiast układy o cząstkach 63-40 μm posiadały kąt zwilżania powierzchni maksymalnie 87.6°. Podobny efekt obserwowano w pracy **[H8]**, gdzie pod uwagę nie brano wielkości cząstek napełniacza, ale jego stężenie i również zaobserwowano tworzenie centrów hydrofilowych na powierzchni kompozytów, gdzie w miarę wzrostu ilości dozowanej ziemi okrzemkowej następowała zmiana charakteru powierzchni z właściwości hydrofobowych (2.5% DE, DSA 102.2°) do właściwości hydrofilowych (15% DE, DSA 85.1°). Zauważalne jest więc, że zarówno stopień rozdrobnienia napełniacza, jak i jego ilość mają wpływ na wtórną aglomerację cząstek w kompozycie, co z kolei powoduje zmianę charakteru powierzchni. W pracy **[H1]** określono również wpływ wielkości cząstek napełniacza na właściwości mechaniczne i reologiczne kompozytów i zauważono, że w przypadku udarności frakcjonowanie napełniacza nie wpłynęło znacząco na ich odporność na uderzenia, a więc zauważony wcześniej problem wtórnej aglomeracji cząstek nie miał wpływu zarówno na wartości udarności, jak i na powtarzalność wyników pomiędzy seriami. W przypadku badania właściwości reologicznych granulatów stwierdzono natomiast prawdopodobny wpływ wtórnej agregacji cząstek na wartości MFR, gdyż różnice pomiędzy poszczególnymi frakcjami są znaczne ($MFR_{PLA+1\%DE\ <40\ \mu m}$ ~7 g/10min; $MFR_{PLA+1\%DE\ 63\text{-}40\ \mu m}$ ~5.5 g/10min). W omawianej pracy stwierdzono również, że symulowane czynniki środowiskowe, takie jak zwiększona wilgotność i podwyższona temperatura (kondycjonowanie przez 72 h w wodzie destylowanej o temperaturze 50°C) mają wpływ na podwyższenie charakteru hydrofobowego kompozytów. Obserwowano znaczący wzrost kąta zwilżania powierzchni kompozytów od wartości DSA 105.2° dla układu zawierającego 1% wag. ziemi okrzemkowej <40 μm do wartości 123.8°,

natomiast dla frakcji o większym rozmiarze cząstek nastąpił bardziej znaczący wzrost DSA, bo aż o 30.8° dla układu o tym samym stężeniu napełniacza i kompozyt ten uzyskał charakter hydrofobowy powierzchni. Efekt ten jest spowodowany zmianami w mikrostrukturze powierzchni analizowanych próbek (dodatkowa strukturyzacja powierzchni). Kondycjonowanie również wpłynęło na poprawę właściwości mechanicznych kompozytów, gdzie nastąpił wzrost wytrzymałości na rozciąganie i modułu sprężystości dla próbek z napełniaczem o niższej frakcji, wydłużenia przy zerwaniu dla układów o wyższej frakcji napełniacza oraz nastąpiła ogólna poprawa udarności dla wszystkich badanych kompozytów. Ponownie zauważono wpływ wielkości cząstek na właściwości kompozytów, w tym przypadku na poprawę ich szeroko rozumianej odporności na warunki środowiskowe. Ponadto można stwierdzić, że opracowane kompozyty finalnie nie tylko cechują się odpornością na warunki środowiskowe, ale też ich właściwości, w zależności od wielkości cząstek napełniacza, ulegają poprawie, a więc z powodzeniem mogą być stosowane do produkcji materiałów m.in. konstrukcyjnych w budownictwie, gdzie istotne są właściwości mechaniczne i odporność na warunki atmosferyczne, w przemyśle motoryzacyjnym, np. do produkcji elementów wnętrza pojazdów, gdzie istotne są właściwości mechaniczne i reologiczne materiału, ale także odporność na warunki środowiskowe.

Jako druga matryca polimerowa do dalszych badań wybrana została żywica epoksydowa w celu pełnego scharakteryzowania ziemi okrzemkowej jako napełniacza kompozytów. W pracach **[H2]** i **[H3]** stosowano żywicę epoksydową sieciowaną trietylenotetraaminą, a jako modyfikator stosowano ziemię okrzemkową frakcjonowaną metodą wykorzystującą zjawisko sedymentacji. Żywica epoksydowa, w przeciwieństwie do używanego wcześniej polilakydu i planowanego do użycia poliamidu 11, nie jest polimerem pochodzenia naturalnego, jednakże jej zastosowanie zostało zaplanowane w celu szerszego przeanalizowania problemu wtórnej aglomeracji cząstek ziemi okrzemkowej w matrycy polimerowej, ze względu na zwiększoną jej gęstość i większą kontrolę pracy podczas przygotowania kompozytów. Zaplanowane prace **[H2]** obejmowały przygotowanie w sposób tradycyjny, tj. metodą odlewania w formach silikonowych, układów żywica-napełniacz o zakresie stężeń 0-70% objętościowych. W celach porównawczych pracowano zarówno na frakcjonowanym napełniaczu (średni rozmiar cząstek ~10 μm, niewielki udział cząstek połamanych i brak cząstek zaglomerowanych), jak i na bazowej, niemodyfikowanej ziemi okrzemkowej (średni rozmiar cząstek ~10 μm, znaczący udział cząstek połamanych i zaglomerowanych). Badania gęstości otrzymanych kompozytów wykazały wpływ zarówno wielkości napełniacza, jak i obecności okrzemek w różnych formach, tj. połamanej

i zaglomerowanej. Gęstość kompozytu wstępnie odgazowanego zawierającego 12% objętościowych bazowej ziemi okrzemkowej wynosiła ~1.1 g/cm^3, natomiast dla układu z frakcjonowanym napełniaczem gęstość wynosiła ponad 1.2 g/cm^3. Ponadto zaobserwowano również różnice w gęstości wyrobów pomiędzy układami ze wstępnym odgazowaniem oraz bez wstępnego odgazowania, co świadczy o złożoności procesów zachodzących w trakcie formowania kompozytów. Udowodniono również, że okrzemki niefrakcjonowane powodują wzrost lepkość żywicy, szczególnie dla wysokich napełnień, co może negatywnie wpływać na proces wstępnego odgazowania mieszanki. Ponadto w toku prac określono, że badane kompozyty można rozpatrywać jako układ trzech faz: napełniacz w postaci okrzemki, żywica oraz pory wypełnione gazem, co stanowi istotną informację dla zrozumienia ich struktury. Zauważono również, że pojedyncze okrzemki nie są wypełnione żywicą w całości co pozwala na uzyskanie lżejszych materiałów.

Kontynuację powyższej pracy stanowi praca **[H3]**, w której badania prowadzono na układach cechujących się takim samym składem, ale różniącą się metodą przygotowania próbek. W celu zminimalizowania problemu niejednorodności wymiarowej wynikającej ze stopniowego zużywania się tradycyjnej silikonowej formy odlewniczej, opracowano metodę odlewania układów żywica-napełniacz w formach szklanych, które dzięki ujednoliconej kontrolowanej metodzie przygotowania formy zapewniały jednolitą grubość próbki kompozytowej, natomiast późniejsze wycinanie próbek za pomocą frezarki CNC pozwoliło na zminimalizowanie odchyleń w pozostałych rozmiarach próbki do badań i wyeliminowanie błędów wynikających z ręcznego dozowania próbki do formy silikonowej. Szklana forma została umieszczona pod określonym, stałym kątem 45° w stosunku do podłoża, dzięki czemu możliwe było przeanalizowanie różnic w stopniu sedymentacji okrzemek w sieciującym kompozycie. Badanie SEM/EDS wykazało, że w przypadku form silikonowych warstwa zsedymentowanych okrzemek naturalnie gromadzi się przy dolnej powierzchni formy, natomiast w przypadku formy szklanej cząstki ziemi okrzemkowej są porywane ku górze wraz z powietrzem, co powoduje różnice w strukturze powierzchni kompozytów otrzymanych tymi dwoma metodami. Zauważono również, że dzięki większej stabilności wymiarowej próbek odlewanych w formach szklanych, wartości wytrzymałości na rozciąganie oraz udarności są znacząco wyższe niż dla układów o identycznym składzie, ale odlewanych w formach silikonowych, a więc dowiedziono, że różne metody otrzymywania kompozytów w istotny sposób mogą wpływać na procesy produkcyjne i właściwości końcowych materiałów. Zastosowanie form szklanych może eliminować wiele problemów związanych z nierównościami powierzchni kompozytu oraz zbyt wczesną

propagacją pęknięć, co z kolei prowadzi do poprawy parametrów mechanicznych. Wnioski te sugerują, że dalsze badania nad optymalizacją procesów produkcyjnych, wyborem odpowiednich form odlewniczych oraz kontrolą procesu odgazowania mogą przyczynić się do poprawy jakości i wydajności kompozytów EP-DE, co może mieć istotne implikacje dla ich zastosowań przemysłowych.

Jak wspomniano wcześniej, w pracy **[H1]** wykorzystano metodę druku 3D FDM w celu otrzymania próbek kompozytów do badań, ale również wykorzystano w celach porównawczych metodę formowania wtryskowego, dlatego też jako kontynuację badań wybrano ostatecznie metodę formowania wtryskowego, która pozwoliła na końcowe przeprowadzenie badań na większej ilości układów o różnych składach. W pracy **[H4]** kontynuowano badania nad kompozytami na matrycy polilaktydowej, a jako modyfikator wybrano, podobnie jak w poprzednich pracach, ziemię okrzemkową frakcjonowaną metodą z wykorzystaniem zjawiska sedymentacji zmodyfikowaną o dwukrotne płukanie. W niniejszej pracy, jak wspomniano wcześniej, uzyskano najbardziej efektywny rozdział napełniacza na frakcje, co pozwoliło na szerokie przeanalizowanie wpływu wielkości cząstek na różne aspekty właściwości kompozytów. Określono wpływ wielkości cząstek napełniacza na właściwości reologiczne i stwierdzono, że dla układu o największych cząstkach ziemi okrzemkowej (Frakcja 2, Dv(50)=8.59 μm, Rysunek 12) już dla wartości 10% napełnienia obserwowany jest najwyższy wskaźnik szybkości płynięcia MFR, a wraz ze zmniejszeniem wielkości cząstek następuje spadek właściwości reologicznych, natomiast dla frakcji o najmniejszych cząstkach (Frakcja 5, Dv(50)=2.17 μm, Rysunek 12) również przy wartości 10% napełnienia obserwowany jest najwyższy MFR; określono również, że zastosowanie niefrakcjonowanej ziemi okrzemkowej, a więc posiadającej pełen przekrój cząstek o różnych rozmiarach, powoduje znaczny spadek MFR, co jest związane ze zmianami w strukturze powodowanymi przez aglomeraty. Analiza właściwości mechanicznych kompozytów wykazała, że próbki zawierające napełniacz o mniejszych cząstkach (Frakcja 4 i Frakcja 5, Rys. 13) charakteryzują się wyższą udarnością, co może mieć istotne znaczenie dla ich wytrzymałości w różnych warunkach eksploatacyjnych.

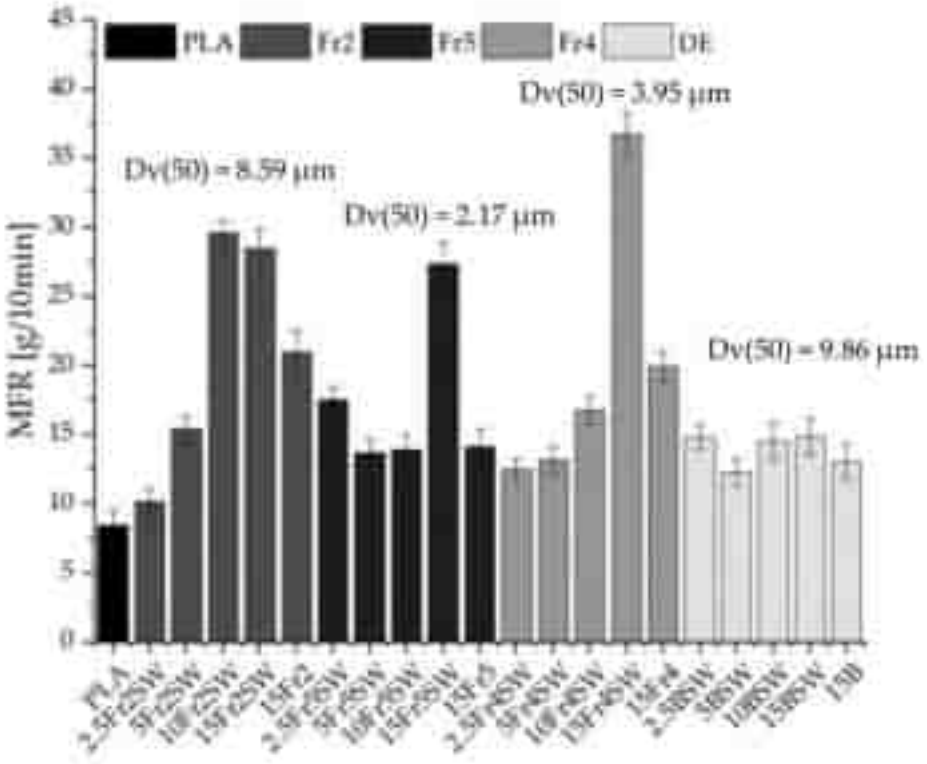

Rysunek 12. Badanie wskaźnika szybkości płynięcia MFR dla kompozytów PLA-DE o różnej wielkości cząstek napełniacza **[H4]**.

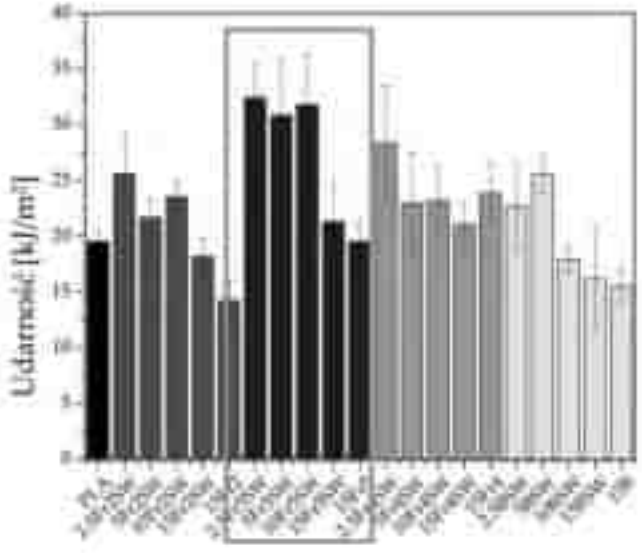

Rysunek 13. Udarność kompozytów o różnej wielkości cząstek napełniacza **[H4]**.

W omawianej pracy zastosowano również, jako czynnik poprawiający właściwości reologiczne, wosk syntetyczny amidowy i zaobserwowano, że zastosowanie jego dodatku pozytywnie wpływa na właściwości przeciwstarzeniowe kompozytów, co sugeruje potencjalne zastosowanie tego składnika w poprawie trwałości materiałów. Odnotowano szczególny wpływ warunków środowiskowych na właściwości mechaniczne kompozytów,

gdzie po 20 dniach ekspozycji na warunki podwyższonej temperatury i wilgotności, zaobserwowano wyraźny wzrost elastyczności, jednoczenie wyższe stężenie napełniacza prowadzi do zmniejszonej transmisji promieniowania do wnętrza kompozytu i tym samym ogranicza stopień fotodegradacji.

W celu kontynuowania badań nad wpływem wielkości cząstek na właściwości kompozytów na osnowie termoplastycznej, do dalszych prac wybrano drugi typ polimeru, jakim był poliamid 11 – podobnie jak polilaktyd, również pozyskiwany ze źródeł odnawialnych, co zostało przedstawione w pracach **[H5, H6]**. Jak wspomniano wcześniej, do modyfikacji poliamidu 11 wykorzystano frakcjonowaną ziemię okrzemkową metodą z wykorzystaniem zjawiska sedymentacji zmodyfikowaną o zwiększoną liczbę płukań poszczególnych osadów, czego wynikiem było uzyskanie napełniacza pozbawionego cząstek o najmniejszych rozmiarach (połamanych). Sam proces frakcjonowania zaprojektowano w taki sposób, aby przebiegał w jak najkrótszym czasie przy jednoczesnym odpowiednim rozdziale cząstek ziemi okrzemkowej, co było na bieżąco kontrolowane metodą DLS. Analizując zbadany wskaźnik szybkości płynięcia kompozytów na osnowie PA11 oraz porównując go ze zbadanym wcześniej dla próbek na osnowie PLA stwierdzono, że ziemia okrzemkowa powoduje zmianę właściwości reologicznych kompozytu w zależności od stosowanego polimeru. Modyfikacja polilaktydu 15% wag. niefrakcjonowanej ziemi okrzemkowej powodowała wzrost wskaźnika szybkości płynięcia, co przedstawiono na Rysunku 14, natomiast dla kompozytów na osnowie PA11 przy podobnej ilości napełniacza zauważalne jest wyraźne pogorszenie MFR o odpowiednio 39.0 i 56.8% (10% wag. niefrakcjonowanej ziemi okrzemkowej i 20% wag. niefrakcjonowanej ziemi okrzemkowej). Skupiając się na wpływie wielkości cząstek na właściwości reologiczne kompozytu zaobserwowano, że wyeliminowanie cząstek o najmniejszych rozmiarach (poniżej 5 μm) pozwoliło na uzyskanie wyższych wartości MFR niż dla układów z niefrakcjonowaną ziemią okrzemkową, a więc kontrola wielkości cząstek jest korzystna z punktu widzenia przetwarzania takiego materiału. Ponadto nawet niewielki dodatek (5% wag.) ziemi okrzemkowej, niezależnie od metody jej wstępnego przygotowania, zwiększa lepkość układów, jednak nie jest to wzrost znaczący, a lepkość takich układów jest niemal stała w całym zakresie zadanych szybkości ścinania. Natomiast efekt wpływu wielkości cząstek jest bardziej widoczny wraz ze wzrostem stężenia napełniacza i przy ilości 20% wag. dochodziło do niemal dwukrotnego wzrostu lepkości, przy czym układ z niefrakcjonowaną ziemią okrzemkową, ze względu na obecność cząstek o najmniejszych rozmiarach (połamanych) cechuje się wyższą lepkością. Kontrola wielkości cząstek w przypadku

frakcjonowanej ziemi okrzemkowej poprawiła przetwarzalność poprzez zmniejszenie tarcia zewnętrznego.

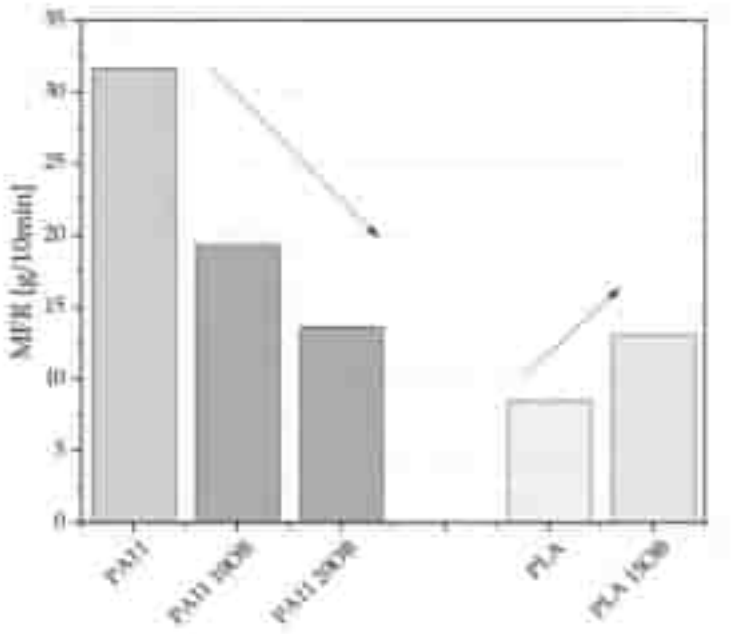

Rysunek 14. Wskaźnik szybkości płynięcia; porównanie kompozytów na matrycy poliamidowej i polilaktydowej.

Analizując właściwości mechaniczne i termomechaniczne uzyskanych układów stwierdzono, że zarówno frakcjonowana, jak i niefrakcjonowana ziemia okrzemkowa nie wykazują tendencji do wtórnej aglomeracji w poliamidowej matrycy, a wręcz wysokie napełnienie wpływa korzystnie zarówno na wytrzymałość na rozciąganie, jak i wytrzymałość na zrywanie, co jest związane z odpowiednią dyspersją napełniacza, dzięki czemu nie następuje zbyt wczesna propagacja pęknięcia. Modyfikacja poliamidu 11 doprowadziła również do wzrostu parametrów termicznych. Zaobserwowano wzrost T_g o 5,8°C dla 5% wag. napełniacza frakcjonowanego, a więc niższe stężenie ziemi okrzemkowej ma korzystniejszy wpływ na stabilność termomechaniczną kompozytów, natomiast analizując różnice w wielkościach cząstek napełniacza, zauważono, że im wyższe jej stężenie tym większa różnica pomiędzy T_g poszczególnych kompozytów, a więc efekt kontroli wielkości cząstek jest bardziej korzystny w tym przypadku dla wyższych stężeń. Analiza charakteru hydrofobowo-hydrofilowego powierzchni kompozytów nie wykazała pozytywnego wpływu napełniacza na właściwości, natomiast analizując układy zawierające 20% wag. ziemi okrzemkowej stwierdzono, że, jak poprzednio, wyeliminowanie cząstek poniżej 5 μm spowodowało brak tendencji napełniacza do aglomeracji, a więc przy

powierzchni kompozytów brak jest dużych aglomeratów powodujących spadek hydrofobowości, co zostało zobrazowane w Tabeli 1.

Tabela 1. Wyniki pomiarów kąta zwilżania kompozytów PA11/DE.

	kąt zwilżania [°]	SD [°]		kąt zwilżania [°]	SD [°]
2.5OB	84,00	0,73	2.5OF	82,70	0,36
5OB	78,00	1,74	5OF	82,10	1,18
10OB	83,60	1,32	10OF	74,40	1,02
20OB	78,80	1,31	20OF	84,00	0,52
PA11	83,90	0,59			

Kontynuację badań nad układami zawierającymi poliamid 11 jako matrycę polimerową stanowił etap modyfikacji chemicznej napełniacza **[H6]**. Do modyfikacji chemicznej ziemi okrzemkowej wykorzystano 1% wag. 3-aminopropylotrietoksysilanu (APTES), co miało na celu poprawę oddziaływań pomiędzy polimerem, a napełniaczem. Efektywność procesu silanizacji badano metodą FT-IR oraz XRD i choć modyfikacja chemiczna nie spowodowała powstania nowych pasm w widmie FT-IR, to zaobserwowano zmianę intensywności i przesunięcie maksimum, natomiast na dyfraktogramach nie stwierdzono obecności charakterystycznych dodatkowych efektów, które pozwoliły być na stwierdzenie, że powierzchniowa modyfikacja napełniacza wpływa na jego tendencję do indukowania zarodkowania, natomiast sam niemodyfikowany chemicznie napełniacz, jak stwierdzono, wpływa na selektywność nukleacji fazy α PA11.

Przeprowadzony proces silanizacji ziemi okrzemkowej miał bardzo istotny wpływ na właściwości mechaniczne wytworzonych kompozytów, w szczególności na wydłużenie przy zerwaniu, co oznacza, że dodatek silanu APTES znacząco zwiększył elastyczność kompozytów. Przy niskim napełnieniu DE (2.5% wag.) i stałej zawartości silanu, efekt wynikający z procesu silanizacji przeważa nad efektem kruchości wywoływanym przez ziemię okrzemkową, natomiast w miarę wzrostu stężenia napełniacza w matrycy polimerowej, charakter napełniacza zaczyna niwelować efekt wynikający ze zwiększonej elastyczności, co w konsekwencji powoduje spadek wydłużenia przy zerwaniu (Rysunek 16).

Podobna zależność występuje w przypadku właściwości reologicznych analizowanych układów. Analizując Rysunek 17. można stwierdzić, że również jak w przypadku właściwości mechanicznych, wpływ silanizacji jest znaczący i już niewielki dodatek silanu (1% wag.) powoduje wzrost parametrów reologicznych niemal trzykrotnie, a w miarę wzrostu stężenia

ziemi okrzemkowej zaczyna przeważać efekt wynikający z charakteru napełniacza, który jest widoczny szczególnie dla układów niepoddawanych silanizacji.

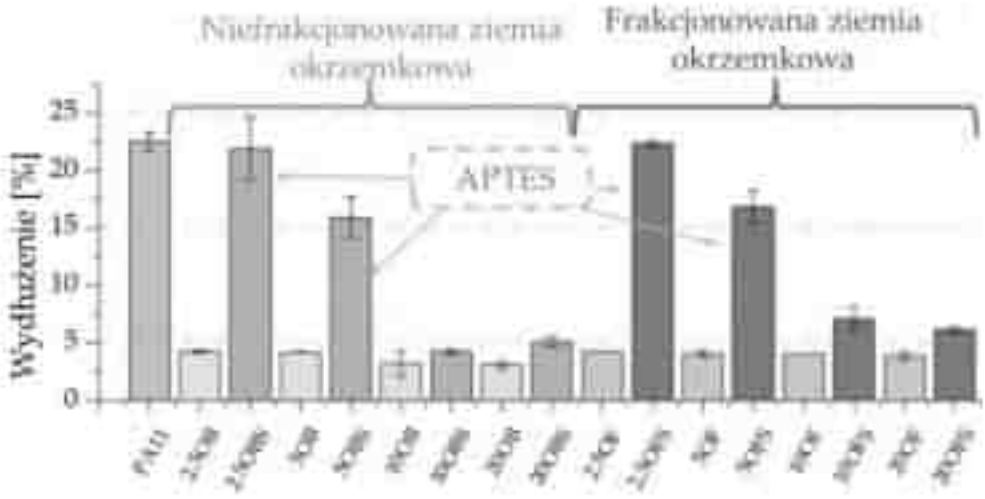

Rysunek 16. Wydłużenie przy zerwaniu; kompozyty na osnowie poliamidowej **[H6]**.

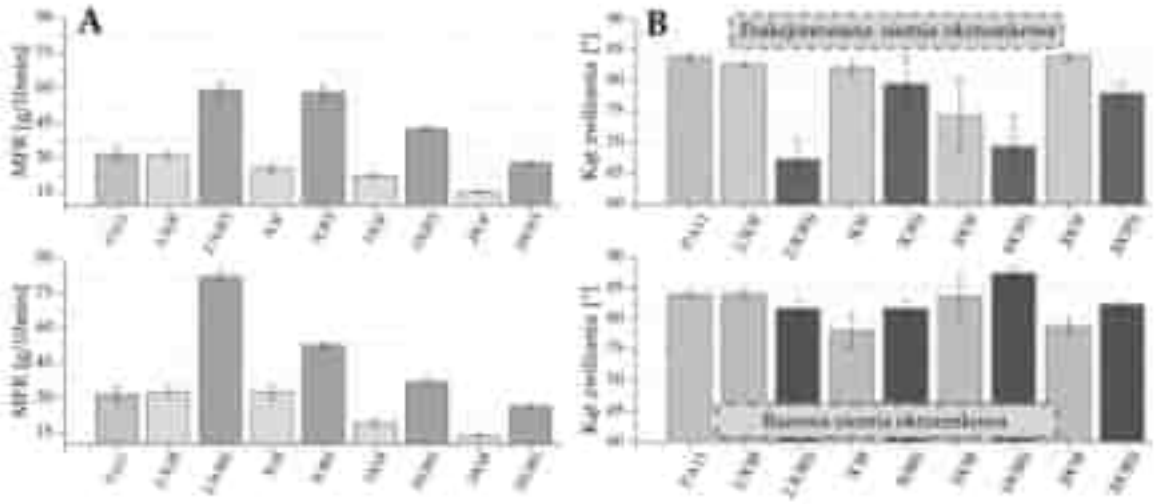

Rysunek 17. Wskaźnik szybkości płynięcia oraz kąt zwilżania; kompozyty na osnowie poliamidowej **[H6]**.

Silan APTES działa jako środek zwiększający szybkość płynięcia kompozytów PA11-DE, zwłaszcza dla niskich stężeń, natomiast analizując badania lepkości przeprowadzone w zakresie szybkości ścinania 1 – 1000 s^{-1} widać wyraźnie, że efekt wynikający z wprowadzenia dodatku silanowego zaczyna być wyraźnie zauważalny dopiero przy wysokich stężeniach napełniacza, gdzie lepkość wzrosła do około 50 Pa×s, w zależności od prędkości ścinania. Zarówno zaobserwowane zależności w zmianie właściwości reologicznych, szczególnie dla kompozytów zawierających niefrakcjonowaną ziemię okrzemkową, jak i pomiary kąta zwilżania (Rysunek 17), gdzie po procesie silanizacji niewielki wzrost charakteru

hydrofobowego powierzchni jest obecny jedynie dla układów z bazową ziemią okrzemkową, pozwalają stwierdzić, że prawdopodobnie aminotrietoksysilan efektywniej łączy się z cząstkami o najmniejszych rozmiarach, które zostały celowo wyeliminowane podczas procesu frakcjonowania ziemi okrzemkowej, stąd efekt silanizacji bazowej ziemi okrzemkowej i związanych z nim zmian we właściwościach kompozytów, jest silniejszy.

Analiza przełomów kompozytów z silanizowaną ziemią okrzemkową skaningowym mikroskopem elektronowym (SEM) oraz badanie siły krycia i płynące z nich obserwacje, tj. zauważalnie niższa siła krycia dla kompozytów silanizowanych, w przypadku 20% wag. napełniacza niższe wartości siły krycia dla układów z frakcjonowaną ziemią okrzemkową oraz widoczne aglomeraty na zdjęciach SEM w przełomach kompozytów z bazową ziemią okrzemkową, pozwoliły zauważyć, że proces silanizacji zmniejsza tendencję ziemi okrzemkowej do aglomeracji, czego efektem jest zwiększona przeźroczystość próbek, a wyeliminowanie najmniejszych cząstek ziemi okrzemkowej podczas procesu frakcjonowania zapobiega tworzeniu aglomeratów w dużym stopniu, co zostało wspomniane powyżej.

5.3. Wpływ rodzaju wosku i procesu silanizacji na właściwości kompozytów

Kolejny etap prac obejmował przygotowanie i scharakteryzowanie kompozytów zawierających, jako matrycę polimerową, polilaktyd, a jako napełniacz bazową, niefrakcjonowaną ziemię okrzemkową oraz dodatki wosków dwóch typów (naturalny, syntetyczny). Zaplanowane prace miały na celu szerszą analizę problemu wpływu ziemi okrzemkowej w niezmienionej postaci na właściwości fizykochemiczne kompozytów, ale również określenie, czy zastąpienie wosku syntetycznego używanego w pracy **[H4]** woskiem naturalnym (pszczelim) będzie miało podobne korzyści m.in. z punktu widzenia właściwości przetwórczych mieszanki. W pracy **[H4]** określono, że w przypadku modyfikacji polilaktydu frakcjonowaną ziemią okrzemkową wpływ dodatku wosku syntetycznego w stężeniu 0.5% wag. powodował znaczy wzrost wskaźnika szybkości płynięcia w porównaniu z kompozytem bez jego dodatku. Szczególnie dla układów zawierających średni oraz najmniejszy rozmiar cząstek, co sugeruje, że wosk syntetyczny szczególnie oddziałuje z cząstkami o rozmiarach poniżej ~5 μm. Natomiast modyfikacja ziemi okrzemkowej niefrakcjonowanej nie spowodowała znaczących różnic we właściwościach reologicznych, dlatego też podjęto dalsze badania nad układami zawierającymi bazową ziemię okrzemkową. Przeprowadzono badania zarówno na układach bez dodatku wosków, jak i z ich różnym stężeniem i typem, a w szczególności skupiono się na zwiększeniu dodatku

wosku naturalnego i zbadaniu jego wpływu na właściwości wytworzonych kompozytów **[H7],** [78]. Największa trudność w produkcji kompozytów wysokonapełnionych wynika ze znacznej lepkości uplastycznionego materiału. Stąd konieczność stosowania dodatków zmniejszających lepkość i poprawiających właściwości przetwórcze. Analiza wskaźnika szybkości płynięcia wykazała, że optymalnym stężeniem dodatku jest 0.5% wag. przy zastosowaniu wosku naturalnego, natomiast jego wyższy dodatek powoduje podobny efekt jak w przypadku zastosowania dodatku wosku syntetycznego, co zostało zobrazowane na Rysunku 18. Sama ziemia okrzemkowa również znacząco zwiększa właściwości przetwórcze polilaktydu, szczególnie przy najwyższym stężeniu, a więc w przypadku matrycy polimerowej jaką stanowi polilaktyd, efekt jest odwrotny niż w przypadku zastosowania poliamidu 11, jednak w tym przypadku jest to związane z obecnością cząstek o dużych rozmiarach.

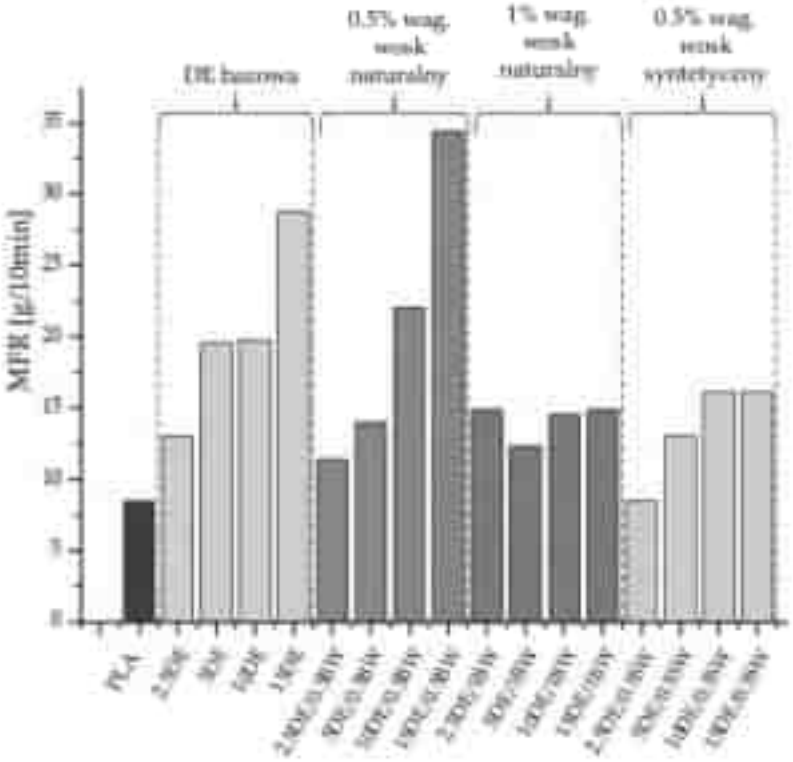

Rysunek 18. Wskaźnik szybkości płynięcia; kompozyty na matrycy polilaktydowej **[H8]**.

Przy zastosowaniu 2.5% wag. ziemi okrzemkowej nie obserwuje się znaczących różnic pomiędzy różnymi rodzajami dodawanych wosków zarówno w badaniu wskaźnika szybkości płynięcia, jak i lepkości. Natomiast 10% wag. napełniacza wskazuje już istotne różnice. Najniższą lepkość odnotowano dla układu z 1% wag. dodatku wosku naturalnego, natomiast pomiędzy 0.5% wag. dodatku wosku naturalnego, 0.5% wag. dodatku wosku syntetycznego i układu bez dodatku wosku nie obserwowano znaczących różnic. Efekt ten może wynikać

z deaglomeracji cząstek, co zwiększa powierzchnię kontaktu napełniacza z matrycą polimerową, a cząstki o mniejszych rozmiarach powodują większy wzrost lepkości w porównaniu z układami zawierającymi aglomeraty. Przy wyższych szybkościach ścinania interakcja matryca-napełniacz staje się mniej istotna, aż lepkość kompozytu osiągnie poziom niemal identyczny z czystym polilaktydem.

Zupełnie odmienne zależności widoczne są we właściwościach mechanicznych kompozytów, gdzie znacząco przeważa efekt związany z dodatkiem 0.5% wag. dodatku wosku syntetycznego na wytrzymałość na rozciąganie. Wartości wydłużenia przy zerwaniu jedynie dla tych układów są zbliżone dla czystego polilaktydu. Dodatek wosku naturalnego, niezależnie od jego stężenia, nie pozwolił na wyeliminowanie efektu zwiększonej kruchości w wyniku zastosowania napełniacza. Jednocześnie nie zaobserwowano różnic w sztywności kompozytów biorąc pod uwagę rodzaj stosowanego wosku. Ponadto każdorazowo wytrzymałość na zginanie próbek była niższa niż odpowiadającym im próbkom bez dodatku wosków.

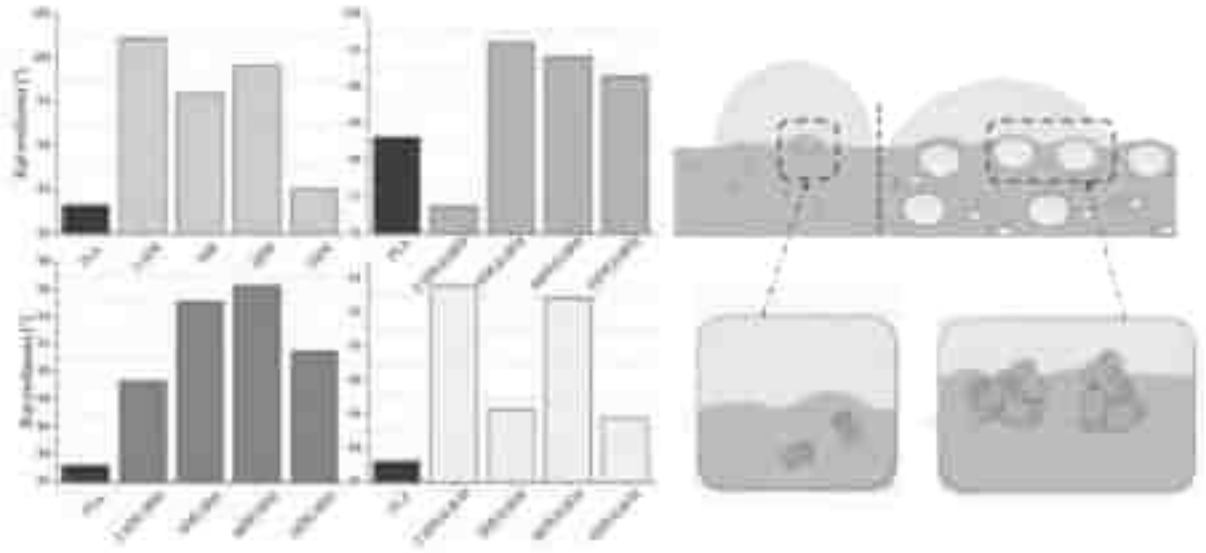

Rysunek 19. Kąt zwilżania kompozytów na matrycy polilaktydowej; schemat centr hydrofilowych **[H8]**.

Hydrofobowy charakter powierzchni kompozytów zawierających ziemię okrzemkowa wynika z wprowadzenia do struktury dodatkowej mikrochropowatości wynikającej z charaktery napełniacza. W poprzednich pracach zauważono efekt tworzenia centrów aktywnych na powierzchni kompozytów, wtedy w wyniku frakcjonowania ziemi okrzemkowej stwierdzono, że eliminacja większych cząstek pozwala osiągnąć efekt hydrofobowy powierzchni. Wykonane na tym etapie badania oraz wykorzystanie ziemi

okrzemkowej o szerokim zakresie wielkości cząstek pozwala stwierdzić, że równie dobre wyniki kąta zwilżania są możliwe do uzyskania dla pełnego zakresu wielkości cząstek. Jednocześnie potwierdza to wcześniejszą tezę, że tendencja cząstek napełniacza do aglomeracji sprzyja tworzeniu centr hydrofilowych (Rysunek 19). Obecność centr hydrofilowych została również zaobserwowana za pomocą obrazowania skaningowym mikroskopem elektronowym (SEM), a ich ilość jest tym większa, im większa zawartość napełniacza. Analizując wpływ dodatku wosków na właściwości hydrofobowo-hydrofilowe nie stwierdzono istotnych różnic pomiędzy rodzajem dodatku i jego ilością, a więc możliwym jest, że dyspersja wosku w matrycy polimerowej nie jest wystarczająca lub też efekt wynikający z mikrostrukturyzacji powierzchni ziemią okrzemkową jest znaczący i przeważa nad wpływem rodzaju wosku na te właściwości.

Kontynuując prace badawcze nad wpływem ziemi okrzemkowej o szerokim zakresie wielkości cząstek na właściwości kompozytów, napełniacz poddano procesowi modyfikacji chemicznej, silanizacji, wykorzystując trzy silany zawierających różne reaktywne grupy **[H8]**. Do badań wykorzystano *n*-oktylotrietoksysilan (OTES), 3-glicydoksypropylotrimetoksysilan (GPTMOS) oraz metylotrimetoksysilan (MTMOS), o wzorach strukturalnych przedstawionych na Rysunku 20. W tym przypadku również zastosowano taką samą kombinację dodatku wosków, jak w pracy **[H7]** i patencie [78]. W opisywanej pracy nie badano wpływu stężenia napełniacza na właściwości kompozytów, dlatego też przygotowano układy zawierające maksymalną możliwą do wprowadzenia ilość ziemi okrzemkowej wynoszącą 25% wag.

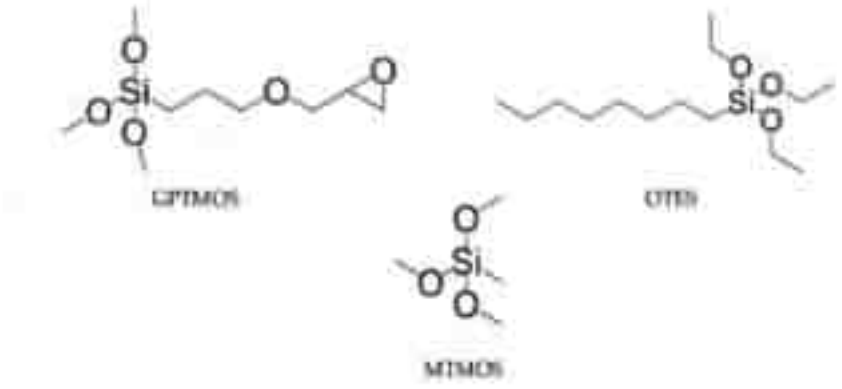

Rysunek 20. Wzory strukturalne wykorzystanych silanów **[H8]**.

Przeprowadzone badania mechaniczne wykazały brak istotnego wpływu zarówno silanizacji, niezależnie od zastosowanego modyfikatora, jak i rodzaju oraz stężenia wosku. Tak wysokie napełnienie kompozytów spowodowało większą kruchość materiałów, co skutkowało znacznym obniżeniem udarności oraz wydłużenia przy zerwaniu, natomiast wartości

wytrzymałości na rozciąganie oraz wytrzymałości na zginanie były podobne w całym zakresie badania, a więc w układach przeważał efekt zmniejszenia wytrzymałości mechanicznej związany z charakterem i stężeniem wprowadzonego napełniacza, natomiast efekty wynikające z zastosowanych wosków i modyfikacji chemicznych mogły zostać stłumione, co jednocześnie może sugerować słabe interakcje matrycą polimer-silanizowana ziemia okrzemkowa-wosk.

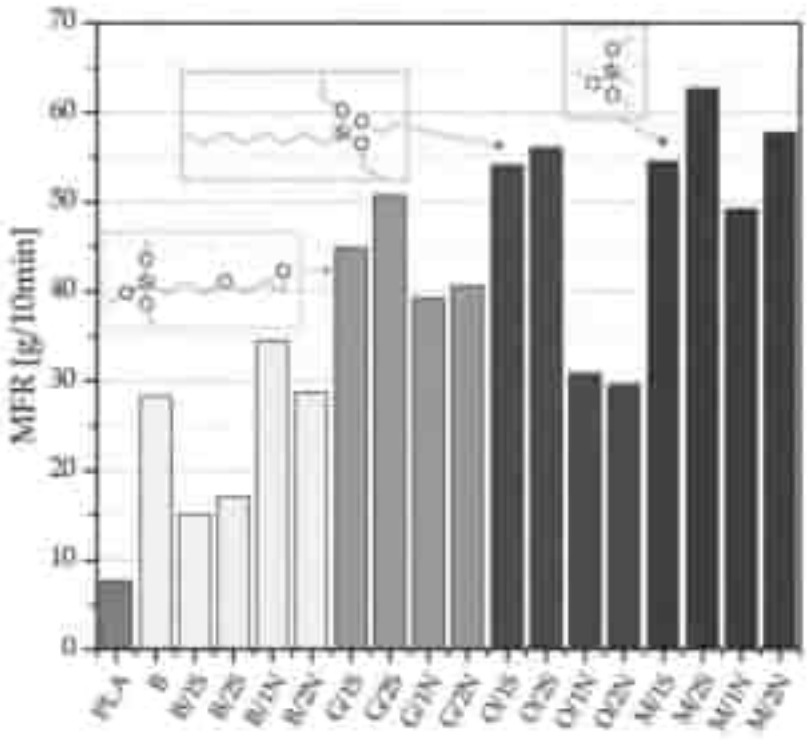

Rysunek 21. Wskaźnik szybkości płynięcia **[H8]**.

Silanizacja oraz dodatek wosków zdecydowanie wpłynęły na właściwości reologiczne kompozytów, obniżając ich lepkość i zwiększając wskaźnik szybkości płynięcia. Lepkość kapilarna nie przekraczała 450 Pa×s niezależnie od szybkości ścinania oraz gwałtownie malała wraz ze wzrostem szybkości ścinania do 100 s^{-1} i pozostawała niemal stała dla wszystkich próbek modyfikowanych, co było spowodowane efektem rozrzedzania ścinaniem typowym dla polimerowych termoplastycznych. Pomiędzy modyfikowanymi kompozytami nie zaobserwowano znaczących różnic, co może oznaczać, że lepkość jest powiązana zarówno z silanizacją jak i z rodzajem wosku, co sugeruje, że możliwa jest interakcja między stosowanym woskiem a powierzchnią silanizowanej ziemi okrzemkowej. Wyraźnie zauważalny zmiany we właściwościach reologicznych zostały zaobserwowane natomiast analizując wskaźnik szybkości płynięcia MFR, co ma istotne znaczenie dla technologii przetwarzania o wysokiej przepustowości. Dodatek syntetycznego wosku

do niefrakcjonowanej ziemi okrzemkowej powodował dwukrotny spadek wskaźnika MFR, niemal niezależnie od stężenia wosku, co może oznaczać zwiększenie tendencji do aglomeracji ziemi okrzemkowej przez ten rodzaj wosku, natomiast zastosowanie wosku pszczelego nie spowodowało wystąpienia tego efektu, a więc między nim, a napełniaczem dochodzi do efektywniejszych interakcji. W przypadku silanizacji ziemi okrzemkowej, najlepszym połączeniem było zestawienie dowolnego silanu z woskiem syntetycznym w stężeniu 2% wag., a więc przeciwnie niż w przypadku czystej ziemi okrzemkowej, co sugeruje, że proces silanizacji spowodował brak możliwości wtórnej aglomeracji cząstek, która nastąpiłaby w wyniku połączenia z woskiem syntetycznym. Obrazowanie wykonane za pomocą SEM zdaje się potwierdzać tą tezę. Zauważono, że w przełomach kompozytów zawierających niemodyfikowaną ziemię okrzemkową i wosk syntetyczny występowała zwiększona aglomeracja, w przeciwieństwie do kompozytów z dodatkiem wosku pszczelego, który wpływał na znaczne uporządkowanie struktury, pomimo dużego stężenia napełniacza. Ponadto zaobserwowano, że silany GPTMOS oraz MTMOS w połączeniu z woskiem syntetycznym wykazują duże rozproszenie pojedynczych okrzemek, co znajduje potwierdzenie również we wspomnianych wcześniej wartościach wskaźnika MFR. Naturalny wosk pszczeli nie wykazywał wystarczających interakcji z powierzchnią okrzemki ze względu na jej hydrofobowy charakter, co skutkowało niższą dyspersją napełniacza i wosku w matrycy polilaktydowej i wpływało na tendencję do aglomeracji, co zaobserwowano we wszystkich układach silanizowanych, gdzie dochodziło do silnego nagromadzenia reszt silanowych i mniejszej zwilżalności powierzchni.

5.4. Badania starzeniowe kompozytów termoplastycznych

Ostatni etap badań obejmował przeprowadzenie badań starzeniowych na dwa sposoby – w warunkach cyklicznie zwiększonej wilgotności i temperatury przez 5 i 20 dni w komorze klimatycznej dla próbek kompozytów na matrycy polilaktydowej modyfikowanych dwoma rodzajami wosków oraz w komorze starzeniowej UV przez 250 i 500 h oraz porównawczo w warunkach naturalnych z jednoczesną ciągłą kontrolą warunków atmosferycznych dla próbek kompozytów na matrycy polilaktydowej modyfikowanych silanizowaną ziemią okrzemkową i dwoma rodzajami wosków. Kompozyty zostały wcześniej poddane badaniom odpowiednio w pracach **[H7, H8]**.

Badania charakteru hydrofobowo-hydrofilowego **[H9, H10]** wykazały, że czysty niemodyfikowany polilaktyd po 5 dniach kondycjonowania w komorze klimatycznej cechował się spadkiem kąta zwilżania powierzchni z 93.2° do 90.5°, a więc nadal charakter

jego powierzchni znajdował się w zakresie hydrofobowym, natomiast po kolejnych 15 dniach następowała hydroliza polimeru, co było związane z częściowym spadkiem jego średniej masy cząsteczkowej i tworzeniem oligomerów kwasu mlekowego na jego powierzchni, co w konsekwencji skutkowało znacznym spadkiem kąta zwilżania do jedynie 70° (Rysunek 22A). Dodatek ziemi okrzemkowej zniwelował konsekwencje hydrolizy polimeru i stabilizował układ podczas kondycjonowania (Rysunek 22B). Zaobserwowano niewielkie zmiany po kondycjonowaniu próbek zawierających ziemię okrzemkową niezależnie od jej stężenia. W przeciwieństwie do polilaktydu, po 5 dniach w komorze klimatycznej kompozyty zyskiwały charakter nieco bardziej hydrofobowy ze względu na obecność okrzemek przy powierzchni. Dodatek wosków wpłynął na badane właściwości, zwłaszcza dla wysokich napełnień. Analizując jedynie układy zawierające 10% wag. ziemi okrzemkowej widoczne jest, że stopień hydrofobowości powierzchni wciąż rośnie w miarę wzrostu czasu kondycjonowania, co sugeruje, że nie tylko woski stabilizują układ, ale również wprowadzają do struktury dodatkowy czynnik hydrofobizujący.

Przeprowadzone badania mechaniczne pozwoliły zaobserwować, że czysty polilaktyd cechuje się nieznacznie wyższą wytrzymałością na rozciąganie po 20 dniach kondycjonowania w komorze klimatycznej niż w warunkach pokojowych, podczas gdy wszystkie układy zawierające ziemię okrzemkową, co spodziewane, uległy obniżeniu tego parametru. Podobnie w przypadku wydłużenia przy zerwaniu. Kondycjonowanie napełnionych kompozytów powodowało zwiększenie sztywności ze względu na większą chłonność wody oraz cykle zamarzania i rozmarzania. Wpływ wosków na wytrzymałość mechaniczną kondycjonowanych kompozytów nie był znaczący, ale zaobserwowano, że zastosowanie dodatku 1% wosku pszczelego pozwala zachować stosunkowo niewielki spadek wytrzymałości na rozciąganie wraz ze wzrostem czasu kondycjonowania oraz układ ten ulega ogólnym najmniejszym zmianom parametru. Podobna zależność wynika z badania udarności, gdzie układ ten również cechował się najmniejszymi zmianami wartości, co może świadczyć o lepszej dyspersji wosku w kompozycie i równomierną degradację próbek. Optymalne parametry dodatku wosków mogą być kluczowe dla uzyskania pożądanych właściwości powierzchniowych kompozytów, takich jak m.in. hydrofobowość. Ponadto, zrozumienie zmian w elastyczności i wytrzymałości materiału po procesie starzenia ma istotne znaczenie dla projektowania kompozytów o odpowiednich właściwościach użytkowych.

W pracy **[H10]** przeprowadzono wspomniany wyżej kontrolowany proces starzenia kompozytów w różnych warunkach w celach porównawczych. Badania przeprowadzono

dla badanych wcześniej **[H8]** próbek na matrycy polilaktydowej napełnionych silanizowaną ziemią okrzemkową w stężeniu 25% wag. i z dodatkiem dwóch rodzajów wosków w dwóch stężeniach (1 i 2% wag,). Badanie prowadzono w komorze starzeniowej UV przez 250 i 500h, gdzie zastosowano naprzemienne cykl jasny (4h, 60°, promieniowanie 0.71 W/m^2) oraz ciemny (4h, 50°) oraz w warunkach naturalnych przez 21 dni, co odpowiada 500h kondycjonowania w komorze klimatycznej, przy stałej kontroli warunków atmosferycznych. Badanie w warunkach naturalnych prowadzono w miesiącach lipiec oraz sierpień w celu zbliżenia tych warunków do warunków zadanych w komorze UV. Kompozyty analizowano przede wszystkim pod kątem stopnia degradacji oraz zmian powierzchni, a w badaniach skupiono się na ocenie warstwy przypowierzchniowej, gdzie przebiegała degradacja.

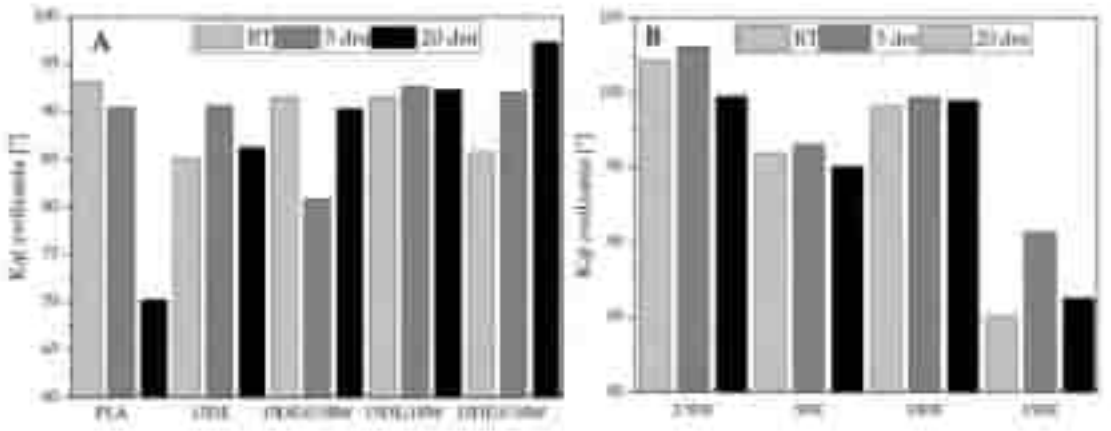

Rysunek 22. Kąt zwilżania; A – kompozyty z dodatkiem wosków, B – kompozyty bez dodatku wosków; na podstawie **[H9]**.

Na podstawie badań degradacji próbek określono, że stopień degradacji czystego polilaktydu wynosi odpowiednio 20.7%, 35.9% oraz 58.5% dla komory UV 250 i 500h oraz dla warunków naturalnych. Na podstawie przesuniętych w stosunku do referencyjnego PLA krzywych rozkładu MWD określono, że dodatek ziemi okrzemkowej oraz wosków zwiększa degradację kompozytów w porównaniu z niemodyfikowanym polilaktydem, co również potwierdzają prace przytoczone w części 2.2.1.

Analizując stopień degradacji kompozytów modyfikowanych 2% wag. dodatku wosków (Rysunek 23) stwierdzono, że modyfikowane kompozyty w większości degradowały w większym stopniu niż PLA. Modyfikacja zmniejszyła stabilność kompozytów w środowisku o wysokim udziale wilgoci działającej jako czynnik hydrolityczny. Jest to związane ze zwiększoną porowatością wprowadzoną przez ziemię okrzemkową, co prowadzi do przyspieszonej dyfuzji wody w polimerze i zwiększa powierzchnię kontaktu wody z fazą polimerową. W porównaniu do referencyjnego polilaktydu, kompozyty

modyfikowane wykazywały większą stabilność barwy w warunkach naturalnych, ale mniejszą po kondycjonowaniu w komorze starzeniowej przez 500h. Wosk naturalny każdorazowo powodował większe odbarwienie kompozytu. Obrazowanie za pomocą SEM potwierdziło jednorodną strukturę powierzchni kompozytów oraz brak defektów w ich strukturze. Kondycjonowanie układów w komorze starzeniowej przez 250h spowodowało krystalizację polilaktydu oraz migrację wosków na powierzchnię, co jest widoczne jako nierównomierne przebarwienia na powierzchni kompozytów. W przypadku dodatku wosku syntetycznego efekt ten był mniej widoczny. Dodatek wosku naturalnego pozytywnie wpłynął na stabilność struktury kompozytów, co jest widoczne jako brak pęknięć i defektów powierzchni po kondycjonowaniu, podczas gdy zarówno polilaktyd, jak i próbki z dodatkiem wosku syntetycznego cechują się defektami w strukturze, co oznacza, że brak jest efektu wosku syntetycznego chroniącego powierzchnię kompozytu przez degradacją. Na Rysunku 24 przedstawiono efekt zmian powodowanych przez czynniki degradujące do wnętrza kompozytów.

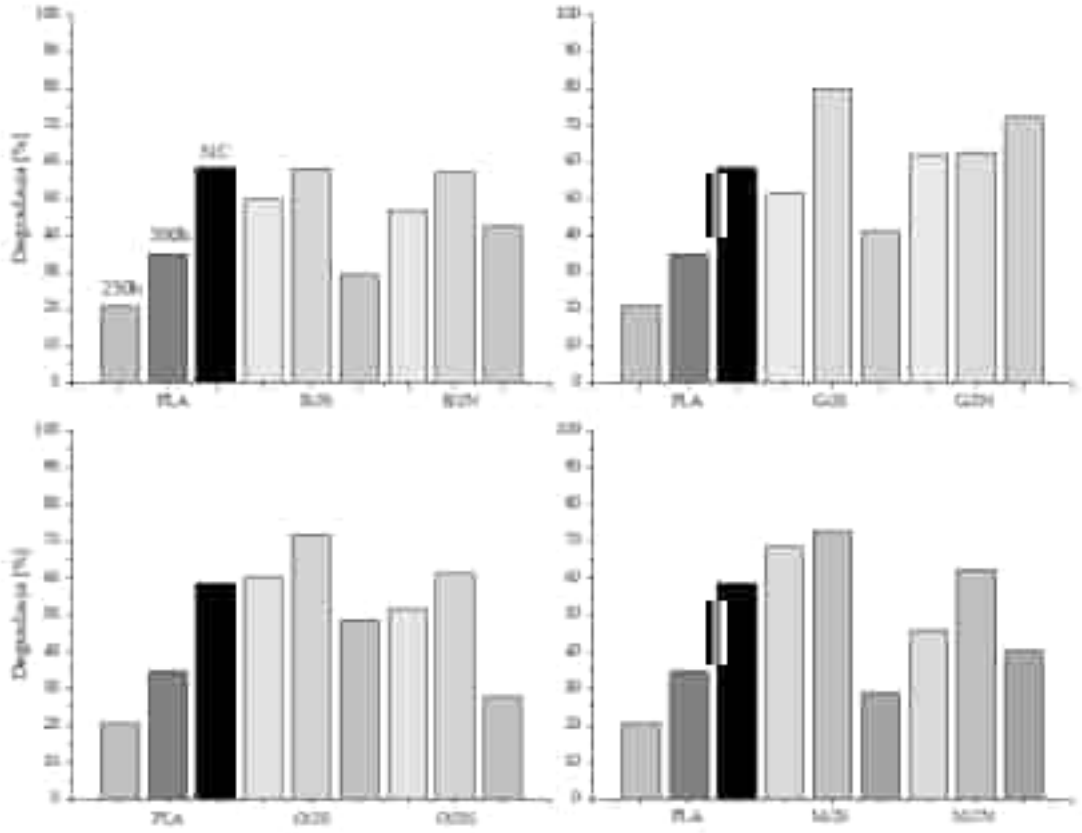

Rysunek 23. Stopień degradacji kompozytów na matrycy polilaktydowej, NC – warunki naturalne; na podstawie **[H10]**.

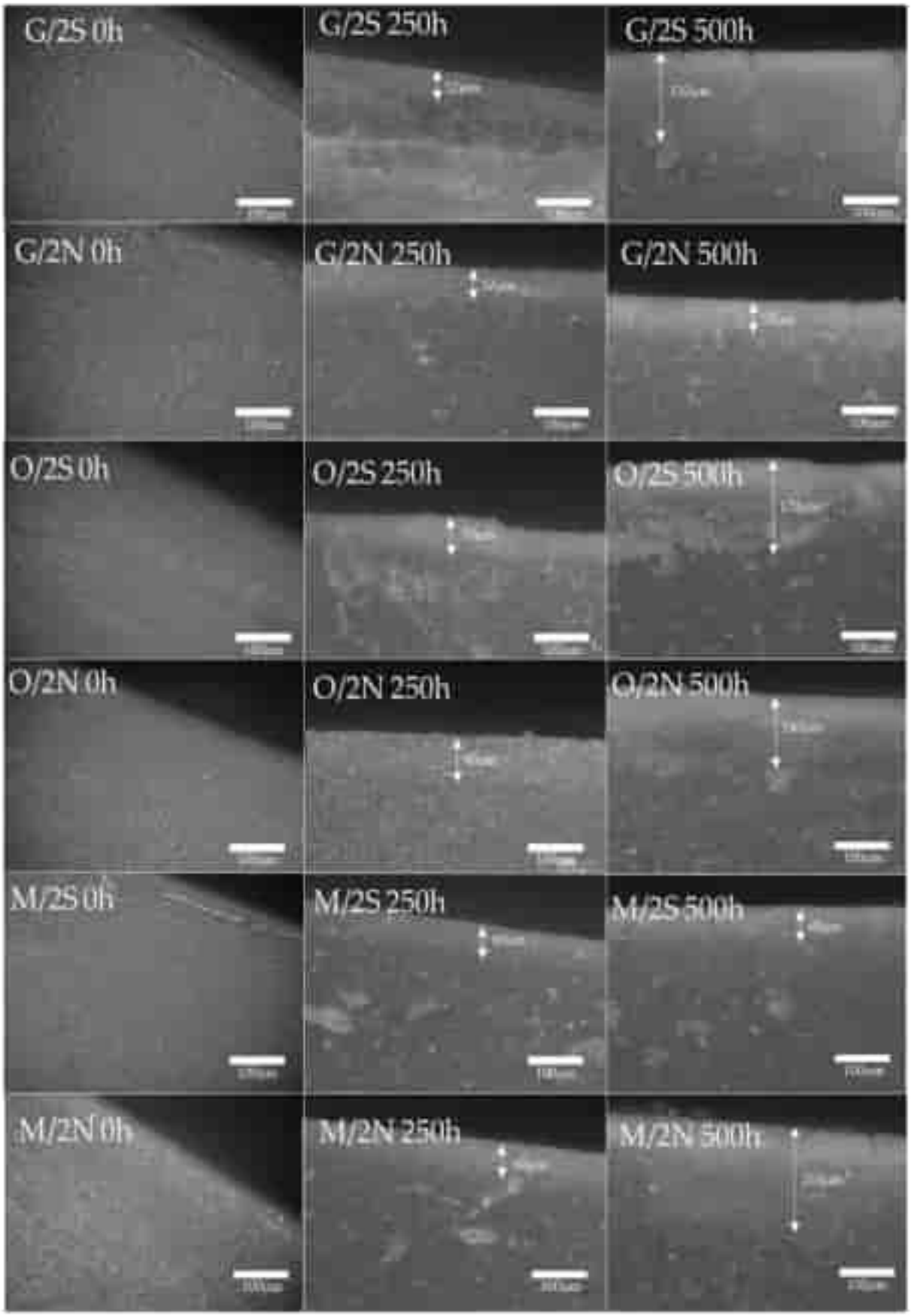

Rysunek 24. Zdjęcia przełomów kompozytów na matrycy polilaktydowej; głębokość degradacji kompozytów **[H10]**.

Czysty PLA wykazuje zmiany w całej objętości już po 250 h w komorze starzeniowej, kompozyty niesilanizowane zachowywały się podobnie, co można wytłumaczyć głównie zmianami poziomu krystaliczności i spadkiem średniego ciężaru cząsteczkowego PLA. W kompozytach zawierających silanizowany napełniacz i dodatek wosków, stopień degradacji powierzchni wzrasta wraz z upływem czasu. Dla kompozytów kondycjonowanych przez 250 h zmiany fizykochemiczne powierzchni zachodziły nie dalej niż na głębokości 90 μm, natomiast dla kompozytów modyfikowanych silanami GPTMOS i MTMOS zachodziły one w zakresie 50-60 μm. Układ zawierający silan OTES charakteryzował się nieco wyższym stopniem degradacji, gdyż w zależności od rodzaju zastosowanego wosku głębokość zmian wynosiła około 70 i 90 μm, odpowiednio dla O/2S i O/2N. Tylko w tym przypadku zaobserwowano niewielki wpływ wosku na szybkość degradacji kompozytu. Po kondycjonowaniu przez 500 h w komorze UV różnice stały się bardziej wyraźne. Zaobserwowano, że głębokość degradacji zwiększała się za każdym razem. Silanizacja może opóźniać dyfuzję wody do głębszych warstw kompozytu, co skutkuje widocznymi różnicami w głębokościach zmian fizykochemicznych. W przypadku kompozytu z napełniaczem modyfikowanym GPTMOS i dodatkiem 2% wosku naturalnego, pomimo stosunkowo wysokiego poziomu degradacji (62%) po 500 h starzenia w komorze UV degradacja występuje tylko na niewielkiej głębokości (52 μm), w warstwie przypowierzchniowej. Ostatecznie stwierdzono, że pomimo iż ziemia okrzemkowa zwiększa szybkość degradacji kompozytu, to możliwe jest kontrolowanie tego efektu poprzez zastosowanie procesu silanizacji, a zastosowanie odpowiedniej kombinacji silan-wosk powoduje większy efekt kontroli zmian degradacyjnych warstwy przypowierzchniowej kompozytu.

6. Podsumowanie najważniejszych rezultatów badań

W treści niniejszej rozprawy, poza przeglądem literaturowym najnowszych rezultatów badań prezentowanych w światowej literaturze, przedstawiono efekty badań własnych, które składają się na cykl 10 spójnych publikacji naukowych, w których analizowano szeroko rozumiany wpływ napełniacza ziemi okrzemkowej na różne właściwości kompozytów na trzy rodzaje matryc polimerowych, żywicy epoksydowej, polilaktydu i poliamidu 11, gdzie dwa z nich stanowią polimery pozyskiwane z surowców odnawialnych. Przeprowadzone prace badawcze pozwoliły opracować efektywną metodę frakcjonowania napełniacza z wykorzystaniem zjawiska sedymentacji **[H1-H4]**. Przeanalizowano wpływ wielkości cząstek ziemi okrzemkowej na właściwości kompozytów **[H1-H5]** oraz zbadano efekt zastosowania niefrakcjonowanego napełniacza **[H8-H12]**. Ponadto określono wpływ rodzaju wosków **[H7-H10]** oraz procesu silanizacji **[H5, H8, H10]** na właściwości fizykochemiczne kompozytów. Zbadano również wpływ poszczególnych typów modyfikacji na proces degradacji wytworzonych materiałów w warunkach naturalnych i kontrolowanych **[H9-H10]**. Do najważniejszych spostrzeżeń oraz wniosków można zaliczyć wymienione poniżej.

Frakcjonowanie ziemi okrzemkowej pozwoliło zaobserwować, że cząstki napełniacza o rozmiarach powyżej 40 μm ulegają wtórnej aglomeracji w kompozycie, co ma istotny wpływ na właściwości mechaniczne, zwłaszcza na obniżenie udarności, a więc zastosowanie niefrakcjonowanej ziemi okrzemkowej nie pozwoli na uzyskanie najwyższych parametrów mechanicznych. Ponadto określono, że rozdział napełniacza na frakcje pozwala na lepszą kontrolę właściwości reologicznych, gdzie cząstki o średnim rozmiarze cząstek ~3 μm i bez udziału cząstek powyżej 10 μm cechują się najwyższym wskaźnikiem MFR, a modyfikacja właściwości reologicznych za pomocą zmiany wielkości cząstek ziemi okrzemkowej jest możliwa. Przy zastosowaniu napełniacza niefrakcjonowanego nie obserwuje się różnic we właściwościach reologicznych w zależności od stężenia ziemi okrzemkowej. Ponadto zauważono, że im wyższa zawartość napełniacza, tym wyższy wskaźnik szybkości płynięcia ($MFR_{2.5\%\ DE}$ = ~15 g/10min; $MFR_{25\%\ DE}$ = ~28 g/10min), jednak tylko w przypadku zastosowania pełnego przekroju wielkości cząstek lub frakcji z obecnością cząstek o mniejszych rozmiarach. Eliminacja cząstek poniżej ~5 μm znacząco wpływa na zmianę trendu i wraz ze wzrostem stężenia napełniacza, MFR ulega obniżeniu. Ważną obserwacją stanowi fakt, że wysokie napełnienie (70% obj.) nie powoduje obniżenia wytrzymałości kompozytów, a więc układy wysokonapełnione również mogą być z powodzeniem stosowane. Wpływ wielkości cząstek napełniacza na właściwości powierzchni kompozytów również są znaczne, gdzie określono, że zarówno wtórna aglomeracja cząstek, jak i obecność

okrzemek o większych średnich rozmiarach wpływa na obniżenie właściwości hydrofobowo-hydrofilowych oraz przy powierzchni obecne są centra hydrofilowe związane z nagromadzeniem aglomeratów dużych cząstek napełniacza, co powoduje punktowy spadek hydrofobowości.

Zastosowanie procesu silanizacji ziemi okrzemkowej spowodowało znaczące zmiany we właściwościach reologicznych kompozytów. Dodatek silanów jedynie w ilości 1% wag. pozwolił na zwiększenie MFR z wartości $MFR_{25\%DE}$ = ~28 g/10min do $MFR_{25\%DE+GPTMOS}$ = ~39 - 51 g/10min, $MFR_{25\%DE+OTES}$ = ~30 - 56 g/10min oraz $MFR_{25\%DE+MTMOS}$ = ~49 - 63 g/10min w zależności od zastosowanego dodatku wosku. Podobny efekt zaobserwowano dla kompozytów na matrycy poliamidowej, gdzie dla 2.5% wag. niefrakcjonowanej ziemi okrzemkowej z MFR = 31 g/10min po procesie silanizacji silanem APTES odnotowano wzrost aż do wartości MFR = ~80 g/10min. Można zatem stwierdzić, że dobór odpowiedniego silanu pozwala na kontrolę parametrów przetwórczych kompozytów napełnionych ziemią okrzemkową. Ponadto przeprowadzony proces silanizacji ziemi okrzemkowej miał bardzo istotny wpływ na właściwości mechaniczne, w szczególności na wydłużenie przy zerwaniu, gdzie dodatek silanu APTES znacząco zwiększył elastyczność kompozytów.

Analizując wpływ dodatku wosków różnych typów stwierdzono, że niemal wszystkie parametry kompozytów są modyfikowalne w zależności od użytego wosku, a więc możliwa jest pełna kontrola właściwości wytworzonych materiałów, gdzie m.in. dodatek wosku pszczelego wpływał pozytywnie na wzrost właściwości przetwórczych, natomiast dla wosku syntetycznego odnotowano nie tylko spadek MFR, ale także brak istotnych jego zmian w miarę wzrostu stężenia napełniacza, natomiast w przypadku wytrzymałości na rozciąganie i wydłużenia przy zerwaniu wyraźnie wyższe wyniki odnotowano dla próbek z woskiem syntetycznym.

Przeprowadzony proces starzenia kompozytów w różnych warunkach (komora klimatyczna, komora UV, warunki naturalne) pozwolił na przeanalizowanie korelacji pomiędzy zastosowanym rodzajem wosku czy silanu i zbadanie ich wpływu na odporność próbek m.in. na działanie promieniowania UV. Zauważono, że elastyczność kompozytów wzrastała wraz ze wzrostem stężenia napełniacza po kondycjonowaniu w warunkach podwyższonej wilgotności i temperatury (komora klimatyczna). Ponadto określono, że dodatek ziemi okrzemkowej oraz wosków zwiększa degradację kompozytów w porównaniu z niemodyfikowanym polilaktydem, co jest zgodne z doniesieniami literaturowymi. Jednakże możliwa jest kontrola stopnia degradacji kompozytów i jego

ograniczenie szczególnie w warstwie przypowierzchniowej próbek poprzez zastosowanie odpowiedniej kombinacji dodatków silan-wosk, m.in. mimo wysokiego stopnia degradacji po 500h kondycjonowana w komorze UV (62.5%) dla kompozytu zawierającego silan GPTMOS oraz 2% wag. wosku naturalnego, degradacja następuje tylko w warstwie przypowierzchniowej do głębokości około 52 μm, natomiast dla kompozytu zawierającego silan MTMOS i 2% wag. wosku naturalnego, pomimo takiego samego stopnia degradacji, zmiany w strukturze następują w większej objętości próbki, bo do głębokości około 210 μm.

7. Bibliografia

1. Völker, C., Kramm, J., and Wagner, M.; On the Creation of risk: framing of microplastics risks in science and media. Global Challeng, 2020, 4, 1900010

2. Miller, S.A.; The capabilities and deficiencies of life cycle assessment to address the plastic problem, Frontiers in Sustainability, 2022, 3

3. Maeda, H.; Aoyama, M.; Kasuga, T. Potential of diatoms as phase change materials. Mater. Lett. 2021, 282, 128673

4. Gültürk, E.; Güden, M.; Tasdemirci, A. Calcined and natural frustules filled epoxy matrices: The effect of volume fraction on the tensile and compression behavior. Compos. Part B Eng. 2013, 44, 491–500

5. Jemutai-Kimosop, S.; Orata, F.; Shikuku, V.O.; Okello, V.A.; Getenga, Z.M. Insights on adsorption of carbamazepine onto iron oxide modified diatomaceous earth: Kinetics, isotherms, thermodynamics, and mechanisms. Environ. Res. 2020, 180, 108898

6. Zhen, Y.; Zhang, J.; Wang, W.; Li, Y.; Gao, X.; Xue, H.; Hayat, T. Embedded SnO2/Diatomaceous earth composites for fast humidity sensing and controlling properties. Sens. Actuators B Chem. 2020, 303, 127137

7. Wang, Y.; Cai, J.; Jiang, Y.; Jiang, X.; Zhang, D. Preparation of biosilica structures from frustules of diatoms and their applications: Current state and perspectives. Appl. Microbiol. Biotechnol. 2012, 97, 453–460

8. Bakr, H.E.G.M.M. Diatomite: Its characterization, modifications and applications. Asian J. Mater. Sci. 2010, 2, 121–136

9. Ivanov, S.E.; Belyakov, V. Diatomite and its applications. Glass Ceram. 2008, 65, 48–51

10. Ruggiero, I.; Terracciano, M.; Martucci, N.M.; De Stefano, L.; Migliaccio, N.; Tatè, R.; Rendina, I.; Arcari, P.; Lamberti, A.; Rea, I. Diatomite silica nanoparticles for drug delivery. Nanoscale Res. Lett. 2014, 9, 329

11. Wang, X.; Zheng, B.; Liu, L.; Li, L. Use of Diatoms in River Health Assessment. Annu. Res. Rev. Biol.2014, 4, 4054–4074

12. Kale, A., Karthick, B. The diatoms. Reson, 2015, 20, 919–930

13. Kieu, K.; Li, C.; Fang, Y.; Cohoon, G.; Herrera, O.D.; Hildebrand, M.; Sandhage, K.H.; Norwood, R.A.Structure-based optical filtering by the silica microshell of the centric marine diatom Coscinodiscus wailesii. Opt. Express 2014, 22, 15992–15999

14. Rakowska, B. Okrzemki—ogranizmy, które odniosły sukces. Kosmos Problemy Nauk Biologicznych 2003, 52, 307–314

15. Sedai, B.R.; Khatiwada, B.K.; Mortazavian, H.; Blum, F.D. Development of superhydrophobicity in fluorosilane-treated diatoma-ceous earth polymer coatings. Appl. Surf. Sci. 2016, 386, 178–186

16. Cacciotti, I.; Mori, S.; Cherubini, V.; Nanni, F. Eco-sustainable systems based on poly(lactic acid), diatomite and coffee grounds extract for food packaging. Int. J. Biol. Macromol. 2017, 112, 567–575

17. Aw, M.S.; Simovic, S.; Yu, Y.; Addai-Mensah, J.; Losic, D. Porous silica microshells from diatoms as biocarrier for drug delivery applications. Powder Technol. 2012, 223, 52–58

18. Sprynskyy, M. The Structural Heterogeneity and Adsorption Properties of Natural Adsorbents (Clinoptilolite, Mordenite, Diatomaceous Earth, Talc, Chrysotile); Scientific Publishing of Nicolaus Copernicus University: Torun, Poland, 2012

19. Leuschel, M.; Llorens, M.; Oliver, J.; Silva, J.; Tamarit, S. SOC. In Proceedings of the 2009 ACM SIGPLAN Workshop on ML—ML ’09, Savannah, GA, USA, 19–20 January 2008; ACM: New York, NY, USA, 2018; Volume 76, pp. 92–98

20. Guan, Y.; Chen, R.; Sun, G.; Liu, Q.; Liu, J.; Yu, J.; Lin, C.; Wang, J. Secretion mechanism and adhesive mechanism of diatoms: Direct evidence from the quantitative analysis. Micron 2021, 140, 102951

21. Bąk M., Witkowski A., Żelazna-Wieczorek J., Wojtal A.Z., Szczepocka E., Szulc K., Szulc B., Klucz do oznaczania okrzemek w fitobentosie na potrzeby oceny stanu ekologicznego wód powierzchniowych w Polsce, Biblioteka Monitoringu Środowiska, ISBN: 978-83-61227-96-0, 2012

22. Mulla, M.Z.; Rahman, M.R.T.; Marcos, B.; Tiwari, B.; Pathania, S. Poly Lactic Acid (PLA) Nanocomposites: Effect of inorganic nanoparticles reinforcement on its performance and food packaging applications. Molecules 2021, 26, 1967

23. Murariu, M.; Benali, S.; Paint, Y.; Dechief, A.L.; Murariu, O.; Raquez, J.M.; Dubois, P. Adding value in production of multi-functional polylactide (PLA)–ZnO nanocomposite films through alternative manufacturing methods. Molecules 2021, 26, 2043

24. Cifuentes, S.C.; Frutos, E.; Benavente, R.; Lorenzo, V.; González-Carrasco, J.L. Assessment of mechanicalbehavior of PLAcomposites reinforced with Mg micro-particles through depth-sensing indentations analysis. J. Mech. Behav. Biomed. Mater. 2017,65, 781–790

25. Tan, L.J.; Zhu, W.; Zhou, K. Recent progress on polymer materials for additive manufacturing. Adv. Funct. Mater. 2020, 30, 2003062

26. Jiang, D.; Ning, F. Fused filament fabrication of biodegradable PLA/316L composite scaffolds: Effects of metal particle content. Procedia Manuf. 2020, 48, 755–762

27. John, R.P., Nampoothiri, K.M., Pandey, A., Solid-state fermentation for L-lactic acid production from agro wastes using Lactobacillus delbrueckii. Proc. Biochem, 2006, 41, 759–763

28. Nampoothiri K.M.; Nair, N.R.; John, R.P; An overview of the recent developments in polylactide (PLA) research, Bioresource Technology 101, 2010, 8493–8501

29. Raquez, J.M.; Habibi, Y.; Murariu, M.; Dubois, P.; Polylactide (PLA)-based nanocomposites, Progress in Polymer Science, 2013, 38, 1504–1542

30. Anderson, K.S.; Schreck, K.M.; Hillmyer, M.A.; Toughening Polylactide, Polymer Reviews, 2008, 48, 1, 85-108

31. Li T., Sun H., Wu B., Han H., Li D., Wang J.-K., Zhang J., Huang J., Sun D., High-performance polylactic acid composites reinforced by artificially cultured diatom frustules, Materials and Design, 2020, 195, 109003

32. Li T., Sun H., Han H., Zhang C., Li B., Huang J., Sun D., Ultrafast bulk degradation of polylactic acid by artificially cultured diatom frustules, Composites Science and Technology, 2022, 22326, 109410

33. Zhang, C.; Sun, J.; Lyu, S.; Lu, Z., Li, T.; Yang, Y.; Li, B.; Han, H.; Wu, B.; Sun, H.; Li, D.; Huang, J.; Sun, D.; Poly(lactic acid)/artificially cultured diatom frustules nanofibrous membranes with fast and controllable degradation rates for air filtration, Advanced Composites and Hybrid Materials, 2022, 5:1221–1232

34. Agüero, A.; Quiles-Carrillo, L.; Jorda-Vilaplana, A.; Fenollar, O.; Montanes, N.; Effect of different compatibilizers on environmentally friendly composites from poly(lactic acid) and diatomaceous earth, Polym. Int., 2019, 68, 5

35. Gonzalez, l.; Agüero, A.; Quiles-Carrillo, L.; Lascano, D.; Montanes N.;, Optimization of the Loading of an Environmentally Friendly Compatibilizer Derived from Linseed Oil in Poly(Lactic Acid)/Diatomaceous Earth Composites, Materials, Materials, 2019, 12, 1627

36. Carrasco, F.; Gamez-Perez, J.; Santana, O.O.; Maspoch, M.L. Processing of poly(lactic acid)/organomontmorillonite nanocomposites: Microstructure, thermal stability and kinetics of the thermal decomposition. Chem. Eng. J. 2011, 178, 451–460

37. Cacciotti, I.; Mori, S.; Cherubini, V.; Nanni, F.; Eco-sustainable systems based on poly(lactic acid), diatomite and coffee grounds extract for food packaging, BIOMAC, 2018, 9072

38. Cerdá-Gandia, R.; Agüero, Á.; Arrieta, M.P.; Fenollar, O. Effect of Different Porous Size of Porous Inorganic Fillers on the Encapsulation of Rosemary Essential Oil for PLA-Based Active Packaging. Polymers 2024, 16, 2632

39. Mei, L., Lixian, Z., Jialin, Y. et al. Polylactic acid/poly(butylene adipate-co-terephthalate)/diatomite composites with antimicrobial properties for green packing. Polym. Bull, 2024, 81, 1729–1742

40. Koranteng E., Jiang S., Xiao F., Weng F., Wu Q., Effects of poly(butanediol adipate ester) based polyurethane prepolymer content on structure and

properties of PLA–diatomaceous earth composites, Journal of Applied Polymer Science, 2023, 140, 29,

41. Łach, M.; Gliścińska, E.; Przybek, A.; Smoroń, K. The Influence of Diatomite on the Sound Absorption Ability of Composites. Materials 2024, 17, 4590

42. Bai, J.; Goodridge, R.D.; Hague, R.J.M.; Okamoto, M. Processing and characterization of a polylactic acid/nanoclay composite for laser sintering. Polym. Compos. 2015, 38, 2570–2576

43. Przekop, R.E.; Kujawa, M.; Pawlak, W.; Dobrosielska, M.; Sztorch, B.; Wieleba, W.; Graphite Modified Polylactide (PLA) for 3D Printed (FDM/FFF) Sliding Elements, Polymers 2020, 12, 1250

44. Popescu, D.; Zapciu, A.; Amza, C.; Baciu, F.; Marinescu, R. FDM process parameters influence over the mechanical properties of polymer specimens: A review. Polym. Test. 2018, 69, 157–166

45. Gaweł, A.; Kuciel, S.; The Study of Physico-Mechanical Properties of Polylactide Composites with Different Level of Infill Produced by the FDM Method, Polymers 2020, 12, 3056

46. Zgłobicka, I.; Joka-Yildiz, M.; Molak, R.; Kawalec, M.; Dubicki, A.; Wroblewski, J.; Dydek, K.; Boczkowska, A.; Kurzydłowski, K.J.; Poly(lactic acid) Matrix Reinforced with Diatomaceous Earth, Materials 2022, 15, 6210

47. Shih, Y-F.; Wang, C-H.; Tsai, M-L.; Jehng, J-M.; Shape-stabilized phase change material/nylon composite based on recycled diatomite, Materials Chemistry and Physics, 2020, 242, 122498

48. Andrusiv, L.;, Experimental Study of Reinforcing Mechanical Properties of Nylon-11 by Selective Laser Sintering †, Phys. Sci. Forum 2022, 4, 22

49. Cheng, Z-L.; Ma, L.; Liu, Z.; A study on synergistic reinforcing effect of halloysite nanotubes/diatomite mixture-filled polymer (PP and PA6) composites, Plastics, Rubber And Composites, 2018, 47, 6, 249–257

50. Liang, J.Z.; Zhu, Z.H.; Research into Melt Flow Properties of Polypropylene/Diatomite Composites, Journal of Reinforced Plastics And Composites, 2010, 29, 10

51. Chen, Y.; Wang, B.; Effect of Diatomite on the Thermal Degradation Behavior of Polypropylene and Formation of Graphene Products, Polymers 2022, 14, 3764

52. Hichem, R.; Said, B.; Effect of the Chemical Modification of Diatomite/Isotactic Polypropylene Composite on the Rheological, Morphological and Mechanical Properties, Advanced Materials Research, 2023, 1177, 8, 121-136

53. Kucinska-Lipka, J.; Sinyavsky, N.; Mershiev, I.; Haponiuk, J.; Study of the Efect of Filling Thermoplastic Medical Polyurethane with PVA, PLA or Diatomite on the Relaxation Times Distributions of 1 H NMR, Applied Magnetic Resonance, 2020, 51, 759–768

54. Mustafov, S.D.; Sen, F.; Seydibeyoglu M.O.; Preparation and characterization of diatomite and hydroxyapatite reinforced porous polyurethane foam biocomposites, Scientific Reports, 2020, 10, 13308

55. Perera, H.J.; Banu, H.; Goyal, A.; Alhassan. S.M.; Low cost fuorinated diatomaceous earth polyurethane foam for the absorption of oil, MRS Energy & Sustainability, 2022, 9, 94–104

56. Kucuk, F.; Sismanoglu, S.; Kanbur, Y.; Tayfun, U.; Optimization of mechanical, thermo-mechanical, melt-flow and thermal performance of TPU green composites by diatomaceous earth content, Cleaner Engineering and Technology, 2021, 4, 100251

57. Leskovac, M.; Kovacevic, V.; Lucic, S.; Perrott, H.R.; Smit, I.; Composites of Poly(Acrylate) Copolymer filled with diatomaceous earth: morphology and mechanical behaviour, Mat Res Innovat, 2002, 6, 206–213

58. Wu, G.; Ma, S.; Bai, Y.; Zhang H.; The Surface Modification of Diatomite, Thermal, and Mechanical Properties of Poly(vinyl chloride)/Diatomite Composite, Journal Of Vinyl And Additive Technology, 2018, 22, 2, 39-47

59. Cacciotti, I.; Rinaldi, M.; Fabbrizi, J.; Nanni, F.; Innovative polyetherimide and diatomite based composites: influence of the diatomite kind and treatment, Journal of Materials Research and Technology, 2019, 8, 2, 1737-1745

60. Ijaz, A.; Miko, A.; Demirel, A.L.; Anti-icing agent releasing diatomaceous earth/SBS composites, New Journal of Chemistry, 2018, 11

61. Tasdemirci, A.; Yuksel, S.; Karsu, D.; Gulturk, E.; Hall, I.W.; Guden, M.; Diatom frustule-filled epoxy: Experimental and numerical study of the quasi-static and high strain rate compression behavior, Materials Science and Engineering A, 2008, 480, 373–382

62. Gültürk, E.A.; Güden, M.; Tasdemirci, A.; Calcined and natural frustules filled epoxy matrices: The effect of volume fraction on the tensile and compression behavior, Composites: Part B, 2013, 44, 491–500

63. Zeren, D.; Guden, M.; The increased compression strength of an epoxy resin with the addition of heat-treated natural nano-structured diatom frustules, Journal of Composite Materials, 2016, 51, 12

64. Perera, H.J.; Khatiwada, B.K.; Paul, A.; Mortazavian, H.; Blum, F.D.; Superhydrophobic surfaces with silane-treated Diatomaceous earth/resin systems, J. Appl. Polym. Sci. 2016, 133, 41

65. Perera, H.J.; Mortazavian, H.; Blum, F.D.; Surface Properties of Silane-Treated Diatomaceous Earth Coatings: Effect of Alkyl Chain Length, Langmuir, 2017, 33, 11, 2799-2809

66. Lv, J.; Sun, B.; Jin, J.; Jiang, W.; Mechanical and slow-released property of poly(acrylamide) hydrogel reinforced by diatomite, Materials Science & Engineering C, 2019, 99, 315–321

67. Liu, W.; Zhuang, L.; Liu, J.; Liu, Y.; Wang, L.; He, Y.; Yang, G.; Shen, F.; Zhang, B.; Zhang, Y.; Make the building walls always clean: A durable and anti-bioadhesive diatomaceous earth@SiO_2 coating, Construction and Building Materials, 2011, 301, 124293

68. Sun, X.; Liu, J.; Zhang, Z.; Zhi, Y.; Jin, L.; Hang, J.; Shi, L.; One-step fabrication of wear-resistant superhydrophobic coating based on aminosilane-functionalized diatomaceous earth, J Appl Polym Sci., 2021, 51227

69. Li, X.; Lin, H.; Jing, H.; Zhang, Y.; Liu, B.; Sun, Y.; Zhao, C.; Preparation and properties of a new bio-based epoxy resin/diatomite composite, Polymer Degradation and Stability, 2021, 187, 109541

70. Pereira, J.; Souza, R.; Moreira, A.; Moita, A. Durable and High-Temperature-Resistant Superhydrophobic Diatomite Coatings for Cooling Applications. Coatings, 2024, 14, 805

71. Lamastra, F.R.; Mori, S.; Cherubini, V.; Scarselli, M.; Nanni, F.; A new green methodology for surface modification of diatomite filler in elastomers, Materials Chemistry and Physics, 2017, 194, 253-260

72. Porobic, S.J.; Markovic, G.; Ristic, I.; Samaržija-Jovanovic, S.; Javonovic, V.; Budinski-Simendi, J.; Marinovic-Cincovi, M.; Hybrid Materials Based on Rubber Blend Nanocomposites, Polymer Composites—2018, 40, 8, 3056-3064

73. Wang, J.; Zhao, D.; Liu, Z.; Chen, H.; Zhou, Y.; Zhou, Y.; Zhu, B.; Effects of biomass diatom frustule on structure and properties of polyurethane elastomer, J. Appl. Polym. Sci. 2019, 137, 10

74. Olewnik-Kruszkowska, E.; Brzozowska, W.; Adamczyk, A.; Gierszewska, M.; Wojtczak, I.; Sprynskyy, M.; Effect of Diatomaceous Biosilica and Talc on the Properties of Dielectric Elastomer Based Composites, Energies, 2020, 13, 5828

75. Zhao, M.; Duan, H.; Han, L.; Glycidyl methacrylate-modified diatomite as reinforcing filler for natural rubber composite. Colloid Polym Sci, 2024

76. Wang, H.; Lou, C.; Yu, J.; Yang, Y.; The effects of the contents of modified-diatomite on the properties of modified-diatomite/epoxy resin composites, Journal of Applied Polymer Science, 2024, 141, 31

77. Zgłoszenie patentowe P.436292 „*Sposób rafinacji ziemi okrzemkowej w skali półtechnicznej*”

78. Patent Pat.243125 „*Biokompozyt składający się z biodegradowalnego poli(kwasu mlekowego), ziemi okrzemkowej i wosku pszczelego oraz sposób wytwarzania biokompozytu*”

8. Wykaz pozostałego dorobku naukowego

Konferencje krajowe i międzynarodowe

1. **M. Dobrosielska**, Dobrucka R., Kurzydłowski K.J., Przekop R.E., Amorficzna ziemia okrzemkowa jako napełniacz w kompozytach polimerowych, VI Ogólnopolska Konferencja Naukowa Biopolimery – źródło nowych materiałów, 27.10.2022
2. **M. Dobrosielska**, Dobrucka R., Kurzydłowski K.J., Przekop R.E., Amorficzna ziemia okrzemkowa jako napełniacz w kompozytach polimerowych, VI Ogólnopolska Konferencja Naukowa Biopolimery – źródło nowych materiałów, 27.10.2022
3. **M. Dobrosielska**, Dobrucka R., Kurzydłowski K.J., Przekop R.E., Nowe aspekty wykorzystania biogenicznej krzemionki jako napełniacza w kompozytach polimerowych, VI Ogólnopolska Konferencja Naukowa Nauki Przyrodnicze na rzecz człowieka i środowiska, 21.10.2022
4. **M. Dobrosielska**, D. Pakuła, M. Jarkowski, M. Popiół, B. Klonowski, D. Brząkalski, B. Marciniec, R. E. Przekop, Wpływ fizykochemii powierzchni napełniaczy stałych na dyspersję w systemie polimocznikowym, XXIII Sympozjum KOMPOZYTY 2019 – Teoria i Praktyka, 24- 26.04.2019, Cedzyna k. Kielc
5. D. Pakuła, **M. Dobrosielska**, M. Jarkowski, M. Popiół, B. Klonowski, D. Brząkalski, B. Marciniec, R. E. Przekop, Nowy mikrokrzemionkowy napełniacz do systemów polimocznikowych, XXIII Sympozjum KOMPOZYTY 2019 – Teoria i Praktyka, 24-26.04.2019, Cedzyna k. Kielc
6. R. Przekop, M. Frydrych, **M. Dobrosielska**, M. Pietrowski, M. Zieliński, A. Martyła, B. Sztorch, Reakcje uwodornienia z wykorzystaniem wysoko zdyspergowanej platyny na dwuskładnikowych nośnikach tlenkowych, X Poznańska Konferencja Naukowa „Chemia – Nauka i Przemysł”, 30.11.– 1.12.2018, Poznań
7. R. Przekop, **M. Dobrosielska**, M. Frydrych, M. Pietrowski, M. Zieliński, A. Martyła, B. Sztorch, Właściwości teksturalne dwuskładnikowych nośników tlenkowych typu Al2O3-MxOy otrzymywanych na drodze procesów zol-żel, X Poznańska Konferencja Naukowa „Chemia – Nauka i Przemysł”, 30.11.– 1.12.2018, Poznań
8. P. Marciniak, B. Sztorch, D. Brząkalski, **M. Dobrosielska**, R. Przekop, M. Frydrych, B. Marciniec, Synteza wielkolaboratoryjna organofunkcyjncyh silseskwioksanów na

drodze reakcji kondensacji hydrolitycznej, X Poznańska Konferencja Naukowa „Chemia – Nauka i Przemysł”, 30.11.–1.12.2018, Poznań

9. D. Brząkalski, B. Sztorch, M. Frydrych, **M. Dobrosielska**, R. Przekop, B. Marciniec, Potencjał aplikacyjny związków typu POSS z mieszanymi grupami funkcyjnymi, X Poznańska Konferencja Naukowa „Chemia – Nauka i Przemysł”, 30 listopada – 1.12.2018, Poznań

10. P. Marciniak, D. Brząkalski, B. Sztorch, **M. Dobrosielska**, R. Przekop, M. Frydrych, B. Marciniec, Synteza wielkolaboratoryjna organofunkcyjnych silseskwioksanów na drodze reakcji hydrosililowania, X Poznańska Konferencja Naukowa „Chemia – Nauka i Przemysł”, 30 listopada – 1.12.2018, Poznań

11. D. Pakuła, K. Jankowska, K. Włodarek, **M. Dobrosielska**, B. Sztorch, R. Przekop, Modyfikacja tlenku glinu silanami o właściwościach hydrofobowych, II Ogólnopolskie Sympozjum Chemii Bioorganicznej, Organicznej i Biomateriałów, 2.12.2017, Poznań

12. M. Frydrych, **M. Dobrosielska**, S. Skonieczna, B. Sztorch, R. Przekop, Hybrydowe materiały Al_2O_3/3-aminopropylotrimetoksysilan i Al_2O_3/3-merkaptopropylotrimetoksysilan, II Ogólnopolskie Sympozjum Chemii Bioorganicznej, Organicznej i Biomateriałów, 2.12.2017, Poznań

13. R. Przekop, M. Stodolny, B. Sztorch, P. Marciniak, K. Wójtowska, A. Czapik, Ł. Majchrzycki, **M. Dobrosielska**, M. Frydrych, A. Reisner, A. Jarmołowicz, A. Marchewka, B. Marciniec, The effect of the reaction system on the direct synthesis of alkoxysilanes, ISOS-18 & ASiS-6 Ji’nan, China, 6-11.04.2017

14. R. Przekop, M. Stodolny, K. Wojtowicz, B. Sztorch, P. Marciniak, **M. Dobrosielska**, A. Jarmołowicz, B. Marciniec, Direct synthesis of alkoxysilanes: the impact of doping contact mass with zinc and aluminum on conversion and selectivity, 8th European Silicon Days, 28-31.08.2016, Poznań

15. Marchewka, A. Jarmołowicz, **M. Dobrosielska**, A. Reisner, M. Frydrych,B. Sztorch, R. Przekop, Właściwości hydrofilowo/hydrofobowe hybrydowych materiałów żelatynowo-siloksanowych, I Wielkopolskie Sympozjum Chemii Bioorganicznej, Organicznej i Biomateriałów, 5.12.2015, Poznań

16. A. Czapik, R. Przekop, B. Sztorch, J. Włodarczak, **M. Dobrosielska**, A. Marchewka, A. Jarmołowicz, Ł. Majchrzycki, A. Martyła, B. Marciniec, Analiza rentgenowska mas

kontaktowych Cu-Si otrzymywanych na drodze mechanochemicznej i termicznej, 8. Kongres Technologii Chemicznej, 30.08-4.09.2015, Rzeszów

17. A. Czapik, R. Przekop, B. Sztorch, J. Włodarczak, **M. Dobrosielska**, A. Marchewka, A. Jarmołowicz, Ł. Majchrzycki, A. Martyła, B. Marciniec Zastosowanie mechanosyntezy w reakcjach krzemu, chlorku miedzi (I) i minerałów miedzionośnych, 8. Kongres Technologii Chemicznej, 30.08-4.09.2015, Rzeszów
18. B. Sztorch, J. Włodarczak, **M. Dobrosielska**, A. Marchewka, A. Jarmołowicz, A. Czapik, R. Przekop, B. Marciniec, Zastosowanie analizy termograwimetrycznej w badaniach reakcji Si+CuClx, 8. Kongres Technologii Chemicznej 30.08-4.09.2015, Rzeszów
19. R. Przekop, B. Sztorch, J. Włodarczak, A. Czapik, M. Stodolny, Ł. Majchrzycki, **M. Dobrosielska**, A. Marchewka, A. Jarmołowicz, N. Gutowska, A. Martyła, B. Marciniec, Nowe metody otrzymywania masy kontaktowej do bezpośredniej syntezy alkoksysilanów, 8. Kongres Technologii Chemicznej, 30.08-4.09.2015, Rzeszów
20. R. Przekop, A. Martyła, P. Marciniak, B. Sztorch, **M. Dobrosielska**, A. Marchewka, Zastosowanie dynamicznej adsorpcji par (DVS) do wyznaczania izoterm adsorpcji wody na żelowych układach Al_2O_3/B_2O_3, II Międzynarodowa Konferencja Naukowa Oxygenalia, 7-8.11.2014, Poznań

Pozostałe publikacje naukowe

1. R.E. Przekop, E. Gabriel, **M. Dobrosielska,** A. Martyła, P. Jakubowska, J. Głowacka, P. Marciniak, D. Pakuła, M. Jałbrzykowski, G. Borkowski, The 3D-Printed (FDM/FFF) Biocomposites Based on Polylactideand Carbonate Lake Sediments—Towards a Circular Economy. Polymers, 15, 2817 , 2023
2. G. Borkowski, A. Martyła, **M. Dobrosielska**, P. Marciniak, J. Głowacka, D. Pakuła, E. Gabriel, R.E. Przekop, Characterisation of carbonate lake sediments asa potential filler for polymer composites, Green Processing and Synthesis, 12: 20228082, 2023
3. G. Borkowski, A. Martyła, **M. Dobrosielska**, P. Marciniak, E. Gabriel, J. Głowacka, M. Jałbrzykowski, D. Pakuła, R.E. Przekop, Carbonate Lake Sediments in the Plastics Processing-Preliminary Polylactide Composite Case Study: Mechanical and Structural Properties. Materials, 15, 6106, 2022

4. D. Brząkalski, R. E. Przekop, M. Frydrych, D. Pakuła, **M. Dobrosielska**, B. Sztorch, B. Marciniec, Where ppm Quantities of Silsesquioxanes Make a Difference—Silanes and Cage Siloxanes as TiO2 Dispersants and Stabilizers for Pigmented Epoxy Resins, Materials, 15, 494, 2022

5. **M. Dobrosielska**, M. Zieliński, M. Frydrych, M. Pietrowski, P. Marciniak, A. Martyła, B. Sztorch, R. E. Przekop, Sol–Gel Approach for Design of Pt/Al2O3-TiO2 System—Synthesis and Catalytic Tests, Ceramics, 4, 667–68, 2021

6. K. Wałęsa, A. Wrzesińska, **M. Dobrosielska**, K. Talaśka, D. Wilczyński, Comparative Analysis of Polyurethane Drive Belts with Different Cross-Section Using Thermomechanical Tests for Modeling the Hot Plate Welding Process, Materials, 14, 3826, 2021

7. R. E. Przekop, M. Kujawa, W. Pawlak, **M. Dobrosielska**, B. Sztorch, W. Wieleba, Graphite Modified Polylactide (PLA) for 3D Printed (FDM/FFF) Sliding Elements, Polymers 12(6), 1250, 2020

8. D. Brząkalski, R. E. Przekop, **M. Dobrosielska**, B. Sztorch, P. Marciniak, B. Marciniec, Highly bulky spherosilicates as functional additives for polyethylene processing—Influence on mechanical and thermal properties, Polymer Composites, 41(8), 1-14, 2020

9. **M. Dobrosielska**, D. Pakuła, B. Sztorch, M. Popiół, B. Klonowski, D. Brząkalski, B. Marciniec, R. E. Przekop, The influence of surface physicochemistry of solid fillers on dispesion in polyurea systems, Composites Theory and Practice, 19:2, 83-90, 2019

10. D. Pakuła, **M. Dobrosielska**, B. Sztorch, M. Popiół, B. Klonowski, D. Brząkalski, B. Marciniec, R. E. Przekop, A new microsilica filler for polyurea systems, Composites Theory and Practice, 19:2, 76-82, 2019

11. A. Martyła, M. Osińska-Broniarz, M. Kopczyk, B. Sztorch, **M. Dobrosielska**, R. E. Przekop, A new method of one-pot synthesis of efficient Au/SnO_2 electrocatalysts for fuel cells, WSEAS Transactions on Fluid Mechanics 13:126-135, 2018

Patent i zgłoszenia patentowe

1. Zgłoszenie patentowe P.436292 „*Sposób rafinacji ziemi okrzemkowej w skali półtechnicznej*”

2. Patent Pat.243125 „*Biokompozyt składający się z biodegradowalnego poli(kwasu mlekowego), ziemi okrzemkowej i wosku pszczelego oraz sposób wytwarzania biokompozytu*”
3. Zgłoszenie patentowe P.440888 *„Biokompozyt polimerowy na bazie polilaktydu PLA i węglanowych osadów jeziornych CLS oraz sposób jego otrzymywania”*
4. Zgłoszenie patentowe P. 442544 *Sposób bielenia ziemi okrzemkowej*
5. Zgłoszenie patentowe P.433343, *Kompozyt termoplastyczny i sposób otrzymywania kompozytu termoplastycznego na bazie polilaktydu do zastosowanego w technice przyrostowej*
6. Zgłoszenie patentowe P.431506, *Kompozyt polimerów termoplastycznych polipropylenu z odpadowym pyłem lotnym Microsilica jako napełniaczem oraz sposób jego wytwarzania*
7. Zgłoszenia patentowe P.431947 *Sposób otrzymywania powłok polimocznikowych*
8. Zgłoszenie patentowe P.431948 *Sposób otrzymywania powłok polimocznikowych*
9. Zgłoszenie patentowe P.431949 *Sposób otrzymywania powłok polimocznikowych*

Granty naukowe

1. Wykonawca w projekcie Lider „Nowe metody otrzymywania masy kontaktowej do syntezy bezpośredniej alkoksyslianów” (NCBiRLIDER/045/631/L-4/12/NCBR/2013) – Centrum Zaawansowanych Technologii UAM w Poznaniu
2. Wykonawca w projekcie Preludium 15 „Funkcjonalizowane układy POSS jako modyfikatory napełniaczy do polimerów termoplastycznych i żywic epoksydowych” (UMO-2018/29/N/ST5/00868) - Centrum Zaawansowanych Technologii UAM w Poznaniu
3. Technolog w projekcie FNP „Zaawansowane biokompozyty dla gospodarki jutra BIOG-NET” (POIR.04.04.00-00-1792/18-00) – Politechnika Warszawska

Część II

Publikacje składające się na rozprawę doktorską

H1

Biogenic Composite Filaments Based on Polylactide and Diatomaceous Earth for 3D Printing

Dobrosielska M., Przekop R.E., Sztorch B., Brząkalski D., Zgłobicka I., Łępicka M., Dobosz R., Kurzydłowski K.J.; Materials 13, 20, 4632, 2020

materials

MDPI

Article

Biogenic Composite Filaments Based on Polylactide and Diatomaceous Earth for 3D Printing

Marta Dobrosielska [1], Robert Edward Przekop [2,*], Bogna Sztorch [2], Dariusz Brząkalski [3], Izabela Zglobicka [4], Magdalena Łępicka [4], Romuald Dobosz [1] and Krzysztof Jan Kurzydłowski [4]

1 Faculty of Materials Science and Engineering, Warsaw University of Technology, 141 Wołoska, 02-507 Warsaw, Poland; marta.dobrosielska@pw.edu.pl (M.D.); romuald.dobosz@pw.edu.pl (R.D.)
2 Centre for Advanced Technologies, Adam Mickiewicz University in Poznań, 10 Uniwersytetu Poznańskiego, 61-614 Poznań, Poland; bs330138@amu.edu.pl
3 Faculty of Chemistry, Adam Mickiewicz University in Poznań, 8 Uniwersytetu Poznańskiego, 61-614 Poznań, Poland; dbl80278@amu.edu.pl
4 Faculty of Mechanical Engineering, Białystok University of Technology, 45C Wiejska, 15-351 Białystok, Poland; i.zglobicka@pb.edu.pl (I.Z.); m.lepicka@pb.edu.pl (M.Ł.); krzysztof.kurzydlowski@pw.edu.pl (K.J.K.)
* Correspondence: rprzekop@amu.edu.pl

Received: 11 September 2020; Accepted: 13 October 2020; Published: 16 October 2020

Abstract: New composites containing a natural filler made of diatom shells (frustules), permitting the modification of polylactide matrix, were produced by Fused Deposition Modelling (3D printing) and were thoroughly examined. Two mesh fractions of the filler were used, one of <40 µm and the other of 40–63 µm, in order to check the effect of the filler particle size on the composite properties. The composites obtained contained diatom shells in the concentrations from 0% to 5% wt. (0–27.5% vol.) and were subjected to rheological analysis. The composites obtained as filaments of 1.75 mm in diameter were used for 3D printing. The printed samples were characterized as to hydrophilic–hydrophobic, thermal and mechanical properties. The functional parameters of the printed objects, e.g., mechanical characteristics, stability on contact with water and water contact angle, were measured. The results revealed differences in the processing behavior of the samples as well as the effect of secondary granulation of the filler on the parameters of the printing and mechanical properties of the composites.

Keywords: diatoms; fused deposition modeling (FDM); polylactide; 3D printing

1. Introduction

Additive technologies, known also as 3D printing, have become a key type of processing of 4.0 Industry. They were developed in the beginning of the 1980s, however their rapid growth started nearly a decade ago, mainly because of finding solutions permitting cost reduction, and cessation of patent protection. Until that time, these technologies were inaccessible for individuals, small companies, research and technology workers concerned with the improvement of technologies and designing new materials. At present, the area of additive technologies has entered a new phase of development and arouses increasing interest in many branches of the industry. A wide range of materials can be applied in this technology, starting from plastics, through ceramics to metal powders. For each type of material, different dedicated techniques and types of 3D printers are used. Fused Deposition Modeling (FDM) is a popular method for the production of elements made of thermoplastic materials [1,2].

The widespread use of FDM is strictly related to the development of printing materials and 3D printers. Additive technologies are used, e.g., in medicine for printing polymer implants, showing high

density and rigidity, which can remain in human body for a longer time than traditionally produced ones [3]. The products of 3D printing find increasing use in the automotive and aviation industry and architecture [4]. The most important challenges in the research and development of FDM include the improvement of mechanical strength and functional properties of the products at a high rate of the printing process. One of the materials most often used for 3D printing is polylactide (PLA), obtained from renewable and biodegradable precursors [5,6]. According to IUPAC (International Union of Pure and Applied Chemistry), its proper simplified name is poly(lactide), however it has been often ambiguously referred to as poly(lactic acid), despite not containing carboxyl groups [7]. The greatest benefits of PLA in the area of material processing is its ability to biodegrade in specific conditions, low glass transition point, small thermal shrinkage upon extrusion molding (also in 3D printing) and no toxic gases emission upon processing. Polylactide is not counted as a good construction material as it shows a low impact strength and low thermal stability [8]. It is used for the production of everyday use goods, including the packaging foil, disposable products and containers, and medical products such as wound dressings, threads and surgical masks [9]. To not compromise the ecologically friendly character of the products, PLA, which is a biopolymer, should be used with additives of natural origin. One of possible additives can be diatom shells made of biosilica. Diatoms are one of the most abundant and diverse groups of algae. Their characteristic feature is the decorated silica shells (frustules) of a variety of shapes and sizes from 1 µm to 1 mm, most often 10–200 µm [10]. Due to their size, diatoms belong to microorganisms. Thanks to their abundant presence in water, the bottoms of all kinds of water bodies are covered with diatomaceous earth formed of diatom shells [11]. Fossil diatoms are found in the form of diatomite or diatomaceous earth. The content of silica in diatomite varies from 60% to 95%, the rest are pollutants such as carbonates, iron oxides, quartz, loams or substances of volcanic origin. One cm^3 of diatomite contains about 2.5 billion of diatom shells [12,13]. Thanks to its attractive properties, e.g., high sorption capacity, abrasive character, insecticide activity and nontoxicity, it is a valuable component used in food and chemical industries, and construction. Diatom shells are covered with a variety of pore systems, different for individual species, but also different in the shell of each diatom. The pores of different shapes and sizes permit the capturing of nutrients and filtering off toxic substances. Diatoms are a renewable source of three-dimensional nanostructural silica that could be used in different devices filtering pathogens (bacteria or viruses). As diatomite shows the ability to adsorb heavy metal ions (nickel, lead, zinc, and titanium) and participate in water oxidation, it is used for water treatment [14,15]. Moreover, diatomite is used for purification and filtration of alcohols, saccharides, paints and varnishes, as well as for protection and thermal insulation. The first report on the application of PLA filaments enriched in diatom shells in FDM has been presented by Aggarwal et al. [16]. From the point of view of processing, the important parameters describing the diatomaceous earth as a filler are the primary and secondary granulation. The primary granulation is the actual size of the diatom shells used in the filler, while the secondary granulation is the size of agglomerated and non-agglomerated diatom shells in the composite filaments. A distinction between these two types of granulation is vital from the point of view of processing and the properties of the composite materials based on diatomaceous earth. Besides the specific properties of diatoms, attractive for 3D printing when in composite with PLA, the application of a biogenic filler can considerably reduce the cost of this process. In this work, we present an approach towards the preparation of composites comprised of PLA as a polymer matrix and diatomite as an extender and structural filler, allowing for an improvement to the mechanical characteristics of PLA and a reduction in the polylactide consumption. The obtained materials were formed into 3D printing filaments and showed satisfactory printability, which was proof of the concept for a new series of highly eco-friendly, biodegradable and multi-purpose materials for the FDM technique. These composite filaments may be exceptionally attractive for the introduction to consumer use due to the amount of globally produced plastic waste of household–3D printing origin, which is often not properly disposed of and usually not recovered for recycling.

2. Materials and Methods

2.1. Materials

Polylactide (PLA) type Ingeo 2003D was purchased from NatureWorks (Minnetonka, MN, USA). Diatomaceous earth—fossilized algae diatoms of Phylum Bacillariophyta from pure Mexican fresh water was purchased from Perma Guard Agro (Otwock, Poland).

2.2. Analyses

Contact angle analyses were performed by the sessile drop technique at room temperature and atmospheric pressure, with a Krüss DSA100 goniometer (KRÜSS GmbH Hamburg, Germany). Three independent measurements were performed for each sample, each with a 5 µL water drop, and the obtained results were averaged to reduce the impact of surface nonuniformity.

Thermogravimetry was performed using a NETZSCH 209 F1 Libra gravimetric analyzer (NETZSCH-Gerätebau GmbH, Selb, Germany). Samples of 5 ± 0.2 mg were cut from each granulate and placed in Al_2O_3 crucibles. Measurements were conducted under nitrogen (flow of 20 mL/min) in the range of 30–800 °C and a 20 °C/min heating rate. Differential scanning calorimetry was performed using a NETZSCH 204 F1 Phoenix calorimeter (NETZSCH-Gerätebau GmbH, Selb, Germany). Samples of 6 ± 0.2 mg were cut from each granulate and placed in an aluminum crucible with a punctured lid. The measurements were performed under nitrogen in the temperature range of −20–290°C and at a 20 °C/min heating rate, and T_g was measured from the second heating cycle.

The effect of the modifier addition on the mass flow rate (MFR) was also determined. The measurements were made using a Instron plastometer, model Ceast MF20 (Instron, Norwood, MA, USA) according to the applicable standard ISO 1133. The measurement temperature was 190 ± 0.5°C, while the piston loading was 2.16 kg.

The dynamic viscosity coefficient was determined by a capillary rheometer Instron Ceast SR 10 (Instron, Norwood, MA, USA), according to ISO 11443:2005, using a capillary tube of 5 mm in length, 1 mm in diameter and the shearing speed range 1–100 (s^{-1}). Measurements were carried out at 190 °C.

For flexural and tensile strength tests, the obtained materials were printed into type 1B dumbbell specimens in accordance with EN ISO 527:2012 and EN ISO 178:2006. Tests of the obtained specimens were performed on a universal testing machine INSTRON 5969 with a maximum load force of 50 kN. The traverse speed for tensile strength measurements was set at 2 mm/min, and for flexural strength was also set at 2 mm/min. Charpy impact test (with no notch) was performed on a Instron Ceast 9050 (Instron, Norwood, MA, USA) impact-machine according to ISO 179–1. For all the series, 6 measurements were performed.

The X-ray diffraction measurements were carried out using a Philips PW1050 diffractometer (Philips, Amsterdam, The Netherlands) working in the θ–2θ geometry with Ni-filtered CuKα radiation. The following measurement conditions were applied: 2θ range of 5°–80°, voltage 35 kV, current 20 mA, scan step 0.040° at 1° per minute. The positions of the reflections were calculated by the Philips APD program version 1.3.

The porous structure was determined by low temperature nitrogen adsorption measurements carried out on a Micromeritics ASAP 2420 apparatus (Norcross, GA, USA) in the standard analysis mode, using 0.8–1.4 g of material with the grain size fraction between 0.1 and 0.2 mm. Prior to nitrogen adsorption, all samples were degassed for about 10 h at 350 °C at 0.4 Pa until reaching a constant weight. Both adsorptive and desorptive branches of the isotherm were recorded in the range of p/p_0 0–1.0. Reports were provided by ASAP 2420 software (Micromeritics Instrument Corp., version 2.09A). Distribution of pore area and pore volume was calculated using de Boer t-plot method and BJH method. The pore volume and pore diameter were established from the adsorptive branch of the isotherm using BJH method, and the surface area was calculated using the BET method.

Hardness of the composite samples was tested by the Shore method using a durometer Bareiss Prüfgerätebau GmbH (Oberdischingen, Germany).

The images of diatomaceous earth as well as composite materials were obtained using a scanning electron microscope Hitachi SU−8000 (Tokyo, Japan) using acceleration voltage of 5.0 kV. Samples were placed on the double-adhesive carbon tape and coated with Cu-Ni, using the PECS coating system made by Gatan (Pleasanton, CA, USA).

The grain size distribution was measured by a Mastersizer 3000 (Malvern Instruments Ltd. Malvern, UK). The measurements were made for the samples in the water suspension (Hydro EV attachment) and for dry powders (Aero S attachment). The parameters of measurements for dry powders: rate of sample supply 27, air pressure 2.7 bar, and nozzle slit 1 mm. The parameters of measurements for wet samples: stirrer revolution speed 2330 rev/min and ultrasound power 60%.

A water absorption study of printed samples was also carried out. The samples were placed in distilled water at 50 °C upon constant stirring with a magnetic stirrer for 72 h. The samples were then pre-dried, placed under vacuum for 1 h, and then in an oven at 40 °C for 24 h.

2.3. Fabrication of Filaments

The filaments were fabricated using the following procedure: (a) preparation of diatom modifier, (b) preparation of concentrated granules, and (c) extrusion of filaments.

(a) Preparation of diatom modifier

Diatomaceous earth was milled in a ball mill and then divided into fractions (on a vibrating table) of the mesh size up to 40 µm and 40–63 µm to be used in further studies.

(b) Preparation of granulates

The polymer and the filler were homogenized using a laboratory two-roll mill ZAMAK MERCATOR WG 150/280 (Krakow, Poland). A portion of 500 g PLA Ingeo™ 2003 D was mixed with 26.5 g diatomite of grain size up to <40 µm or from the range 63–40 µm, until the final concentration of the filler of 5% w/w. The mixing was performed at the rolls temperature of 200 °C for 15 min., getting to full homogeneity of the concentrates. Masterbatch was granulated by a grinding mill WANNER C17.26 sr. (Wanner Technik GmbH, Reicholzheim, Germany) The granulates were diluted with pure PLA up to the final filler concentrations of 1% or 2.5% w/w upon extrusion molding of a stream with consequent cold granulation on the twin-screw extrusion setup line HAAKE Rheomex OS (Thermo Fisher Scientific, Waltham, MA, USA), and then dried for 24 h at 40 °C.

(c) Extrusion of Filaments

The granulates obtained as above were used for molding of filaments of 1.75 mm in diameter by a single-screw extrusion setup HAAKE Rheomex OS (Thermo Fisher Scientific, Waltham, MA, USA).

3D Printing (FDM)

Using a 3D printer FlashForge Finder (Warsaw, Poland) two types of samples were printed by FDM: oars and bars, according to PN-EN- ISO 527−2. Parameters of printing are given in Table 1.

Table 1. Process parameters for sample printing.

Layer height	0.18 mm
Top layer height	0.27 mm
Shells	2
Top and bottom layers number	3
Bottom layers number	3
Infill density	100%
Infill pattern	Hexagonal
Printing speed	60 mm/s
Idle speed	80 mm/s
Extruder temp.	220 °C

3. Results and Discussion

3.1. Low-Temperature Nitrogen Sorption

Diatomaceous earth has a triple hierarchical structure as it shows three types of pore systems: micropores of 2–3 nm, mesopores of 10–50 nm and macropores of 3–10 μm in diameter. Thus, diatom shells are nanoporous materials of hierarchic porous structure [17]. Specific surface area of diatomite varies depending on its origin. The mean volume of pores obtained from the desorption branch of nitrogen sorption was 0.063 cm^3/g and 0.070 cm^3/g for the fractions of <40 μm and 63–40 μm, respectively. The mean pore diameter obtained by the same method was 13.51 nm and 11.70 nm, which confirm the presence of small mesopores in the frustule. The specific surface area of the fractions was 24.40 ± 0.18 m^2/g for the diatomite fraction of <40 μm, while 27.60 ± 0.16 m^2/g for the fraction of 63–40 μm, respectively. The results are given in Figure 1a,b. The specific surface areas of other fillers vary in a wide range, e.g., the specific surface areas of aluminum oxide (Al_2O_3), silica (SiO_2), magnetite (Fe_3O_4), zinc oxide (ZnO), magnesium hydroxide ($Mg(OH)_2$) are 12–250 m^2/g [18], 50–1000 m^2/g [19], 6–90 m^2/g [20], 8–75 m^2/g [21,22], and 4–10 m^2/g [23], respectively. The surface area of the diatomite is not as well-developed as that of, e.g., aluminum oxide, but it still has been successfully used as an adsorbent thanks to its porous structure [24].

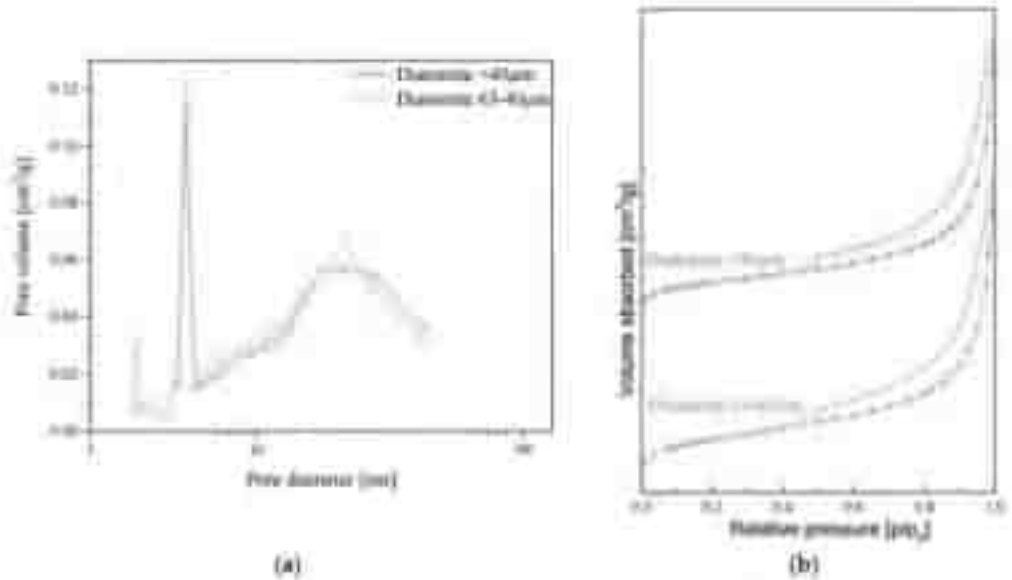

Figure 1. (a) Pore volume versus diameter and (b) isotherms of nitrogen sorption.

3.2. Particle Size Measurements by Dynamic Light Scattering (DLS)

Amorphous diatomaceous earth was sieved into two mesh size fractions: one of grains smaller than 40 μm and the other of grain size 40–63 μm, in order to elucidate the problem of formation of diatom shells agglomerates in the diatomaceous earth. Figure 2 shows many agglomerates of diatom shells whose appearance may imply poorer dispersion of the filler in the PLA matrix. Determination of the size of particles in dry powders and in water suspension in the two size fractions (Figure 2) revealed differences in particle distribution in them. The fraction of particles size 63–40 μm shows a greater contribution of particles smaller than 6 μm, classified on the basis of SEM images as fragments of broken diatom shells (cf. 3.3 SEM). This fraction contains a smaller number of the largest particles of sizes close to 40 μm. Both mesh fractions contain the greatest number of particles of sizes close to ~10 μm (the fraction <40 μm contains about 15% more). Measurements performed in water permitted further observations. The fraction <40 μm after immersion in water showed a minimum increase in the maximum particle size, which was still below 40 μm, although their contribution significantly

increased. The fraction 40–63 µm shows the appearance of a small contribution of particles whose size reaches up to 90 µm. This observation indicates the agglomeration of diatom shell particles in water. The diversity of particle sizes in both mesh fractions 40–63 µm and <40 µm is visible in the corresponding SEM images shown in Figure 3.

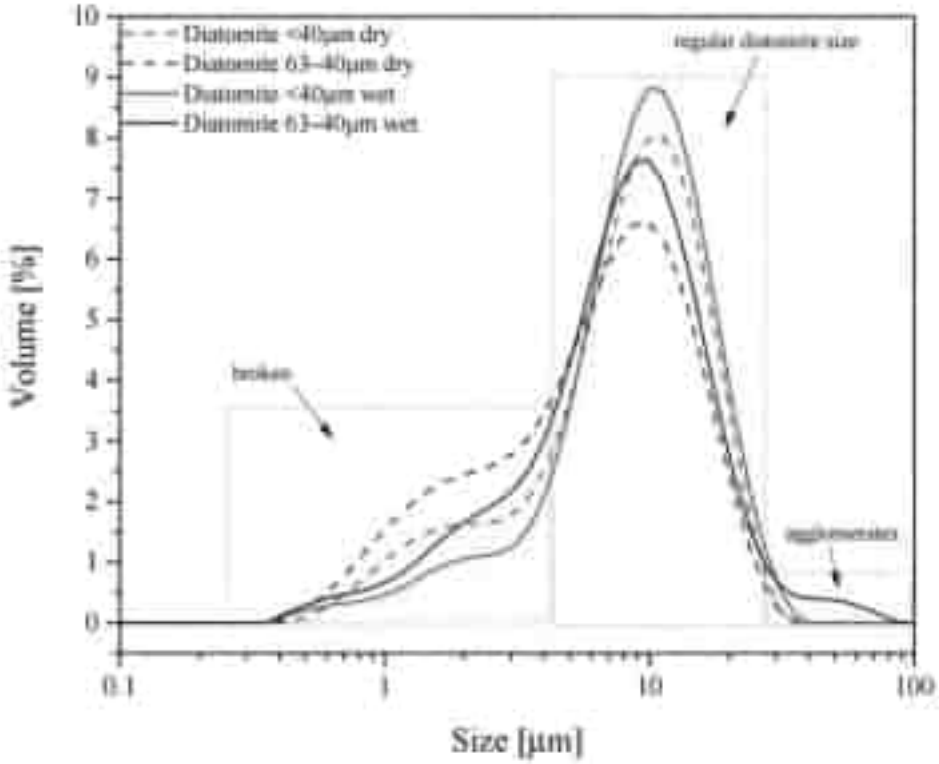

Figure 2. Particle size distribution of diatom shells for the two mesh size fractions; measurements in water and in dry powder.

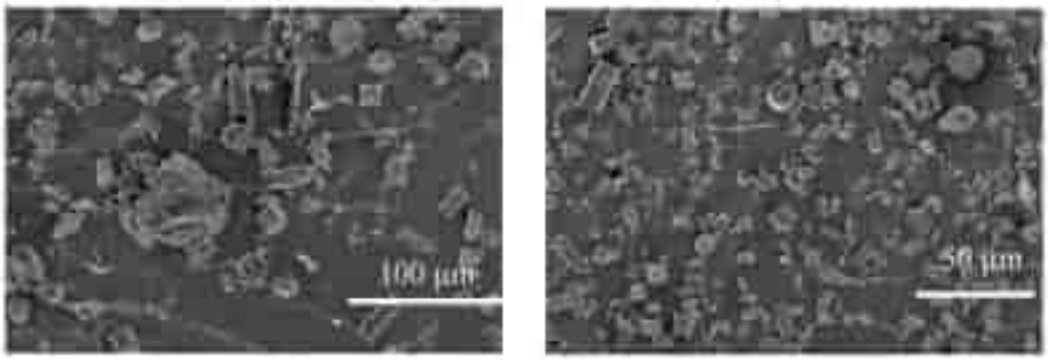

Figure 3. SEM image of dry powder of amorphous diatomaceous earth.

The DLS method was chosen to gain information on the actual behavior of the particles. The measurements for dry powders provides more reliable particle sizes, and thanks to the way the samples were supplied, there is no problem with particle agglomeration. The particle size profile obtained from such measurements corresponds to that of the primary particles. The measurements in water do not eliminate the problem of particle agglomeration (as seen in the particle size profile), but are useful for the estimation of the actual secondary particle size in composite systems in which the filler of polar surface shows a tendency to agglomerate in a much less polar polymer matrix. Thus, to get a wider picture of particle size distribution, the two methods have to be employed side-by-side.

3.3. SEM

The SEM imaging of the samples broke the cross sections and revealed the presence of diatom shells in the PLA matrix and permitted the evaluation of the size, morphologies and defects of the filler particles, as well as their distribution and agglomerations (Figure 4a–f). The figures show diatom shells of different shapes and sizes. SEM images of raw fossil diatomaceous earth showed that it contained unbroken diatom shells of a cylindrical shape of 8 to 20 µm in diameter, along with broken shells of sizes below 8 µm and shell agglomerates of 20 to 80 µm in size. With increasing concentrations of diatoms in the matrix, their agglomerates become larger, irrespective of the fraction. The majority of the diatom shells were visible in the SEM images and assumed the shape of a cylinder and had numerous openings; only few are built of smooth walls. This characteristic feature of diatom shells permitted living diatoms to absorb nutrients and excrete products of metabolism. In the context of their effect on the properties of diatom shells as a filler, these openings can be treated as pores. The pores play an important role in the process of the filler binding with the polymer matrix, which has been confirmed by SEM image analyses.

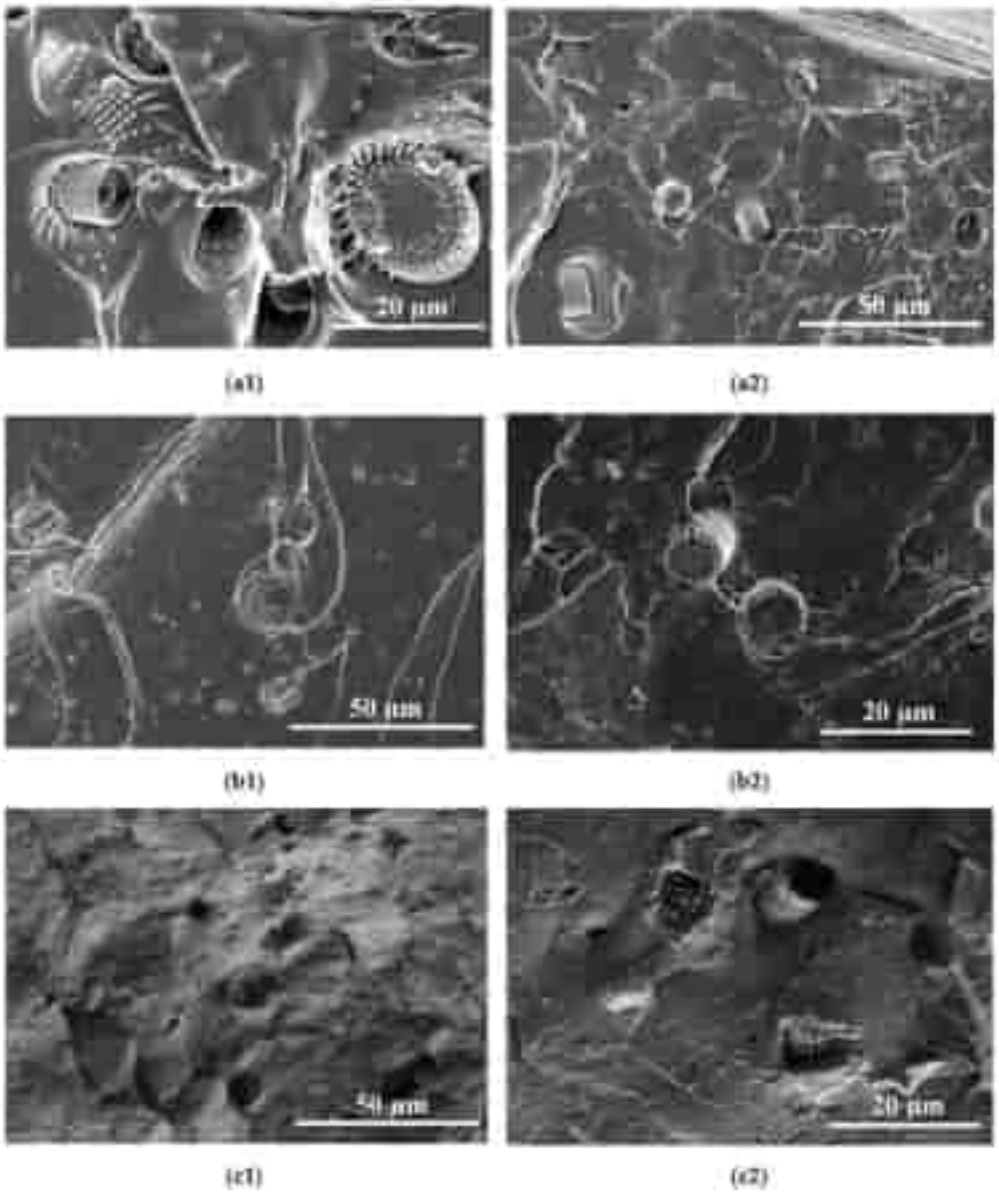

Figure 4. Cont.

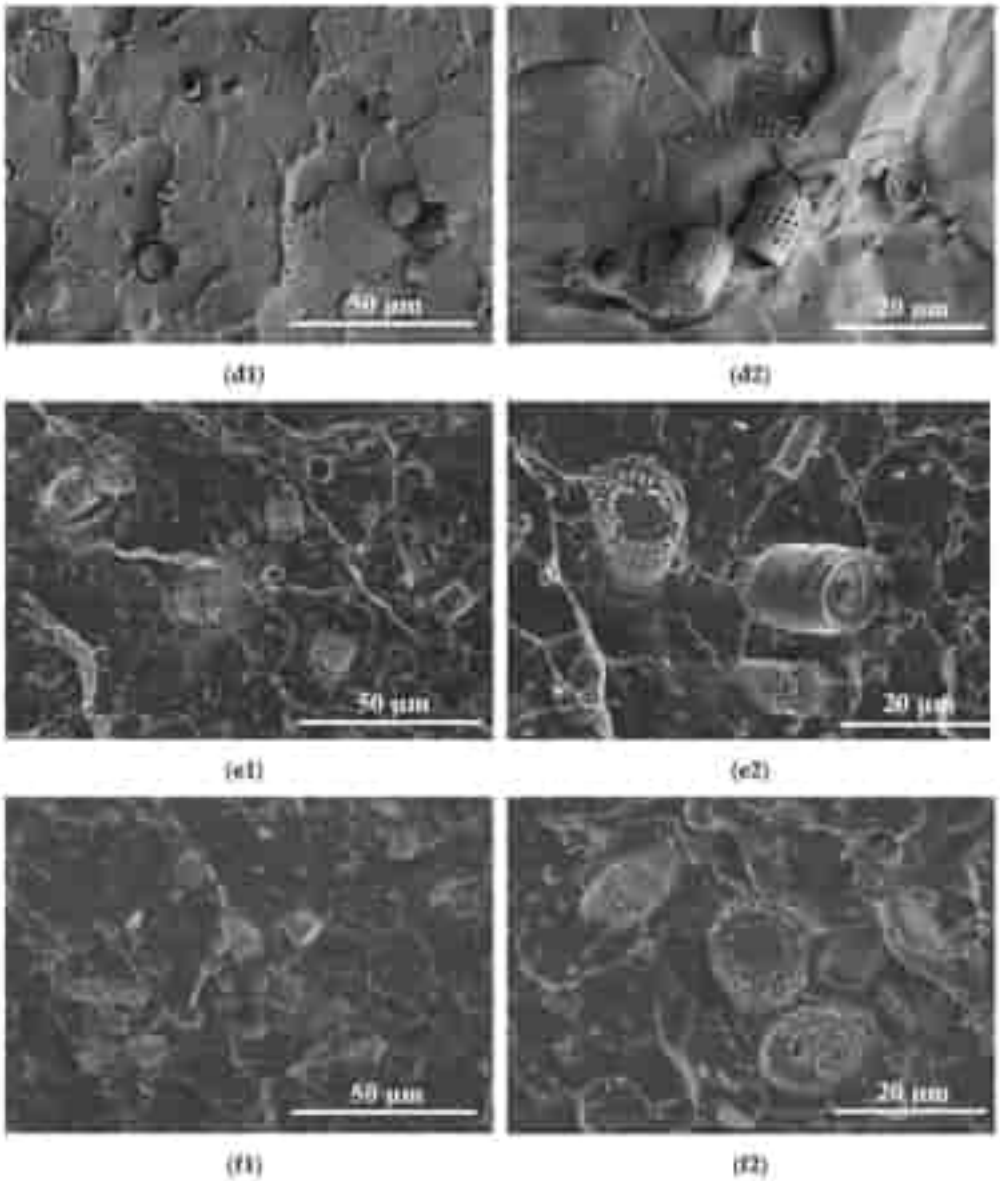

Figure 4. SEM images of PLA composites with diatoms: **(a1)** 1% diatomite fraction <40 µm, scale 50 µm, **(a2)** 1% diatomite fraction <40 µm, scale 20 µm, **(b1)** 1% diatomite fraction 63–40 µm, scale 50 µm, **(b2)** 1% diatomite fraction 63–40 µm, scale 20 µm, **(c1)** 2.5% diatomite fraction <40 µm, scale 50 µm, **(c2)** 2.5% diatomite fraction <40 µm, scale 20 µm, **(d1)** 2.5% diatomite fraction 63–40 µm, scale 50 µm, **(d2)** 2.5% diatomite fraction 63–40 µm, scale 20 µm, **(e1)** 5% diatomite fraction <40 µm, scale 50 µm, **(e2)** 5% diatomite fraction <40 µm, scale 20 µm, **(f1)** 5% diatomite fraction 63–40 µm, scale 50 µm, and **(f2)** 5% diatomite fraction 63–40 µm, scale 20 µm.

Figure 4 presents images of composites of PLA with diatomites of different particle size fractions and added in different concentrations. The images reveal distinct non-agglomerated diatom shells, usually of cylindrical shape. They have different diameters, varying from about 7 µm to 20 µm, however those of the external diameter of approx. 15 µm and 9–12 µm in length dominate. The shells are covered with clearly marked pores of 0.5–0.6 µm in diameter (Figure 5).

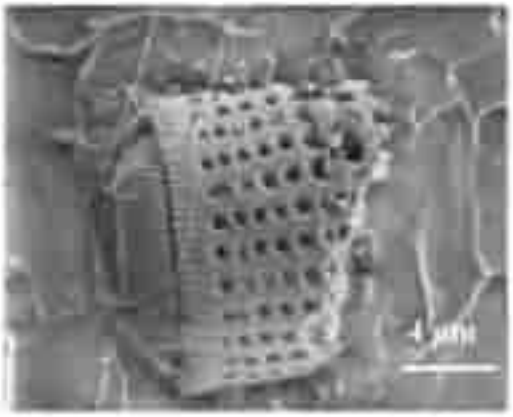

Figure 5. SEM image of the sample of PLA with 1% w/w loading of diatomite, fraction <40 µm.

Usually, the well-defined oval shape pores make a network. As a result of the processing, the secondary particles underwent de-agglomeration, which points to good dispersion of the diatom shells in the PLA matrix and high miscibility of the filler with the matrix. The images also show the traces of polymer flow through the pores in diatom shells, Figure 6a, as trails of PLA running from the pore mouth to the bulk polymer. This observation indicates a very good penetration of frustules by the molten polymer and good mechanical contact of the filler with the matrix, which means that this filler has an effective reinforcing phase.

3.4. DSC and TGA Results

Results of the TGA and DSC measurements, in the form of DSC curves, are presented in Figure 6a,b, and the parameters determined, including the percentage of the mass loss, temperature at the maximum rate of mass loss and glass transition temperature are given in Tables 2 and 3. The processes of decomposition of the reference sample and composites of PLA with diatom shells occur in a single stage. Thermal decomposition of both fractions of the filler in the form of dry powder takes place in three stages. The first one in the range of 228.8–234.8 °C is interpreted as the evaporation of water physically and chemically adsorbed in the pores of diatom shells. The mass loss accompanying the process is 8–9%. The second mass loss is observed in the range 450.7–457.5 °C is interpreted as corresponding to the decomposition of organic and inorganic substances as well as the elimination of remaining silanol groups. The third stage was noted to take place in the range of 962.9–983.5 °C could be explained by the total dehydration of the sample and decomposition of carbonates [25]. On the basis of the derivatographic curves, it was possible to establish the temperature of thermal decomposition (pyrolysis) of molten mixtures of PLA and diatomaceous earth. On the basis of T_{onset} it can be concluded that in the first phase of the samples decomposition, the presence of diatom shells has a stabilizing effect on the matrix, for instance through hindering of free radicals transfer between the polymer chains and slower radical migration in more viscous polymer melt. The sample of pure PLA was characterized by the lowest T_{onset} from among all samples, of 348.3 °C. However, when comparing the temperatures of the fastest mass loss (T_{DTG}), the sample of pure PLA showed the highest from among all the samples, at 376.0 °C. In these conditions, diatom shells acted as catalyst of thermal decomposition, similarly as zeolites used in the catalytic pyrolysis of organic matter, including polymers. The decrease in T_{DTG} being rather small was related to a low contribution of diatom shell mass in the composites [26]. The dry mass left after pyrolysis increased, as expected, with a growing concentration of the filler and with an increasing size of the filler fraction used. The differences between the dry mass left after pyrolysis (Table 2) and the actual content of the filler in the composite follow from the fact that the process of pyrolysis is rapid (a steep mass loss curve) and pyrolytic gases carry out some fragments of diatom shells [27].

Table 2. Results of thermogravimetric analysis.

	1% Mass Loss [°C]	Onset Temperature, [°C]	Temperature at the Maximum Rate of Mass Loss [°C]	Dry Mass Left after Pyrolysis [%]
Neat PLA	305.8	348.3	376.0	0.00
PLA + 1% diatomite < 40 µm	292.9	354.1	366.7	0.21
PLA + 2.5% diatomite < 40 µm	311.3	352.2	373.8	1.73
PLA + 5% diatomite < 40 µm	301.2	350.5	372.3	3.25
PLA + 1% diatomite 63–40 µm	312.1	353.2	373.5	0.60
PLA + 2.5% diatomite 63–40 µm	313.0	352.4	373.6	2.01
PLA + 5% diatomite 63–40 µm	311.4	351.4	372.5	3.74
Diatomite < 40 µm powder	66.9	194.5	234.8	86.09
Diatomite 63–40 µm powder	74.4	185.5	228.8	86.90

The glass transition temperature (T_g), determined on the basis of the second cycle of heating is clearly lower for all the samples containing diatom shells, than for the reference sample (59.9 °C, Table 3). It is most probably related to the presence of additional stress in the sample detected by the XRD method and the presence of additional amorphous interphases at the PLA-filler interface or to a negative influence of the filler on the orientation ability of PLA chains. Exothermic peak appearing on the heating curve at about ~120 °C is assigned to "cold crystallization", T_{cc}. In this process a small amount of the polymer undergoes crystallization upon heating [28]. The decrease in T_{cc} is interpreted as due to the presence of internal stress in the sample. An important parameter of sample processing is the time of the cycle, which should be the shortest possible, to maximize the efficiency of production. For this reason the process of cooling is fast and short lasting, which is not conducive to crystal phase development. The melting point of the PLA crystalline fraction is in the range of 150–154 °C, the signals area was higher for neat PLA than for the samples with the filler (Table 3, k +5%a-b). This observation can be explained by the fact that diatom shells may act as the nuclei of crystallization and boosts the formation of crystallites [29]. An addition of diatomaceous earth to the polymer significantly reduced the contribution of the amorphous fraction and increased that of the crystalline phase. Moreover, with increasing content of diatom shells the crystallization point was noted to decrease. No significant effect of the filler addition on the melting point of the composites was observed.

Table 3. Analysis of DSC results for the composite samples.

	T_g [°C]		T_{cc} [°C]		T_m [°C]	
	Granulate	Print	Granulate	Print	Granulate	Print
PLA natural	59.9	57.7	126.4	124.6	153.3	151.5
PLA + 1% diatomite < 40 µm	57.0	57.6	121.6	123.1	152.5	152.8
PLA + 2.5% diatomite < 40 µm	58.2	59.6	119.5	119.1	153.3	150.5
PLA + 5% diatomite < 40 µm	57.3	58.3	116.3	117.8	151.5	151.6
PLA + 1% diatomite 63–40 µm	57.2	59.4	122.9	124.1	152.5	153.9
PLA + 2.5% diatomite 63–40µm	57.5	59.0	117.0	120.9	152.6	153.1
PLA + 5% diatomite 63–40 µm	58.0	59.1	118.6	118.7	152.0	152.5

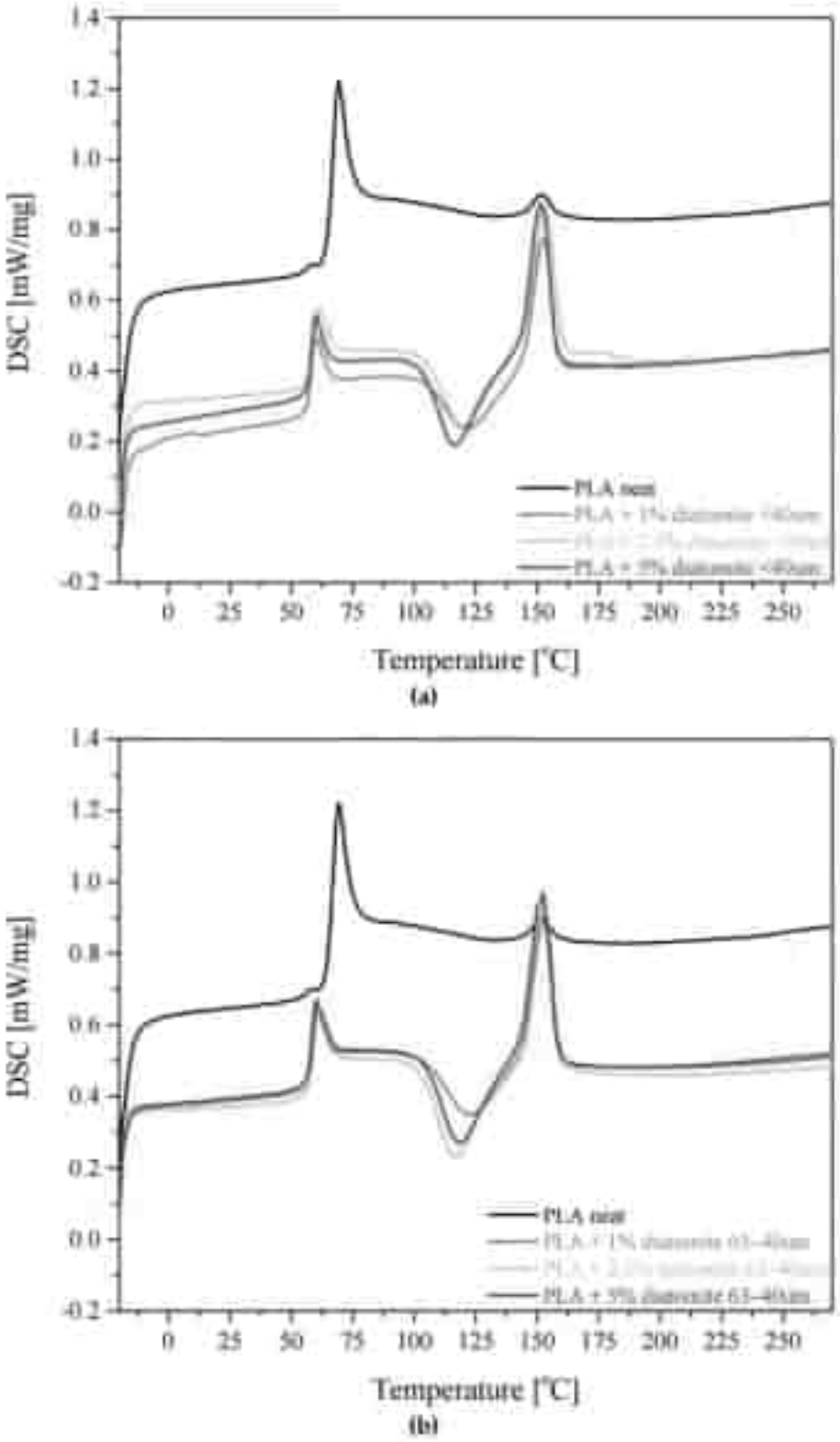

Figure 6. DSC curves recorded for samples of PLA composite with diatomite (**a**) <40 μm and (**b**) 63–40 μm.

3.5. *Contact Angle Measurements*

Water contact angle (WCA) was measured for dry samples and the samples subjected to distilled water at 50 °C (chemical treatment). Results of the measurements are given in Table 4. Diatomaceous

earth is a hydrophilic filler, characterized by a water contact angle of 0°. The degree of hydrophobicity decreases with the increasing particle size of the diatom shells. The samples containing diatomite of particle size fraction 63–40 µm are characterized by a smaller water contact angle (below 90°) than neat PLA (93.5°) so are hydrophilic. However, the composites of 40 µm particle fraction are more hydrophobic than the neat PLA. This difference between the WCA of two mesh fraction composite series is the result of the difference in the particle size of these two fractions, which in turn introduces additional porosity to the sample surface in the case of 63–40 µm fraction. However, while the 40 µm fraction contains smaller particles, which also modify the composite surface facture, it does so without introducing much porosity. It is a known fact that materials with more complex surface facture often show increased hydrophobicity if the base material is hydrophobic itself. The composites studied were subjected to distilled water at 50 °C in order to check the effects of such conditions on the degree of hydrophobicity, mechanical properties and to assess the water tightness of the printed objects. After the samples treatment with water at 50 °C, the contact angle values increased considerably to above 113°. Higher water contact angles were measured for the composites containing diatom shells fraction of smaller particle sizes <40 mm. With an increasing content of the filler, the water contact angle decreased. The greatest increase in the WCA relative to that of the reference sample was obtained for the composites containing the diatomite size fraction 63–40 µm (by about 30.2°). A significant increase in WCA was caused by changes in the microstructure of the sample surface (additional surface structuration). Additionally, PLA is a semicrystalline polymer and there are phases that undergo hydrolysis faster (amorphous phase) and slower (crystalline phase, also known as spherulites). Therefore, during hydrolysis, different spots of the surface hydrolyze with different ratios, resulting in additional factorization. It is visible as the neat PLA also becomes more hydrophobic after the water treatment. The WCA of the composites is a superposition of two effects: a physical structural one and a chemical one on the surface. The physical effect is dominant for samples on the inhomogeneous surface. The use of greater particle size fraction of the filler and its greater content lead to a decrease in the degree of hydrophobicity, thanks to its hydrophilic properties. The samples containing the fraction <40 µm are characterized by higher WCA than those containing the fraction of particle sizes 40–63 µm, which is explained by the fact that smaller filler particles do not lead to the appearance of large hydrophilic defects on the sample surface that would decrease the degree of hydrophobicity. With an increasing concentration of the filler, WCA decreases as a greater amount of hydrophilic filler is present on the sample surface.

Table 4. Water contact angle [°].

			Contact Angle [°]		
Storage Condition	**Fraction**	**Neat PLA**	**PLA + 1% Diatomite**	**PLA + 2.5% Diatomite**	**PLA + 5% Diatomite**
24 h, 40 °C	<40 µm	93.5	105.2	104.9	105.3
	63–40 µm		86.6	87.6	83.1
72 h, 50 °C, H_2O	<40 µm	112.9	123.8	115.2	113.8
	63–40 µm		117.4	116.3	114.3

PLA subjected to chemical treatment in water undergoes hydrolysis. On the basis of measurements of the composites mass before and after the conditioning in water it was proven that water remains in the samples' pores. The mass increase was the greatest for the samples of neat PLA. The samples containing diatomaceous earth were more resistant to water; their mass increased by almost 1.04%, while the mass increase of neat PLA was almost five times greater. While the water absorption by the samples studied was rather poor, their hydrophobic properties significantly increased. The hydrolysis of hydrophobic PLA led to a stronger binding of the polymer with polar filler, which caused an additional effect on the micro-structuration of the samples' surfaces, leading to partial pore closing and an increase in the samples hydrophobicity (Figure 7).

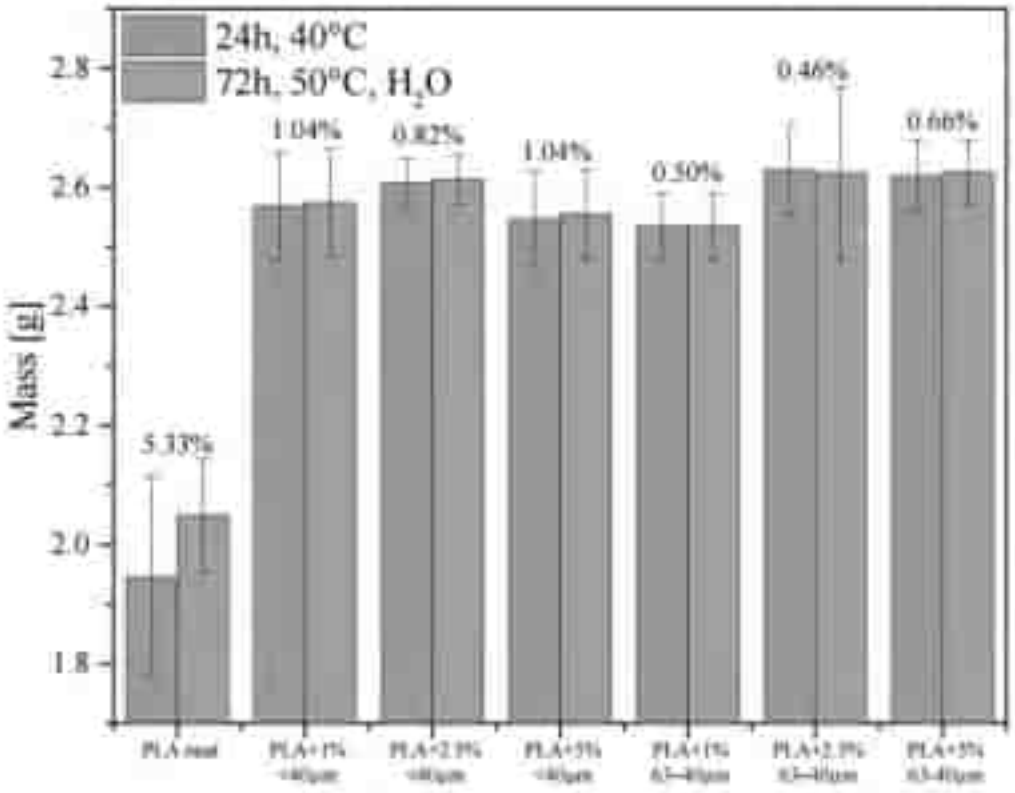

Figure 7. Masses of the as-obtained samples and the samples conditioned in distilled water at 50 °C for 72 h.

3.6. XRD

All the PLA/diatomite composites, as well as starting materials, neat PLA and diatomite of both diameter fractions, were subjected to XRD measurements (Figure 8). Due to the low crystallinity levels of the materials, the diffractograms present broad diffraction peaks instead of sharp reflexes. PLA shows two peaks, at. 2θ 16.0°, coming from (110) and (200) lattices, and a low-intensity 32.4°, coming from the (216) lattice. The observed crystalline phase is the most common α type [30]. Diatomite also shows two crystalline peaks at ~21° and ~35° (depending on the defects of the crystalline structure in the particular material grade and species of the diatoms the material is derived from). For the PLA/diatomite composites, it can be observed that although particular reflexes or peaks cannot be distinguished, the moderately intense 16.0° peak of PLA is broadened and its maximum is shifted to higher angles, which is a result of diatomite 21° peak contribution. This effect is stronger for 63–40 µm diatomite composites. Moreover, an interesting effect was observed for the 2.5% composite of 63–40 µm diatomite/PLA, where application of the filler resulted in improved polymer crystallinity, visible as the increase of peak intensity. The unexpected shift in the peak maximum, however, may be explained by the internal stress of the sample, residual from the composite processing (known also as the material processing memory). The effect, non-observable for the 5% composite of 63–40 µm diatomite, may be due to low control over material crystallization behavior, which was not a factor studied in this work.

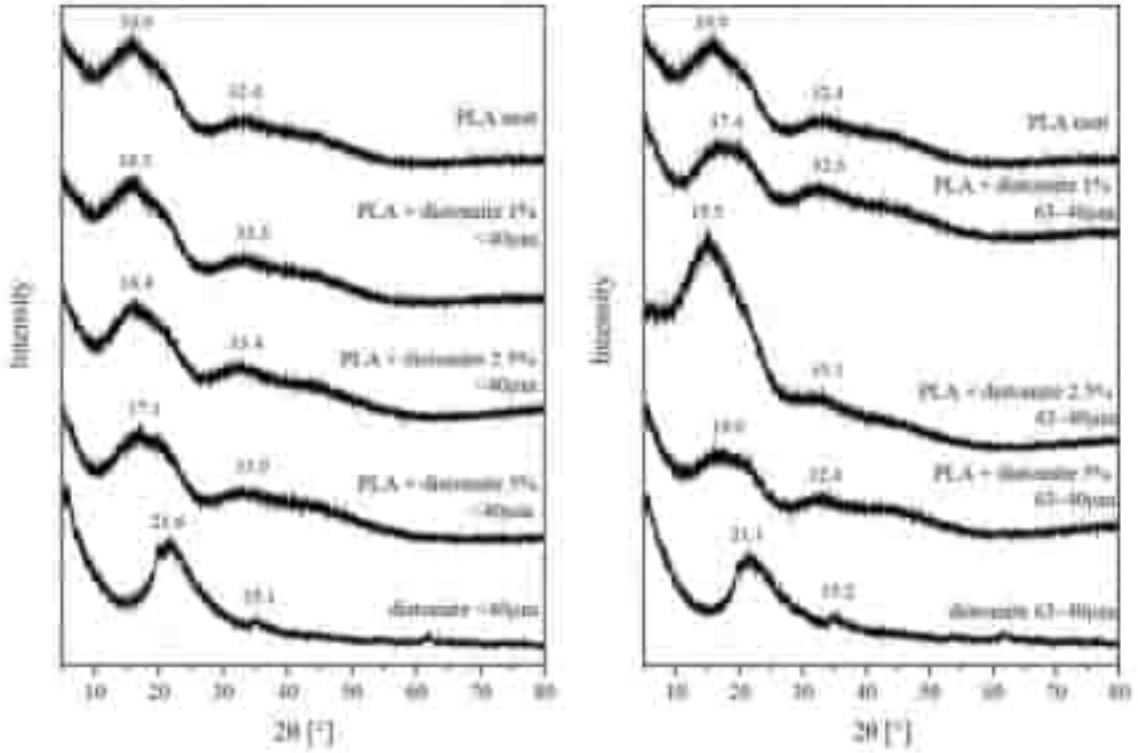

Figure 8. Diffractograms of PLA composites with diatom shells.

3.7. Mechanical Properties

3.7.1. Tensile Strength and Flexural Strength

Neat PLA samples for tests, printed out by the FDM method, showed tensile strength of 15.5–72.2 MPa, elongation at rupture of 0.5–9.2 %, bending strength of 52–115.1 MPa and elasticity modulus of 2.39–4.93 GPa [31,32]. The samples of PLA composites with diatom shells printed out by the same method showed almost a twice as high tensile strength (maximum value of 63.7 ± 2 MPa) relative to the value for neat PLA (37.7 ± 3 MPa). The greatest mechanical strength was noted for the samples containing 1% of diatomaceous earth. Higher concentrations of the filler result in a decrease in the tensile strength, which is related to a too high number of discontinuities in the polymer. Elongation at rupture was at a similar level for all the samples, however, the samples containing 1% or 2.5% of the filler of particle size <40 μm showed a small increase in the value of this parameter, up to >3% (Figure 9). After examination of water absorbability at 50 °C, the tensile strength increased, both for neat PLA and for PLA composites with diatomaceous earth fraction <40 μm. The composite samples with the filler particle size fraction 63–40 μm revealed a subtle decrease in tensile strength. More pronounced differences were observed for elongation at rupture. The elongation of neat PLA samples remained basically the same, but for the composites containing 2.5% or 5% of the filler of grain size 40–63 μm, the values of this parameter increased to about 3.5 and 3.0, respectively, so the increase reached 20% to 40%. For all samples, high values of standard deviation were obtained, which is characteristic of the samples printed by FDM.

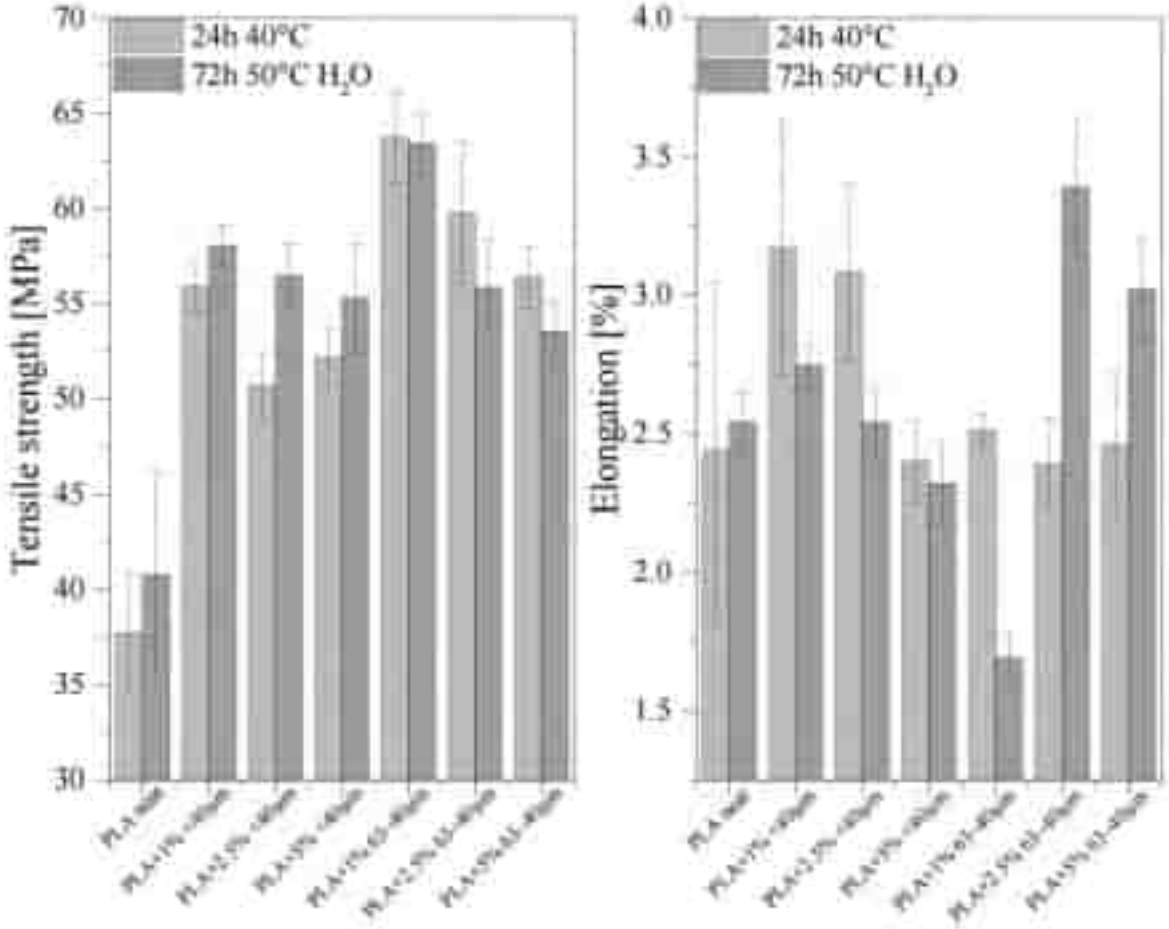

Figure 9. Results of tensile tests.

The elasticity modulus in bending and bending strength of the samples were measured by the three-point bending flexural test at the rate of 2 mm/min, (Figure 10). The samples of composites showed higher elasticity modulus in bending and higher flexural strength than neat PLA.

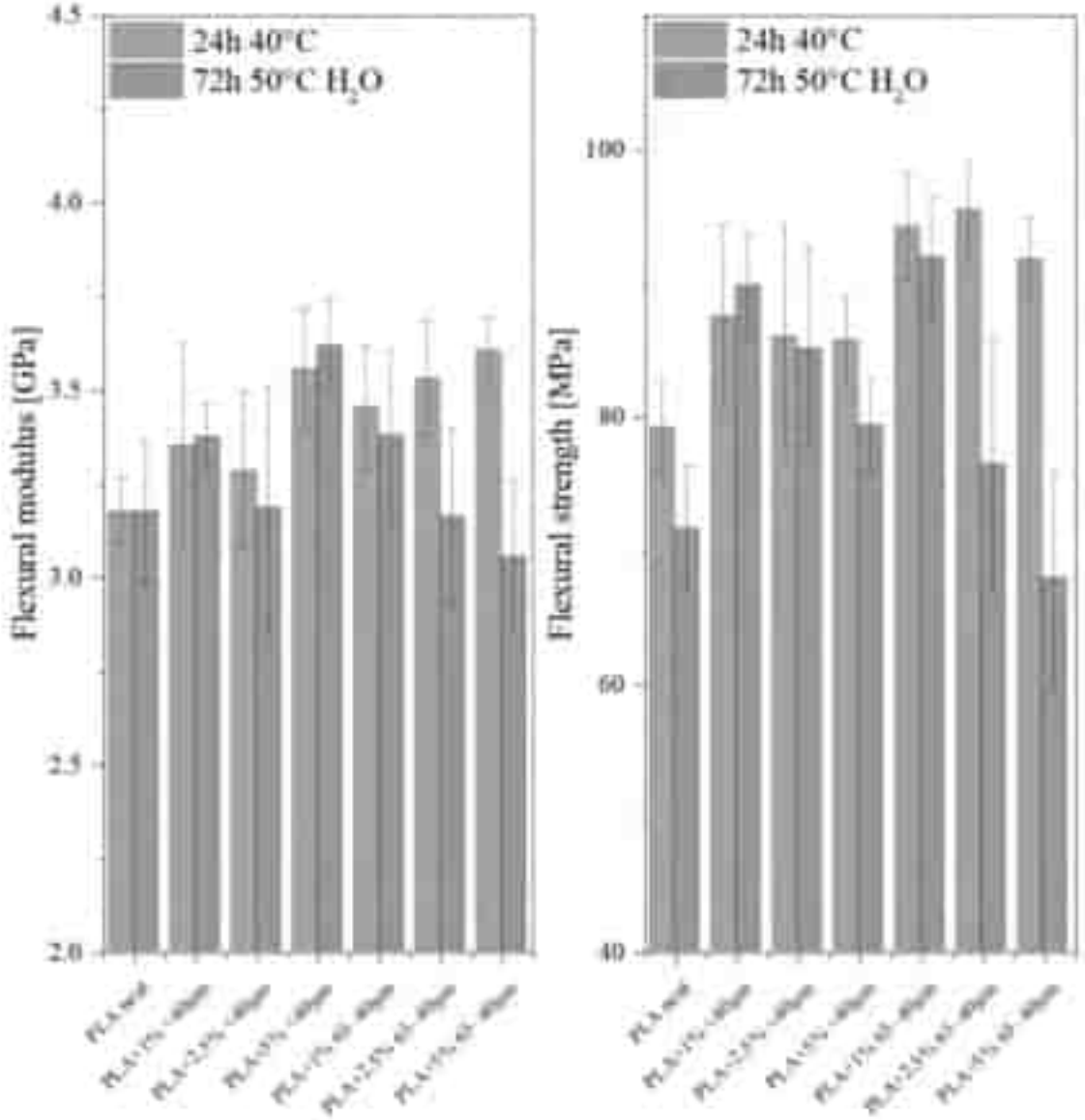

Figure 10. Results of bending tests.

The value of elasticity modulus significantly depends on the content of the filler in the composites; it increases with increasing filler concentration. The addition of diatomaceous earth also increases the flexural strength of the samples, which is more pronounced for the samples containing the particle size fraction 40–63 µm, but the differences between the concentrations are within the standard deviation. After the studies of water absorbability, the mechanical strength parameters decreased for the majority of samples. While water absorption by the composite does not induce changes in the final mass of the samples appreciably (Figure 7), it modifies the structure of the samples and thus affects their mechanical properties. The considerable deterioration of mechanical strength parameters is explained by a decrease in the average molecular mass and degree of crystallinity caused by the polymer hydrolysis. The loss of mechanical properties correlated with the increasing loadings of the fillers, especially visible for 63–40 µm fraction, may be due to hydrophilic properties of the diatomite component, increasing water penetration through the sample.

3.7.2. Impact Strength and Hardness

The impact strength of neat PLA varies in the range 13.3 ± 4.4 kJ/m^2 (Table 5). For all samples of the composites, the values of Kc are higher and vary in the range 18.5–21.8 kJ/m^2. The hardness of the composites in the Shore D scale takes values from the range 79–83°, while the PLA hardness is close to 83, which is consistent with the literature data. After the exposition of the samples to water at 50 °C, the hardness of all the samples decreased slightly, which can be linked to the hydrolytic depolymerization of PLA. After treatment with water at 50 °C, the impact strength of neat PLA and PLA +1% diatomite <40 µm significantly decreased, by 83% and 65%, respectively, which was attributed to the degradation of PLA in water. For the other samples, the impact strength increased by from 4% to 20%. With increasing content of the filler, the effect of diatomite in the mechanical properties of the composite begins to dominate the influence of PLA degradation in water; moreover, the interaction between PLA and the filler increases. Thus, the samples of composites are more resilient and less brittle.

Table 5. Impact test results and shore hardness.

	Impact Strength [kJ/m^2] (24 h, 40 °C)	Impact Strength [kJ/m^2] (72 h, 50 °C, H_2O)	Hardness Shore D [°] (24 h, 40°C)	Hardness Shore D [°] (72 h, 50 °C, H_2O)
Neat PLA	13.35 ± 4.42	2.22 ± 0.52	82 ± 2	77 ± 3
PLA + 1% diatomite < 40 µm	20.90 ± 4.39	7.37 ± 2.14	81 ± 1	79 ± 1
PLA + 2.5% diatomite < 40 µm	20.52 ± 3.78	24.59 ± 4.14	80 ± 1	78 ± 2
PLA + 5% diatomite < 40 µm	18.51 ± 3.47	18.3 ± 6.97	83 ± 2	79 ± 1
PLA + 1% diatomite 63–40 µm	21.81 ± 4.42	27.19 ± 2.64	81 ± 3	75 ± 2
PLA + 2.5% diatomite 63–40 µm	20.24 ± 5.10	21.66 ± 4.60	80 ± 1	78 ± 1
PLA + 5% diatomite 63–40 µm	20.54 ± 3.14	25.11 ± 1.38	79 ± 1	77 ± 1

3.8. Rheology

The melt flow index (MFR) of pure PLA at 190 °C is 6.705 g/10 min (Figure 11). For the PLA compositions with diatomaceous earth of grain size <40 µm the MFR value increased with increasing concentrations of the filler. The composite samples containing the filler fraction of 63–40 µm are characterized by smaller MFR value, although still MFR increases with increasing filler concentration. A higher MFR means that a given material can be easier processed and used for different applications. For the composites with the filler fraction of 63–40 µm, this parameter takes lower values as larger grains may cause greater turbulences in the polymer stream so the friction increases and MFR decreases.

A capillary rheometer was used to determine the relation between shear rate and viscosity (Figure 12). At the lowest shear rate, the viscosities of all compositions are greater than that of pure PLA, as a consequence of the presence of the filler. The highest increase in viscosity was noted for the sample containing 5% of the filler. With an increasing shear rate, the values of viscosity decrease, which is known as the shear thinning. Some of the samples, mainly containing 63–40 µm diatomite fraction and also 5% of 40 µm fraction, revealed an increase in viscosity near the shear rate of 50 1/s, attributed to the onset of composition turbulent flow.

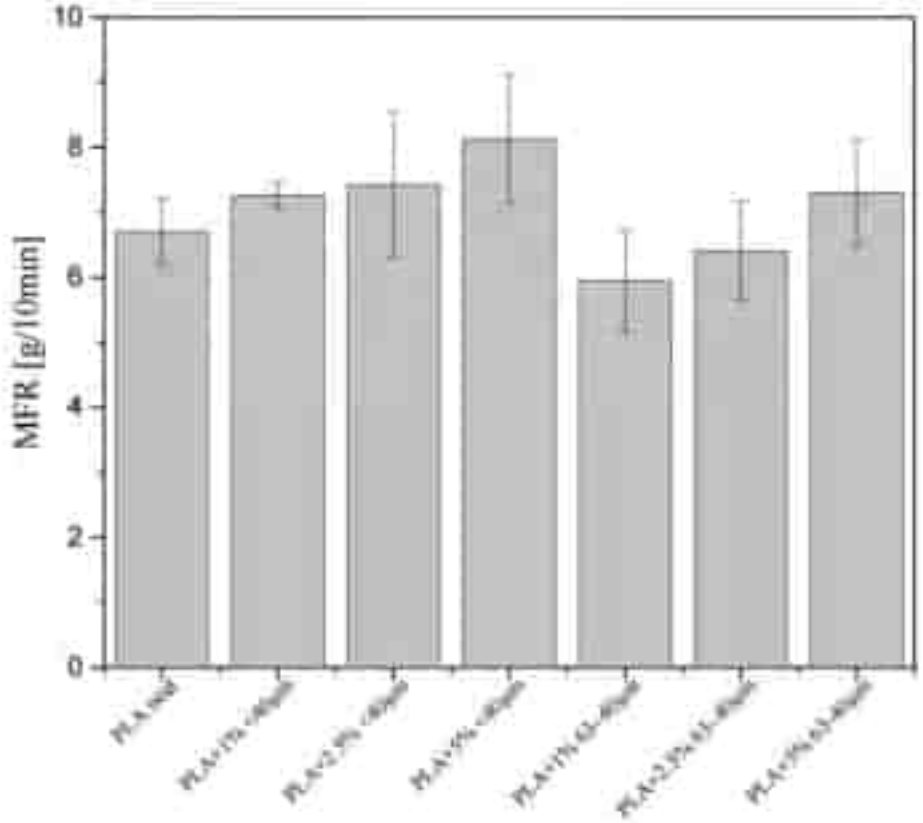

Figure 11. Results of flow coefficient measurements (tests carried out at 190 °C).

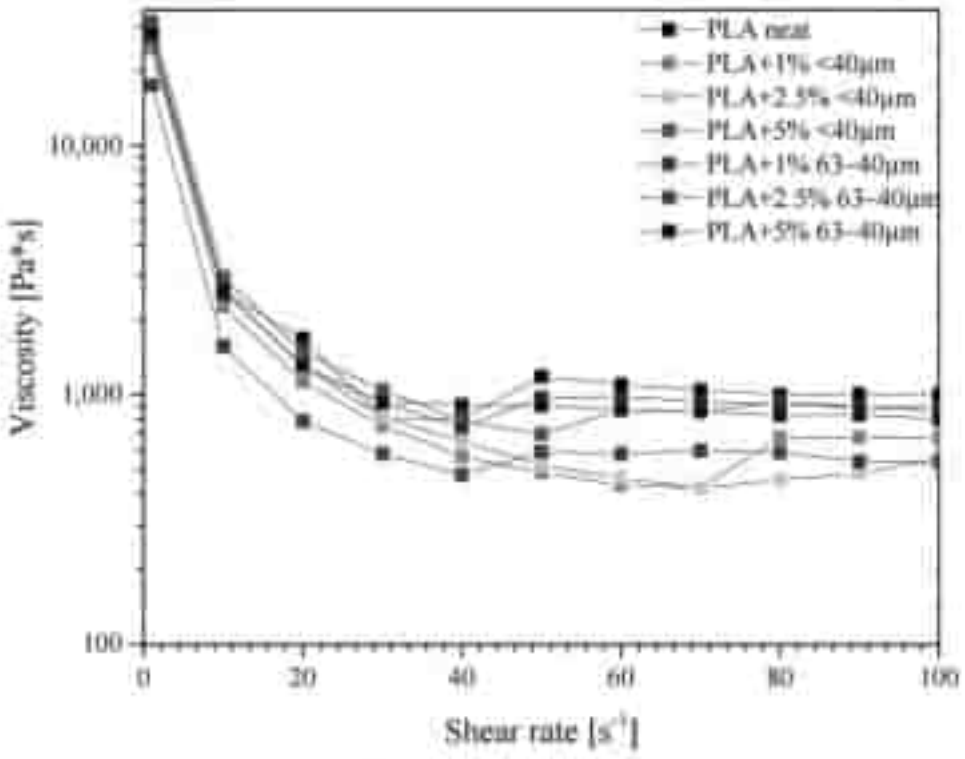

Figure 12. Viscosity measurement results.

3.9. Density Measurements

Densities of all samples were measured by the hydrostatic method and the results are given in Figure 13. Measurements were performed for the samples of 1 cm in length. The lowest value of density was found for neat PLA (~1.24 g/cm^3). For the composites, with an increasing concentration of the filler, the density slightly increased up to 2.5% of the filler loading and at 5% loading, the density was abruptly reduced.

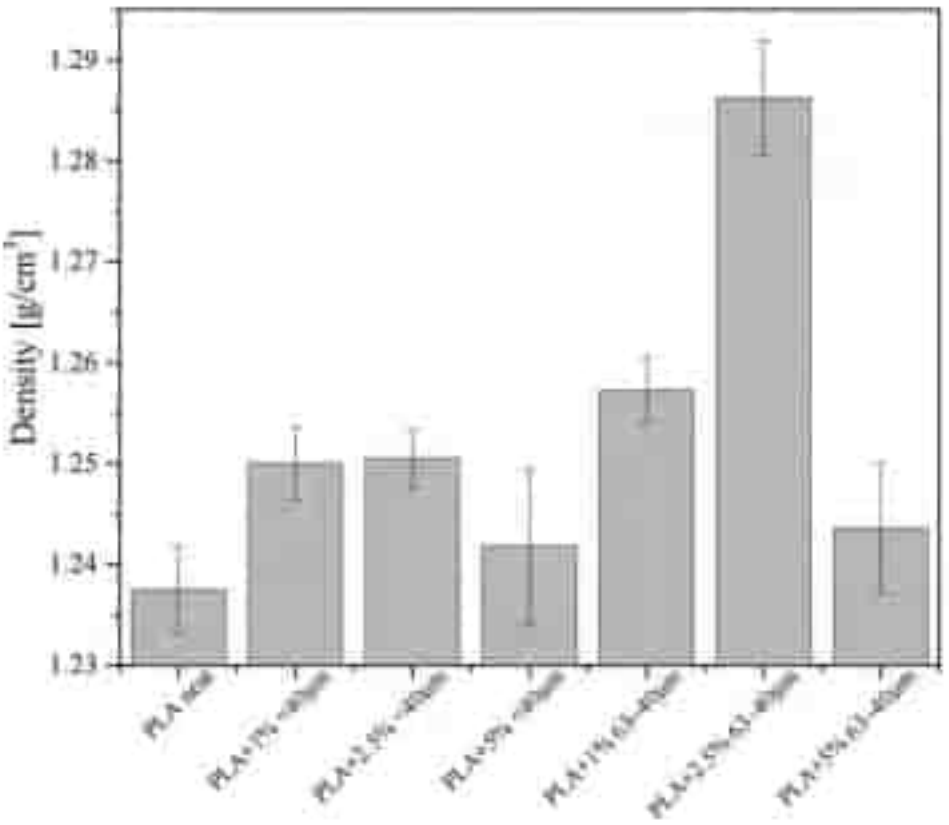

Figure 13. Densities of the extruded samples.

The greatest density was obtained for the sample containing 2.5% of the 63–40 μm fraction. The experimentally determined neat PLA density is in agreement with the literature value [53]. In parallel, densities of the samples printed out for bending tests were measured and the results are given in Figure 14. Their densities were calculated on the basis of measurements of their thicknesses, lengths, widths and masses. The samples studied were printed out on a 3D printer with 100% infill ratio. The samples of composites were found to have much higher density than that of pure PLA, which means that even a small addition of diatomite results in denser packing of the composition during printing and that the theoretical 100% infill ratio is not actually the most effective material packing to obtain. Irrespective of the mesh fraction of the filler, the sample containing 5% of the filler showed the highest density. These samples caused considerable problems during printing, e.g., blocking of the extruder, detaching of the sample from the printer table, in particular the samples containing the filler fraction of 63–40 μm.

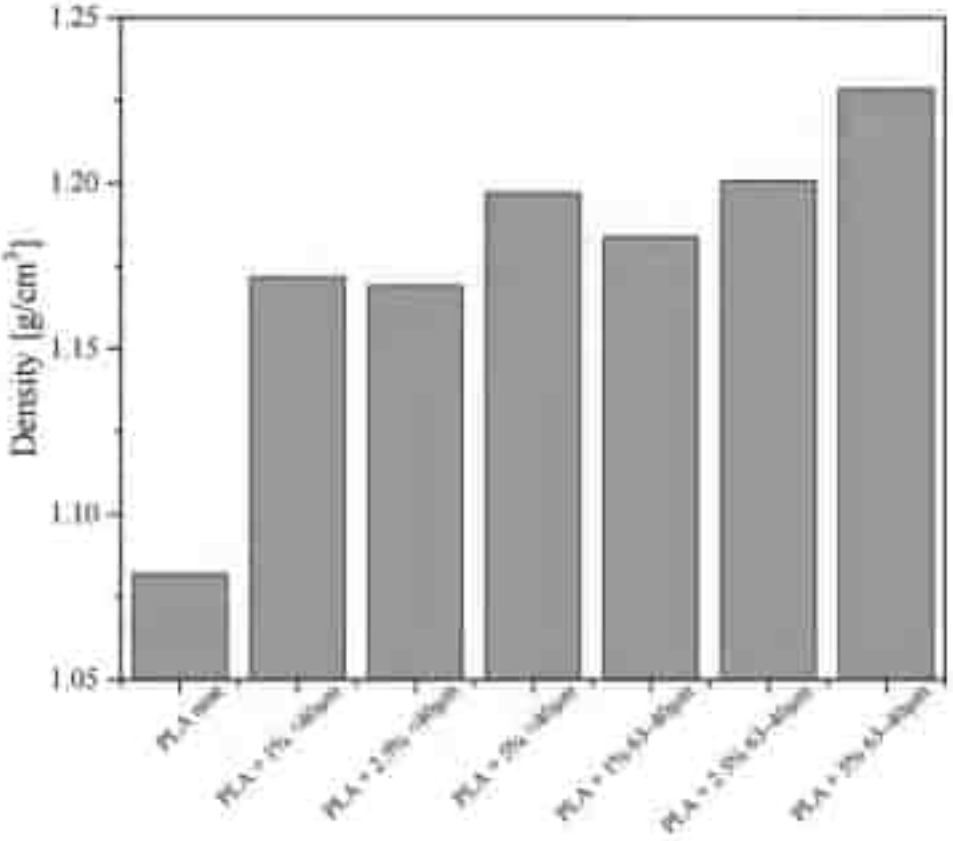

Figure 14. Densities of the 3D-printed samples for bending tests.

4. Conclusions

The composites obtained by the modification of polylactide (PLA) with diatomaceous earth were characterized by higher thermal stability and a greater degree of hydrophobicity than neat PLA. Moreover, the composites were observed to show a higher WCA after treatment with water and its reduced absorbability (small mass change) than neat PLA. As to the mechanical strength parameters, the measurements for the composites revealed an increase in tensile strength and an improved elongation at rupture in some cases. Additionally, the samples were characterized by improved flexural durability. Modification of polylactide with diatomaceous earth results in increasing the melt flow in proportion to the concentration of the modifier. The use of different mesh fractions of the filler is reflected in different mechanical and rheological parameters of the composites, as well as in the density of the filaments. The composites obtained with the diatomite mesh fraction <40 µm show higher hydrophobicity, and after conditioning in water, higher melt flow index and higher values of most mechanical strength parameters. However, those obtained with the diatomite mesh fraction of 63–40 µm show greater thermal stability, greater tensile strength and the filaments made of such composites show greater densities.

The obtained composite filaments may be viewed as an attractive alternative to the ones currently available commercially for 3D printing and made from neat PLA, offering improved mechanical properties, a cut back on the PLA used for their manufacturing and being made solely from non-toxic, bio-friendly and biodegradable materials. The impact of the diatomite as a filler for PLA on its biodegradation kinetics and pathways will be the subject of further studies, as it is substantial from the perspective of an environmental sustainability-oriented development of new materials.

Author Contributions: Conceptualization, R.E.P. and K.J.K.; methodology, M.D., R.E.P., and B.S.; validation, M.D., and R.E.P.; formal analysis, M.D., B.S., D.B., I.Z., M.L., and R.D.; investigation, R.E.P. and M.D.; data curation,

M.D., and R.E.P.; writing—original draft preparation, R.E.P., M.D., B.S., and D.B.; writing—review and editing, M.D., R.E.P., B.S., I.Z., and K.J.K.; visualization, M.D., R.E.P., and B.S.; project administration, R.E.P.; funding acquisition, K.J.K. All authors have read and agreed to the published version of the manuscript.

Funding: This research was funded from the sources of Foundation for Polish Science, TEAM-NET program, POIR.04.04.00–00–1792/18 (BIOG-NET) grant.

Conflicts of Interest: The authors declare no conflict of interest.

References

1. Upcraft, S.; Fletcher, R. The rapid prototyping technologies. *Assem. Autom.* **2003**, 23, 318–330. [CrossRef]
2. Gibson, I.; Rosen, D.W.; Stucker, B. *Additive Manufacturing Technologies Rapid Prototyping to Direct Digital Manufacturing*; Springer: Boston, MA, USA, 2010.
3. Molitch-Hou, M. The First 3 D Printed Polymer Implant to Receive FDA Approval. 2013. Available online: https://3dprintingindustry.com/news/the-first-3d-printed-polymer-implant-to-receive-fda-approval-5821/ (accessed on 12 August 2020).
4. Kellner, T. Jet Engines with 3 D-Printed Parts Power Next-Gen Airbus Passenger Jet. 2015. Available online: https://trprojects.lanews.com/reports/post/119709422770/jet-engines-with-3d-printed-parts-power-next-gen/ (accessed on 12 August 2020).
5. Palumbo, J. Inside the Race to Perfect the 3 D-Printed Home. Available online: https://www.artsy.net/article/artsy-editorial-inside-race-perfect-3d-printed (accessed on 12 August 2020).
6. Vuković-Kwiatkowska, I.; Kaczmarek, H. Innowacyjne kompozyty poli(kwasu mlekowego)) do produkcji folii opakowaniowych. *Chemik* **2014**, 68, 135–140. (In Polish)
7. Vert, M.; Chen, J.; Hellwich, K.-H.; Hodge, P.; Nakano, T.; Scholz, C.; Slomkowski, S.; Vohlidal, J. Nomenclature and terminology for linear lactic acid-based polymers (IUPAC Recommendations 2019). *Pure Appl. Chem.* **2020**, 92, 193–211. [CrossRef]
8. Żenkiewicz, M.; Richert, J. Synteza, właściwości i zastosowania polilaktydu. *Przetwórstwo Tworzyw* **2009**, 5, 192–199. (In Polish)
9. Bates-Green, K.; Howie, T. Technical Education in Additive Manufacturing & Materials TEAMM. Available online: http://www.teamm.org/ (accessed on 12 August 2020).
10. Leuschel, M.; Llorens, M.; Oliver, J.; Silva, J.; Tamarit, S. SOC. In Proceedings of the 2009 ACM SIGPLAN Workshop on ML—ML '09, Savannah, GA, USA, 19–20 January 2008; ACM: New York, NY, USA, 2018; Volume 76, pp. 92–98. [CrossRef]
11. Wang, Y.; Cai, J.; Jiang, Y.; Jiang, X.; Zhang, D. Preparation of biosilica structures from frustules of diatoms and their applications: Current state and perspectives. *Appl. Microbiol. Biotechnol.* **2012**, 97, 453–460. [CrossRef] [PubMed]
12. Ruggiero, I.; Terracciano, M.; Martucci, N.M.; De Stefano, L.; Migliaccio, N.; Tatè, R.; Rendina, I.; Arcari, P.; Lamberti, A.; Rea, I. Diatomite silica nanoparticles for drug delivery. *Nanoscale Res. Lett.* **2014**, 9, 329. [CrossRef]
13. Wang, X.; Zheng, B.; Liu, L.; Li, L. Use of Diatoms in River Health Assessment. *Annu. Res. Rev. Biol.* **2014**, 4, 4054–4074. [CrossRef]
14. Kieu, K.; Li, C.; Fang, Y.; Cohoon, G.; Herrera, O.D.; Hildebrand, M.; Sandhage, K.H.; Norwood, R.A. Structure-based optical filtering by the silica microshell of the centric marine diatom Coscinodiscus wailesii. *Opt. Express* **2014**, 22, 15992–15999. [CrossRef]
15. Rakowska, B. Okrzemki—organizmy, które odniosły sukces. *Kosmos Problemy Nauk Biologicznych* **2003**, 52, 307–314.
16. Aggarwal, S.; Johnson, S.; Saloni, D.; Hakovirta, M. Novel 3D printing filament composite using diatomaceous earth and polylactic acid for materials properties and cost improvement. *Compos. B Eng.* **2019**, 177, 107310. [CrossRef]
17. Seckbach, J.; Gordon, R. *Diatoms: Fundamentals and Applications*; Scrivener Publishing LLC: Beverly, MA, USA, 2019.
18. Goldberg, S.; Lebron, I.; Suarez, D.L.; Hinedi, Z.R. Surface Characterization of Amorphous Aluminum Oxides. *Soil Sci. Soc. Am. J.* **2001**, 65, 78–86. [CrossRef]
19. Hans, E.; Johansson Bo, V. Larsson, Silica Sols Having High Surface Area. U.S. Patent 5368833 A, 29 November 1990.

20. Dry, M.; Du Plessis, J.; Leuteritz, G. The influence of structural promoters on the surface properties of reduced magnetite catalysts. *J. Catal.* **1966**, *6*, 194–199. [CrossRef]
21. Legodi, M.; DeWaal, D. The preparation of magnetite, goethite, hematite and maghemite of pigment quality from mill scale iron waste. *Dye. Pigment.* **2007**, *74*, 161–168. [CrossRef]
22. Li, J.; Deng, H.; Michalatos, P. TransVision. *ACM SIGGRAPH 2019 Art Gallery* **2019**, *2780*, 2759. [CrossRef]
23. Rothon, R.N. Mineral Fillers in Thermoplastics: Filler Manufacture and Characterisation. In *Advances in Polymer Science*; Springer Science and Business Media LLC: Berlin/Heidelberg, Germany, 2007; Volume 139, pp. 67–107.
24. Li, J.P.H.; Adesina, A.; Kennedy, E.; Stockenhuber, M. A mechanistic study of the Knoevenagel condensation reaction: New insights into the influence of acid and base properties of mixed metal oxide catalysts on the catalytic activity. *Phys. Chem. Chem. Phys.* **2017**, *19*, 26630–26644. [CrossRef]
25. Ibrahim, S.S.; Selim, A.Q. Heat treatment of natural diatomite. *Physicochem. Probl. Miner. Process.* **2012**, *48*, 413–424.
26. Miandad, R.; Rehan, M.; Barakat, M.A.; Aburiazaiza, A.S.; Khan, H.; Ismail, I.M.I.; Dhavamani, J.; Gardy, J.; Hassanpour, A.; Nizami, A.-S. Catalytic Pyrolysis of Plastic Waste: Moving Toward Pyrolysis Based Biorefineries. *Front. Energy Res.* **2019**, *7*. [CrossRef]
27. Brzakalski, D.; Przekop, R.E.; Dobrosielska, M.; Sztorch, B.; Marciniak, P.; Marciniec, B. Highly bulky spherosilicates as functional additives for polyethylene processing—Influence on mechanical and thermal properties. *Polym. Compos.* **2020**, *41*, 3389–3402. [CrossRef]
28. Hesami, M.; Jalali-Arani, A. Cold crystallization behavior of poly(lactic acid) in its blend with acrylic rubber; the effect of acrylic rubber content. *Polym. Int.* **2017**, *66*, 1564–1571. [CrossRef]
29. Gonzalez, L.; Aguero, A.; Quiles-Carrillo, L.; Lascano Almacana, D.S.; Montanes, N. Optimalization of the Loading of an Environmentally Friendly Copatibilizer Derived from Linseed Oil in Pol(Lactic Acid)/Diatomaceous Earth Composites. *Materials* **2019**, *12*, 1627. [CrossRef]
30. Puchalski, M.; Kowalek, S.; Szparaga, G.; Chrzanowski, M.; Krucińska, I. Investigation of the Influence of PLA Molecular Structure on the Crystalline Forms (α' and α) and Mechanical Properties of Wet Spinning Fibres. *Polymers* **2017**, *9*, 18. [CrossRef] [PubMed]
31. Ranakoti, R.; Javadpour, S.; Delfanian, F.; Leicher, T. Failure Analysis and Mechanical Characterization of 3D Printed ABS with Respect to Layer Thickness and Orientation. *J. Fail. Anal. Prev.* **2016**, *16*, 467–481. [CrossRef]
32. Tymrak, B.M.; Kreiger, M.; Pearce, J.M. Mechanical properties of components fabricated with open-source 3-D printers under realistic environmental conditions. *Mater. Des.* **2014**, *58*, 242–246. [CrossRef]
33. Tarrazo-Serrano, D.; Castiñeira-Ibáñez, S.; Sánchez-Aparisi, E.; Uris, A.; Rubio, C. MRI Compatible Planar Material Acoustic Lenses. *Appl. Sci.* **2018**, *8*, 2634. [CrossRef]

Publisher's Note: MDPI stays neutral with regard to jurisdictional claims in published maps and institutional affiliations.

© 2020 by the authors. Licensee MDPI, Basel, Switzerland. This article is an open access article distributed under the terms and conditions of the Creative Commons Attribution (CC BY) license (http://creativecommons.org/licenses/by/4.0/).

H2

A New Method of Diatomaceous Earth Fractionation—A Bio-Raw Material Source for Epoxy-Based Composites

Dobrosielska M., Dobrucka R., Gloc M., Brząkalski D., Szymański M., Kurzydłowski K.J., Przekop R.E.; Materials, 14, 1663, 2021

materials

MDPI

Article

A New Method of Diatomaceous Earth Fractionation—A Bio-Raw Material Source for Epoxy-Based Composites

Marta Dobrosielska [1], Renata Dobrucka [1,2,*], Michał Głuc [1], Dariusz Brząkalski [3], Marcin Szymański [4], Krzysztof J. Kurzydłowski [1] and Robert E. Przekop [4,*]

[1] Faculty of Materials Science and Engineering, Warsaw University of Technology, ul. Wołoska 141, 02-507 Warsaw, Poland; Marta.Dobrosielska@pw.edu.pl (M.D.); michal.gluc@pw.edu.pl (M.G.); krzysztof.kurzydlowski@pw.edu.pl (K.J.K.)

[2] Department of Non-Food Products Quality and Packaging Development, Institute of Quality Science, Poznań University of Economics and Business, al. Niepodległości 10, 61-875 Poznań, Poland

[3] Faculty of Chemistry, Adam Mickiewicz University in Poznań, ul Uniwersytetu Poznańskiego, 61-614 Poznań, Poland; d.brzakalski@gmail.com

[4] Centre for Advanced Technologies, Adam Mickiewicz University in Poznań, ul. Uniwersytetu Poznańskiego 10, 61-614 Poznań, Poland; marcin.szymanski@amu.edu.pl

* Correspondence: Renata.Dobrucka@pw.edu.pl or renata.dobrucka@ue.poznan.pl (R.D.); rprzekop@gmail.com (R.E.P.)

Abstract: The authors of this paper use an original method of diatomaceous earth fractionation, which allows for obtaining a filler with a specific particle size distribution. The method makes it possible to separate small, disintegrated and broken diatom frustules from those which maintained their original form in diatomaceous earth. The study covers a range of tests conducted to prove that such a separated diatomic fraction (5–30 µm) shows features different from the base diatomite (from 1 to above 40 µm) used as an epoxy resin filler. We have examined the mechanical properties of a series of diatomite/resin composites, considering the weight fraction of diatoms and the parameters of the composite production process. The studied composites of Epidian 603 epoxy resin cross-linked with amine-based curing agent Z-1 contained 0 to 70% wt. of diatoms or diatomaceous earth. Samples were produced by being casted into silicone molds in vacuum degassing conditions and, alternatively, without degassing. The results have shown that the size and morphology of the filler based on diatomaceous earth affects mechanical and rheological properties of systems based on epoxy resin. Elongation at rupture and flexural stress at rupture were both raised by up to 35%, and impact strength by up to 25%.

Keywords: diatomite; bio-composites; mechanical properties; fractionation; purification of diatomaceous earth; bio-raw materials

check for updates

Citation: Dobrosielska, M.; Dobrucka, R.; Głuc, M.; Brząkalski, D.; Szymański, M.; Kurzydłowski, K.J.; Przekop, R.E. A New Method of Diatomaceous Earth Fractionation—A Bio-Raw Material Source for Epoxy-Based Composites. *Materials* **2021**, *14*, 1663. https://doi.org/10.3390/ma14071663

Academic Editor: Dibyan Gupta

Received: 9 March 2021
Accepted: 25 March 2021
Published: 30 March 2021

Publisher's Note: MDPI stays neutral with regard to jurisdictional claims in published maps and institutional affiliations.

Copyright: © 2021 by the authors. Licensee MDPI, Basel, Switzerland. This article is an open access article distributed under the terms and conditions of the Creative Commons Attribution (CC BY) license (https://creativecommons.org/licenses/by/4.0/).

1. Introduction

The engineering of new polymer-based composites with a reduced fraction of petroleum-based material matrix is one of the trends in designing novel products containing natural raw materials. Due to their functional properties such as adhesion, flame resistance or chemical and thermal stability, epoxy resins are used in various sectors of industry. Despite having many benefits, they are fragile and have a low impact and crack propagation resistance, which considerably limits their scope of use. The curing of epoxy resins is accompanied by a very low shrink, so a cured epoxy resin precisely represents the shape and dimensions of the mold. This creates great possibilities to produce elements of different shapes [1]. However, it is still necessary to increase the toughness and strength of such a material in order to satisfy the increasing demands of specific applications [2]. This is despite the significant improvement of the already excellent resins by using them for modification and as composite matrices [3,4]. Fillers, having a high surface area/volume ratio, are generally expected to show better mechanical properties. A high surface area is

usually associated with a small filler size and with extremely rough surfaces [5]. Diatoms as biogenic materials have a complex porous hierarchical structure, which makes them micrometric fillers with a highly developed specific surface. It is estimated that diatoms produce even up to 25% of organic matter in the ocean and approximately 25% of oxygen on the Earth [6]. Their cell wall is saturated with silica, which has a great potential as a raw material. The principal source of bio-silica is the so-called diatomaceous earth (diatomite). It is a mixture of diatom frustules with various sizes and morphologies, including significant amounts of damaged and broken structures being smaller than 2–3 µm.

The Earth's crust is composed of 93 elements, eight of which represent 99.5% of its weight. These eight most important elements are oxygen, silicone, aluminium, iron, calcium, potassium, and magnesium (Figure 1). We should point out that diatomaceous earth is, on the one hand, a representation of the most common elements existing in the Earth's crust, and on the other hand one of the most efficient sources of biogenic silica with a great potential for commercial use.

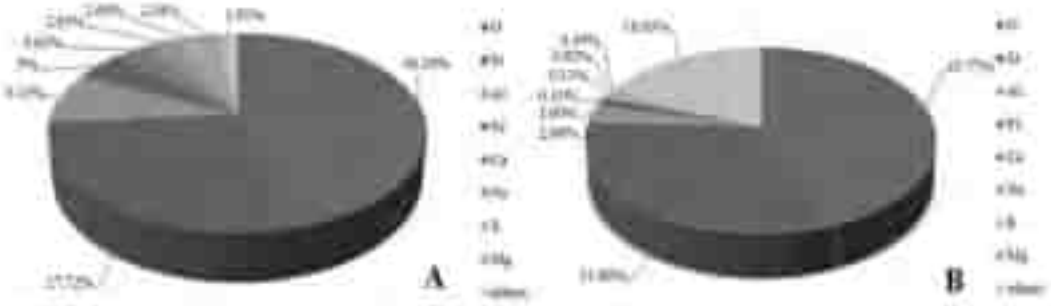

Figure 1. Elemental composition of Earth crust (**A**) and diatom frustule (**B**).

Diatomaceous earth contains 60–95% amorphous silica. Diatoms are one of the most spectacular examples of biologically derived nano-structured materials [7]. Each diatom frustule has species-specific, regularly arrayed features: pores, ridges and protuberance [8]. The skeleton of diatoms, known as the frustule or siliceous shell, is made of nano-size silica with a three-dimensional intricate framework [9]. The mechanical properties of individual diatom frustules vary with the location of measurement, which is attributed to the different stages of the bio-mineralization process [10]. The energy required to break the frustules and the area of fracture were further shown to be relatively high, as the cracks travelled for around 40 nm through silica particles of the diatom frustules [11].

Due to their peculiar characteristics, diatoms have been recently proposed to be employed in nanotechnology as natural fillers [12]. The variety of unique frustule architectures were attractive materials for optical, mechanical, and transport properties. Diatomaceous earth has been modified in different ways and, after treatments of different kinds, used in the construction of advanced devices for light harvesting, photonics, molecular separation, sensing, and drug delivery. Diatomaceous earth has also been used in photo-catalysis, the synthesis of zeolites, removal of dyes, wastewater treatment, cement production, filtration, nanotechnology, chromatography, and mostly as an adsorbent [13].

As mentioned above, diatomaceous earth contains diatom frustules of various sizes, a lot of fractions that are mechanically damaged, as well as agglomerates and colonies. In the literature, there are methods for purifying diatomaceous earth with the use of thermal and thermo-chemical treatments [14]. Sun et al. [15] cleaned diatomaceous earth using sodium hexametaphosphate as a dispersant combined with centrifugation. Other scientists [16] used cold and hot acidic solutions. Various methods of the purification and separation of diatomaceous earth before its final use are known. Hydraulic industrial separation methods are among the most efficient. These processes use cyclones or hydrocyclones to achieve high separation efficiency. However, their main purpose is to separate sand and other inclusions [17].

We have proposed and described a method of fractioning and purifying raw diatomaceous earth which allows for the generation of a fraction with a narrow size distribution of diatom frustules.

We prepared degassed and non-degassed composites based on epoxy resin, which contained a variable amount (0, 12, 24, 36, 48, 60, 70% vol.) of base and fractionated diatomite. The prepared systems were cast in silicone molds, cross-linked and then subjected to mechanical and functional property testing and imaging with the use of a scanning electron microscope. The tests allowed us to determine whether the methodology of composite production is appropriate from the perspective of the following variables: the degassing of the prepared systems, contents of the filler (% vol.) in the tested systems, and the method of preparing the applied modifier (fractionated and base diatomite).

2. Experimental Section

2.1. Materials

For the tests, we used epoxy resins produced by Zakłady Chemiczne Organika Sarzyna: Epidian 601 (Nowa Sarzyna, Poland) with an epoxide equivalent of 0.50–0.55 mol/100 g and a viscosity of 700–1100 [mPa·s], cured with triethylenetetramine (curing agent Z-1). Diatomaceous earth (Perma-Guard, Bountiful, UT, USA) was derived from diatomite deposits. It was provided in a powder form and used as received for "base diatomite" preparations and fractionated according to the procedure described further for "fractionated diatomite" preparations. It mostly contains the cells of Aulacoseira, a planktonic freshwater diatom. They have a perforated scutellum specific to that species (Figure 2). Diatoms have a mechanism that allows them to create colonies (chains). The mechanism ("zipper") is presented in Figure 3. The diversified size of diatoms is due to their life cycle. Along with cell division, diatoms shrink until they are no longer capable of dividing. They sexually multiply, as a result of which their cells reach their maximum size, which is followed by vegetative division where the cells start to shrink. For this reason, diatomaceous earth is a filler that features a high heterogeneity of particle size, which has already been mentioned (Figure 2), and a high structural heterogeneity (Figure 4) [6].

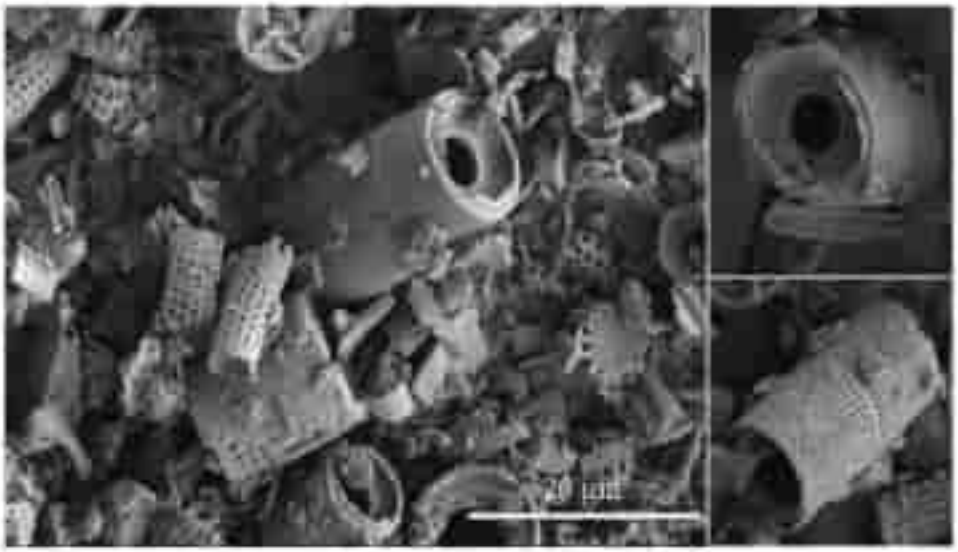

Figure 2. Base diatomaceous earth containing both fractured and non-fractured frustules, with a dominant content of Aulacoseira.

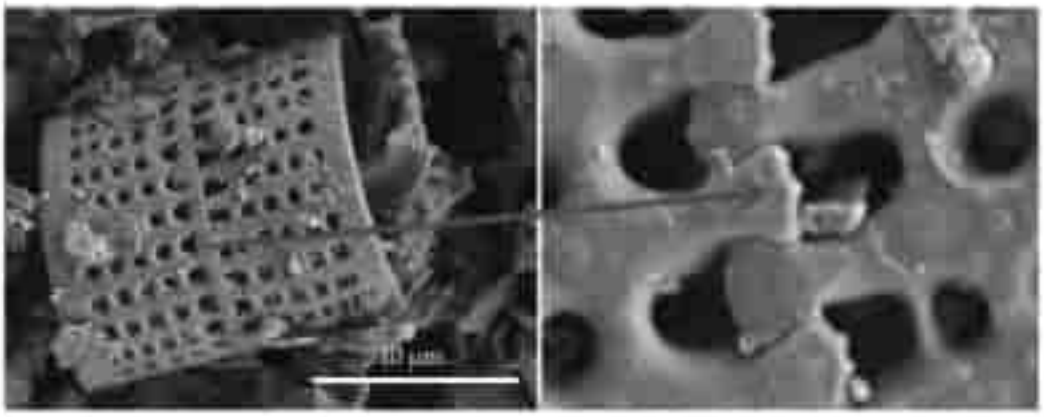

Figure 3. The "zipper" mechanism for counting colonies.

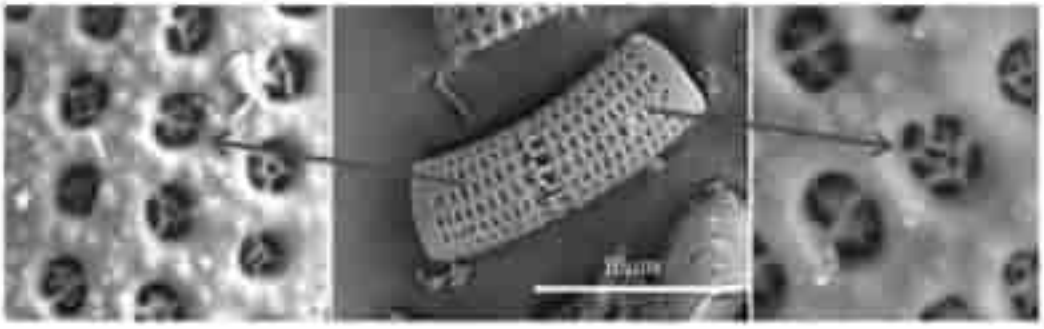

Figure 4. Pores present in the frustule wall.

2.2. Sample Preparation

Raw diatomaceous earth contains broken, mechanically damaged structures which differ by the geometry of their inner structure, shape, and size. For the purpose of this study, raw diatomite was mechanically mixed with water and fractionated with the use of sedimentation. The small, broken frustule pieces were partly removed, along with bigger agglomerates/colonies, by suspending the diatomite in water and subjecting the suspension to sedimentation. Based on interacting gravitational forces, particles of different sizes settled out at different ratios.

The fractionation was performed by placing 1 kg of diatomite in a 50 dm^3 tank, adding 40 dm^3 of demineralized water and mixing mechanically for 10 min, and leaving it for 3.5 h to cause sedimentation of the heavier precipitate fraction PRE1 (Figure 5). The next step was to pour off the suspension from above the precipitate to obtain suspension 1 (SUS1) and precipitate 1 (PRE1). SUS1 was mixed for 10 min with 40 dm^3 of water and then left for 24 h to obtain SUS2 and PRE2. SUS2 was left for 48 h for sedimentation to obtain PRE3 (which, once dried, was marked as tail fraction 0a) and SUS3 which was left for 168 h to obtain tail fraction 0b. The PRE2 was filled with 40 dm^3 of water, mixed for 10 min and left for 24 h to obtain SUS4 and PRE4 (which, once dried, was marked as tail fraction 1b). SUS4 was left for 24 h to obtain tail fraction 1a. The PRE1 was filled with 40 dm^3 of water, mixed for 10 min and left for two hours to obtain SUS5, which was left for 48 h to obtain tail fraction 2. The PRE5 was filled with 40 dm^3 of demineralized water, mixed for 10 min and left for 30 min to obtain PRE6 (fraction 4) and SUS6, which was left for 48 h to obtain fraction 3. The diatom precipitate (individual fractions) was dried with a thin layer at 80 °C to obtain a stable weight. The percentage share of each precipitate is shown in Figure 5. The total share of the fractions is 95.7%, which arises from the contents of extremely small fragments of bio-silica coming from the diatoms that did not sediment

in the process and were rejected along with the operating liquid. The morphology of diatoms in each fraction was characterized by scanning electron microscopy (SEM, Hitachi, Tokyo, Japan). On the basis of dynamic light scattering (DLS) (Figure 6) and SEM analyses (Figure 7), fraction 3 was chosen for further study, as explained in the "Discussion". The developed method allows for the purification of raw diatomaceous earth by removing smaller and broken fragments of diatom frustules and by de-agglomeration (Figure 6). Additionally, this method enables us to separate the fractions with bigger frustules (tail fraction 4) from those having a smaller geometric size (tail fraction 3); see Figure 6.

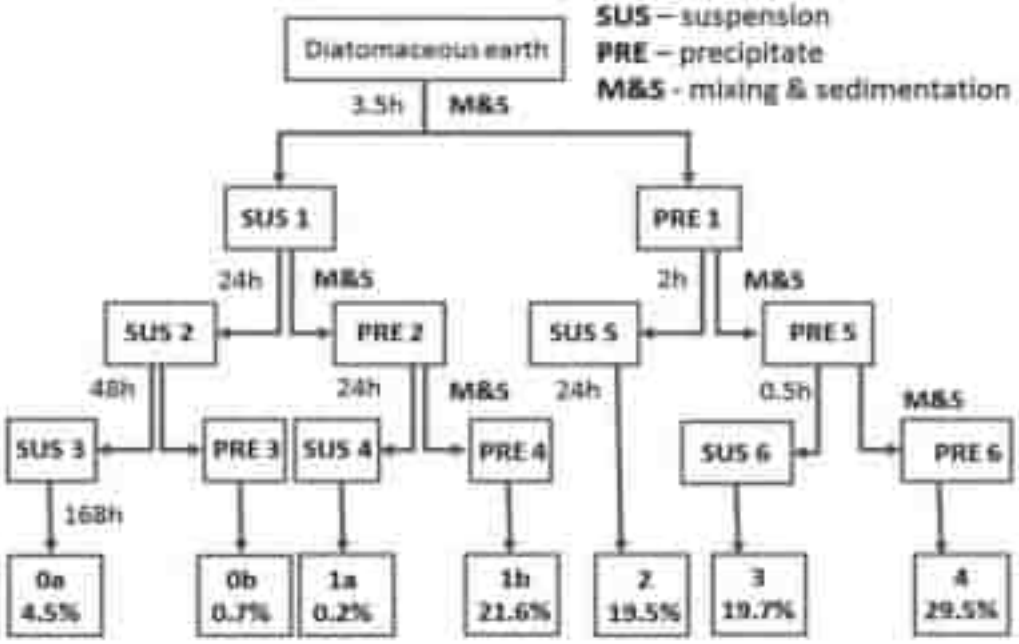

Figure 5. Fractionation of diatomaceous earth and the percentage share of each fraction of diatomaceous earth after fractionation.

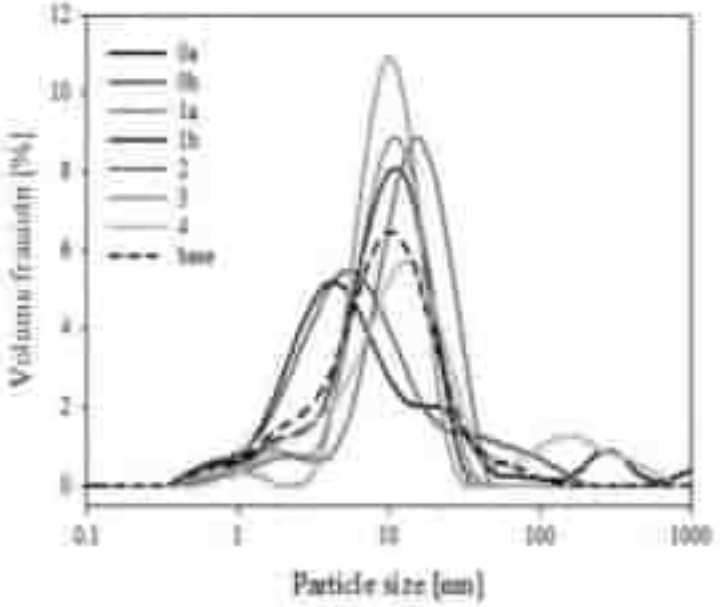

Figure 6. Separation of particles of fractionated diatomaceous earth by size.

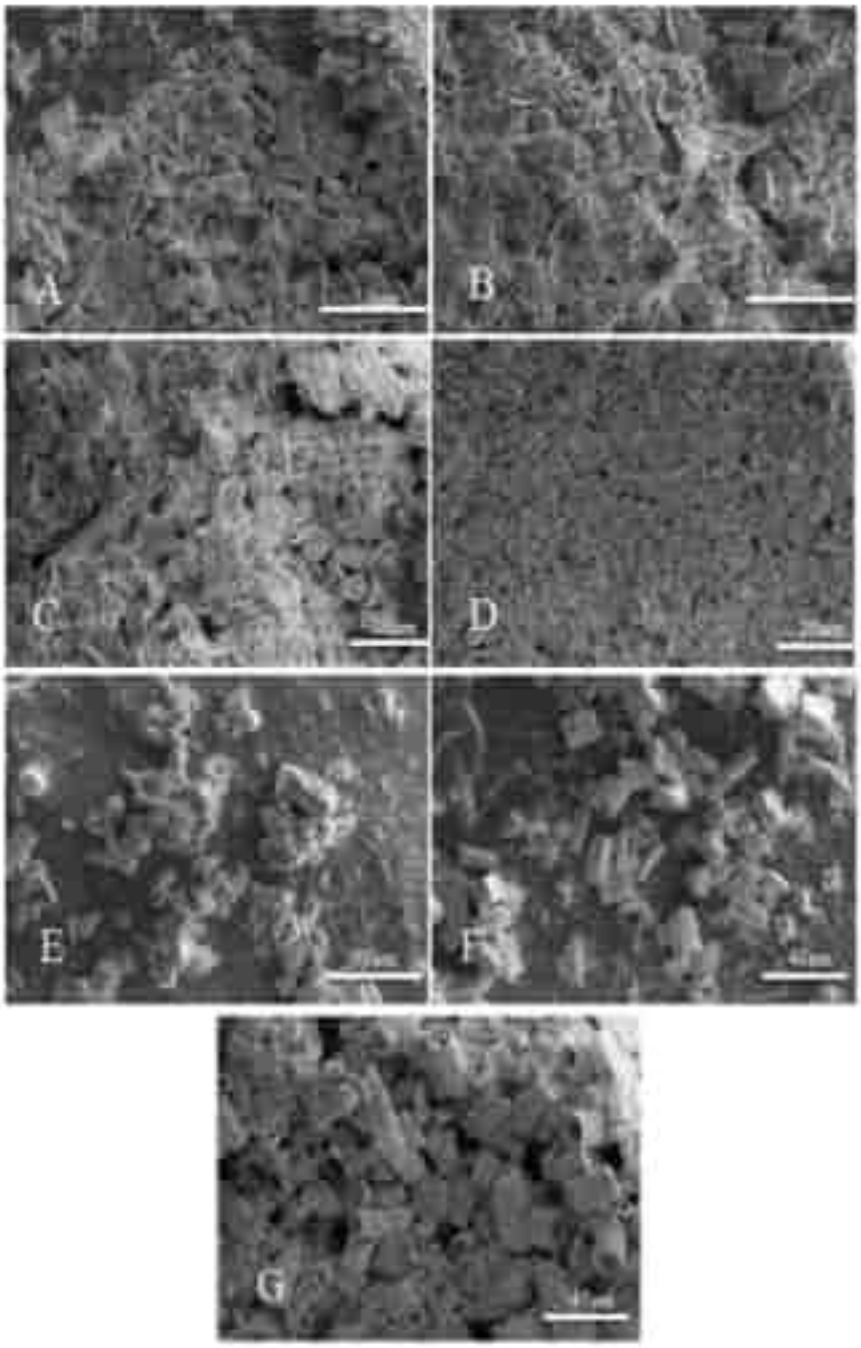

Figure 7. Microscopic images of fractionated diatomaceous earth (A) 1a, (B) 1b, (C) 1a, (D) 1b, (E) 2, (F) 3, (G) 4.

The studied composites of epoxy resin Epidian 601 (epoxy number (mol/100g) 0.5–0.55, viscosity at 25 °C (mPa·s) 800–1500), cross-linked with amine-based curing agent Z-1 (triethylenetetramine, viscosity at 25 °C (mPa·s) 20–30; amine number (mg KOH/g) min 1100), contained different quantities (0, 12, 24, 36, 48, 60, 70% vol.) of base and fractionated diatoms with an average particle size distribution of approx. 10 µm (Figure 8). The choice of the resin/hardener system was dictated, on the one hand, by the necessity to obtain a low viscosity of the mixture, and on the other hand, by the optimal time of its final gelation.

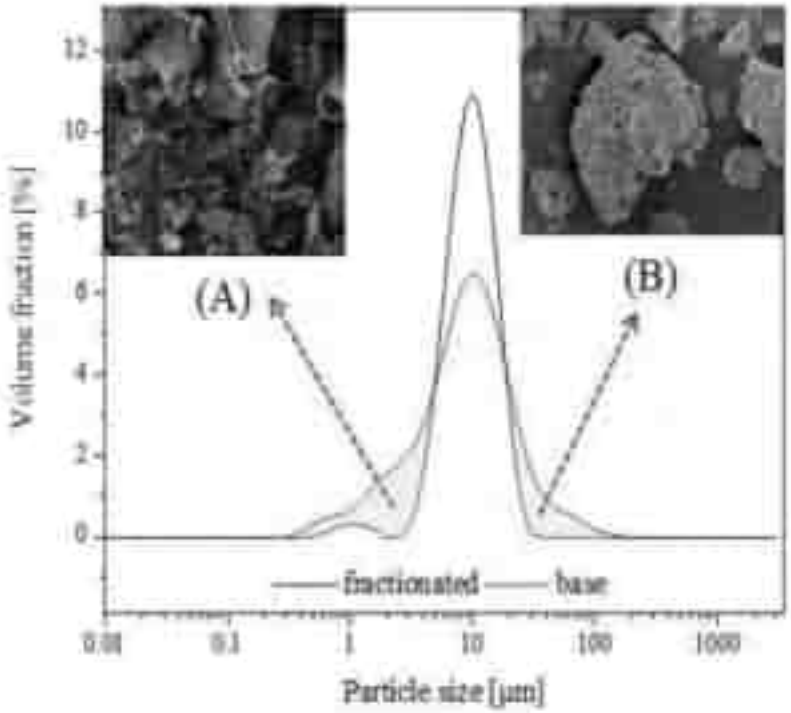

Figure 6. Particle size distribution for (A) base and (B) fractionated diatoms.

The epoxy resin with diatom frustules was mixed mechanically in plastic vessel, using steel propeller (600 rpm, 10 min). The samples were cast in silicone molds, as in work of Zolghadr et al. [16]. The test samples were prepared according to EN ISO 527 [19] and EN ISO 178 [20]. The tests were performed after three weeks of samples curing at 20 °C.

2.3. Characterization Methods

The size of the diatoms used to prepare the composites was measured with Mastersizer 3000 (Malvern Instruments Ltd., Malvern, UK). The measurements were made for the samples in water suspension (Hydro EV attachment). The parameters of measurements for wet samples were stirrer revolution speed: 2330 RPM, and ultrasound power: 70%. Fourier transform-infrared (FT-IR) spectra were recorded on a Nicolet i550 Fourier transform spectrophotometer (Thermo Fisher Scientific, Waltham, MA, USA) equipped with a diamond ATR unit with a resolution of 0.09 cm^{-1}. Spectra were collected in the 400–4000 cm^{-1} range, with 16 scans being collected for each spectrum. Contact angle analyses were performed by the sessile drop technique (5 µL) at room temperature and atmospheric pressure, with a Krüss DSA100 goniometer (KRÜSS GmbH, Hamburg, Germany). For flexural and tensile strength tests, the materials obtained were printed into type 1B dumbbell specimens in accordance with EN ISO 527-1:2012 and EN ISO 178:2010. Tests of the obtained specimens were performed on a universal testing machine INSTRON 5969 with a maximum load force of 50 kN (Instron, Norwood, MA, USA). The traverse speed for tensile strength measurements was set at 2 mm/min, and for flexural strength it was also set at 2 mm/min. A Charpy impact test (with no notch) was performed on an Instron Ceast 9050 impact machine according to ISO 179-1 [21] (Instron, Norwood, MA, USA). The density of the composites obtained was determined with the hydrostatic method using a Sartorius YCP04MS analytical balance at 20 °C with the use of distilled water (Sartorius, Göttingen, Germany). Thermogravimetry was performed using a NETZSCH 209 F1 Libra gravimetric analyzer (Netzsch Group, Selb, Germany). Samples of 5 ± 0.2 mg were cut from each composition and placed in Al_2O_3 crucibles. Measurements were conducted under nitrogen (flow of 20 mL/min) in the range of 30–1000 °C and a 10 °C/min heating

rate. The morphology and microstructure of the prepared composites were observed by scanning electron microscopy. Samples in the form of powders and molds were dusted with cupro-nickel using a GATAN duster. Observations were conducted with a Hitachi SU 8000 scanning microscope with an accelerating voltage of 5 kV to image the preparations (Hitachi, Ltd., Chiyoda, Tokyo, Japan). The imaging was performed in three SE modes. Viscosity tests were carried out with an MCRAnton Paar 302 rotational rheometer at a shear velocity range of 0.01–100 1/s, at room temperature (Anton Paar GmbH, Graz, Austria). A 1 mm measuring gap was used, and each measurement was performed three times.

3. Results and Discussion

3.1. Particle Size Measurements by Dynamic Light Scattering (DLS)

It can be seen that the base diatomaceous earth contained a wide spectrum of particles sized from ~0.5 µm up to over 100 µm (Figure 5). According to our previous research, for the species of diatoms used for this study, the particles smaller than 6 µm can be attributed to broken frustules (pieces thereof), while particles larger than approx. 40 µm are mostly agglomerates or colonies of frustules, as well as some single specimens of a bigger size [22]. It was observed that fraction 3 obtained by sedimentation of diatomaceous earth shows much narrower distribution of particle size, ranging from approx. 3 to 30 µm, with some additional fraction of broken frustule particles and dust particles (~1 µm) (Figure 6) which, due to small size, are always present in the sedimented material together with traces of residual suspension liquid. It appears that a large portion of broken frustule particles and agglomerates of high diameter was discarded (Figure 6). The results indicate that the proposed fractionation method allows for the obtainment of a raw material with a more uniform design and morphology, which thus provides specific properties of the finished product (Figure 8).

3.2. Density of Composites

Density is one of the most important physical properties of the composite material. Figures 9 and 10 show the determined density of composites with different contents (0, 12, 24, 36, 48, 60, 70% vol.) of base and fractionated diatoms, which have or have not been degassed. Density was determined based on the formula below:

$$d = V_{diatomite} \times d_{diatomite} + (1 - V_{diatomite}) \times d_{epoxy}$$

$V_{diatomite}$—volume fraction of diatomite;
$d_{diatomite}$—density of solid diatomite excluding porous structures (considered 2 g/cm^3);
d_{epoxy}—density of cured epoxy (measured to be 1.12 g/cm^3).

The bulk density of the base and fractionated diatoms is 0.271 g/cm^3 and 0.249 g/cm^3, respectively. For the degassed resin without diatoms, the average density was 1.131 g/cm^3, and for the non-degassed resin, 1.080 g/cm^3. For composites (both degassed and non-degassed) with base diatoms, we observed a slight growth in density (Figure 9). A higher density was observed for the composites containing fractionated diatoms, both degassed and non-degassed (Figure 10). A system containing 70% vol. of diatomaceous earth has a density of nearly 1.3 g/cm^3, which is almost 10% higher than in a system containing the same amount of base diatoms.

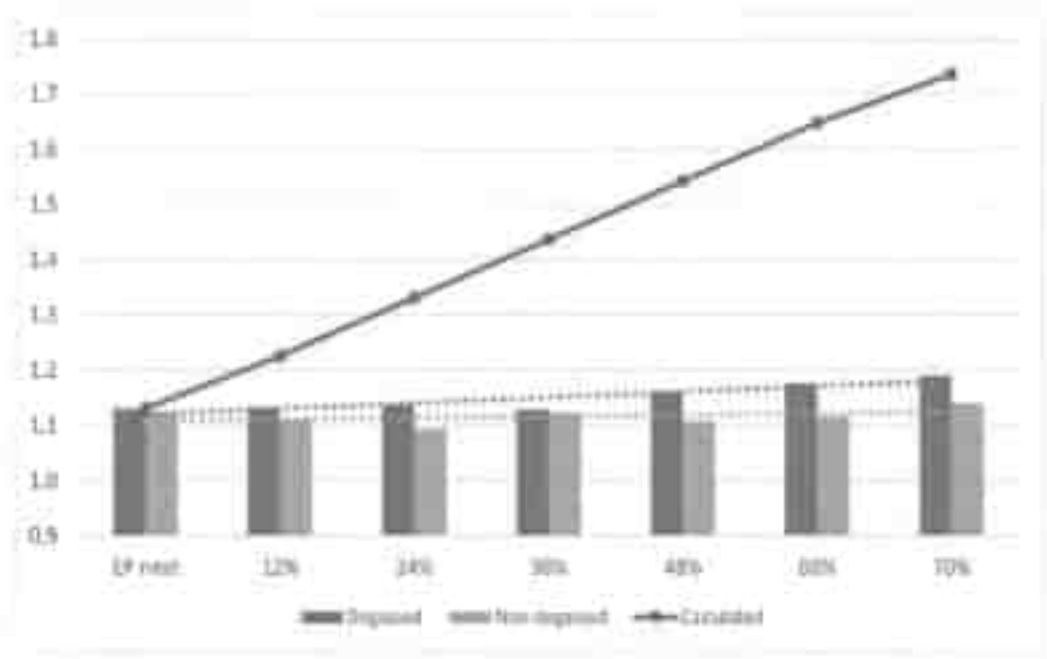

Figure 9. Density of degassed and non-degassed epoxy resin containing base diatomite earth.

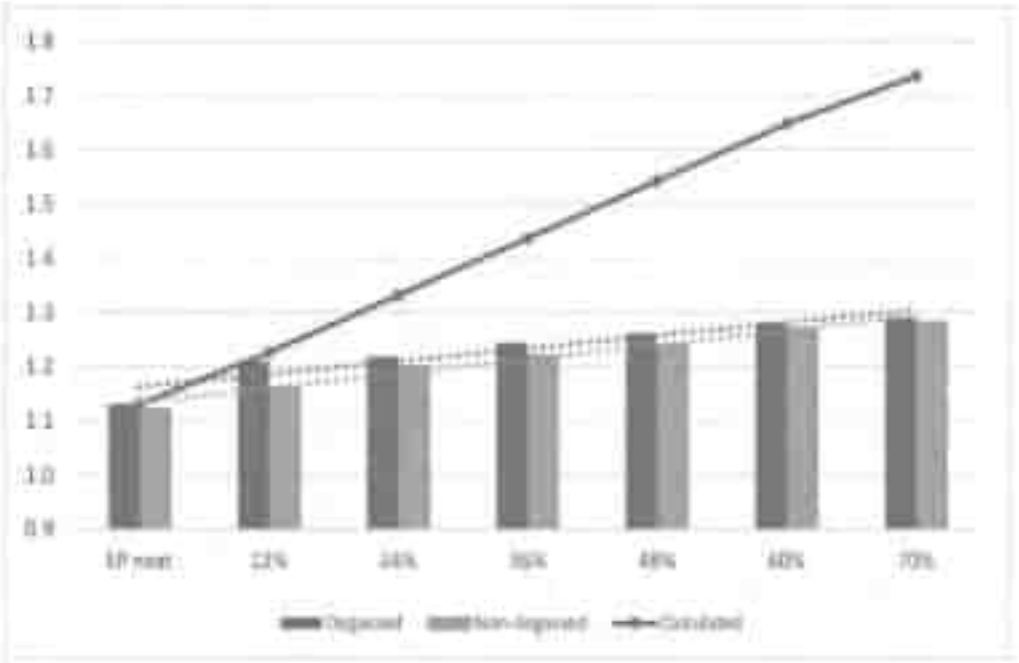

Figure 10. Density of degassed and non-degassed epoxy resin containing fractionated diatomite.

An increase in density up to 1.3 g/cm^3 was also observed by [7], who used centric type diatom frustules as filler in an epoxy resin (degassing was applied) with a weight percentage of 15%. It has been observed that an increasing number of supplied fractionated diatoms went along with a linear growth in the density of composites obtained. Deviation from the theoretical value calculated for fully degassed composites with frustules completely filled with epoxy (Figures 9 and 10) arises from the fact that resin does not fully penetrate into the diatom structure and the nanostructure of the diatom frustule. We can also observe silica substructures present in frustule holes (Figure 4). Due to viscosity,

despite the applied degassing process, the resin is not capable to penetrate into diatom frustules, since the holes are covered by the substructures. Diatomaceous earth is characterized by quite a low specific weight due to its highly porous structure, being much lower than that of neat epoxy resin, but its main component is nano- and microstructured silica, which itself is characterized by a density of ~2 g/cm^3. The frustules' density is defined as 1.4–2.2 g/cm^3 [23]. Therefore, along with a successful infusion of frustules with the epoxy resin, a raise in the composites' density is to be expected, along with increasing loading; however, it is highly dependable on the fraction of air eliminated from the frustules during infusion. Additionally, mostly for base diatomite earth, with increasing loading, the effect of composition degassing on the material density becomes more substantial, as the diatomite traps significant amounts of air. Therefore, a bigger difference between degassed and non-degassed samples can be observed. Moreover, in general, higher values of density were observed for the samples with fractionated diatomite. This effect can be linked to stronger the thixotropic effect of micron-sized particles of broken frustules, as proven by (DMA) rheology (Figure 11), which in turn causes the entrapment of more air in the samples and bigger differences between degassed and non-degassed samples for base diatomite earth. It can be seen that with low loadings, viscosity is low and barely dependable on the diatomite type or degassing procedure. With increasing loading, viscosity raises significantly and the differences between diatomite types become substantial, as base filler imparts much higher viscosity. A reduction in the viscosity of base diatomite earth-loaded epoxy after degassing may be due to the agglomeration of micron-sized particles during degassing.

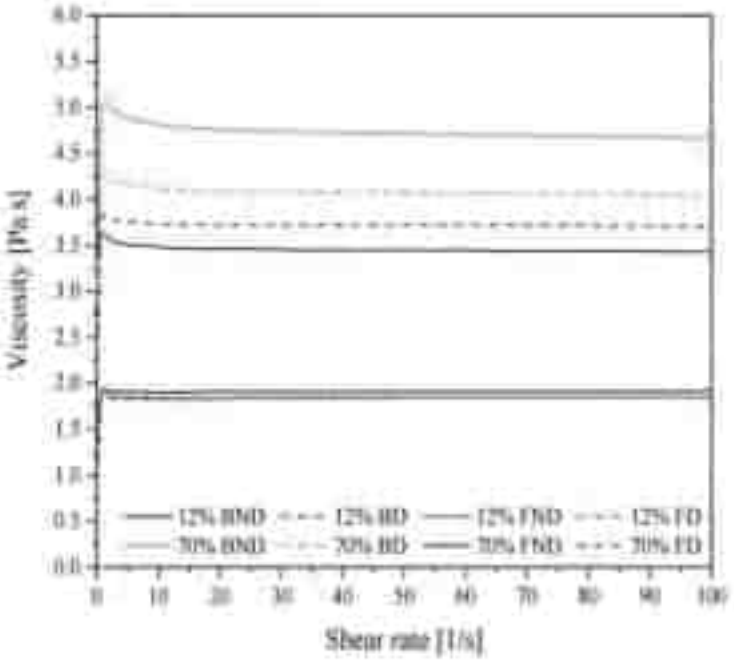

Figure 11. DMA rheology diatomo/epoxy resin composition. BND—base diatomite non degassed, BD—base degassed, FND—fractionated non degassed, FD—fractionated degassed.

3.3. FTIR Analysis

Figure 12 shows the FT-IR spectra of degassed composites containing base diatoms. For resin samples, we can observe characteristic bands at a wavelength of 2953–2800 cm^{-1} for C–H aliphatic bonds, 1450–1400 cm^{-1} for C–O bonds, 1258 cm^{-1}, and 1100–650 cm^{-1} for different C–H bonds [24]. The strong band at 2962 cm^{-1} is typical for the vibration of CH, CH_2, and terminal methyl groups. The peak at around 864 cm^{-1} can be assigned to 1,4-substitution of aromatic ring for epoxy resin. The band characteristics of ester groups,

representing the C-O-C bond stretching, are found at 1258 cm^{-1} and 1015 cm^{-1} [25]. For degassed composites with base diatoms, there emerged weak bands at wavelengths of 3566 and 3394 cm^{-1}, related to stretching vibrations of O-H bonds in silanol groups as well as in hydrogen-bonded molecular water [26]. We also observed an additional band at a wavelength of 797 cm^{-1}, which is caused by symmetric bending vibrations of Si-O-Si bonds [27]. The band at 1646 cm^{-1} is due to bending vibrations of H-O-H bonds of bound molecular water [22]. We additionally observed bands at a wavelength of 1015 cm^{-1}, which could be attributed to the asymmetric stretching of Si–O–Si bond, while the 661 cm^{-1} belong to symmetric stretching [28].

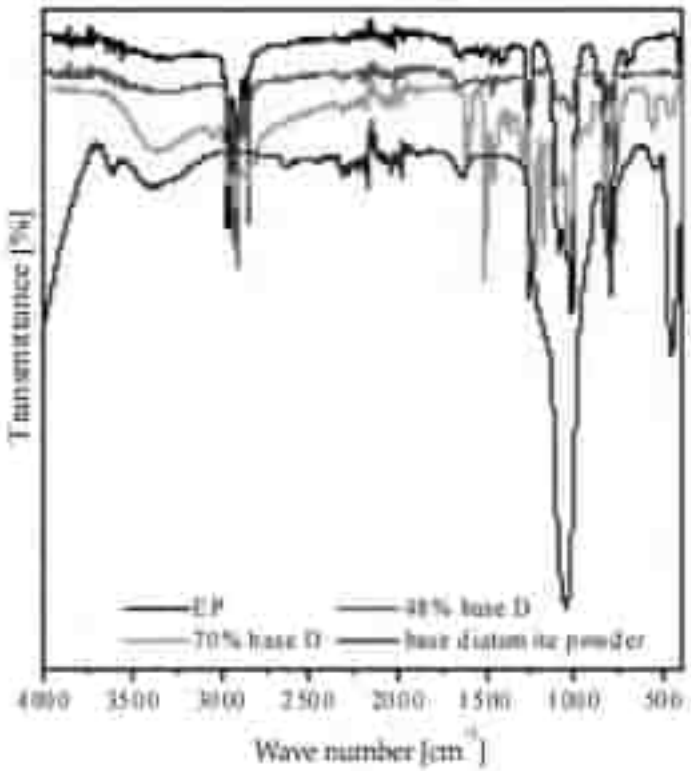

Figure 12. FT-IR spectra of degassed composites containing base diatoms and base diatomite powder. Base D: base diatomite. EP: neat epoxy resin.

3.4. Mechanical Properties

As for the mechanical properties of the obtained composites, we examined their tensile strength, three-point flexural strength, and impact strength.

3.4.1. Tensile Strength

Figure 13 shows the results for the tensile strength (A) and elongation at break (B) of the prepared composites. The degassed samples of neat epoxy were characterized by a higher tensile strength than the non-degassed counterparts, that is 19.91 and 18.26 MPa, respectively. For base diatomite, at low filler concentration, a slight increase in tensile strength was observed. At higher loadings, a small decline was observed, down to 15.09 and 14.82 MPa for 70% degassed and non-degassed compositions, respectively. For the compositions with fractionated diatomite, the tensile strength reached higher values than for the composites with base diatomite, up to 22.78 MPa for 24% composition. As we know, the strengthening effect of the filler is determined by interfacial action forces, which largely depend on the break-up of the filler and the development of the surface. It proves that the elimination of agglomerated particles during diatomite preparation, as well as the degassing of the epoxy composition both have positive effects on the mechanical

properties of the composites obtained. Tensile strength may be linked to the amount of resin introduced into the frustules' internal structure during composition degassing, as observed in SEM images (see Microstructural analysis). Frustules with more resin introduced into their porous structure and penetrating inside their internal volume induce slightly more mechanical reinforcement, due to improved mechanical contact between the matrix and the filler. In the work [8] that studied calcined and natural frustules filled epoxy matrices, they observed variations of tensile elastic modulus and tensile strength with vol. % of frustules addition. In the work, two main tensile failure mechanisms were described for calcinated frustule filled epoxy composites: frustules debonding and frustules fracture/crushing, followed by partial pull-out. Similar failure mechanisms were observed with SEM imaging during this investigation. Debonding and pull-out may be the reason for small levels of difference in mechanical properties when comparing neat epoxy resin and differently filled composites thereof—the limited wetting of the filler surface by the matrix epoxy.

The elongation at break was also investigated (Figure 13B). Due to the brittleness of epoxy resins being one of their main weak spots, as well as the sample preparation method, it was difficult to observe a particular trend for the elongation at break, as the results show a rather high standard deviation. The non-degassed resin without diatoms showed lower elongation at break (1.033%) than the degassed resin (1.528%). The samples containing base frustules without degassing showed slightly lower elongation at break than their counterparts with fractionated filler. It can be explained on the basis of the frustule agglomerates observed in the base diatomite earth forming defect sites. Additionally, for low loadings, the entrapped air in both systems also contributes to material failure at low elongation. Likely for this reason, the difference was poorly visible for degassed samples. In general, as expected, the degassed samples showed improved elongation at break when compared to the non-degassed ones. From the practical point of view, for the studied systems, it is important that even at high loadings the obtained composites show mechanical parameters comparable to those of the neat epoxy resin, being a reasonable option for more eco-friendly materials with a high content of biogenic filler.

3.4.2. Flexural Strength

Figure 14 shows the maximum flexural stress and flexural modulus for degassed and non-degassed composites containing base (A) diatoms and fractionated (B) diatoms. The flexural stress for degassed and non-degassed epoxy resin was 42.48 MPa and 47.15 MPa, respectively. For degassed samples, the stress at three-point bending gradually increases at base diatom contents of 12 and 24% vol. to reach 53.09 MPa and 55.78 MPa, respectively, and then, at base diatom contents of 48, 60 and 70% vol., the stress gradually decreases to reach values down to 35.74 MPa. For degassed composites containing fractionated diatoms, the flexural stress reaches higher values than for the composites with base diatoms, the maximum value of 61.87 MPa being reached for 48% vol. The non-degassed samples showed lower values of flexural stress than the degassed ones, both for base and fractionated diatoms. For the non-degassed samples, we observed much lower values regardless of the filler used. In general, the conclusions are similar to those for tensile tests and prove that both the purification of diatomite to the desired fraction containing single, undamaged frustules, and the degassing of the composition give the best results and improve flexural strength of the composites at the highest loadings, while leaving the flexural modulus similar to the base value. Additionally, for non-degassed composites, a decline of the flexural modulus was observed, as the air gaps increase the elasticity of the material.

For degassed composites, the maximum value of flexural modulus is higher than for degassed composites. The initial value for resin with degassing was approx. 2.5 GPa. Degassed composites with fractionated diatoms showed a higher maximum flexural modulus than those with base diatoms. This could be due to the uniformity of the raw material used. However, in both cases (base and fractionated diatoms), at 70% vol., the value of flexural

modulus reached around 6.7 GPa. For non-degassed resin without a modifier, the value of flexural modulus was 3.2 GPa. The addition of 12 and 70% vol. of base diatoms caused a slight growth of the maximum flexural modulus up to 3.7 GPa. In other cases, the value was even higher than the initial value. The use of fractionated diatoms also did not cause any considerable increase in flexural strength. The addition of 36–60% vol. of fractionated diatoms caused a slight increase in the value, and the further addition of the modifier resulted in a significant deterioration of properties. The maximum value of flexural stress, existing at a 60% content of fractionated diatomite, is approximately 4.6 GPa.

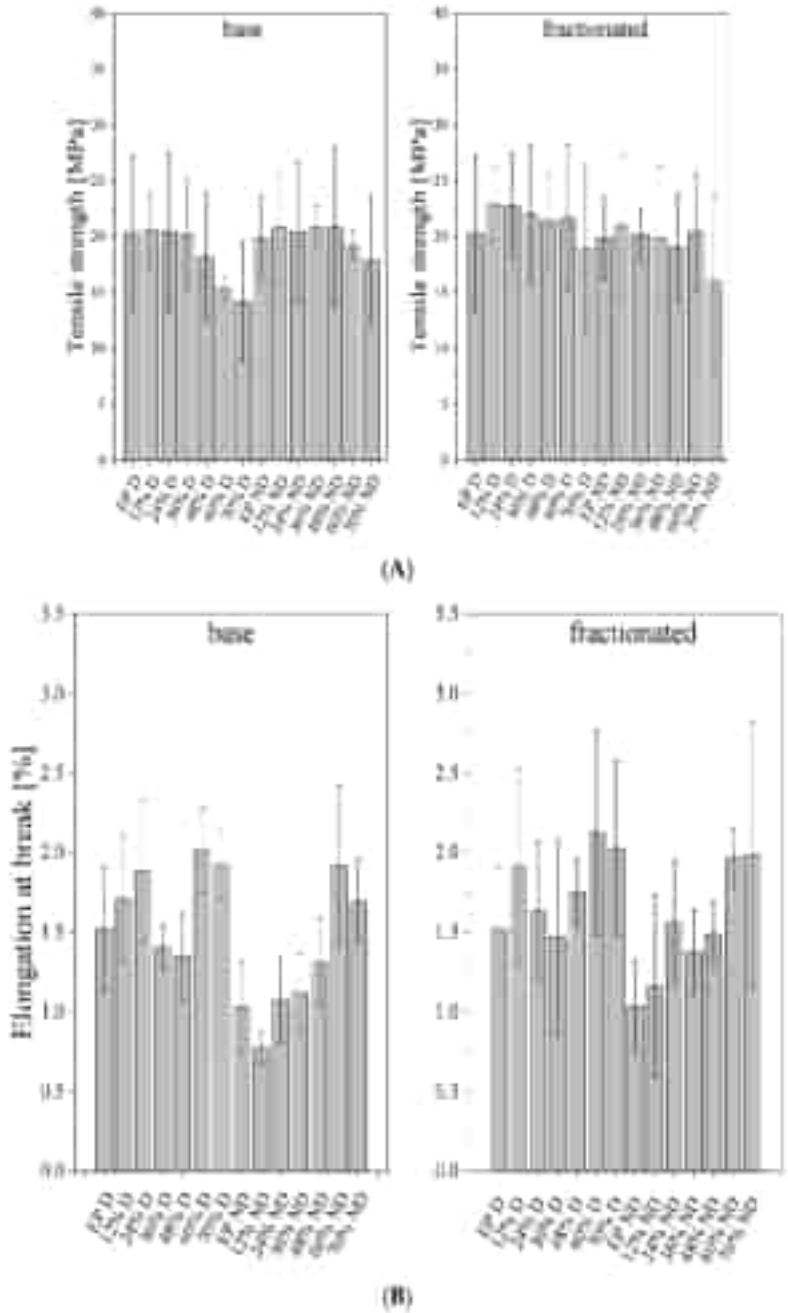

Figure 13. Tensile strength (**A**) and elongation at break (**B**) for degassed ("D") and non-degassed ("ND") composites containing base diatoms and fractionated diatoms.

The use of fractionated diatoms (degassed samples) in a polymer matrix caused a growth in flexural stress. The non-degassed samples showed lower flexural stress values than the degassed samples, both for base and fractionated diatoms, as the presence of air bubbles reduced the strength of the material. Due to degassing, we could see more clearly the strengthening impact of the filler. For the determination of the flexural modulus, the degassing of the sample was important. Non-degassed samples showed comparable (and in certain cases, reduced) flexural modulus values, which were caused by a high share of air and a weaker resin–filler interaction. Changes in flexural strength were observed only for degassed composites, where we observed a slight increase in the flexural modulus. The presence of air bubbles had a considerable impact on the results.

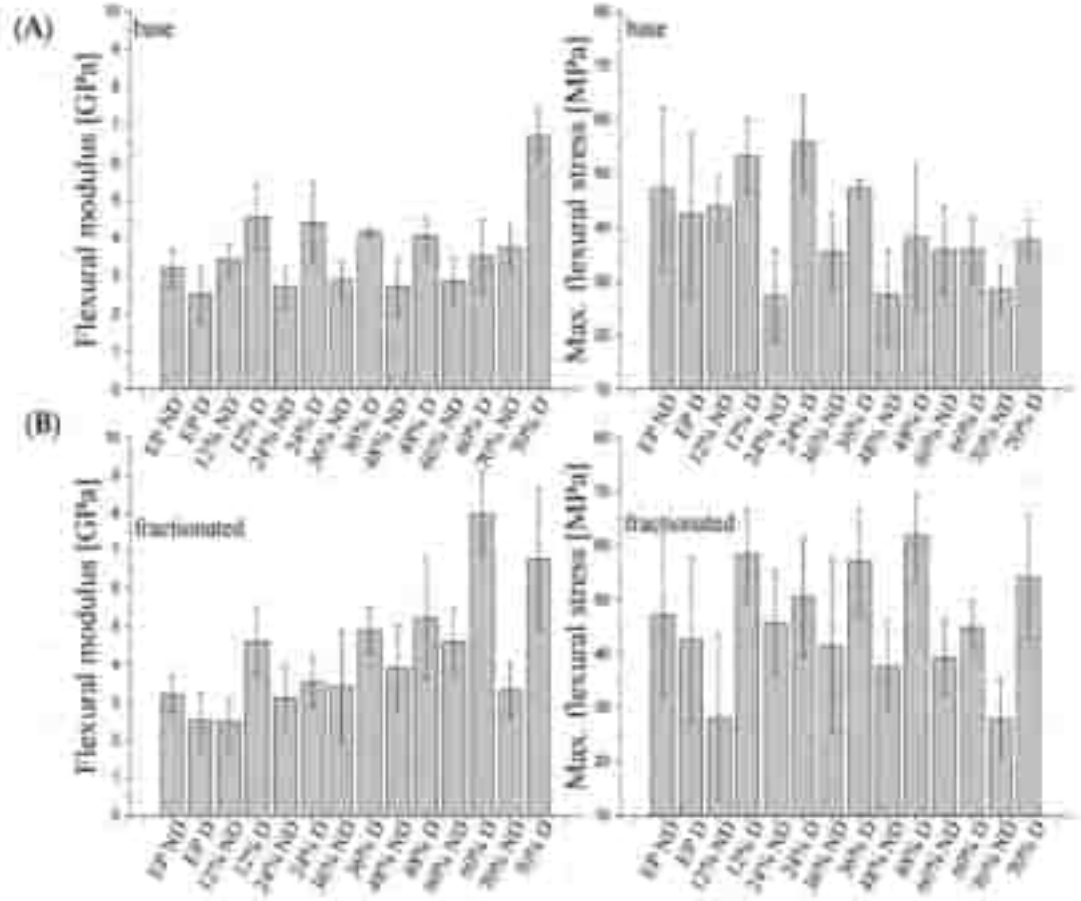

Figure 14. Flexural modulus and max. bending stress for degassed and non-degassed ("D" and "ND") composites containing base (**A**) and fractionated (**B**) samples diatoms.

3.4.3. Impact Strength

For impact strength (Figure 15), two main reasons for decreased values of non-degassed composites should be considered. One of them is the presence of air bubbles introducing mechanical discontinuities, and the other one may be the lower bonding between the matrix and the filler, which in turn causes tearing of the frustules from the resin and increased crack propagation during impact. Impact strength is usually lower for non-degassed samples; this is caused by the presence of air bubbles, which have a significant impact on mechanical properties. A higher impact strength is shown by the samples modified with fractionated diatomite, which may be caused by a more even distribution of diatom particles. Most of the analyzed samples have an impact strength ranging from 2 to 5 kJ/m^2. The values grow along with increasing filler content. The best results were

attained by degassed samples containing 60% vol. of diatomite (base and fractionated: 6 and 9 kJ/m^2, respectively). In general, the impact strength was comparable to the base material regardless of the filler loading, and only sample degassing played a visible role in increasing the material durability.

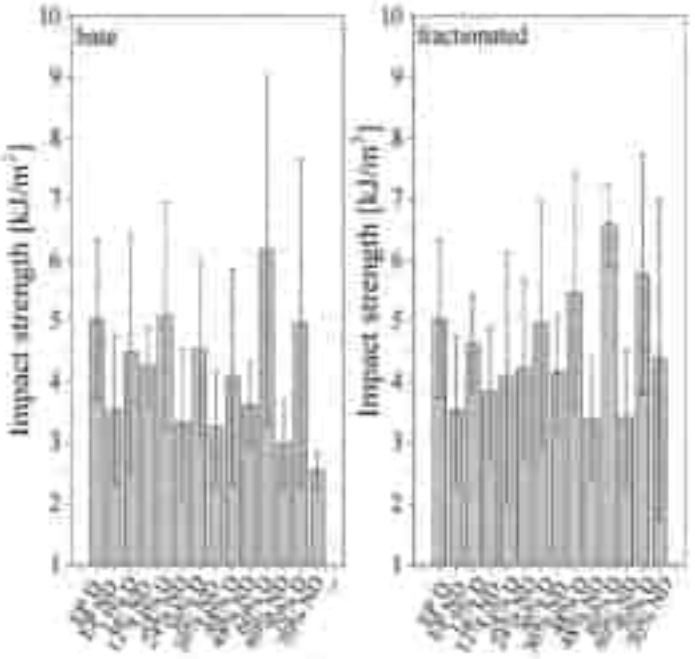

Figure 10. Impact strength for degassed and non-degassed composites containing base and fractionated diatoms.

In the measurements, we observed a large dispersion of results. It may be due to the following reasons: (a) the structural heterogeneity of the composite; (b) the use of silicone molds for casting, whose edges leave defects in the composite (as confirmed by SEM, the edges of the samples were highly irregular); (c) the presence of air bubbles, marking the start of cracking (the presence of air bubbles (both for degassed and non-degassed composites) at random spots of the samples); (d) cracking of the agglomerates for base diatomite. Therefore, in further tests, we may consider whether it is appropriate to use a silicone mold to prepare epoxy resin composites.

3.5. Water Contact Angle

Wettability is a physical feature of materials that specifies their interaction with liquids, mostly water, and determines the basic material properties such as adhesion. The contact angle is an important parameter for determining the hydrophobic or hydrophilic nature of polymers. The contact angle test was conducted on samples shaped as dumbbells. We tested the top and bottom parts of the dumbbells. The angle value for each type of composite was given as the average value obtained in the measurements (Figure 16). Example pictures of a droplet are presented in Figure 17. The samples of degassed and non-degassed resin without diatoms showed hydrophilic properties. As we know, 85% of diatomite consists of SiO_2. The stable tetrahedral structure of SiO_2 makes diatomite a hydrophobic material [29]. However, depending on the degree of purification, diatomite is available with hydrophilic or hydrophobic surface properties [30]. Composites modified with diatomaceous earth showed hydrophobic properties, both in the top and bottom parts. This was except for systems with degassing that contained 12 and 24% vol. of base diatoms and 12% of fractionated diatoms. The values of contact angle in this case are below 90°. Hydrophobic properties of the tested systems increased along with the growing concentration of modifier

in the samples and showed higher values for the systems containing fractionated diatomite. We may therefore conclude that the incorporation of diatomite into the epoxy resin matrix resulted in a considerable increase in the overall hydrophobicity.

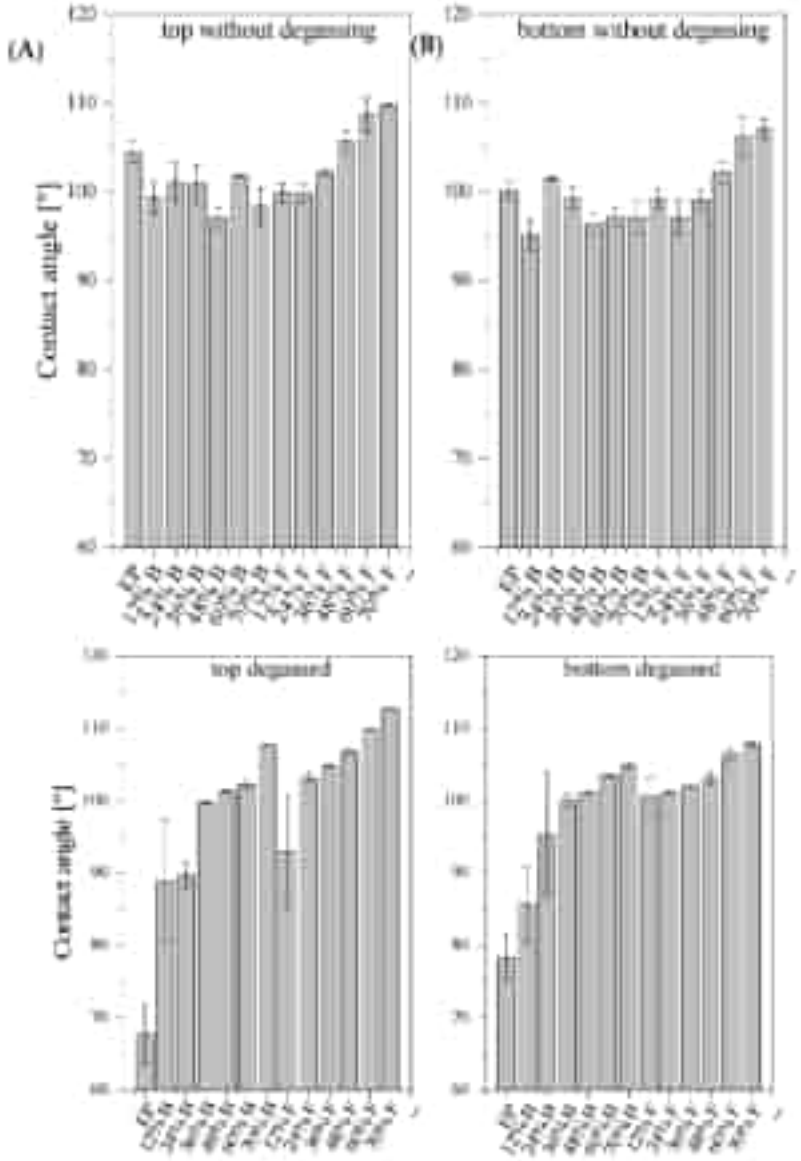

Figure 16. Contact angle bottom (**A**) and top (**B**) for degassed and non-degassed composites containing base ("B") diatoms and fractionated ("F") diatoms.

Figure 17. Droplets applied on the bottom part of the dumbbells for samples containing 20% vol. (**A**) with non-degassed base diatoms, and (**B**) with non-degassed fractionated diatoms.

3.8. Changes in Weight/Rate of Changes with Increasing Temperature (TG/DTG) Analysis

TG thermograms and DTG for degassed and non-degassed composites containing base (A,B) and fractionated diatomite (C,D) (Figure 18). In the samples obtained, we measured the changes in weight (TG) and the rate of these changes along with increasing temperature (DTG). The decomposition of both fractions of diatomaceous earth in the atmosphere takes place in a single stage. This is due to the decomposition of the epoxy resin itself. The addition of diatomite, regardless of the fraction used, increases thermal stability of resin–filler systems. Temperature at a 5% weight loss is, in each case, lower for degassed samples than for non-degassed samples, by nearly 10% maximum (for 48% fractionated samples), whereas the samples containing fractionated diatoms generally show lower temperature values at a 5% weight loss than base diatoms. Temperature at the maximum weight change rate is at a similar level for all the analyzed systems, and ranges from 375 to 381 °C.

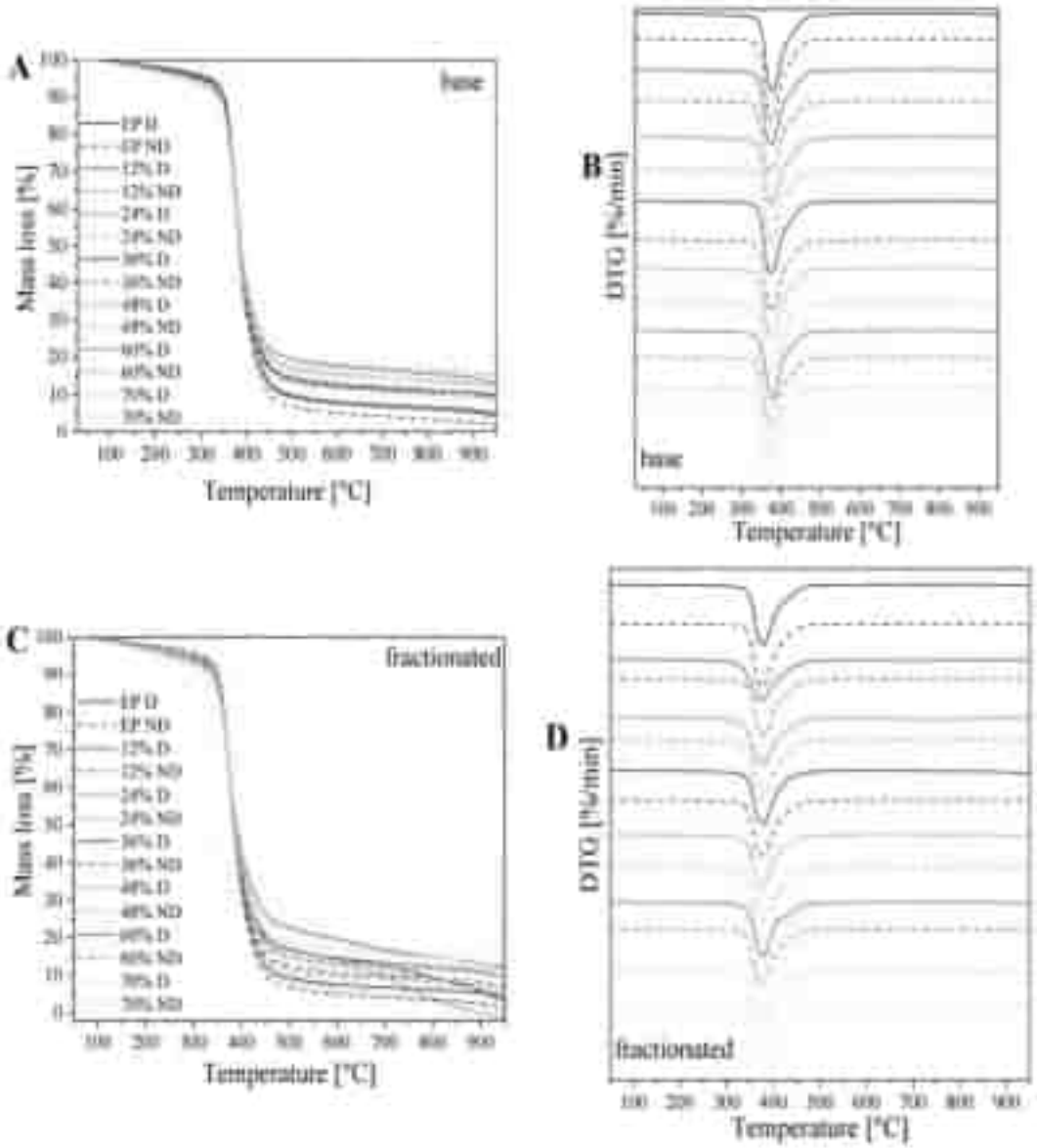

Figure 18. Changes in weight (TG) and the rate of changes with increasing temperature (DTG) curves for degassed and non-degassed composites containing base diatoms (**A**,**B**) and fractionated diatoms (**C**,**D**).

3.7. Microstructural Analysis

We have analysed the side, fracture and meniscus of the samples. For both degassed and non-degassed samples, we observed air bubbles, which are smaller for degassed samples. The observations of sample surfaces (Figures 19–21) allowed us to conclude that the surface is rough. The superficial irregularity decreased along with the growing concentration of diatoms in the system. On the surface of non-degassed samples, we can clearly see air bubbles, while in the degassed systems the air bubbles are either small or do not exist at all.

Observations of sample fractures (Figures 22–24) have shown that the analysed surface is mostly homogeneous. In non-degassed samples, we can observe small air bubbles located on the entire fractured surface as well as larger bubbles located in the upper section of the sample (closer to the meniscus). The fractured surface of degassed samples shows a similar degree of uniformity regardless of diatomite concentration. The samples containing fractionated diatoms feature air bubbles that are slightly bigger than those in the samples containing base diatomite.

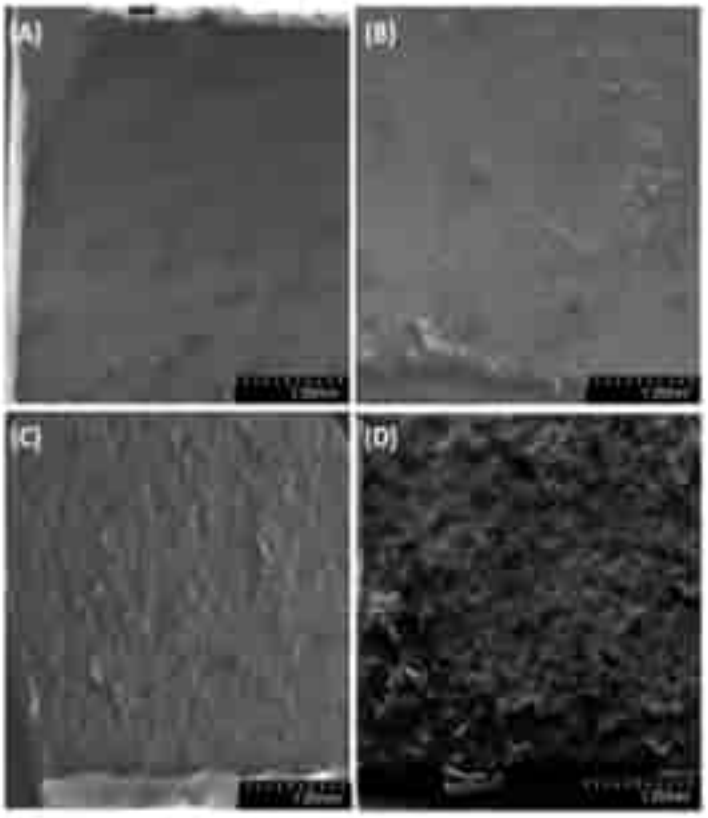

Figure 19. SEM images of the surface of samples with 30% vol. of diatomite (A)—base deg, (B)—base no deg, (C)—fractionated deg, (D)—fractionated no deg.

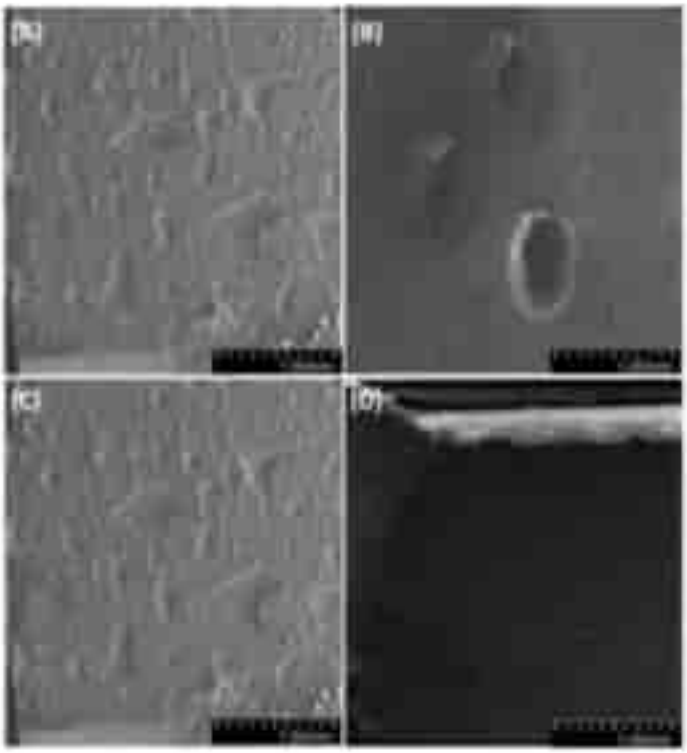

Figure 20. SEM images of the surface of samples with 40% vol. of diatoms (A)—base deg, (B)—base no deg, (C)—fractionated deg, (D)—fractionated no deg.

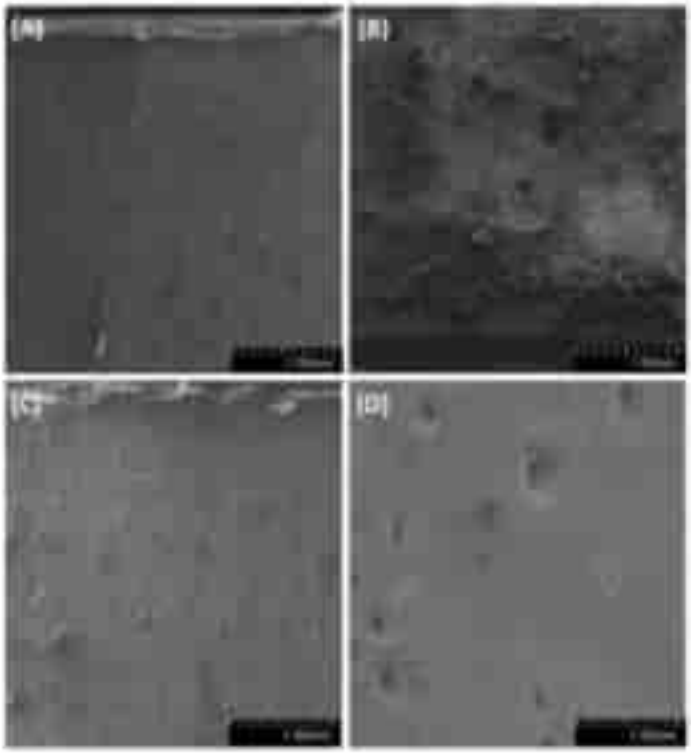

Figure 21. SEM images of the surface of samples with 70% vol. of diatoms (A)—base deg, (B)—base no deg, (C)—fractionated deg, (D)—fractionated no deg.

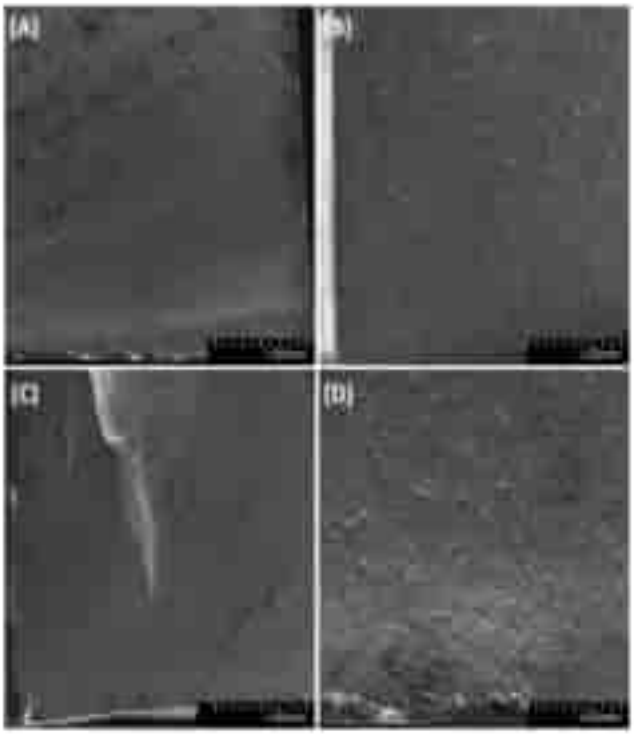

Figure 22. SEM images of the fractures of samples with 30% vol. of diatoms: (A)—base deg, (B)—base no deg, (C)—fractionated deg, (D)—fractionated no deg.

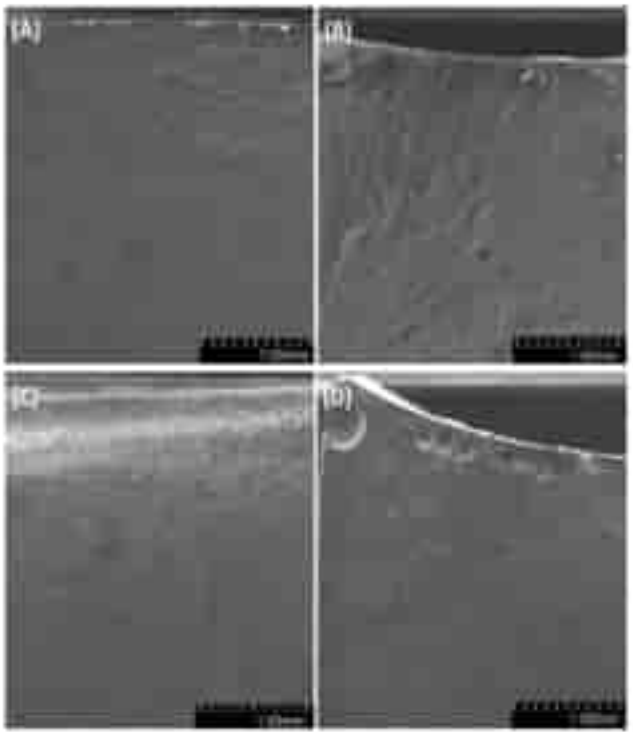

Figure 23. SEM images of sample fractures: 40% vol. of diatoms: (A)—base deg, (B)—base no deg, (C)—fractionated deg, (D)—fractionated no deg.

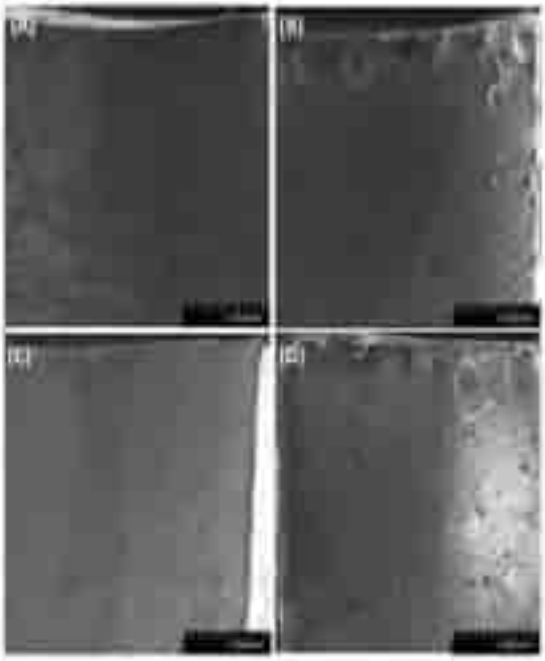

Figure 24. SEM images of the fractures of samples with 20% vol. of diatoms: (A)—base deg, (B)—base no deg, (C)—fractionated deg, (D)—fractionated no deg.

By observing the wall of the mold that contained the tested samples (Figures 25–27), we found a significant heterogeneity in its structure, which, in the results, was also present in the composite samples. In most of the examined systems, the mold walls have irregular projections which are due to the fact that the samples adhere to the silicone molds. As the diatomite concentration in the system raises, the surface roughness drops. Systems that contain over 40% vol. of diatomaceous earth showed a lower inclination to adhere to the silicone mold during sample preparation, so the mold walls in those systems seems to be smoother. Non-degassed systems show the presence of air bubbles. Their size depends both on diatom concentration in the system and on filler preparation. Samples with base diatoms without degassing have bigger air bubbles, while the samples with fractionated diatoms have air bubbles that are much smaller. Along with the growing quantity of diatoms in polymer matrix, the share of bubbles is usually lower. In addition, in all the tested samples, whether degassed or non-degassed, we observed that diatoms were torn off the polymer matrix, leaving a clear mark, or were sheared and partially left in the matrix. This proves that the place where a diatom frustule is bonded with resin is more exposed to damage than the structure of base resin. This arises from low adhesion between the mineral and organic parts of the composite. Additionally, as mentioned in Results—Mechanical Properties, in all the tested samples we observed the supersaturation of resin into the diatomic structure (Figure 28 on the right) as well as the mark it left after debonding (Figure 28 on the left). We have noticed that the resin partially penetrated into the micropores in diatom frustule, creating mechanical links with the polymer matrix.

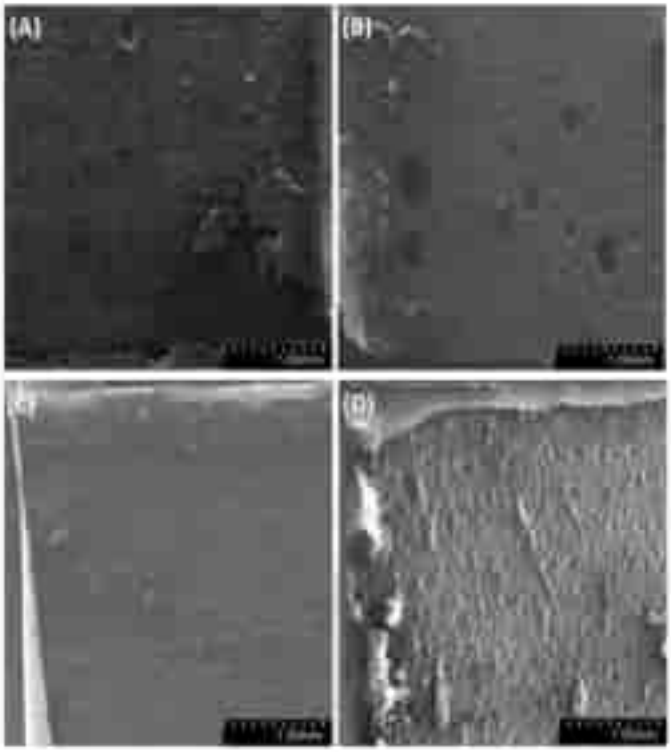

Figure 25. SEM images of mold wall with 36% vol. of diatoms: (A)—base deg, (B)—base no deg, (C)—fractionated deg, (D)—fractionated no deg.

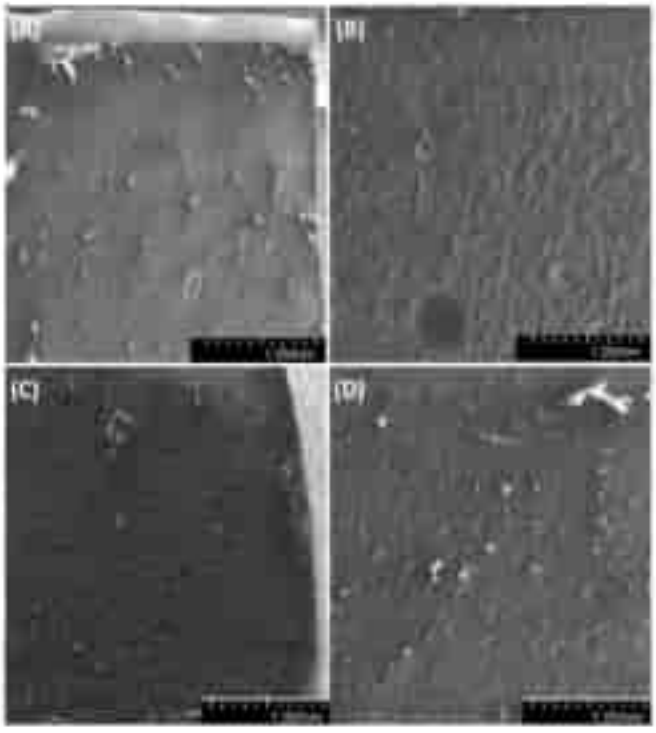

Figure 26. SEM images of mold wall with 48% vol. of diatoms: (A)—base deg, (B)—base no deg, (C)—fractionated deg, (D)—fractionated no deg.

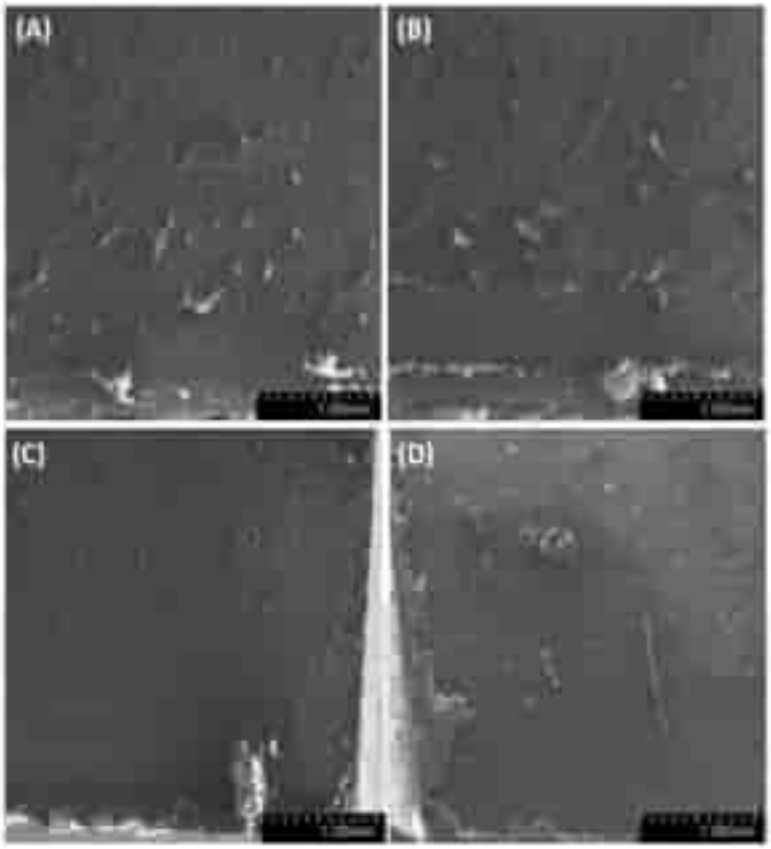

Figure 27. SEM images of mold wall with 70% vol. of diatoms: (A)—base deg, (B)—base no deg, (C)—fractionated deg, (D)—fractionated no deg.

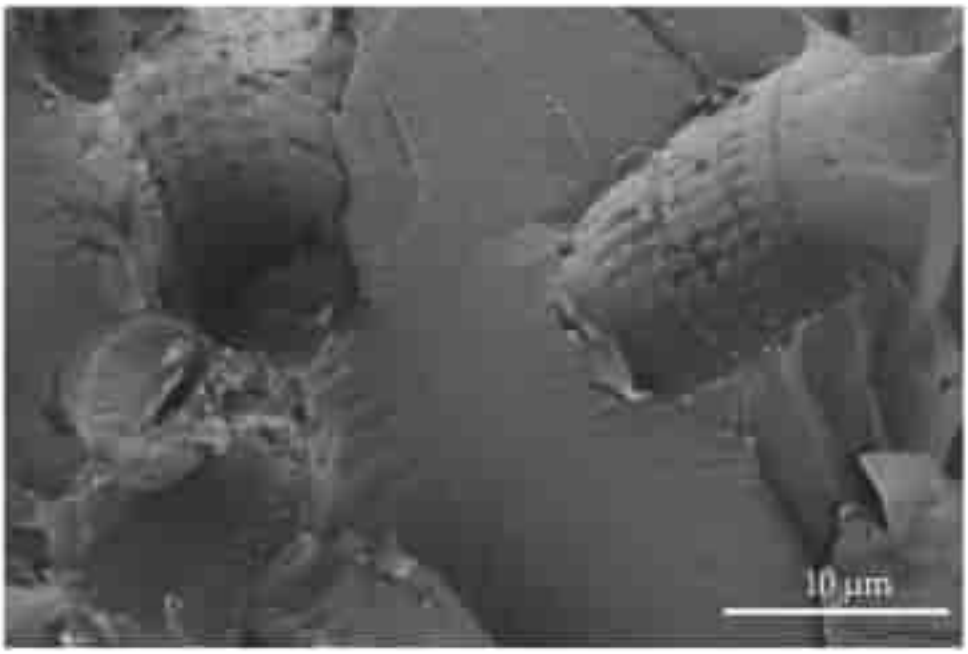

Figure 28. SEM image of diatoms filled with resin (right) and the mark after diatom debonding (left).

4. Conclusions

The tests were aimed to experimentally verify the assumptions on the technology of the fractionation of raw diatomaceous earth to obtain resin–diatomite composites for a specific fraction of diatom frustule structures. We have verified the impact of fractionation as a function of diatom content as well as of process factors such as the degassing of samples. The applied methods of separating diatoms by fractionation and sedimentation enables the removal of diatom agglomerates and a large part of fractured frustules and dusts. It is possible to separate diatom frustule fractions with a specific size distribution. The effective density of diatoms is higher than the density of resin, so the density of obtained composites grows along with the increasing weight share of diatoms. What is important, however, is that the relation between density and weight share of diatoms is not linear and depends on the size of diatom frustule and on the degassing degree of the mixtures. Non-fractionated diatoms increase resin viscosity, which hinders its effective degassing. Samples obtained by degassing technology and those with fractionated diatoms featured higher density, which proves that the tested composites can be considered as a system of three phases: diatoms + resin + pores filled with gas. Based on calculations, we have estimated the expected density of composites with a theoretical 100% filling level, which has shown that with the applied method of preparing composites, diatoms are not completely filled with resin. At the same time, based on SEM, we can conclude that this is not required to obtain good wetting of the filler surface with resin, plus it allows us to obtain lighter materials.

The degassed composites (so those with fewer pores) featured higher tensile strength. Their mechanical properties were also affected by the method of diatom preparation. Samples with fractionated diatoms showed higher tensile strength values than composites with base diatoms, but the effect was more noticeable for non-degassed systems. The slight differences in the strength of samples containing different amounts of filler could be caused by the separation of diatoms from resin during tension (debonding, pulling out). This was similar for elongation at break, which was higher for composites with fractionated diatoms, especially for non-degassed systems. As we know, the strengthening effect of the filler is determined by interfacial action forces, which largely depend on the break-up of the filler. Since diatoms after fractionation are smaller than diatoms as delivered (they do not contain the agglomerates imaged by SEM), the composites based on them feature higher tensile strength. An important observation is that the composites maintain good strength parameters despite a high degree of filling (even for 70% vol.). The addition of fractionated diatoms to the matrix in sample degassing technology affects the hydrophobicity of their surface. The effect is due to the formation of surface microstructure in a diatom frustule–epoxide resin arrangement. The addition of diatoms (whether base or fractioned) caused an increase in the thermal stability of resin–filler systems. The comparative tests carried out (without degassing and degassing) allowed us to conclude that the presence of gas in the composite does not result from the degassing method (which could be a methodological objection in the process of evaluating our results) but is related to the release of gas from the inside of the diatom during the cross-linking process (system heating up). Studies have shown that standard methods adopted as good industrial practice are not sufficient to remove the air contained in diatom shells. The specificity of diatom frustules' morphology is unusual for commonly used fillers. They have a hierarchical porous structure (nanopores, micropores and macro pores). It is necessary to use other factors, such as auxiliary means, but this is not the subject of this work.

Tests have shown that diatom frustules can be used as a biologically friendly filling phase of natural origin in polymer composites, which allows for the reduction in the consumption of production with a high degree of chemical treatment such as epoxy resins.

Author Contributions: Conceptualization, R.E.P.; measurements, evaluation and interpretation, M.D., D.B., R.D., R.E.P., SEM measurements, M.G.; diatomaceous earth sedimentary process, M.S.; writing—original draft, R.D., R.E.P., D.B., M.D.; writing—review and editing, M.D., D.B., R.E.P., R.D.; supervision, R.D., R.E.P., K.J.K. All authors have read and agreed to the published version of the manuscript.

Funding: This work was financially supported in the frame of the project "Advanced Biocomposites for Tomorrow's Economy BIOG-NET", FNP POIR.04.04.00-00-1792/18-00, project is carried out within the TEAM-NET programme of the Foundation for Polish Science co-financed by the European Union under the European Regional Development Fund.

Institutional Review Board Statement: Not applicable.

Informed Consent Statement: Not applicable.

Data Availability Statement: Data available in a publicly accessible repository.

Acknowledgments: Acknowledgement for Andrzej Witkowski for consultation regarding the identification of diatom species in the tested raw material.

Conflicts of Interest: The authors declare no conflict of interest.

References and Notes

1. Chmielewska, D.; Sterzyński, T.; Dudkiewicz, M. Estimation of processing properties of epoxy resin modified with silsesquioxanes (POSS). *Inorganic Appl. Chem.* **2015**, *3*, 337–338.
2. Huskić, M.; Bolka, S.; Vesel, A.; Mozetič, M.; Anžlovar, A.; Vizintin, A.; Žagar, E. One-step surface modification of graphene oxide and influence of its particle size on the properties of graphene oxide/epoxy resin nanocomposites. *Eur. Polym. J.* **2018**, *101*, 211–217. [CrossRef]
3. Kisiel, M.; Mossety-Leszczak, B. Development in liquid crystalline epoxy resins and composites—A review. *Eur. Polym. J.* **2020**, *124*, 109507. [CrossRef]
4. Hsu, Y.-I.; Huang, L.; Asoh, T.-A.; Uyama, H. Anhydride-cured epoxy resin reinforcing with citric acid-modified cellulose. *Polym. Degrad. Stab.* **2020**, *178*, 109213. [CrossRef]
5. Taşdemirci, A.; Yüksel, S.; Karsu, D.; Gültürk, E.; Hall, I.W.; Güden, M. Diatom frustule-filled epoxy: Experimental and numerical study of the quasi-static and high strain rate compression behavior. *Mater. Sci. Eng. A* **2008**, *480*, 373–382. [CrossRef]
6. Sprynskyy, M. *The Structural Heterogeneity and Adsorption Properties of Natural Adsorbents (Clinoptilolite, Mordenite, Diatomaceous Earth, Talc, Chrysotile)*; Scientific Publishing of Nicolaus Copernicus University: Torun, Poland, 2012.
7. Maeda, H.; Aoyama, M.; Kasuga, T. Potential of diatoms as phase change materials. *Mater. Lett.* **2021**, *282*, 128673. [CrossRef]
8. Gültürk, E.; Güden, M.; Taşdemirci, A. Calcined and natural frustules filled epoxy matrices: The effect of volume fraction on the tensile and compression behavior. *Compos. Part B Eng.* **2013**, *44*, 491–500. [CrossRef]
9. Guan, Y.; Chen, R.; Sun, G.; Liu, Q.; Liu, J.; Yu, J.; Lin, C.; Wang, J. Secretion mechanism and adhesive mechanism of diatoms: Direct evidence from the quantitative analysis. *Micron* **2021**, *140*, 102951. [CrossRef] [PubMed]
10. Almqvist, N.; Delamo, Y.; Smith, B.L.; Thomson, N.H.; Bartholdson, A.; Lal, R.; Brzezinski, M.; Hansma, P.K. Micromechanical and structural properties of a pennate diatom investigated by atomic force microscopy. *J. Microsc.* **2001**, *202*, 518–532. [CrossRef] [PubMed]
11. Crawford, S.A.; Higgins, M.J.; Mulvaney, P.; Wetherbee, R. Nanostructure of the diatom frustule as revealed by atomic force and scanning electron microscopy. *J. Phycol.* **2001**, *37*, 543–554. [CrossRef]
12. De Stefano, L.; Maddalena, P.; Moretti, L.; Rea, I.; Rendina, I.; De Tommasi, E.; Mocella, V. Nano-biosilica from marine diatoms: A brand new material for photonic applications. *Superlattices Microstruct.* **2009**, *46*, 84–89. [CrossRef]
13. Sedai, B.R.; Khatiwada, B.K.; Mortazavian, H.; Blum, F.D. Development of superhydrophobicity in fluorosilane-treated diatomaceous earth polymer coatings. *Appl. Surf. Sci.* **2016**, *386*, 178–186. [CrossRef]
14. Mohamed, F.M.; Li, Z.; Zayed, A.M. Carbon nanotube impregnated anthracite (An/CNT) as a superior sorbent for azo dye removal. *RSC Adv.* **2020**, *10*, 25586–25601. [CrossRef]
15. Sun, Z.; Yang, X.; Zhang, G.; Zheng, S.; Frost, R.L. A novel method for purification of low grade diatomite powders in centrifugal fields. *Int. J. Miner. Process.* **2013**, *125*, 18–26. [CrossRef]
16. Goren, R.; Baykara, T.; Marsoglu, M. A study on the purification of diatomite in hydrochloric acid. *Scand. J. Met.* **2002**, *31*, 115–119. [CrossRef]
17. Koulcheris, A.P. Beneficiation of Diatomaceous Earth. U.S. Patent 3572500A, 30 March 1971.
18. Zolghadr, M.; Zohuriaan-Mehr, M.J.; Shakeri, A.; Salimi, A. Epoxy resin modification by reactive bio-based furan derivatives: Curing kinetics and mechanical properties. *Thermochim. Acta* **2019**, *673*, 147–157. [CrossRef]
19. EN ISO 527-1:2012 Plastics—Determination of tensile properties—Part 1: General principles. PKN, 2013.
20. EN ISO 178:2010 Plastics—Determination of flexural properties. PKN, 2011.
21. ISO 179-1:2010 Plastics—Determination of Charpy impact properties—Part 1: Non-instrumented impact test. PKN, 2010.
22. Dobrosielska, M.; Przekop, R.E.; Sztorch, B.; Brząkalski, D.; Zgłobicka, I.; Łępicka, M.; Dobosz, R.; Kurzydłowski, K.J. Biogenic Composite Filaments Based on Polylactide and Diatomaceous Earth for 3D Printing. *Materials* **2020**, *13*, 4632. [CrossRef]
23. Miklasz, K.A.; Denny, M.W. Diatom sinkings speeds: Improved predictions and insight from a modified Stokes' law. *Limnol. Oceanogr.* **2010**, *55*, 2513–2525. [CrossRef]

24. Fernandes, I.J.; Santos, R.Y.; Dos Santos, F.C.A.; Rocha, T.L.A.C.; Junior, N.S.D.; Moraes, C.A.M. Replacement of Commercial Silica by Rice Husk Ash in Epoxy Composites: A Comparative Analysis. *Mater. Res.* **2018**, *21*. [CrossRef]
25. Pandit, R.; Lach, R.; Grellmann, W.; Michler, G.; Henning, S.; Saiter, J.; Berkowski, A.; Adhikari, R. Chemical modification of SBS star block copolymer for templating nanostructures in epoxy resin blends. *Mater. Today Proc.* **2020**, *29*, 1158–1160. [CrossRef]
26. Jiang, W.; Luo, S.; Liu, P.; Deng, X.; Jing, Y.; Bai, C.; Li, J. Purification of biosilica from living diatoms by a two-step acid cleaning and baking method. *Extremophiles Biol. Fishes* **2014**, *26*, 1511–1518. [CrossRef]
27. Hernández-Ortiz, M.; Hernández-Padrón, G.; Bernal, R.; Cruz-Vázquez, C.; Castaño, V.M. Nanocrystalline nematic opals: Synthesis and comparative characterization vs. natural stones. *Int. J. Basic Appl. Sci.* **2015**, *4*, 238. [CrossRef]
28. Zhang, Y.; Guo, W.W.; Zheng, T.X.; Zhang, Y.X.; Fan, X. Engineering hierarchical Diatom@ Co_3O_4 MnO_2 hybrid for high performance supercapacitor. *Appl. Surf. Sci.* **2018**, *427*, 1158–1165. [CrossRef]
29. Akyuz, L.; Kaya, M.; Koc, B.; Mujtaba, M.; Ilk, S.; Labidi, J.; Salaberria, A.M.; Cakmak, Y.S.; Yildiz, A. Diatomite as a novel composite ingredient for chitosan film with enhanced physicochemical properties. *Int. J. Biol. Macromol.* **2017**, *105*, 1403–1411. [CrossRef]
30. Ehrhart, A. Materials today energy. *Mater. Today* **2017**, *5*, 37–57.

H3

Methodological Aspects of Obtaining and Characterizing Composites Based on Biogenic Diatomaceous Silica and Epoxy Resin

Dobrosielska M., Dobrucka R., Brząkalski D., Gloc M., Rębiś J., Głowacka J., Kurzydłowski K.J., Przekop R.E.; Materials, 14, 4607, 2021

materials

MDPI

Article

Methodological Aspects of Obtaining and Characterizing Composites Based on Biogenic Diatomaceous Silica and Epoxy Resins

Marta Dobrosielska [1], Renata Dobrucka [2,3,*], Dariusz Brząkalski [3], Michał Gloc [1], Janusz Ryński [1], Julia Głowacka [4], Krzysztof J. Kurzydłowski [1,3] and Robert E. Przekop [4,*]

[1] Faculty of Materials Science and Engineering, Warsaw University of Technology, ul. Wołoska 141, 02-507 Warsaw, Poland; Marta.Dobrosielska@pw.edu.pl (M.D.); michal.gloc@pw.edu.pl (M.G.); janusz.rynski@pw.edu.pl (J.R.); krzysztof.kurzydlowski@pw.edu.pl (K.J.K.)

[2] Department of Non-Food Products Quality and Packaging Development, Institute of Quality Science, Poznań University of Economics and Business, al. Niepodległości 10, 61-875 Poznań, Poland

[3] Faculty of Chemistry, Adam Mickiewicz University in Poznań, ul Uniwersytetu Poznańskiego, 61 - 614 Poznań, Poland; d.brzakalski@gmail.com

[4] Centre for Advanced Technologies, Adam Mickiewicz University in Poznań, ul. Uniwersytetu Poznańskiego 10, 61-614 Poznań, Poland; julia.glowacka@amu.edu.pl

[5] Faculty of Mechanical Engineering, Białystok University of Technology, Wiejska 45c, 15-351 Białystok, Poland

* Correspondence: Renata.Dobrucka@pw.edu.pl (R.D.); rprzekop@amu.edu.pl (R.E.P.)

Abstract: Diatomaceous earth are sediments of unicellular algal skeletons with a well-defined hierarchical structure. Despite many tests conducted on systems using diatomaceous earth and epoxy resins, we can find many differences in the methods of acquisition and characteristics of the composite, which may considerably affect the results. In our study, we have conducted tests to verify the impact of the method of obtaining samples and the degassing of the composite on its mechanical properties and standard deviations. The samples were cast in glass moulds and silicone moulds and then subjected to testing for their mechanical and functional properties, imaging with the use of an optical microscope and a scanning electron microscope. The tests have shown that, for samples cast in glass moulds, there is no heterogeneity within the area of the tested sample, as in the case of samples cast in silicone moulds. Silicone moulds allow for quite effective self-degassing of the resin due to the large area-to-mass ratio, and the small remaining air vesicles have a limited effect on the mechanical properties of the samples. The filler used also played a significant role. For systems containing base and rinsed diatomite, it is clear that the degassing of mixtures increases the tensile strength. For rinsed diatomite, the elongation at break grew along with increasing filler concentration, while for base diatomite, the improvement was observed for flexural strength and impact strength. A non-modified epoxy resin shows a tensile strength at 18.91 MPa (silicone mould cast). At the same time, the degassed, glass mould-cast systems containing 12% of base and rinsed diatomite showed a tensile strength of 27.4 MPa and 44.7 MPa, respectively. We have also observed that the higher the filler concentration, the higher were the tensile strength values, which for the rinsed diatomite reached over 50.1 MPa and for the base diatomite were maximum of 43.8 MPa. The tests, therefore, constitute a set of guidelines and recommendations for testing with the use of fillers showing an extended inner structure.

Keywords: epoxy resin; diatomaceous earth; diatomite; silicone mould; glass mould; bio-composite; degassing

check for updates

Citation: Dobrosielska, M.; Dobrucka, R.; Brząkalski, D.; Gloc, M.; Ryński, J.; Głowacka, J.; Kurzydłowski, K.J.; Przekop, R.E. Methodological Aspects of Obtaining and Characterizing Composites Based on Biogenic Diatomaceous Silica and Epoxy Resins. *Materials* **2021**, *14*, 4607. https://doi.org/10.3390/ma14164607

Academic Editor: Francesca Lionetto

Received: 29 June 2021
Accepted: 11 August 2021
Published: 17 August 2021

Publisher's Note: MDPI stays neutral with regard to jurisdictional claims in published maps and institutional affiliations.

Copyright: © 2021 by the authors. Licensee MDPI, Basel, Switzerland. This article is an open access article distributed under the terms and conditions of the Creative Commons Attribution (CC BY) license (https://creativecommons.org/licenses/by/4.0/).

1. Introduction

Diatomaceous earth is an amorphous, naturally existing material with unique physical and chemical properties [1]. Moreover, it is a porous biological sedimentary rock consisting mostly of SiO_2, with small quantities of Al, Fe, Ca, Na, Mg, and other elemental oxides

as well as small organic impurities that fill its pores and are adsorbed on its surface [2]. Besides, raw diatomaceous earth contains non-defective structures, i.e., diatom frustules, as well as many structures that are defective, fractured, mechanically damaged and different in terms of external structural geometry, shape, and size. The literature describes methods of purifying diatomaceous earth.

From the practical point of view, deposits containing diatoms have the broadest application in composite materials. Despite a high spread of diatoms in the sea and freshwater, their acquisition directly from the environment is expensive and economically unreasonable. For this reason, the methods of extracting and purifying diatomaceous earth are an important direction in the use of that material to obtain composites. The most common method for large-scale production of diatomite is surface-mining of geologic formations containing fossilized diatomite layers [3]. Heavy equipment, including bulldozers and power shovels, is used. We know methods of purifying raw diatomaceous earth using thermochemical treatments with minimum calcination combined with acid treatment [4]. Based on these studies, it has been observed that a hot acid significantly affects the composition and structure of diatoms. Along with the increasing time and temperature, the natural diatomite was dissolving [5]. Raw diatomaceous earth was also subjected to chemical treatment with acids such as HF [6], HCl [7], or HNO_3 [8]. The chemical treatment additionally allowed for removing contamination from diatomaceous earth, reducing the size of particles, and obtaining a material with a high SiO_2 content. Yang et al. 2014 [9] used physical purification of raw diatomaceous earth with a laminar-flow centrifugal separator. Jung et al. [10] have developed a method to improve the porous structure of raw diatomaceous earth by using an electric field. The electric field allowed them to effectively remove contaminants from raw diatomaceous earth and to uncover any clogged and hidden small pores in the diatomite. Diatomaceous earth was also purified by rinsing with sodium hexametaphosphate (SHMP) used as a dispersant, in combination with centrifuging [11] or high-gradient magnetic separation (HGMS) to remove magnetic contaminants. In our previous tests [12], we used a method of fractioning and purifying raw diatomaceous earth by sedimentation, which allows for obtaining a fraction with a narrow distribution of diatom frustules. In our study, raw diatomite was mechanically mixed with water and fractionated with the use of sedimentation. This method, after modification involving the use of large-scale centrifuges, is economical on an industrial scale. The small, fractured frustule pieces were partly removed, along with bigger agglomerates/colonies, by suspending the diatomite in water and subjecting the suspension to sedimentation. Based on interacting gravitational forces, particles of different sizes were settling out at different rates. The method we propose allows for producing a raw material with a more uniform design and morphology, which thus provides specific properties of the finished product. The proposed method makes it possible to refine diatomaceous earth and obtain economically added value, e.g., in the form of reduction of resistance during filtration or improvement of the properties of composite materials. The application of diatomite as a filler may not only reduce the price of epoxy composites and coatings but also improve their performance. Lee et al. reported epoxy resin composition containing titanium dioxide and diatomaceous earth to increase the hydrophobicity of the surface of coatings and provide them photocatalytic self-cleaning ability [13]. The application of mineral fillers such as diatomite is superior in terms of stability towards naturally occurring decay when compared to organic filler-based composites [14].

In this study, a mechanically fractionated raw diatomaceous earth was used as an epoxy resin filler. Among all polymers used, epoxy resins are not only widely used in adhesives, coatings, and the aerospace and electronics industries but also play an important role in marine engineering because of their easy processability, good mechanical and thermal properties, high chemical and corrosion resistance, good adhesion to various substrates, and low shrinkage on curing. However, the curing system has many shortcomings due to the high cross-linking density of the resin, such as inherent brittleness, poor toughness, and impact resistance. It is necessary to improve the above characteristics, especially the

toughness, to apply the epoxy resin in the industry on a global scale for packaging, adhesives, paints, and coatings, [15–18]. In addition, despite the significant improvement of the already resins, composite materials based on the epoxy resin are still a subject of intensive research. Recent years have witnessed an increasing amount of research conducted to improve mechanical properties. However, the effect of different filler contents on the mechanical properties of epoxy resin polymers still requires further investigation, even though it is already known that the dispersion state, shape, and size of the filler could affect the inherent properties of epoxy resin [19].

Tests conducted on epoxy resin-based systems require the preparation of samples in the form of casts. Moulds made of silicone, steel, aluminium, or Teflon are widely used. Each of these materials has various advantages and disadvantages. Steel or Teflon moulds are more difficult to prepare and require more financial outlays, but they feature a lower wear and tear. Silicone moulds are made of relatively cheap materials, but they are less durable and repeatable. The type of mould used has the biggest impact on the dimensional compliance of the produced samples and the ease of casting and releasing the sample. In case of the limited possibility of proper resin degassing, the construction and orientation of the mould will affect the manner and location of the air bubbles forming in the sample. Moreover, the application of a silicone mould may result in the absorption of anti-adhesive (release) agents on the surface layer of the epoxy during casting, which affects its composition, surface appearance and properties, as well as other performance aspects of the final component [20]. From the point of view of designers and manufacturers of moulded components, the properties of the contaminated epoxy surface layer will be different to those of the bulk resin. In their work, Nogueira et al. prepared the tested epoxy resin-based systems with the use of silicone moulds [21]. They carried out mechanical tests that showed, among others, that the application of the said moulds causes standard deviations of tensile strength values ranging from 14.1% to 31.8%. Similarly, in a study [22] where silicone moulds were used to prepare the samples, the standard deviation was a maximum of 10.2%. In another study [23], composites were prepared with steel moulds. The authors have tested, for example, tensile strength, flexural strength, and flexural modulus. Standard deviations from the said values were approximately 6.3–24.6%, 5.1–10.1% and 4.3%–9.7%, respectively. Similarly, in study [24], authors also used steel moulds, and the deviation from the flexural strength was around 7% and 0.75 GPa. In addition, study [25] covered the testing of mechanical properties of epoxy resin/ZrO_2 composites, which were prepared using moulds made of aluminium. The deviation from the tensile strength was a maximum of 17.9%. In study [26], composites were prepared with moulds made of Teflon, and the deviation from the tensile strength was similar to that in other types discussed above (maximum of 14%). For this study, we have prepared resin/filler systems using conventional silicone moulds as well as glass moulds with CNC cutting of the samples.

2. Materials and Methods

2.1. Materials

For the tests, we used epoxy resins produced by Zakłady Chemiczne Organika Sarzyna: Epidian 601 with an epoxide equivalent of 0.50–0.55 mol/100 g and a viscosity of 700–1100 [mPa·s], cured with triethylenetetramine (curing agent Z-1). Diatomaceous earth (Perma-Guard, Bountiful, UT, USA) was derived from diatomite deposits.

2.2. Preparation of Samples

The tested composites of epoxy resin Epidian 601, cross-linked with amine-based curing agent Z-1, contained different quantities (0, 12, 24, 36, 48, 60, 70% vol.) of base and fractionated diatoms according to the methodology described in the previous study [12]. The tested composites of epoxy resin Epidian 601 (epoxy number [mol/100 g] 0.5–0.55, viscosity at 25 °C [mPa·s] 800–1500), cross-linked with amine-based curing agent Z-1 (triethylenetetramine, viscosity at 25 °C [mPa·s] 20–30, amine number [mg KOH/g] min. 1100), contained different quantities (0, 12, 24, 36, 48, 60, 70% vol., corresponding to 0, 2.6,

5.5, 8.0, 10.4, 12.7, and 14.5% by weight, accordingly) of base and fractionated diatoms with an average particle size distribution of approx. 10 µm. The choice of the resin/hardener system was dictated, on the one hand, by the necessity to obtain a low viscosity of the mixture, and on the other hand, by the optimal time of its final gelation. The epoxy resin with diatom frustules was mixed mechanically in a plastic vessel using a steel propeller (600 rpm, 10 min). The samples were cast in silicone and glass moulds. The glass moulds were used to obtain 4 mm thick panels which were then cut with a CNC milling cutter to produce profiles for testing. The test samples were prepared after three weeks of resin curing at ambient temperature. The test samples were prepared according to EN ISO 527-1 [27] and 178:2010 [28]. The tests were performed after three weeks of samples curing at 20 °C. Table 1 includes the sample designations used in the study.

Table 1. Designations of the tested samples.

Nazwa Skniczna	Sample Name
EP	Reference
RDG	Rinsed with degassing glass mould
BDG	Base with degassing glass mould
RNDG	Rinsed without degassing glas mould
BNDG	Base without degassing glass mould
RDS	Rinsed with degassing silicon mould
BDS	Base with degassing silicon mould
RNDS	Rinsed without degassing silicon mould
BNDS	Base without degassing silicon mould

2.3. Characterization Methods

For flexural and tensile strength tests, the materials obtained were printed into type 1B dumbbell specimens in accordance with EN ISO 527:2012 and EN ISO 178:2006. Tests of the specimens obtained were performed on a universal testing machine INSTRON 5969 with a maximum load force capacity of 50 kN. The traverse speed for tensile strength measurements was set at 2 mm/min, and for the flexural strength, it was also set at 2 mm/min. Charpy impact test (with no notch) was performed on an Instron Ceast 9050 impact machine(Instron, Norwood, MA, USA) according to ISO 179-1 [29]. The density of the composites obtained was determined with the hydrostatic method using a Sartorius YCP04MS analytical balance (Sartorius, Göttingen, Germany) at 20 °C with the use of distilled water. The morphology and microstructure of the prepared composites were observed by scanning electron microscopy. Samples in the form of powders and moulds were dusted with cupro-nickel using a GATAN duster. Observations were conducted with a Hitachi SU 8000 scanning microscope (Hitachi, Ltd., Chiyoda, Tokyo, Japan) with an accelerating voltage of 5 kV to image the preparations. The imaging was performed in three SE modes. Surface structure and breakthroughs were analysed under a Digital Light Microscope Keyence VHX 7000 with 100× to 1000× VH-Z100T lens (Osaka, Japan). All pictures were recorded with a VHX 7020 camera (Keyence International, Mechelen, Belgium). Differential scanning calorimetry was performed using a NETZSCH 204 F1 Phoenix calorimeter (Netzsch Group, Selb, Germany). Samples of 6 ± 0.2 mg were cut from each granulate and placed in an aluminium crucible with a punctured lid. The measurements were performed under nitrogen in the temperature range of 20–200 °C and at a 10 °C/min heating rate, and T_g was measured from the second heating cycle.

3. Results and Discussion

3.1. Influence of Gravity and Degassing

For the produced resin-based composite materials, filler sedimentation processes are important for particles exceeding 5 µm. Sedimentation is used to obtain quartz-epoxy conglomerates with a high filling rate. These effects were also observed for resin/diatomaceous earth systems [12].

Figure 1 schematically shows sections of systems cast in silicone moulds and in glass moulds. The silicone mould during casting is positioned transversally to the gravitation direction (Z axis), so we can observe the concentration of mineral material in the lower part of the mould, with a proportional distribution towards the XY axes. For the glass mould, deviation from the XY plane was 60°. Such a position causes significant differences in filler sedimentation in the tested sample. If the glass mould was angled at 60°, this could cause a non-uniform concentration of the filler and the sedimentation being in line with the gravitation direction but not in line with the direction of CNC cutting. The tests have shown that, for samples cast in glass moulds, there is no heterogeneity within the area of the tested sample, unlike in the case of samples cast in silicone moulds. SEM/EDS images (Figure 2) show an even dispersion of diatomaceous earth in epoxy resin and the layout of filler particles being in line with the direction of CNC cutting. The systems cast in the silicone mould show an inclination to collect the filler closer to the bottom surface of the sample (Figure 2c), whereas the layout of particles in the samples cast in the glass shows that they are more homogeneous (Figure 2d). In addition, in non-degassed systems, we can observe floatation. Particles of diatomaceous earth are "entrained" along with air bubbles and gather by the top surface of the sample. (Figure 2d). This results in a slight accumulation of the filler in the upper layout of the composites.

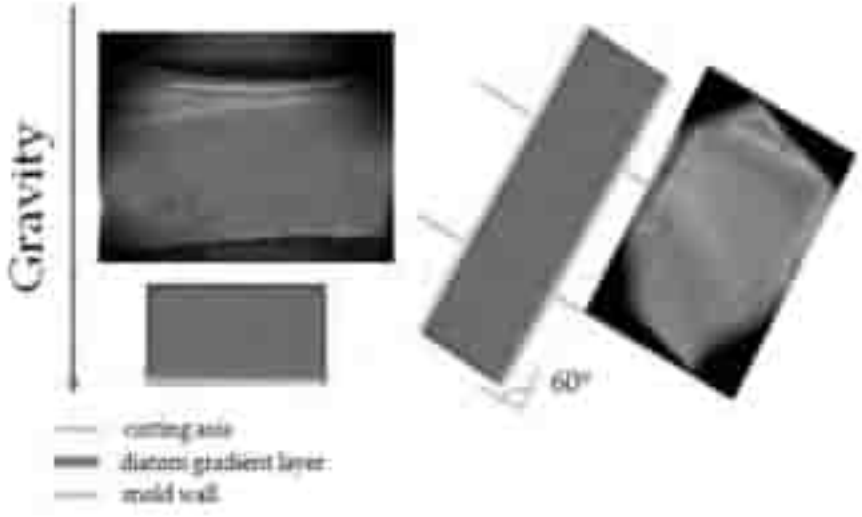

Figure 1. A glass mould, a silicone mould, inclination, and sedimentation direction of diatomaceous earth.

Another of the studied issues regarding the application of silicone moulds is the difference in the dimensions of test samples. Systems cast in silicone moulds are exposed to the meniscus effect (Figure 3), which does not occur in samples prepared in glass moulds. The meniscus is caused by uneven casting or, on the contrary, a slight casting-on of the top surface of the samples, which consequently leads to differences in the sample thickness being difficult to reduce and causes higher deviations in the values of the tested parameters. Samples cast in glass moulds feature constant dimensions, and their preparation by cutting out a measuring profile with CNC gives a dimension deviation lower than 0.03 mm. The SEM images show both a difference in composite thickness and the impact of the meniscus. Figure 2a clearly shows a concave meniscus produced by slight uneven casting of the sample, which causes non-heterogeneity of the samples in the series and a

subsequent problem in testing mechanical properties, whereas the sample cast in a glass mould (Figure 2b) has its top surface flat, so the differences in dimensions between the samples in the series are minimal. The dispersion of diatomaceous earth in epoxy resin requires (intensive) mechanical mixing of constituents, which causes aeration of the system. Additionally, diatomaceous earth has internal voids of micrometric dimensions, filled with air. The choice of the mould type affects the degassing mechanism of the composite system. A silicone mould enables a free release of gas to the environment during gelation and cross-linking due to the relatively large sample-to-environment contact area (Figure 4). Any air bubbles that may remain in the samples are small and have a lower impact on mechanical properties. On the contrary, in the case of glass moulds, there are difficulties with air extraction. Gas bubbles accumulate on the mould's top wall (according to the direction of buoyancy) and often merge into larger formations. An air bubble layer in a non-degassed sample might be 400 to even 900 µm thick depending on filler concentration.

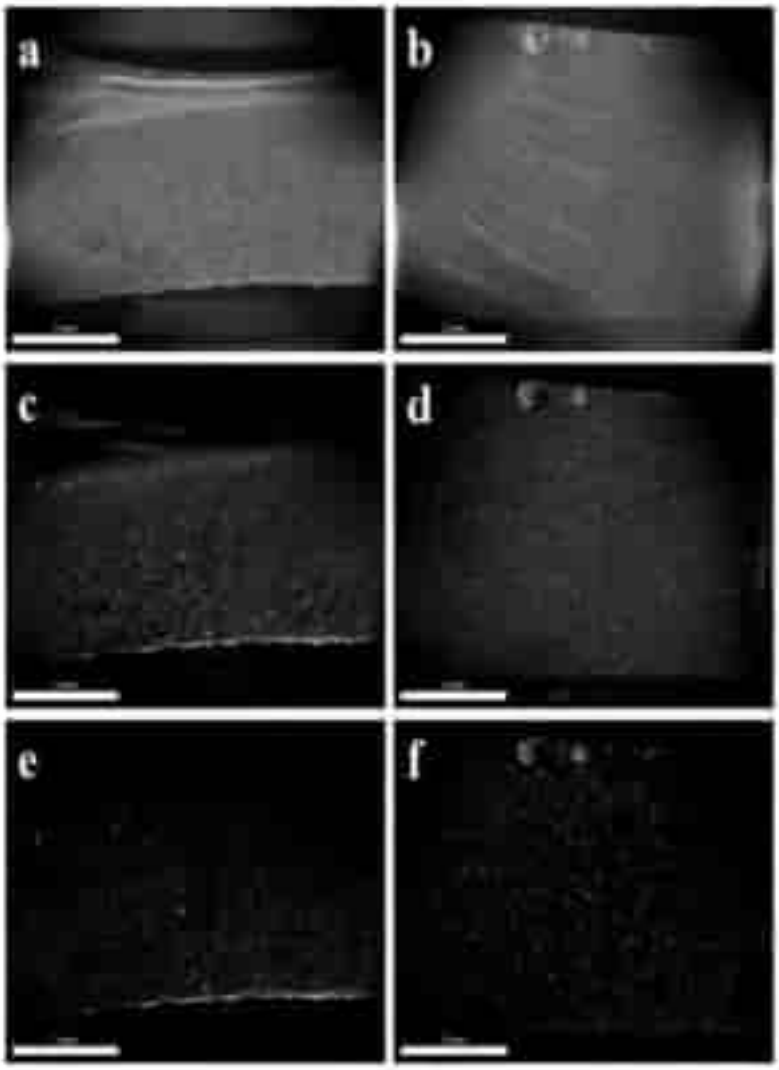

Figure 2. SEM/EDS images of diatoms/resin composites; (a,c,e)—image of a composite cast in a silicone mould; (b,d,f)—SEM image of a composite cast in a glass mould.

Figure 3. The issue of a convex and concave meniscus, casting in silicone.

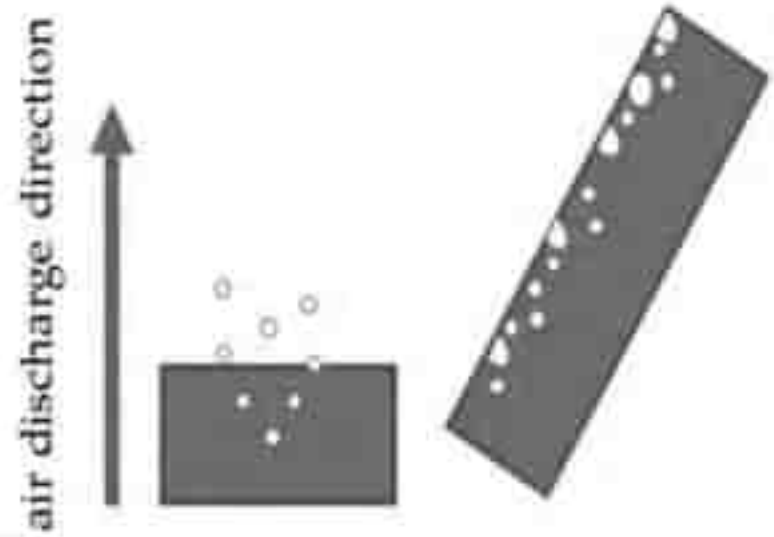

Figure 4. Degassing direction, a silicone mould on the left, and a glass mould on the right.

A high content of air, which is difficult to remove given the structure of diatoms, causes the formation of untypical composites. Prior to cross-linking, a typical composite forms a three-phase system, i.e., it consists of a liquid phase (epoxy resin), solid-phase (powder filler), and gaseous phase (entrapped air), while after degassing and cross-linking it becomes a single-phase system that only consists of the solid phase. For composites with diatomaceous earth, we originally also deal with a three-phase system, but due to difficulties with extracting air, for example from the inside of diatom frustules, after cross-linking the system becomes two-phased: the solid phase is formed by a cross-linked, filled resin, and the gaseous phase, by air entrapped inside the composite, including in diatom frustules. A small amount of air is also present in pre-degassed systems. Such samples will show properties (for example, mechanical properties) different from those of single-phase composites.

As mentioned above, systems cast in glass moulds feature an untypical distribution of air bubbles. Figure 5a presents both the upper and the lower parts of an epoxy panel filled in 70% with diatomaceous earth without degassing. On the top surface, we can clearly see a layer of cavities caused by air bubbles, which do not exist on the bottom surface, where the panel is smooth. Figure 5b presents the system with the highest filling level, which was degassed before being cast into a mould. Both for the upper and the lower part of the panel, the cavities caused by air bubbles are virtually non-existent, which proves very good degassing and possibly better mechanical properties of the systems. The photos in Figures 6–9 were taken to observe the surface structure and any defects in the composites. The photos in Figure 6 show the difference for the top surface of the samples cast in glass and in silicone, with and without degassing. The samples cast in glass and in silicone, which have been degassed, do not show any cavities caused by air bubbles, unlike the samples that have not been degassed. The large size of the cavities (Figure 6b) comes from the accumulation of bubbles by the surface.

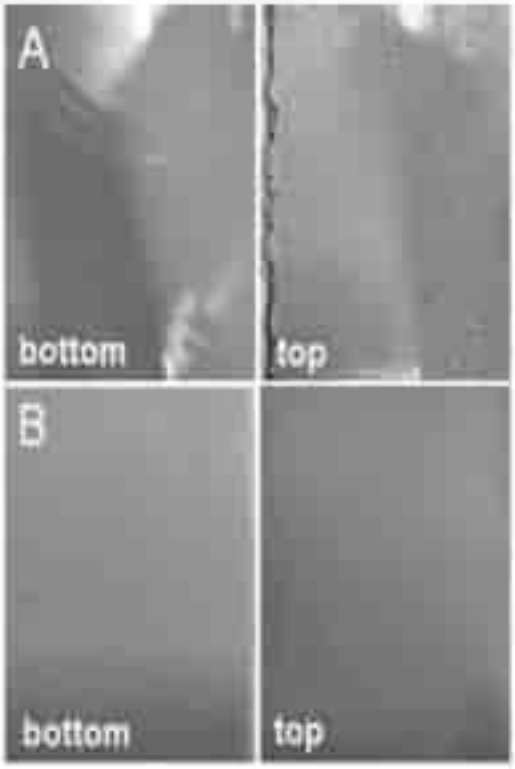

Figure 5. Panels cast in a glass mould, 70% of filling, (A)—without degassing, (B)—with degassing.

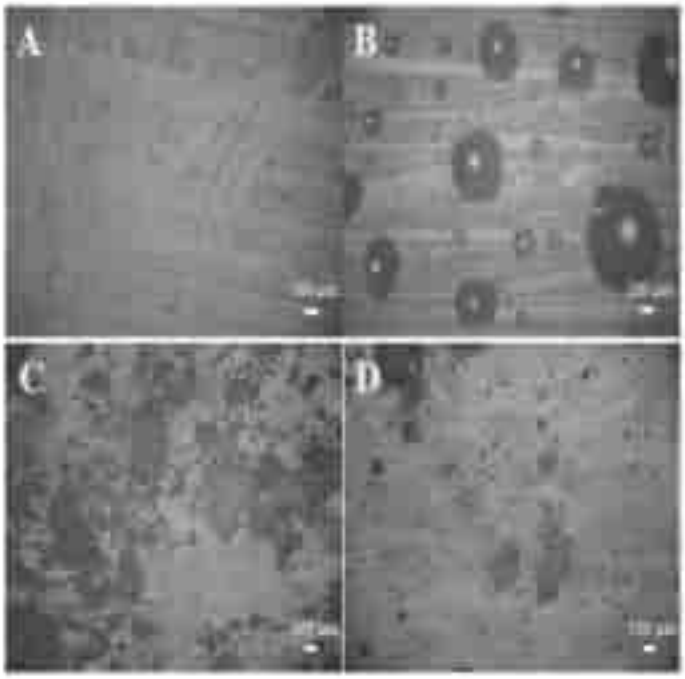

Figure 6. Photos of the samples' surfaces, upper part, (A)—glass, degassed; (B)—glass, non-degassed; (C)—silicone, degassed; (D)—silicone, non-degassed.

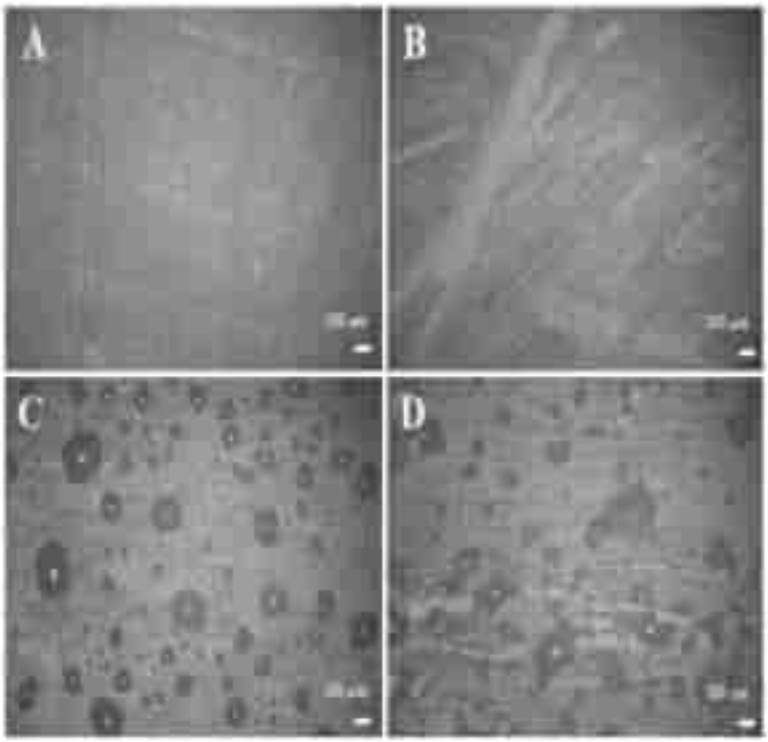

Figure 7. Surface of the samples: lower part. (A)—glass, degassed; (B)—glass, non-degassed; (C)—silicone, degassed; (D)—silicone, non-degassed.

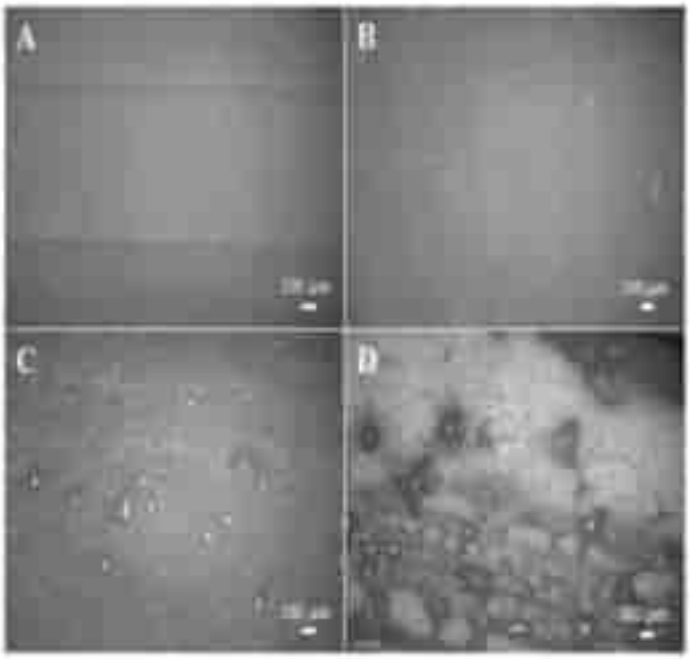

Figure 8. Photos of a side of the samples. (A)—glass, degassed; (B)—glass, non-degassed; (C)—silicone, non-degassed; (D)—silicone, degassed.

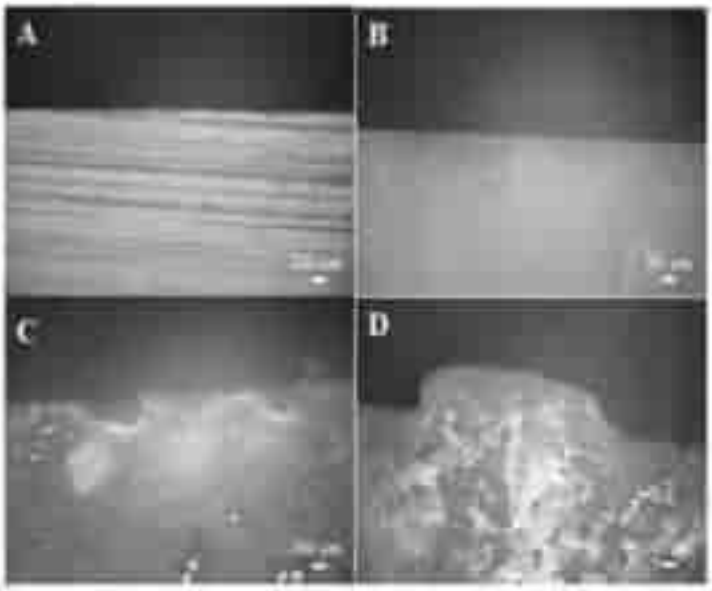

Figure 9. Photos of side edges of the samples. (**A**)—glass, degassed; (**B**)—glass, non-degassed; (**C**)—silicone, degassed; (**D**)—silicone, non-degassed.

Figure 7A–D present the bottom surface of the samples. We observed no difference between the samples cast in glass (Figure 7A,B); despite their different preparation (with or without degassing), their surfaces were almost identical. The air bubbles present in the non-degassed sample (Figure 7B) accumulated by the top surface, as mentioned above. The systems cast in silicone moulds (Figure 7C,D) also do not show any major differences in terms of the presence of air. Visible defects come from the reuse of the silicone moulds (missing fragments of the mould). The non-degassed sample (Figure 7D) contains partially embedded fragments of the silicone mould. The silicone mould, due to its short life and fast wear, adheres to the surface of composites, makes it difficult to remove the cross-linked sample, and, consequently, silicone fragments often remain on the bottom surface of the samples. This affects, for example, the hydrophobic and hydrophilic properties, as the removal of silicone before testing is hindered.

Figure 8A–D present the lateral section of the composites. The systems cast in glass must be cut with a CNC milling cutter prior to testing in order to obtain standardised samples. When a milling cutter moves across the sample, it leaves a characteristic mark after every plane of the milling path (Figure 8A). If the milled sample is not properly clamped during milling, and vibrations occur, the material gets chipped by the milling cutter (Figure 8B). The side wall of the samples cast in silicone includes cavities caused by mould defects (Figure 8C) but also many fragments being detached (Figure 8D). Both the degassed and non-degassed samples cast in glass moulds have a surface that is much more uniform than that of the samples cast in silicone moulds.

The photos of side edges (Figure 9A–D) of the samples allow us to obtain information on any defects that influence the systems' properties. The degassed samples cast in glass have an almost completely even edge with no defects, whereas the non-degassed samples produced with the same method show small, shallow cavities by their edge, which are caused by the presence of air bubbles. The composites cast in silicone moulds also have more defects. These include deep cavities caused by air bubbles, silicone fragments (Figure 9C) and large projections (Figure 9D), which are caused by the wear of the silicone mould, so by cavities that form on it, into which the resin penetrates. The observed defects have a considerable influence on the mechanical properties of the tested samples, as described further in this paper.

3.2. Density

The fractioning of diatomaceous earth by sedimentation causes a change in particle size distribution in the system. Base diatomaceous earth contains particles ranging from 0.5 to 200 µm, which form fractured bubbles (<4 µm), non-fractured bubbles (4–50 µm) and agglomerates (50–200 µm) [12], whereas fractionated diatomaceous earth contains a small quantity of fractured particles and does not contain any particles bigger than 30 µm. For this reason, the packing of diatomite particles in epoxy resin is lower than in a fractionated system (due to the absence of fractions smaller than 5 µm). Any air remaining in the inner structure of a diatom is released by being replaced with resin, thus increasing the liquid phase aeration, which in turn hinders degassing in a vacuum chamber. In consequence, the higher the filler concentration and its packing in the resin, the higher the air content in the final product. Particles of diatomaceous earth may be subject to the sedimentation of epoxy resin and to floatation (Figure 10C,D).

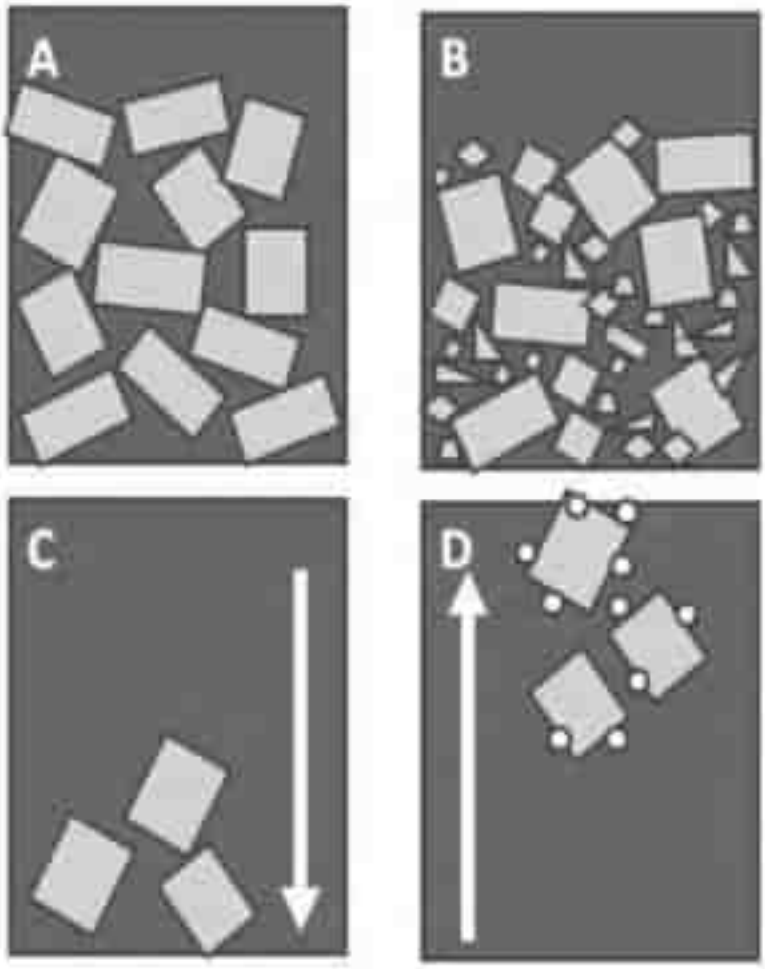

Figure 10. The mechanisms of packing and mobility of diatom frustules in an epoxy resin system. (A)—Manner of packing for a narrow particle size distribution, (B)—manner of packing for a wide particle size distribution (base diatoms), (C)—filler sedimentation in a resin, and (D)—filler floatation in a resin.

The bulk density of base diatoms is 0.271 g/cm^3, and of rinsed diatoms is 0.248 g/cm^3. A higher value for the base diatoms relates to the presence of particles of various sizes, which were removed from the sieved fraction during rinsing. Their presence increases the packing of particles and, consequently, reduces the air content between diatom frustules.

The rinsed fraction consists of diatoms with more uniform sizes, between which more air is accumulated (Figure 11). Depending on their size, diatoms force a high quantity of air into the epoxy resin. The base fraction, due to its higher packing and the presence of smaller particles as well, causes lower aeration of the system, whereas the rinsed fraction contains larger spaces between bubbles and more uniform fractules, which causes higher aeration. Gas extraction from systems modified with base diatoms is more difficult given the formation of agglomerates, while rinsed diatoms after the same degassing time contain less gas. A higher quantity of air remaining in non-fractionated systems compared to fractionated systems causes a dilution of the effects related to filler content; the trend becomes flattened. At high filling levels, density is compensated for by the quantity of air entrapped. For silicone moulds, we can clearly see the secondary degassing effect.

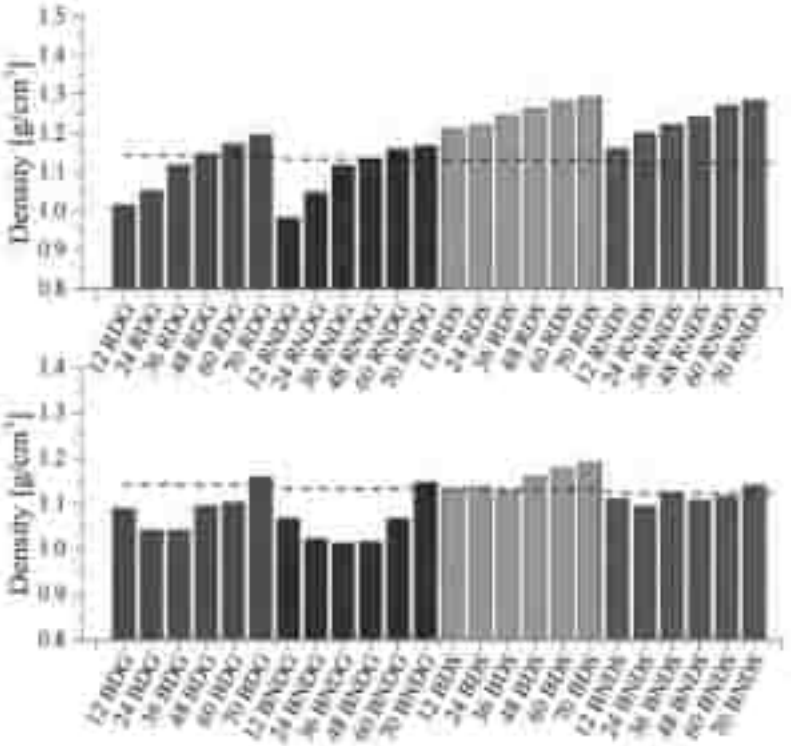

Figure 11. Density of degassed and non-degassed composites containing base diatoms and rinsed diatoms.

3.3. Mechanical Properties

3.3.1. Tensile Strength

Both for systems containing base diatoms and rinsed diatoms, it is clear that the degassing of mixtures before casting into moulds increases the tensile strength (Figure 12A,B). That increase is clearer for base diatoms, even at lower concentrations. A non-modified epoxy resin shows a tensile strength at 19.91 MPa, whereas in almost any system containing diatomaceous earth that value is higher, sometimes over two-fold. In addition, the rinsing process also contributes to the growth of strength parameters. Degassed systems containing 12% of base diatoms and those after rinsing show a tensile strength of 27.4 MPa and 44.7 MPa. The higher is the filler concentration, the higher are the values, which for the rinsed diatoms reach over 55.1 MPa and for the base diatoms are maximum of 43.8 MPa. Composites cast in silicone moulds, due to their structural defects, feature lower strength characteristics. The changing trend as a function of filler content is generally linear. This indicates that defects in the sample prevail over the behaviour of the composite. The use of glass moulds allows for observing real dependencies for the characterised

material. Difficulties with removing air from the composites also cause differences in the samples' mechanical strength. Systems with base diatoms show a lower tensile strength than systems with rinsed diatoms, which is caused by the presence of a higher quantity of air in the base diatoms after degassing. Both the breaking strength and the elongation at break (see Figure S1) grow along with increasing filler concentration. A higher quantity of diatomaceous earth facilitates degassing, which reduces the brittleness of materials. If composites are not degassed before being cast into moulds, their mechanical properties are reduced, whether for base or rinsed diatoms. The reduction is proportional to the content of filler, which is caused by the growing number of air bubbles pressed into the systems by the diatoms. Gülltürk, Taşdemirci et al. studied calcined and natural frustules filled epoxy matrices. The authors observed that debonding and pull-out may be the reason for the difference in mechanical properties when comparing neat epoxy resin and composites (the limited wetting of the filler surface by the matrix epoxy) [30,31].

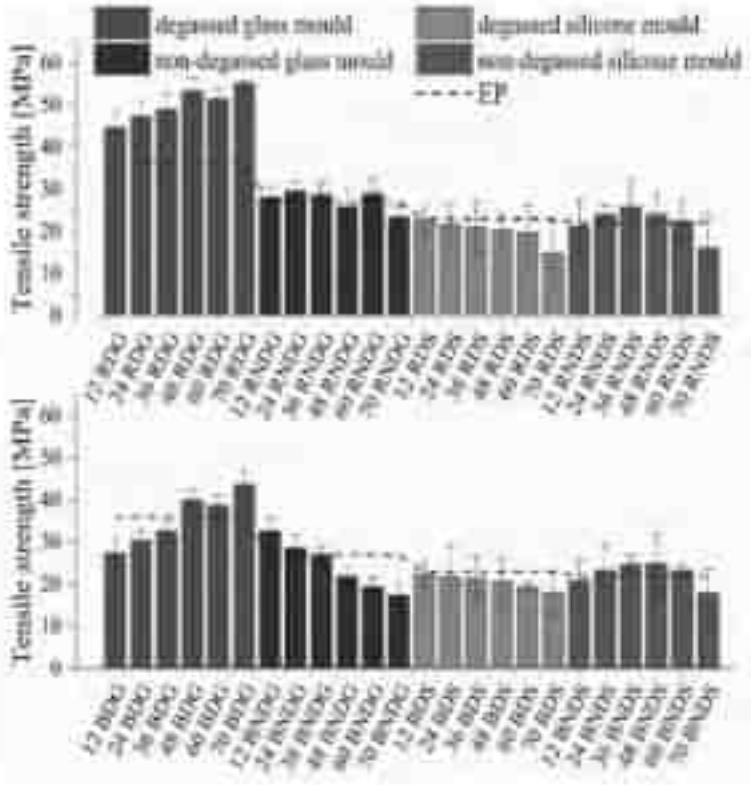

(A)

Figure 12. Cont.

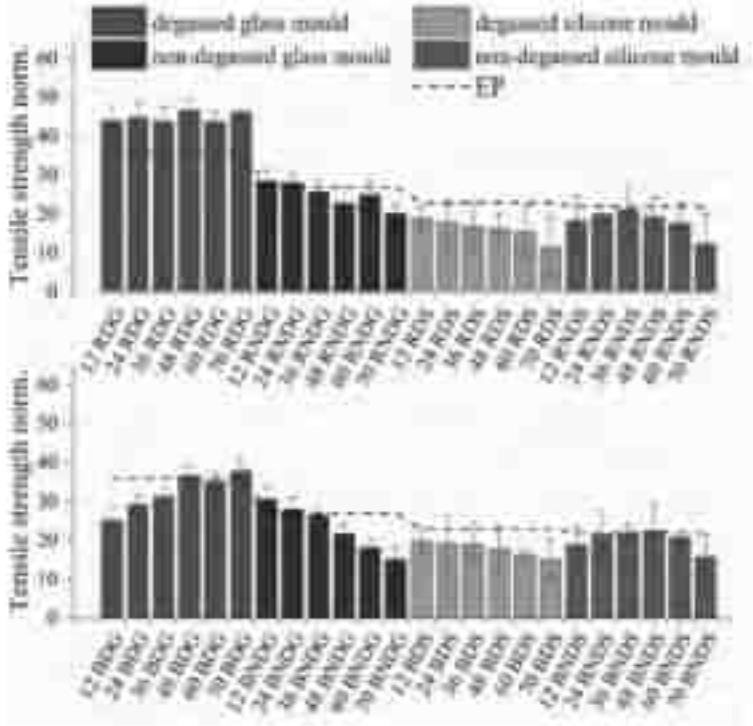

(B)

Figure 12. (**A**) Tensile strength for degassed and non-degassed composites containing base diatoms and rinsed diatoms. (**B**) Tensile strength for degassed and non-degassed composites containing base diatoms and rinsed diatoms, density normalized.

3.3.2. Flexural Strength

Flexural testing is considered an appropriate measure of strength because it combines elements of compression, tension, and shear, which more closely mimics in vivo stresses than either compression or tension testing alone [32]. Also, the produced composites were subjected to flexural testing with a three-point loading.

Figure 13 present the flexural module and flexural stress of diatom/epoxy resin composites. Degassed systems cast in glass moulds, containing both base and fractionated diatoms, feature a flexural modulus ranging from 4 to 5 GPa. There is no impact of filler concentration on mechanical properties. Higher differences are observed in non-degassed systems cast in glass. Flexural modulus values grow in line with the growing filler content in the system, which applies in particular to the samples with base diatoms. For the highest concentration (70% vol.) of base diatoms, the flexural modulus is 7.5 GPa, whereas at the same concentration the value for fractionated diatoms is 1.2 GPa lower. Degassed systems show a lower air content, so their flexural modulus values increase. This is caused by a reduced brittleness of the samples. For systems cast in silicone moulds, this trend is reversed. Flexural modulus for the degassed samples increases along with the growing concentration of modifier, whereas for the non-degassed samples the values are similar in the entire series, regardless of the modifier used. An addition of diatomaceous earth, irrespective of its type, reduces flexural stress in each case (see Figure S2A,B) compared to a non-modified resin, which is caused by the presence of air bubbles in diatomaceous earth. Non-degassed systems show an elongation at break that drops in line with the growing modifier concentration, which relates to the fact that a higher quantity of the added filler contains more air entrapped in form of vesicles. Degassed systems show an opposite relation: flexural stress grows (up to 92.5 MPa) in line with the growing diatom

concentration. As mentioned above, mixtures containing a higher quantity of modifier were easier to degas before cross-linking, thus the air content and, consequently, the brittleness of materials are lower. Systems cast in silicone moulds, whether degassed or non-degassed, have a similar flexural stress ranging from 27 to 61 MPa. We have neither observed any influence of filler type on flexural stress nor any presence of air in the systems.

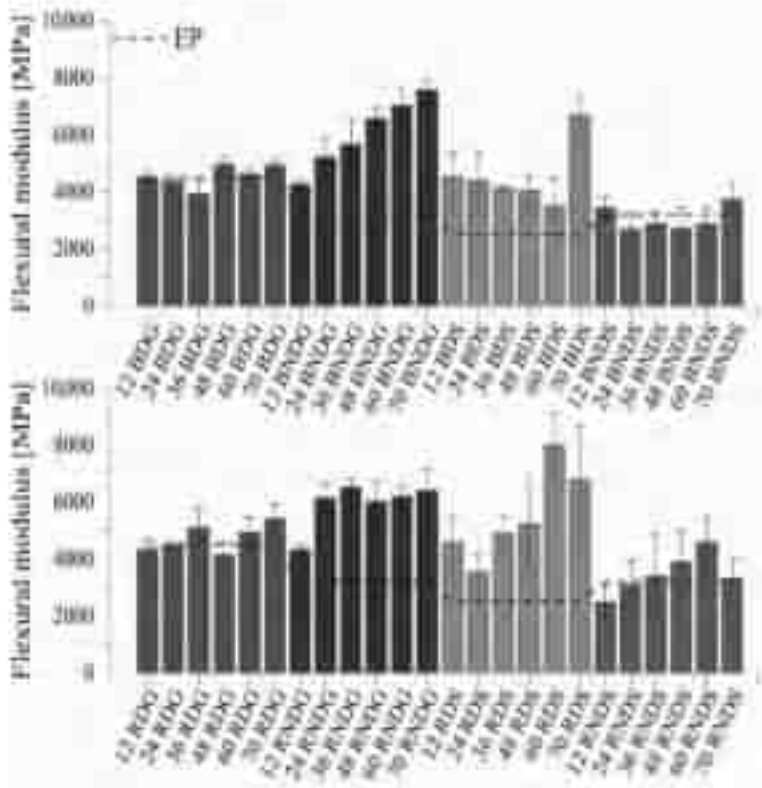

Figure 13. Flexural modulus for degassed and non-degassed composites containing base diatoms and rinsed diatoms.

3.3.3. Impact Strength

Figure 14A,B present the impact strength values. For most systems, it is similar and does not exceed 10 kJ/m^2, whereas degassed systems cast in glass moulds feature higher values. Both the samples containing base diatoms and those containing fractionated diatoms show an impact strength of over 10 kJ/m^2 up to nearly 26 kJ/m^2. The addition of base diatoms caused a linear growth of the value along with the growing modifier concentration, whereas fractionated diatomaceous earth shows the highest impact strength for systems containing 12% vol. (13 kJ/m^2); with a higher addition of modifier, the values linearly decrease. The differences in impact strength arise from the use of rinsing and from the degassing process. Systems containing air bubbles will have much lower impact strength values. The use of silicone moulds significantly contributes to the impairment of mechanical properties. Both degassed and non-degassed systems show, in most cases, impact strength values lower than that of a reference epoxy resin. It can be seen that, in this case, the deterioration of mechanical properties is not influenced by the filler type or the degassing of the systems prior to casting.

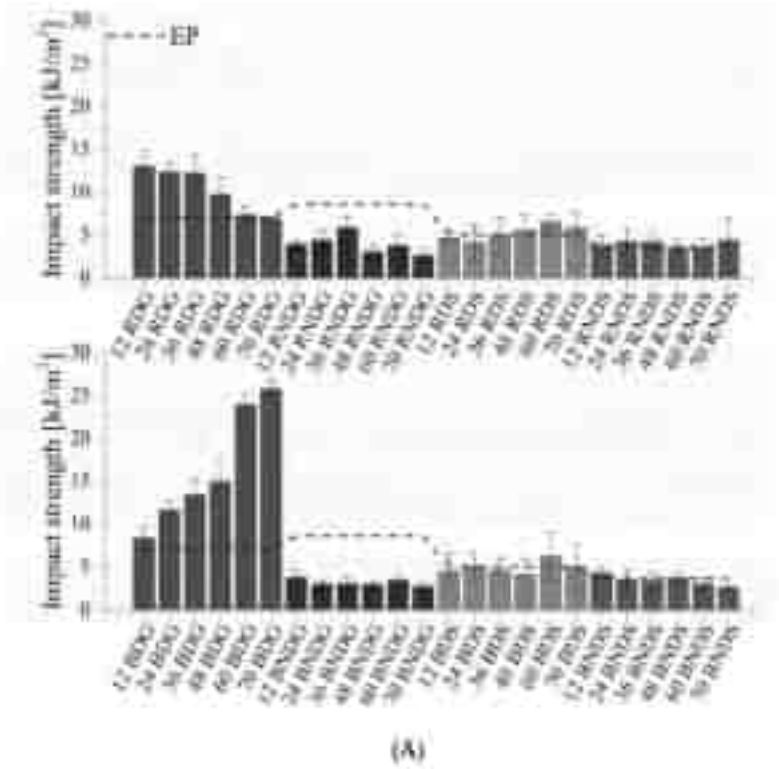

(A)

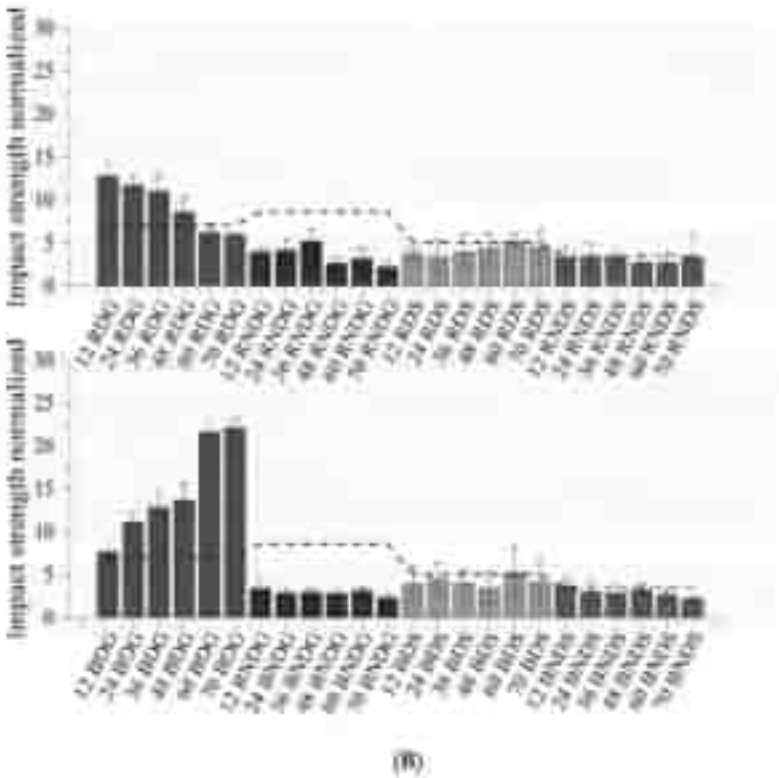

(B)

Figure 11. (A) Impact strength for systems containing base and fractionated diatoms. (B) Impact strength for systems containing base and fractionated diatoms, density normalized.

3.3.4. Standard Deviations

As mentioned above, a number of factors have an influence on the uniformity of the results of mechanical property tests conducted on filled composites. Figure 17 presents the standard deviations from the tensile strength value.

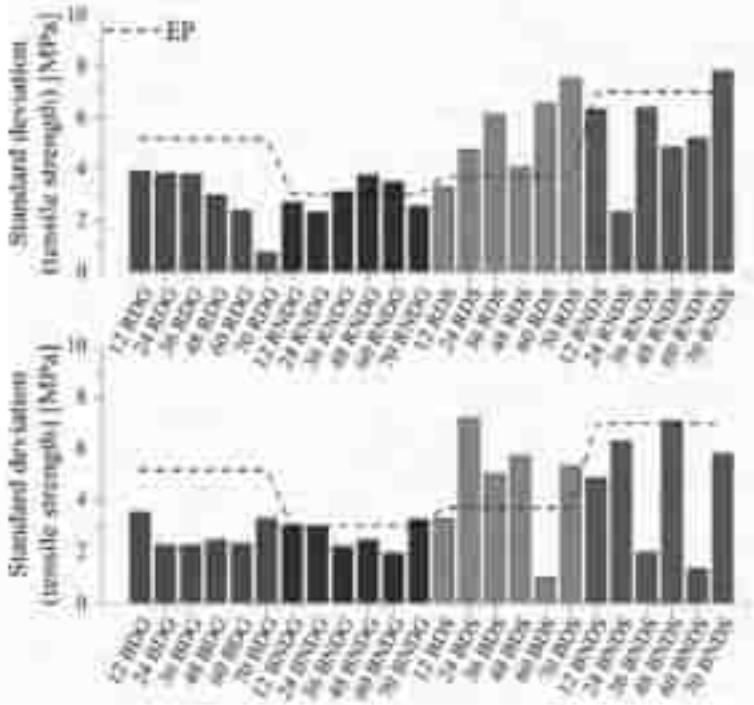

Figure 18. Standard deviations from the tensile strength value for systems containing base and fractionated diatoms.

Standard deviations for systems modified with base diatoms and rinsed diatoms fall within similar ranges. The maximum value of 4 MPa is reached by systems cast in glass moulds, while the value of 8 MPa is reached by a standard deviation for samples cast in silicone moulds. Rinsed systems cast in glass moulds, where degassing was used, indicate that the higher is the modifier content, the lower is the error bar, which is due to the higher homogeneity of material and the absence of defects caused by air bubbles. The values of standard deviation at the maximum elongation (see Figure 53) are much lower for systems containing base diatoms. This proves a better filler dispersion in the composite matrix. In addition, there are no significant differences between the deviation for samples cast in glass and in silicone moulds. Clearer differences exist in systems modified with rinsed diatoms. Higher standard deviation values exist for systems cast in silicone moulds.

The standard deviations from the flexural modulus (Figure 16) for systems cast in glass moulds do not differ considerably between samples modified with rinsed diatoms and with base diatoms. In each case, the deviation is lower than that for a reference epoxy resin. Much higher deviation values exist for systems cast in silicone moulds (up to nearly 1900 MPa for 70% of rinsed diatoms), while an analogical sample cast in a glass mould shows a deviation of 530 MPa. This is similar to the results of the standard deviation in flexural stress (see Figure 54). Systems filled with base diatoms show lower deviations than those filled with rinsed diatoms. The standard deviation from the impact strength value (see Figure 55) is similar for systems modified with rinsed diatoms and with base diatoms. We can see a difference between the values for degassed and non-degassed samples. The values for non-degassed systems are lower, whether for glass or silicone moulds. Secondary agglomerates of the diatomite formed in the curing resin are a source

of irregular mechanical defects (stress concentration centres or crack propagation sites), which result in unpredictable mechanical failure of the samples, which in turn causes an increased standard deviation. This secondary agglomeration effect is increased during degassing of the resin/filler compositions. This observation leads to a conclusion that diatomite should be initially properly surface-treated to improve the stabilization of its particles in epoxy compositions.

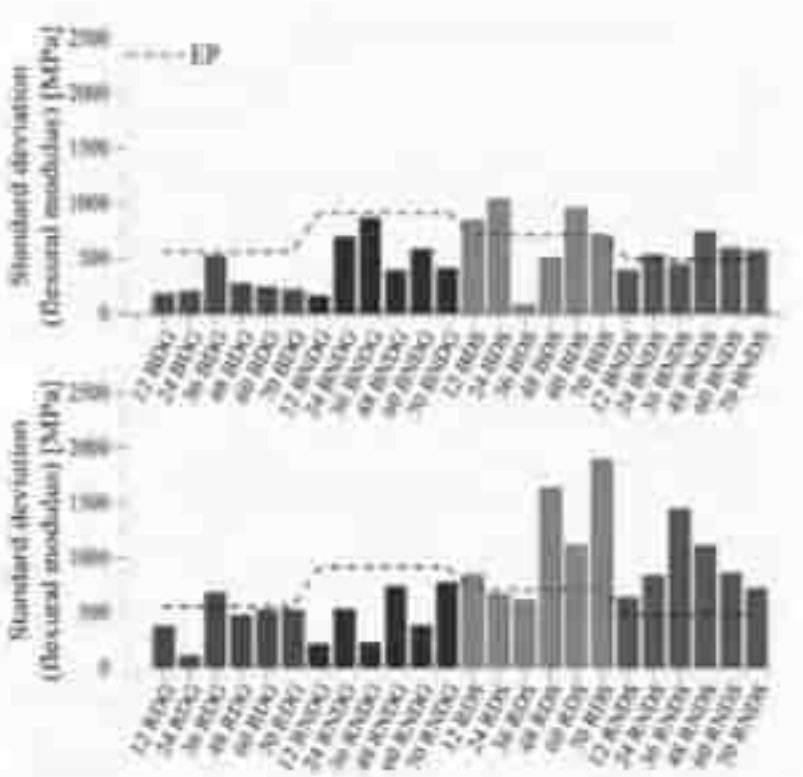

Figure 16. Standard deviations from the flexural modulus value for systems containing base and fractionated diatomite.

3.4. Thermal Analysis Results

DSC analysis was performed to study thermal behaviour of the composites (Figure 17). Two heating cycles were performed to register the most characteristic features of the thermal behaviour of the epoxy resin materials during their thermal treatment. In the first cycle, a sharp, low-temperature peak is observed at ~65 °C, which corresponds to the glass transition of the residually uncured resin (T_{gu}). The residually uncured resin has much more polymer chain freedom due to lower cross-linking density when compared to fully cured resin, which results in a stronger endothermic effect. It can be seen that the diatomaceous earth/epoxy composites show slightly higher T_{gu} values, which can be explained by the fact that the filler acts as a heat insulator that delays the flow of heat into the samples. In the 80–160 °C range we can observe post-curing, as the remaining reactive epoxy and amino groups undergo a cross-linking reaction. During the second heating cycle, glass transition (T_g) is observed at a higher temperature and with a significantly lower endothermic effect, which are both related to a reduced freedom of the cross-linked polymer chains. Again, a heat-insulating effect of the filler is observed, as the T_g of the diatomite composites is notably higher. This effect can be correlated with the filler loading, as the samples with a higher filling ratio showed higher temperatures.

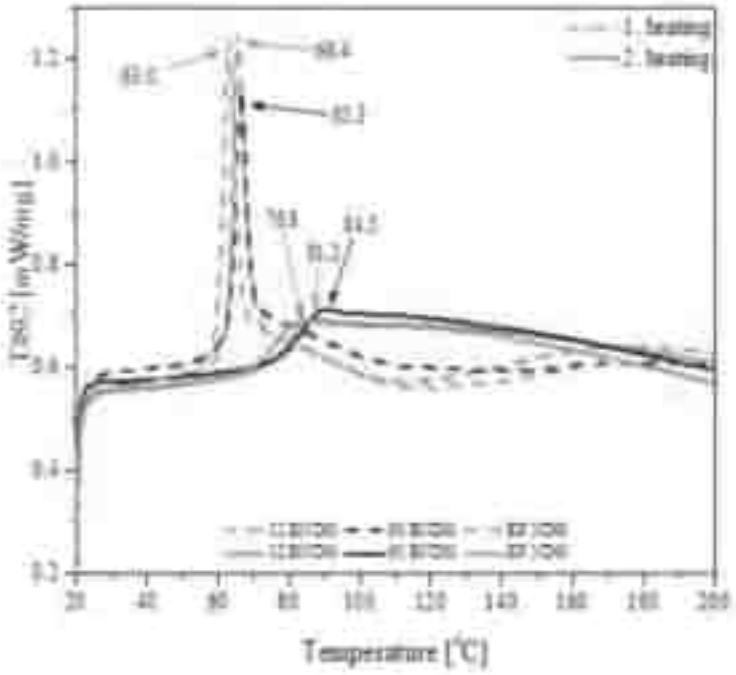

Figure 17. DSC curves recorded for samples of neat epoxy resin, and 12% and 40% BNDG.

4. Conclusions

The conducted tests were aimed to determine the impact of the manner of obtaining tests samples of epoxy/diatom frustule composites on the results of mechanical property measurements and on the existence of measuring errors. The tests have shown a significant impact of the applied method of casting test samples on a statistical dispersion of measuring results and on the mechanical properties obtained. The use of a silicone mould, given its relatively large area of contact with the environment, facilitates the degassing of any air that remains in the samples during cross-linking of the composite. At the same time, reusable silicone moulds cause defects on the test samples, which translates into repeating measurement errors. In the event of an improper degassing of the resin, the use of a glass mould angled at 60° causes sedimentation of air bubbles on the top surface of the composite and the formation of a porous layer that is 400 to 900 µm thick. Additionally, composites cast in a glass mould have a more homogeneous composition than those cast in silicone moulds, where the filler accumulates in the upper part of the sample. When using a specific filler such as diatom frustules (extended inner microstructure containing air), degassing issues grow along with the growing content of the filler in the resin. In such a case, complete removal of gas from the diatom frustule space for fast cross-linking resins is virtually impossible. The use of a silicone mould, unlike a glass mould, causes dimensional heterogeneity of the obtained composite samples, which also translates into measuring errors, and additionally, a (concave or convex) meniscus was observed, which had an impact on the low repeatability of dimensions of the samples and on measuring errors. The systems produced in glass moulds showed even edges, constant dimensions and, consequently, a higher repeatability of results. The systems cast in glass moulds feature a higher tensile strength and elongation at break than the systems cast in silicone, which is probably due to (samples were non-coaxial or out of the plane of measurement) misalignment of the samples cast in silicone, which causes faster cracking (the impact of complex stresses on the sample). The tests constitute a set of guidelines and recommendations for testing with the use of fillers showing an extended inner structure.

Supplementary Materials: The following are available online at https://www.mdpi.com/article/10.3390/ma14216607/s1, Figure S1: Elongation at break for degassed and non-degassed composites containing base diatoms and rinsed diatoms; Figure S2: (**A**) Flexural stress for degassed and non-degassed composites containing base diatoms and rinsed diatoms, (**B**) Flexural stress for degassed and non-degassed composites containing base diatoms and rinsed diatoms, density normalized; Figure S3: Standard deviation at the maximum elongation for degassed and non-degassed composites containing base diatoms and rinsed diatoms; Figure S4: Standard deviation at the flexural stress for degassed and non-degassed composites containing base diatoms and rinsed diatoms; Figure S5: Standard deviations at the impact strength for degassed and non-degassed composites containing base diatoms and rinsed diatoms.

Author Contributions: Conceptualization, R.E.P.; measurements, evaluation, and interpretation, M.D., J.G., D.B., R.D. and R.E.P.; imaging, M.G. and J.B.; writing—original draft, R.D., R.E.P., D.B. and M.D.; writing—review and editing, M.D., D.B., R.E.P., R.D. and K.J.K.; supervision, R.D., R.E.P. and K.J.K. All authors have read and agreed to the published version of the manuscript.

Funding: This work was financially supported in the frame of the project "Advanced Biocomposites for Tomorrow's Economy BIOG-NET", FNP POIR.04.04.00-00-1792/18-00, project is carried out within the TEAM-NET programme of the Foundation for Polish Science co-financed by the European Union under the European Regional Development Fund.

Institutional Review Board Statement: Not applicable.

Informed Consent Statement: Not applicable.

Data Availability Statement: Data available in a publicly accessible repository.

Conflicts of Interest: The authors declare no conflict of interest.

References

1. Jemutai-Kimosop, S.; Orata, F.; Shikuku, V.O.; Okello, V.A.; Getenga, Z.M. Insights on adsorption of carbamazepine onto iron oxide modified diatomaceous earth: Kinetics, isotherms, thermodynamics, and mechanisms. *Environ. Res.* **2020**, *180*, 108898. [CrossRef] [PubMed]
2. Zhen, Y.; Zhang, J.; Wang, W.; Li, Y.; Gao, X.; Xue, H.; Hayat, T. Embedded SnO_2/Diatomaceous earth composites for fast humidity sensing and controlling properties. *Sens. Actuators B Chem.* **2020**, *303*, 127137. [CrossRef]
3. Ghobara, M.M.; Mohamed, A. Diatomite in use: Nature, modifications, commercial applications and prospective trends. In *Diatoms: Fundamentals and Applications*; Seckbach, J., Gordon, R., Eds.; Wiley: Hoboken, NJ, USA, 2019.
4. Mohamed, E.A.; Selim, A.Q.; Zayed, A.M.; Komarneni, S.; Mobarak, M.; Seliem, M.K. Enhancing adsorption capacity of Egyptian diatomaceous earth by thermo-chemical purification: Methylene blue uptake. *J. Colloid Interface Sci.* **2019**, *534*, 408–419. [CrossRef] [PubMed]
5. Aphirak, C. Effects of thermal and acid treatments on some physico-chemical properties of lampang diatomite. *Suranaree J. Sci. Technol.* **2004**, *11*, 289–299.
6. Tsai, W.T.; Lai, C.W.; Hsien, K.J. Characterization and adsorption properties of diatomaceous earth modified by hydrofluoric acid etching. *J. Colloid Interface Sci.* **2006**, *297*, 749–754. [CrossRef]
7. Şan, O.; Gören, R.; Özgür, C. Purification of diatomite powder by acid leaching for use in fabrication of porous ceramics. *Int. J. Miner. Process.* **2009**, *93*, 6–10. [CrossRef]
8. Benkacem, T.; Hamdi, B.; Chamayou, A.; Balard, H.; Calvet, R. Physicochemical characterization of a diatomaceous upon an acid treatment: A focus on surface properties by inverse gas chromatography. *Powder Technol.* **2016**, *294*, 498–507. [CrossRef]
9. Yang, X.; Sun, Z.; Zheng, S. Physical purification of diatomite based on laminar-flow centrifugal separation. *Physicochem. Probl. Miner. Process.* **2014**, *50*, 705–718. [CrossRef]
10. Jung, K.W.; Jang, D.; Ahn, K.H. A novel approach for improvement of purity and porosity in diatomite (diatomaceous Earth) by applying an electric field. *Int. J. Miner. Process.* **2014**, *131*, 7–11. [CrossRef]
11. Sun, Z.; Yang, X.; Zhang, G.; Zheng, S.; Frost, R.L. A novel method for purification of low grade diatomite powders in centrifugal fields. *Int. J. Miner. Process.* **2013**, *125*, 18–26. [CrossRef]
12. Dobrosielska, M.; Dobrucka, R.; Gloc, M.; Brząkalski, D.; Szymański, M.; Kurzydłowski, K.J.; Przekop, R.E. A new method of diatomaceous earth fractionation—A bio-raw material source for epoxy-based composites. *Materials* **2021**, *14*, 1663. [CrossRef] [PubMed]
13. Lee, B.S.; Feng, C.T.; Lin, K.H.; Lin, W.C.; Shu, Y.L.; Shu, C.M. Effectiveness and application of modified wind turbine coating: Adding ionic liquids to titanium dioxide and diatomaceous earth. *J. Loss Prev. Process Ind.* **2021**, *72*, 104566. [CrossRef]
14. Udele, K.E.; Morrell, J.J.; Sinha, A. Biological durability of cross-laminated timber—The state of things. *For. Prod. J.* **2021**, *71*, 124–132.

15. Zhang, T.; Si, H.; Wang, Z.; Zhang, X.; Wang, Y.; Qiao, Y.; Wang, X. The curing kinetics and mechanical properties of epoxy resin composites reinforced by PEEK microparticles. *Polym. Test.* **2020**, *91*, 106781. [CrossRef]
16. Gómez-Laserna, O.; Irizar, P.; Lando, G.; Kortazar, L.; Irto, A.; Ruiz-Rubio, L.; Olazabal, M.A. Design of epoxy-silica hybrids based on cycloaliphatic diol of natural origin for conservation of lithic materials. *Prog. Org. Coat.* **2021**, *151*, 106028. [CrossRef]
17. Chiou, Y.C.; Chou, H.Y.; Shen, M.Y. Effects of adding graphene nanoplatelets and nanocarbon aerogels to epoxy resins and their carbon fiber composites. *Mater. Des.* **2019**, *178*, 107869. [CrossRef]
18. Kiroski, L.; Dongel, N. Effect of the layer structure of wooden floorings on dimensional stability under different relative humidity and water retention conditions. *For. Prod. J.* **2020**, *70*, 122–131.
19. Guo, S.Y.; Zhang, X.; Ren, J.; Chen, J.Z.; Zhao, T.J.; Li, T.W.; Zhang, L. Preparation of TiO_2/epoxy resin composite and its effect on mechanical and bonding properties of OPC mortars. *Constr. Build. Mater.* **2021**, *272*, 121960. [CrossRef]
20. Shaikh, A.J.; Hepburn, D.M.; Kemp, I.J.; Cooper, J.M. The absorption of mould release agent by epoxy resin. *Polym. Degrad. Stab.* **2000**, *70*, 253–258. [CrossRef]
21. Nogueira, P.; Ramirez, C.; Torres, A.; Abad, M.J.; Cano, J.; Lopez, J.; Barral, L. Effect of water sorption on the structure and mechanical properties of an epoxy resin system. *J. Appl. Polym. Sci.* **2001**, *80*, 71–80. [CrossRef]
22. Cheng, J.; Wang, J.; Yang, S.; Zhang, Q.; Huo, S.; Zhang, Q.; Ding, G. Benzimidazolyl-substituted cyclotriphosphazene derivative as latent flame-retardant curing agent for one-component epoxy resin system with excellent comprehensive performance. *Compos. Part B Eng.* **2019**, *177*, 107440. [CrossRef]
23. Wan, Y.J.; Gong, L.X.; Tang, L.C.; Wu, L.B.; Jiang, J.X. Mechanical properties of epoxy composites filled with silane-functionalized graphene oxide. *Compos. Part A Appl. Sci. Manuf.* **2014**, *64*, 79–89. [CrossRef]
24. Pan, L.; Ben, J.; Lu, S.; Chen, G.; Yang, J.; Luo, Q.; Yu, J. Improving thermal and mechanical properties of epoxy composites by using functionalized graphene. *RSC Adv.* **2015**, *5*, 60596–60607. [CrossRef]
25. Medina, R.; Haupert, F.; Schlarb, A.K. Improvement of tensile properties and toughness of an epoxy resin by nanozirconium-dioxide reinforcement. *J. Mater. Sci.* **2008**, *43*, 3245–3252. [CrossRef]
26. Ruamcharoen, P.; Umaree, S.; Ruamcharoen, J. Relationship between tensile properties and morphology of epoxy resin modified by epoxidised natural rubber. *J. Mater. Sci. Eng.* **2011**, *5*, 504–510.
27. *EN ISO 527-1:2012 Plastics—Determination of Tensile Properties—Part 1: General Principles*; PKN: Warsaw, Poland, 2013.
28. *EN ISO 178:2010 Plastics—Determination of Flexural Properties*; PKN: Warsaw, Poland, 2011.
29. *ISO 179-1:2010 Plastics—Determination of Charpy Impact Properties—Part 1: Non-Instrumented Impact Test*; PKN: Warsaw, Poland, 2010.
30. Gültürk, E.; Güden, M.; Taşdemirci, A. Calcined and natural frustules filled epoxy matrices: The effect of volume fraction on the tensile and compression behavior. *Compos. Part B Eng.* **2013**, *44*, 491–500. [CrossRef]
31. Taşdemirci, A.; Yüksel, S.; Karsu, D.; Gültürk, E.; Hall, I.W.; Güden, M. Diatom frustule-filled epoxy: Experimental and numerical study of the quasi-static and high strain rate compression behavior. *Mater. Sci. Eng. A* **2008**, *480*, 373–382. [CrossRef]
32. Farid, M.Y.; Raji, R.; Chattopadhyay, A. The ratio of flexural strength to uniaxial tensile strength in bulk epoxy resin polymeric materials. *Polym. Test.* **2014**, *40*, 156–162. [CrossRef]

H3 - supplementary

Methodological Aspects of Obtaining and Characterizing Composites Based on Biogenic Diatomaceous Silica and Epoxy Resin

Dobrosielska M., Dobrucka R., Brząkalski D., Gloc M., Rębiś J., Głowacka J., Kurzydłowski K.J., Przekop R.E.; Materials, 14, 4607, 2021

materials

MDPI

Article

Methodological Aspects of Obtaining and Characterizing Composites Based on Biogenic Diatomaceous silica and Epoxy Resins

Marta Dobrowielska [1], Renata Dobrucka [2,3,*], Dariusz Brząkalski [1], Michał Głuc [1], Janusz Rębiś [1], Julia Głowacka [1], Krzysztof J. Kurzydłowski [1,3] and Robert E. Przekop [4,5]

[1] Faculty of Materials Science and Engineering, Warsaw University of Technology, ul. Wołoska 141, 02-507 Warsaw, Poland; Marta.Dobrowielska@pw.edu.pl (M.D.); michal.gluc@pw.edu.pl (M.G.); janusz.rebis@pw.edu.pl (J.R.); krzysztof.kurzydlowski@pw.edu.pl (K.J.K.)

[2] Department of Non-Food Products Quality and Packaging Development, Institute of Quality Science, Poznań University of Economics and Business, al. Niepodległości 10, 61-875 Poznań, Poland

[3] Faculty of Chemistry, Adam Mickiewicz University in Poznań, ul Uniwersytetu Poznańskiego, 61-614 Poznań, Poland; d.brzakalski@gmail.com

[4] Centre for Advanced Technologies, Adam Mickiewicz University in Poznań, ul. Uniwersytetu Poznańskiego 10, 61-614 Poznań, Poland; julia.glowacka@amu.edu.pl

[5] Faculty of Mechanical Engineering, Białystok University of Technology, Wiejska 45c, 15-351 Białystok, Poland

* Correspondence: Renata.Dobrucka@pw.edu.pl (R.D.); r.przekop@gmail.com, rprzekop@amu.edu.pl (R.E.P.)

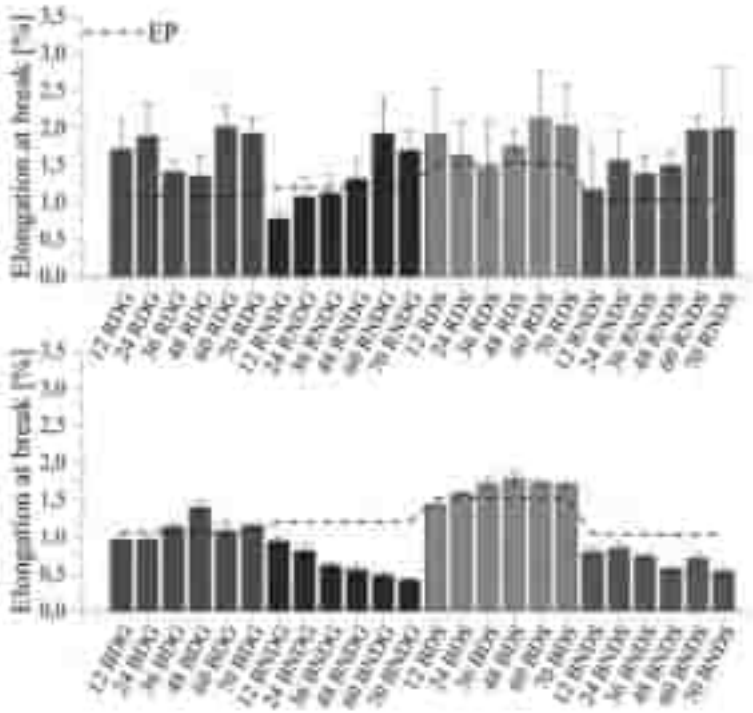

Figure 51. Elongation at break for degassed and non-degassed composites containing base diatoms and crushed diatoms.

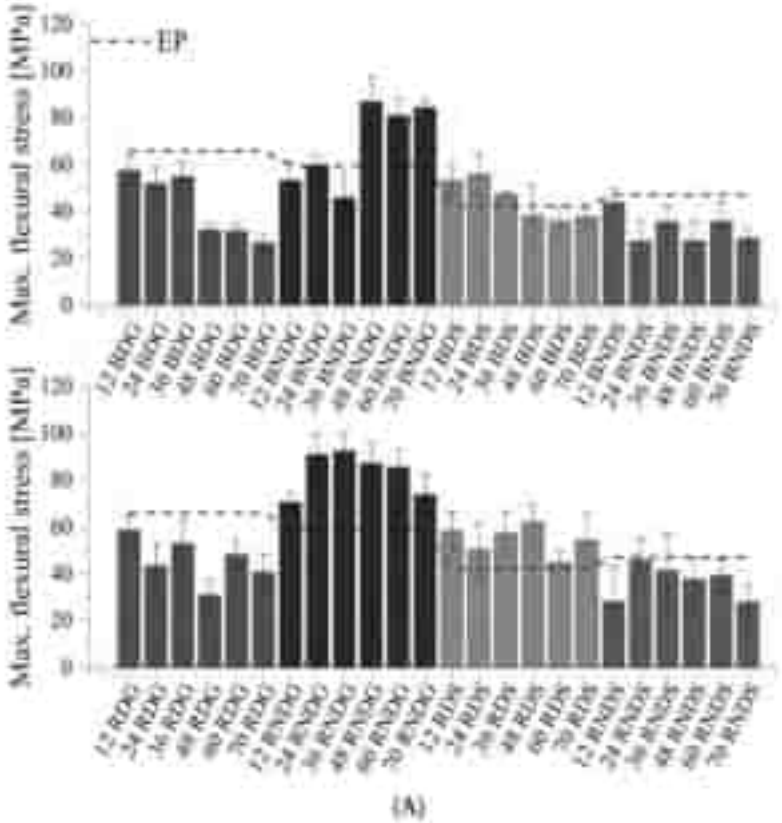

(A)

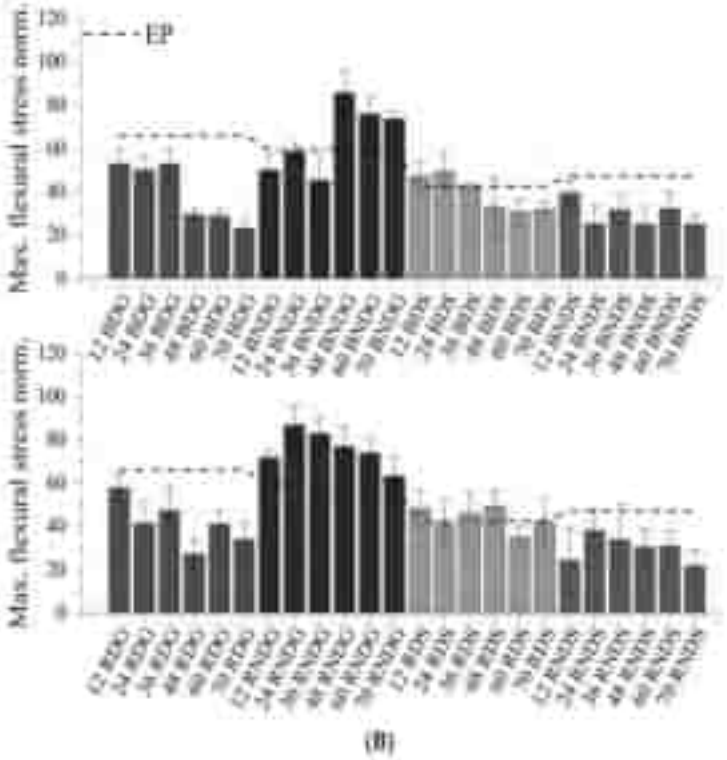

(B)

Figure 52 (A) Flexural stress for degassed and non-degassed composites containing base diatoms and rinsed diatoms; (B) Flexural stress for degassed and non-degassed composites containing base diatoms and rinsed diatoms, density normalized.

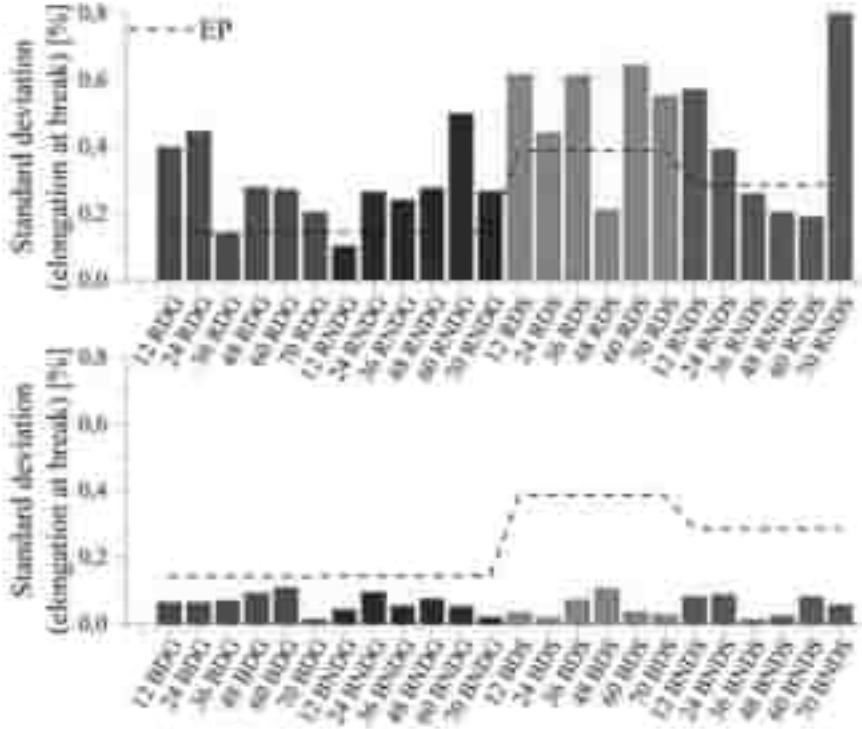

Figure S3. Standard deviation at the maximum elongation for degassed and non-degassed composites containing base diatoms and rinsed diatoms.

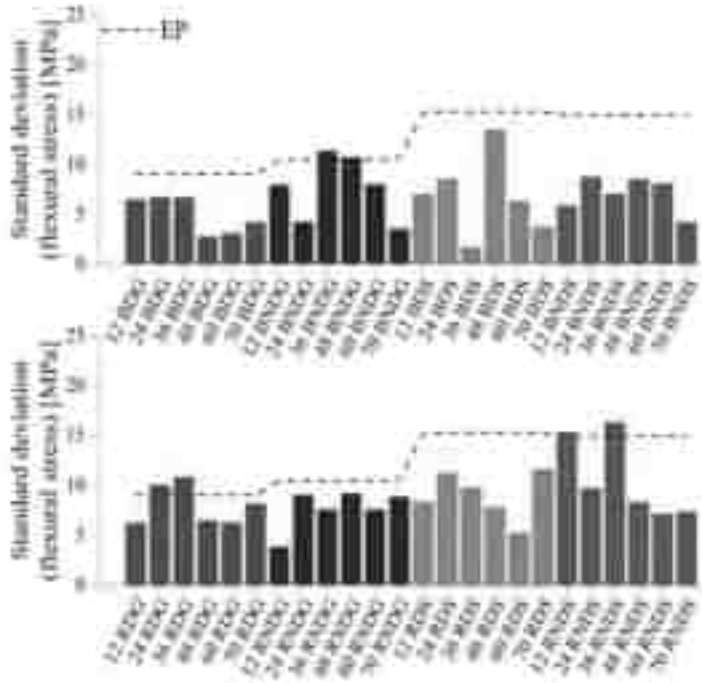

Figure S4. Standard deviation at the flexural stress for degassed and non-degassed composites containing base diatoms and rinsed diatoms.

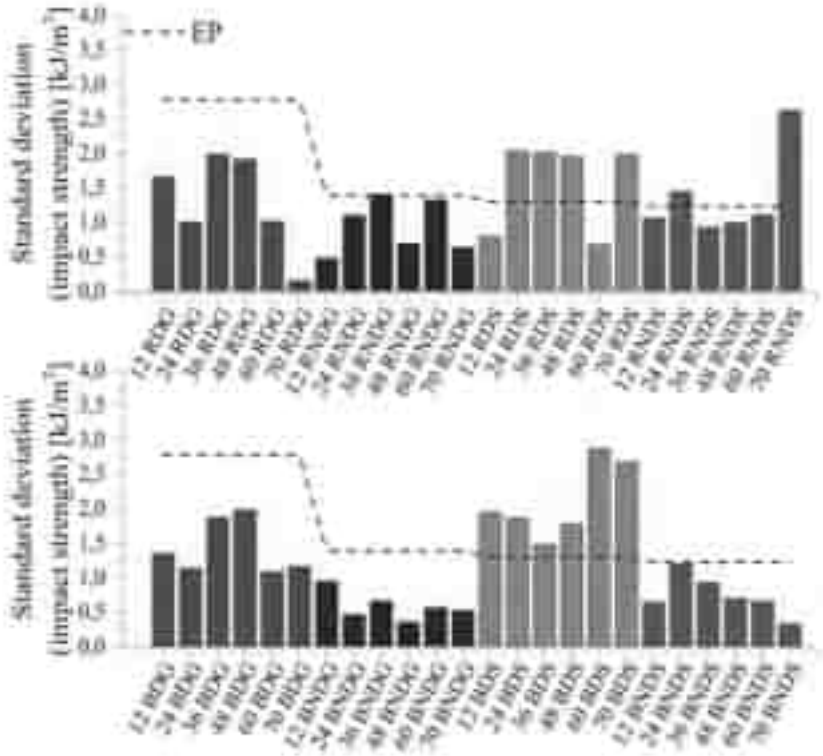

Figure 55. Standard deviation at the impact strength for degassed and non-degassed composites containing base diabetes and rinsed diatoms.

H4

Influence of Diatomaceous Earth Particle Size on Mechanical Properties of PLA/Diatomaceous Earth Composites

Dobrosielska M., Dobrucka R., Brząkalski D., Frydrych M., Kozera P., Wieczorek M., Jałbrzykowski M., Kurzydłowski K.J., Przekop R.E., Materials, 15, 3607, 2022

materials

MDPI

Article

Influence of Diatomaceous Earth Particle Size on Mechanical Properties of PLA/Diatomaceous Earth Composites

Marta Dobrosielska [1], Renata Dobrucka [2,*], Dariusz Bezgkalski [3], Miłosz Frydrych [3], Paulina Kozera [3], Monika Wieczorek [3], Marek Jałbrzykowski [4,5], Krzysztof J. Kurzydłowski [4] and Robert E. Przekop [5,*]

[1] Faculty of Materials Science and Engineering, Warsaw University of Technology, ul. Wołoska 141, 02-507 Warsaw, Poland; marta.dobrosielska@pw.edu.pl (M.D.); paulina.kozera@pw.edu.pl (P.K.); monika.wieczorek.dokt@pw.edu.pl (M.W.)

[2] Department of Non-Food Products Quality and Packaging Development, Institute of Quality Science, Poznań University of Economics and Business, al. Niepodległości 10, 61-875 Poznań, Poland

[3] Faculty of Chemistry, Adam Mickiewicz University in Poznań, ul. Uniwersytetu Poznańskiego 8, 61-614 Poznań, Poland; d.bezgkalski@gmail.com (D.B.); frydrych@amu.edu.pl (M.F.)

[4] Faculty of Mechanical Engineering, Bialystok University of Technology, ul. Wiejska 45c, 15-351 Białystok, Poland; m.jalbrzykowski@pb.edu.pl (M.J.); krzysztof.kurzydlowski@pw.edu.pl (K.J.K.)

[5] Centre for Advanced Technologies, Adam Mickiewicz University in Poznań, ul. Uniwersytetu Poznańskiego 10, 61-614 Poznań, Poland

* Correspondence: renata.dobrucka@put.poznan.pl or renata.dobrucka@ue.poznan.pl (R.D.); rprzekop@amu.edu.pl or rprzekop@gmail.com (R.E.P.)

check for updates

Citation: Dobrosielska, M.; Dobrucka, R.; Bezgkalski, D.; Frydrych, M.; Kozera, P.; Wieczorek, M.; Jałbrzykowski, M.; Kurzydłowski, K.J.; Przekop, R.E. Influence of Diatomaceous Earth Particle Size on Mechanical Properties of PLA/Diatomaceous Earth Composites. *Materials* **2022**, *15*, 3607. https://doi.org/10.3390/ma15103607

Academic Editor: Sandra Maior Fernandes Carvalho

Received: 20 March 2022
Accepted: 9 May 2022
Published: 18 May 2022

Publisher's Note: MDPI stays neutral with regard to jurisdictional claims in published maps and institutional affiliations.

Copyright: © 2022 by the authors. Licensee MDPI, Basel, Switzerland. This article is an open access article distributed under the terms and conditions of the Creative Commons Attribution (CC BY) license (https://creativecommons.org/licenses/by/4.0/).

Abstract: The fractionation of diatomaceous earth (DE) using sedimentation made it possible to obtain separate unbroken diatom fractions from broken or agglomerated bodies with a range of particle sizes. The produced filler was used to prepare polylactide (PLA)/diatomaceous earth biocomposite samples containing different particle sizes, which were subjected to mechanical testing (tensile strength, flexural strength, impact strength), colloidal testing (contact angle, color change test, SEM/EDS), and thermal testing (TGA, DSC, DMA). Modification of the PLA containing the smallest particle size with diatomaceous earth (Fraction 5) resulted in a higher impact strength compared to both the pure PLA and the PLA/DE composite that contained base diatomaceous earth. Furthermore, the melt flow rate was improved by more than 80 and 80% for the composite modified with fractionated diatomaceous earth (Fraction 4) compared to pure PLA and base diatomaceous earth, respectively. The elasticity of the composite was also improved from 3.3 GPa for pure polylactide to 4.4 GPa for the system containing the smallest diatomaceous earth particles (Fraction 5).

Keywords: diatomaceous earth; polylactide; particle size; mechanical properties; biocomposite

1. Introduction

For many years, an intense increase in the global production of plastic has been observed. This is due, among other factors, to the easy access to their raw materials, improved living standards, and thus a higher consumption. Domka [1] identified that the main objection to the production of plastics is the problem of their resistance to biodegradation and, hence, they remain unchanged in landfills for centuries. In the next few years, the plastics industry is expected to face challenges that are posed by the amendments to relevant directives, such as the requirement to reduce the environmental impact of certain plastic products, especially single-use plastics (SUP). Moreover, societal engagement and pro-environmental action can effectively counteract destruction to the environment [2]. The initiatives presented in the relevant directive are also seen in the wider context of the European Union's transition toward the idea of a circular economy, which is one of the key areas for the development of the European Union.

Degradation of the natural environment, development of climate policies, new pro-environmental regulations, and increasing consumer awareness/expectations are changing

how business is conducted. A circular economy linked to biological and technical cycles is guided by the following three main principles:

- Preserving and enhancing natural capital by the control of limited resources and the balancing of renewable resource flows;
- Optimizing raw material use by keeping products, components, and materials in circulation with their highest utility in both cycles;
- Developing system efficiency by identifying and removing negative externalities.

The developed concept of the circular economy is, therefore, an approach in which products and materials remain in circulation as long as possible, resulting in reduced waste at landfills. In response, the search for new materials to replace conventional thermoplastics has begun.

A ubiquitous thermoplastic, with many applications, that requires a reduction in its environmental impact is PLA. The latter is a biodegradable polymer derived from renewable resources with very attractive properties (good mechanical properties, biocompatibility, and good transparency) [3,4]. The main disadvantages of PLA include: rigidity, brittleness, possibility of a partial degradation during processing, the need for drying before processing, and a low resistance to deformation at higher temperatures [5]. To use PLA in certain applications, the properties of such a polymer are modified using various techniques, methods, and technologies. The properties of PLA can be modified by introducing different types of fillers and plasticizers [6], of either natural or synthetic origin. Examples of polylactide reinforced with, for example, natural fibers of various types [7], natural and synthetic zeolites [8], or carbon nanotubes [9] are described in the literature. Examples of synthetic additives to PLA, such as polyadipates, epoxidized oils, citrate esters, poly (ethylene glycol), and lactic acid oligomers, can be found in the literature [10]. Polylactide could also be modified with metallic particles such as silver, magnesium, iron and steel, silicon, boron nitride, hydroxyapatite, and other alternatives [11–13]. In addition, polylactide can be successfully modified with nanoparticles and made into films and used as packaging material in the food industry. For example, inorganic metal/metallic oxide, graphite and silica-based nanoparticles [14], zinc oxide (ZnO) nanofiller [15], nanoclay, nanocelluloses, carbon nanotube, and graphene [16] are used to produce PLA nanocomposites.

In this study, a naturally occurring filler (i.e., diatomaceous earth) is used. With this in mind, our paper acts as a response to the search for suitable alternatives to conventional polymer composites. Diatomaceous earth is chosen because of its unique properties and wide availability. Diatomite is characterized by its porous structure, developed specific surface area, and high silica content [17,18]. Moreover, diatomaceous frustules have a variety of particle sizes, averaging from 3 µm to 200 µm and sometimes up to 1 mm. In raw diatomite, there are both broken, unbroken frustules, and agglomerates particles [19]. Composites with diatomaceous earth are used in many fields, for example, in the packaging industry due to their reinforcement properties, as well as limiting diffusion of gases into the packaging [20]. Diatomaceous earth is also widely used in applications such as a filler material, an additive for dental fillings, a natural insecticide, an additive for membranes [21], and drug carriers [22]. To obtain individual fractions of diatomaceous earth, a sedimentation process is performed, which involves the time-dependent rate of descent of diatoms. Large particles drop more quickly, while smaller particles remain in suspension much longer, which enables their separation.

In previous papers [23,24], we focused on the creation of epoxy resin/diatomaceous earth composites, which allowed for an observation of the effects of the modifier on changes in the parameters of the uncured epoxy resin. Moreover, we investigated the effects of diatomaceous earth on the process of manufacturing composites and related difficulties. In this paper, we focus on polylactide-based composites that are modified with fractionated diatomaceous earth. The choice of this polymer is dictated by the desire to produce a fully ecological biocomposite, which enables biodegradation under appropriate environmental conditions and, thus, reduces the environmental impact compared to PP/PE-based composites. PLA/diatomaceous earth composites can potentially be used as packaging materials.

cutlery, cups, etc. The rationale for this potential application is two-fold: first, its superior biodegradability creates less environmental pollution and, secondly, the properties of the diatomaceous earth naturally imply that the product would be completely safe.

In this study, diatomaceous earth is fractionated using a sedimentation process and the fractions that result are then used to modify the polylactide and create composites. Composites that contain four different diatomaceous earth particle sizes (fraction 2, fraction 4, fraction 5, and base) and four different modifier concentrations (2.5%, 5%, 10%, and 15%) are obtained. Next, particle size tests (Dynamic Light Scattering—DLS) are conducted and SEM images of the sediments after fractionation are produced. In addition, mechanical, rheological, surface (contact angle), and ageing tests are performed on the composites.

2. Materials and Methods

2.1. Materials

Polylactide (PLA)-type Ingeo 4043D was purchased from NatureWorks (Minnetonka, Minneapolis, MN, USA). Diatomaceous earth (Perma-Guard, Beautiful, UT, USA) was derived from diatomite deposits. Synthetic wax WTH-8 microbeads were bought from WTH GmbH (Hamburg, Germany).

2.2. Preparation of Samples

2.2.1. Preparation of Diatomaceous Earth

Amorphous diatomaceous earth (Perma-Guard, Beautiful, UT, USA) (28 kg) was placed into Barrel 3 that can hold 180 L, which was then filled with demineralized water to approximately 100 L. The suspension was then mechanically stirred for 3 min (at a speed of 2000 rpm) and left to undergo sedimentation. After 2 h, the supernatant liquid was pumped into Barrel 4 by using a water pump and again left to undergo sedimentation; Barrel 3 was refilled with demineralized water to about 120 L. After 24 h, the supernatant liquid from Barrel 4 was transferred to Barrel 5. The suspension in Barrel 3 was mechanically stirred and, after 2 h, the supernatant liquid was pumped into Barrel 4. The sediment remaining in Barrel 3 was put into Barrel 2, and Barrel 2 was then filled with demineralized water of volume 140 L. As shown in Figure 1, the process was repeated until each sediment had been washed twice. After this event, the sediments were moved into barrels with lower numbers, while the supernatant liquid was pumped into barrels with higher numbers. At the end of the process, the remaining supernatant liquids were decanted, while the sediments were left to dry at 60 °C for 24 h. The obtained filler fractions together with masses of the sediments are shown in Table 1. The material loss of 1.358 kg, with an initial input of 28 kg of diatomaceous earth, arises because the smallest particles of diatomite do not sediment completely and they are removed together with the discarded supernatant liquid when pumping out.

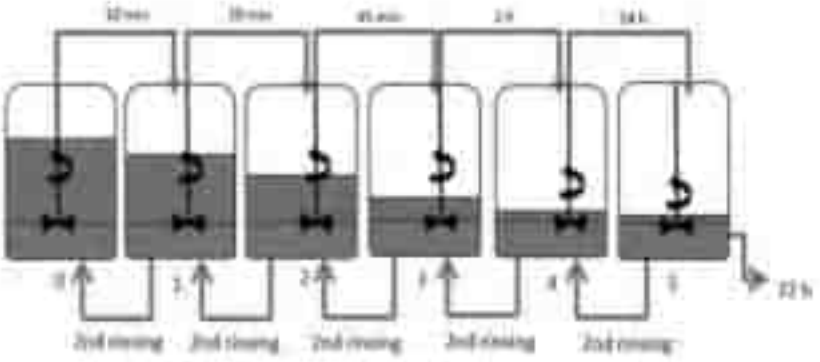

Figure 1. Diagram of diatomaceous earth fractionation.

Table 1. Percentage of individual diatomaceous earth fractions after fractionation using sedimentation.

	Sediment Mass [kg]	Percentage [%]
Sediment 0	0.592	2.23
Sediment 1	0.206	0.76
Sediment 2	1.934	7.25
Sediment 3	1.778	6.73
Sediment 4	16.730	62.78
Sediment 5	5.402	20.27
In total	26.642	100

The following diatomaceous earth fractions were selected for further testing: base, Fraction 2, Fraction 4, and Fraction 5. The detailed study of these fractions is given in Section 3.1. Characterization of the fillers. Base diatoms have every type of frustules (broken, unbroken, and agglomerates) and the proportion of the largest number of particles is average compared to fractionated diatoms. Fraction 2 was chosen because of the absence of agglomerates and an average particle size larger than the others, but also due to the relatively high percentage of sediment mass that is available for further testing. Fractions 4 and 5 have the smallest particle sizes but differ in both small and large particles. This choice of sediments enabled the possibility of testing the properties of the diatomaceous earth, which comprehensively depends on the particle size.

2.2.2. Preparation of Granulates

The ZAMAK MERCATOR WG 150/280 laboratory mill (Skawina, Poland) was used to homogenize polylactide (PLA 4043D) with base and fractionated diatomaceous earth. For this purpose, 300 g of PLA was plasticized at 210 °C for 15 min with diatomaceous earth added in portions so that the concentrations of 5, 10, 20, and 30% and 1% of WTH-B Microbeads synthetic wax were obtained. Wax-free systems were also prepared for comparison purposes. The systems were then ground using the WANNER C17.26 er mill (Łódź, Poland) and dried for 24 h at 80 °C.

2.2.3. Preparation of Final Samples

The prepared masterbatches were diluted 1:1 with PLA using the Engel e-victory 170/80 (Warsaw, Poland) injection molding machine. Table 2 shows the injection parameters. A holding pressure of linear increment over time was applied. The mold temperature was maintained at 80 °C. Test specimens for the mechanical testing, which accords with EN ISO 20753:2019-01, were obtained. The final concentrations of the systems are shown in Table 3.

Table 2. Injection parameters.

Temperature [°C]	Zone 1	Zone 2	Zone 3	Die
	195.0	200.0	185.0	190.0
Holding pressure		t [s] P [bar]	0.0 300.0	6.0 1500.0
Clamping force [kN]		Holding time [s]	cooling time [s]	screw diameter [mm]
600		6.0	50.0	25.0

2.3. Characterization Methods

For flexural and tensile strength tests, the materials obtained were printed into type-1B dumbbell specimens, in accordance with EN ISO 527:2012 and EN ISO 178:2006. The tests of the obtained specimens were performed on the INSTRON 5969 universal testing machine (Instron, Norwood, MA, USA) with a maximum load force of 50 kN. The traverse speed for the tensile strength and the flexural strength measurements were set at 2 mm/min.

The Charpy impact test (with no notch) was performed on the Instron Ceast 9050 impact-machine (Instron, Norwood, MA, USA) and accorded with ISO 179-1 (ISO 179-1:2010 Plastics—Determination of Charpy impact properties—Part 1: Non-instrumented impact test, PKN, 2010). The powder morphology was characterized by a scanning electron microscope (SEM, TM 1000 Hitachi, Tokyo, Japan) operating at an applied voltage of 5 kV. Before observations via the SEM, the samples surfaces were sputtered with a gold-palladium layer for 90 s at an electric current of 10 mA and voltage of 2 kV. The size of the diatoms used to prepare the composites was measured with a Mastersizer 3000 (Malvern Instruments Ltd., Malvern, UK). The measurements were taken for samples in water suspension (Hydro EV attachment). The parameters of the measurements for the wet samples were a stirrer revolution speed of 2330 RPM and an ultrasound power of 70%. Contact angle analyses were performed by use of the sessile drop technique (5 µL) at room temperature and atmospheric pressure, with the Krüss DSA100 goniometer (Krüss Optronic GmbH, Hamburg, Germany). Ageing tests were performed in the ESPEC ARS-0220 environmental stress chamber using 10 heating and cooling cycles of −10 °C ÷ 50 °C at an 85% humidity. The melt flow rate (MFR) was measured using the Instron CEAST MF20 melt flow tester (Instron, Norwood, MA, USA), which accords to EN ISO 1133 at 210 °C for a load of 2.16 kg. The thermal properties of the materials were studied using a Q1000 Differential Scanning Calorimeter (TA Instruments, New Castle, DE, USA). Samples with a weight of 8.0 ÷ 0.2 mg were placed into an aluminium hermetic pan. First, the samples were equilibrated at −90 °C, then heated to 280 °C with a scan rate of 10 °C/min, and cooled to −90 °C with a scan rate of 10 °C/min. Finally, they were again heated to 280 °C with a scan rate of 10 °C/min. The process was conducted in a nitrogen atmosphere. Using Universal V4.5A TA software (TA Instruments, New Castle, DE, USA), the glass transition temperature (T_g) was determined as the midpoint of the glass transition temperature range. The cold crystallization temperature (T_c) and melting temperature I were taken as the peak temperatures of the cold crystallization and melting, respectively. The measurements for the hiding power were performed by placing samples of the prepared resin systems into the optical path between the light source (LED) and the UV-NIR spectrophotometer, a AvaSpec-Mini2048CL (Avantes, Louisville, CO, USA). Dynamic mechanical analysis (DMA) was performed using a Q800 DMA (TA Instruments, New Castle, DE, USA) using a dual cantilever mode that accords to ASTM D4065-01. From each composite, three rectangular specimens, which were 60 mm long and 10 mm wide, were cut and used in the testing. The analysis was conducted from 0 °C to 130 °C, with a heating rate of 3 °C/min at a frequency of 1 Hz and amplitude of 30 µm. The glass transition temperature (T_g) was determined from the peak value in the storage modulus, the loss modulus, and the damping factor curves.

Table 3. Final concentrations of the tested systems.

Sample Name	Short Name	Sample Name	Short Name
PLA + 2.5% Fraction 2 + 0.5% WTH-II	2.5Fr2SW	PLA + 2.5% Fraction 4 + 0.5% WTH-II	2.5Fr4SW
PLA + 5% Fraction 2 + 0.5% WTH-II	5Fr2SW	PLA + 5% Fraction 4 + 0.5% WTH-II	5Fr4SW
PLA + 10% Fraction 2 + 0.5% WTH-II	10Fr2SW	PLA + 10% Fraction 4 + 0.5% WTH-II	10Fr4SW
PLA + 15% Fraction 2 + 0.5% WTH-II	15Fr2SW	PLA + 15% Fraction 4 + 0.5% WTH-II	15Fr4SW
PLA + 15% Fraction 2	15Fr2	PLA + 15% Fraction 4	15Fr4
PLA + 2.5% Fraction 5 + 0.5% WTH-II	2.5Fr5SW	PLA + 2.5% base + 0.5% WTH-II	2.5BSW
PLA + 5% Fraction 5 + 0.5% WTH-II	5Fr5SW	PLA + 5% base + 0.5% WTH-II	5BSW
PLA + 10% Fraction 5 + 0.5% WTH-II	10Fr5SW	PLA + 10% base + 0.5% WTH-II	10BSW
PLA + 15% Fraction 5 + 0.5% WTH-II	15Fr5SW	PLA + 15% base + 0.5% WTH-II	15BSW
PLA + 15% Fraction 5	15Fr5	PLA + 2.5% base	15B
PLA			

3. Results and Discussion

3.1. Characterization of the Fillers

Figure 2 shows the particle sizes of the fractionated diatomaceous earth. The base diatomaceous earth has broken (0.5–2 µm) and unbroken (2–40 µm) frustules alongside agglomerated particles (above 40 µm). The fractionation process results in both the removal of agglomerated particles and the broken frustules depending on the diatomaceous earth fraction. Furthermore, it can be observed that the longer the sedimentation time, the smaller the diatomaceous earth particles (Fraction 4 and Fraction 5 have sedimentation times of 24 and 72 h, respectively), while short rinsing times enable the extraction of particles with larger sizes (Fraction 0 and Fraction 1 have sedimentation times of 10 and 20 min, respectively). Fractions 2 and 3, which have the respective sedimentation times of 45 min and 2 h, do not differ from the base diatomaceous earth in terms of the small particle size. However, it is possible to eliminate the largest-diameter agglomerates. Some of the agglomerations visible in Fraction 5 arise due to a secondary particle aggregation in the water suspension, which was also observed in the previous report [19]. On the basis of DLS and SEM images (discussed in Section 3.1), the SEM images produced (Figure 3) confirm the relationships mentioned above. As the fraction number increases, the diatomaceous earth particle size decreases and the proportion of the broken frustules increases. The SEM image of Fraction 0 clearly shows that a large number of agglomerates formed for both broken and unbroken frustules. Similarly for Fraction 1, the proportion of the largest particle size is smaller, while Fraction 2 and Fraction 3 have similar particle sizes. It is Fraction 2 that has, by far, the most particles with unbroken frustules, which is consistent with the DLS measurements given above. Fractions 4 and 5, as measured with DLS, show the presence of mostly the smallest particle sizes and a high proportion of broken frustules. For Fraction 5, the presence of such small particles results in the further formation of agglomerates. The base diatomaceous earth contains the combination of all the characteristics described above.

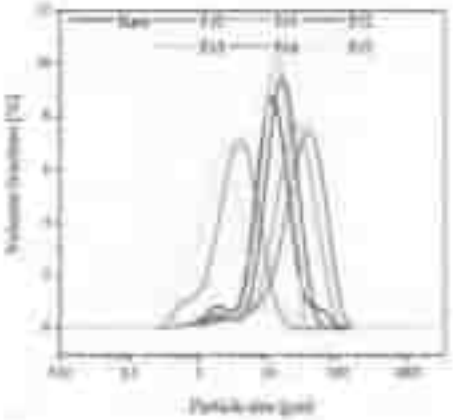

Figure 2. Particle size distribution of individual diatomaceous earth fractions.

3.2. Rheology

The melt flow rate was measured for the samples after the injection process (Figure 4). It showed significant differences between the samples that were analyzed. The reference polylactide has an MFR value of approximately 8.5 g/10 min, which is slightly higher than the values found in the literature [25], due to the injection molding. Modifications due to the diatomaceous earth result in a significant increase in the flow rate for all the systems. Fractionated systems with added waxes show a mostly linear increase in the value with an increase in the content of diatomaceous earth. Unmodified diatoms, regardless of their concentration, show similar values at ~12–15 g/10 min. For Fraction 2 and Fraction 4, the effect of the addition of the synthetic wax on the MFR values is observed (15Fr2 and 15Fr4 systems compared to 15Fr2SW and 15Fr4SW), i.e., the value increases dramatically (from 20.978, 19.940 to 29.978, 36.747, respectively). Furthermore, the addition of the

diatomaceous earth alone increases the melt flow rate, even without the addition of the waxes. This can be seen by comparing the systems that contain 15% diatomaceous earth without wax and with lower concentrations of wax (2.5% and 5%). The diatomaceous earth particle size has a significant effect on the processing parameters. As mentioned above, base diatomaceous earth is characterized by the lack of correlation between its content and an increase or decrease in the MFR, while the system that contains the larger particle sizes (Fraction 2) already clearly display improved properties at a concentration of 10%.

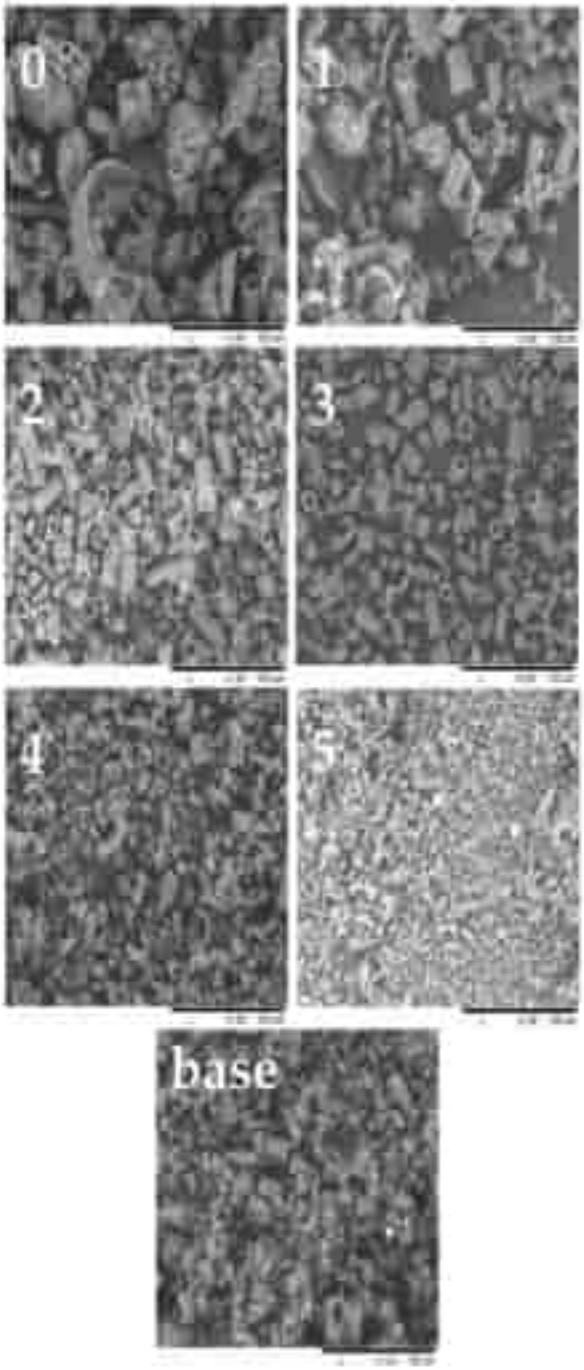

Figure 3. SEM images of fractionated diatomaceous earth, 0—Fraction 0, 1—Fraction 1, 2—Fraction 2, 3—Fraction 3, 4—Fraction 4, 5—Fraction 5, base—base diatomaceous earth.

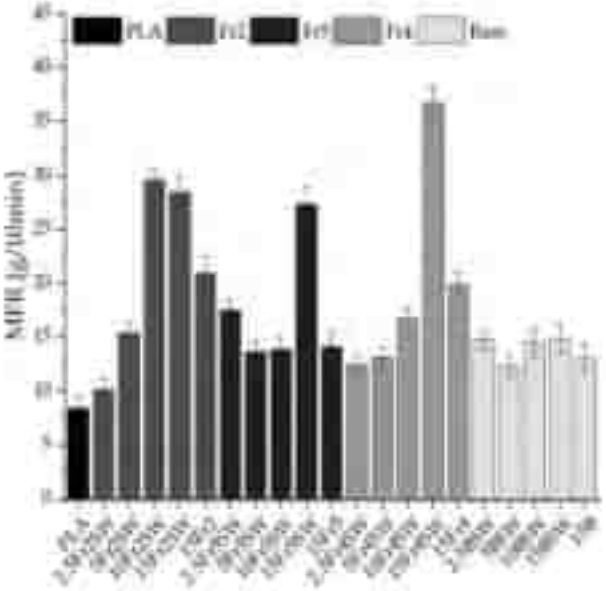

Figure 6. Melt flow rate of granulates.

3.3. Mechanical Properties

A study was conducted to investigate the effect of the particle size on the mechanical properties of the composites (Figures 5–7 and S1). It is shown that the diatomaceous earth decreases the strength of the material due to, among other factors, the application of rigid particles as the filler, the presence of air in the frustule, and the tendency of the diatomite to agglomerate, which increases the concentration of the point stresses. The last aspect is the lack of chemical surface treatment of the filler, resulting in limited adhesion on the composite interphase. This implies that pure polylactide shows both a higher elongation at break and tensile strength parameters [28]. When using diatomite loadings in the range of ~2.5–15%, we can conclude that the optimum amount of additive, for testing mechanical properties at the break point, includes the addition of 5% fractionated diatomaceous earth. However, the base diatomaceous earth shows an inverse relationship between the tensile strength and concentration. The aspects of the PLA-diatom interaction and the mechanical behavior of PLA-diatomaceous earth, as well as the filler particle size distribution, have been discussed in detail in the previous work [29]. The addition of the synthetic wax (WTH-8) has a significant effect on reducing the mechanical strength of the systems under investigation, while improving the flow rate. The systems modified with Fraction 2 (5% of the additive), i.e., with a medium range of particles but without any agglomerated particles, have the highest parameters, while Fraction 5 (the smallest particles) boasts a relative stability based on their measurements irrespective of the additive concentration.

The flexural strength of the composite systems is also examined. Pure PLA is characterized by the flexural modulus and maximum flexural stress values of 3.52 GPa and 96.15 MPa, respectively. Systems filled with diatomaceous earth, with the addition of synthetic wax, have lower maximum flexural stress values compared to pure polylactide (except for the system 5Fr95W at 96.53 MPa), which is due to the low adhesion of the polymer to the filler particles. Compared to the tensile tests, the synthetic wax does not cause a significant deterioration in the mechanical parameters relating to flexure. However, the particle size of the filler has a significant effect on the flexural strength of the systems. Fraction 2, which has the highest average particle diameter, causes the greatest decrease in the tensile strength parameters for the highest filling. In each case, the flexural modulus is higher for the filled samples compared to the base PLA (which is typical for filled composites), with an increasing trend with more filling. Moreover, the fractions with the largest and smallest particles show the highest values of the flexural modulus, especially for the

highest concentration (15%). The systems that are modified with the base diatomaceous earth, and Fraction 4, show a similar tendency.

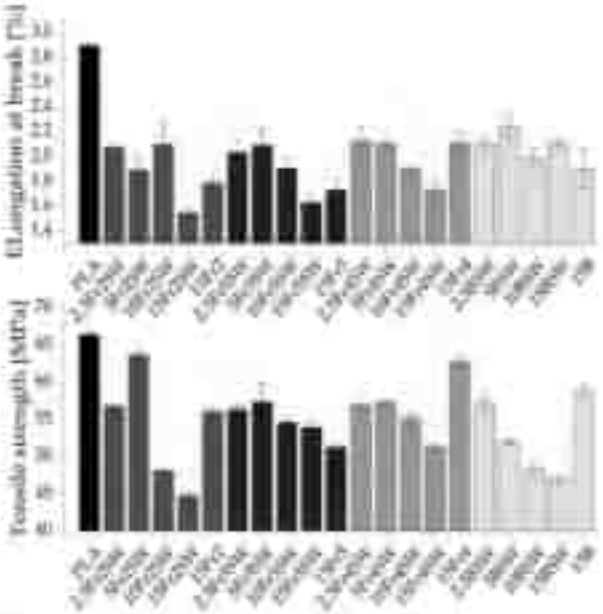

Figure 5. Tensile strength and elongation at break of composites.

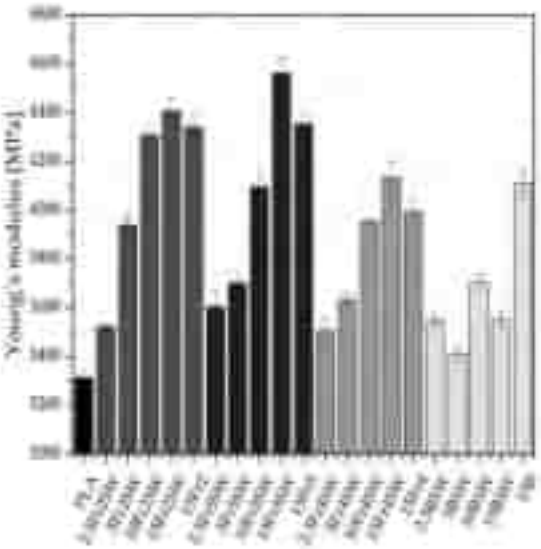

Figure 6. Young's modulus of composites.

The addition of diatomaceous earth to the polylactide, irrespective of the fraction, results in an initial increase and then a decrease in the impact strength at most concentrations (Figure 8). The optimum results are obtained for the fraction with the smallest particles, in the filling range up to 10%. The impact strength of the obtained samples is undoubtedly influenced by the particle size of the diatomite and its agglomeration. The fraction that contains the largest-diameter particles has the lowest impact strength parameters, but this is only slightly lower than the systems with the base diatoms, which indicates that the presence of large-diameter particles has a negative effect on the impact strength.

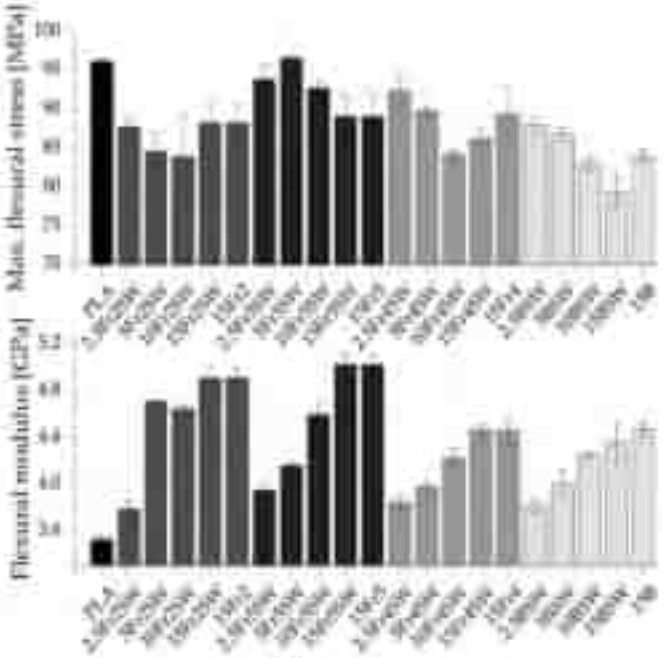

Figure 7. Max. flexural stress and flexural modulus of composites.

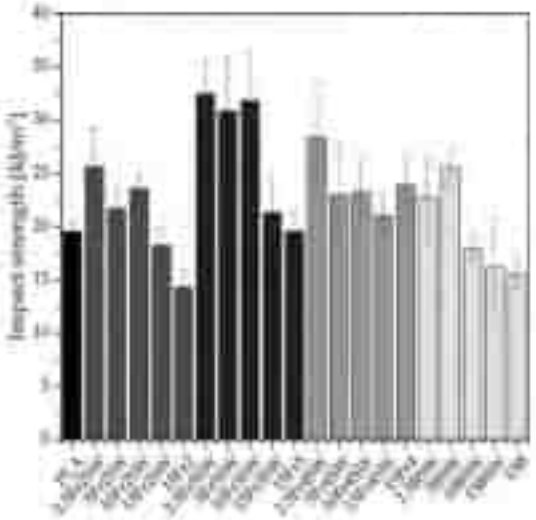

Figure 8. Impact strength of composites.

Diatomaceous earth is also shown to affect the brittleness of the material; the higher its addition, the lower the impact strength values. This correlation is the most and least visible for Fraction 5 (the smallest particles) and Fraction 4 (the largest particles, without agglomerates), respectively. In the latter case, the addition of 5% or more does not cause any significant changes, so the impact strength remains at a similar, constant level.

To assess the influence of atmospheric conditions, i.e., the effects of the differences in humidity and temperature on the mechanical and visual properties (Figures S2 and S3), the samples were placed into a climate chamber. Regardless of the fraction used, a decrease in the strength of the composites is minimal for most systems on the addition of wax. In contrast to the systems with wax, the composites without wax show a noticeably higher degradation of their mechanical properties, except for Fraction 5, in which the anti-ageing effect is already caused by the high filler dispersion in the plastic. The correlation between the decrease in the mechanical properties of the samples and the filler concentration (and

its fraction) is related to the increased porosity of the samples and, therefore, water has a great impact on them, which result in the hydrolytic degradation of the polylactide under the above-mentioned environmental conditions. The wax acts as a barrier that prevents water from passing through the pores of the filler, as it enables the formation of a hydrophobic layer.

Conditioning the composites in a climatic chamber for 5 days results in a slight increase in the elongation at the break point. However, further exposure of the samples to harsher climatic conditions (for 20 days) cause clear changes in the structure, which manifest in terms of an increased flexibility and, thus, an increased elongation at the break point. The smallest changes are observed, each time, for the highest proportion of the filler, which relates to the lowest light transmission (which is the factor responsible for the photodegradation) within the samples. Photodegradation, together with the hydrolysis, results in a reduction in the average molecular weight of the polymer, which translates into higher sample tensility. The lack of any significant differences between the samples with and without wax is due to a low proportion of photodegradation for samples with a high proportion of the filler. This also indicates that, at higher filling levels, the tensile strength of the samples is so low that their degradation has little to no further effect on this parameter.

Conditioning of the samples in a climate chamber also affects their flexural strength (Figure S4). The flexural modulus, depending on the particle size of the filler used, either remains relatively constant or even increases slightly, as in the case of Fr4 and Fr2 diatomaceous earth systems, or decreases with the time spent in the climatic chamber, as in the case of Fraction 5 and Fraction 2. Compared to pure polylactide, the flexural modulus for the modified samples is maintained at a much higher level, even despite the unfavorable conditioning conditions, indicating the positive effect of the filler on the mechanical properties of the composites, regardless of the particle size. In most cases, the impact strength (Figure S5) reaches its maximum value for samples that are conditioned for 5 days in the climatic chamber, while any further conditioning over the next 20 days partly weakens the structure of the composites, and also lowers the impact strength values, but the results are still higher than for those for unconditioned samples. Young's modulus decreased slightly for most of the specimens after they were placed in the climate chamber (Figure S6). The optimum results are achieved for systems that contain a 5% addition of diatomaceous earth for the fraction with the smallest particle sizes, i.e., Fraction 5 and Fraction 2, while fractions containing both the larger particle sizes and agglomerates (in the case of the base diatomaceous earth) have significantly lower values. Small-sized particles result in improved energy transfer through the sample. Moreover, the partial degradation of the polymer, which occurs during the first days of the conditioning, causes a reduction in the brittleness of the polymer that, as written above, arises due to the lower average molecular weight. At the highest filling level, in all systems, the presence of the filler reduces the ageing effect on the impact strength of the samples.

3.4. Hydrophilic and Hydrophobic Properties of the Obtained Composites

For each system, the maximum contact angle is observed for a given proportion of the filler in the composite. This relates to the balance between the increasing proportion of porous filler and an intensifying micro-roughness of the sample, and the impact of the polar character of the filler surface on the polarity of the composite surface. However, the polar effect is observed to a lesser extent in the presence of wax in the composites. As the size of particle diatoms in the systems increases, the hydrophobicity also increases. The lowest values are observed for the systems that are modified with Fraction 5 (69.3° on average), while for Fraction 4 and Fraction 5, the results are comparable: 86.7 and 84.8° (Table 4). Systems that contain the full range of sizes of particle diatoms, i.e., the base systems, have by far the highest values for the contact angle, which averages to 92.3°. The hydrophobicity of systems, therefore, is affected by both large- and small-sized particles, but a predominance arises for particles above 3 nm. However, an adverse effect on the

hydrophilic and hydrophobic properties of the composite surface occurs on addition of synthetic wax. By considering systems with a 15% diatomaceous earth content, the higher contact angle values are obtained for systems that are not modified with synthetic wax (except for the base system, in which the values are slightly higher for the system with wax).

Table 4. Contact angle for the reference samples after 5 and 20 days in the climate chamber (CCh).

	Contact Angle RT [°C]	Contact Angle after 5 Days in CCh [°C]	Contact Angle after 20 Days in CCh [°C]
PLA	83.4	90.5	70.6
2.5Fr25W	80.4	81.7	82.1
5Fr25W	84.5	95.6	90.1
10Fr25W	90.9	87.2	88.6
15Fr25W	82.8	69.0	69.7
15Fr2	85.7	110.0	74.6
2.5Fr50W	83.2	76.1	91.0
5Fr50W	91.5	93.3	89.2
10Fr50W	80.6	90.8	92.0
15Fr50W	61.8	72.0	84.0
15Fr5	93.4	95.0	87.6
2.5Fr45W	86.9	86.5	94.7
5Fr45W	90.0	83.3	91.8
10Fr45W	84.7	90.0	80.1
15Fr45W	85.5	79.5	81.1
15Fr4	92.3	87.3	88.9
2.5B5W	95.6	96.9	77.0
5B5W	94.4	91.2	84.2
10B5W	85.8	58.2	93.5
15B5W	93.3	91.8	96.4
15B	85.7	90.5	87.5

The exposure of the composites to increased humidity, and variable temperature conditions (within the climatic chamber), causes changes in their properties. The system with the smallest diatomaceous earth particles has a higher contact angle for the whole series, regardless of the modifier concentration. Similarly, for systems that are not modified with synthetic wax, the 15% diatom sample for Fraction 2 achieves the highest contact angle result (of all the tested samples) of 110.05°. Holding the systems in the climate chamber for a longer period of time results in decreased values for the contact angle for most systems, which can be explained by the degradation of the polylactide, the latter is evidenced by the decrease in the contact angle for pure PLA after 20 days from 83.4° to 70.6°. The initial increase in the contact angle is related to the development of a microporous structure on the polymer surface [37]. Further ageing of the polymer leads to the formation of larger breaks and the creation of a greater number of polar groups on the PLA surface.

3.5. Electron Microscopy—The Effects of Modifier Particle Sizes on Dispersion within the Polymer Matrix

Figure 9 shows the images of the composite surface, at magnification of 1000×, that derive from the scanning electron microscope (SEM). As mentioned above, Fraction 2 is characterized by the largest diatom particle size, as confirmed by the SEM Figure 9A image. Here, cylindrical diatoms that are surrounded by the polylactide are clearly visible. Similarly for Fraction 4 (Figure 9B), where cylindrical diatoms are also seen, it is clear that they have a slightly smaller size compared to those in Fraction 2. Figure 9C shows Fraction 5, which contains the smallest particle size; here, it can clearly be observed that the diatomaceous earth disperses uniformly within the polymer matrix, and only one secondary agglomerate formation of the diatomaceous earth particles is present. Base diatomaceous earth (Figure 9D), which tends to agglomerate, is not uniformly dispersed within the polymer.

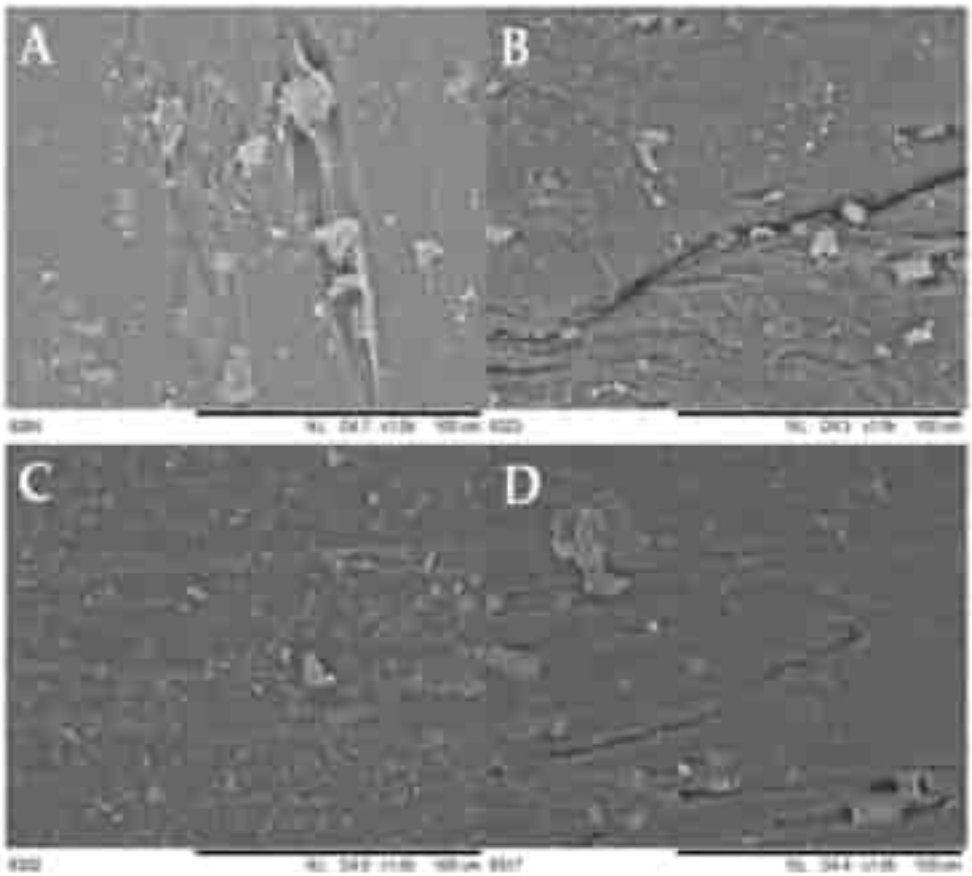

Figure 9. SEM images of various surfaces (**A**–**D**): (**A**)—15Fr2SW; (**B**)—15Fr4SW; (**C**)—15Fr6SW; and (**D**)—15BSW.

The electron microscope is also used to provide images of the fractures that are formed after the impact testing of the composites (Figures 10 and S7). The composite that is modified with Fraction 2 (with the largest particles, see Figure 10A) is characterized by the presence of diatoms with a maximum length of 13 µm and a diameter around 10 µm. Here, whole diatoms are visible, without any broken frustules. The breaking of the test sample does not cause the diatoms to disintegrate into fragments, and no voids remain after diatoms become visible in the matrix. This suggests that the polymer fracture occurs at the filler–polymer interface during a composite failure, rather than a filler pull-out, which is probably due to the low length-to-diameter ratio of the diatom frustules. A 15% concentration for the modifier results in a high local accumulation of the filler, but the agglomeration phenomenon is not observed in this case. The composite that is modified with Fraction 4 (Figure 10B) has a significantly smaller filler size (i.e., a maximum diameter of 9 µm). The proportion of broken diatom frustules is significantly higher than those in Fraction 2, and the imprints in the polymer matrix that result from the pull-out are also present. The composite is modified with diatomaceous earth that has the smallest particle size (Fraction 5, Figure 10C), which are characterized by the presence of the mainly broken diatom fragments; only a small number of whole diatoms are seen and their sizes do not exceed 6 µm. The base diatomaceous earth (Figure 10D) contains both the larger and smaller diatoms.

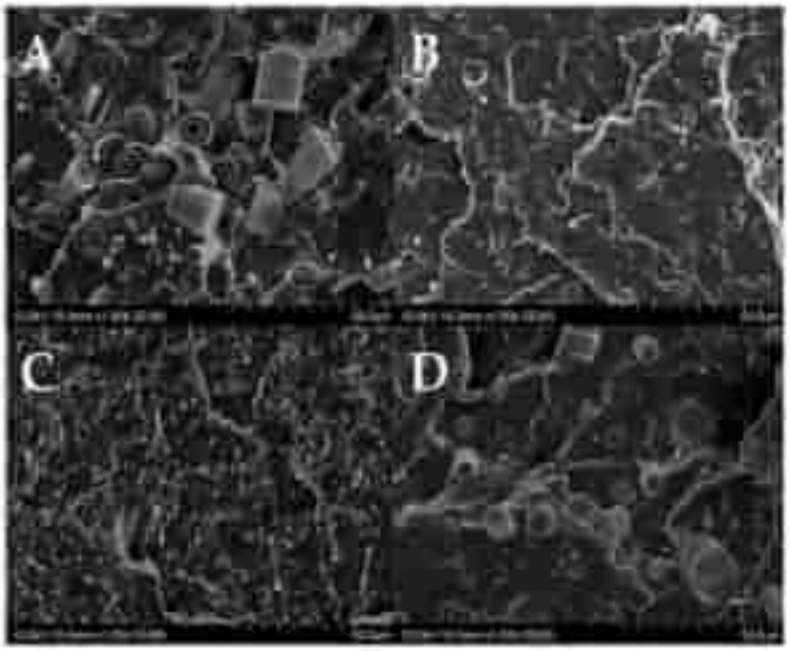

Figure 10. SEM images of the (A–D) fractures: (A)—15Fr25W, (B)—15Fr45W, and (C)—15Fr55W, (D)—15Fr85W.

3.6. Hiding Power Tests

Hiding power tests, based on the visible light transmittance of the samples, show the impact of both the diatomaceous earth content and the particle size of the individual fractions on the pigmentation efficiency of the composites. The higher the DE content, irrespective of the modifier type, the higher the hiding power. Once again, the highest results are obtained for fractions that contain the diatomaceous earth with the smallest particle size, i.e., Fraction 5. This occurs due to the excellent dispersion characteristics of the particles with small sizes in the polymer matrix, as confirmed by the SEM images (Figure 11). The composites that contain the base diatoms have the lowest hiding power, which is due to the proportion of the agglomerated fraction. A relatively low hiding power is observed for the composites that contain Fraction 4, despite the high proportion of small-diameter particles in the composition.

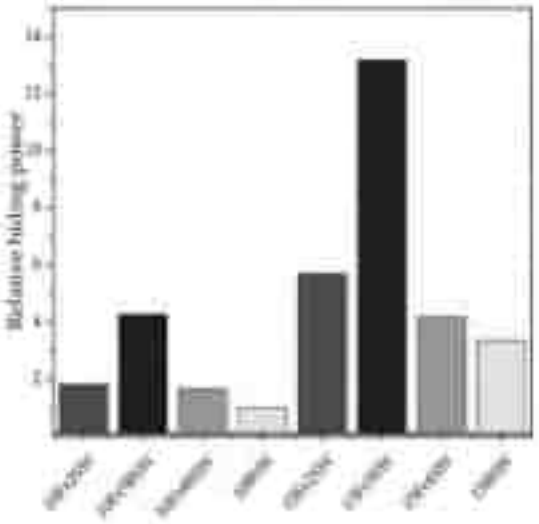

Figure 11. Relative hiding power of the PLA/DE composites.

3.7. DMTA Tests

Table 5 shows the influences on the storage modulus (E') due to addition of different volume fractions of diatomaceous earth (Figure 12); this involves the loss modulus (E"), and the damping factor (tan d) for the composites that are based on PLA and diatoms. The T_g of neat PLA is less pronounced and observed in the 60–63 °C range. The application of the fractionated diatomite leads to a slight change in the dynamic mechanical properties of the composites. Most importantly, the T_g transition is significantly more distinctive. Moreover, it can be observed that the addition of a different fraction of DE enables an increase in the glass transition temperature (T_g), which is determined from the storage modulus (E'), loss modulus (E"), and the damping factor (tanδ). A sharp decrease in the storage modulus, the loss modulus (E"), and the damping factor (tanδ) of the composites with diatomaceous earth is related to the glass transition of PLA. The glass transition temperature (T_g) increases slightly when the filler particle size decreases. This shows that the presence of a different volume fraction of DE restricts the segmental motion of the polymer chains.

Table 5. Summary of the determined values for the glass transition temperature from the DMTA curves.

Sample Name	T_g [°C]		
	E' [MPa]	E" [MPa]	tanδ
15BSW	59.8	61.7	65.2
15Fr25W	56.7	57.8	62.2
15Fr45W	58.8	59.8	63.9
15Fr55W	58.8	59.6	64.4

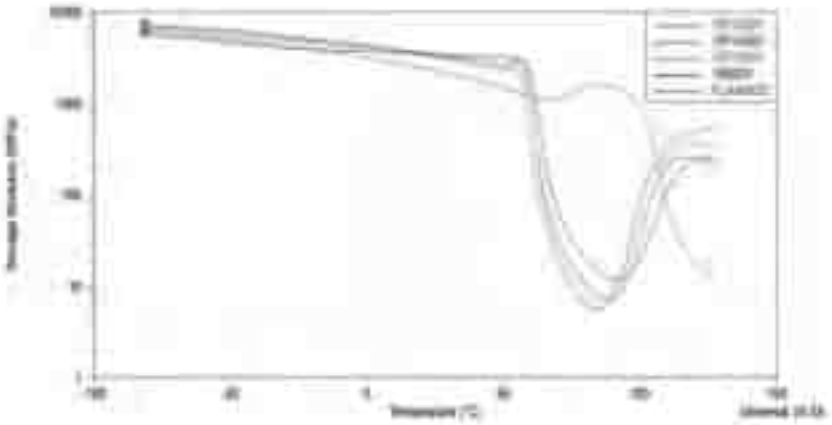

Figure 12. Storage modulus curves of the samples on a logarithmic scale.

Based on the DMTA curves at normal scale, cold crystallization and subsequent melting are observed after the glass transition temperature. In the process of cold crystallization, a new fraction of crystallites is formed due to improved mobility and ordering ability of the polymer chains in the amorphous phase, which consequently results in an increase in modulus, and a significant peak in the tan delta curve is observed, with an onset at ~90 °C for PLA composites. This phenomenon was discussed in the review by Cristea et al. [70]. As the DSC and DMTA measurements are based on different measuring principles, the cold crystallization event during the DSC measurement occurs at a slightly different temperature. Crystallites that form at relatively low temperatures during cold crystallization are not stable and undergo crystal perfection. Then, as the temperature increases, the decrease in the modulus indicates the beginning of the crystallite melting process.

3.8. Thermal Studies

A DSC analysis is performed to investigate the thermal behavior of the PLA and PLA/diatoms composites. Figure 13 shows the DSC thermograms of the PLA and PLA/diatom composites during the second heating stage. When the temperature increases from 52 °C to 153 °C, each DSC curve possesses three thermal characteristics: (a) a glass transition temperature (T_g) near 55 °C, (b) a cold crystallization peak (T_{cc}), and (c) an endothermic melting peak (T_m).

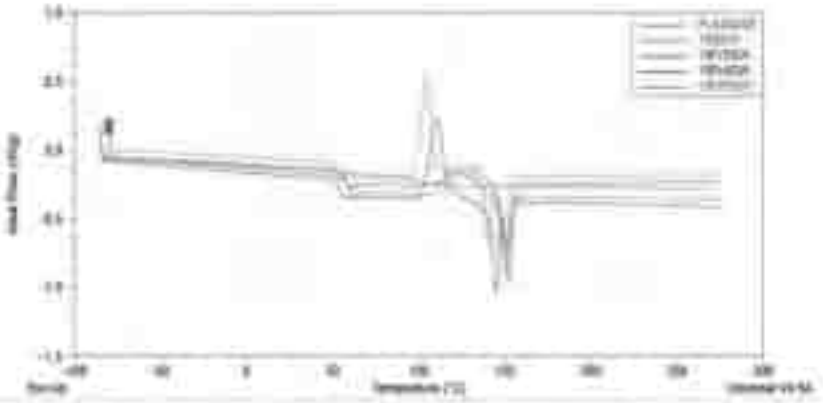

Figure 13. DSC curves of unmodified PLA, and the composites based on PLA, with a different weight fraction of the diatoms obtained during the second heating procedure.

The values of the glass transition temperature, cold crystallization temperature, specific cold crystallization enthalpy, melting temperature, and the specific melting enthalpy are listed in Table 6. It can be observed that the unmodified PLA and the 15Fr25W composite have a single melting peak, while the 15Fr45W and 15Fr55W composites involve two distinct melting peaks (Tm_1 and Tm_2). For the 15B5W and 15Fr25W materials, there is only one melting peak, and hence, in Tm_1 equals Tm_2. Figure 2 and Table 1 reveal that the glass transition temperature decreases with an increase in the weight fraction of the diatoms from 58.3 to 52.1 °C, which indicates that the presence of the diatoms has an effect on the chain mobility of the PLA, by creating more mobile polymer phases on the matrix-filler interphase. This effect is known for composites with no chemical attraction between the polymer matrix and filler surface [29–31].

Table 6. Thermal characteristics of the PLA, and composites based on PLA, with a different weight fraction of the diatoms.

Sample	T_g (°C)	T_{cc} (°C)	ΔH_{cc} (J/g)	Tm_1 (°C)	Tm_2 (°C)	ΔH_m (J/g)
PLA	100.0	-	-	-	-	-
15B5W	58.3	122.2	19.0	150.5	150.5	20.4
15Fr25W	58.2	129.0	16.9	150.6	150.6	17.1
15Fr45W	55.1	110.6	33.6	144.9	152.6	34.4
15Fr55W	52.1	104.5	35.0	141.1	150.1	31.3

With regard to cold crystallization, Figure 13 shows that the unmodified PLA and the 15Fr25W composite show a wide cold crystallization peak, which represents its slow crystallization behavior over time; the presence of any diatoms significantly narrows this cold crystallization peak. Moreover, the temperature of the cold crystallization decreases with an increase in the diatom content. Based on these results, it can be determined that the diatoms can greatly promote crystallization of the PLA due to its outstanding nucleating effect.

With a further increase in the temperature, the crystals that are generated during cold crystallization begin to melt. As a result, a melting peak appears in the DSC thermograms.

It can be observed that the unmodified PLA and the 15Fr25W composite show a single melting peak, and its melting temperature (T_m) is around 150 °C. While the PLA/GF composites reveal a double melting peak with two melting temperatures (Tm_1 and Tm_2), the double melting peak could be related to the recrystallization of the generated crystals. For the 15Fr45W and 15Fr55W composites that crystallize around 110 °C, the crystals typically show a less-than-perfect structure and they are much thinner than the crystals generated at the higher temperatures during cold crystallization. However, these thinner crystals can melt and recrystallize to generate a closer to perfect and thicker structure. Due to a temperature increase, melting again occurs and the second melting peak (Tm_2) is achieved [32,33].

4. Conclusions

Fractionation of the diatomaceous earth, using the phenomenon of sedimentation, allows for fractions of different grain sizes to become distinguishable. This process enables the separation of broken, unbroken, and agglomerated diatoms. The diatomaceous earth particle size, which is used as a polylactide filler, affects both the rheological and the mechanical properties of the composites. As the filler concentration increases, the melt flow rate (MFR) increases, which varies depending on the diatomaceous earth fraction. It was also determined that the MFR of the unfractionated diatoms has significantly lower values compared to the others. When measuring the tensile strength of the composites, the optimum amount of additive is 5% diatomaceous earth, which produces the highest obtained results; this is regardless of particle size. The highest impact strength is obtained for the composites that are modified with diatomaceous earth that contain the smallest particle size (Fraction 5). The highest hiding degree is achieved for composites that have diatomaceous earth with the smallest particles (Fraction 5). With an increase in the modifier concentration within the system, the hiding degree also increases. The thermal analysis revealed that the particle size of the diatomaceous earth, and its tendency to form agglomerates, both have an effect on the blocking the PLA chain. The addition of synthetic wax provides the PLA composites with diatoms and the resulting anti-ageing properties, which has a positive effect on the mechanical properties after an acceleration of the ageing.

Supplementary Materials: The following materials are available online at https://www.mdpi.com/article/10.3390/ma15103607/s1, Figure S1: Example of tensile stress-strain curves of composites before climate chamber. Figure S2: Tensile strength for samples before and after 5 and 20 days in climate chamber. Figure S3: Elongation at break for samples before and after 5 and 20 days in climate chamber. Figure S4: Flexural modulus for samples before and after 5 and 20 days in climate chamber. Figure S5: Impact strength for samples before and after 5 and 20 days in climate chamber. Figure S6: Young's modulus for samples before and after 5 and 20 days in climate chamber. Figure S7: Photograph of fractured specimens after impact test.

Author Contributions: Conceptualization, R.E.P.; methodology, R.E.P., M.D. and M.W.; formal analysis, R.E.P., M.D., R.D. and M.J.; investigation, R.E.P., M.D., M.F., M.W. and P.K.; data curation, M.D., D.B., M.F. and P.K.; writing—original draft preparation, M.D., R.E.P. and R.D.; writing—review and editing, M.D., R.E.P., D.B. and R.D.; visualization, M.D. and P.K.; supervision, R.E.P., R.D., M.J. and K.J.K.; project administration, R.D. and K.J.K.; funding acquisition, R.D. and K.J.K. All authors have read and agreed to the published version of the manuscript.

Funding: This work was financially supported in the frame of the project "Advanced Biocomposites for Tomorrow's Economy BIOG-NET", FNP POIR.04.04.00-00-1792/18-00; the project was carried out within the TEAM-NET programme of the Foundation for Polish Science co-financed by the European Union under the European Regional Development Fund.

Institutional Review Board Statement: Not applicable.

Informed Consent Statement: Not applicable.

Data Availability Statement: Not applicable.

Conflicts of Interest: The authors declare no conflict of interest.

References

1. Domka, F. Biodegradable "plastic" waste in the strategy of environmental sustainability. *Fiber Text. East. Eur.* **2004**, *4*, 14–17.
2. Domka, F. Knowledge and sustainable development of the natural environment. *Ekopol* **2004**, *7*, 65–66.
3. Oksiuta, Z.; Jalbrzykowski, J.; Mystkowska, J.; Romanczuk, E.; Osiecki, T. Mechanical and thermal properties of polylactide(PLA) composites modified with Mg, Fe, and Polyethylene (PE) Additives. *Polymers* **2020**, *12*, 2939. [CrossRef] [PubMed]
4. Wootthikanokkhan, J.; Chanchon, T.; Sombatsompop, N.; Thumsorn, S.; Kaabbuathong, N.; Wongta, N.; Wong-On, J.; Isarankura Na Ayutthaya, S.; Kositchaiyong, A. Crystallization and thermomechanical properties of PLA composites: Effects of additive types and heat treatment. *J. Appl. Polym. Sci.* **2013**, *129*, 215–223. [CrossRef]
5. Domb, A.J.; Kumar, N. *Biodegradable Polymers in Clinical Use and Clinical Development*; John Wiley & Sons: Hoboken, NJ, USA, 2011; ISBN 978-0-470-42475-9.
6. Fiore, V.; Botta, L.; Scalici, R.; Valenza, A.; Pirrotta, A. PLA based biocomposites reinforced with arundo donax fibers. *Compos. Sci. Technol.* **2014**, *105*, 110–117. [CrossRef]
7. Rahman, R.; Putra, S.Z.F.S. Mechanical and Physical Testing of Biocomposites, Fibre-Reinforced Composites and Hybrid Composites. In *Composites Science and Engineering*; Woodhead Publishing Series; Elsevier: Cambridge, UK, 2019; pp. 81–102.
8. Yuzay, I.E.; Auras, R.; Soto-Valdez, H.; Selke, S. Effects of synthetic and natural zeolites on morphology and thermal degradation of poly(lactic acid) composites. *Polym. Degrad. Stab.* **2010**, *95*, 1769–1777. [CrossRef]
9. Erpek, C.E.Y.; Oyku, G.; Yilmazer, U. Comparison of natural halloysite with synthetic carbon nanotubes in poly(lactic acid) based composites. *Polym. Compos.* **2017**, *38*, 2337–2346. [CrossRef]
10. Sessini, V.; Palenzuela, M.; Damian, J.; Mosquera, M.E.G. Bio-based polyether from limonene oxide catalytic ROP as green polymeric plasticizer for PLA. *Polymer* **2020**, *210*, 123003. [CrossRef]
11. Cifuentes, S.C.; Frutos, E.; Benavente, R.; Lorenzo, V.; González-Carrasco, J.L. Assessment of mechanicalbehavior of PLA composites reinforced with Mg micro-particles through depth-sensing indentation analysis. *J. Mech. Behav. Biomed. Mater.* **2017**, *65*, 781–790. [CrossRef]
12. Tan, L.J.; Zhu, W.; Zhou, K. Recent progress on polymer materials for additive manufacturing. *Adv. Funct. Mater.* **2020**, *30*, 2003062. [CrossRef]
13. Jiang, D.; Ning, F. Fused filament fabrication of biodegradable PLA/316L composite scaffolds: Effects of metal particle content. *Procedia Manuf.* **2020**, *48*, 755–762. [CrossRef]
14. Molla, M.Z.; Rahman, M.R.T.; Mazen, B.; Tiwari, B.; Pathania, S. Poly Lactic Acid (PLA) Nanocomposites: Effect of inorganic nanoparticles reinforcement on its performance and food packaging applications. *Molecules* **2021**, *26*, 1967. [CrossRef]
15. Murariu, M.; Benali, S.; Paint, Y.; Dechief, A.L.; Murariu, O.; Raquez, J.M.; Dubois, P. Adding value in production of multi-functional polylactide (PLA)–ZnO nanocomposite films through alternative manufacturing methods. *Molecules* **2021**, *26*, 2043. [CrossRef] [PubMed]
16. Ritima, R.; Suprakas, S.R. An overview of the recent advances in polylactide-based sustainable nanocomposites. *Polym. Eng. Sci.* **2021**, *61*, 617–649.
17. Bakr, H.E.G.M.M. Diatomite: Its characterization, modifications and applications. *Asian J. Mater. Sci.* **2010**, *2*, 121–136.
18. Ivanov, S.E.; Bobyakov, V. Diatomite and its applications. *Glass Ceram.* **2008**, *65*, 48–51. [CrossRef]
19. Dobrowolska, M.; Przekop, R.E.; Sobczyk, B.; Brzakalski, D.; Zgłobicka, I.; Łępicka, M.; Dobosz, R.; Kurzydłowski, K.J. Biogenic composite filaments based on polylactide and diatomaceous earth for 3D Printing. *Materials* **2020**, *13*, 4632. [CrossRef]
20. Cacciotti, I.; Mori, S.; Cherubini, V.; Nanni, F. Eco-sustainable systems based on poly(lactic acid), diatomite and coffee grounds extract for food packaging. *Int. J. Biol. Macromol.* **2017**, *101*, 567–575. [CrossRef]
21. Gonzalez, L.; Agüero, A.; Quiles-Carrillo, L.; Lascano, D.; Montanes, N. Optimization of the loading of an environmentally-friendly compatibilizer derived from linseed oilin Poly(Lactic Acid)/Diatomaceous earth composites. *Materials* **2019**, *12*, 1627. [CrossRef]
22. Aw, M.S.; Simovic, S.; Yu, Y.; Addai-Mensah, J.; Losic, D. Porous silica microshells from diatoms as biocarrierfor drug delivery applications. *Powder Technol.* **2012**, *223*, 52–58. [CrossRef]
23. Dobrowolska, M.; Dobrucka, R.; Gloc, M.; Brzakalski, D.; Szymański, M.; Kurzydłowski, K.J.; Przekop, R.E. A new method of diatomaceous earth fractionation—A bio-raw material source for epoxy-based composites. *Materials* **2021**, *14*, 1663. [CrossRef]
24. Dobrowolska, M.; Dobrucka, R.; Brzakalski, D.; Gloc, M.; Rybki, J.; Głowacka, J.; Kurzydłowski, K.J.; Przekop, R.E. Methodological aspects of obtaining and characterizing composites based on biogenic diatomaceous silica and epoxy resins. *Materials* **2021**, *14*, 4607. [CrossRef] [PubMed]
25. Olejnik, O.; Masek, A. Bio-based packaging materials containing substances derived from coffee and tea plants. *Materials* **2020**, *13*, 5719. [CrossRef] [PubMed]
26. Rhim, J.W.; Park, H.M.; Ha, C.S. Bio-nanocomposites for food packaging applications. *Prog. Polym. Sci.* **2013**, *38*, 1629–1652. [CrossRef]
27. Lin, W.; Xie, G.; Qiu, Z. Effects of ultraviolet aging on properties of wood flour-poly(lactic acid) 3D printing filaments. *BioResources* **2019**, *14*, 8699–8710.
28. Cristea, M.; Ioanita, D.; Iftime, M.M. Dynamic mechanical analysis investigations of PLA-based renewable materials: How are they useful? *Materials* **2020**, *13*, 5302. [CrossRef] [PubMed]
29. Meyer, A.M. Softer at the boundary. *Nat. Mater.* **2003**, *4*, 651–652. [CrossRef] [PubMed]

30. Bansal, A.; Yang, H.; Li, C.; Cho, K.; Benicewicz, B.C.; Kumar, S.K.; Schadler, L.S. Quantitative equivalence between polymer nanocomposites and thin polymer films. *Nat. Mater.* **2005**, *4*, 693–698. [CrossRef]
31. Ash, B.J.; Schadler, L.S.; Siegel, R.W. Glass transition behavior of alumina/polymethylmethacrylate nanocomposites. *Mater. Lett.* **2002**, *55*, 83–87. [CrossRef]
32. Wang, G.; Zhang, D.; Li, B.; Wan, G.; Zhao, G.; Zhang, A. Strong and thermal-resistance glass fiber-reinforced polylactic acid (PLA) composites enabled by heat treatment. *Int. J. Biol. Macromol.* **2019**, *129*, 448–459. [CrossRef]
33. Sarasua, J.R.; Prud'Homme, R.E.; Wisniewski, M.; Le Borgne, A.; Spassky, N. Crystallization and melting behavior of polylactides. *Macromolecules* **1998**, *31*, 3895–3905. [CrossRef]

H4 - supplementary

Influence of Diatomaceous Earth Particle Size on Mechanical Properties of PLA/Diatomaceous Earth Composites

Dobrosielska M., Dobrucka R., Brząkalski D., Frydrych M., Kozera P., Wieczorek M., Jałbrzykowski M., Kurzydłowski K.J., Przekop R.E., Materials, 15, 3607, 2022

materials

MDPI

Supplementary materials

Influence of Diatomaceous Earth Particle Size on Mechanical Properties of PLA/Diatomaceous Earth Composites

Marta Dobrowolska [1], Renata Dobrucka [2,*], Dariusz Brząkalski [3], Miłosz Frydrych [3], Paulina Kosmela [1], Monika Wieczorek [1], Marek Jałbrzykowski [4,5], Krzysztof J. Kurzydłowski [4] and Robert E. Przekop [3,*]

[1] Faculty of Materials Science and Engineering, Warsaw University of Technology, ul. Wołoska 141, 02-507 Warsaw, Poland; marta.dobrowolska@pw.edu.pl (M.D.); paulina.kosmela@pw.edu.pl (P.K.); monika.wieczorek@pw.edu.pl (M.W.)

[2] Department of Non-Food Products Quality and Packaging Development, Institute of Quality Science, Poznań University of Economics and Business, al. Niepodległości 10, 61-875 Poznań, Poland

[3] Faculty of Chemistry, Adam Mickiewicz University in Poznań, ul. Uniwersytetu Poznańskiego 8, 61-614 Poznań, Poland; d.brzakalski@gmail.com (D.B.); frydrych@amu.edu.pl (M.F.)

[4] Faculty of Mechanical Engineering, Białystok University of Technology, ul. Wiejska 45 c, 15-351 Białystok, Poland; m.jalbrzykowski@pb.edu.pl (M.J.); krzysztof.kurzydlowski@pw.edu.pl (K.J.K.)

[5] Centre for Advanced Technologies, Adam Mickiewicz University in Poznań, ul. Uniwersytetu Poznańskiego 10, 61-614 Poznań, Poland

* Correspondence: renata.dobrucka@pw.edu.pl (R.D.) or renata.dobrucka@ue.poznan.pl (R.D.); rprzekop@amu.edu.pl (R.E.P.) or r.przekop@gmail.com (R.E.P.)

Citation: Dobrowolska, M.; Dobrucka, R.; Brząkalski, D.; Frydrych, M.; Kosmela, P.; Wieczorek, M.; Jałbrzykowski, M.; Kurzydłowski, K.J.; Przekop, R.E. Influence of Diatomaceous Earth Particle Size on Mechanical Properties of PLA/Diatomaceous Earth Composites. *Materials* **2022**, *15*, 3607. https://doi.org/10.3390/ma15103607

Academic Editor: Sandra Maria Fernandes Carvalho

Received: 29 March 2022
Accepted: 9 May 2022
Published: 18 May 2022

Publisher's Note: MDPI stays neutral with regard to jurisdictional claims in published maps and institutional affiliations.

Copyright: © 2022 by the authors. Licensee MDPI, Basel, Switzerland. This article is an open access article distributed under the terms and conditions of the Creative Commons Attribution (CC BY) license (https://creativecommons.org/licenses/by/4.0/).

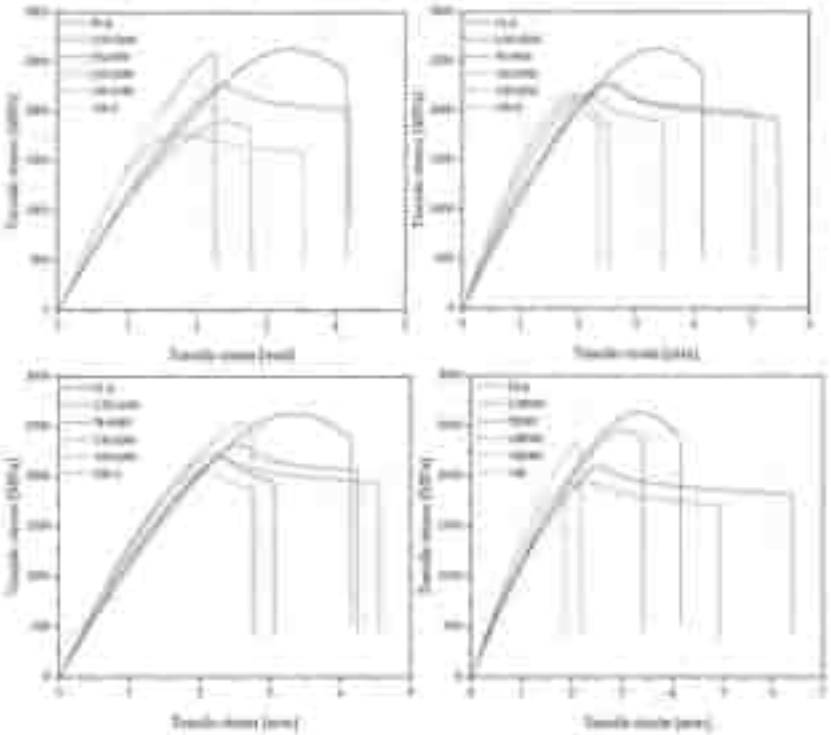

Figure S1. Example of tensile stress–strain curves of composites before climate chamber.

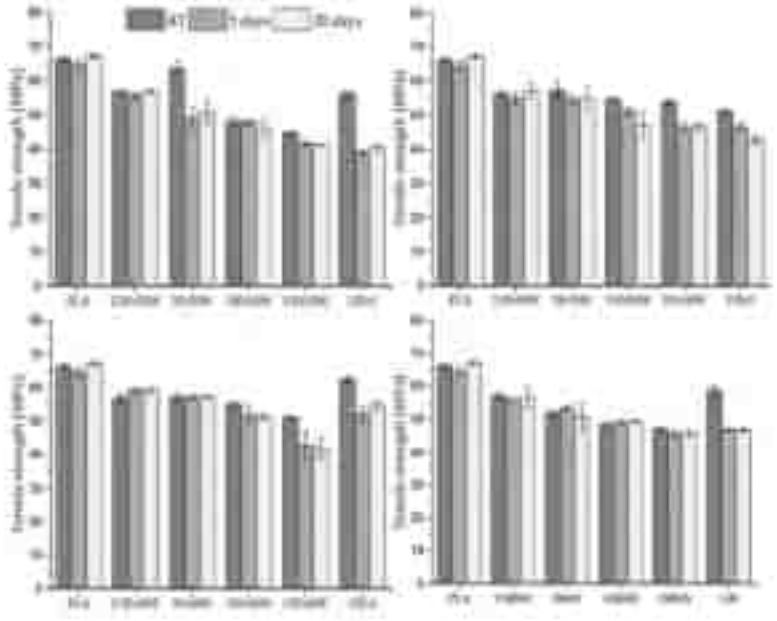

Figure S2. Tensile strength for samples before and after 5 and 20 days in climate chamber.

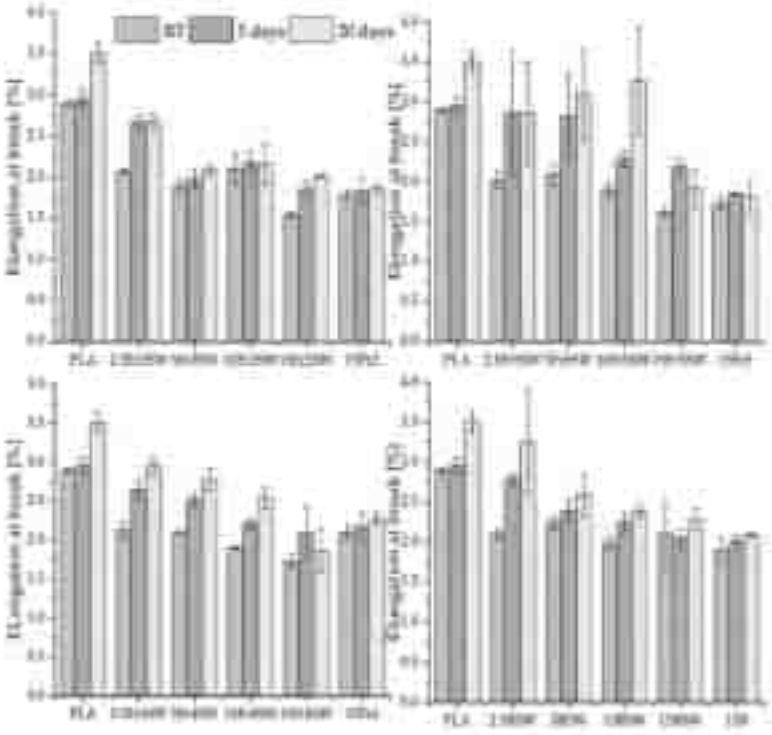

Figure S3. Elongation at break for samples before and after 5 and 20 days in climate chamber.

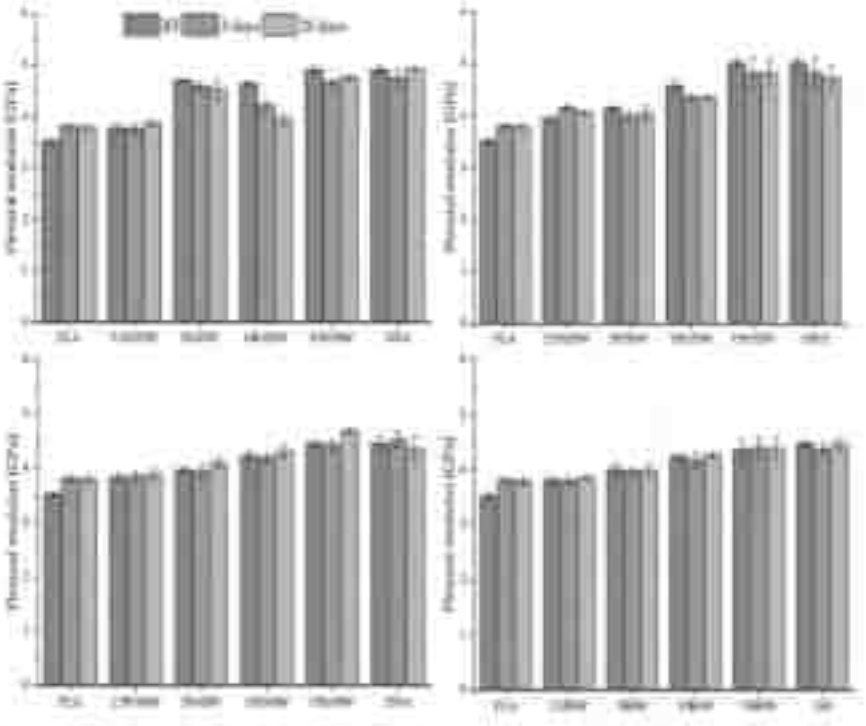

Figure 54. Flexural modulus for samples before and after 5 and 20 days in climate chamber.

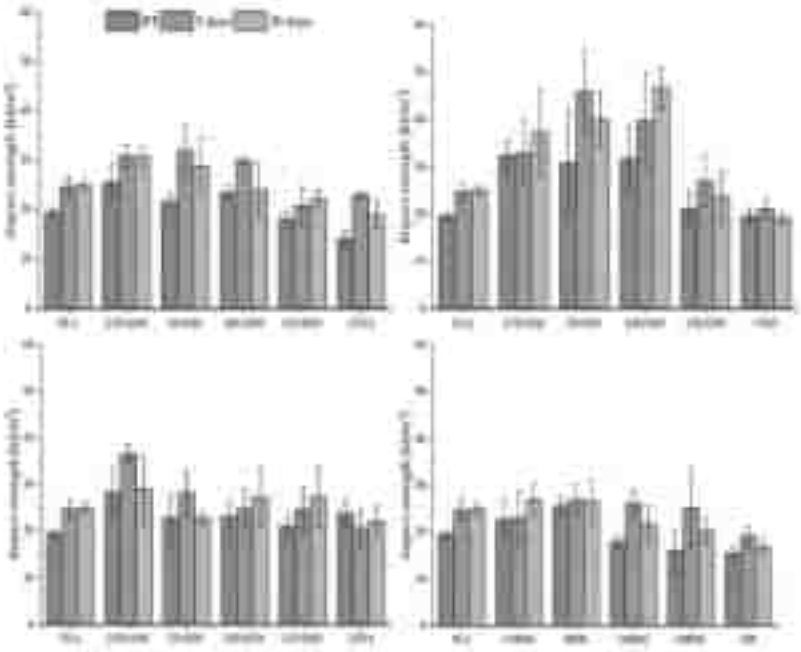

Figure 55. Impact strength for samples before and after 5 and 20 days in climate chamber.

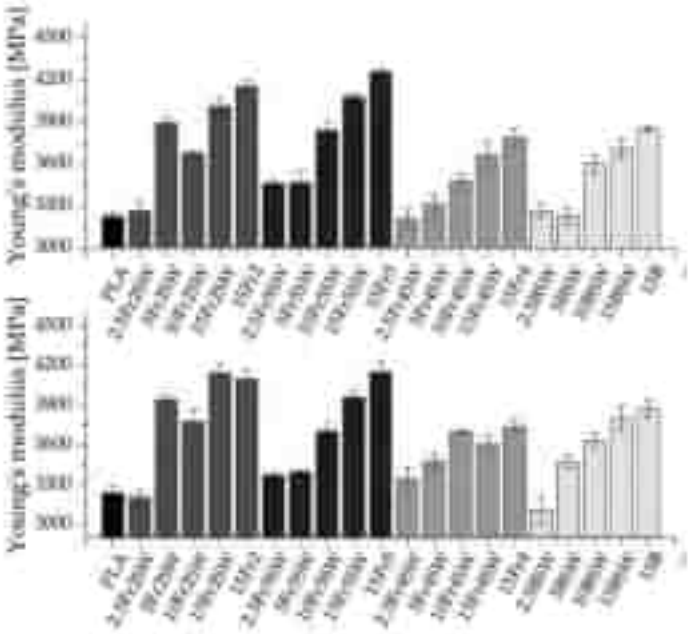

Figure 56. Young's modulus for samples before and after 5 and 20 days in climate chamber.

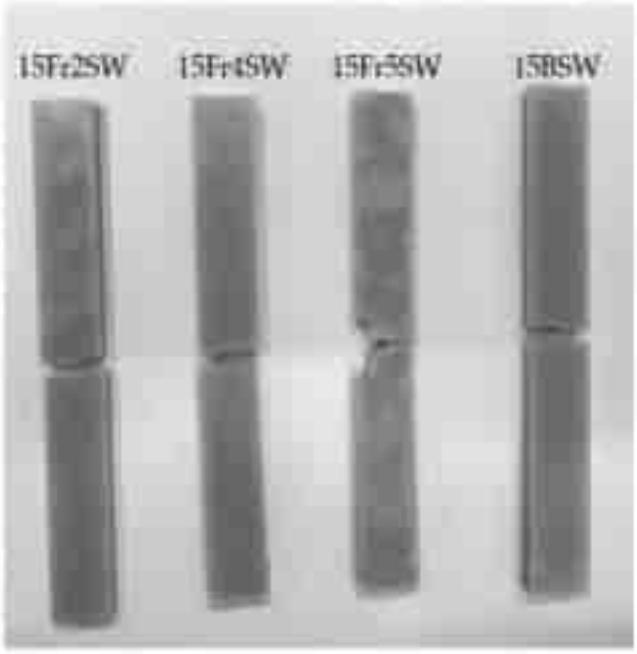

Figure 57. Photograph of fractured specimens after impact test.

H5

Biocomposites Based on Polyamide 11/Diatoms with Different Sized Frustules

Dobrosielska M., Dobrucka R., Kozera P., Kozera R., Kołodziejczak M., Gabriel E., Głowacka J., Jałbrzykowski M., Kurzydłowski K.J., Przekop R.E.; Polymers, 14, 3153, 2022

polymers

MDPI

Article

Biocomposites Based on Polyamide 11/Diatoms with Different Sized Frustules

Marta Dobrowolska [1], Renata Dobrucka [1,2,*], Paulina Kozera [1], Rafał Kozera [1], Marta Kołodziejczak [3], Ewa Gabrzel [4], Julia Głowacka [5], Marek Jałbrzykowski [4,5], Krzysztof J. Kurzydłowski [6] and Robert E. Przekop [4,*]

[1] Faculty of Materials Science and Engineering, Warsaw University of Technology, ul. Wołoska 141, 02-507 Warsaw, Poland; marta.dobrowolska@pw.edu.pl (M.D.); paulina.kozera@pw.edu.pl (P.K.); rafal.kozera@pw.edu.pl (R.K.)

[2] Department of Non-Food Products Quality and Packaging Development, Institute of Quality Science, Poznań University of Economics and Business, al. Niepodległości 10, 61-875 Poznań, Poland

[3] Faculty of Chemistry, Adam Mickiewicz University in Poznań, Uniwersytetu Poznańskiego, 61-614 Poznań, Poland; martakolodziejczak97@gmail.com (M.K.); julia.glowacka@amu.edu.pl (J.G.)

[4] Centre for Advanced Technologies, Adam Mickiewicz University in Poznań, 10 Uniwersytetu Poznańskiego, 61-614 Poznań, Poland; ewa.gabrzel@amu.edu.pl (E.G.); m.jalbrzykowski@ph.edu.pl (M.J.)

[5] Faculty of Mechanical Engineering, Bialystok University of Technology, ul. Wiejska 45c, 15-351 Białystok, Poland; krzysztof.kurzydlowski@pw.edu.pl

* Correspondence: renata.dobrucka@inc.poznan.pl or renata.dobrucka@pw.edu.pl (R.D.); rprzekop@gmail.com or rprzekop@amu.edu.pl (R.E.P.)

Abstract: Amorphous diatomite was used as a filler for a thermoplastic polymer of polyamide 11 obtained from natural sources. The diatomite particles of different sizes were previously fractionated by sedimentation to obtain powders with varying particle size distribution, including powders with or without frustule particles, crushed, uncrushed or agglomerated. Biocomposites containing 2.5, 5, 10 and 20% filler were tested for their mechanical properties, including tensile strength, flexural strength and impact strength. In addition, a particle size analysis (by Dynamic Light Scattering, DLS) was performed and the dispersion of the filler in the polymer matrix (Scanning Electron Microscopy, SEM), thermal parameters (Differential Scanning Calorimetry, DSC, and Dynamic Mechanical Analysis, DMA) were determined. Testing showed that biocomposites modified with diatomaceous earth have a higher mechanical strength than the reference system, especially with larger amounts of the filler (10 and 20%), e.g., the tensile strength of pure PA11 is about 46 MPa, while 20I38 and 20I0F 47.9 and 47 MPa, respectively, while an increase in mass, flexural strength and flexural modulus is also observed compared to pure PA11 by a maximum of 63 and 54%, respectively. Diatomaceous earth can be obtained in various ways—it is commercially available or it is possible to breed diatoms in laboratory conditions, while the use of commercially available diatomite, which contains diatoms of different sizes, eliminates the possibility of controlling mechanical parameters by filling biocomposites with a filler with the desired particle size distribution, and diatom breeding is not possible on an industrial scale. Our proposed biocomposite based on fractionated diatomaceous earth using a sedimentation process addresses the current need to produce biocomposite materials from natural sources, and moreover, the nature of the process, due to its simplicity, can be successfully used on an industrial scale.

Keywords: polyamide 11; diatomite; mechanical properties; particle size; biocomposite

check for updates

Citation: Dobrowolska, M.; Dobrucka, R.; Kozera, P.; Kozera, R.; Kołodziejczak, M.; Gabrzel, E.; Głowacka, J.; Jałbrzykowski, M.; Kurzydłowski, K.J.; Przekop, R.E. Biocomposites Based on Polyamide 11/Diatoms with Different Sized Frustules. *Polymers* **2022**, *14*, 3153. https://doi.org/10.3390/polym14153153

Academic Editor: Luigi Ambrosio

Received: 1 July 2022
Accepted: 29 July 2022
Published: 2 August 2022

Publisher's Note: MDPI stays neutral with regard to jurisdictional claims in published maps and institutional affiliations.

Copyright: © 2022 by the authors. Licensee MDPI, Basel, Switzerland. This article is an open access article distributed under the terms and conditions of the Creative Commons Attribution (CC BY) license (https://creativecommons.org/licenses/by/4.0/).

1. Introduction

Polyamide 11 (PA 11) is a thermoplastic polymer obtained from renewable sources derived from castor oil. Compared to polyamide 12, the production of PA 11 is by far more environmentally sustainable as it utilizes natural oil derivatives. In addition, PA 11 has excellent heat resistance, is stable under natural weather conditions and is characterized

by high mechanical strength on the level comparable to that of PA 12 (Table 1). Since it is derived from natural sources, polyamide 11 is also biodegradable, which reduces its carbon footprint. Considering the abovementioned advantages, PA 11 is a good answer to traditional oil-derived polymers used, including the commonly used PA 12, in terms of environmental protection [1,2]. Polyamides are polymers whose chain structure contains amide groups (R-CO-NH-R'), widely used in many industries, such as automotive [3], aerospace [4], 3D printing [5], production of housings for power tools and machinery [6]. The polyamide varieties most widely used and discussed in the literature include: PA 6, PA 6,6, PA 12 and PA 11. The properties of the selected polyamide grades are compiled in Table 1. Polyamides can be obtained by polycondensation of dicarboxylic acids and diamines (PA 6,6), ω-aminocarboxylic acids (PA 11, PA 12) and by the ring opening reaction (ROP) of lactams (PA 6) [7]. Óvári, Zsófia, et al., in their review [8], described the recent developments in the production of PA 6 and composites thereof, including the thermoplastic resin transfer molding (TRTM) process, which is a promising method for large-scale fabrication of reinforced PA 6 composites. Polyamide 12 is produced on an industrial scale from lauric lactam by ROP. Due to the increasing environmental pollution and the depleting crude oil resources, the extraction of which could become economically unviable, alternative methods of polyamide synthesis are being sought worldwide. Evonik has developed a biotechnology for the production of PA 12 using ω-aminolauric acid derived from palm kernels [9]. Research is also being conducted on the synthesis of Bio-PA 6 as described by Oelmann and Meier [10]. The reaction scheme for the production of polyamide 6 is shown in Figure 1.

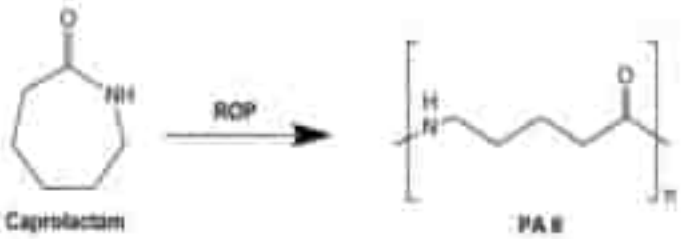

Figure 1. The reaction scheme for obtaining polyamide 6 from caprolactam.

Nylon 11 [poly(imino-1-oxoundecamethylene)] has been produced on an industrial scale since 1940 by step-growth polymerization. The ricinoleic acid obtained from castor oil is successively pyrolyzed and brominated (HBr) in the presence of oxygen. The resulting 11-bromododecanoic acid is then treated with aqueous NH_3, leading to the precipitation of a crystalline amino acid (11-aminoundecanoic acid). Polycondensation of this amino acid with aqueous extraction leads to obtaining polyamide 11 [11]. The utilization of castor oil for production of PA 11 renders it a bio-based polymer. The reaction scheme for the production of polyamide 11 is shown in Figure 2. Monomers of individual polyamides are presented in Figure 3.

Polyamide 11 can be processed in several ways. Among the most popular are injection molding and extrusion. In addition, rotational molding is a relatively new form of processing [10]. PA 11 is also successfully used in 3D printing as a powder for selective laser sintering (SLS) [19,20]. Due to its very good mechanical and chemical properties, it found applications for fabrication of components of both underwater and land-based pipelines, plastic car parts and housings for electronic equipment. It is also used as a coating material and in medicine [21,22].

As with other polymers of technical importance in structural applications, PA 11 has a long record on preparation of composites thereof containing various types of reinforcing phases. PA 11 reinforced with glass fibers (PA 11GF) is commercially available. Other examples cover the use of carbon fibers [23], basalt fibers [24] or graphene, the latter being introduced to increase wear resistance of coating-application-dedicated polyamide composites [25]. However, as mentioned above, due to its environmental friendliness

and biodegradability, the most favorable modification procedures for PA 11 are carried out with natural raw materials. Polyamide can be reinforced with bamboo fibers [26], basalt/flax interwoven fibers [27], cellulose fibers [28], lignocellulosic pine fibers [29] or beech fibers [30]. Such biofillers are considered to be economically viable, less-contributing to the carbon footprint, and environmentally non-burdening when reaching material end-of-life [31]. The development of novel, biopolymer-based and/or biofiller containing, high performance biocomposites, constituting a large part of the bioplastics group, is an important trend in the development of circular economy [32,33].

Table 1. Comparison of the properties among PA 11 [12–14], PA 12 [14–16] and PA 6 [14,17].

	PA 11	PA 12	PA 6
Tc (°C)	142–159.8	147–148	191.8–193.2
Tm (°C)	176–198	174–185	220–260
Tg (°C)	35–46	35	50–75
Polydisperity Mw/Mn	1.72–2.30	1.54–3.5	1.7–2.4
Crystallinity (%)	16.6–36	30–52	24.4–50
Tensile strength (MPa)	40.53–42	50–70	74–106
Tensile modulus (MPa)	1288.83–1300	1.600–1.608	780–3.000
Izod impact strength (kJ/m^2)	13.49	30	17
Charpy impact strength (kJ/m^2)	5–15	6–25	3.5–42
Flexural strength (MPa)	~45	60.7	101
Flexural modulus (MPa)	290–1080	560–1260	2.603
Shore D hardness	64–75	63–79	78.5–82

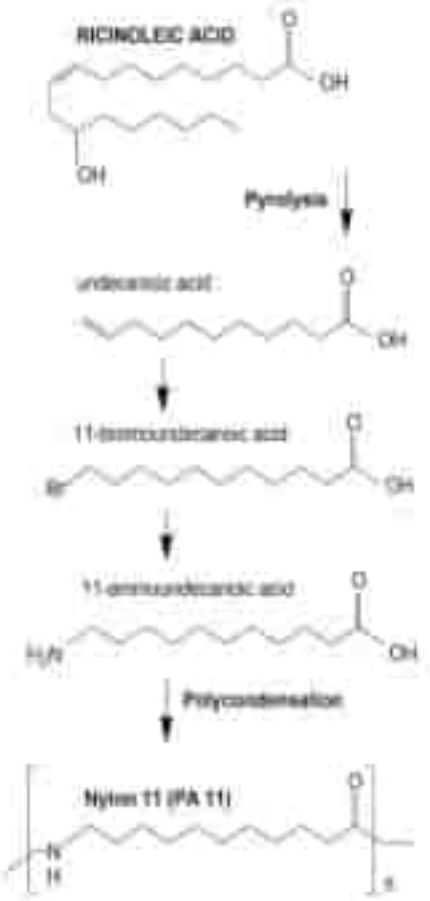

Figure 2. The reaction diagram for obtaining polyamide 11 from castor acid.

Among the biofillers group, one deserving special attention is diatomaceous earth (DE), or in short, diatomite. It is a leftover mineral material constituting of frustules of dead diatoms, with particle size from single up to hundreds of micrometers. From a physicochemical point of view, it can be seen as porous microsilica doped with compounds of Al, Fe, Mg, Ca and traces of other elements [34]. Diatomite is considered biofriendly, non-toxic, and used for multiple applications, including as an adsorbent and filtering medium in wastewater treatment and other purification procedures, cement production and as a polymer filler [35]. In our previous works, we tested diatomaceous earth as a filler in different polymer systems, including epoxy composites [36,37], injection-molded PLA [38] and PLA-based composite filaments for FDM 3D printing [39].

In this work, we developed methodology of preparation of PA 11/DE biocomposites and tested their processing behavior and service performance. For this purpose, polyamide 11 was filled with an amorphous diatomaceous earth which was previously fractionated by sedimentation, so that fractions with varied diatom grain sizes could be obtained. Biocomposites containing 2.5, 5, 10 and 20% of the filler (neat and fractionated diatomite) were prepared by extrusion and injection molding. The biocomposites were tested for mechanical strength, processing properties, heat resistance and filler dispersion in the polymer matrix. The tested samples were conditioned at room temperature, 23 °C (RT).

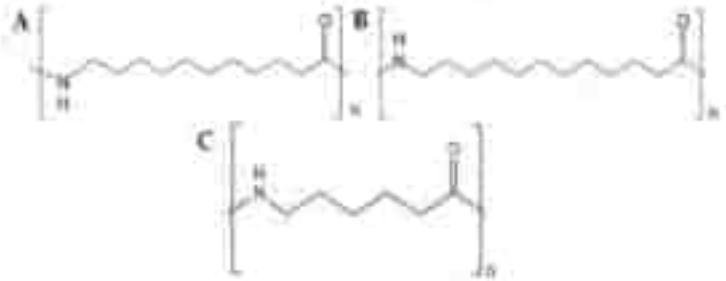

Figure 1. Monomers of polyamides: (A)—PA 11, (B)—PA 12, (C)—PA 6.

2. Materials and Methods

2.1. Materials

Polyamide 11 (Rilsan® BESNAT Natural) (density = 1.03 g/cm³, MFI index = 30 g/10 min) in pellet form was purchased from Arkema (Colombes, France). Diatomaceous earth (PermaGuard, Bountiful, UT, USA) in the form of powder was derived from diatomite deposits.

2.2. Preparation of Diatomite

The original diatomaceous earth was fractionated in a similar way as in the previous works [36–39], according to Figure 4. Amorphous diatomite weighing 15 kg was placed in barrel 1, which was filled to a volume of 140 L with demineralized water. The whole mixture was mixed with a mechanical stirrer for 5 min and sedimented for 2 h. After this time, the supernatant liquid was pumped into the next barrel (2) with a pressure booster pump. The sludge remaining in the first barrel was again filled up with demineralized water and the washing was performed in the same way. The rinsing process was repeated 5 times, and the supernatant liquids (barrel 1) were pumped to obtain suspended solids in barrel 2. Another series of washes of the remaining sludge in the first barrel was carried out. This time the procedure included 1 h of sedimentation. Barrel number 1 with the sediment was filled up with demineralized water to a volume of 140 L and stirred for 5 min with a mechanical stirrer. The suspension was allowed to settle for 1 h and then the supernatant liquid was pumped into barrel 3. The procedure was repeated 5 times and a suspension in barrel 3 was obtained from the liquids poured together. One week after the end of fractionation, the remaining supernatant liquids were pumped out of barrels 2 and 3. The sludge from barrels 1, 2 and 3 were dried at 70 °C for 24 h. Eventually, 3 fractions of diatomite with different particle size distributions were obtained. Table 2 shows the

weights of the obtained sludges after the respective number of washes and their percentage in relation to the used diatomite (15 kg). The loss of material was due to the removal of supernatant liquid, which partly contained dispersed diatomite particles. Fraction 2 of the washed diatomaceous earth was used to obtain the polyamide-based biocomposites, because a large amount of diatomite was obtained and the particle size distribution is significantly different from the original diatomite, which also allowed us to investigate the effect of particle size on the properties of the biocomposites produced.

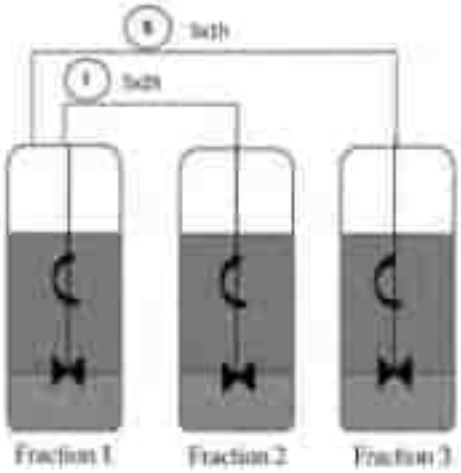

Figure 4. Fractionation of diatomite: I—5-fold sedimentation, 2 h each time; II—5-fold sedimentation, 1 h each time.

Table 2. The weight of sediments obtained.

	Weight of Sediment (kg)	Percentage (%)	Times Washed
Fraction 1	1.785	11.90	10
Fraction 2	**10.361**	**70.40**	**5**
Fraction 3	0.952	6.35	5
Total	13.298	88.65	-

2.3. Extrusion of Biocomposite

The extrusion of biocomposites was carried out on a process line RHEO DRIVE 16 from Haake PolyLab OS (Thermo Scientific) (Waltham, MA, USA). The process was carried out with a twin-screw extruder. Before extrusion polyamide 11 was dried out for 8 h in 90 °C. A mixture of PA 11 and original diatomaceous earth was fed into the hopper in portions (of 50 g) at four concentrations of 2.5%, 5%, 10% and 20%, respectively. The screws were used to plasticize and stir the materials. The extrudates were dried at 70 °C for 24 h, and then ground in WANNER C17.26 ev plastic mill (Łódź, Poland). Four compositions of polyamide 11 with diatomaceous earth were obtained in concentrations of 2.5%, 5%, 10% and 20%. The remaining biocomposites were extruded in a similar way. The parameters of the extrusion process are shown in Table 3.

Table 3. The parameters of the extrusion process.

Temperature at heating zones (°C)	Nozzle	TS6	TS5	TS4	TS3	TS2	TS1
	235	250	250	235	255	250	250
Torque, M (Nm)		**Nozzle pressure, P_M (bar)**			**Revolutions per minute, N (1/min)**		
20–70		16			14		

2.4. Injection Molding—To Obtain Standardized Measurement Paddles

The injection was performed on a column-free e-victory 170/80 injection molding press from Engel (Warsaw, Poland). Table 4 shows the process parameters. A holding pressure of linear increment over time was applied. The mold temperature was maintained at 80 °C. Standard measuring preforms of the type 1A were obtained according to ISO 527 (Figure 3). Finally, 4 biocomposite types and a reference system (Table 5) were obtained.

Table 4. Injection process parameters.

Temperature (°C)	Nozzle	Zone 1	Zone 2	Zone 3	Traverse
	215	220	215	220	40
Mold closing force (kN)	Clamping time (s)		Cooling down time (s)	Screw diameter (mm)	
800	4		30	25	

Figure 3. Biocomposites obtained by injection.

Table 5. Biocomposites to be tested.

Biocomposite Type	Filler Concentration	Abbreviation
PA11 + original diatoms	2.5%	2.5OB
	5%	5OB
	10%	10OB
	20%	20OB
PA11 + fractionated diatoms	2.5%	2.5OF
	5%	5OF
	10%	10OF
	20%	20OF
PA11	-	PA11

2.5. Characterization Methods

Paddle-shaped specimens prepared in accordance with EN ISO 527-1 were used for the strength tests: 2012 and EN ISO 178:2010. Testing was carried out on the INSTRON 5969 strength testing machine with a peak load force of 50 kN (Instron, Norwood, MA, USA). The traverse rate for the tensile strength measurements and flexural strength measurements

was set at 5 mm/min. Charpy impact strength (with V-notch) was performed using Instron's Ceast 9050 impact device with pendulum hammer with a maximum energy of 25 J according to ISO 179-1:2000 (Instron, Norwood, MA, USA). The impact strength test was conducted in accordance with PN-EN ISO 178-1. The notch was machined and positioned in the center of the preform according to ISO 179-1/1eA. A V-shaped 2 mm-deep notch with a 45° angle was produced. According to the standard, the impact direction was aligned with the edge. Dynamic mechanical analysis (DMA) was performed using a Q800 DMA (TA Instruments, USA) in dual cantilever mode according to ASTM D4065-01. Three rectangular specimens with 60 mm length and 10 mm width were cut from each biocomposite and used in the test. The analysis was conducted from 0 to 130 °C with a heating rate of 3 °C/min at a frequency of 1 Hz and an amplitude of 30 µm. The glass transition temperature (Tg) was determined from the peak value in the storage modulus using TA Universal Analysis software. The powder morphology was characterized using a scanning electron microscope (SEM, TM 1000 Hitachi, Japan) operating at an applied voltage of 5 kV. Before observations with the SEM, the surfaces of the specimens were sputtered with a gold-palladium layer for 90 s at a current of 10 mA and voltage of 2 kV. The melt flow rate (MFR) was measured using the Instron CEAST MF20 melt flow tester (Instron, Norwood, MA, USA), which complies with EN ISO 1133 at 235 °C for a load of 2.16 kg. The size of the diatoms used to prepare the biocomposites was measured with Mastersizer 3000 (Malvern Instruments Ltd., Malvern, GB). The measurements were made for the samples in water suspension (Hydro EV attachment). The parameters of the measurements for the wet samples: stirrer speed: 2330 RPM; ultrasound power: 70%. Thermal properties of materials were studied using a Q1000 Differential Scanning Calorimeter (TA Instruments, New Castle, DE, USA). Samples with a weight of 8.0 ± 0.2 mg were placed in an aluminum hermetic pan. Firstly, the samples were equilibrated at −90 °C, then heated to 230 °C with a scan rate of 10 °C/min, and cooled to −90 °C with a scan rate of 10 °C/min. Finally, they were heated again to 230 °C with a scan rate of 10 °C/min. The process was conducted in a nitrogen atmosphere (20 mL/min). Using the Universal V4.5A TA software, the glass transition temperature (Tg) was determined as the midpoint of the glass transition temperature range. The melting temperature was determined as the peak temperatures of cold crystallization and melting, respectively. Moreover, the degree of crystallinity was calculated. The heat of fusion of 100%-crystalline Nylon 11 was equal to 206 J g^{-1} [11]. The viscosity of the biocomposite was determined by the capillary method and using the Instron CEAST SR10 Smart RHEO 1000 capillary rheometer. The measurement was carried out at 235 °C using a capillary tube with a diameter of 1 mm and a length of 20 mm. Viscosity was determined for 6 shear rates, that is, 10, 30, 100, 500 and 1000 (1/s). Images of the surface and fractures of the biocomposites were taken using KEYENCE VHX-7000 digital microscope (KEYENCE INTERNATIONAL, BELGIUM, NV/SA) with a VH-Z100R wide-angle zoom lens at 100× magnification. Images were taken with depth composition and 3D imaging. Total coaxial illumination was used. Mechanical properties, i.e., tensile breaking strength, flexural strength, impact strength and wetting angle were tested for biocomposites, which were previously conditioned at room temperature. Viscosity testing, fracture imaging (SEM) and thermal tests (DSC, DMTA) were performed on selected biocomposites, i.e., those containing 5 and 20% filler in order to compare the effects of low and high filling on rheological, mechanical and thermal properties.

3. Results

3.1. Particle Size Distribution of the Modifier (Determined Using DLS)

The fractionation of raw diatomaceous earth resulted in three fractions that differed in particle size distribution, as shown in Figure 6. The original diatomite has a particle size distribution ranging from 1 µm to about 100 µm with particles with an average size of approx. 10 µm making up the largest volume fraction. Fraction 1, which was washed 10 times, has particles ranging in sizes of approx. 3 to 100 µm, with the largest number of particles of about 40–50 µm, indicating that this number of washes resulted in the

removal of low-diameter particles but enriched the material with large-diameter particles. Fractions 2 and 3 do not show any significant differences from each other. The two fractions have a significant proportion of particles ranging in size from 4 to about 35 µm and the elimination of ultrafine particles that remained suspended in the supernatant after washing the diatomite. This method of fractionating diatomite made it possible to obtain sediments with completely different particle size distributions. One of the resulting fractions had larger particles that were probably agglomerated, and the other contained no agglomerates and particles smaller than 4 µm, i.e., diatoms with crushed frustules. Similar results, i.e., partial separation of the crushed particles from the uncrushed and agglomerated particles, were obtained in previous work [39], which shows the repetition of the sedimentation, which is a process of deposition.

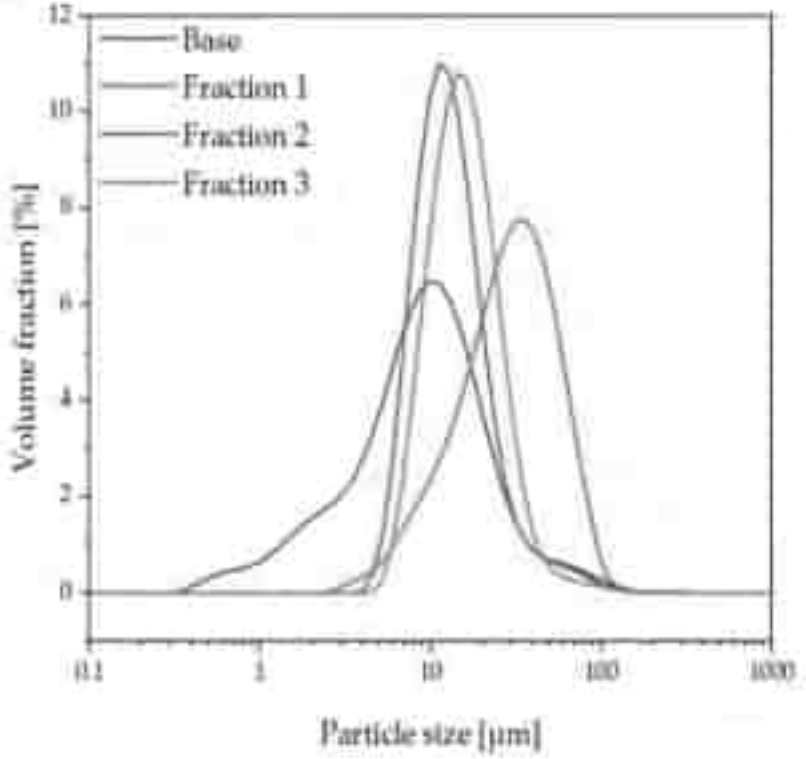

Figure 6. Particle size distribution of fractionated diatomite.

3.2. Rheology—Melt Flow Rate (MFR) and Capillary Rheology

Melt flow rate testing showed that pure polyamide 11 has a relatively high MFR (about 30 g/10 min), which is consistent with literature reports [40]. The modification of PA11 with original diatomite at a low concentration, that is up to 5 wt%, does not cause significant changes in processing properties, while higher addition of modifier (10 and 20%) results in almost twice as low values (~20 and ~15 g/10 min, respectively) (Figure 7). The modification with fractionated diatomite and the addition of as little as 5% modifier resulted in a linear decrease in the MFR when the concentration was lowered, but the final values are similar to those for the original diatomite. The addition of up to 20% modifier does not cause any general difficulties in the processing of biocomposites, as the melt flow rate of 15 g/10 min is still sufficient for both extrusion and injection of small components, the standardized preforms studied in this work.

As expected, the reference polyamide 11 has the lowest viscosity of all tested samples (Figure 8). Filling the biocomposite to a concentration as low as 5% causes an increase in viscosity for the samples with both the original and the fractionated diatomite, although the effects are small at high shear rates. In addition, for low-filled systems, the viscosity is

almost constant at a shear rate of 100–1000 1/s. Highly filled systems with 20 wt% filler exhibit a completely different relationship. They have a much higher viscosity than the others, on average more than double, with the system containing the original diatomite having a higher viscosity due to the proportion of micro and sub-micro fractions. A similar effect was described in a previous paper [36]. Diatom particles, due to their size, penetrate between the biopolymer chains and consequently disrupt their ordering. This effect results in smaller interactions between the chains, which reduce the viscosity of the biocomposites. In addition, the viscosity curves show a different tendency than low-filled systems. The shear thinning effect is more pronounced [41]. From the above correlations, a small addition of diatomite filler does not significantly worsen the viscosity of the biocomposite systems in the melt, while at high filler levels (20%) the use of sedimented filler can keep the melt viscosity at a lower level. Filler particle size also affects the viscosity of biocomposites. For 20% filler concentration, particle size control improved processability by reducing external friction. The addition of diatomaceous earth with a smaller particle size range (Fraction 2, Figure 6) resulted in lower viscosity compared to unfractionated diatomite.

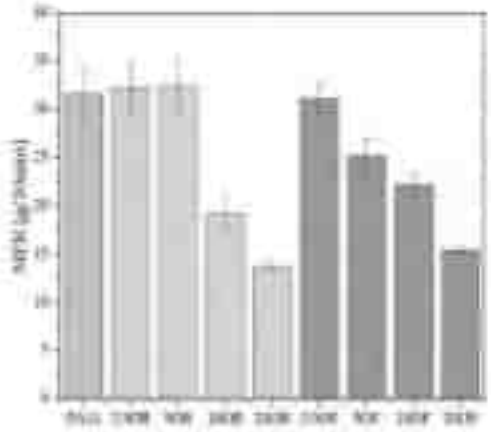

Figure 7. Melt flow rate (MFR) of biocomposites.

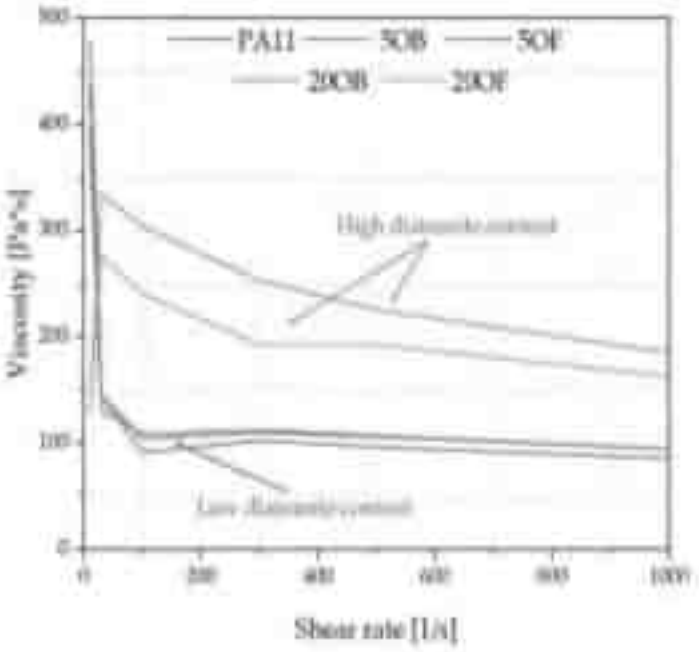

Figure 8. The viscosity of biocomposites of PA11 and diatoms after the injection (capillary rheology).

3.3. Mechanical Tests

3.3.1. Tensile Strength

Mechanical tests were carried out on biocomposites conditioned at room temperature, as shown in Figures 9–11. As expected, modification of pure polyamide 11 with both original and fractionated diatomite resulted in a slight decrease in tensile strength for low filler concentration compared to neat PA11 (Figure 9). Both the tensile strength and the Young's modulus increased with increasing filler concentration, with fractionation of diatomite resulting in slightly higher tensile strength values as soon as for the lowest concentration, compared to the original diatomite. By filling at a level of 20%, values were achieved that were higher than those of pure polyamide. This could indicate that it is important to eliminate the matrix effect on the mechanical strength of the polyamide in favor of the natural filler. In our previous work, the reinforcing effect of diatomite filler on polylactide [38,39] and epoxy resin [36,37] was also observed for different ways of obtaining composites. Due to the structure of diatoms, there can be an effect of penetration of biopolymer molecules into the filler particles; thus, strengthening the structure of the biocomposite. Diatoms acts asan excellent anchor where hydrocarbon chains can bond together strengthening the structure. There is also a limiting concentration of diatomaceous earth at which the structure strengthening effect begins to prevail, as observed in the form of increased tensile strength. For both base and fractionated diatomaceous earth, this concentration is more than 10% filler.

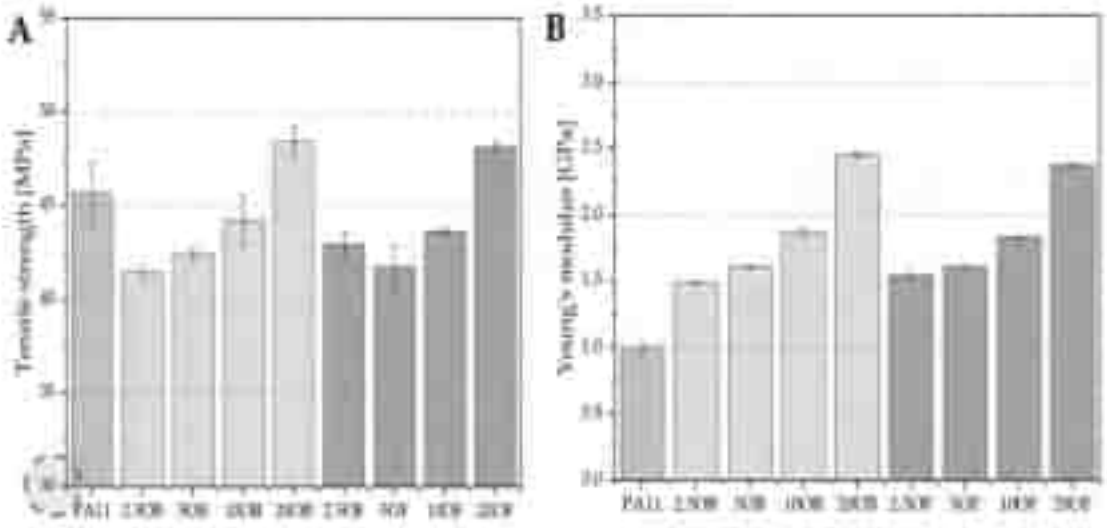

Figure 9. The results of the static tensile test are as follows: (**A**) the tensile strength and (**B**) the Young's modulus of the biocomposites conditioned at room temperature (RT).

3.3.2. Flexural Strength

The modification of the pure polyamide 11 with diatomaceous earth improved the mechanical parameters, including the flexural strength (Figure 10). Pure PA11 withstands a peak bending stress of 40 MPa, and has a modulus of elasticity of 1.25 GPa, which is the lowest measured value for the tested samples previously conditioned at room temperature. As the modifier concentration in the series increases, both parameters increase linearly. Although the particle sizes were different in the original diatomite compared to the fractionated diatomite, no significant differences were found in the flexural strength values for the corresponding samples in the series.

3.3.3. The Charpy Impact Test (V-Notch Test)

The impact strength of pure polyamide 11 is relatively high, approximately 7 kJ/m^2 on average. Filling the biocomposite with diatomite reduces the impact strength due to

the nature of the filler (powder filler). The higher the filling ratio of the biocomposite, the lower the impact strength values, which is due to the fact that air is trapped in the diatom particles, causing early crack propagation (Figure 11). The more filler added, the greater the amount of air present.

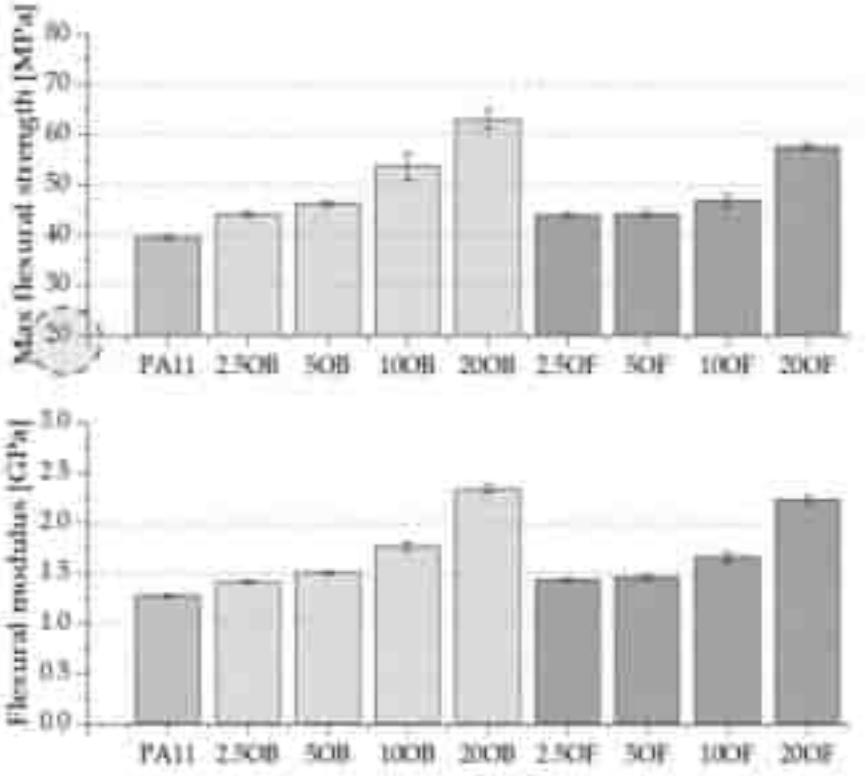

Figure 10. The results of static flexural strength test: maximum bending stress and modulus of elasticity.

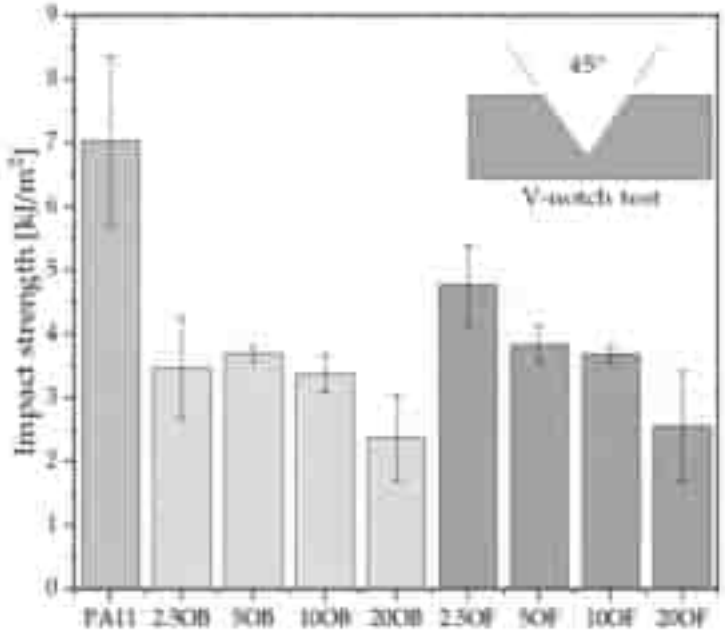

Figure 11. The results of the Charpy impact test (Charpy V-notch test).

3.4. Morphology of Biocomposite Surfaces

Images of biocomposite fractures taken with a scanning electron microscope at a magnification of 200 µm are shown in Figure 12. Once fractured, the pure polyamide 11 delaminates and its structure remains homogeneous. Biocomposites containing diatomaceous earth show similar behavior. In most cases, numerous furrows are present on the fracture surfaces. Only the biocomposites modified with 5% original diatomite show a smooth fracture structure, without furrows. The diatomaceous earth is uniformly dispersed in the polymer matrix and no tendency to agglomeration is observed. SEM images confirm that the amount of diatom particles increases with the increasing concentration of the modifier.

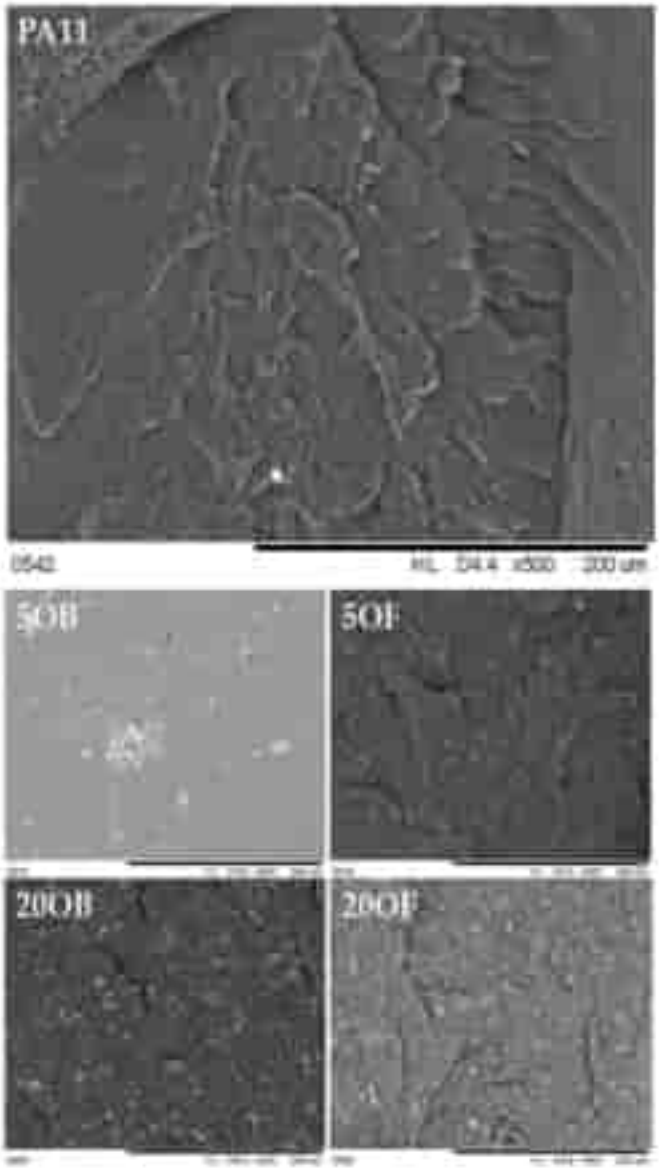

Figure 12. SEM images of biocomposite fractures.

An optical microscope was used to image the surface of the biocomposites (Figure 13), and their fractures that occurred after the notched impact strength testing (Figure 14). The reference system used was pure polyamide 11 (PA11). Polyamide has a relatively smooth surface, but small furrows are locally present, indicating the relatively poor scratch resistance of the polyamide, which is mostly absent in the biocomposites filled with diatomite.

The samples modified with original diatomite show color differences both between concentrations within the system and compared to the samples filled with fractionated diatomite, possibly due to the different particle arrangement (agglomeration) of the original diatomite, which does not occur for fractionated diatomite due to the narrower range of particle sizes. As the concentration of the original or fractionated filler increases, the surface of the biocomposite becomes irregular and numerous protrusions are formed. This effect is more evident when only 10% of the original diatomite is added, while irregularities appear on the surface when the filler concentration is only 20%. Examination of the biocomposite fractures showed that the fractionation of diatomite had no significant effect on the type or brittleness of a crack. Regardless of the modifier used, the fractures are very similar. At concentrations between 2.5% and 10%, furrows and numerous "wrinkles" formed in the material when the biocomposite particles were pulled out. For highly filled samples (20%), the effect is much less. There are a few changes in the material structure that can be attributed to high-energy impact.

Gloss testing was performed in a 60° geometry (Table 6). Pure polyamide 11 exhibited surface gloss values of 31.5 GU, making it a medium gloss system. The addition of diatomaceous earth resulted in a decrease in gloss and the formation of a surface towards matte. The gloss of the biocomposites decreased linearly as the filler concentration of the base diatomaceous earth increased. This was different for diatomaceous earth fractionation, where the highest results of 35.7 and 26.1 GU were recorded for biocomposites filled at 5 and 10%, respectively. The surface of all tested samples, both pure polyamide 11 and biocomposites modified with diatomaceous earth, have hydrophilic character due to the value of wetting angle below 90° (Figure 13). No linear relationship between filler content and surface character was observed. Both fractionated and base diatomaceous earth show similar values of 75–84°. High filling of polyamide 11 with diatomaceous earth (20%) did not result in loss of surface properties, especially for fractionated DE.

Table 6. Gloss of biocomposite surfaces.

	Gloss 60° (GU)	SD (GU)		Gloss 60° (GU)	SD (GU)
2.5DE	24.53	0.50	2.5DF	23.00	0.08
5DE	21.90	0.54	5DF	35.70	1.13
10DE	17.50	2.12	10DF	26.10	0.75
20DE	15.07	0.74	20DF	16.57	0.12
PA11		31.50		1.93	

3.5. Thermal Tests

The DMA thermograms of the PA11 biocomposite materials were created to determine the stiffness of the materials with the change in the temperature. As shown in Figure 14, the evolution of the storage modulus (E') and tan δ of PA11 and the biocomposites as a function of temperature showed a transition in the studied range, related to the glass temperature of the polymer matrix. The measured values of the Tg are presented in Table 7.

Table 7. Summary of the determined values of the glass transition temperature from storage modulus E' curves.

Sample	T_g (°C)
PA11	50.0
5DE	53.6
5DF	53.7
20DE	52.7
20DF	53.9

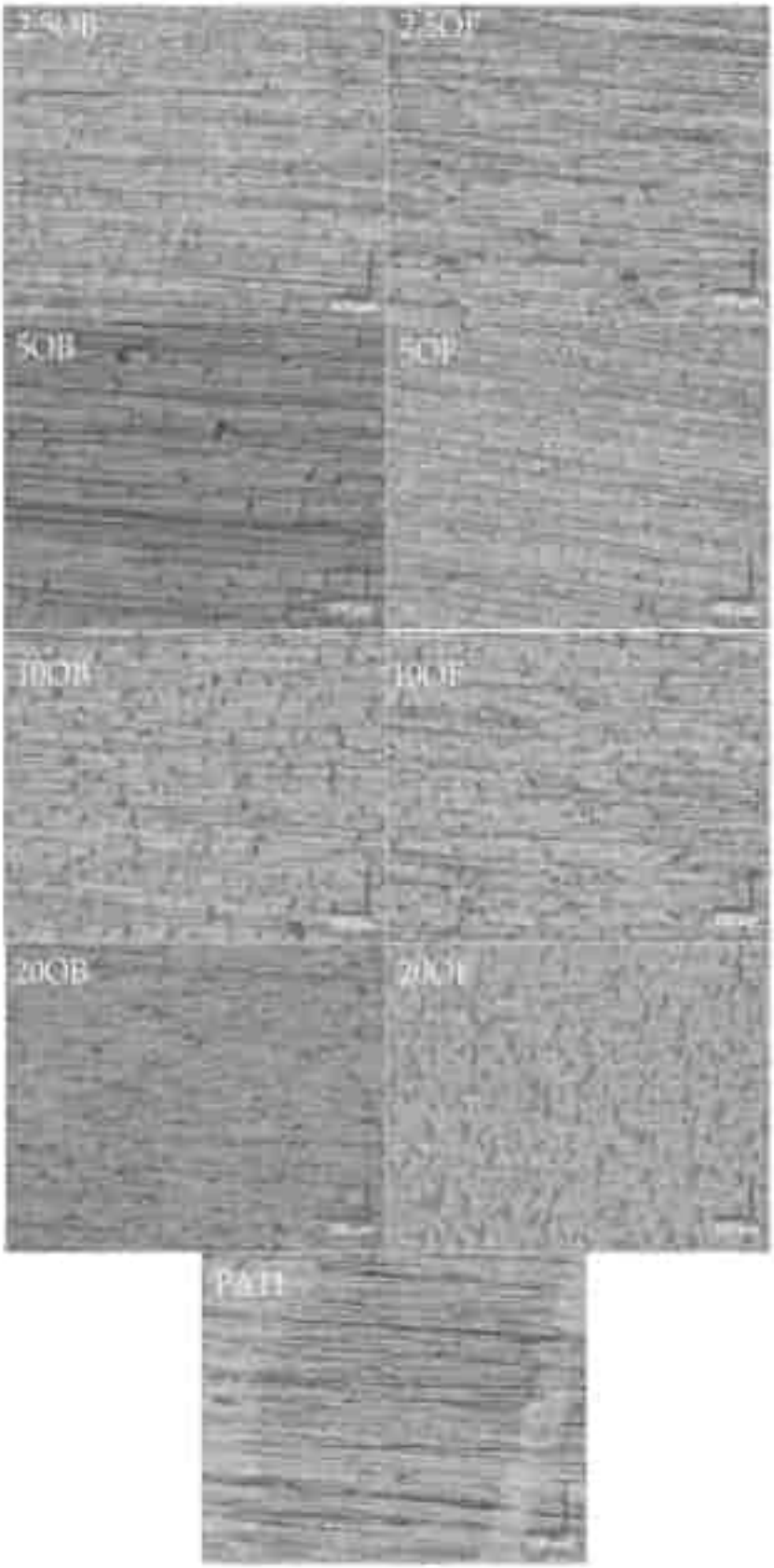

Figure 13. Surface of the biocomposites.

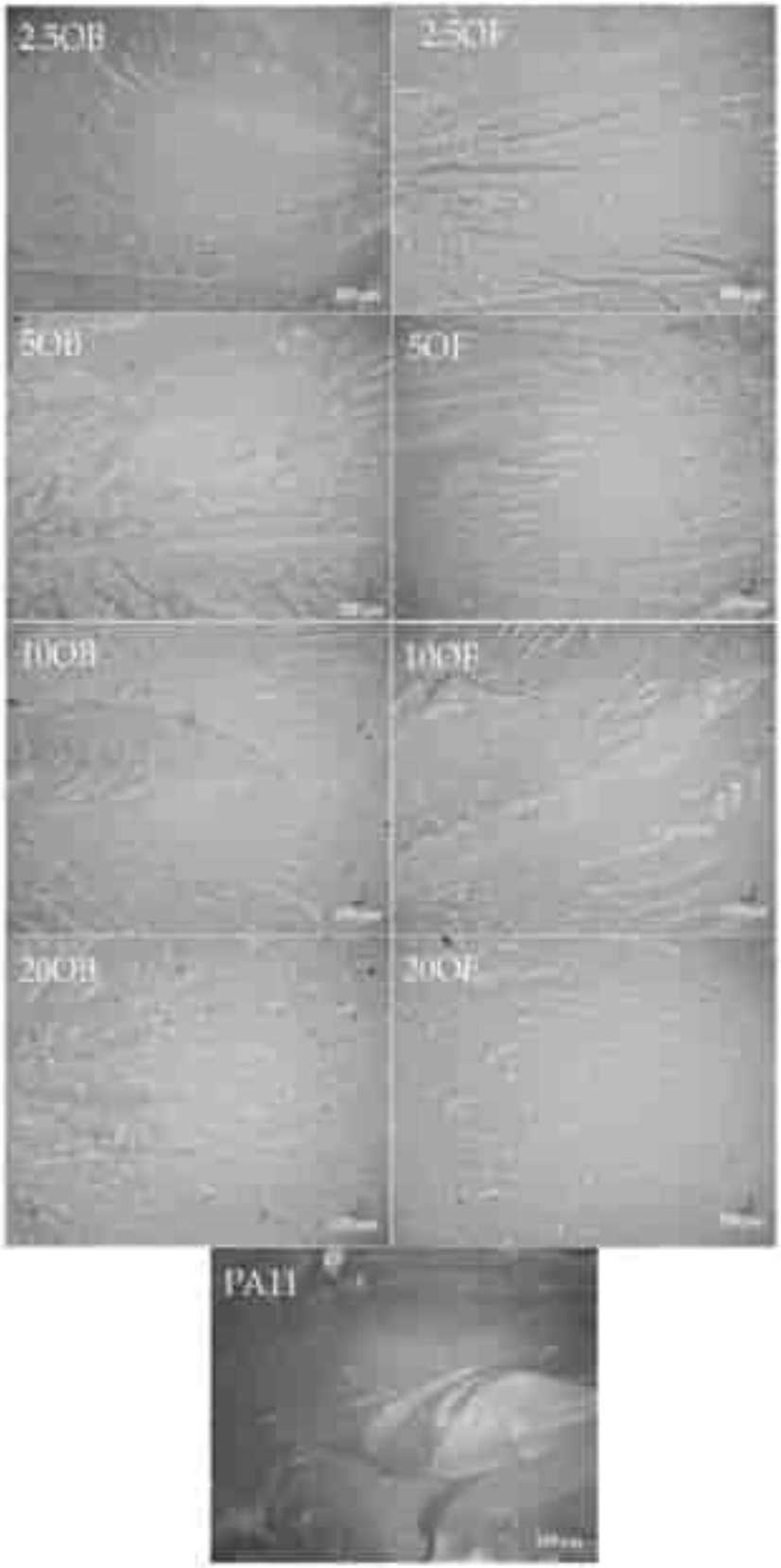

Figure 14. Biocomposite fractures after notched impact strength testing.

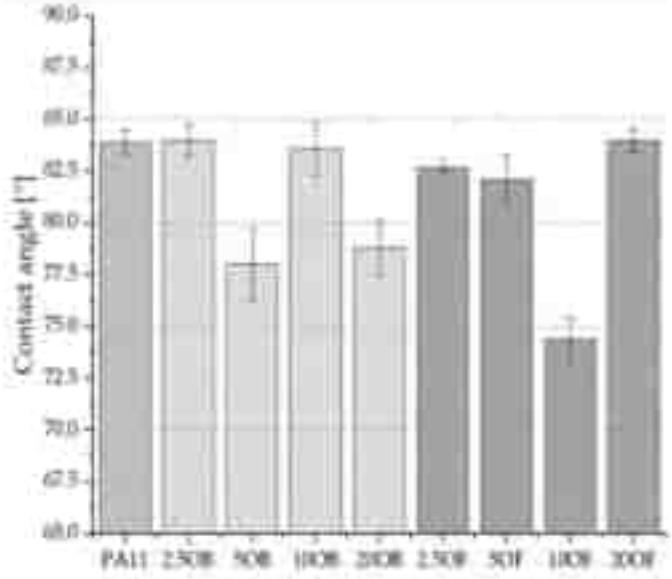

Figure 15. Contact angles of biocomposites' surfaces.

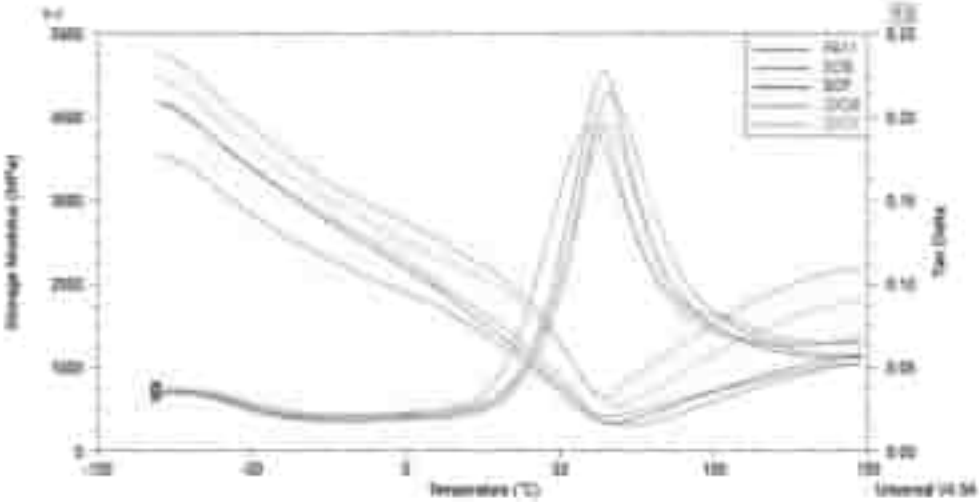

Figure 16. The results of the storage modulus and tan δ of PA11/diatoms biocomposites.

Figure 16 shows how the addition of different contents and different types of diatomaceous earth influenced the storage modulus (E') of biocomposites based on PA11 and diatoms. For comparison, the results were compared with the Tg of pure PA11. No considerable differences were observed in the Tg of the biocomposites by the effect of diatom content. Only a distinct increase in the Tg value was observed. However, the addition of 5 weight fractions of OB and OF to biocomposites caused a higher change in the glass transition temperature than the application of 20 wt% components. The fractionated diatomaceous earth increases the Tg value by 1.3° compared to the original when 20 wt% diatomite was added. Thus, the fractionation of diatoms has a beneficial effect on the thermal properties of PA11-based biocomposites, especially in the higher concentration range. The addition of diatoms into the PA11 polymer allowed for obtaining stiffer material with higher values of storage moduli due to the stiffening effect of the reinforcement. As it was found in [42], an increase in the weight fraction of the reinforcement causes an increase in the storage modulus of the biocomposite. Once the temperature was over the Tg, the storage modulus values were decreased, indicating high mobility of the polymer molecules corresponding to the amorphous phase of the PA11. The presence of diatoms in

the biocomposite structure was found to significantly reduce the mobility of the polymer chains at temperatures higher than its Tg.

DSC analysis was performed to investigate the thermal behavior of PA11 and PA11/diatom biocomposites. Figure 17 shows the DSC thermograms of PA11 and PA11/diatom biocomposites during the first heating and the second heating stage, respectively, and Table 8 shows the measured values. With increasing temperature, DSC curves of the first heating showed two thermal characteristics: a glass transition temperature (Tg) of nearly 50 °C, and an endothermic melting pt(Tm) of nearly 190 °C. It was found that the addition of diatoms resulted in a slight decrease in Tg and Tm temperatures. The inverse dependency was obtained during cooling. The use of diatomaceous earth had an influence on the increase of the crystallization temperature. For the second heating curves, it was observed that the unmodified PA11 and 5B and 5OF biocomposite showed two distinct melting peaks (Tm1 and Tm2) while 20OB and 20OF biocomposite had a single melting peak. It was found that PA11 and 5B and 5OF biocomposite presented the main peak at about 188 °C, preceded by a shoulder with a maximum at about 182 °C as rearrangement in the structure. Depending on temperature and processing conditions, PA11 has different crystalline structures which can be interconverted. This double peak corresponded to the melt-crystallization process of the γ phase to the α' crystalline form of PA11. The secondary peak seemed to decrease when the diatomaceous earth content was increased in the biocomposite material [34–43]. In addition, the peak of the glass transition temperature broadened considerably, and it is difficult to determine the Tg from the DSC curves during the second heating. The heat-of-fusion values determined from the second heating stage were used to obtain the crystallinity values, and these are tabulated in Table 8. Although the changes were very small, the crystallinity content consistently appears to increase with the content of diatoms. Moreover, higher degrees of crystallinity were obtained for composites with fractioned diatoms. Similar results were obtained in [44], which also observed an increase in the degree of crystallinity depending on the rise in the content of the additive to the polymer matrix.

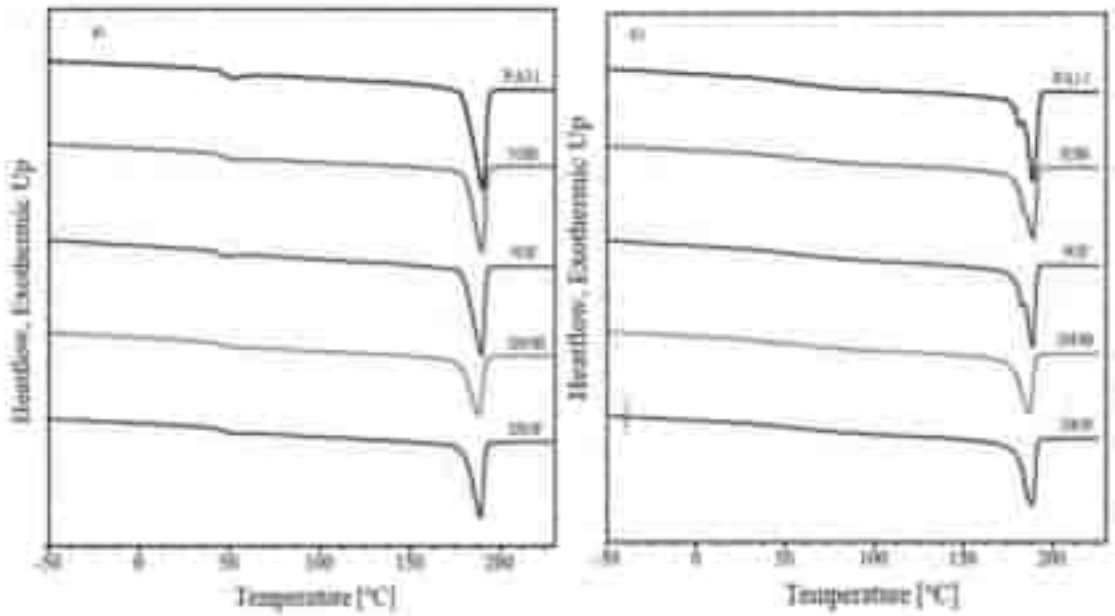

Figure 17. DSC curves of unmodified PA11 and biocomposites based on PA11 with different weight fractions of diatoms obtained during first heating procedure (a) and second heating procedure (b), respectively.

Table 8. Thermal characteristics of PA11 and biocomposites based on PA11 with different weight fractions of diatoms.

	1st Heating			Cooling		2nd Heating			
Sample	T_g (°C)	T_m (°C)	ΔH_m (J/g)	T_c (°C)	ΔH_c (J/g)	T_{mI} (°C)	T_{mII} (°C)	ΔH_m (J/g)	X_c (%)
PA11	48.7	190.0	56.9	163.9	53.2	181.4	189.0	51.6	25.0
5OB	46.8	189.5	44.6	167.6	50.4	182.6	189.0	45.0	22.9
5OF	44.0	189.5	48.7	167.1	49.11	182.8	188.6	50.3	25.7
20OB	44.6	187.6	36.4	167.8	50.7	-	186.6	44.1	26.7
20OF	46.6	188.7	39.2	169.7	51.5	-	188.4	44.7	27.1

4. Conclusions

Fractionation of the original diatomite using a simple vessel system and the sedimentation phenomenon allowed the obtaining of fractions with different particle size distributions. The resulting fractions differ in their content of crushed, uncrushed, and agglomerated diatom particles. The use of a sedimented and submicron-free fraction resulted in a lower increase in the viscosity of the melt, which is an advantageous effect from a processing point of view. Both the original diatomaceous earth and fraction 2, which were used as biocomposite fillers, do not tend to agglomerate and thus do not worsen the mechanical parameters. A suitable dispersion of the filler in the polymer matrix eliminates the problem of too early crack propagation. The effect is significantly less prominent in the case of tensile strength, though, as a considerable drop in its values is observed for 2.5–10% loadings, and only at 20% loading the biocomposites are characterized by statistically improved tensile strength. As the filler concentration increases, the above parameters improve significantly. The modification of polyamide 11 with diatomite also led to an increase in the thermal parameters of the biocomposites. An increase in Tg of 5.8 °C was observed. A lower filler concentration has a more favorable effect on the thermomechanical stability of the biocomposites. High filling of diatomaceous earth (20%) did not result in a decrease in the hydrophilic-hydrophobic character of the surface, especially for fractionated DE.

Author Contributions: Conceptualization, R.E.P.; methodology, R.E.P. and M.D.; formal analysis, R.E.P., M.D., R.D. and M.J.; investigation, R.E.P., M.D., P.K., R.K. and M.K.; data curation, M.D., P.K., M.K., E.G. and J.G.; writing—original draft preparation, M.D., R.E.P. and R.D.; writing—review and editing, M.D., R.E.P. and R.D.; visualization, M.D., P.K., R.K., M.K., E.G. and J.G.; supervision, R.E.P., R.D., M.J. and K.J.K.; project administration, R.D. and K.J.K.; funding acquisition, R.D. and K.J.K. All authors have read and agreed to the published version of the manuscript.

Funding: This work was financially supported in the frame of the project "Advanced Biocomposites for Tomorrow's Economy BIOG-NET", FNP POIR.04.04.00-00-3792/18-00, project is carried out within the TEAM-NET programme of the Foundation for Polish Science co-financed by the European Union under the European Regional Development Fund.

Institutional Review Board Statement: Not applicable.

Informed Consent Statement: Not applicable.

Data Availability Statement: The data presented in this study are available on request from the corresponding author.

Conflicts of Interest: The authors declare no conflict of interest.

References

1. Wypych, G. PA-11 polyamide-11. In *Handbook of Polymers*; Elsevier: Amsterdam, The Netherlands, 2016; pp. 241–245.
2. Jariyavidyanont, K.; Mallardo, S.; Cerruti, P.; Di Lorenzo, M.L.; Boldt, R.; Rhoades, A.M.; Androsch, R. Shear-Induced Crystallization of Polyamide 11. *Rheol. Acta* **2021**, *60*, 231–240. [CrossRef]
3. He, D.; Kim, H.C.; De Kleine, R.; Inac, V.K.; Kiziltas, A.; Compston, P.; Doolan, M. Life cycle energy and greenhouse gas emissions implications of polyamide 12 recycling from selective laser sintering for an injection-molded automotive component. *J. Ind. Ecol.* 2022, early view.

4. Qiao, M.; Xu, X.; Qin, Z.; Yan, S. Silicon carbide whiskers enhance mechanical and anti-wear properties of PA6 towards potential applications in aerospace and automobile fields. *Compos. Part B Eng.* **2019**, 175, 107096. [CrossRef]
5. Arun, M.; Sathishkumar, N.; Kumar, K.N.; Ajai, S.S.; Aswin, S. Development of patient specific bio-polymer incisor teeth by 3D printing process: A case study. *Mater. Today Proc.* **2021**, 39, 1303–1308. [CrossRef]
6. Winnacker, M.; Rieger, B. Biobased Polyamides: Recent Advances in Basic and Applied Research. *Macromol. Rapid Commun.* **2016**, 37, 1391–1413. [CrossRef] [PubMed]
7. Zia, K.; Akram, N.; Tabasum, S.; Noreen, A.; Akbar, M. *Processing Technology for Bio-Based Polymers*, 1st ed.; Elsevier: Amsterdam, The Netherlands, 2021.
8. Oroszi, Z.; Szilke, A.; Pinzies, S.; Zavoczki, L.; Szarka, G.; Iván, B. Recent Advances in the Synthesis and Analysis of Polyamide 6 and Products therefrom: From Polymerization Chemistry of ε-caprolactam to Thermoplastic Resin Transfer Moulding (t-rtm). *Acad. J. Polym. Sci.* **2020**, 4, 555629.
9. Dadbin, L. Polyamide (Nylon) 12 Degradation during the Selective Laser Sintering (SLS) Process: A Quantification for Recycling Optimization. Master's Thesis, Mechanical Engineering, University of Wisconsin, Madison, WI, USA, 2015.
10. Oelmann, S.; Meier, M.A.R. Synthesis of Modified Polycaprolactams Obtained from Renewable Resources. *Macromol. Chem. Phys.* **2015**, 216, 1972–1981. [CrossRef]
11. Meier, M.A.R. Plant-Oil-Based Polyamides and Polyurethanes: Toward Sustainable Nitrogen-Containing Thermoplastic Materials. *Macromol. Rapid Commun.* **2019**, 40, 1800524. [CrossRef]
12. Hao, A.; Wong, I.; Wu, H.; Lisco, B.; Ong, B.; Sallam, A.; Butler, S.; Londa, M.; Koo, J. Mechanical, thermal, and flame-retardant performance of polyamide 11–halloysite nanotube nanocomposites. *J. Mater. Sci.* **2015**, 50, 157–167. [CrossRef]
13. Magniez, K.; Iftikhar, R.; Fox, B.L. Properties of bio-based polymer nylon 11 reinforced with short carbon fiber composites. *Polym. Compos.* **2015**, 36, 668–674. [CrossRef]
14. Wypych, G. *Handbook of Polymers*; Elsevier: Amsterdam, The Netherlands, 2022; Volume 230–236, pp. 256–267.
15. Dong-Hun, L.; Chang, Y.W.; Jang, K.S. Morphology, mechanical properties and shape memory effects of polyamide12/polyolefin elastomer blends compatibilized by glycidylisobutyl POSS. *Materials* **2020**, 14, 27.
16. Stojšić, J.; Raos, P.; Milinović, A.; Damjanović, D. A Study of the Flexural Properties of PA12/Clay Nanocomposites. *Polymers* **2022**, 14, 434. [CrossRef]
17. Satheesh Kumar, S.; Kanagaraj, G. Investigation on mechanical and tribological behaviors of PA6 and graphite-reinforced PA6 polymer composites. *Arab. J. Sci. Eng.* **2016**, 41, 4347–4357. [CrossRef]
18. Oliveira, M.J.; Botelho, G. Degradation of polyamide 11 in rotational moulding. *Polym. Degrad. Stab.* **2008**, 93, 139–146. [CrossRef]
19. Sherman, L.M. Additive manufacturing: Materials for 'real-world' parts. *Plast. Technol.* **2014**, 60, 42–47.
20. Bai, J.; Yuan, S.; Shen, F.; Zhang, B.; Chua, C.K.; Zhou, K.; Wei, J. Toughening of polyamide 11 with carbon nanotubes for additive manufacturing. *Virtual Phys. Prototyp.* **2017**, 12, 235–240. [CrossRef]
21. Kohan, M.I. (Ed.) Chapter 13 Commercial nylon plastics and their applications. In *Nylon Plastics Handbook*; Hanser Publishers: Munich, Germany, 1995; pp. 487–599.
22. Bello, J.O.; Wood, R.J.K. Micro-abrasion of filled and unfilled poly-amide 11 coatings. *Wear* **2005**, 258, 294–302. [CrossRef]
23. Kausar, A. Advances in Carbon Fiber Reinforced Polyamide-Based Composite Materials. *Adv. Mater. Sci.* **2019**, 19, 67–82. [CrossRef]
24. Libera, V.; Papa, I.; Lopresto, V.; Mocerino, D.; Filippone, G.; Russo, R. Manufacturing of Bio-Polyamide 11/Basalt Thermoplastic Laminates by Hot Compaction: The Key-Role of Matrix Rheology. *J. Thermoplast. Compos. Mater.* **2022**. [CrossRef]
25. Pan, B.; Xu, G.; Zhang, B.; Ma, X.; Li, H.; Zhang, Y. Preparation and Tribological Properties of Polyamide 11/Graphene Coatings. *Polym.-Plast. Technol. Eng.* **2012**, 51, 1163–1166. [CrossRef]
26. Haddou, G.; Dandurand, J.; Dantras, E.; Maiduc, H.; Thai, H.; Vu Giang, N.; Trung, T.H.; Ponteins, P.; Lacabanne, C. Mechanical properties of continuous bamboo fiber-reinforced biobased polyamide 11 composites. *Int. J. Appl. Polym. Sci.* **2019**, 136, 47623. [CrossRef]
27. Russo, P.; Simeoli, G.; Vitiello, L.; Filippone, G. Bio-Polyamide 11 Hybrid Composites Reinforced with Basalt/Flax Interwoven Fibers: A Tough Green Composite for Semi-Structural Applications. *Fibers* **2019**, 7, 41. [CrossRef]
28. Venkatraman, P.; Gohn, A.M.; Rhoades, A.M.; Foster, E.J. Developing high performance PA 11/cellulose nanocomposites for industrial-scale melt processing. *Compos. Part B Eng.* **2019**, 174, 106988. [CrossRef]
29. Oliver-Ortega, H.; Méndez, J.; Espinach, F.; Tarrés, Q.; Ardanuy, M.; Mutjé, P. Impact Strength and Water Uptake Behaviors of Fully Bio-Based PA11-SGW Composites. *Polymers* **2018**, 10, 717. [CrossRef] [PubMed]
30. Zierdt, P.; Theumer, T.; Kulkarni, G.; Däumlich, V.; Klehm, J.; Hirsch, U.; Weber, A. Sustainable wood-plastic composites from bio-based polyamide 11 and chemically modified beech fibers. *Sustain. Mater. Technol.* **2015**, 6, 6–14. [CrossRef]
31. Chang, B.P.; Gupta, A.; Muthuraj, R.; Mekonnen, T.H. Bioresourced fillers for rubber composite sustainability: Current developments and future opportunities. *Green Chem.* **2021**, 23, 5337–5378. [CrossRef]
32. Rosenboom, J.G.; Langer, R.; Traverso, G. Bioplastics for a circular economy. *Nat. Rev. Mater.* **2022**, 7, 117–137. [CrossRef] [PubMed]
33. Zheng, J.; Suh, S. Strategies to reduce the global carbon footprint of plastics. *Nat. Clim. Change* **2019**, 9, 374–378. [CrossRef]

34. Danil de Namor, A.F.; El Gamouz, A.; Frangie, S.; Martinez, V.; Valiente, L.; Webb, O.A. Turning the volume down on heavy metals using tuned diatomite. A review of diatomite and modified diatomite for the extraction of heavy metals from water. *J. Hazard. Mater.* **2012**, *241–242*, 14–31. [CrossRef]
35. Sedai, B.R.; Khatiwada, B.K.; Mortazavian, H.; Blum, F.D. Development of superhydrophobicity in fluorosilane-treated diatomaceous earth polymer coatings. *Appl. Surf. Sci.* **2016**, *366*, 178–186. [CrossRef]
36. Dobrowolska, M.; Dobrucka, R.; Głuc, M.; Brzakalski, D.; Szymański, M.; Kurzydłowski, K.J.; Przekop, R.E. A New Method of Diatomaceous Earth Fractionation—A Bio-Raw Material Source for Epoxy-Based Composites. *Materials* **2021**, *14*, 1663. [CrossRef]
37. Dobrowolska, M.; Dobrucka, R.; Brzakalski, D.; Głuc, M.; Bobel, J.; Głowacka, J.; Kurzydłowski, K.J.; Przekop, R.E. Przekop. Methodological Aspects of Obtaining and Characterizing Composites Based on Biogenic Diatomaceous Silica and Epoxy Resins. *Materials* **2021**, *14*, 4607. [CrossRef] [PubMed]
38. Dobrowolska, M.; Dobrucka, R.; Brzakalski, D.; Frydrych, M.; Konera, P.; Wiecinek, M.; Jabrzykowski, M.; Kurzydłowski, K.J.; Przekop, R.E. Influence of Diatomaceous Earth Particle Size on Mechanical Properties of PLA/Diatomaceous Earth Composites. *Materials* **2022**, *15*, 3607. [CrossRef] [PubMed]
39. Dobrowolska, M.; Przekop, R.E.; Sztorch, B.; Brzakalski, D.; Zgłobicka, I.; Łępicka, M.; Dobosz, K.; Kurzydłowski, K.J. Biogenic Composite Filaments Based on Polylactide and Diatomaceous Earth for 3D Printing. *Materials* **2020**, *13*, 4632. [CrossRef]
40. Zhu, F.; Yu, R.; Su, J.; Han, J. Study on PLA/PA11 bio-based toughening multi-blown nanowovens. *AUTEX Res. J.* **2020**, *20*, 24–31. [CrossRef]
41. Gug, J.; Sobkowicz, M.J. Effect of Catalyst on Compatibilization of Poly(lactic acid)/Polyamide Blends. In Proceedings of the Annual Technical Conference—ANTEC, Orlando, FL, USA, 23–25 March 2015.
42. Ortega, H.O.; Méndez, J.A.; Mutjé, P.; Tarrés, Q.; Espinach, F.X.; Mònica Ardanuy, M. Evaluation of Thermal and Thermomechanical Behaviour of Bio-Based Polyamide 11 Based Composites Reinforced with Lignocellulosic Fibres. *Polymers* **2017**, *9*, 522. [CrossRef]
43. Stoclet, G.; Seguela, M.; Devaux, J. Relations between structure and property of polyamide 11 nanocomposites based on raw clays elaborated by water-assisted extrusion. *J. Appl. Polym. Sci.* **2013**, *127*, 4809–4824. [CrossRef]
44. Castagnet, S.; Thilly, L. High-pressure dependence of structural evolution in polyamide 11 during annealing. *J. Polym. Sci. Part B Polym. Phys.* **2009**, *47*, 2015–2025. [CrossRef]
45. Marcic, L.; Osman, R.F.M.; Costa, A.M.L.M.; d'Almeida, J.R.M.; Marcinkowic, R.A.; Rizzo, F.C. Thermal and mechanical properties of polyamide 11 based composites reinforced with surface modified titanate nanotubes. *Mater. Des.* **2015**, *83*, 459–467. [CrossRef]
46. Feng, N.; Wang, X.; Wu, D. Surface modification of recycled carbon fiber and its reinforcement effect on nylon 6 composites: Mechanical properties, morphology and crystallization behaviors. *Curr. Appl. Phys.* **2013**, *13*, 2038–2050. [CrossRef]

H6

Polyamide 11 Composites Reinforced with Diatomite Biofiller—Mechanical, Rheological and Crystallization Properties

Dobrosielska M., Dobrucka R., Pajewska-Szmyt M., Brząkalski D., Kozera P., Martyła A., Gabriel E., Kurzydłowski K.J., Przekop R.E.; Polymers, 15, 1563, 2023

polymers

MDPI

Article

Polyamide 11 Composites Reinforced with Diatomite Biofiller—Mechanical, Rheological and Crystallization Properties

Marta Dobrowolska [1], Renata Dobrucka [2,3,*], Dariusz Bezpalski [3], Paulina Kozera [1], Agnieszka Mattyla [3], Ewa Gabriel [3], Krzysztof J. Kurzydłowski [4] and Robert E. Przekop [2,4]

[1] Faculty of Materials Science and Engineering, Warsaw University of Technology, ul. Wołoska 141, 02-507 Warsaw, Poland
[2] Department of Non-Food Products Quality and Packaging Development, Institute of Quality Science, Poznań University of Economics and Business, al. Niepodległości 10, 61-875 Poznań, Poland
[3] Centre for Advanced Technologies, Adam Mickiewicz University in Poznań, ul. Uniwersytetu Poznańskiego 10, 61-614 Poznań, Poland
[4] Faculty of Mechanical Engineering, Białystok University of Technology, ul. Wiejska 45c, 15-351 Białystok, Poland
* Correspondence: renata.dobrucka@ue.poznan.pl or renata.dobrucka@amu.edu.pl (R.D.); rprzekop@amu.edu.pl or r.przekop@gmail.com (R.E.P.)

Abstract: Amorphic diatomaceous earth is derived from natural sources, and polyamide 11 (PA11) is produced from materials of natural origin. Both of these materials show a low harmfulness to the environment and a reduced carbon footprint. This is why the combination of these two constituents is beneficial not only to improve the physicochemical and mechanical properties of polyamide 11 but also to produce a biocomposite. For the purpose of this paper, the test biocomposite was produced by combining polyamide 11, as well as basic and pre-functionalized diatomaceous earth, which had been subjected to silanization. The produced composites were used to carry out rheological (melt flow rate-MFR), mechanical (tensile strength, bending strength, impact strength), crystallographic (X-ray Diffraction-XRD), thermal and thermo-mechanical (differential scanning calorimetry-DSC, dynamic mechanical thermal analysis-DMTA) analyses, as well as a study of hydrophobic-hydrophilic properties of the material surface (wetting angle) and imaging of the surface of the composites and the fractured specimens. The tests showed that the additive 3-aminopropyltriethoxysilane (APTES) acted as an agent that improved the elasticity of composites and the melt flow rate. In addition, the produced composites showed a hydrophilic surface profile compared to pure polylactide and polyamide 11.

Keywords: polyamide 11; diatomaceous earth; diatomite; silanization; silanes; surface properties; mechanical strength; hydrophilic composite system

check for updates

Citation: Dobrowolska, M.; Dobrucka, R.; Bezpalski, D.; Kozera, P.; Mattyla, A.; Gabriel, E.; Kurzydłowski, K.J.; Przekop, R.E. Polyamide 11 Composites Reinforced with Diatomite Biofiller—Mechanical, Rheological and Crystallization Properties. Polymers 2021, 13, 2565. https://doi.org/10.3390/polym13152565

Academic Editors: Nick Virgilio and Gisele Hbaieb

Received: 28 February 2021
Revised: 15 March 2021
Accepted: 14 March 2021
Published: 31 March 2021

Copyright: © 2021 by the authors. Licensee MDPI, Basel, Switzerland. This article is an open access article distributed under the terms and conditions of the Creative Commons Attribution (CC BY) license (https://creativecommons.org/licenses/by/4.0/).

1. Introduction

Filled polymer composites have been successfully applied for many years in various sectors of the economy, such as automotive, aerospace and construction industries [1–3]. The most popular fillers include wood flour [4,5], carbon fibres [6,7], glass fibre [8,9], clays [10,11], white titanium [12,13], cellulose [14,15], basalt [16,17] and flax fibre [18]. However, the most important vice of conventional polymer products is their harmful impact on the natural environment, which is a result of ineffective waste management and the growing consumer demand for new products. Even so, the marketing of new, advanced materials based on biopolymers faces many obstacles and has been broadly discussed in the literature by researchers with both academic and industrial backgrounds. It has consistently been shown that an additive to mineral and fibrous fillers has a positive impact on mechanical properties, thermal stability and abrasion resistance, and in many cases, it helps considerably reduce production costs, which is important for many entrepreneurs.

Such a cost-effective mineral filler is diatomaceous earth (EUR 0.80/kg on average). In addition to the favourable impact on the mechanical or rheological properties of polymer composites, diatomaceous earth is also used as a filtration medium to remove harmful substances, and its porous structure makes it easy to modify its surface [19].

The use of inorganic fillers in polymer composites entails not only benefits but also challenges. This is because the final properties of the designed materials depend on the interaction (adhesion) at the interface between the filler and the polymer matrix. The improved interactions at the filler-polymer interface are an important issue for researchers.

Silanization is a well-known method for improving adhesion between different materials, which is also well described in the literature. Silanes are hybrid compounds that consist of the organic and inorganic parts with a general formula $(XCH_2)_nSiR_3$, with 'n' usually being 0–3, which makes them applicable as the promoters of adhesion between materials dissimilar in terms of the chemical structure, such as ceramics–polymer and polymer–metal [20–22]. The hybrid, inorganic and organic structures of silanes allow us to form stable chemical bonds between organic and inorganic materials. The organic part of silane consists of groups that are chemically reactive or compatible with organic materials (depending on the choice of X substituent and the materials to be compatibilized), such as polymers (e.g., amine, epoxy or vinyl groups). The R substituents are groups susceptible to hydrolysis (alkoxy or chloride groups) responsible for forming siloxane links with the surface of inorganic materials [23].

Silane-based couplers form a thin film between incompatible materials, thus improving the interface interactions in composites, which in turn translates into improved mechanical properties of the filled polymeric composites. When placed on an inorganic surface, silanol oligomers react with one another to create branched hydrophobic siloxane bonds -Si-O-Si-. They form metal–siloxane bonds -Si-O-M- (where M = metal) on the surface of the inorganic matrix (for example, silica, diatomaceous earth or metal oxides containing hydroxyl groups, -OH). Figure 1 shows a diagram representing the structure of a single diatom particle comprising diatomite earth, while Figure 2 shows a diagram of its surface silanization with APTES. More details on the microstructure of diatomite have been discussed in our previous works [24], as well as the silanization thereof [25].

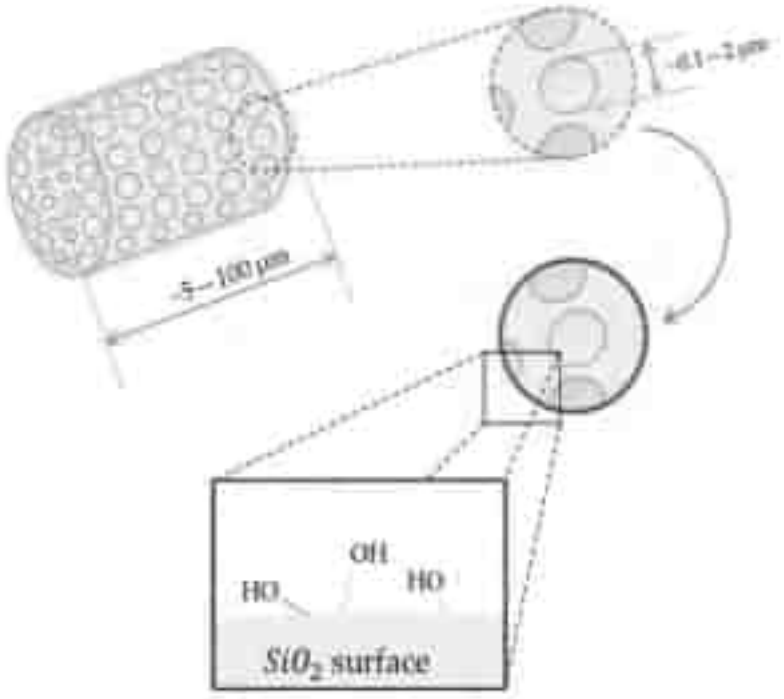

Figure 1. Diagram representing diatomaceous earth microstructure and surface chemistry.

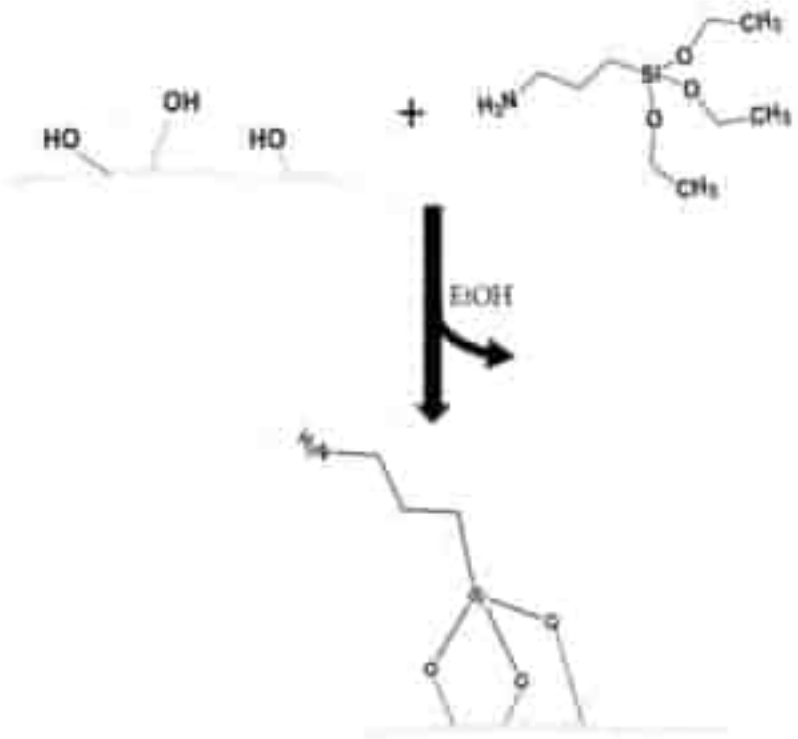

Figure 2. Diagram representing the diatomaceous earth surface silanization process with APTES.

Composites based on the PA11 matrix, loaded with silanized fillers for reinforcement, are not commonly known. The literature has recorded few works devoted to PA11 with silanized fillers. We know the methods of strengthening polyamide 11 with organically modified clay [26], organically modified layered silicate (Cloisite 30B) [30], silane (3-aminopropyltriethoxysilane (APTES)) grafted titanate nanotubes [27], and Palygorskite nanofiber clay silanized by the same silane (APTES) [28]. Adding silanes is aimed mainly at improving the interface interactions between the filler and polyamide 11. Additionally, a natural filler is added to produce a biocomposite whose ingredients are derived from renewable sources that can be strengthened and, consequently, we can improve its tensile strength, impact strength or Young modulus. A key point in terms of the industrial application of the PA11/filler composite is its weather resistance, which has been obtained in, for example, the work of Cong et al., which used jute fibres silanized by vinyltrimethoxysilane (VTMOS) [29].

As we had no references in the bibliographical references regarding the use of silanized diatomaceous earth as a filler for polyamide 11, we attempted to produce such composites. In our previous work, we also performed the silanization of diatomaceous earth and examined the impact of the modification on the physicochemical and mechanical properties of composites on the polylactide matrix [31]. Tests have shown that, depending on the silane applied, it is possible to modify individual parameters; for instance, methyltrimethoxysilane causes the greatest growth in processing properties (MFR), n-octyltriethoxysilane reduces the composite degradation, and (3-glycidyloxypropyl)trimethoxysilane helps inhibit the penetration of UV rays into the composite, so the degradation progresses only down to a specified depth. The use of 3-aminopropyltriethoxysilane as a diatomaceous earth modifier may further improve the physicochemical parameters of composites, but this time, for a broader analysis, the composite matrix was polyamide 11 acquired from renewable sources.

In this work, we carried out a chemical modification (silanization) of basic diatomaceous earth pre-fractionated with the use of sedimentation. The prepared material was

used as a filler for polyamide 11 to produce composites with a diatomaceous earth content of 2.5, 5, 10 and 20% by weight with a 1% addition of APTES. The produced composites were tested for the impact of silanization on their mechanical and processing characteristics. Furthermore, we compared the thermal and thermomechanical properties of the composites (DSC and DMTA) and tested their surfaces and fractures with an optical microscope. The degree of dispersion of a filler in a polymer was determined using a scanning electron microscope. Our reference systems were the composites produced in a previous work [30], which made it possible to fully specify the impact of both the diatomaceous earth alone and the silanized diatomaceous earth on the characteristics of the obtained composites.

2. Materials and Methods

Polyamide 11 (Rilsan® BESNO Natural) was purchased from Arkema (Colombes, France). Diatomaceous earth (Perma-Guard, Bountiful, UT, USA) was derived from diatomite deposits. Silane APTES (3-Aminopropyltriethoxysilane) was purchased from Sigma-Aldrich (Saint Louis, MO, USA).

2.1. Preparation of Diatomite

The fractionation of amorphic diatomaceous earth was performed using the hydraulic method, according to the procedure presented in previous works [30,31], with the use of gravitational sedimentation. Fifteen kilograms of amorphic diatomaceous earth (particle size between 1 µm and 100 µm) was washed with demineralised water in order to separate particles of different sizes. We obtained three fractions of diatomaceous earth with disparate particle size distributions. In further testing, we used a fraction with a medium particle size (Fraction 2, particle size between 4 and 35 µm), where we eliminated the content of the smallest diatomite particles.

2.2. Preparation of Modified Diatomaceous Earth

We placed 1 kg of diatomaceous earth in a 14-L glass reactor equipped with a mechanical stirrer. Then, we added to the reactor 4 L of isopropanol, 10 mL of demineralised water, and 1% by weight of APTES (3-aminopropyltrimethoxysilane), and we left it for 24 h, stirring continuously (300 rpm). Then, the mixture was poured into a separate container and left for sedimentation. Once the liquid was poured out from above the sediment, the diatomaceous earth was washed with demineralised water and put into a dryer at 60 °C for 24 h.

2.3. Extrusion of the Biocomposite

The biocomposite extrusion process was performed on a RHEO DRIVE 16 process line made by Haake PolyLab OS (Thermo Scientific) (Waltham, MA, USA). The process was carried out using a double-screw extruder. We added to the charge the mixture of PA 11 with basic diatomaceous earth, in portions (50 g), modified with the APTES at four concentrations of 2.5%, 5%, 10% and 20%, in that particular order. The materials became plasticised and mixed at the screws. The extruded substance was dried for 24 h at 70 °C and then milled in a plastics mill WANNER CT7.26 w (Lodz, Poland). We obtained 4 compositions of polyamide 11 with diatomaceous earth at concentrations of 2.5%, 5%, 10% and 20%. Other composites were extruded in a similar way. The extrusion parameters are shown in Table 1.

Table 1. Extrusion parameters.

Temperature at Heating Zones (°C)	Nozzle	TS6	TS5	TS4	TS3	TS2	TS1
	220	250	250	255	250	250	250
Torque, M (Nm)		**Nozzle Pressure, P50 (bar)**			**Revolutions per Minute, N (1/min)**		
20–70		0.6			14		

2.4. Injection Moulding—The Production of Standardised Measuring Paddles

The injection moulding procedure was performed on an e-victory 170/80 made by Engel (Schwertberg, Austria). Table 2 shows the process parameters. The mould temperature was maintained at 80 °C. We obtained standardised type 1A measuring paddles according to ISO 527 [32]. Finally, we produced 4 types of composites and a reference system (Table 3).

Table 2. Injection moulding parameters.

Temperature [°C]	Nozzle	Zone 3	Zone 2	Zone 1	Traverse
	215	220	215	210	40
Mold Closing Force (kN)	**Clamping Time (s)**		**Cooling Down Time (s)**	**Screw Diameter (mm)**	
600	4		30	25	

Table 3. Composites obtained for testing.

Biocomposite Type	Filler Concentration	Abbreviation
PA11 + original diatoms + 1% wt. APTES[a]	2.5%	2.5OB5
	5%	5OB5
	10%	10OB5
	20%	20OB5
PA11 + fractionated diatoms + 1% wt. APTES[a]	2.5%	2.5OF5
	5%	5OF5
	10%	10OF5
	20%	20OF5
PA11	-	PA11

a—APTES was applied in 1 wt% ratio of the diatomite.

2.5. Characterisation Methods

For the mechanical analysis, we used dumbbell-shaped samples prepared according to EN ISO 527-1: 2020 [32] and EN ISO 178: 2010 [33] norms. The test was conducted on a universal testing machine INSTRON 5969 with a maximum loading force of 50 kN (Instron, Norwood, MA, USA). The transverse travel speed for tensile and flexural strength measurements was set at 5 mm/min.

The Charpy impact test with a notch was performed on an impact testing device, Instron Ceast 9050 (Instron, Norwood, MA, USA), according to ISO 179-1: 2010 [34]. The impact test was carried out according to PN-EN ISO 178-1 [32]. The notch was made by machining in the centre of the test sample according to ISO 179-1/1 eA [35]. The V-notch was angled at 45° and 2 mm deep. The side impact direction was applied in the line axis normal to the sample plane.

Dynamic mechanical thermal analysis (DMTA) was performed using a Q800 DMA (TA Instruments, USA) in dual cantilever mode according to ASTM D4065-01. From each composite, three rectangular specimens 60 mm in length and 10 mm in width were cut and used in the test. The analysis was conducted from 0 °C to 130 °C with a heating rate of 3 °C/min at a frequency of 1 Hz and an amplitude of 30 µm. The glass transition temperature (Tg) was determined from the peak value in the storage modulus using VALSA TA Universal Analysis software.

Powder morphology was characterised by a scanning electron microscope (SEM, TM 1000 Hitachi, Tokyo, Japan) operating at an applied voltage of 5 kV. Before observations via SEM, the sample surfaces were sputtered with a gold-palladium layer for 90 s at an electric current of 10 mA and voltage of 2 kV.

The melt flow rate (MFR) was measured using the Instron CEAST MF20 melt flow tester, which accords with EN ISO 1133 [36], at 235 °C for a load of 2.16 kg.

Thermal properties of materials were studied by the DSC (differential scanning calorimetry) technique, using a Q1000 Differential Scanning Calorimeter (TA Instruments,

New Castle, DE, USA). Samples with a weight of 8.0 ± 0.2 mg were placed in an aluminium hermetic pan. First, the samples were equilibrated at −90 °C, then heated to 230 °C with a scan rate of 10 °C/min, and cooled to −90 °C with a scan rate of 10 °C/min. Finally, they were heated again to 230 °C with a scan rate of 10 °C/min. The process was conducted in a nitrogen atmosphere. Using Universal V4.5A TA software, the glass transition temperature (Tg) was determined as the midpoint of the glass transition temperature range. The melting temperature was taken as the peak temperatures of cold crystallisation and melting, respectively. For the calculation of the composite crystallinity, the following formula was used, which is in accordance with the general methodology for DSC analysis of polymer composites [37].

$$X = \frac{H_m^0}{H_0} \cdot \frac{100}{100 - a}$$

a—filler loading [wt%]
H_m—measured melting enthalpy [J/g]
H_0—melting enthalpy of fully crystalline PA11, 206 J/g [38].

The viscosity of the composites was determined with a capillary method, using a capillary rheometer Instron CEAST SR10 Smart RHEO 1000. The measurement was performed at 235 °C, and the capillary tube used was 1 mm in diameter and 20 mm in length. The viscosity was determined for 6 shear velocities: 10, 30, 100, 500 and 1000 [1/s].

The images of surfaces and fractures were made with a digital microscope KEYENCE VHX-7000 (KEYENCE INTERNATIONAL (BELGIUM) NV/SA) with a wide-angle zoom lens VH-Z100R with 100-fold magnification. The images were made using depth composition and 3D imaging features. We used full coaxial illumination.

Contact angle analyses were performed by the sessile drop technique (5 µL) at room temperature and atmospheric pressure with a Krüss DSA100 goniometer.

Surface gloss measurements were recorded at 23 °C according to the ISO 2813 [39] standard using a compact gloss meter (GM04, 3Color®, Naruma, Poland) using 20°, 60° and 85° geometry. The device was calibrated between various specimen measurements using dedicated standard black glass. Three gloss unit (GU) values were recorded from each specimen and averaged. Before the measurements, the samples were stored in the same lighting conditions to prevent possible colour changes.

The phase identification and the relationship between the sediment fraction depth and its composition were determined using an X-ray diffraction (XRD) powder diffractometer Bruker AXS D8 Advance (Bruker, Karlsruhe, Germany) using CuKα lamp radiation and an Ni filter. X-ray diffractograms were recorded in the angular range of 5–80° (2θ).

The measurements for hiding power were performed by placing samples of the prepared resin systems into the optical path between the light source (LED) and the UV-NIR spectrophotometer AvaSpec-Mini2048CL (Avantes, Louisville, CO, USA).

Fourier Transform-Infrared (FT-IR) spectra were recorded on a Nicolet i550 Fourier transform spectrophotometer (Thermo Fisher Scientific, manufacturer Madison, WI, USA) equipped with an ATR unit (5000–60 cm^{-1}).

For the washability test, two types of markers were used: a water-resistant permanent marker (green) and removable board markers in two colours (black, blue). Having applied a thin layer of each of the tested markers, the following test steps were planned:

- One-time wiping of the surface with a clean, dry cotton cloth;
- One-time wiping of the surface with a clean cotton cloth soaked with tap water;
- One-time wiping of the surface with a clean cotton cloth soaked with methanol;
- One-time wiping of the surface with a clean cotton cloth soaked with acetone.

The last step was not carried out as all traces of the markers had been removed previously by methanol.

The measurements for hiding power were performed by placing samples of the composites into the optical path between the light source (LED) and the UV-NIR spectrophotometer, an AvaSpec-Mini2048CL (Avantes, Louisville, CO, USA).

The size of the diatoms used to prepare the composites was measured with a Mastersizer 3000 (Malvern Instruments Ltd., Malvern, UK). The measurements were taken for samples in water suspension (Hydro EV attachment). The parameters of the measurements for the wet samples were a stirrer revolution speed of 2330 RPM and an ultrasound power of 70%. The tensile, bending and impact strength tests, rheological tests (MFR, viscosity), thermal tests (DSC, DMTA) and microscope observations were compared to the composites produced by direct injection moulding, which are described in a previous paper [30]. Additionally, the tests were complemented with a surface analysis, that is, the analysis of wetting angle and the test of gloss at the composite surface for all samples, whether or not they were modified by the APTES.

The particle size distribution of the filler was performed by Dynamic Light Scattering (DLS) on a Mastersizer 3000 instrument (Malvern Panalytical, Malvern, UK) with a Hydro EV measuring attachment.

3. Results and Discussion

3.1. Infrared Spectroscopy (FT-IR)

Figure 3 shows the FTIR spectra of unmodified diatomaceous earth and fractionated diatomaceous earth silanized with APTES, used for modifying polyamide 11.

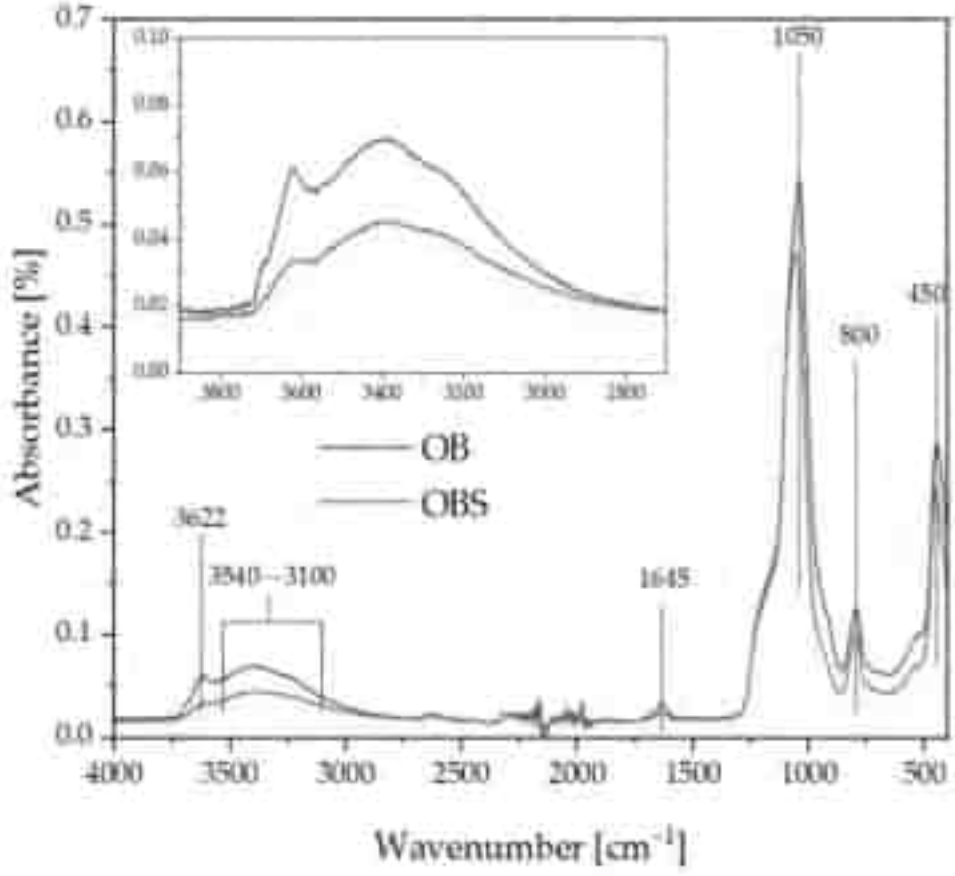

Figure 3. FT-IR spectra of neat, base diatomaceous earth (OB) and silanized diatomaceous earth (OBS)

Both modified and unmodified diatomaceous earth are characterised by the presence of bands at 3622, 3540–3100, 1645, 1050, 800 and 450 cm^{-1}. The silanization process did not produce new bands in the FT-IR spectrum, while a change in the intensity and peak maximum shift of the bands after the silanization process was observed.

The presence of a broad band in the range of 3540–3100 cm^{-1} is related to the presence of stretching vibrations of surface -OH groups, and a band at 1645 cm^{-1} being -OH bending vibrations of coordinated H_2O molecules [39] or Si-OH silanol groups [40], while the band present at 3622 cm^{-1} is related to the O-H vibrations of adjacent SiOH groups forming intermolecular hydrogen bonds [41]. Silanization of diatomite resulted in a significant reduction of the O-H bands, both the main, broad one, and the sharp one at 3622 cm^{-1}. The band present at 450 cm^{-1} is related to the muscovite present in the samples. The bands present at 1050 cm^{-1} and 800 cm^{-1} come from Si-O bond vibrations, as in the band in [42].

3.2. Particle Size Distribution

Particle size distribution analysis was performed by Dynamic Light Scattering (DLS) for diatomaceous earth before and after the sedimentation fractionation process. The fractionation process allowed for the removal of the smallest diatomaceous earth particles, i.e., less than 4 µm, as shown in Figure 4. In addition, the effect of the sedimentation fractionation process on the tendency to form agglomerates is also observed, which can be seen as an increased proportion of particles with sizes in the 50–200 µm range. It is also observed that the largest amount of diatomaceous earth particles with a size of 7–12 µm is present, which is the main fraction of the material.

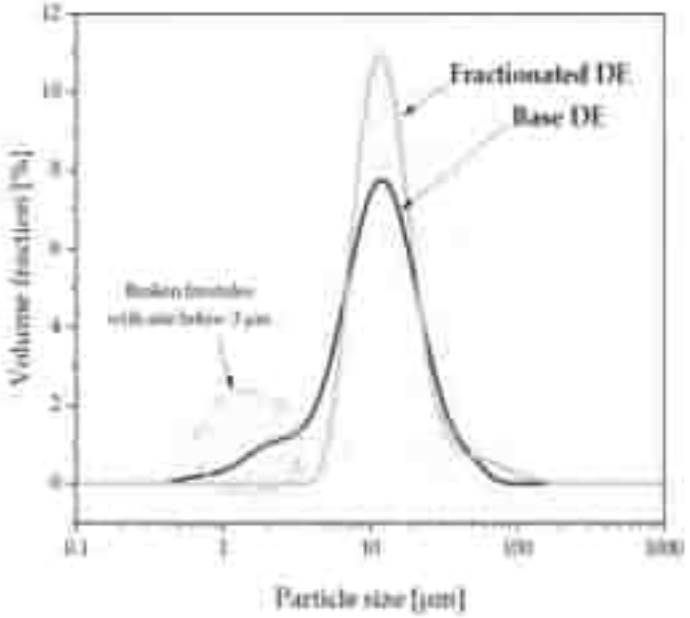

Figure 4. Particle size of the fillers, basic and fractionated diatomaceous earth.

3.3. Crystallinity Analysis (XRD)

XRD analysis of all studied materials was performed in order to investigate the effect of the diatomite filler on the crystallisation of the polymer matrix and to study the crystalline structure of neat PA11 processed under the same conditions. It is known that PA11 and other polyamide types are characterised by polymorphism, resulting in overlapping XRD reflexes, making the crystallographic analysis of composites based thereof a challenging task. Common polymorphs observed are α, γ, δ′ (smectic) and amorphous phases, and a high temperature δ phase forming above 95 °C (known as Brill transition temperature) in a reversible transition of α phase [43]. In addition, various crystalline phases have been reported in diatomite, including quartz, cristobalite, calcite, feldspar, kaolinite and vermiculite [44–46]. Analysis of neat PA11 (Figure 5) showed that the commonly observed α phase is present, as a reflex at 2θ of 7.3 is visible, corresponding to the (001) lattice, which is in agreement with available reports [47]. For a diffraction pattern of neat PA11

a phase, additional reflexes in 2θ of 20.0–20.5 and 22.9–23.5 ranges should be present, corresponding to the (200) and (010) + (210) lattices, respectively. In the studied case, a right-side broadened reflex at 2θ of 21.1 with another smaller maximum at 2θ ~22.3 is visible. This shift can be explained by the presence of an additional metastable γ phase, which is reported to give reflexes at 2θ of 21.6 and 22.4 [47]. The presence of some amounts of the δ′ smectic phase was also plausible, but the obtained data did not allow for its unambiguous confirmation.

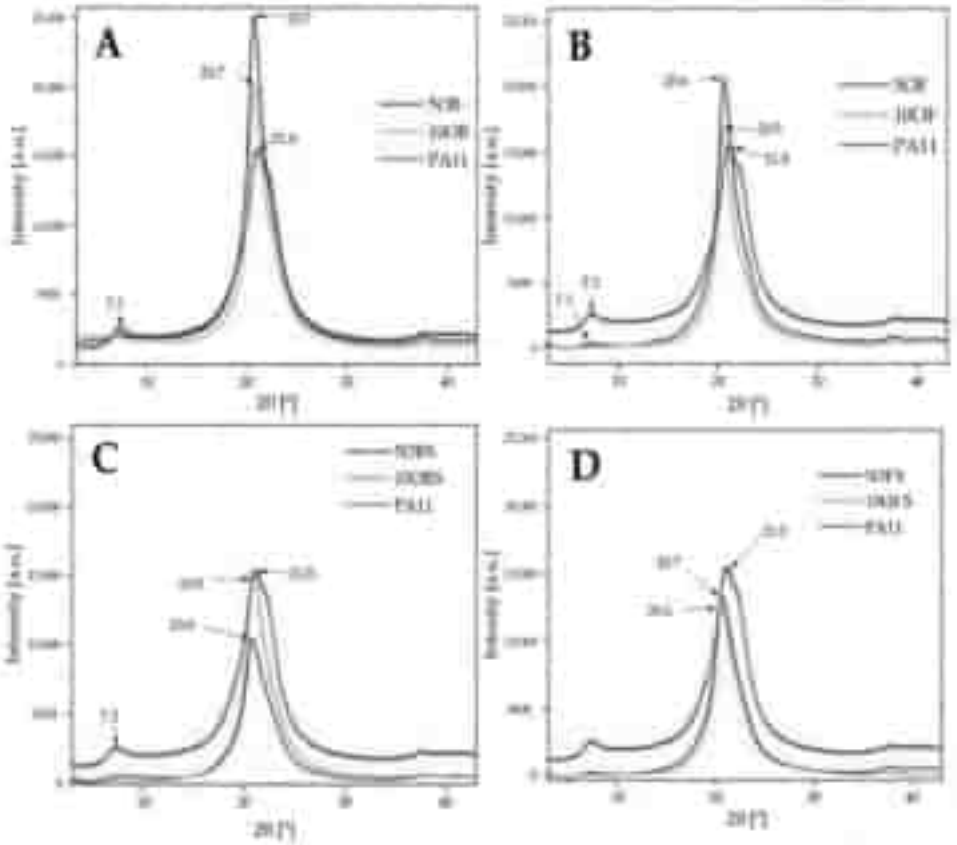

Figure 5. XRD PA11/diatomite with and without silane APTES; (**A**)—samples with base diatomite; (**B**)—samples with fractionated diatomite and APTES; (**C**)—samples with base diatomite; (**D**)—samples with fractionated diatomite and APTES.

In the case of non-silanized filler composites, both fractionated and non-fractionated diatomite, strong and well-pronounced reflexes of the δ′ smectic phase, were observed in each system, with the maximum at 2θ ~20.6. The presence of a correlating α phase was confirmed by the still visible reflex at ~7.2; however, the abundance thereof decreased together with increasing filler content. It was initially thought that the application of the filler could have also caused changes in polymer crystallinity; however, DSC analysis (Section 3.4) revealed that the differences in the crystallinity index (CI) of the produced samples was barely noticeable. Therefore, the filler presence affects the selectivity of the PA11 α phase nucleation, while the obtained CI levels are comparable and, rather, the result of the injection moulding parameters kept constant for all the produced materials. The analysis of composites filled with APTES-silanized diatomite allowed us to draw the same conclusions, showing no particular effect of the filler surface treatment on its nucleation-inducing behaviour.

3.4. Test of the Composites' Mechanical Characteristics

The notch impact test was conducted for the composites both with the addition of silane and, comparatively, without silane, which was presented previously in [30]. Neat polyamide was characterised by the highest impact strength amongst the tested samples, 7 kJ/m^2 (Figure 6). The relatively low impact strength values arose from the high elasticity of the composites and from the requirement to test samples that were previously notched. For this reason, the impact strength values are lower than those recorded in the literature [48]. As in the previous work, we observed an impact of the size of diatomaceous earth particles on the composite impact strength. Composites containing fractionated diatomaceous earth showed a higher impact strength, but the differences were not too big. The silanization of PA11/DE composites in most cases caused a slight reduction in impact strength; a greater decline was recorded for the fractionated diatomaceous earth, while most of the modified composites showed a lower standard deviation, which means that the addition of silane had a positive impact on this aspect, i.e., probably on the filler dispersion in the polymer matrix, while for higher filling levels it could affect the secondary agglomeration of particles in the composite, which caused the slight reduction in impact strength.

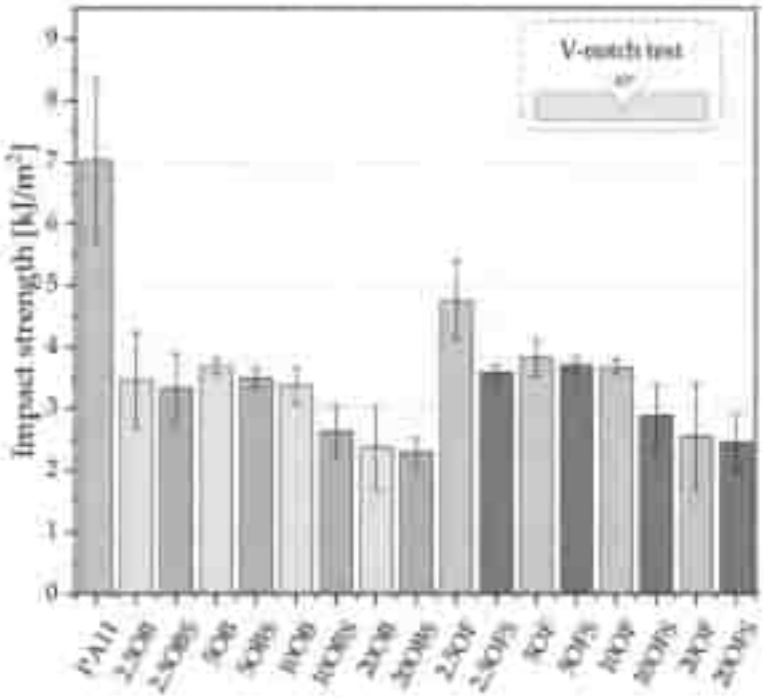

Figure 6. Impact strength of the composites after injection moulding: comparison of the composites containing diatomite filler with and without APTES silanization.

The silanization of diatomaceous earth had a very significant impact on the composites' mechanical properties, in particular on the elongation at the yield point, which is shown in Figure 7. Composites containing pure diatomaceous earth show elongation at a yield point of around 5%, whereas, in particular for the low filling with silanized diatomaceous earth, we recorded an over 4-fold growth in that parameter irrespective of the pre-fractionation of the fillet. The higher the diatomaceous earth concentration, the smaller the differences. The relationships presented above indicate that the addition of APTES increased the elasticity of the composites. That relationship might be associated with the fact that, if the level of filling the composite with diatomaceous earth is low (2.5%) and the content of the silane-based modifier is stable, the effect of silanization alone prevails over the effect of

increased brittleness caused by the diatomaceous earth. As the filler concentration grows, the filler starts to prevail over the silanization effect, which consequently causes a decline of elongation at break. In contrast, the yield point was reduced after silanizing the filler, being lowest for systems with 10% concentration, whereas further filling of the composites caused the growth of the yield point.

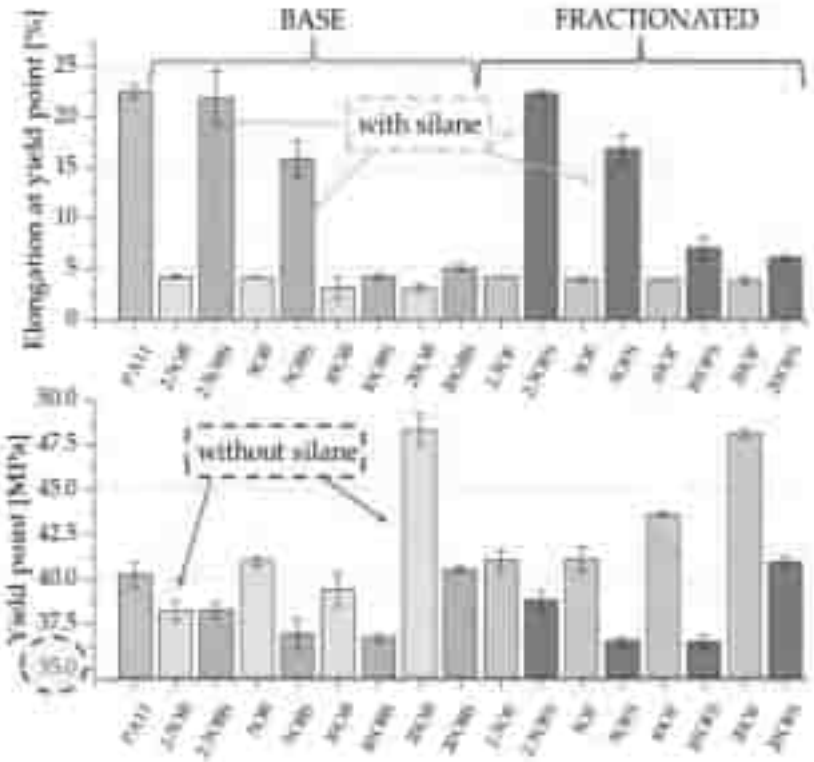

Figure 7. Elongation at yield point and yield point of PA11 composites containing silanized and non-silanized diatomite.

Composites that contain the silanized filler show somewhat lower values of Young's modulus, tensile strength, flexural modulus or maximum flexural stress, but these parameters remain acceptable, particularly for high concentrations (Figures 8 and 9). High-filled samples show values that are higher than those for the reference polyamide 11, and thus we can conclude that a high filling level (20%) is beneficial not only due to reduced costs of production of the composites but also due to the fact that they maintain acceptable mechanical parameters. Lower results, e.g., for the yield point of the composites, particularly those highly filled, may result from the fact that diatom agglomerates are formed in the composite, where the accumulation of APTES is higher, so there may also occur local cross bonds between the silane particles inoculated on diatomaceous earth [28]. Although it was tempting to correlate the observed differences between the mechanical properties and the crystalline polymorphism of neat PA11 and composite samples thereof, the literature data on the mechanical properties of the PA11 polymorphs was found insufficient to discuss the phenomenon of filler-induced crystallisation of PA11. The reports covered the XRD analysis of PA11-based composites; however, either no correlation between polymorphism and mechanical properties was discussed, or it was explained that the data did not allow us to discuss such a relationship [19,30].

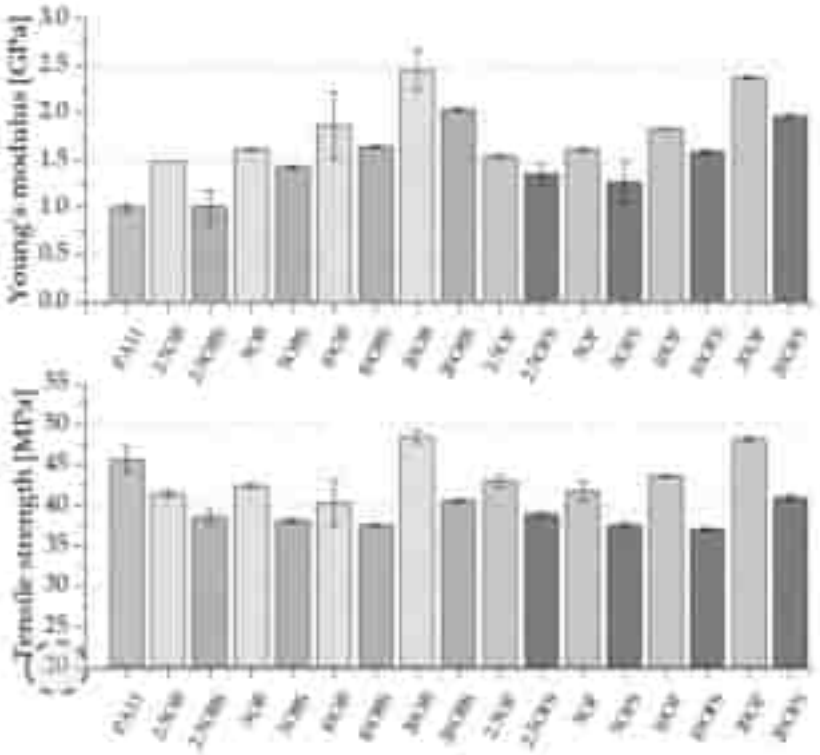

Figure 8. Young's modulus and tensile strength of PA11 composites containing silanized and non-silanized diatomite.

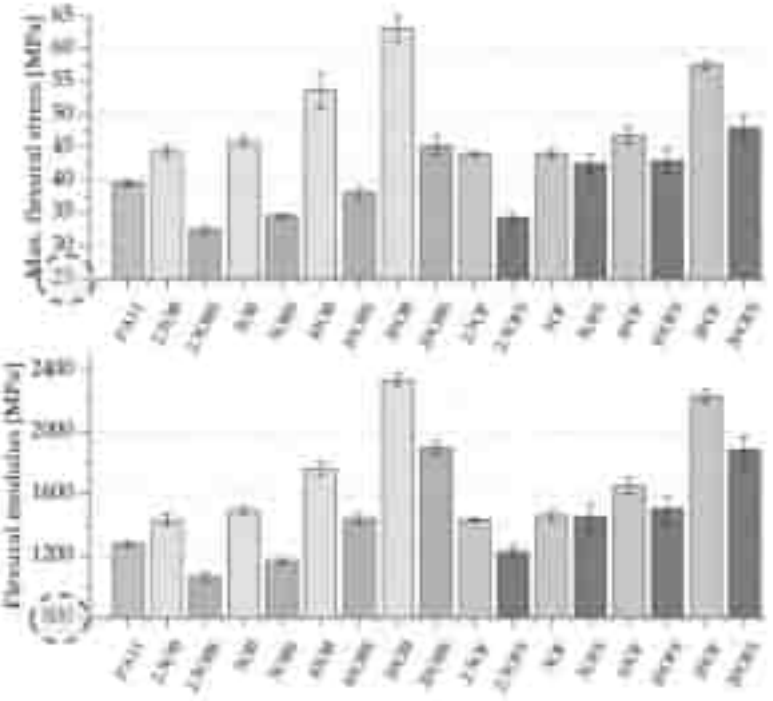

Figure 9. Maximum flexural stress and flexural modulus of PA11 composites containing silanized and non-silanized diatomite.

3.5. Rheology—Melt Flow Rate (MFR) and Viscosity

Silanization of diatomaceous earth positively affected the melt flow rate of PA11/DE composites. We observed considerable growth in processing parameters, especially at the lowest concentrations. As the filler concentration grows, the MFR reduction effect starts to prevail, which arises from the nature of the filler; however, we still recorded a twofold growth in MFR compared to the composites without silane (Figure 10). In earlier research [23], where the polymer matrix was formed by a polylactide, a similar effect was observed, where the MFR index grew even higher once silane was introduced to the system. The apparent dynamic viscosity of polyamide 11 was around 60–65 Pa·s regardless of the range of shear velocity (Figure 11), whereas the introduction of silanized diatomaceous earth to the systems caused a growth of that value along with increasing concentration, but at low DE concentrations the viscosity curve was similar to that of the reference sample. Upon exceeding 10% by weight of the filler, the viscosity at the initial values of shear velocity grew approximately twofold, particularly for the system containing basic diatomaceous earth. The functioning of diatomite and the filling of the composite with diatomaceous earth with a limited particle size distribution resulted in somewhat lower values of apparent dynamic viscosity. The added (3-Aminopropyl)trimethoxysilane acts as an agent that increases the melt flow rate (MFR), especially for low filling levels, and increases the viscosity of composites at high concentrations. The viscosity grew to around 50 Pa·s, depending on the shear velocity.

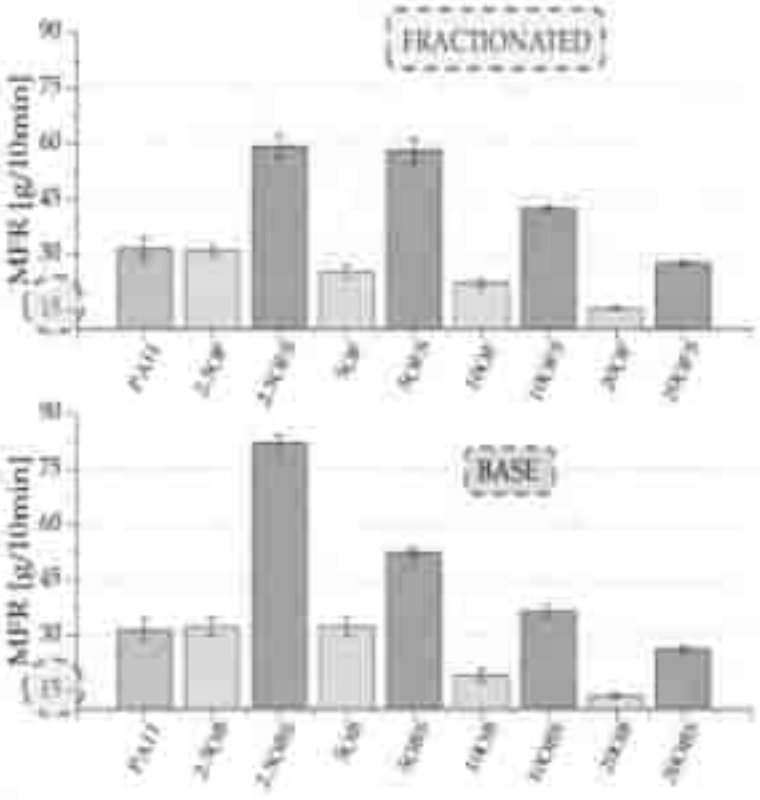

Figure 10. Melt flow rate (MFR) of the granulates of PA11/DE composites after injection moulding.

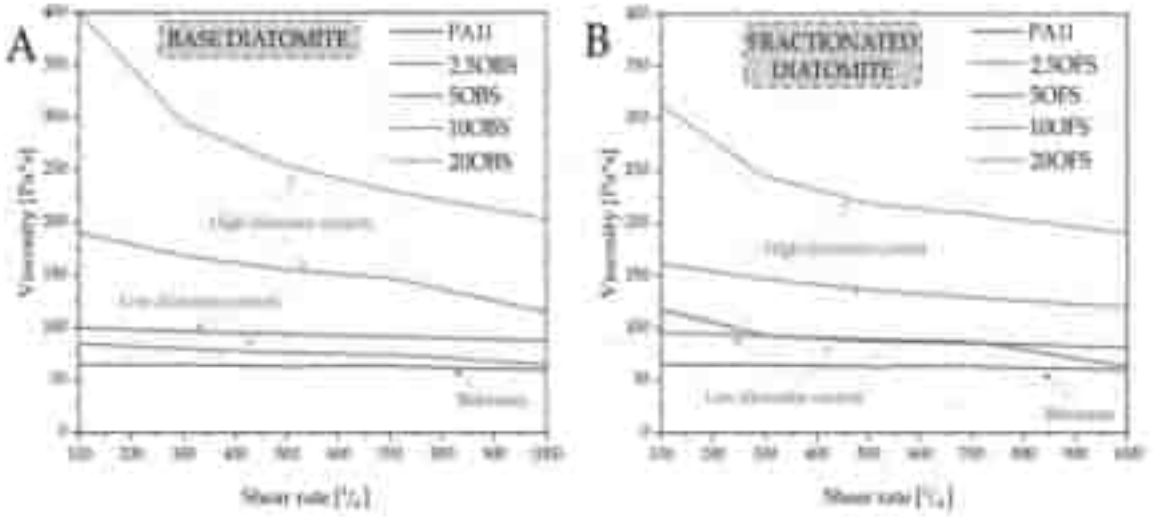

Figure 11. Viscosity of PA11/DE composites after injection moulding: (**A**)—PA11 and 2.5–20% OBS, (**B**)—PA11 and 2.5–20% OFS.

3.6. Thermal Analysis (DSC, DMTA)

DSC analysis was performed to investigate the thermal behaviour of the PA11 and PA11/diatomite composites. Figures 12–15 show the DSC thermograms of PA11 and PA11/diatomite composites during the first and second heating cycles for 5% and 20% loading, respectively, and Tables 4 and 5 present thermal characteristics of the materials with and without silane treatment obtained during two heating cycles. With increasing temperature, DSC curves show two thermal events: a glass transition (T_g) near 50 °C, and a single endothermic melting event near 190 °C. It was found that the addition of diatomite did not affect T_g or T_m to any significant extent. On the other hand, in the previous work [30], a more significant drop in T_g was observed upon the addition of diatomite, showing that untreated diatomite presence causes formation of a filler–matrix interphase of weak interaction, with additional polymer freedom, while the filler treatment with APTES increases this interaction. The addition of diatomite caused a slight increase in the crystallisation temperature, showing some nucleation properties of the filler; however, silanization thereof caused no difference in this matter. Therefore, silanization does not affect the diatomite efficacy of PA11 nucleation, although it significantly affects the selectivity of nucleating the polymer towards either α or γ polymorph, as proven by XRD (see Section 3.3). For the second heating cycle, significant differences in PA11 behaviour were observed, mainly the reduction in T_g slope to the point where its exact determination was unfeasible. Additionally, both the unmodified PA11 and all 5% composites showed two melting peaks (T_{m1} and T_{m2}) during the second heating cycle, and for 20%-composites this double melting effect was still visible for all the materials by broadening and left-side shouldering of the endotherm signal, while being much better resolved for 20OFU13. While the main (larger) melting event was still observed at around 189 °C, the additional melting peaks were characterised by a maximum of around 182 °C, which was a result of formation of the abovementioned γ crystalline phase (smectic phase), accompanying the α phase melting at ~189 °C [47]. Depending on the processing conditions, PA11 may crystallise into different polymorphs that can be transformed from one to another. This double peak corresponded to the melt-crystallisation process of the γ phase to the α′ crystalline form of PA11. The secondary peak seemed to decrease when the additive content was increased in the composite material [51–53]. In addition, the glass transition temperature peak broadened considerably, and it was difficult to determine T_g from the DSC curves during the second heating. We did not observe a significant impact of the added (3-aminopropyl)trimethoxysilane on thermal stability of the composites; however, as noted also in a previous work [30], the size of diatomite

particles did have a slight importance and, for the fractionated diatoms, we observed an increase in temperature T_g by around 1 °C for the first heating cycle.

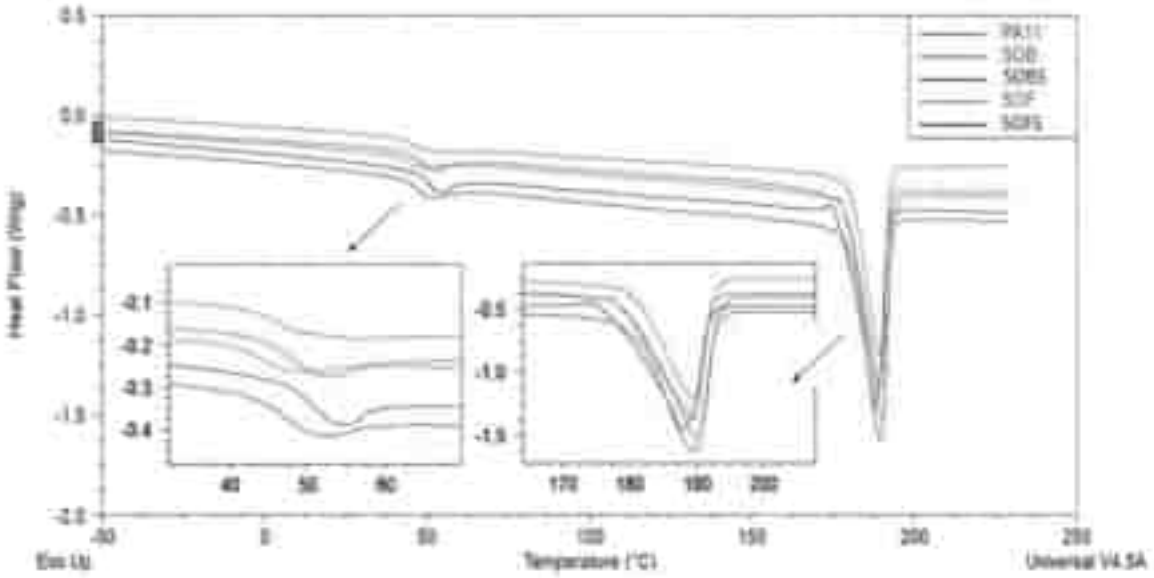

Figure 12. DSC curves of unmodified PA11 and composites, first heating; samples with 5% of diatoms.

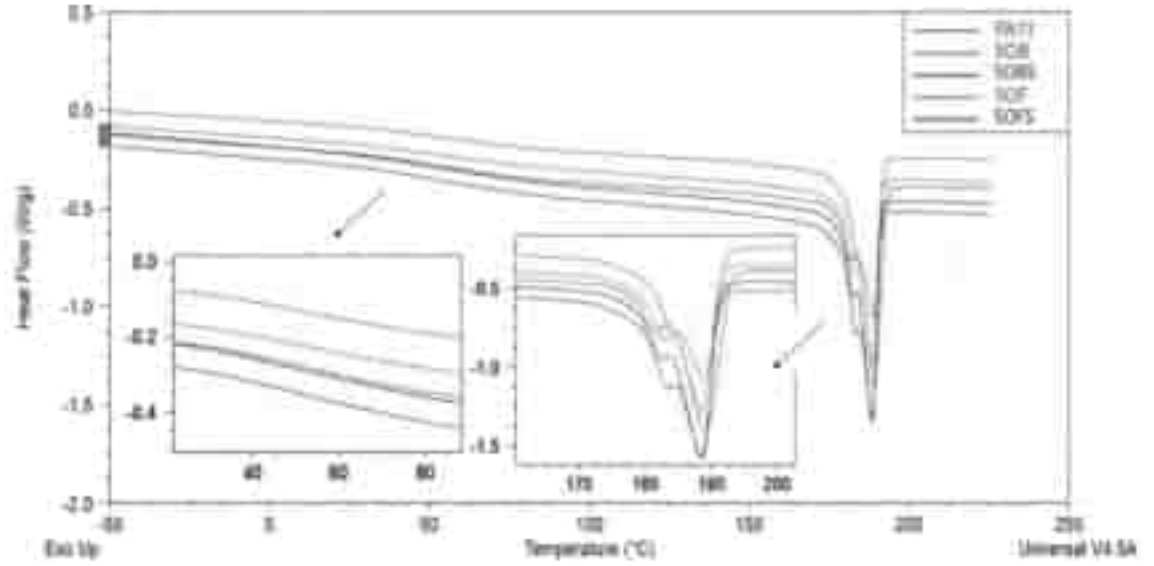

Figure 13. DSC curves of unmodified PA11 and composites, second heating; samples with 5% of diatoms.

Table 4. Thermal characteristics of PA11 and composites with silane.

Sample	1st Heating				Cooling	2nd Heating			
	T_g (°C)	T_m (°C)	H_m (J/g)	X (%)	T_c (°C)	T_{m1} (°C)	T_{m2} (°C)	H_m (J/g)	X (%)
PA11	48.7	190.0	56.9	27.6	163.9	181.4	189.0	51.6	25.0
5OBS	47.9	189.4	52.0	26.6	167.8	183.4	188.5	50.5	25.8
5OFS	49.8	188.7	48.8	24.9	167.8	182.7	188.5	51.7	26.4
20OBS20OBU13	46.9	189.9	44.3	26.9	169.5	-	188.3	43.7	27.7
20OFS	48.2	188.5	34.6	23.0	169.2	-	188.6	32.1	19.5

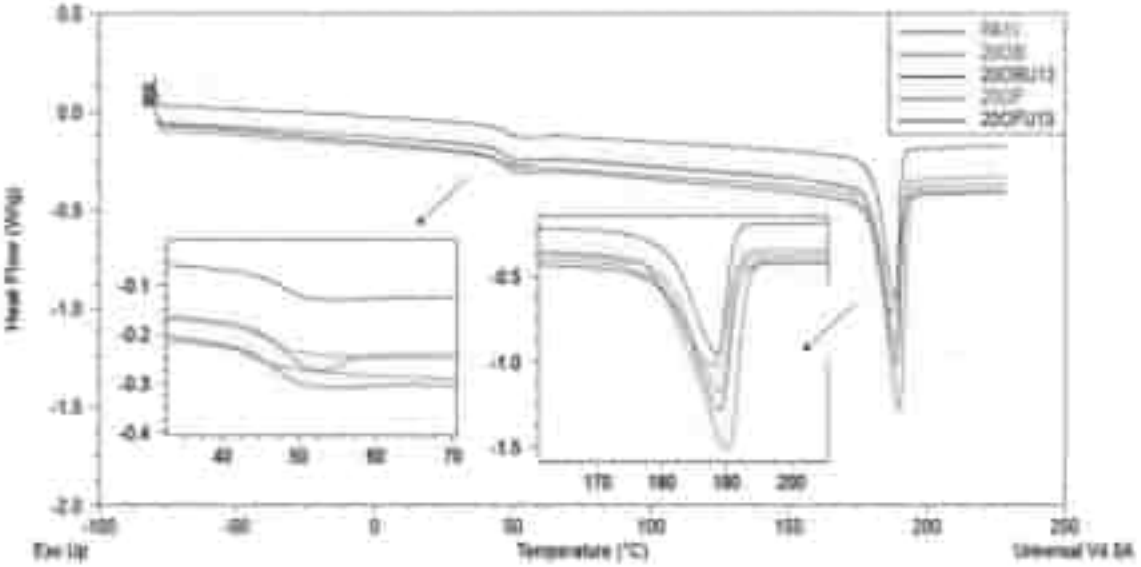

Figure 14. DSC curves of unmodified PA11 and composites, first heating, samples with 20% of diatoms.

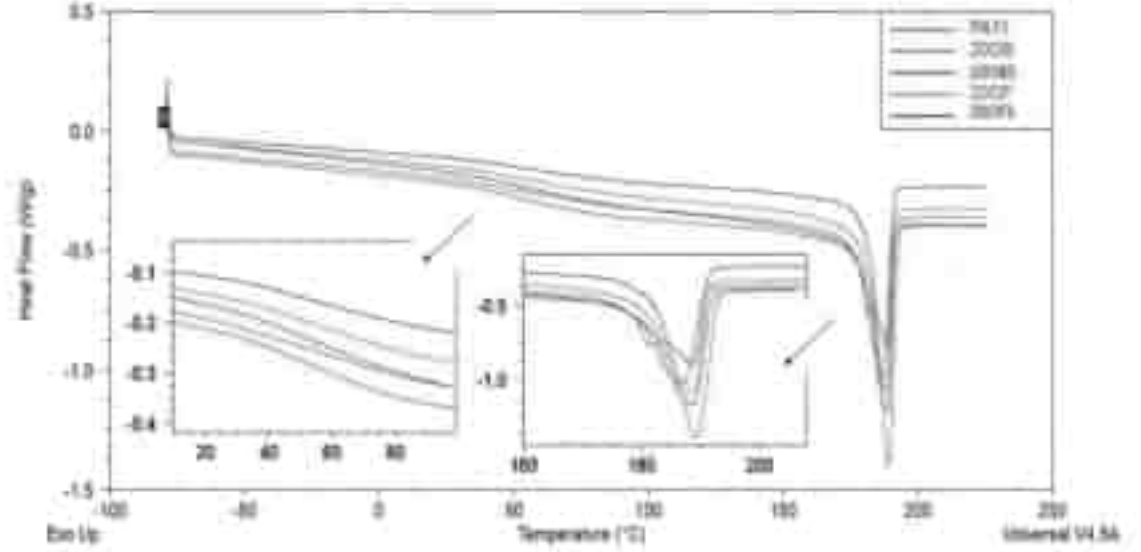

Figure 15. DSC curves of unmodified PA11 and composites, second heating, samples with 20% of diatoms.

Table 5. Thermal characteristics of composites without silane obtained in a previous work [17].

Sample	1st Heating				Cooling	2nd Heating			
	T_g (°C)	T_m (°C)	H_m (J/g)	X (%)	T_c (°C)	T_{cc1} (°C)	T_{cc2} (°C)	H_m (J/g)	X (%)
PA11	46.7	190.0	56.9	27.6	163.9	181.4	189.0	51.6	25.0
5OB	46.8	189.5	44.6	22.8	167.6	182.6	189.0	45.0	23.0
5OF	44.0	189.5	48.7	24.9	167.1	182.8	188.6	50.3	25.7
20OB	44.6	187.6	36.4	22.1	167.8	-	186.6	44.1	26.8
20OF	46.6	188.7	39.2	23.8	168.7	-	188.4	44.7	27.1

The effect of the diatom concentration and addition of (3-aminopropyl)trimethoxysilane silane on the viscoelastic behaviour of composites was studied by DMTA. The curves of the

storage modulus (E') and tan δ as the temperature's function are shown in Figures 16 and 17, while the obtained results are summarised in Table 6. The storage modulus or viscoelastic modulus corresponds to the elastic response of the material and is associated with the energy absorbed (stored) by the material and recovered in each load cycle. Generally, the increase in storage modulus is caused by mechanical viscoelastic stiffness raise [54]. The glass transition temperature (T_g) was determined from the tan δ curve, which is defined as the ratio of the loss modulus E'' to the storage modulus E'. The peak of the tan δ curve occurs as a result of the relaxation of the polymer chains, and the glass transition temperature is attributed to it [55].

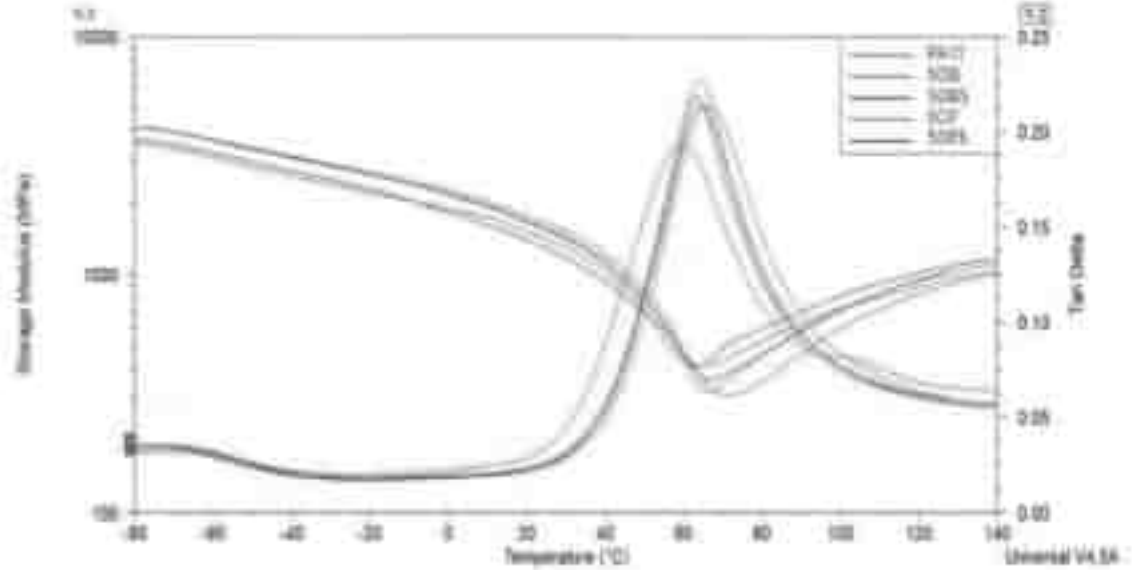

Figure 16. The storage modulus and tan δ curves of unmodified PA11 and composites samples with 5% of diatoms.

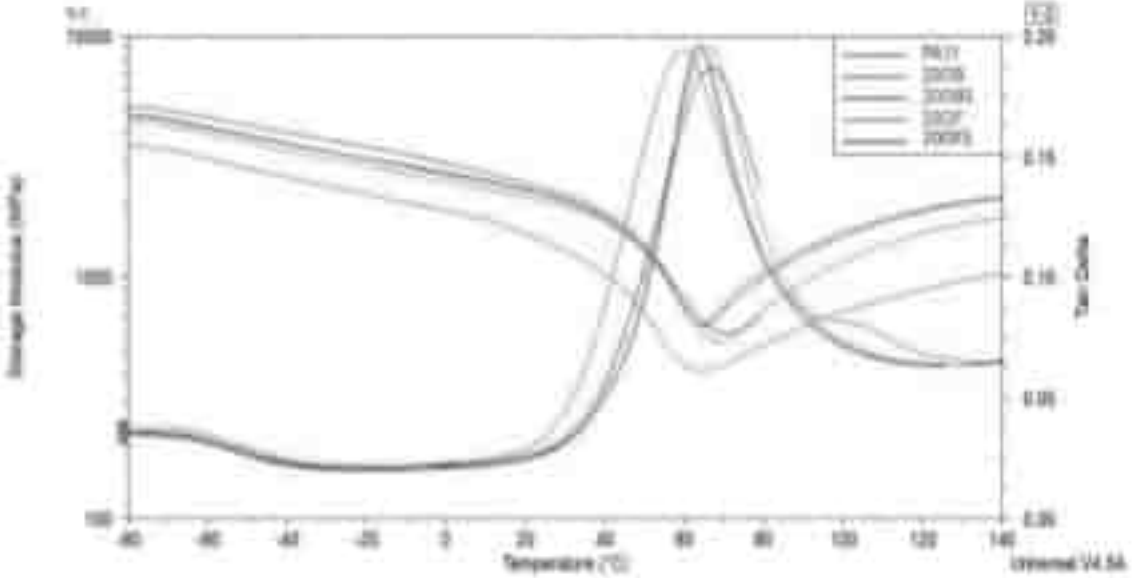

Figure 17. The storage modulus and tan δ curves of unmodified PA11 and composites samples with 20% of diatoms.

Table 6. Summary of the determined values of the glass transition temperature from tan δ curves and storage modulus E' curves.

Sample	T_g (°C)	E' (MPa)	tan δ
PA11	59.6	1409	0.194
5OH	66.4	1649	0.214
5OH5	63.2	1591	0.219
5OF	64.2	1534	0.227
5OF5	64.2	1560	0.214
20OH	63.4	2222	0.196
20OH5	64.0	2340	0.196
20OF	65.8	2062	0.196
20OF5	66.9	2190	0.187

It can be seen that for neat PA11 the glass temperature was under 60 °C. In the presence of 20 wt% diatoms and (3-aminopropyl)trimethoxysilane, T_g increased to 66.9 °C. It was found that the addition of diatoms with different sized frustules and silane shifted the Tg peak towards higher values of about 5 °C. This confirms a good dispersion of diatoms in the PA11 matrix, which limits the polymer chains' mobility and causes mechanical viscoelastic stiffness to increase. A similar tendency was confirmed by other researchers [34]. The addition of APTES silane did not change the glass temperature much, which was related to not affecting the polymer chains' movement. These results were correlated with the obtained mechanical parameters. The addition of silane did not increase Young's modulus and tensile strength composites relative to chemical unmodified materials.

Looking into the presented curves, it should also be noted that the addition of diatoms into the PA11 polymer allowed for obtaining stiffer material with higher values of storage moduli investigated at room temperature and tan δ value due to the stiffening effect of the reinforcement. As observed, the increase of the diatom content tends to increase the value of E' from 1409 MPa to 2340 MPa, suggesting an improvement in the material's mechanical viscoelastic performance. At the same time, tan δ presented a slight increase for composites with 20 wt% of the diatom concentration, probably due to reducing the polymer's relaxation caused by the reinforcing effect of diatoms that hinders the mobility of the PA11 molecular chains [34]. In comparison, Stoclet et al. indicated that the increase in the clay content and improvement of its dispersion involves an enhancement of thermomechanical properties of polyamide 11 nanocomposites [31].

3.7. Surface Properties

Composite fracture imaging showed a relationship between both the method of preparing the filler and the tendency for secondary agglomeration of particles and between its concentration and the distribution of agglomerates in the polymer matrix (Figure 18). The higher the filler concentration, the more clusters of diatom particles were present, which was observed for both the basic and the fractionated diatomaceous earth. Basic diatomaceous earth showed a greater tendency towards secondary agglomeration than fractionated diatomaceous earth, which was due to the presence of particles of various sizes. Based on the comparison of SEM images showing the fractures of composites without silane, we found that it had an impact on the structure of the surface. The silanization of diatomaceous earth made the composite surface smoother, regardless of the fraction used and of its concentration. In addition, the share of grooves visible at the fracture declined.

Images of the surfaces and fractures of the composites with an optical microscope were made (Figures 19 and 20). Along with the growing filler concentration on the surface of the composites, we observed an increasing non-uniformity in colour due to the presence of hydrophilic centres (black spots) on the composite surface, which was in turn directly attributable to the values of the wetting angle and the hydrophobic-hydrophilic properties of the composites (Figure 21 wetting angle). In addition, there were differences in colour between the composites filled with basic and fractionated diatomaceous earth. This was

caused by eliminating the systems of the smallest DE particles, which gave the composite an even, uniform colour, whereas larger, agglomerated particles were visible, as the dark spots discussed above. That effect was also slightly visible in the images of the composite fractures, while much larger differences were noticed on the surface of the samples. For the fractures, it was easier to see the colour difference arising from the more concentration of the filler, so as the concentration grew, the colour of the composite changed towards that of diatomaceous earth alone, with a gentle difference due to the filler particle size.

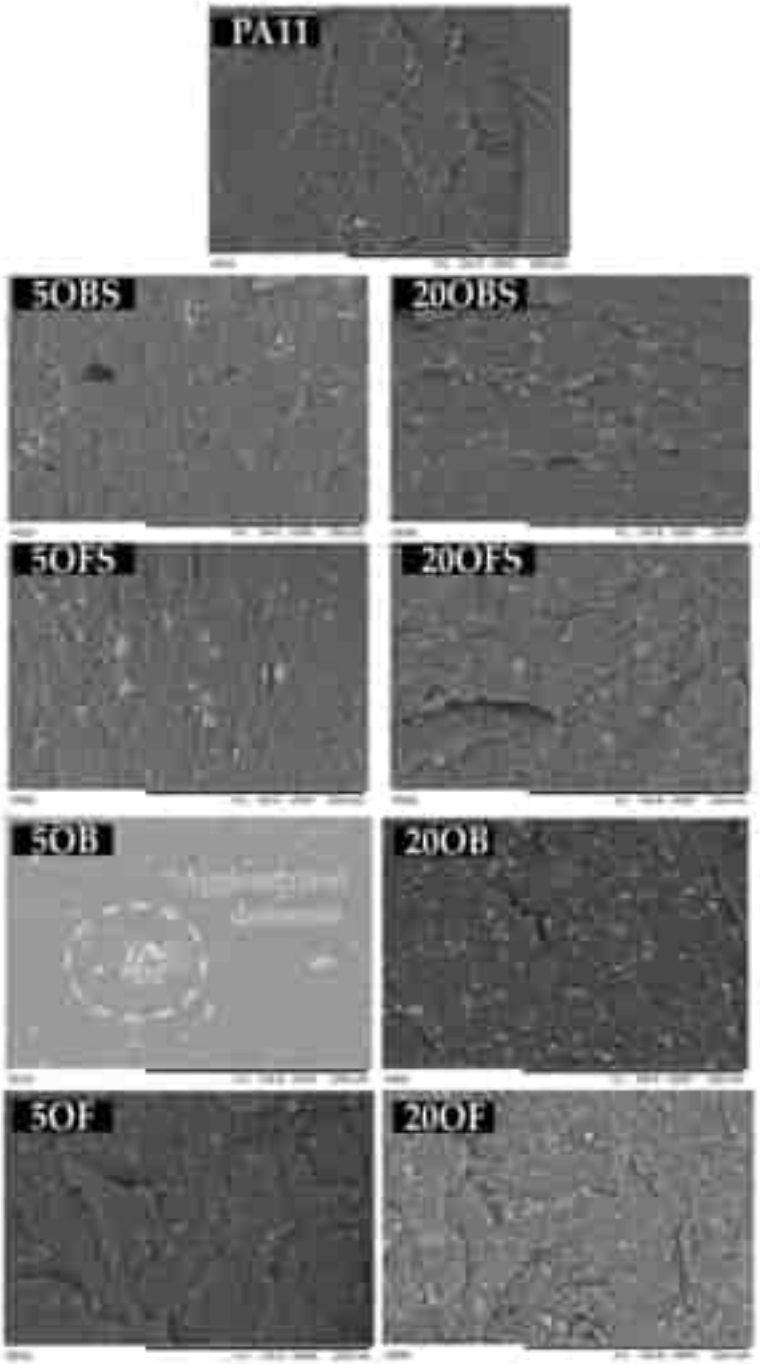

Figure 18. SEM images of composite fractures after testing the notch impact test; comparison to the systems without silane APTES.

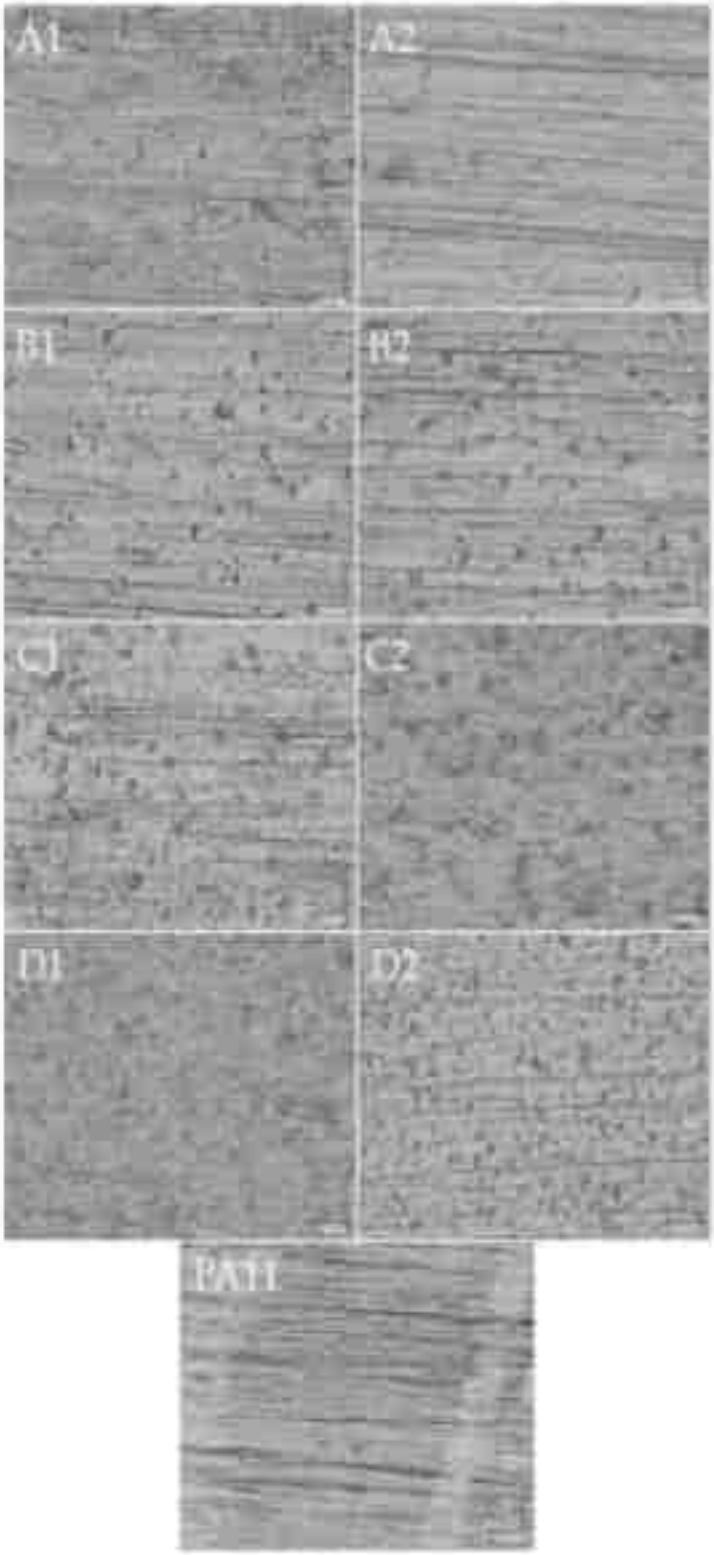

Figure 19. Surface of the composites: (A1)—2.5OH5, (A2)—2.5OH5, (B1)—5OH5, (B2)—5OH5, (C1)—10OH5, (C2)—10OH5, (D1)—20OH5, (D2)—20OH5, (PA11)—Polyamide 11.

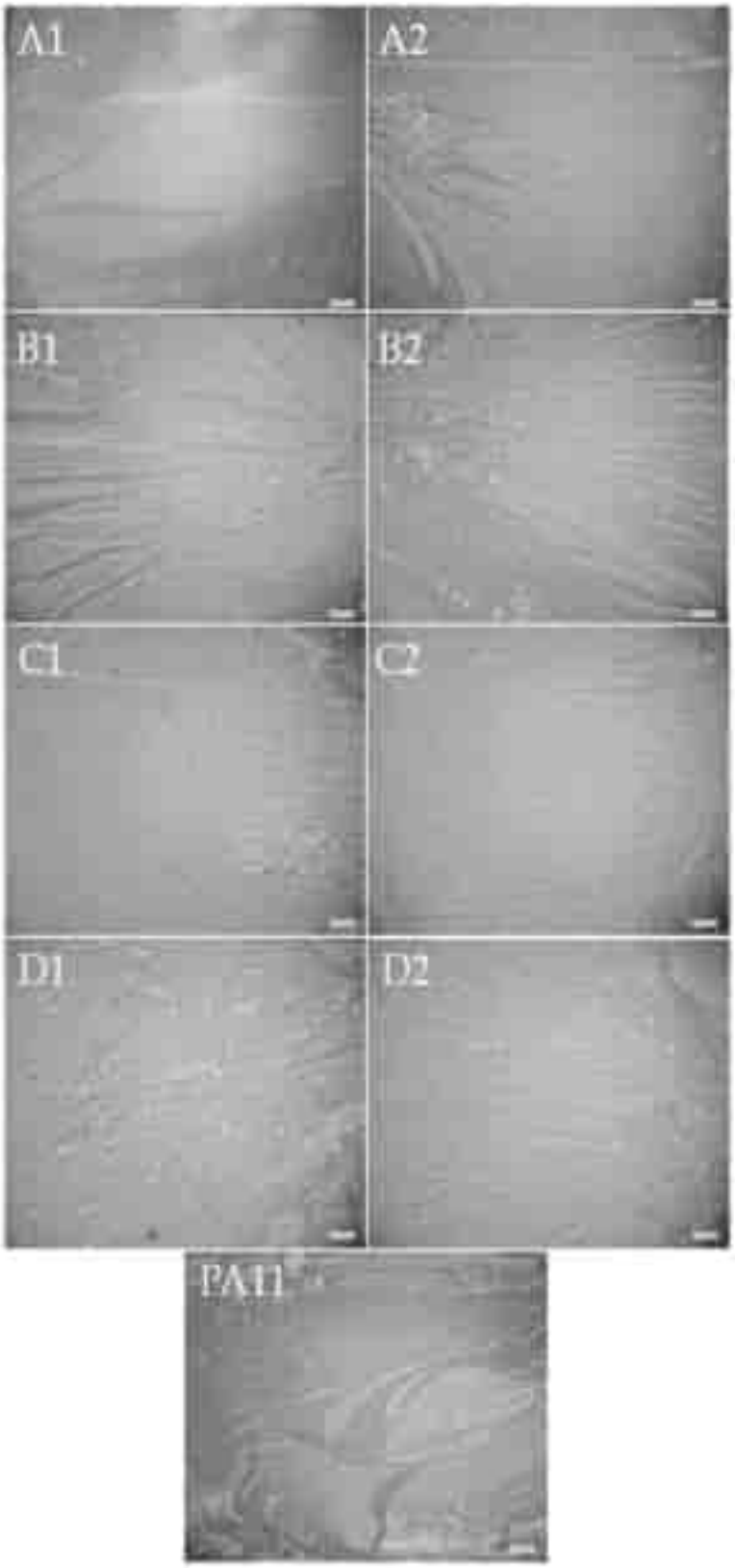

Figure 20. Fractures of the composites after the notch impact test: (A1)—2.5OH5, (A2)—2.5OH5, (B1)—5OH5, (B2)—5OH5, (C1)—10OH5, (C2)—10OH5, (D1)—20OH5, (D2)—20OH5, (PA11)—Polyamide 11.

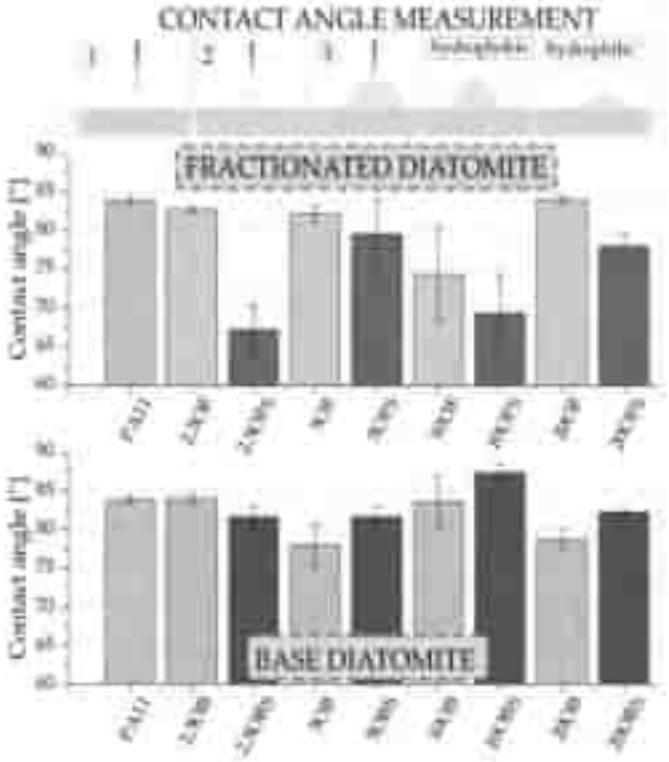

Figure 21. Wetting angle.

The gloss tests were carried out both for the composites modified with silanized diatomaceous earth and for the composites without U-13 to make a comparison, as presented in Table 7. The test was carried out at 60° geometry. Neat polyamide 11 is characterised by a surface gloss of 31.5 GU, which makes it a medium gloss system. The addition of diatomaceous earth reduced the gloss, which decreased linearly along with the growing concentration of the filler having the form of basic diatomaceous earth. The modification of base systems with silane further reduced the gloss and, for the high-filled samples, the formation of systems with a near-matte surface. An exception is the system filled in 5%, subjected to silanization, as in this case we can observe a slight growth in gloss value, which is also visible for the fractionated sample 5OF. In this case, at the initial abrupt increase of gloss and achieving the limit for system 5OF, the values start declining along with further growth of the filler. It is similar after modification with APTES, but in this case the limit filling value turned out to be 10%, and each addition of silane caused a gloss reduction and the formation of systems with surfaces approaching matte.

Table 7. Gloss on the composite surface measured at 60° geometry.

	Gloss 60° [GU]	SD [GU]		Gloss 60° [GU]	SD [GU]		Gloss 60° [GU]	SD [GU]		Gloss 60° [GU]	SD [GU]
2.5OH	24.53	0.30	2.5OH6	22.20	0.36	2.5OF	23.80	0.08	2.5OF6	22.97	1.13
5OH	21.90	0.54	5OH6	22.20	1.12	5OF	25.70	1.13	5OF5	20.70	0.36
10OH	17.50	2.12	10OH6	21.30	1.45	10OF	26.10	0.75	10OF6	27.03	0.62
20OH	15.07	0.74	20OH6	12.47	0.17	20OF	16.57	0.12	20OF6	15.47	0.42
PA11				31.50						1.93	

The addition of APTES enabled us to obtain a hydrophilic composite system. The tests of hydrophobic-hydrophilic properties (Figure 21) showed that neat polyamide 11 had a

wetting angle of around 84°, making it hydrophilic. This was similar to composites filled with diatomaceous earth, whose surfaces were also hydrophilic. Those based on polylactide were hydrophilic systems. The addition of base, silanized diatomaceous earth in most cases (except 2.5% loading), caused a slight growth in surface hydrophobicity, which might have been due to the presence of smaller filler particles, which do not exist in fractionated DE, and to the combination with APTES, which is likely to interact more effectively with smaller particles. The silanization of fractionated diatomaceous earth and the elimination of the smallest particles allowed us to obtain a more hydrophilic composite system compared to the others, but we found no relationship between the filler concentration and the wetting angle values.

Washability tests were conducted (Figure 22) to determine whether PA11/diatoms are useful in industrial applications, for example in the overprinting of foils and packaging materials. We selected a composite characterised by the lowest degree of surface hydrophobicity (2.5OFS) and, for reference, a corresponding composite without silanization (2.5OF) and pure Polyamide 11 (PA11). The test showed that, after the first step of the washability test conducted on the surface of composite 2.5OF (without silanization), the green (permanent) marker was partially removed, which did not occur for the other samples; additionally, for that composite, we also found that the removable board marker (blue) remained on the surface to the greatest extent. Despite the much lower wetting angle for the silanized sample compared to pure polyamide 11, after using water, the trace of the permanent marker remained unchanged and had a similar intensity. Only methanol used to clean the surface completely removed each type of marker used. Based on the described tests, we concluded that a silanized composite showed higher resistance to surface washing than a composite containing pure diatomaceous earth, despite the difference in wetting angle, which was 16° on average, whereas pure polyamide 11 and composite 2.5OE, despite the nearly identical hydrophobicity level (~84° and 83°, respectively), showed significant differences in the behaviour of their surfaces when coloured.

Figure 22. Washability test.

The relative hiding power tests (Figure 23) of the composites indirectly permitted us to determine the composites' colouring degree and transmittance. The relative hiding power increased along with the growing filler concentration, but that increase was not so significant up to 10% DE. In the case of composites modified with basic DE, the maximum recorded relative hiding power was around 5%, and 3% for fractionated DE, which indicates that the elimination of the smallest particles (<3 µm) increased the transmittance of the composites (Figure 4), implying a change in colour in this case. Composites filled with base diatomaceous earth at 20% showed the lowest relative hiding power values, while for fractionated DE, they were lower by half, which means that the effect of absence of the smallest particles was visible considerably better at higher concentrations. Figure 24 shows an SEM image of a composite containing 20% basic diatomaceous earth without silanization, which was made in a random location at the fracture of the sample. We observed large amounts of agglomerated diatomaceous earth containing broken and unbroken frustules. The filler agglomeration in the polymer matrix had a direct impact on the very high values of relative hiding power due to the hindered permeation of rays through the sample. Each modification of the systems with APTES reduced the relative hiding power, which was best visible for systems 20OF. The SEM images presented in Figure 25 show composites containing 20% of the filler. We observed a considerably higher dispersion of the filler in the polymer matrix, implying a lower hiding power for composite surfaces, which applies in particular to the systems with fractionated diatomaceous earth.

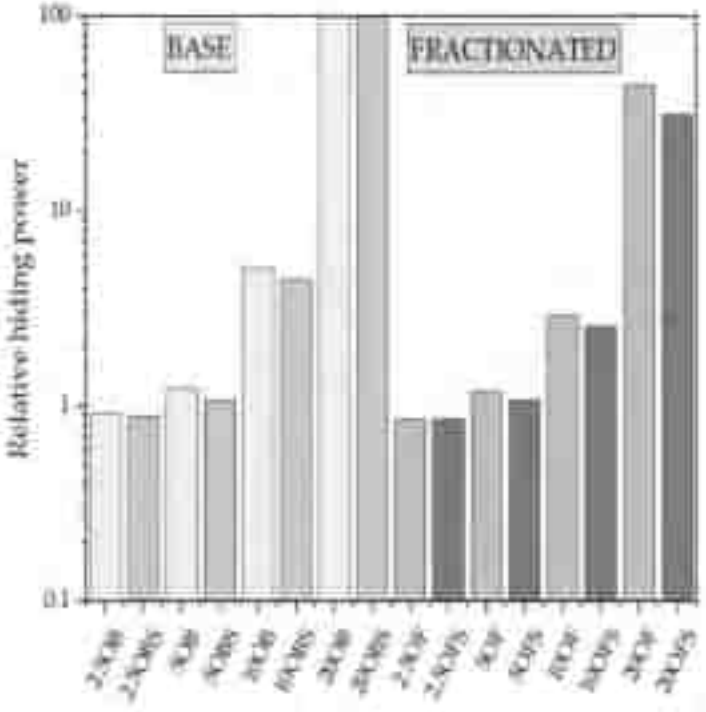

Figure 23. Relative hiding power.

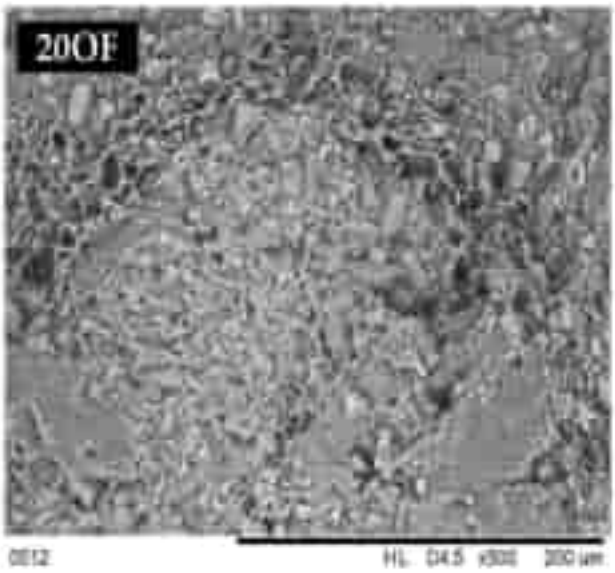

Figure 24. An SEM image of a composite containing 20% of basic diatomaceous earth.

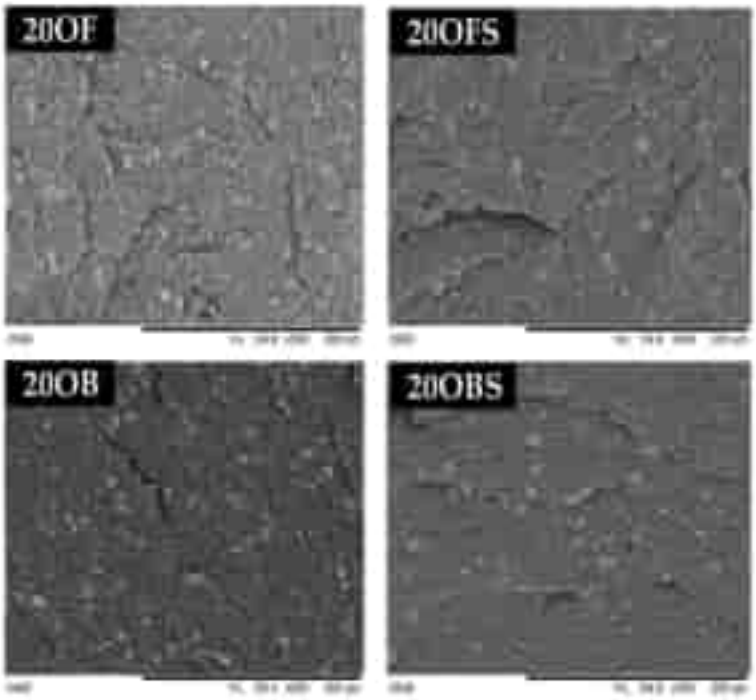

Figure 25. SEM images of composites containing 20% silanized and non-silanized diatomaceous earth.

4. Conclusions

The tests allowed us to make conclusions on the effect of diatomaceous earth's introduction into PA11 on the number of properties of such fabricated composites, as well as the impact of diatomite hydraulic fractionation and silanization. The addition of the diatomite filler results changed the crystalline structure of PA11 and the formation of δ' smectic phase, as opposed to α + γ phases for neat PA11. The modification of diatomaceous earth favourably affected the elongation at the break of PA11/DE composites; we observed a significant improvement in their elasticity, particularly at low filler concentrations. The addition of APTES also contributed to a considerable improvement in the

composites' processing capacity, particularly at low filler concentrations, whereas, along with the growing content of DE, the effect brought by the characteristics of diatomaceous earth started to prevail. With the silanization of fractionated diatomaceous earth, we obtained a hydrophilic composite system, while the addition of APTES to basic diatomaceous earth increased the hydrophobic–hydrophilic properties of the surface. Depending on the desired parameters of the composite, the system properties were controlled by silanizing fillers of various particle sizes. On the surface of the composites, many hydrophilic centres were visible, the amount of which grew along with the increasing filler concentration. The centres had a direct impact on both the morphology of the surface of the composite and its hydrophobic–hydrophilic properties.

Author Contributions: Conceptualization, R.E.P., R.D. and M.D.; methodology, R.E.P. and M.D.; formal analysis, R.D.; investigation, M.D., P.K., E.G. and A.M.; data curation, M.D., P.K., E.G. and A.M.; writing—original draft preparation, M.D. and D.R.; writing—review and editing, M.D., D.R., R.E.P. and R.D.; visualization, M.D.; supervision, R.E.P., R.D. and K.J.K.; project administration, R.D. and K.J.K.; funding acquisition, R.D. All authors have read and agreed to the published version of the manuscript.

Funding: This work was financially supported in the frame of the project "Advanced Biocomposites for Tomorrow's Economy BIOG-NET", FNP POIR.04.04.00-00-1792/18-00. The project was carried out within the TEAM-NET programme of the Foundation for Polish Science co-financed by the European Union under the European Regional Development Fund.

Institutional Review Board Statement: Not applicable.

Informed Consent Statement: Not applicable.

Data Availability Statement: Not applicable.

Conflicts of Interest: The authors declare no conflict of interest.

References

1. Friedrich, K.; Almajid, A.A. Manufacturing Aspects of Advanced Polymer Composites for Automotive Applications. *Appl. Compos. Mater.* **2013**, *20*, 107–128. [CrossRef]
2. Muhammad, A.; Rahman Md, R.; Baini, R.; Bakri, M.K.B. *Applications of Sustainable Polymer Composites in Automobile and Aerospace Industry. Advances in Sustainable Polymer Composites*; Woodhead Publishing Series in Composites Science and Engineering: Cambridge, UK, 2021; pp. 185–207.
3. Motavalli, M.; Czaderski, C.; Schumacher, A.; Gsell, D. *4—Fibre Reinforced Polymer Composite Materials for Building and Construction. Textiles, Polymers and Composites for Buildings*; Woodhead Publishing: Cambridge, UK, 2010; pp. 69–128.
4. Polec, I.; Hine, P.J.; Bonner, M.J.; Ward, I.M.; Barton, D.C. Die drawn wood polymer composites. I. Mechanical properties. *Compos. Sci. Technol.* **2010**, *70*, 45–52. [CrossRef]
5. Borah, J.S.; Kim, D.S. Recent development in thermoplastic/wood composites and nanocomposites: A review. *Korean J. Chem. Eng.* **2016**, *33*, 3035–3049. [CrossRef]
6. Durmaz, B.U.; Aytac, A. Investigation of the mechanical, thermal, morphological and rheological properties of bio-based polyamide11/poly(lactic acid) blend reinforced with short carbon fiber. *Mater. Today Commun.* **2022**, *30*, 103030. [CrossRef]
7. Rahmani, H.; Najafi, S.H.M.; Ashori, A. Mechanical performance of epoxy/carbon fiber laminated composites. *J. Reinf. Plast. Compos.* **2014**, *33*, 733–740. [CrossRef]
8. Kuram, E. Hybridization effect of talc/glass fiber as a filler in polycarbonate/acrylonitrile-butadiene-styrene composites. *Compos. Part B Eng.* **2019**, *173*, 106954. [CrossRef]
9. Jubinville, D.; Abdelwahab, M.; Mohanty, A.K.; Misra, M. Comparison in composite performance after thermooxidative aging of injection molded polyamide 6 with glass fiber, talc, and a sustainable biocarbon filler. *J. Appl. Polym. Sci.* **2020**, *137*, 48618. [CrossRef]
10. Halim, K.A.A.; Farrell, J.B.; Kennedy, J.E. Preparation and characterisation of polyamide 11/montmorillonite (MMT) nanocomposites for use in angioplasty balloon applications. *Mater. Chem. Phys.* **2013**, *143*, 336–348. [CrossRef]
11. Guo, F.; Aryana, S.; Han, Y.; Jiao, Y. A Review of the Synthesis and Applications of Polymer–Nanoclay Composites. *Appl. Sci.* **2018**, *8*, 1696. [CrossRef]
12. Cazan, C.; Enesca, A.; Andronic, L. Synergic Effect of TiO_2 Filler on the Mechanical Properties of Polymer Nanocomposites. *Polymers* **2021**, *13*, 2017. [CrossRef]

13. Brząkalski, D.; Przekop, R.E.; Frydrych, M.; Pakuła, D.; Dobrosielska, M.; Sztorch, B.; Marciniec, B. Where ppm Quantities of Silsesquioxanes Make a Difference—Silanes and Cage Siloxanes as TiO_2 Dispersants and Stabilizers for Pigmented Epoxy Resins. *Materials* **2022**, *15*, 494. [CrossRef] [PubMed]
14. Oliver-Ortega, H.; Méndez, J.A.; Mutjé, P.; Tarrés, Q.; Espinach, F.X.; Ardanuy, M. Evaluation of Thermal and Thermomechanical Behaviour of Bio-Based Polyamide 11 Based Composites Reinforced with Lignocellulosic Fibres. *Polymers* **2017**, *9*, 522. [CrossRef]
15. Bajwa, D.S.; Adhikari, S.; Shojaeiarani, J.; Bajwa, S.G.; Pandey, P.; Shanmugam, S.R. Characterization of bio-carbon and ligno-cellulosic fiber reinforced bio-composites with compatibilizer. *Constr. Build. Mater.* **2019**, *204*, 193–202. [CrossRef]
16. Balaji, K.V.; Shirvanimoghaddam, K.; Rajan, G.S.; Ellis, A.V.; Naebe, M. Surface treatment of Basalt fiber for use in automotive composites. *Mater. Today Chem.* **2020**, *17*, 100334.
17. Saleem, A.; Medina, L.; Skrifvars, M. Mechanical performance of hybrid bast and basalt fibers reinforced polymer composites. *J. Polym. Res.* **2020**, *27*, 61. [CrossRef]
18. More, A.P. Flax fiber–based polymer composites: A review. *Adv. Compos. Hybrid Mater.* **2022**, *5*, 1–20. [CrossRef]
19. Ediz, N.; Bentli, İ.; Tatar, İ. Improvement in filtration characteristics of diatomite by calcination. *Int. J. Miner. Process.* **2010**, *94*, 129–134. [CrossRef]
20. Chróścika, E.; Sobiecki, J.R.; Święszkowski, W.; Kurzydłowski, K.J. Silanization as a method for improving PLLA coating adhesion to the intramedullary nails—Preliminary studies. *Eng. Biomater.* **2010**, *96–98*, 88–92.
21. Watanabe, R.; Sugahara, A.; Hagihara, H.; Sakamoto, K.; Nakajima, Y.; Naganawa, Y. Mechanical Properties of Multiscale Graphene Oxide/Basalt Fiber/Epoxy Composites. *Fibers Polym.* **2019**, *20*, 138–146.
22. Watanabe, R.; Sugahara, A.; Hagihara, H.; Sakamoto, K.; Nakajima, Y.; Naganawa, Y. Polypropylene-Based Nanocomposite with Enhanced Aging Stability by Surface Grafting of Silica Nanofillers with a Silane Coupling Agent Containing an Antioxidant. *ACS Omega* **2020**, *5*, 12431–12439. [CrossRef]
23. Ahangaran, F.; Navarchian, A.H. Recent advances in chemical surface modification of metal oxide nanoparticles with silane coupling agents: A review. *Adv. Colloid Interface Sci.* **2020**, *286*, 102298. [CrossRef] [PubMed]
24. Dobrosielska, M.; Dobrucka, R.; Kozera, P.; Brząkalski, D.; Gabriel, E.; Głowacka, J.; Jałbrzykowski, M.; Kurzydłowski, K.J.; Przekop, R.E. Beeswax as a natural alternative to synthetic waxes for fabrication of PLA/diatomaceous earth composites. *Sci. Rep.* **2023**, *13*, 1161. [CrossRef] [PubMed]
25. Dobrosielska, M.; Dobrucka, R.; Pajewska-Szmyt, M.; Kozera, P.; Gabriel, E.; Głowacka, J.; Brząkalski, D.; Kurzydłowski, K.J.; Przekop, R.E. Effect of Wax Additives and Silanization of Diatom Surfaces on Thermomechanical Properties of Polylactide Composites. *Polymers* **2022**, *14*, 5511. [CrossRef] [PubMed]
26. Liu, T.; Lim, K.P.; Tjiu, W.C.; Pramoda, K.P.; Chen, Z.-K. Preparation and characterization of nylon 11/organoclay nanocomposites. *Polymer* **2003**, *44*, 3529–3535. [CrossRef]
27. Mancic, L.; Pontón, P.I.; Letichevsky, S.; Costa, A.M.; Marinkovic, B.A.; Rizzo, F.C. Application of silane grafted titanate nanotubes in reinforcing of polyamide 11 composites. *Compos. Part B Eng.* **2016**, *93*, 153–162. [CrossRef]
28. Benobeidallah, B.; Benhamida, A.; Dorigato, A.; Sola, A.; Messori, M.; Pegoretti, A. Structure and Properties of Polyamide 11 Nanocomposites Filled with Fibrous Palygorskite Clay. *JRM* **2019**, *7*, 1. [CrossRef]
29. Cong, D.V.; Giang, N.V.; Trung, T.H.; Hoang, T.; Lam, T.D. Biocomposites from polyamide 11 reinforced by organic silane modified jute fibers: Fabrication and characterization. *J. Appl. Polym. Sci.* **2022**, *139*, 11. [CrossRef]
30. Dobrosielska, M.; Dobrucka, R.; Kozera, P.; Kozera, R.; Kołodziejczak, M.; Gabriel, E.; Głowacka, J.; Jałbrzykowski, M.; Kurzydłowski, K.J.; Przekop, R.E. Biocomposites Based on Polyamide 11/Diatoms with Different Sized Frustules. *Polymers* **2022**, *14*, 3153. [CrossRef]
31. Dobrosielska, M.; Dobrucka, R.; Brząkalski, D.; Frydrych, M.; Kozera, P.; Wieczorek, M.; Jałbrzykowski, M.; Kurzydłowski, K.J.; Przekop, R.E. Influence of Diatomaceous Earth Particle Size on Mechanical Properties of PLA/Diatomaceous Earth Composites. *Materials* **2022**, *15*, 3607. [CrossRef]
32. *PN-EN ISO 527-1:2020-01*; Plastics—Determination of Mechanical Properties under Static Stretching—Part 1: General Principles. PKN: Płock, Poland, 2020.
33. *EN ISO 178:2010*; Plastics—Determination of Flexural Properties. PKN: Płock, Poland, 2010.
34. *EN ISO 179-1:2010*; Plastics—Determination of Charpy Impact Properties—Part 1: Non-Instrumented Impact Test. PKN: Płock, Poland, 2010.
35. *PN-EN ISO 178:2019-06*; Plastics—Determination of Bending Properties. PKN: Płock, Poland, 2019.
36. *EN ISO 1133-1:2022*; Plastics—Determination of the Melt Mass-Flow Rate (MFR) and Melt Volume-Flow Rate (MVR) of Thermoplastics—Part 1: Standard Method. PKN: Płock, Poland, 2022.
37. Patel, A.K.; Bajpai, R.; Keller, J.M. On the crystallinity of PVA/palm leaf biocomposite using DSC and XRD techniques. *Microsyst. Technol.* **2014**, *20*, 41–49. [CrossRef]
38. *EN ISO 2813:2014*; Paints and Varnishes—Determination of Gloss Value at 20°, 60° and 85°. PKN: Płock, Poland, 2014.
39. Zemnukhova, L.A.; Panasenko, A.E.; Artem'yanov, A.P.; Tsoy, E.A. Dependence of Porosity of Amorphous Silicon Dioxide Prepared from Rice Straw on Plant Variety. *BioResources* **2015**, *10*, 3713–3723. [CrossRef]
40. Wardhani, G.; Nurlela, N.; Azizah, M. Silica Content and Structure from Corncob Ash with Various Acid Treatment (HCl, HBr, and Citric Acid). *Molekul* **2017**, *12*, 174–181. [CrossRef]

41. Peng, Z.-W.; Hsieh, P.-T.; Liu, Y.-J.; Huang, C.-J.; Li, C.-C. Investigation on blistering behavior for n-type silicon solar cells. 5th International Conference on Silicon Photovoltaics, SiliconPV. *Energy Procedia* **2015**, *77*, 827–831. [CrossRef]
42. Reka, A.A.; Pavlovski, B.; Fazlija, E.; Berisha, A.; Pacarizi, M.; Daghmehchi, M.; Sacalis, C.; Jovanovski, G.; Makreski, P.; Oral, A. Diatomaceous Earth: Characterization, thermal modification, and application. *Open Chem.* **2021**, *19*, 451–461. [CrossRef]
43. Ricou, P.; Pinel, E.; Juhasz, N. Temperature Experiments for Improved Accuracy in The Calculation of Polyamide-11 Crystallinity by X-ray Diffraction. International Centre for Diffraction Data. *Adv. X-ray Anal.* **2005**, *48*, 170–175.
44. Flores-Rojas, E.; Schmalzl, D.; Jasso-Cabrera, E.; Solorza-Feria, O.; Poggi-Varaldo, H.M.; Bretón-Deval, L. Using Nano Zero-Valent Iron Supported on Diatomite to Remove Acid Blue Dye: Synthesis, Characterization, and Toxicology Test. *Sustainability* **2021**, *13*, 13699. [CrossRef]
45. Lutyński, M.; Sakiewicz, P.; Lutyńska, S. Characterization of Diatomaceous Earth and Halloysite Resources of Poland. *Minerals* **2019**, *9*, 670. [CrossRef]
46. Ilia, I.K.; Stamatakis, M.G.; Perraki, T.S. Mineralogy and technical properties of clayey diatomites from north and central Greece. *Cent. Eur. J. Geosci.* **2009**, *1*, 393–403. [CrossRef]
47. Thomas, P.; Ashokbabu, A.; Vaish, R. Structural, thermal and dielectric properties and thermal degradation kinetics of nylon 11/$CaCu_3Ti_4O_{12}$ (CCTO) nanocomposites. *J. Therm. Anal. Calorim.* **2020**, *141*, 1125–1138. [CrossRef]
48. Moriyama, T.; Sumiya, N.; Saito, T. Impact strength improvement of polyamide 11 without flexural modulus reduction by dispersing poly(butylene succinate) particles. *Polym. J.* **2016**, *48*, 221–224. [CrossRef]
49. Latko, P.; Kolbuk, D.; Kozera, R.; Boczkowska, A. Microstructural Characterization and Mechanical Properties of PA11 Nanocomposite Fibers. *J. Mater. Eng. Perform.* **2016**, *25*, 68–75. [CrossRef]
50. Bahrami, M.; Abenojar, J.; Martínez, M.A. Comparative Characterization of Hot-Pressed Polyamide 11 and 12: Mechanical, Thermal and Durability Properties. *Polymers* **2021**, *13*, 3553. [CrossRef]
51. Stoclet, G.; Sclavons, M.; Devaux, J. Relations between structure and property of polyamide 11 nanocomposites based on raw clays elaborated by water-assisted extrusion. *J. Appl. Polym. Sci.* **2013**, *127*, 4809–4824. [CrossRef]
52. Castagnet, S.; Thilly, L. High-pressure dependence of structural evolution in polyamide 11 during annealing. *J. Polym. Sci. Part B Polym. Phys.* **2009**, *47*, 2115–2125. [CrossRef]
53. Mancic, L.; Osman, R.F.M.; Costa, A.M.L.M.; d'Almeida, J.R.M.; Marinkovic, B.A.; Rizzo, F.C. Thermal and mechanical properties of polyamide 11 based composites reinforced with surface modified titanate nanotubes. *Mater. Des.* **2015**, *83*, 459–467. [CrossRef]
54. Da Cruz, R.D.S.M.; Tienne, L.G.P.; Gondim, F.F.; da Silva Candido, L.; Chaves, E.G.; Marques, M.D.F.V.; da Luz, F.S.; Monteiro, S.N. Graphene nanoplatelets reinforced Polyamide-11 nanocomposites thermal stability and aging for application in flexible pipelines. *J. Mater. Res. Technol.* **2022**, *18*, 1842–1854. [CrossRef]
55. Nash, N.H.; Ray, D.; Young, T.M.; Stanley, W.F. The influence of hydrothermal conditioning on the Mode-I, thermal and flexural properties of Carbon/Benzoxazine composites with a thermoplastic toughening interlayer. *Compos. Part A Appl. Sci. Manuf.* **2015**, *76*, 135–144. [CrossRef]

Disclaimer/Publisher's Note: The statements, opinions and data contained in all publications are solely those of the individual author(s) and contributor(s) and not of MDPI and/or the editor(s). MDPI and/or the editor(s) disclaim responsibility for any injury to people or property resulting from any ideas, methods, instructions or products referred to in the content.

H7

Beeswax as a natural alternative to synthetic waxes for fabrication of PLA/Diatomaceous earth composites

Dobrosielska M., Dobrucka R., Kozera P., Brząkalski D., Gabriel E., Głowacka J., Jałbrzykowski M., Kurzydłowski K.J., Przekop R.E.; Scientific Reports, 12, 1161, 2023

scientific reports

OPEN

Beeswax as a natural alternative to synthetic waxes for fabrication of PLA/diatomaceous earth composites

Marta Dobrosielska[1], Renata Dobrucka[1,2]✉, Paulina Kozera[1], Dariusz Brząkalski[1], Ewa Gabriel[1], Julia Głowacka[1], Marek Jałbrzykowski[3,4], Krzysztof J. Kurzydłowski[1] & Robert E. Przekop[5]✉

In this study, injection moulding was applied to produce biocomposites consisting of polylactide (PLA) and amorphous diatomaceous earth used as a filler at different concentrations. Natural wax and synthetic wax were added to improve processing properties, comparing the resulting biocomposites. The use of natural beeswax makes the composite environmentally friendly. The prepared composites contained 2.5, 5, 10 and 15% w/w filler. The test samples have been injection moulded. Rheological, mechanical, surface and other properties were assessed for the fabricated composites. The testing has shown that the use of wax additives has a significant influence on the mechanical properties (tensile strength, flexural strength, impact strength) and the hydrophilicity/hydrophobicity of composite surfaces. The addition of natural wax, especially at lower concentration, has a positive effect on the rheological properties of composites (melt flow rate, MFR), flexural modulus and impact strength. Different composite parameters are modified by different wax types so both natural and synthetic waxes, can be used interchangeably, depending on the required final material characteristics.

Amorphous diatomaceous earth (diatomite, DE) consists mainly of SiO_2 (weight content of 60–95%) and small quantities of other additives, including ferrous compounds (Fe_2O_3) and aluminium compounds (Al_2O_3)[1–4]. Diatomite is a great modifier for thermoplastic polymer-based composites, including polyamide or polylactide. Due to its properties (high porosity, low density, high content of amorphous silica), diatomite is used as an adsorbent, germicide, plant protection product and for other applications[5–9].

Diatomaceous earth is a good alternative to other natural or synthetic fillers. It has a simple chemical composition and a hierarchical micro-/nano-porous structure. Additionally, it can be successfully used as a carrier of active substances. Diatomaceous earth has many advantages, such as porous structure, resistance to acids, neutrality to various types of chemicals and very low density. These characteristics make it possible to find a number of applications, e.g. as an absorbent of harmful gases, as a filtration medium, or a filler for thermoplastics or thermosets to reinforce their structure[1–3].

Neat diatomite is of natural origin, and hence ideal to be added as a filler for various types of polymers, reducing the cost of manufacturing products, but above all making the production process more sustainable. The use of diatomite to modify polylactide, feedstock of which is also obtained from natural sources, results in an organic biocomposite that is biodegradable under certain conditions. The use of diatomaceous earth as a modifier is known in the literature. Gonzalez used diatomaceous earth as a filler material for polylactide, with linseed oil in various concentrations as an additional compatibilizer[11]. On the other hand, Perera used diatomite modified with fluorosilanes and alkylsilanes as fillers for polyurethane to form superhydrophobic surfaces[12]. In contrast, Aguero presented environmentally friendly composites of poly(lactic acid) (PLA) filled with diatomaceous earth (DE), and the composites were prepared by extrusion and injection moulding[13]. A series of compatibilizers/coupling

[1]Faculty of Materials Science and Engineering, Warsaw University of Technology, Ul. Wołoska 141, 02-507 Warsaw, Poland. [2]Department of Non-Food Products Quality and Packaging Development, Institute of Quality Science, Poznań University of Economics and Business, Al. Niepodległości 10, 61-875 Poznań, Poland. [3]Faculty of Chemistry, Adam Mickiewicz University in Poznań, Ul. Uniwersytetu Poznańskiego, 61-614 Poznań, Poland. [4]Centre for Advanced Technologies, Adam Mickiewicz University in Poznań, Ul. Uniwersytetu Poznańskiego 10, 61-614 Poznań, Poland. [5]Faculty of Mechanical Engineering, Białystok University of Technology, Ul. Wiejska 45C, 15-351 Białystok, Poland. ✉email: renata.dobrucka@pw.edu.pl; rprzekop@amu.edu.pl

agents, such as 3-glycidyl oxypropyltrimethoxysilane, epoxy-based styrene-acrylic oligomer, and industrial linseed oil were also used to improve the polymer-filler interaction.

Polylactide is a thermoplastic polymer of natural origin that is susceptible to hydrolytic degradation and industrial composting, making it more environmentally friendly than most petroleum-based polymers. Neat polylactide has quite good physical and chemical properties, but the constant need for product improvement has led to additives being used with this polymer to improve its parameters or to obtain other interesting properties; especially, PLA suffers from limited impact resistance and elongation at break. Therefore, improvement of its mechanical properties is constantly sought, which may be achieved through addition of fillers, plasticizers or other types of processing and functional additives. Liu added *N*-ethyl- and *N*-2-hydroxyethyl-substituted maleimide-styrene graft-block copolymer to the polylactide, while in our previous work, it was found that the addition of graphite to PLA is a step towards obtaining material that is cheap and suitable for 3D printing of sliding spare parts. In addition, a polylactide-based material with proper additives can help produce fibre-reinforced composite intended for use in agriculture or metal alginate grafted PLA aerogels (PLA-g-M alginate; M: Ca^{2+}, Co^{2+}, Ni^{2+}, Cu^{2+}). It was previously reported that diatomaceous earth may also be used to reinforce PLA, which is beneficial for both mechanical and thermal properties of such obtained composites. These findings were later confirmed in our studies concerning PLA-based composites.

Depending of the additive concentration, the polylactide filled with amorphous diatomaceous earth varies in the melt flow rate, which directly affects the production by injection moulding. To improve the processing properties, various synthetic/natural waxes are used at specified concentrations. The patent application WO2013100006A1 describes the production of a biolaminate made of PLA and natural soy wax. Righetti et al. described the biocomposite made from polylactide with the addition of plasticizer (tributyl O-acetylcitrate), $CaCO_3$, potato pulp and a non-ionic emulsion of beeswax, carnauba wax or modified polypropylene wax. In our previous work, we have determined the effect of the synthetic wax, as well as natural beeswax addition on the properties of PLA/DE composites. Studies have shown that both types of wax, particularly at high concentrations, improve the processing properties of composites (increase melt flow rate, reduce melt viscosity under shear conditions), and influence many other parameters, including mechanical ones. On top of that, the possible mechanisms of wax interaction with the filler and polymer were discussed, being found highly dependable on the surface treatment of the filler. The effects of wax additives on filler behaviour was studied by Gigante et al. for PLA composites with wheat and rice bran.

Beeswax consists of more than 300 chemical substances, including about 12–16% hydrocarbons with chain length C27–C33, 12–14% free fatty acids with chain length C24–C32, 35–45% fatty acid esters, and other substances. The content of each chemical compound may vary between the different wax producing bee species and the area in which they occur, due to differences in their diet and genetic predispositions. The structural formula of the polyamide wax WTH-R is presented in Fig. 1, and the composition of beeswax and the structural formulae of the individual components in Table 1 and in Fig. 2.

The PLA/DE composite, to which beeswax is added instead of synthetic wax, not only has better processing properties but also many other parameters. In this work, a number of composites were made with different concentrations of diatomite as a filler material (2.5, 5, 10 and 15%) and different wax content and type. Natural and synthetic waxes were used as modifiers in different concentrations to compare their effect on the properties of the composites produced. Mechanical testing was performed for tensile strength, flexural strength, impact strength and other parameters. In addition, the hydrophobic and hydrophilic character of the surface was examined, the

Figure 1. The structural formula of polyamide wax WTH-R.

Component designation	Name of components	Content (%)
A	Hydrocarbons (C_{21}–C_{33})	14
B	Monoesters (C_{40}–C_{48})	35
C	Diesters (C_{56}–C_{64})	14
D	Hydroxy monoesters (C_{40}–C_{50})	4
E	Hydroxy polyesters (no data)	8
F	Free fatty acids (C_{24}–C_{32})	12
G	Free fatty alcohols (no data)	1
H-I	Triesters (no data)	3
J	Acid monoesters (C_{40}–C_{48})	1
K	Acid polyesters (no data)	2
	Unidentified	6

Table 1. Composition of beeswax.

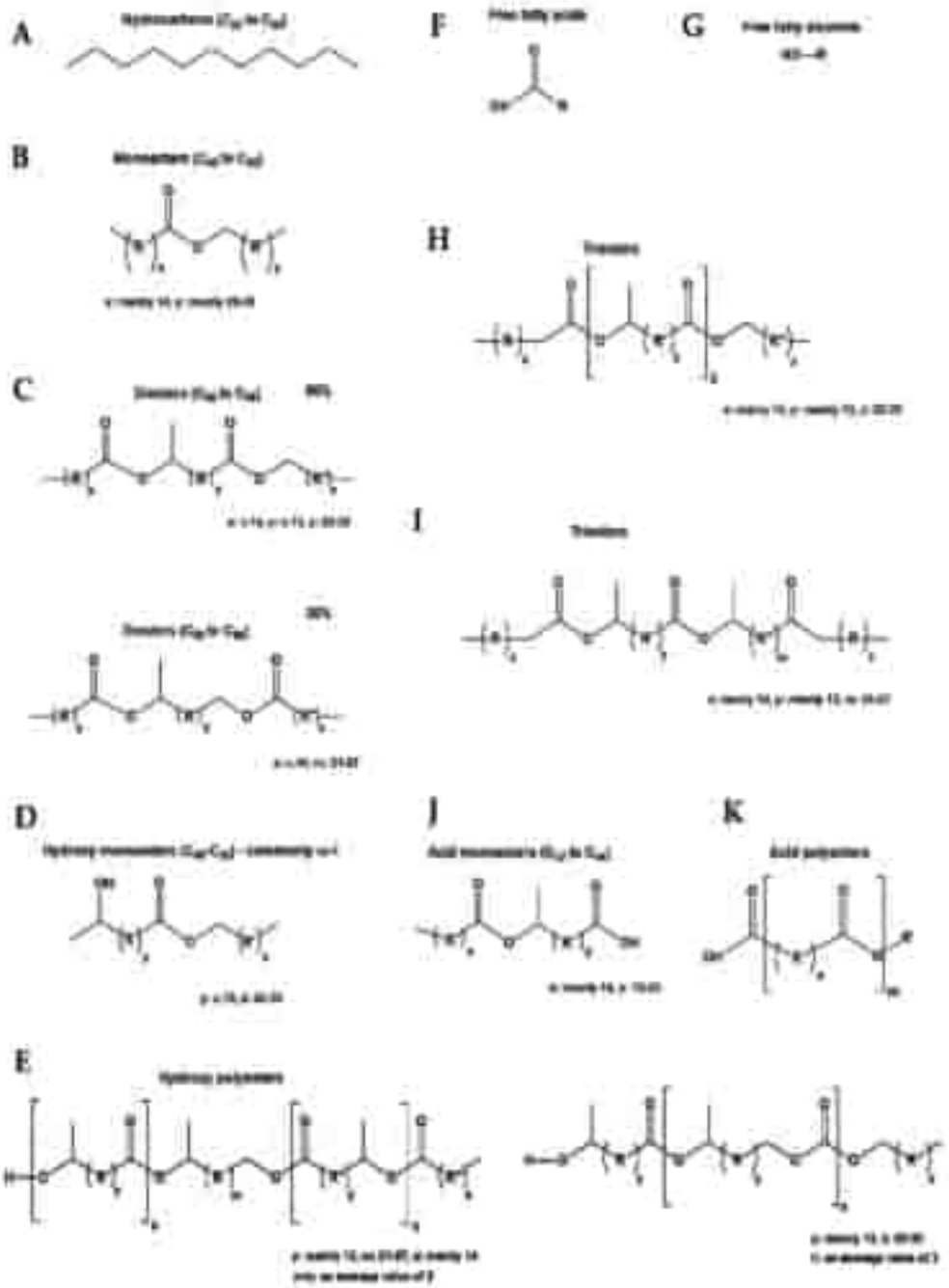

Figure 2. Structural formulae of individual components of beeswax.

filler material's dispersion in the polymer matrix was assessed and the waxes' effect on the diatomite agglomeration was assessed. Thermal stability tests were also performed on the samples obtained, including differential scanning calorimetry (DSC) and dynamic mechanical analysis (DMA). The resulting composites were conditioned at room temperature. The test composites were obtained by widely used injection moulding method.

Experimental section

Materials. Polylactide (PLA) of Ingeo 4043D type was purchased from NatureWorks (Minnetonka, MN, USA). Diatomaceous earth (Perma Guard, Bountiful, UT, USA) was derived from diatomite deposits. Synthetic wax WTH B Microbeads was sourced from WTH GmbH (Hamburg, Germany). Beeswax was purchased from Spółdzielnia Pszczelarska APIS (Lublin, Poland).

Preparation of samples. *Preparation of granulate.* The polymer and the filler were homogenized using a laboratory two-roll mill ZAMAK MERCATOR WG 150/280. A portion of 500 g PLA Ingeo™ 4043 D was mixed with diatomaceous earth and wax, until the final concentration of the diatomaceous earth was 5%, 10%, 20% and 30% w/w, 1% and 2% concentration of beeswax or 1% concentration of synthetic wax. The mixing was performed at the rolls temperature of 215 °C for 20 min., to achieve full homogeneity of the concentrates. The masterbatch was granulated with a grinding mill WANDER C17.26 sr and then dried for 24 h at 60 °C.

Injection moulding. The prepared masterbatches were diluted 1:1 with PLA directly in the Engel e-victory 170/80 injection moulding machine. Table 2 shows the injection moulding parameters. A holding pressure of linear increment over time was applied. The mould temperature was maintained at 80 °C. Standardized specimens for mechanical tests were obtained according to PN-EN ISO 20753:2019-01. Final system concentrations are shown in Table 3.

Characterization methods. For flexural and impact strength tests, the obtained materials were injection moulded into dumbbell specimens of type 1B in accordance with PN-EN ISO 527-1:2020-01[37] and PN-EN ISO 178:2019-06; for tensile tests, 1A specimens were injection moulded[38]. Tensile and flexural tests of the obtained specimens were performed on a universal testing machine DOETBDN 5969 with a maximum load force of 50 kN. The traverse speed for the tensile strength measurements was set at 2 mm/min, and for the flexural strength also at 2 mm/min. Charpy impact test (with no notch) was performed on an Instron Ceast 9050 impact-machine according to ISO 179-1[39]. The morphology and microstructure of the prepared composites were observed by scanning electron microscopy (SEM). The imaging was performed in three SE modes. The surface observations were analysed using a Hitachi SU70 scanning electron microscope equipped with an energy dispersive spectrometer (EDS) for chemical analysis. Prior to the observation, the surface samples were coated with electroconductive layer of Au–Pd with a thickness of 5 nm. Observations were conducted in SE mode with an acceleration voltage of 5 kV. Contact angle analysis was performed by the sessile drop technique (5 µL) at room temperature and atmospheric pressure, with a Krüss DSA100 goniometer. The melt flow rate (MFR) was measured using the Instron CEAST MF20 melt flow tester according to the standard EN ISO 1133 at 210 °C and for the load of 2.16 kg. Thermal properties of the materials were examined using a Q1000 Differential Scanning Calorimeter (TA Instruments, New Castle, DE, USA). Samples weighing 8.0 ± 0.2 mg were placed in an aluminium hermetic

Table 2. Injection parameters.

Table 3. Composition of the composites obtained.

pan. Firstly, the samples were equilibrated at −90 °C, then heated to 230 °C at a scan rate of 10 °C/min, and cooled to −90 °C with a scan rate of 10 °C/min. Finally, they were heated again to 230 °C at a scan rate of 10 °C/min. The process was conducted in a nitrogen atmosphere. Using the Universal V4.5A TA software, the glass transition temperature (T_g) was determined as the midpoint of the glass transition temperature range. The melting temperature (T_m) was determined as the peak temperatures of cold crystallization and melting, respectively. The rheological properties of the composites were examined using the capillary rheometer Instron CEAST SR10 Smart RHEO 1000. The measurement was carried out at 190 °C using a capillary tube with a diameter of 1 mm and a length of 20 mm. The force was measured using a force converter at specific piston speeds with the range corresponding to apparent shear rates ($\dot{\gamma}$) i.e. 10, 30, 100, 300, 500 and 1000 [1/s].

$$\dot{\gamma} = \frac{4v^2}{r^3} \cdot s$$

R bore radius (set in test parameters), r die radius (set in test parameters), v piston speed calculated from shear rate value. Apparent viscosity was calculated from the formula below:

$$\eta = \frac{\tau}{\dot{\gamma}},$$

where τ is the apparent shear stress expressed by the following formula:

$$\tau = \frac{Rr}{2\pi R^2 L},$$

L die length (set in test parameters), F force measured with load cells.

Light microscopy images of the surface and fractures of the composites were taken using KEYENCE VHX-7000 digital microscope (KEYENCE INTERNATIONAL, BELGIUM, MY/5A) with VH-Z100R wide angle zoom lens at × 100 magnification. Images were taken with depth composition and the aid of 3D imaging built-in software. Total coaxial illumination was used. Surface gloss measurements were recorded at 23 °C according to the ISO 2813 standard using a compact gloss meter (GM58, 3Color®, Poland) using 20°, 60° and 85° geometries. The device was calibrated between various specimens measurements using dedicated standard black glass. Three values for each specimen were recorded in gloss units (GU) and averaged. Before the measurement, the samples were stored under the same lighting conditions to prevent possible colour changes. Fourier Transform-Infrared (FT-IR) spectra were recorded on a Nicolet iS50 Fourier trans-form spectrophotometer (Thermo Fisher Scientific) equipped with a diamond ATR unit with a resolution of 0.09 cm^{-1}.

Mechanical properties, i.e. ultimate tensile strength, flexural strength, impact strength, and additionally water contact angle were tested for composites, which were previously conditioned at a room temperature (5 days, 23 °C, atmospheric pressure). Imaging of fractures (SEM, EDS, optical microscope) and thermal tests (DSC, DMTA) were performed on selected composites, i.e. containing different concentrations of the filler to compare the effect of different filling on mechanical and thermal properties.

Results and discussion

Analysis of the function groups of modifiers (waxes). An analysis of infrared spectroscopy has shown significant differences in structure between the beeswax (natural) and the polyamide wax (synthetic), where beeswax has a simpler structure (Fig. 3). The common bands characterizing both types of wax are those at 2915, 2850, 1470, 1432 and 720 cm^{-1}, which originate from asymmetric and symmetric stretching of aliphatic

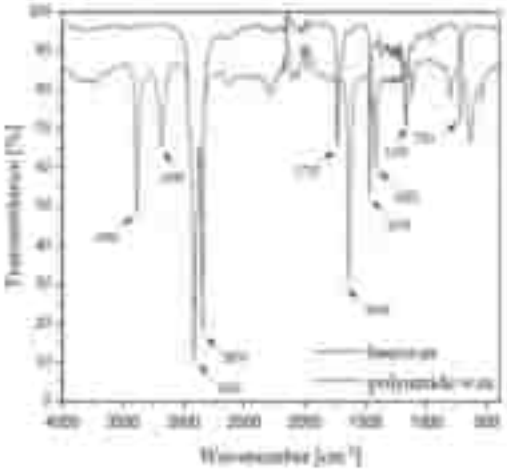

Figure 3. FT-IR spectra of beeswax and polyamide wax.

hydrocarbons (2919 and 2850 cm^{-1}), the in-plane vibrations of aliphatic hydrocarbons (1470, 1422 cm^{-1}) and peak due to the rocking of the same vibrational group (720 cm^{-1})[36]. In beeswax, there are also bands at 1735 cm^{-1} and 1165 cm^{-1} due to the presence of carbonyl groups of fatty acids and esters[37,38]. In addition to the common bands with beeswax, synthetic wax is characterised by additional bands at 1946 and 3186 cm^{-1} derived from the amide group CONH, and at 1640 cm^{-1} derived from the carbonyl group.

Rheology—melt flow rate (MFR) and capillary viscosity. The melt mass flow rate was measured for ground moulded pieces after the injection moulding. Neat polylactide, according to literature data[39], has an MFR value of 6 g/10 min at 210 °C. Modification with the original diatomite alone (Fig. 4) added in the range of 2.5–10%, results in a near-constant increase in melt flow rate to 15 g/10 min, which is equivalent to improved processing performance. Each of the compositions prepared was characterised by increased melt flow rate in comparison to the neat PLA (besides of 2.5DE/0.5BW), with the greatest increase recorded for systems modified with beeswax at a concentration of 0.5%. Such a concentration is optimal, because a further addition (1%) of natural wax results in the drop of MFR, which reaches the value similar to that of samples modified with synthetic wax.

The greatest difficulty in producing high-fill composites is due to high melt viscosity of the processed material. It is important to use additives to facilitate the processing of the material, especially at high concentrations. Beeswax at a concentration of 0.5% per composition has increased the melt flow rate compared to the system containing the same amount of pure diatomaceous earth.

Figure 5 shows the rheological properties (capillary viscosity) of the compositions with different filler and processing aids content. While the concentration of the filler added increases, the viscosity of the composite is reduced. Within the range of shear rates examined, the molten composite is a non-Newtonian fluid subjected to shear-thinning, which is common for thermoplastics. The viscosity curves of compositions containing 2.5% diatomaceous earth show similar behaviour at increasing shearing rates, i.e. above approximately 200 s^{-1}. In this case, the addition of beeswax or synthetic wax at any concentration is irrelevant. At low shearing rates, the viscosity of the samples with 2.5% filler varies considerably and decreases once waxes are added. As beeswax content, the viscosity is further reduced. Interestingly, for 10% filler loading, 0.5% of either wax content, viscosity of the composition is higher than with no wax, while the addition of beeswax at 1% content results in a significant decrease with increasing shear rate. The effect may be due to the particles deagglomeration, which increases filler matrix contact surface area and smaller particles cause higher viscosity rise in comparison to the agglomerated systems. Under higher shear rates, the matrix-filler interaction becomes less relevant, until viscosity of PLA/DE compositions reaches level almost identical to that of neat PLA.

Diatomaceous earth is a rheological agent for the molten polymer, which means that it increases the melt flow rate of the composite when compared to neat PLA. There is a very sharp decrease in viscosity over the full range of shear rates as the concentration of diatomaceous earth (10%) increases.

In direct injection moulding manufacturing which was used in this work to obtain PLA/DE composites, the process shear rates start at 100 [1/s] and often exceed the limit of 1000 [1/s] up to which the capillary rheometer tests were performed as shown in Fig. 6[40]. The difference in viscosity decreases as the shear rate changes. The graphs of all the tested composites flatten out at high shear rates and can be approximated to remain constant as the shear rate increases further during injection moulding. The neat polylactide had the highest viscosity among the analysed samples in the shear rate range tested, which means that by modifying the polymer with diatomaceous earth and waxes, composites with lower processing resistance or with less stringent processing parameters could be obtained. Figure 6 shows the shear rate ranges accompanying the most common processing, i.e. injection moulding, extrusion and 3D printing[40–42].

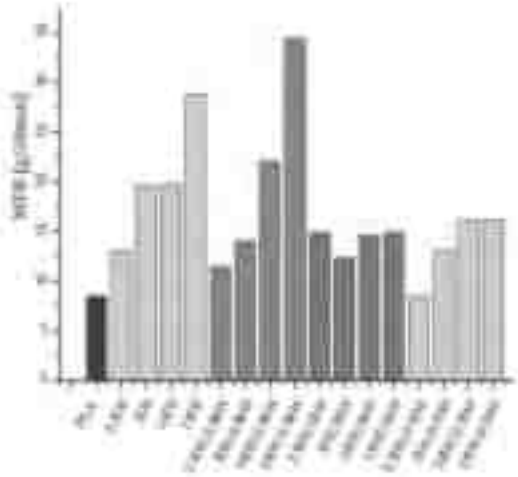

Figure 4. Melt flow rate (MFR) for granulates after injection moulding.

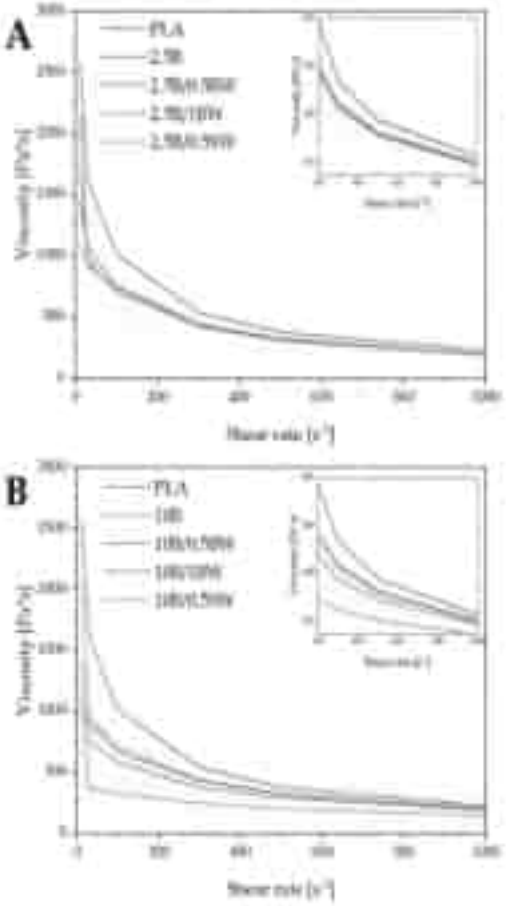

Figure 5. Viscosity of composites after injection moulding. (A) composites with 2.5% DE, (B) composites with 10% DE.

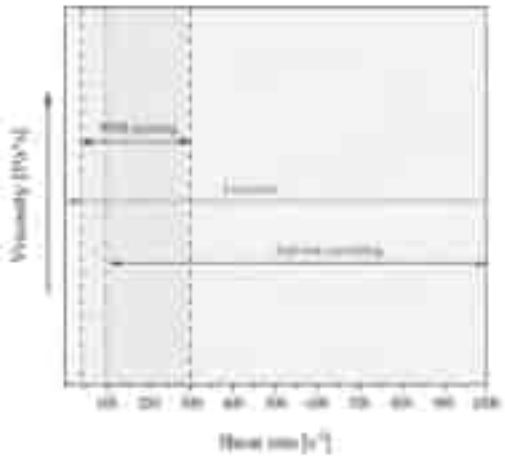

Figure 6. Areas of manufacturing technology: 3D processing area, extrusion technology area, injection moulding technology area.

Mechanical properties. The addition of diatomaceous earth to the polylactide results in a decrease in mechanical properties (tensile strength, elongation at break), which is expected due to the particulate filler nature of diatomite, with its relatively high average particle size and low aspect ratio, the filler particles causing discontinuity of the polymer phase and reducing the elasticity of the system. In addition, diatomaceous earth can agglomerate during the composite production, and the deposited particles can cause a concentration of local stresses and consequently a decrease in elongation at break[35]. In the case of modification with diatomaceous earth alone, as well as with addition of DE and 0.5% beeswax, a tendency to decrease the elasticity of the samples with increasing filler concentration is observed (Fig. 7). The situation is different for the other modifications. For the systems containing 1% beeswax, the highest values were recorded for the sample with 5% DE, while for the series without added wax, the values are constant up to a concentration of 10% DE. The decrease in tensile strength for 1% natural wax may be due to the concentration of too much wax at the filler/PLA interphase and a decrease in PLA adhesion to the filler (polymer-filler phase separation).

Tensile strength values for the systems modified with diatomite alone, diatomite and 0.5% beeswax, and diatomite and 0.5% synthetic wax, are at similar levels, both in modifications and in series (Fig. 7). No significant effect of filler concentration on the mechanical strength of the composites was observed, besides of LBW series, where together with the filler loading, tensile strength dropped due to non-reinforcing behaviour of the filler having no wetting action of the polymer phase, caused by wax overloading, as explained above.

The modification of the polylactide with diatomite has an effect on the flexural strength, which, as already mentioned, is due to the nature of the filler, i.e. the limited adhesion or filler wetting by PLA, lack of flexibility of the filler grains, the filler's particulate structure and the presence of agglomerates that are structural defects in the composite. Increasing the filler loading to 15% also increases the amount of air injected into the composite due to the porous structure of the diatomite frustules. Therefore, the greater the addition of diatomite to the composite, the lower the flexural stress it is able to carry. This relationship is shown in Fig. 8, where each time the filler loading increases, the maximum flexural stress decreases. A slight positive effect of adding 0.5% beeswax is observed for the sample containing 5% DE, since in this case the maximum flexural stress is the highest and the concentration diatomite in the system is the most favourable. The resulting composites are simultaneously characterized by lower tensile strength, but higher flexural strength. Similar effects have been observed for other PLA-based composite systems before and discussed[37]. This effect may be due to the mixed-mode mechanical stress during the flexural measurements, where both tensile and compressive forces are present, while for tensile strength measurements, the latter are not present. Composites and low compressibility materials, such as concretes, often show higher compressive strength than tensile strength[35,38].

Even for the lowest diatomite concentrations (2.5%), the flexural moduli are higher than those for the reference sample. With increasing filler concentration, these values increase as well. A similar linear upward trend is observed for systems without wax and with 0.5% beeswax addition. Slightly lower values, with a similar trend, were determined for the other systems. The effect of a decrease in flexural modulus for 1% natural wax compared to 0.5% may also be due to the concentration of compatibilizer at the polymer-filler boundary. While the particles' rigidity reduces the polymer matrix ability of deforming under load, thus increasing flexural modulus, the large particle size, together with limited matrix-filler wetting action (depending on the methodology of filler pretreatment and composite processing) result in limited capacity of the filler phase to effectively transfer the mechanical load from the matrix phase. Filler pull-out and filler-matrix debonding may occur, which results in mechanical failure of the composite. It can be seen that this effect is more pronounced for higher loadings, where the negative effects of filler agglomeration emerge, as it results in formation of additional mechanical defects in the composite, therefore reducing flexural strength.

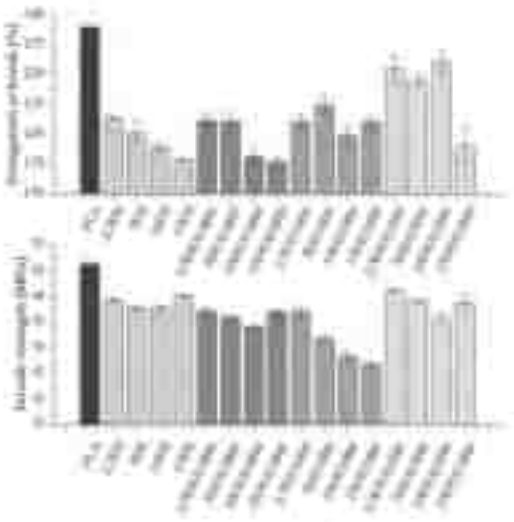

Figure 7. Tensile strength and elongation at break for samples conditioned at room temperature.

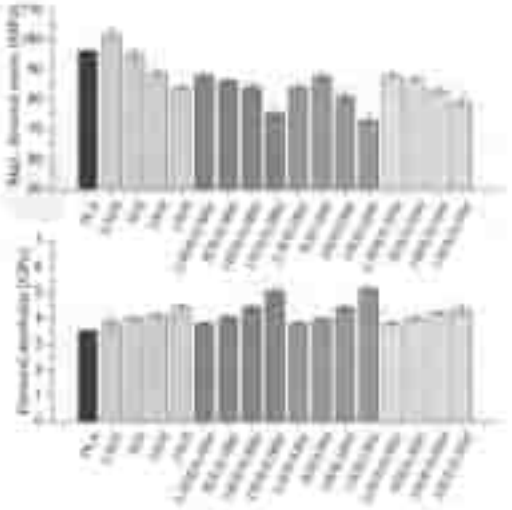

Figure 8. Maximum flexural stress and flexural modulus for samples conditioned at room temperature.

The impact strength of neat polylactide after injection moulding is around 19 kJ/m^2. The addition of as little as 2.5% diatomite results in a significant increase in impact strength, up to about 25 kJ/m^2, demonstrating the positive effect of diatomite alone on the impact strength of the composite. Increasing the diatomite concentration results in an increase in brittleness and hence a decrease in impact strength, which is expected due to the nature of the filler. The addition of 1% beeswax resulted in impact strengths above 25 kJ/m^2 for 5% DE, which is higher than for pure diatomite and samples with 0.5% beeswax (Fig. 9). The higher error bars obtained for composites containing diatomite, especially at high concentrations, are related to the dispersion of the filler in the polymer matrix and the above mentioned air introduction into the samples, which both are defects of the composite structure.

Thermal studies. DSC analysis was performed to investigate the thermal behaviour of PLA and PLA/diatomite composites. Figure 10 and 11 showed the DSC thermograms of PLA and PLA/diatomite composites during the second heating stage. As the temperature increases, each DSC curve exhibits three thermal characteristics: (a) a glass transition temperature (T_g), (b) a cold crystallization peak (T_{cc}), and (c) an endothermic melting peak (T_m). The values of the glass transition temperature, cold crystallization temperature, specific cold crystallization enthalpy, melting temperature, and specific melting enthalpy are listed in Table 4.

The neat PLA used in this study basically does not have a well-defined crystalline phase presence. No T_g or T_{cc} was observed, and only a small endothermic event at ~ 100 °C, suggesting either melting of a metastable phase (T_m) without further crystal perfection and resulting or relaxation of some polymer chains, but without subsequent cold crystallization, as the temperature of this transition is in the typical range of T_{cc}. It can be observed

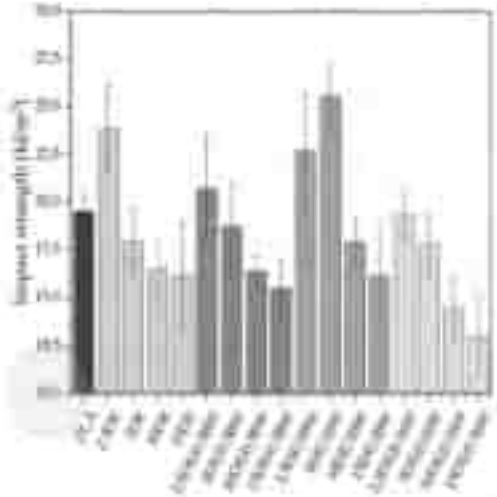

Figure 9. Impact strength for samples conditioned at room temperature.

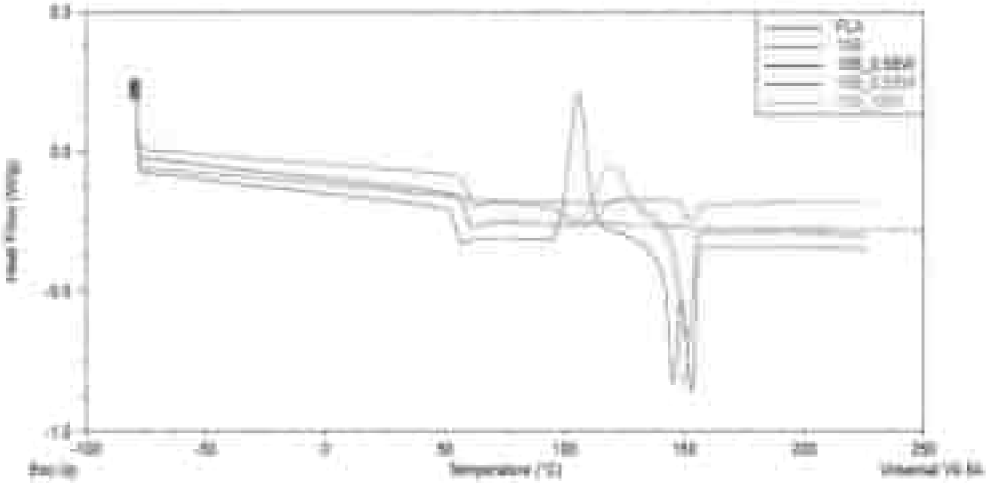

Figure 10. DSC curves of unmodified PLA and 10% DE composites with different type and loading of waxes obtained during second heating cycle.

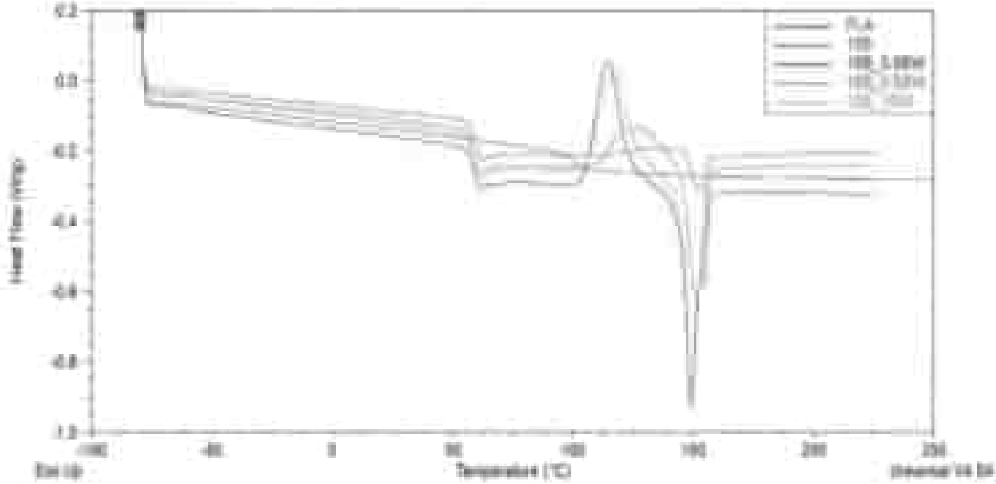

Figure 11. DSC curves of unmodified PLA and 15% DE composites with different type and loading of waxes obtained during second heating cycle.

Sample	2nd heating				
	T_g (°C)	T_c (°C)	ΔH_c (J/g)	T_m (°C)	ΔH_m (J/g)
PLA	52.6	–	–	–	–
10E	59.5	118.2	1.8	153.0	2.5
10E_0.5BW	53.0	103.9	31.4	143.5 and 153.0	35.2
10E_0.5TW	59.0	126.5	11.2	152.0	13.7
10E_1BW	59.6	126.6	20.6	150.1	21.0
15E	59.9	114.0	1.7	152.1	2.1
15E_0.5BW	59.6	114.7	25.1	149.1 and 154.6	25.5
15E_0.5TW	58.8	137.5	14.3	151.2	14.3
15E_1BW	59.5	124.6	21.6	149.6	22.6

Table 4. Thermal characteristics of PLA and composites based on PLA with different weight fraction of diatoms and different kind of waxes.

that the application of diatoms and waxes changed the character of the DSC curves. For neat PLA, no T_{c1} and T_{m1} events were observed. The glass transition temperature for the composites was determined about 60 °C. For the rest of the composites a glass transition temperature, a temperature and enthalpy of cold crystallization peak, and temperature and enthalpy of an endothermic melting peak were determined. It was also found that 10B_0.5BW and 15B_0.5BW composites had two distinct melting peaks (T_{m1} and T_{m2}), which can be attributed to the melting of metastable and perfect crystals, respectively[45]. The addition of 0.5% of beeswax reduces the melt viscosity and facilitates wetting action of PLA on the diatomite filler, which results in improved nucleation, which is visible by the occurrence of a well-defined cold crystallization (T_{c2}) event. At higher loading of BW or when SW was applied, the nucleation was obstructed and observed at higher temperatures, as most likely too much wax was aggregated on the matrix-filler interphase. Moreover, application of 15%BW or filler loading of 15% affected both the T_{c2} and T_{m2}, showing that when the cold crystallization occurs at the higher temperature, it prevents formation of the low melting point metastable crystals, and instead, a single melting event is observed, however of slightly lower temperature than that of the perfect crystals for double melting event observed earlier.

Surface properties. *Contact angle of the composites' surface.* The contact angle has been measured for systems conditioned at room temperature (Table 5). The reference polylactide is characterized by a hydrophilic surface. Samples containing neat diatomite are characterized by a contact angle in the range of approximately 86°–104° regardless of concentration and conditioning regime, making the surface hydrophobic in most cases. This is due to the additional micro-roughness created by the filler. Composites containing beeswax, have the highest values for systems containing 5 and 10% diatomite. Modification with synthetic wax did not result in significant differences between systems with beeswax and synthetic wax. As the filler concentration increases, the contact angle also increases, reaching more than 95° for the highest concentration of DE.

The hydrophobicity of the composites is mainly influenced by the diatomite itself and not by the addition of waxes. Even small addition (2.5%) of diatomite increases the contact angle from 83.2° for the reference polylactide to 102.2°. For such a DE concentration, the increase in hydrophobicity is related to the geometry of the composite surface, i.e. an effect of micro roughness on the hydrophobic–hydrophilic character of the surface is observed. At higher concentrations of diatomite, the decrease in hydrophobicity is related to the formation of hydrophilic centres at the composite/water interface. The hydrophilic centres are formed due to the large accumulation of diatomite, which tends to agglomerate. Diagrams of hydrophilic centres are presented in Fig. 12.

Gloss of composite surfaces. The gloss of composite surfaces was analysed for samples conditioned at room temperature. The test was performed at 23 °C in the geometry of 60° since the results were in the range 10–70 GU in accordance with ISO 2813. Systems with 2.5 and 10% filler were selected for comparative testing. All composites are characterized by medium gloss properties. Of all the samples analysed, the low-fill systems have the highest gloss (2.5B–57.9 GU, Table 6), while the addition of a larger amount of diatomite to the composites resulted in a reduction of gloss by more than 40% (10B–21.7 GU), with neat polylactide characterized by the gloss value of 32.1 ± 0.90 GU, which shows the strong influence of neat diatomite on the gloss of polylactide. Key factors affecting the optical properties of diatomite-filled composites are the structural features of the diatomite particles (surface roughness, number of porous silica layers, thickness, and pore diameter) and the refractive index of silica content. The periodic distribution of holes in the diatom forms a kind of mesh. The periodicity and porous structure allow interaction between light and frustules (photon–matter interaction), so the incident light waves can undergo diffraction, scattering and guiding, and other phenomena. Therefore, the size, number and distribution of the diatom particles in the polymer structure (PLA) influence the change in the gloss of the samples[46]. Referring to structural factors, it can be said that with increasing diatom concentration, the light waves are more scattered, are partially attenuated, so that the detector of the gloss measurement system receives a weaker signal compared to the reflection from the neat polymer, which is interpreted as a lower gloss of the test sample (lower GU value).

This effect is expected due to the nature of the filler and its ability to increase the brittleness and porosity of the composite surface. After the addition of 0.5% beeswax, composites with a much lower surface gloss than without the additive were obtained, i.e. for the 2.5% filler the gloss decreased to 23 GU, while for the 10% filler to 16.2 GU, which is the lowest result obtained. In contrast, a higher addition of the modifier (1%) in the form of natural wax did not result in a loss of surface gloss, as the results before and after modification are within the standard deviation. In the case of a 10% filling, it was even possible to achieve an improvement in gloss compared to the system without modification. Similar but slightly lower results were recorded for composites, to which synthetic wax was added. This leads to the conclusion that, in view of the abovementioned correlations, the addition of beeswax at a higher concentration is advantageous for the surface behaviour of PLA/DE composites.

Contact angle (RT) [°]							
PLA				BEE			
2.5DE	102.2	2.5DE/0.5BW	73.6	2.5DE/1BW	89.1	2.5DE/0.5SW	93.6
5DE	96.0	5DE/0.5BW	96.1	5DE/1BW	95.1	5DE/0.5SW	96.3
10DE	99.1	10DE/0.5BW	94.2	10DE/1BW	96.3	10DE/0.5SW	92.9
15DE	95.3	15DE/0.5BW	94.9	15DE/1BW	96.3	15DE/0.5SW	93.8

Table 5. Contact angle of the composites after conditioning at room temperature (RT).

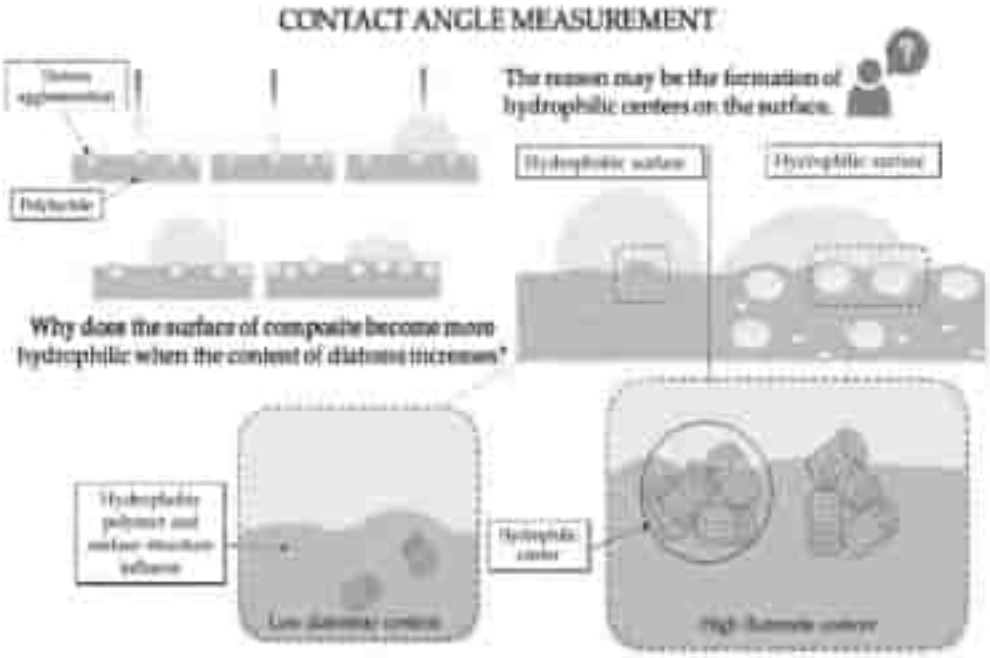

Figure 11. Loading-dependent hydrophilic-hydrophobic nature of PLA/diatomite composites' surface.

	1/10		10/0	
–	37.87	1.86	33.75	0.11
0.5WF	33.09	0.92	16.29	0.01
1WF	35.36	0.37	23.76	0.79
6.0WS	31.83	0.00	22.00	2.68

Table 6. The gloss of composites conditioned at room temperature.

Morphology of composite fractures. Images taken with a scanning electron microscope have revealed the effects of applied waxes at different concentrations on the filler dispersion in the polymer matrix. The 10% and 15% systems (high fill) were selected for tests, and the filler dispersion in their matrix was assessed as accurately as possible (Fig. 13). Neat diatomaceous earth embedded in polylactide is characterised by an even distribution of diatom particles for the 10/0 system. Higher concentration of the filler resulted in more non-uniform edges after the impact test, indicating increased brittleness of the composite. The addition of 0.5% beeswax caused an agglomeration of the diatomite particles, especially for its highest concentration, but this did not negatively affect the mechanical properties of the composite. In this system, the diatoms are present on the surface of the fracture, and not below the crack line as in a system without added wax. In addition, diatom frustules did not break, since whole diatoms can be observed with unchanged shape, which indicates that the addition of wax causes filler pull-out during fracture. The larger, i.e. 1% addition of beeswax had a different effect on the fracture structure of the composite. The agglomeration still occurs, even at lower concentrations, which shows that the higher the concentration of beeswax, the stronger the tendency towards agglomeration, which is not present only at the highest filling. The addition of synthetic wax had a negative effect on the dispersion of the filler in the matrix even at lower concentrations although 0.5% wax was added.

Using the SEM/EDS mapping (Figs. 14, 15), the presence of carbon, silicon and oxygen in composites was confirmed. The content of these elements is similar regardless of the modifier used, i.e. the type and concentration of wax. The most important element to observe is silicon, as it allowed to localize diatomite particles embedded in the PLA matrix. On the basis of area on the mapping image, it was possible to detect agglomerates discussed above.

Using an optical microscope we were able to observe the surface features and composite fractures on a microscale to determine the effects of varying diatomite concentration and the type and quantity of wax added on the microstructural properties of composites. Figure 16 shows the images taken from the surfaces of the samples. Systems with 2.5% and 10% diatomite were studied in detail. The surface of all the composites with the lowest filling is very similar. Numerous furrows are the result of wear on the injection mould. Furthermore, even at low concentrations of diatomite, its small agglomerations are visible, which become larger with increasing

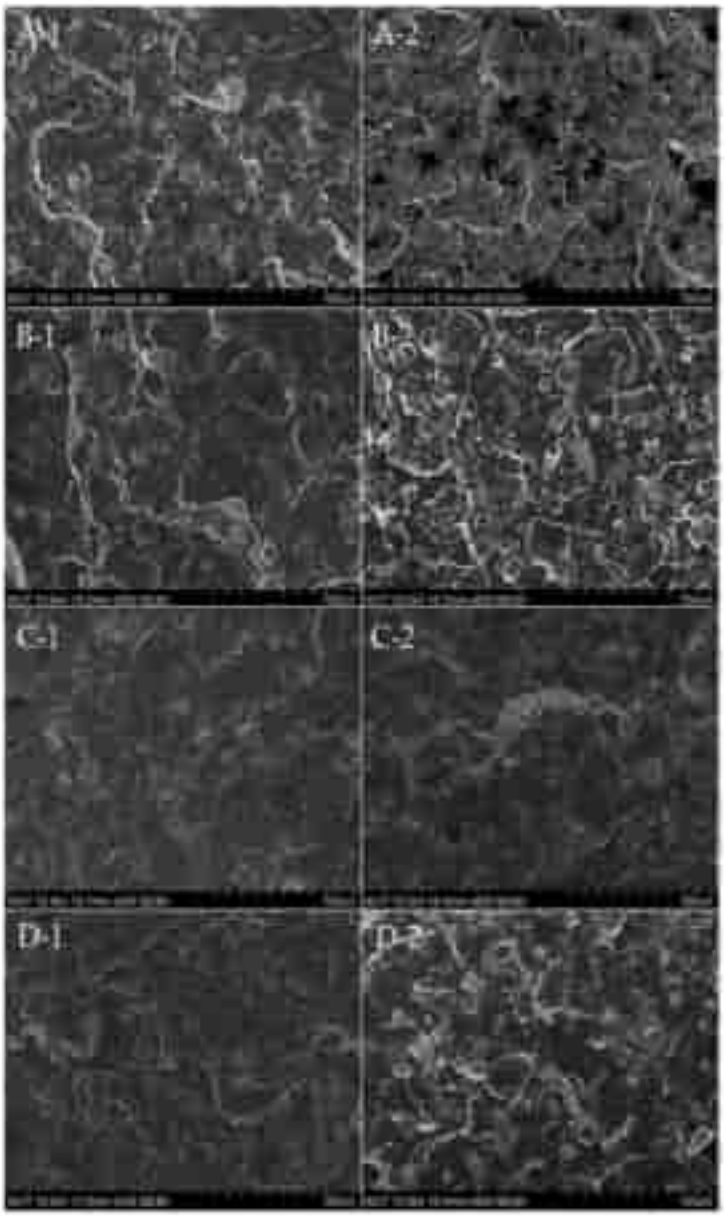

Figure 15. SEM images of composites: (**A-1**) 10B, (**A-2**) 15B, (**B-1**) 10B/0.5BW, (**B-2**) 15B/0.5BW, (**C-1**) 10B/1BW, (**C-2**) 15B/1BW, (**D-1**) 10B/0.55W, (**D-2**) 15B/0.55W.

concentration (Fig. 16). In systems filled with 10% of diatomaceous earth, numerous agglomerations of DE can be seen (Fig. 16A2), which were more dispersed in the polymer matrix after the addition of 0.5% beeswax (Fig. 16B2). The addition of 1% of beeswax and the addition of synthetic wax do not improve the performance of the surface structure of the composites. In the case of system 10B/1BW, there are also slight ripples on the surface, which may indicate that the excess wax has penetrated outside the composite.

Observation of the composite fractures also showed the effect of the modification on the behaviour of the composite surface during the impact strength testing (Fig. 17). In low-fill systems, especially in the system modified by adding 0.5% beeswax, numerous furrows and ripples are present on the material. However, no clear edges caused by the impact are visible. There are also numerous whitened areas, which probably origin from diatomaceous earth, and are due to insufficient dispersion of the filler in the polylactide matrix. This effect is more pronounced for systems containing 10% DE, where, as expected, the filler dispersion is even lower, due to the high addition of diatomite. In contrast, the addition of 1% beeswax seems to compensate for this effect and probably has a positive effect on the dispersion of the filler in the matrix, as shown in Fig. 17C2. The structure of this composite is significantly smoother than that of the others and no whitening or other defects are present.

The use of the light microscope for viewing composites containing the mineral filling is an excellent complement to the SEM, with which it is not possible to determine the colour of the individual components of the

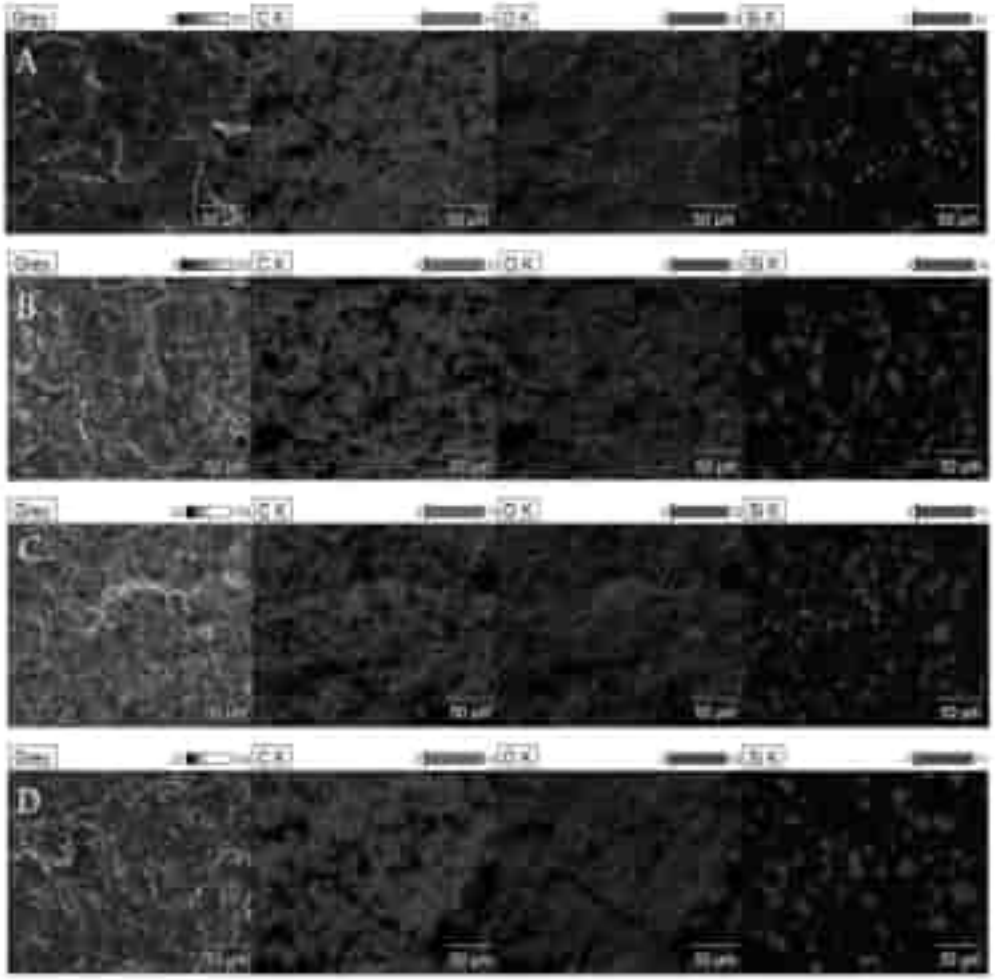

Figure 14. EDS; (A) 15B, (B) 15B/0.5BW, (C) 15B/1BW, (D) 15B/0.5SW.

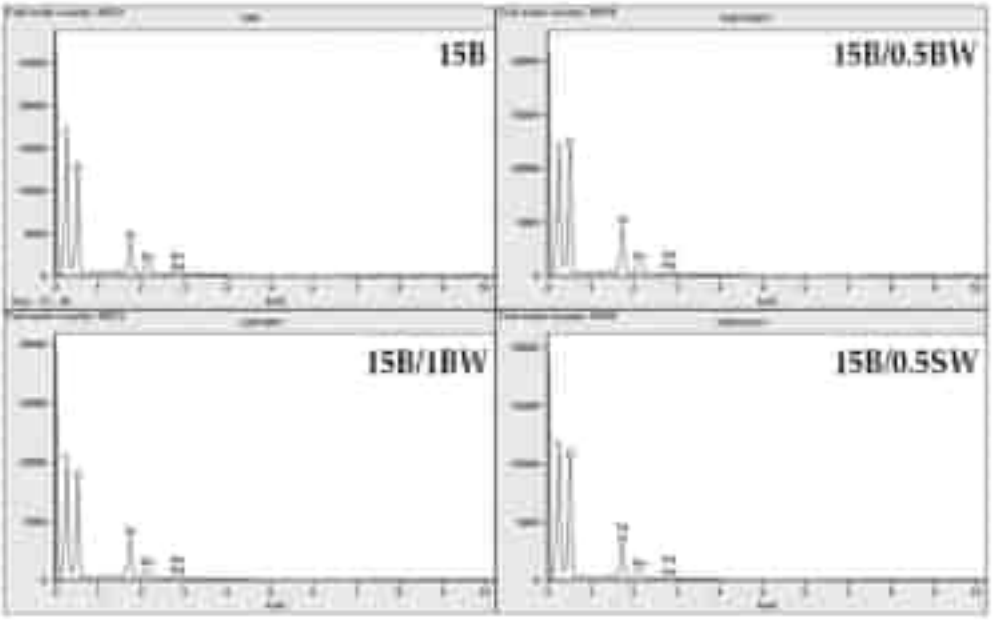

Figure 15. EDS mapping of composite fractures.

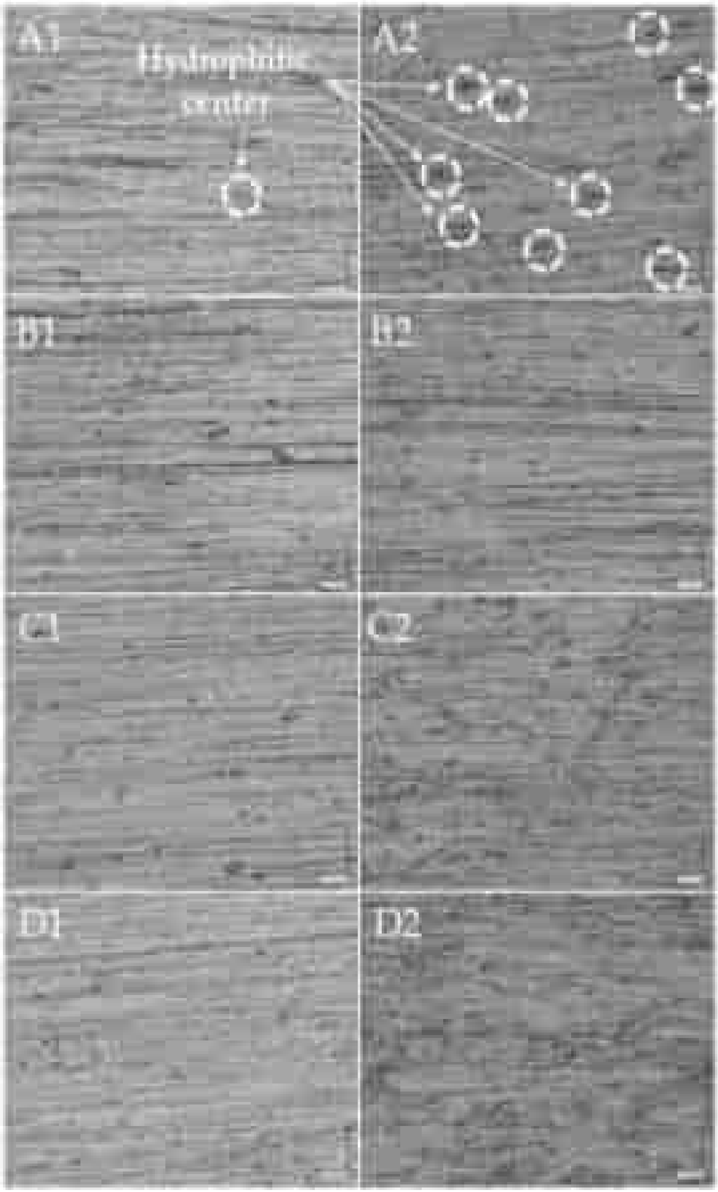

Figure 16. Composite surfaces: (**A1**) 2.5B, (**A2**) 10B, (**B1**) 2.5B/0.5BW, (**B2**) 10B/0.5BW, (**C1**) 2.5B/1BW, (**C2**) 10B/1BW, (**D1**) 2.5B/0.5CW, (**D2**) 10B/0.5CW.

composite, and therefore the individual phases of the composite cannot be easily identified. Using SEM, composite components can often be interpreted as a uniform structure, whereas a light microscope shows different phases. In contrast, it is not possible to distinguish small (crushed) particles of diatomite cannot be distinguished from large particles (not crushed) (Fig. 18). Only when all these techniques are combined, we can get a full picture of the diatomite-filled composites. Diatomite takes on different colours depending on the fragmentation (crushed frustules appear whiter). The fact that the diatomite colour changes according to particle size is due to differences in the refraction and the wavelength of the light that the diatomite absorbs. Under the light microscope, the diatomite takes on a white colour, while the polymer (polylactide) takes on a slightly yellowish colour, which is clearly visible in the photos of the composite fractures (Fig. 17), and on this basis it is easy to identify the dispersion of the filler in the polymer matrix.

Conclusions

The modification of polylactide with diatomaceous earth and the addition of waxes had a positive effect on the processing, microstructural, mechanical and surface properties of the composites. Already an addition of 0.5% beeswax resulted in a significant improvement of the processing properties not only compared to neat PLA, but also to PLA/DE with different filler concentrations. Moreover, the addition of natural wax also contributes

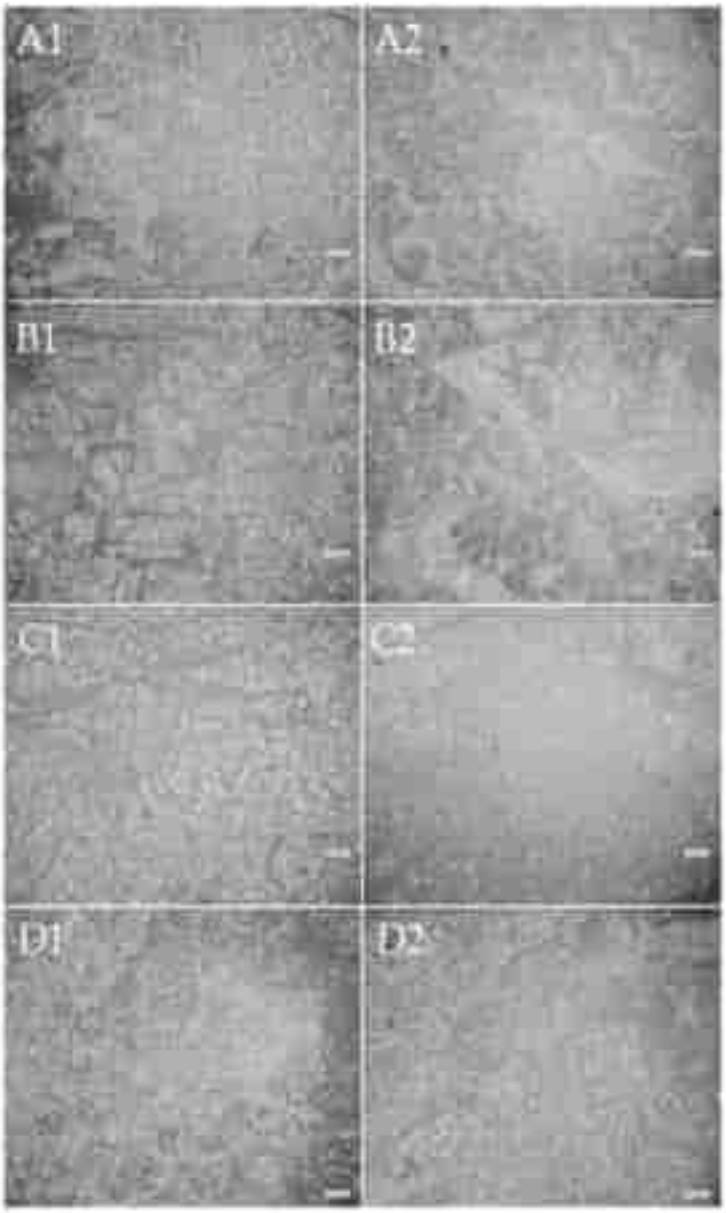

Figure 17. Composite fractures: (**A1**) 2.5B, (**A2**) 10B, (**B1**) 2.5B/0.5BW, (**B2**) 10B/0.5BW, (**C1**) 2.5B/1BW, (**C2**) 10B/1BW, (**D1**) 2.5B/0.5SW, (**D2**) 10B/0.5SW.

to the flexural strength and impact resistance of composite materials. These properties vary depending on the concentration of the additive used, so it is possible to adjust mechanical parameters according to given requirements. The use of the above additives has improved the hydrophilic and hydrophobic properties of the polylactide surface and enabled the production of hydrophobic composites. It was also found that diatomite used in low concentrations results in an increase in hydrophobic properties due to the geometry of the composite surface, while the higher loading of DE results in the formation of hydrophilic centres at the boundary of the composite surface and a decrease in the contact angle. The effects of the waxes on the dispersion of the fillers in the matrix and the changes in the thermal stability of the composites were also noted. The addition of synthetic wax used for comparative purposes also has advantages. Its content has a positive effect on the tensile strength of composites conditioned at room temperature, but natural waxes have an advantage over synthetic waxes as an addition to the composite due to their environmental friendliness. Both the filler and the wax additive have a significant influence on the crystallisation of PLA and the type of crystallites formed. Due to application of biopolymer PLA, biofiller diatomite and a fully natural beeswax as a processing aid and functional additive, a material meeting the today's definition of biocomposite was developed, thus offering a green, environment-friendly option of limited carbon footprint when compared to conventional composites based on petrochemical substrates.

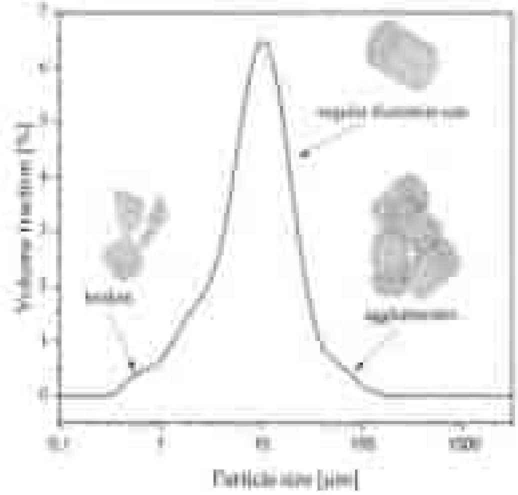

Figure 18. Particle size distribution of the original diatomite.

Data availability

The datasets used and/or analysed during the current study available from the corresponding author on reasonable request.

Received: 12 August 2022; Accepted: 18 January 2023
Published online: 20 January 2023

References

1. Dobrosielska, M. *et al.* Biogenic composite filaments based on polylactide and diatomaceous earth for 3D printing. *Materials* **13**, 4633 (2020).
2. Saidi, T. & Hasan, M. The effect of partial replacement of cement with diatomaceous earth (DE) on the compressive strength and absorption of mortar. *J. King Saud Univ. Eng. Sci.* **34**(4), 250–259 (2022).
3. Hasan, M., Saidi, T. & Afifuddin, M. Mechanical properties and absorption of lightweight concrete using lightweight aggregate from diatomaceous earth. *Constr. Build. Mater.* **277**, 122324 (2021).
4. Hasan, M., Saidi, T. & Husaini, H. Properties and microstructure of composite cement paste with diatomaceous earth powder (DEP) from Aceh Besar district—Indonesia. *Asia Pac. J. Sci. Technol.* **27**(1), 27. https://doi.org/10.14456/apst.2022.3 (2021).
5. Kim, K. *et al.* Structure-based optical filtering by the silica microshell of the centric marine diatom *Coscinodiscus wailesii*. *Opt. Express* **22**, 13992–13999 (2014).
6. Rakowska, B. Okrzemki—Organizmy, które zdumiały naukę. *Kosmos Problemy Nauk Biologicznych* **52**, 307–314 (2003).
7. Dobrosielska, M. *et al.* A new method of diatomaceous earth fractionation—A bio-raw material source for epoxy-based composites. *Materials* **14**, 1663 (2021).
8. Aw, M. S., Simovic, S., Yu, Y., Addai-Mensah, J. & Losic, D. Porous silica microshells from diatoms as biocarrier for drug delivery applications. *Powder Technol.* **223**, 52–58 (2012).
9. Cacciotti, I., Mori, S., Cherubini, V. & Nanni, F. Eco-sustainable systems based on poly(lactic acid), diatomite and coffee grounds extract for food packaging. *Int. J. Biol. Macromol.* **112**, 567–575 (2018).
10. Dermehzadeh, S., Ghasemi, M., Khezri, K. & Bahadorikhalili, S. Poly(styrene-co-butyl acrylate)/mesoporous diatomaceous earth mineral nanocomposites by in situ AGET ATRP. *J. Therm. Anal. Calorim.* **131**, 2513–2523 (2018).
11. Medarevic, D. P., Losic, D. & Ibric, S. R. Diatoms—Nature materials with great potential for bioapplications. *Hem. Ind.* **70**, 613–627 (2016).
12. Özen, I., Şimşek, S. & Okyay, G. Manipulating surface wettability and oil absorbency of diatomite depending on processing and ambient conditions. *Appl. Surf. Sci.* **332**, 22–31 (2015).
13. Gonzalez, L., Agüero, A., Quiles-Carrillo, L., Lascano, D. & Montanes, N. Optimization of the loading of an environmentally friendly compatibilizer derived from linseed oil in poly(lactic acid)/diatomaceous earth composites. *Materials* **12**, 1627 (2019).
14. Perera H. J. & Blain F. D. Superhydrophobic fluorosilane and alkylsilane diatomaceous earth particles treated polyurethane. In *Conference: 2022 Advances in Science and Engineering Technology International Conferences (ASET)* (2022).
15. Agüero, A., Quiles-Carrillo, L., Jorda-Vilaplana, A., Fenollar, O. & Montanes, N. Effect of different compatibilizers on environmentally friendly composites from poly(lactic acid) and diatomaceous earth. *Polymer Int.* **68**(5), 893–903 (2019).
16. Schneiderman, D. K. & Hillmyer, M. A. 50th anniversary perspective: There is a great future in sustainable polymers. *Macromolecules* **50**, 3733–3749 (2017).
17. Tokiwa, Y., Calabia, B. P., Ugwu, C. U. & Aiba, S. Biodegradability of plastics. *Int. J. Mol. Sci.* **10**, 3722–3742 (2009).
18. Södergård, A. & Stolt, M. Properties of lactic acid based polymers and their correlation with composition. *Prog. Polym. Sci.* **27**, 1123–1163 (2002).
19. Garlotta, D. A literature review of poly (lactic acid). *J. Polym. Environ.* **9**, 63–84 (2001).
20. Lee, R., Maher, M. J., Schiffer, H. J., Hillmyer, M. A. & Bates, F. S. Toughening polylactide with graft block polymers. *ACS Appl. Polym. Mater.* **4**(5), 3408–3416 (2022).
21. Prashop, R. E. *et al.* Graphite modified polylactide (PLA) for 3D printed (FDM/FFF) sliding elements. *Polymers* **12**, 1250 (2020).
22. Tertyshnaya, Y. V., Jeleshko, M., Olkhov, A., Shibryaeva, L. & Ivanitskikh, A. Polylactide fiber materials and their application in agriculture. *Key Eng. Mater.* **910**, 617–622 (2022).
23. Raptopoulos, G., Choinopoulos, I., Kontonasaki, E. & Paraskevopoulou, P. Polylactide-grafted metal-alginate aerogels. *Polymers* **14**, 1254 (2022).

24. Zhu, Z., Ye, C., Fu, W. & Wu, H. Improvement in mechanical and thermal properties of polylactic acid biocomposites due to the addition of hybrid sisal fibers and diatomite particles. *Int. J. Polym. Anal. Charact.* **21**(5), 365–377. https://doi.org/10.1080/1023666x.2016.1160529 (2016).
25. Biebel, M. J. & Biebel, M. *Biolaminate Composite Assembly Including Polylactic Acid and Natural Wax Laminate Layer, and Related Methods* WO2013/[illegible] (2013).
26. Righetti, M. C. *et al.* Thermal, mechanical, viscoelastic and morphological properties of poly(lactic acid) based biocomposites with potato pulp powder treated with waxes. *Materials* **12**(6), 990 (2019).
27. Dobrosielska, M. *et al.* Influence of diatomaceous earth particle size on mechanical properties of PLA/diatomaceous earth composites. *Materials* **15**, 3607 (2022).
28. Dobrosielska, M. *et al.* Effect of wax additives and silanization of diatom surfaces on thermomechanical properties of polylactide composites. *Polymers* **14**, 3511. https://doi.org/10.3390/polym14173511 (2022).
29. Gigante, V. *et al.* Improvement of interfacial adhesion and thermomechanical properties of PLA based composites with wheat/rice bran. *Polymers* **14**, 3389 (2022).
30. Fratini, F., Cilia, G., Turchi, B. & Felicioli, A. Beeswax: A mini review of its antimicrobial activity and its application in medicine. *Asian Pac. J. Trop. Med.* **9**(9), 839–843 (2016).
31. Tulloch, A. P. Beeswax—Composition and analysis. *Bee World* **61**, 47–62 (1980).
32. Tulloch, A. P. Beeswax: Structure of the esters and their component hydroxy acids and diols. *Chem. Phys. Lipids* **6**, 235–265 (1971).
33. *PN-EN ISO 527-1:2020-01—Tworzywa sztuczne—Oznaczanie właściwości mechanicznych przy statycznym rozciąganiu—Część 1: Zasady ogólne. PKN* (2020).
34. *PN-EN ISO 178:2019-06—Tworzywa sztuczne—Oznaczanie właściwości przy zginaniu* (2019).
35. *ISO 179-1:2010 Plastics—Determination of Charpy Impact Properties—Part 1: Non-instrumented Impact Test. PKN* (2010).
36. Baglioni, M. *et al.* A triton X-100-based microemulsion for the removal of hydrophobic materials from works of art: SAXS characterization and application. *Materials* **11**, 1144 (2018).
37. Missar, M. *et al.* Thermo-physical characterization of paraffin and beeswax on cotton fabric. *Int. J. Sci. Technol.* **19**, 69–77 (2013).
38. Svečnjak, L. *et al.* An approach for routine analytical detection of beeswax adulteration using FTIR-ATR spectroscopy. *J. Apic. Sci.* **59**, 37–49 (2015).
39. Oksuzh, D. & Maschi, A. Bio-based packaging materials containing substances derived from coffee and tea plants. *Materials* **13**, 5719 (2020).
40. Carneiro, V., Alonso, C., Otto, M. J., Sanchez, E. & Moreno, R. Microfluidic rheology: A new approach to measure viscosity of ceramic suspensions at extremely high shear rates. *Open Ceram.* **5**, 100053 (2021).
41. Chen, G., Chen, N. & Wang, Q. Preparation of poly(vinyl alcohol)/ionic liquid composites with improved processability and electrical conductivity for fused deposition modeling. *Mater. Des.* **157**, 273–283 (2018).
42. Gilmer, E. L. *et al.* Model analysis of feedstock behavior in fused filament fabrication: Enabling rapid materials screening. *Polymer* **152**, 51–61 (2018).
43. Akbari, A., Jawaid, M., Hassan, A. & Balakrishnan, H. Epoxidized natural rubber toughened polylactic acid/talc composites: Mechanical, thermal, and morphological properties. *J. Compos. Mater.* **48**, 1–13 (2013).
44. Kaszyńska, M. & Zieliński, A. Influence of mixture composition on shrinkage cracking of lightweight self-consolidating concrete. *Brittle Matrix Compos.* **10**, 265–327 (2012).
45. Mehdizadeg, J. F., Lurie, A. S., Tábi, T. & Kovács, J. Comparison of injection moldable natural fiber-reinforced composites with PP and PLA as matrices. *J. Thermoplast. Compos. Mater.* **25**(8), 937–948 (2011).
46. Nichols, A. *et al.* Optical properties of nanostructured silica structures from marine organisms. *Front. Mar. Sci.* **5**, 123 (2018).

Author contributions

Conceptualization, R.E.P.; methodology, R.E.P. and M.D.; formal analysis, R.E.P., M.D., R.D. and M.J.; investigation, R.E.P., M.D., P.K.; data curation, M.D., P.K., E.G., J.G.; writing—original draft preparation, M.D., R.E.P., R.D. and D.B.; writing—review and editing, M.D., R.E.P., R.D. and D.B.; visualization, M.D., P.K.; supervision, R.E.P., R.D., M.J. and K.J.K.; project administration, R.D. and K.J.K.; funding acquisition, R.D. and K.J.K. All authors have read and agreed to the published version of the manuscript.

Funding

This work was financially supported in the frame of the project "Advanced Biocomposites for Tomorrow's Economy BIOG-NET", FNP POIR.04.04.00-00-1792/18-00, project is carried out within the TEAM-NET programme of the Foundation for Polish Science co-financed by the European Union under the European Regional Development Fund.

Competing interests

The authors declare no competing interests.

Additional information

Correspondence and requests for materials should be addressed to R.D. or R.E.P.

Reprints and permissions information is available at www.nature.com/reprints.

Publisher's note Springer Nature remains neutral with regard to jurisdictional claims in published maps and institutional affiliations.

Open Access This article is licensed under a Creative Commons Attribution 4.0 International License, which permits use, sharing, adaptation, distribution and reproduction in any medium or format, as long as you give appropriate credit to the original author(s) and the source, provide a link to the Creative Commons licence, and indicate if changes were made. The images or other third party material in this article are included in the article's Creative Commons licence, unless indicated otherwise in a credit line to the material. If material is not included in the article's Creative Commons licence and your intended use is not permitted by statutory regulation or exceeds the permitted use, you will need to obtain permission directly from the copyright holder. To view a copy of this licence, visit http://creativecommons.org/licenses/by/4.0/.

© The Author(s) 2023

H8

Effect of Wax Additives and Silanization of Diatom Surfaces on Thermomechanical Properties of Polylactide Composites

Dobrosielska M., Dobrucka R., Pajewska-Szmyt M., Kozera P., Gabriel E., Głowacka J., Brząkalski D., Kurzydłowski K.J., Przekop R.E.; Polymers, 14, 5511, 2022

polymers

MDPI

Article

Effect of Wax Additives and Silanization of Diatom Surfaces on Thermomechanical Properties of Polylactide Composites

Marta Dobrosielska [1], Renata Dobrucka [2,3,*], Martyna Pajewska-Szmyt [2], Paulina Kozera [1], Ewa Gabriel [3,4], Julia Głowacka [3,4], Dariusz Brząkalski [5], Krzysztof J. Kurzydłowski [5] and Robert E. Przekop [3,*]

[1] Faculty of Materials Science and Engineering, Warsaw University of Technology, ul. Wołoska 141, 02-507 Warsaw, Poland
[2] Department of Non-Food Products Quality and Packaging Development, Institute of Quality Science, Poznań University of Economics and Business, al. Niepodległości 10, 61-875 Poznań, Poland
[3] Centre for Advanced Technologies, Adam Mickiewicz University in Poznań, ul. Uniwersytetu Poznańskiego 10, 61-614 Poznań, Poland
[4] Faculty of Chemistry, Adam Mickiewicz University in Poznań, ul. Uniwersytetu Poznańskiego 8, 61-614 Poznań, Poland
[5] Faculty of Mechanical Engineering, Bialystok University of Technology, ul. Wiejska 45c, 15-351 Białystok, Poland
* Correspondence: renata.dobrucka@ue.poznan.pl or renata.dobrucka@ue.poznan.pl (R.D.); r.przekop@interia.edu.pl or r.przekop@gmail.com (R.E.P.)

Abstract: In the present study, tests were conducted on high-filled composite samples on a polylactide matrix, modified with diatomaceous earth, three types of silanes, and natural and synthetic wax. The obtained samples were characterized in terms of the effect of modifications on mechanical properties (tensile strength, flexural strength, and impact resistance) or processing properties, e.g., melt flow rate (MFR). The study showed that the modification had a favorable effect on the processing properties of the composites, associated with up to an eight-fold increase in flow rate index compared with the reference sample, especially for samples treated with methyltrimethoxysilane (MTMOS), and up to a ten-fold increase under low shear rate flow conditions. The effect of the addition of waxes of different origins (synthetic and natural) was also determined, and it was shown that beeswax tended to reduce the flow rate of the composites regardless of the silane used. The addition of synthetic wax to composites increased the tendency to agglomerate diatomaceous earth, while natural wax had a positive effect on filler dispersion.

Keywords: polylactide; diatomaceous earth; beeswax; diatomite; silanes; chemical modification; mechanical properties; PLA

check for updates

Citation: Dobrosielska, M.; Dobrucka, R.; Pajewska-Szmyt, M.; Kozera, P.; Gabriel, E.; Głowacka, J.; Brząkalski, D.; Kurzydłowski, K.J.; Przekop, R.E. Effect of Wax Additives and Silanization of Diatom Surfaces on Thermomechanical Properties of Polylactide Composites. *Polymers* **2022**, *14*, 5111. https://doi.org/10.3390/polym14235111

Academic Editors: Rafaca Navarro Donn Nitti and Maria Rapa

Received: 24 October 2022
Accepted: 9 December 2022
Published: 1st December 2022

Publisher's Note: MDPI stays neutral with regard to jurisdictional claims in published maps and institutional affiliations.

Copyright: © 2022 by the authors. Licensee MDPI, Basel, Switzerland. This article is an open access article distributed under the terms and conditions of the Creative Commons Attribution (CC BY) license (https://creativecommons.org/licenses/by/4.0/).

1. Introduction

Today, due to ubiquitous environmental pollution, there is an increasing emphasis on producing more goods from renewable raw materials, decreasing carbon emissions, and increasing the biodegradability or recyclability of different types of products. We can also see a clear shift away from the production of materials that use petroleum-based compounds. Additionally, generating large amounts of waste is undesirable from an environmental point of view. Therefore, new environmentally friendly solutions are constantly being sought. Polylactide (PLA) has a number of advantages and in many cases can be used to replace petroleum-based polymers due to its good physicochemical and mechanical properties. Various types of fillers, including fillers of natural origin such as diatomaceous earth [1–3], cellulose fibers [4,5], and even wood flour/fibers [6,7], are used as modifiers of the physicochemical properties of PLA. They can also be used to modify the properties of a range of other polymers. Mineral fillers such as talc, kaolinite [8], montmorillonite [9,10], hydroxyapatite [11,12], fumed silica (aerosil), bentonite, and mica [13] are also used. This

makes it possible to obtain different composite properties depending on the desired purpose. Often, natural fillers tend to agglomerate in the polymer matrix, and therefore the use of dispersion-enhancing additives can favorably affect the mechanical properties of composites as the problems of early cracking or low-energy crack propagation are limited or eliminated. Positive effects of the silanization of fillers resulting in improved dispersion in the matrix are described in the literature. Silane coupling agents are used for the modification of inorganic compounds as they are capable of reacting with surface hydroxyl groups and contain various types of functional groups in their structure that determine the chemical compatibility of the modified surface with the polymer matrix, as well as the mechanism of its interaction with the matrix [14]. Surface silanization is a conventional and low-cost method of improving the interfacial interaction between the filler surface and the polymer matrix. Silane coupling agents act as adhesion promoters and reduce the tendency of fillers to form agglomerates in the polymer matrix. They have the ability to form covalent bonds between organic and inorganic materials in some cases. During the modification process, the hydrolysed silane modifier converts to silanol and reacts with hydroxyl groups on the material's surface to form strong hydrogen bonds [15]. Kucuk et al. described the effect of silane coupling agents with different functional groups on the properties of thermoplastic polyurethane/diatomaceous earth (TPU/DE) composites. The surface modification of diatomaceous earth, among other procedures applied, improved mechanical properties and reduced the formation of filler agglomerates. The authors schematically presented interfacial interactions via silane surface modifiers between the mineral filler and the TPU [16]. The addition of natural fillers, including diatomaceous earth or various types of sludge or fibers, especially in high concentrations, can adversely affect the processing and performance properties of composites, including processing rheology and mechanical properties. In order to eliminate these effects, it is advantageous to use processing additives, primarily, from the ecological point of view, agents of natural origin, which not only have a positive effect on the processing properties but can also help increase certain mechanical and physicochemical parameters. Typical processing additives of natural origin are waxes and oils of plant or animal origin and their semi-synthetic derivatives. Various types of waxes are used for this purpose, including jojoba oil-wax [17], mango seed wax [18], paraffin wax [19], epoxidized jatropha oil [20], epoxidized soybean oil methyl ester [21], and maleinized linseed oil [22]. In previous work [23], it was shown that the particle size of diatomaceous earth used as a filler for PLA matrix composites has a significant effect on the mechanical properties of the obtained materials. The smaller the particle size, the higher the impact resistance of the composite, while as the particle size increases, the mechanical properties deteriorate. In the present study, PLA-based composites with processing additives in the form of natural and synthetic waxes were also tested. However, the filler, i.e., base diatomaceous earth containing a full cross-section of diatoms of different sizes, was pre-silanized. The effect of the addition of waxes in varying amounts on the properties of the produced composites, especially their processing properties and degradation rates, was investigated. The dispersion of the filler in the polymer matrix was also determined in terms of the differences caused by the addition of waxes of different origins.

2. Materials and Methods

2.1. Materials

PLA, type Ingeo 4043D, was purchased from NatureWorks (Minnetonka, Minneapolis, MN, USA). Diatomaceous earth (Perma-Guard, Bountiful, UT, USA) was derived from diatomite deposits. Synthetic wax WTH-B microbeads (behenamide, $C_{22}H_{45}NO$) were purchased from WTH GmbH (Hamburg, Germany). Beeswax was received from APIS Apiculture Cooperative (Lublin, Poland). n-octyltriethoxysilane (OTES), 3-glycidoxypropyltrimethoxysilane (GPTMOS), and methyltrimethoxysilane (MTMOS) were purchased from Sigma-Aldrich (Saint Louis, MO, USA).

2.2. Preparation of Modified Diatomaceous Earth

1 kg of diatomaceous earth was placed in a 20 L glass reactor equipped with a mechanical stirrer. Then, 4 L of iPrOH, 10 mL of demineralized water, and 1% *w*/*w* of the appropriate silane (GPTMOS, OTES, or MTMOS) were added to the reactor and left for two hours with constant stirring (300 rpm). After 2 h, 10 mL of concentrated hydrochloric acid (HCl) was added in portions. After 24 h of continuous mixing, the mixture was transferred to a separate container and allowed to settle. After the liquid was decanted from the precipitate, the diatomaceous earth was washed with demineralized water and placed in an oven at 60 °C for 24 h. The silane formulas are shown in Figure 1a and a scheme of the silanization process is shown in Figure 1b.

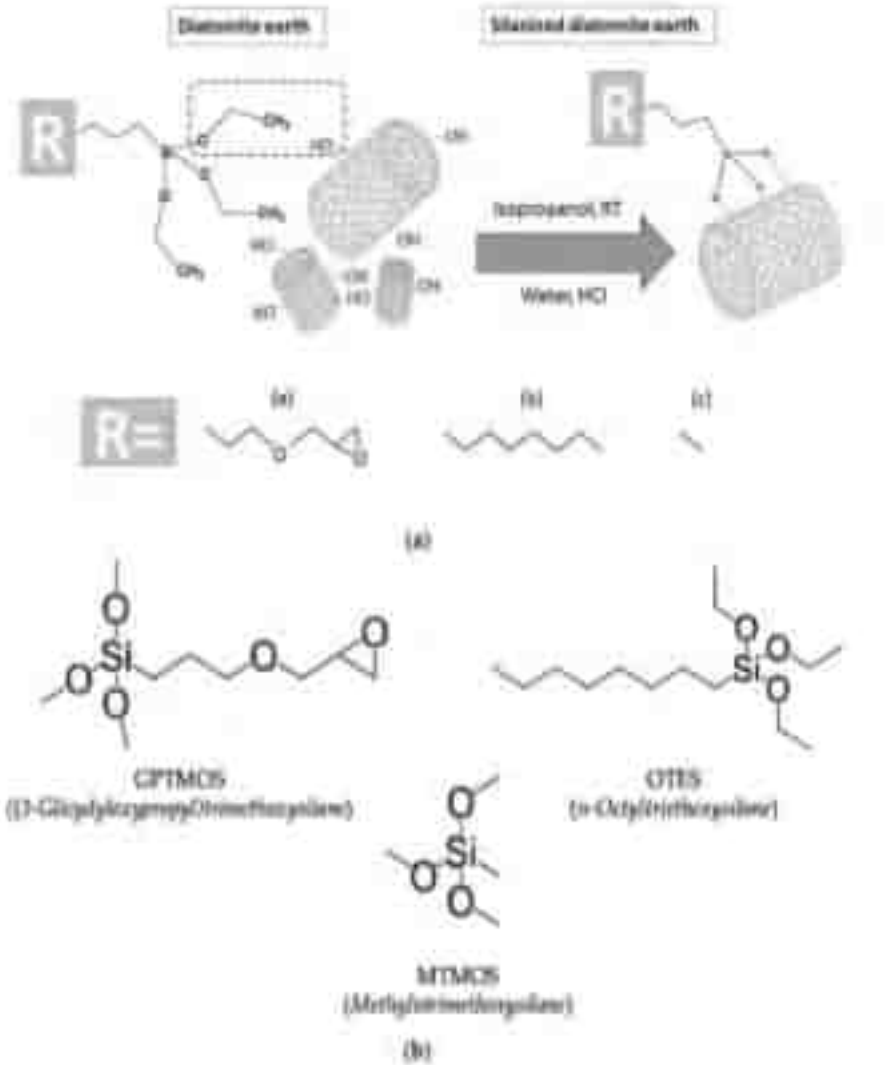

Figure 1. (a) Silanization process. (b) Structural formulas of organofunctional silanes used to modify diatomaceous earth.

2.3. Preparation of Granulates

PLA-based composites were prepared using a ZAMAK MERCATOR WG 150/280 (Zamak Mercator, Skawina, Poland) laboratory two-roll mill. For this purpose, 250 g of PLA 4043D was mixed at 210 °C together with 250 g of modified or base diatomaceous earth and 2% or 4% by weight of natural (beeswax) or synthetic (WIH-8) wax, respectively. The process was carried out until homogeneous mixtures were obtained. The resulting

systems were then ground using a WANNER C17.26 sr mill and dried for 24 h at 60 °C. Analogous systems containing unmodified diatomaceous earth were also prepared.

2.4. Preparation of Final Samples

The finished masterbatches were diluted 1:1 with PLA directly on an Engel e-victory 170/80 injection molding machine. Table 1 shows the injection molding parameters. A holding pressure with a linear increment over time was applied. The mold temperature was maintained at 80 °C. Standardized specimens for mechanical testing in accordance with PN-EN ISO 20753:2019-01 were fabricated. The final concentrations of the systems, together with sample symbols, are shown in Table 2.

Table 1. Injection molding parameters.

Temperature (°C)	Nozzle	Zone 3	Zone 2	Zone 1	Feed
	190.0	195.0	200.0	185.0	40.0
Holding pressure		I (s) P (bar)		8.0 500.0	9.0 1500.0
Clamping force (kN)		Holding pressure time (s)	Cooling time (s)		Screw diameter (mm)
600		9.0	50.0		25.0

Table 2. The resulting compositions.

Full Name	Short Name
PLA	PLA
PLA/DE	B
PLA/DE + 1% [w] SW	B/1S
PLA/DE + 2% SW	B/2S
PLA/DE + 1% NW	B/1N
PLA/DE + 2% NW	B/2N
PLA/DE + 1% GPTMOS + 1% SW	G/1S
PLA/DE + 1% GPTMOS + 2% SW	G/2S
PLA/DE + 1% GPTMOS + 1% NW	G/1N
PLA/DE + 1% GPTMOS + 2% NW	G/2N
PLA/DE + 1% OTES + 1% SW	O/1S
PLA/DE + 1% OTES + 2% SW	O/2S
PLA/DE + 1% OTES + 1% NW	O/1N
PLA/DE + 1% OTES + 2% NW	O/2N
PLA/DE + 1% MTMOS + 1% SW	M/1S
PLA/DE + 1% MTMOS + 2% SW	M/2S
PLA/DE + 1% MTMOS + 1% NW	M/1N
PLA/DE + 1% MTMOS + 2% NW	M/2N

DE: diatomaceous earth; PLA/DE: PLA + 25% by weight DE; SW: synthetic wax; NW: natural wax; GPTMOS: GPTMOS; OTES: OTES; MTMOS: MTMOS; [w]: in all cases, additive % is given in weight by weight (w/w) ratio.

2.5. Characterization Methods

For flexural and tensile strength tests, the materials obtained were cut down into type 1B bar specimens in accordance with EN ISO 527:2012 and EN ISO 178:2006. Tests of the obtained specimens were performed on an INSTRON 5969 universal testing machine with a maximum load force of 50 kN. The traverse speed for tensile strength measurements was set at 2 mm/min, and for flexural strength it was also set at 2 mm/min. A Charpy impact test (with no notch) was performed on an Instron Ceast 9050 impact machine (Instron, Norwood, MA, USA) according to ISO 179-1: 2010 Plastics—Determination of Charpy impact properties—Part 1: Non-instrumented impact test, PKN, 2010. The melt flow rate (MFR) was measured using the Instron CEAST MF20 melt flow indexer (Instron, Norwood,

MA, USA), which accords with EN ISO 1133, at 210 °C for a load of 2.16 kg. The thermal properties of the materials (T_g, T_{cc}, T_m) were studied using a Q1000 differential scanning calorimeter (TA Instruments, New Castle, DE, USA). Samples with a weight of 8.0 ± 0.2 mg were placed into an aluminum hermetic pan. First, the samples were equilibrated at −90 °C, heated to 230 °C with a scan rate of 10 °C/min, and cooled to −90 °C with a scan rate of 10 °C/min. Finally, they were again heated to 270 °C with a scan rate of 10 °C/min. The process was conducted in a nitrogen atmosphere. Using Universal V4.5A TA software, the glass transition temperature (T_g) was determined as the midpoint of the glass transition temperature range. The cold crystallization temperature (T_{cc}) and melting temperature (T_m) were taken as the peak temperatures of the cold crystallization and melting, respectively. Dynamic mechanical analysis (DMA) was performed using a Q800 DMA (TA Instruments, New Castle, DE, USA) in a dual cantilever mode that accords with ASTM D4065-01. From each composite, three rectangular specimens 60 mm long and 10 mm wide were cut and used in the testing. The analysis was conducted from 0 °C to 130 °C, with a heating rate of 3 °C/min at a frequency of 1 Hz and amplitude of 30 µm. The glass transition temperature (T_g) was determined from the storage modulus curve. The size of the diatoms used to prepare the composites was measured with a Mastersizer 3000 (Malvern Instruments Ltd., Malvern, UK). The measurements were made for the samples in water suspension (Hydro EV attachment). For the wet samples, the stirrer revolution speed was 2330 RPM and the ultrasound power was 70%. The FT-IR measurements were carried out using a Thermo Scientific Nicolet iS50FT-IR spectrometer in transmission mode. Samples weighing 4 mg were mixed with 200 mg KBr and pressed at 10 tons into the form of discs. The spectra were recorded using eight scans of background measurements and sixteen scans of sample measurements in the 400–4000 cm^{-1} range using a DTGS detector and a KBr beam splitter at 0.5 nm resolution.

3. Results and Discussion

3.1. Characterization of Silane-Modified Diatomaceous Earth

FT-IR analysis of the neat diatomaceous earth (DE) and silane-modified diatomaceous earth (DE/OTES, DE/GPTMOS, and DE/MTMOS) was carried out (Figure 2). The analysis showed differences in band intensities after the silanization process. A reduction in the -OH stretching band surface area in the 3000–3700 cm^{-1} range and the appearance of a -CH stretching band in the 2800–3000 cm^{-1} range after the silanization process were observed, with the strongest effect seen for the GPTMOS and similar observations recorded for the other two silanes (OTES and MTMOS). These features confirm the successful silanization reaction of the diatomite surface.

3.2. Rheology—Melt Flow Rate (MFR) and Capillary Viscosity

Neat, unmodified PLA has a melt flow rate (MFR) of 7.6 g/10 min, which is consistent with reports in the literature [24]. Modification of the PLA with diatomaceous earth in each case resulted in a significant improvement in the processing parameters, which was also observed in our previous work [23] (Figure 3). The positive effect of the addition of waxes on the magnitude of the MFR parameter is clearly visible—as little as a 1% addition of synthetic wax resulted in a two-fold increase in MFR (B/1S). The highest result for the composite containing unmodified diatomaceous earth was achieved for a 1% concentration of beeswax (B/1S, MFR = 34.5 g/10 min). Further increases in the concentration of wax in the system resulted in a slight, in most cases further, increase in MFR values. Preparation of samples of composites containing silane-modified diatomaceous earth (GPTMOS, MTMOS, and OTES) produced a positive effect on the melt flow rate, i.e., MFRs in the range of 29.5–62.7 g/10 min. Modification of the systems with MTMOS resulted in the greatest changes in melt flow rate, reaching values of up to 62.7 g/10 min, which caused minor difficulties in obtaining composites by injection molding. The difference between the MFRs of the O/xS and O/xN systems were due to the effect of the nonpolar octyl-substituted silane displacing the more polar, synthetic wax from the filler to the polymer phase, while

the highly apolar synthetic wax (being composed mostly of fatty acid esters of long-chain alcohols [75]) was likely in higher concentration at the filler surface or filler-matrix interphase. On the other hand, more polar methyl-substituted silane in the M/xS and M/xN systems did not result in such behavior to a meaningful extent.

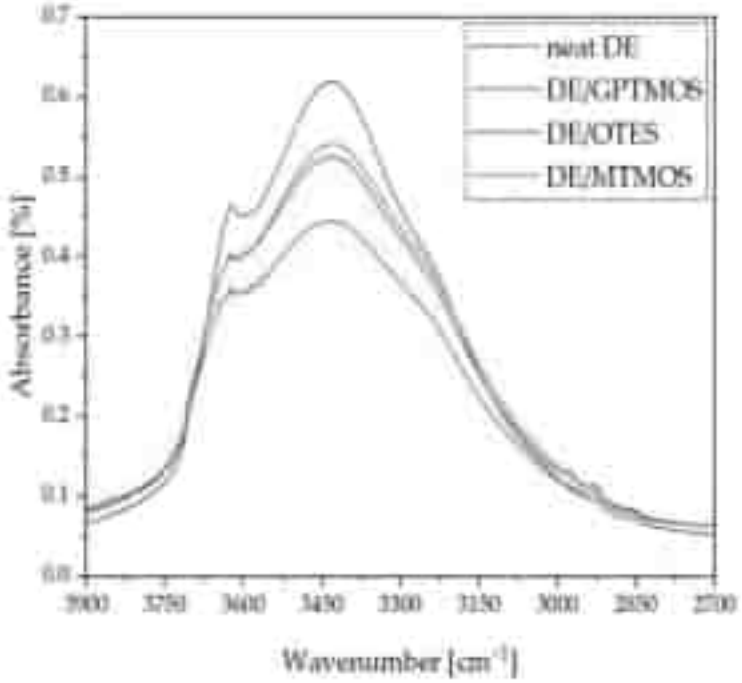

Figure 2. FT-IR spectra of neat diatomaceous earth and silane-modified diatomaceous earth.

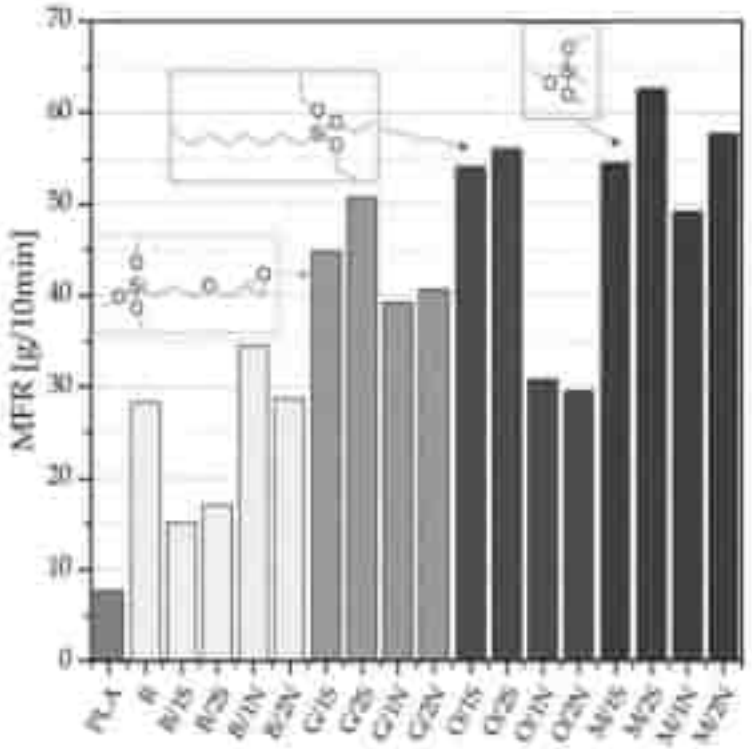

Figure 3. Melt flow rate of granules after the injection process.

Capillary viscosity tests were conducted for selected composites. The viscosity of the PLA/DE composites modified with silanes was significantly lower than that of the pure PLA (Figure 6) and did not exceed 450 Pa*s independently of the shear rate, with the viscosity decreasing sharply with the increasing shear rate. Once the shear rate reached 100 1/s, viscosity reached a plateau and remained relatively constant for all composites, which was due to the shear thinning effect typical of polymer thermoplastics. The highest viscosity among the composites was recorded for the O/2S system, while the lowest was observed for the O/2N system. It is not clear from the above study which silane additive has the greatest effect on the viscosity of the composites, since the viscosity curves of the produced composites are too similar, but based on this observation it can be stated that the viscosity is both related to the choice of silane and the wax, meaning that there is an interaction between the wax additive and the surface of the silanized filler.

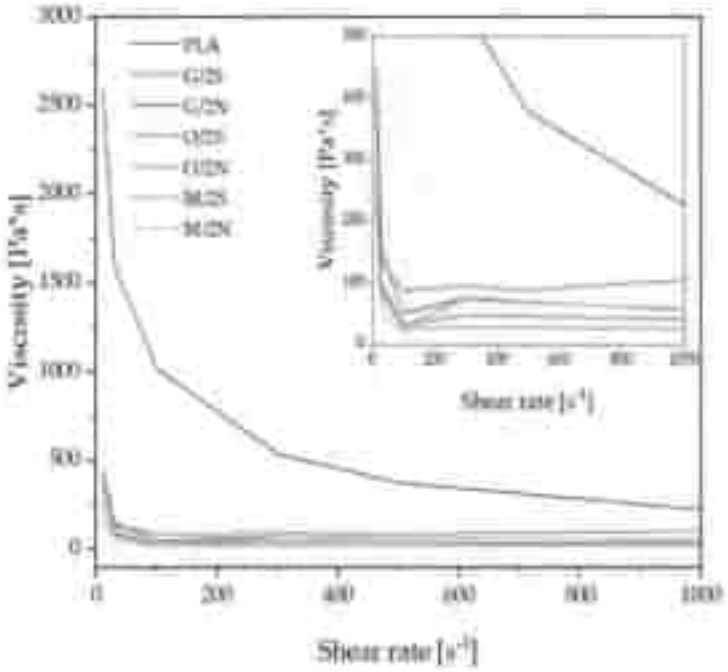

Figure 6. Capillary viscosity of selected composites.

3.3. Mechanical Tests

Tensile tests carried out on the composites containing diatomaceous earth and silanes showed that the addition of 25% filler resulted in a decrease in both the tensile strength and elongation at break, which was expected due to the properties of diatomaceous earth, the geometry of the filler grains classifying it as a particulate microfiller (Figure 7). Despite this, the decrease in tensile strength was not so drastic (even >80% of the strength of the base PLA is retained), especially for the composites containing natural beeswax. The addition of the wax, especially the natural wax, regardless of concentration, resulted in improved dispersion (lower error bars) of the diatomaceous earth in the PLA. The modification of the diatomaceous earth with the silanes and the simultaneous addition of the synthetic wax, especially at a concentration of 2% by weight, resulted in a definite reduction in tensile strength values below 40 MPa, depending on the modifier. On the other hand, regardless of the type of silane used, its combination with natural wax resulted in the composites being almost as resistant to tensile stress as neat PLA, while improving other parameters, including processing (the aforementioned improvement in melt flow rate and capillary viscosity). The elongation at break was highest for neat PLA due to the continuity of the polymer phase, and its decrease was caused by its discontinuity introduced by the rigid, non-deformable filler grains. In addition, the introduction of diatomite also caused

the introduction of air into the plastic, which can further affect crack propagation. The composites modified with the addition of beeswax again showed higher values than those modified with synthetic wax, while the highest elongation at break was recorded for the composite modified with GPTMOS silane and 2% beeswax.

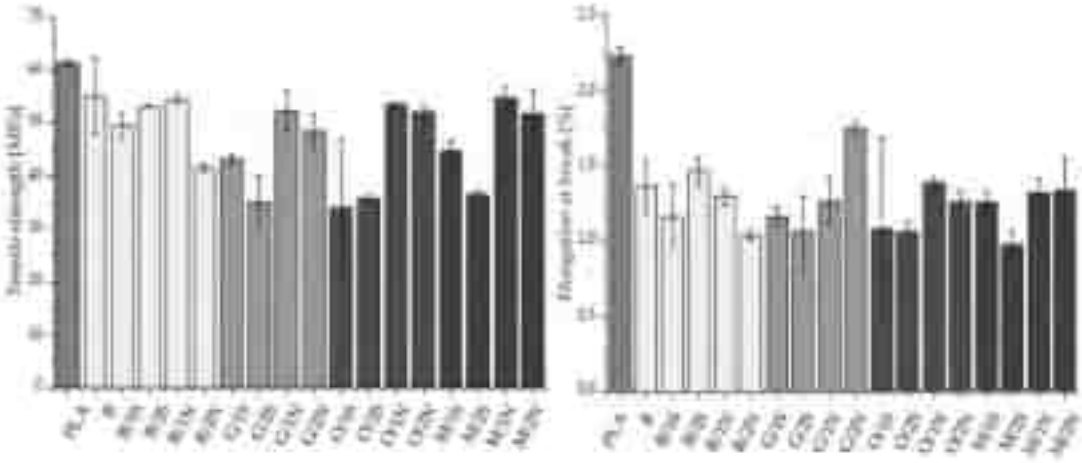

Figure 5. Tensile strength and elongation at break of PLA matrix composites.

The flexural modulus for the diatomaceous earth-modified composites increased compared with the reference sample, a phenomenon typical of polymer composites (Figure 6). The maximum flexural stress determined for the composites was in almost all cases noticeably lower than that of neat PLA, for similar reasons as those relating to the static tensile tests. For the silane-modified systems, the highest values were recorded for samples with added synthetic wax, especially at higher concentrations, while the addition of natural wax in combination with silanes adversely affected the strength of the composites. This was different for the samples modified with diatomaceous earth alone, without silanes. In this case, the highest values were recorded for the systems containing beeswax.

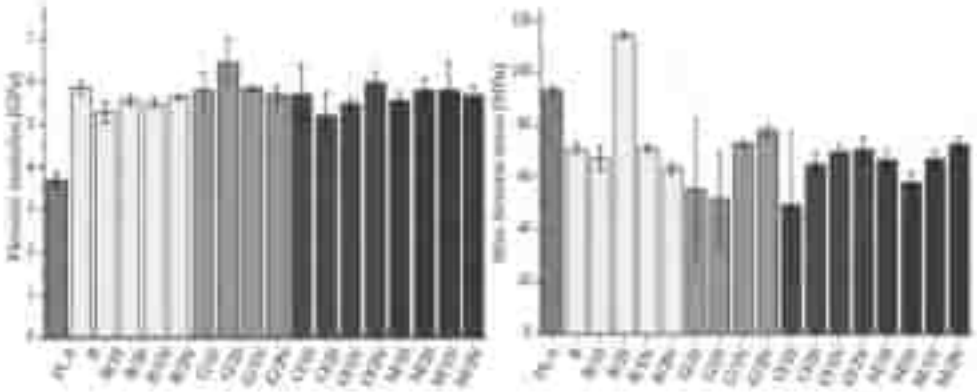

Figure 6. Flexural modulus and maximum flexural stress of PLA matrix composites.

Neat PLA showed moderate impact resistance, while the standard deviation of the measurement series measurements was as high as about 5 kJ/m^2, which may have been due to the low repeatability of the polymer crystallization (PLA is known for its low crystallization ability) during the process of obtaining the injection-molded specimens. The composites modified with diatomite earth showed slightly lower impact resistance values, but their standard deviations were significantly lower than that of the PLA, which may indicate the positive effect of diatomite on the processing of the PLA itself. The decrease in impact resistance when diatomaceous earth was introduced into the system was due,

as previously mentioned, to the powder nature of the filler and its effect on the brittleness of the composite, especially at the relatively high fill tested for this paper (Figure 7). The addition of beeswax, depending on the silane used, resulted in an increase in impact resistance compared with analogous samples modified with synthetic wax. This effect was particularly evident for GPTMOS, and to a lesser extent for MTMOS. The opposite trend was observed for systems with OTES. In this case, the modification with synthetic wax caused a slight increase in this parameter, which indicated the incompatibility of the natural wax and the silane with a relatively long alkyl group, which was responsible for the formation of an interphase on the surface of the filler with a significantly increased hydrophobic character. This was evident in the MFR analysis as a large difference in the viscosity coefficient values for the O/xN and O/xS samples suggested that for these systems, the synthetic wax showed a higher wetting action on the filler action, creating a polymer/wax/filler interface, while the natural wax accumulated in a different phase and a polymer/filler interphase with a small proportion of wax was formed. This was also confirmed by static stretching, where the O/xS samples had a lower tensile strength than the O/xN samples due to the additional interphase reducing the polymer/filler interaction effect.

3.4. Thermal Tests

3.4.1. DMTA

Table 3 and Figure 8 show how both the modification of diatomaceous earth with silanes and the addition of waxes influenced the storage modulus (G') of the composites based on PLA and diatoms. For comparison, the results were collated with the glass transition temperature (T_g) of the neat PLA. It can be observed that the modification led to the emergence of a T_g signal due to the nucleation effect, whereas for the neat PLA, no apparent relaxation was observed during heating, and only cold crystallization (T_{cc}) onset at ~80 °C was visible as a small rise in E'.

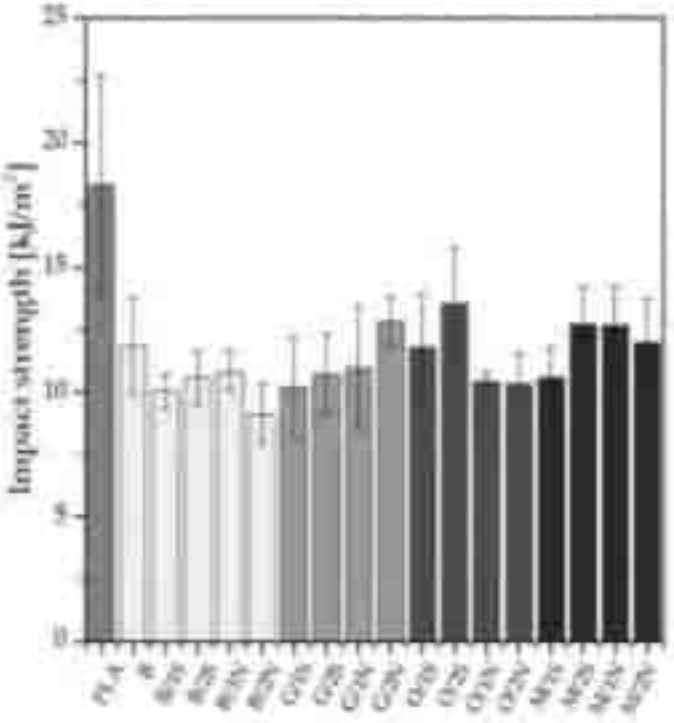

Figure 7. Impact strength of PLA matrix composites.

Table 3. Summary of the determined values of the glass transition temperature from storage modulus G' curves.

Sample	T_g (°C)	Sample	T_g (°C)	Sample	T_g (°C)	Sample	T_g (°C)
PLA	N/A [a]	–	–	–	–	–	–
B	61.6	–	–	–	–	–	–
B/2S	59.9	G/2S	58.5	O/2S	59.9	M/2S	59.5
B/5S	61.1	G/5S	57.7	O/5S	58.6	M/5S	60.0

[a] T_g event not visible.

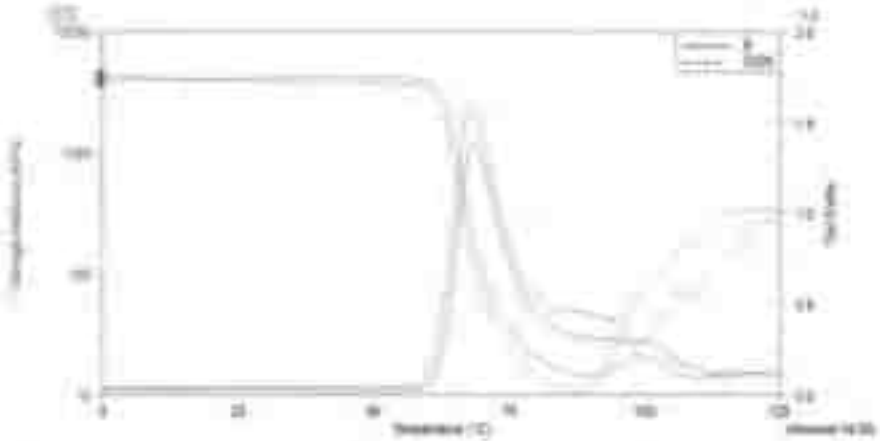

Figure 8. Representative results of the storage modulus and tan δ of the B and O/2N composites.

The dynamic mechanical analysis allowed us to investigate the storage modulus (E') and damping factor (tanδ) as a function of temperature. As can be seen in representative Figure 8, the temperature dependence of the storage modulus and damping factor for the PLA composites was similar. The obtained curves demonstrate a significant peak in the tan delta and a drop in the storage modulus at its narrow glass transition range. It should be noted that the storage moduli at 25 °C for the PLA composites with silane-treated diatomite were higher than the value for the neat PLA and the composites with untreated diatomaceous earth. Moreover, the relaxation intensities in the glass transition region of the composites containing silane were lowered and the peaks of the tanδ curves were shifted to lower temperatures compared with the PLA modified with untreated diatomaceous earth. This can be explained by the fact that the viscoelastic reaction of the polymeric chain was prevented by the formation of silane bonds. As a result, the glass transition temperatures were lowered gradually. These observations were confirmed for the PLA hybridized with epoxide-functionalized silane (GTMS) through reactive extrusion [28]. Looking into the curves, further G' growth in the temperature range above 90 °C can be seen. This may have been caused by an increase in the mobility of the PLA macromolecules related to the cold crystallization of the PLA and its composites [27].

3.4.2. DSC

A DSC analysis was performed to investigate the thermal behavior of the PLA and PLA/diatom composites. The results of the second heating cycle for the studied materials are collected in Table 4. With the temperature increasing in the 40–155 °C range, each DSC curve of the composites possessed three thermal characteristics: (a) a glass transition temperature (T_g), (b) a cold crystallization event (T_{cc}), and (c) an endothermic melting peak (T_m) (Figure 9). The differences between the curves of the neat PLA and the composites are evident, as the curve of the neat PLA shows no apparent crystallinity or glass transition, and only a slight relaxation at ~60 °C, suggesting the onset of cold crystallization. The polymer, however, failed to undergo this event, probably due to a lack of nucleating agents and the heating rate applied in the experiment. This observation is in line with

the DMTA analysis results, for which no glass transition was observed either, while a small local maximum of E' was registered at −90 °C. The addition of diatomite and silanes changed the thermal characteristics significantly. The composites showed a distinct glass transition temperature, an event of cold crystallization, and a melting event, where several endotherms were determined. Moreover, it was found that all the composites showed two distinct melting peaks (T_{m1} and T_{m2}). The double melting peak was related to the recrystallization of the imperfect metastable crystals (T_{m1}) and the melting of the perfected crystals (T_{m2}) [20]. The application of silanized diatomite in combination with natural wax resulted in a reduction in T_{cc} temperature in comparison with the base diatomite composites, likely due to a reduction in melt viscosity and improved wetting action between the filler and the polymer, resulting in nucleation. In turn, however, the observed melting events occurred at lower temperatures, suggesting more crystal imperfections. On the other hand, silanization in combination with the application of synthetic wax, or the application of waxes in systems with base diatomite, showed that T_{cc} occurs at higher temperatures than in the PLA/base diatomite system, which results in the formation of both metastable and perfected PLA crystals with either fewer imperfections or larger diameters (higher T_{m1} and T_{m2}, respectively). This was especially visible in the B/2N system and can be explained by the fact that the molten wax needed to be displaced from the diatomite surface before the nucleating effect occurred, while for the silanized diatomite, this effect took place at a lower temperature.

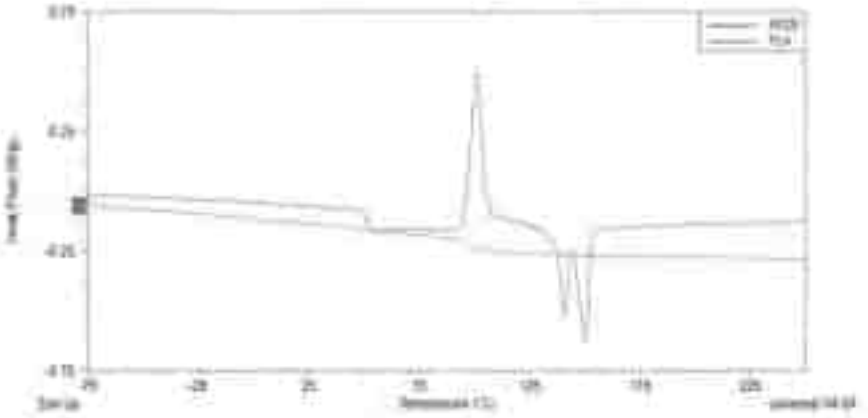

Figure 8. Representative DSC curves of unmodified PLA and M/2S composite obtained during second heating cycle.

Table 4. Thermal characteristics of PLA and composites based on PLA with diatomite, silanes, and waxes.

Sample	Tg [°C]	T_{cc} [°C]	ΔH_{cc} [J/g]	T_{m1} [°C]	T_{m2} [°C]	ΔH_m [J/g]
PLA	N/A [a]	–	–	–	–	–
B	46.1	99.9	25.3	131.0	142.4	24.8
B/2S	53.0	101.0	30.4	140.4	149.8	30.4
B/2N	55.4	109.9	26.8	143.5	151.9	29.5
G/2S	47.8	97.8	28.1	135.6	146.6	30.5
G/2N	52.1	92.9	24.3	124.9	137.7	24.7
O/2S	52.1	101.2	28.7	140.8	150.4	29.4
O/2N	43.5	93.4	24.3	128.1	140.9	26.4
M/2S	43.8	98.3	29.1	130.1	142.0	26.7
M/2N	41.1	92.5	21.4	122.6	136.7	23.6

[a] Tg event not visible.

3.5. SEM Images of Composites

Using a scanning electron microscope, images of fractured samples of neat reference PLA and silane-free samples (Figure 10) and silane-modified composites (Figure 11) were taken. The images allowed us to assess the distribution of the diatomite particles in the PLA/DE composites. In the images taken of the composites modified with synthetic wax (2S), one can clearly see individual broken diatoms embedded in the polymer matrix. The PLA enters deep into the diatom frustule pores, which makes the connection permanent (the effect of the wetting action of the filler with the polymer). The use of a natural wax additive (2N) resulted, at least in part, in a lack of penetration of the PLA into the center of the diatom frustules. The filler particles appear to be on the surface of the polymer without being tightly bound to it. Moreover, in this case, a higher proportion of unbroken diatoms of smaller sizes (that is, in the range from 1 µm to a maximum of about 50 µm) is observed (Figure 12). It was not only the addition of various types of waxes that affected the surface image of the composites. The composites had particles of similar average size compared with the base diatomaceous earth, but did not tend to agglomerate, as seen in the SEM images taken. The number of diatoms in the systems was high, resulting in a large accumulation of diatoms, but they did not aggregate into large clusters. Despite the same filler concentration (25%) having been used, the fractures look different due to the silanization of the diatoms that was carried out before they were embedded in the composite. WH-8 synthetic wax caused increased agglomeration of the particles in the system, unlike natural wax, which caused significant ordering of the composite structure, i.e., individual diatoms are clearly visible and mostly have unbroken frustules. The differences between the silane-modified systems are significant. The aforementioned GPTMOS silane caused an even dispersion of diatomaceous earth in the PLA, similar to MTMOS silane, but with the addition of synthetic wax. In other cases, particle agglomeration occurred, and, in addition, the addition of beeswax to the O and M composites resulted in disordered structures in which there was a strong accumulation of the silanes used for the modification on the surface of the diatom frustules. Natural wax showed a lower wettability of the diatom surface due to its hydrophobic nature, so that the diatomaceous earth with smaller frustule size showed a lower dispersion in the polymer matrix, as seen in Figure 11 in the O/2N sample, among others.

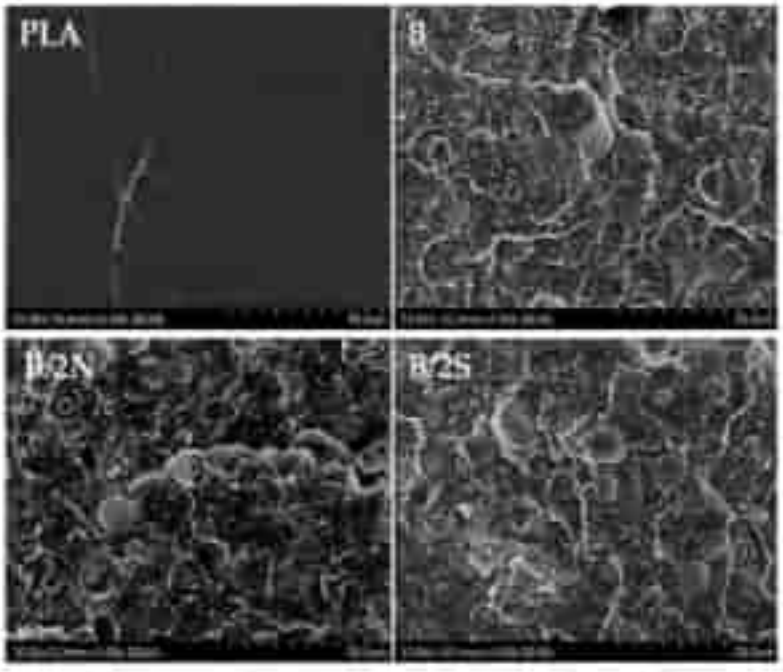

Figure 10. SEM images of fractured samples of composites without added silanes.

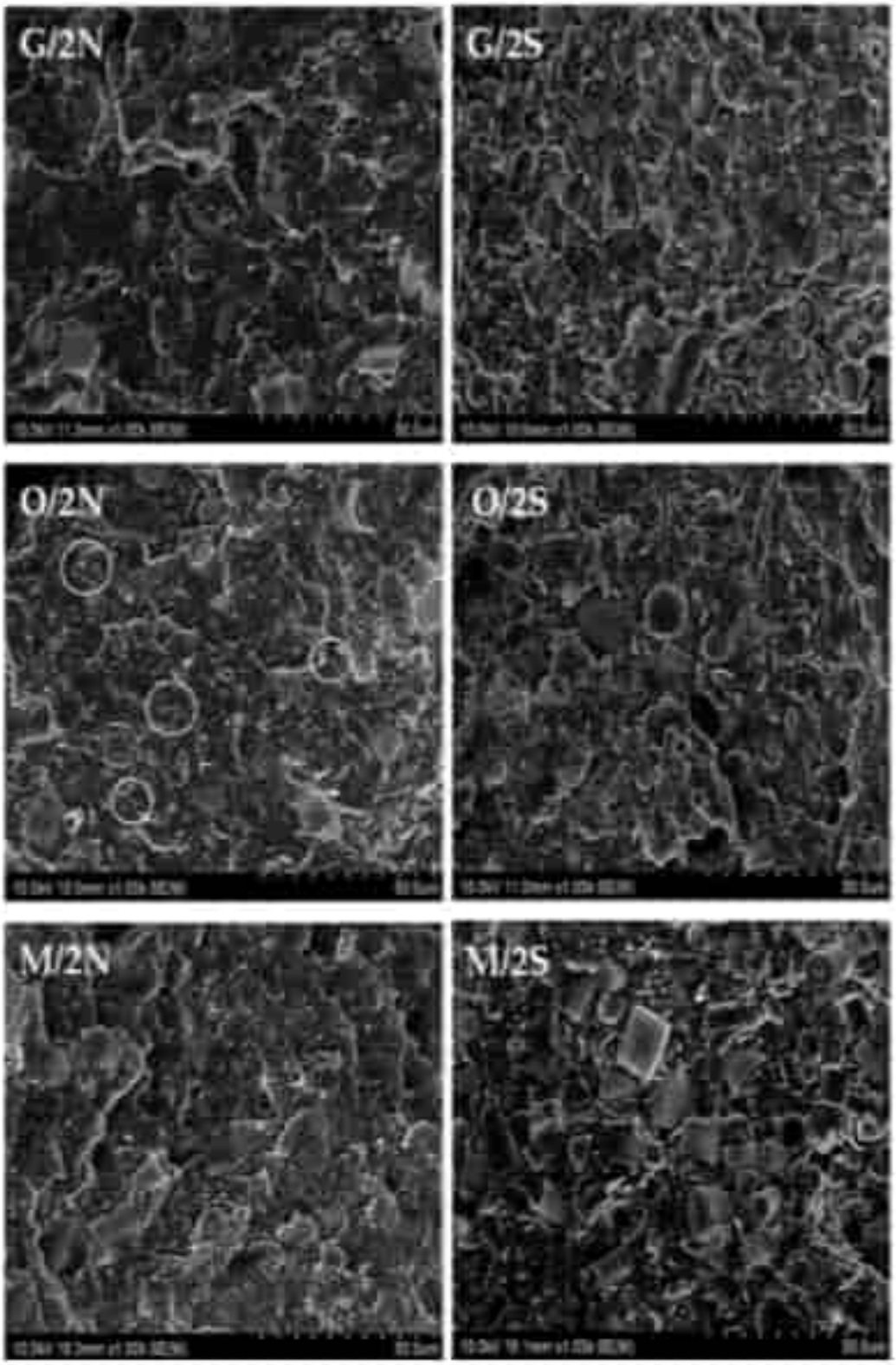

Figure 11. SEM images of fractured samples of selected modified composites.

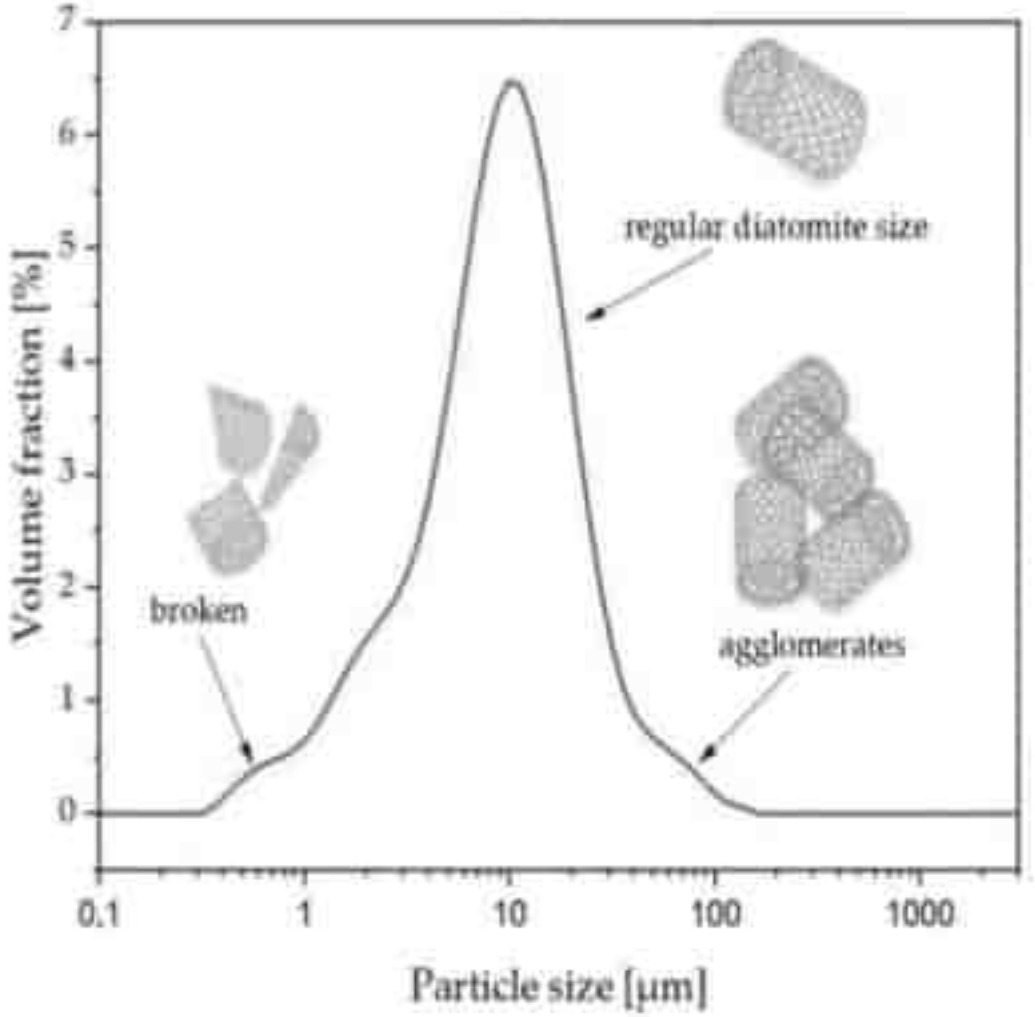

Figure 12. Particle size distribution of diatomaceous earth.

Using an optical microscope, images were taken of the edges of the composites and the reference PLA (Figure 13). The neat PLA showed low scratch resistance, while no scratches or other defects were found on the surface of PLA/DE composites. The edge of the PLA, like the rest of the analyzed samples, was characterized by the presence of a thin layer with a different structure located near the surface. Depending on the filler and type of wax, its depth changed. The addition of the waxes alone resulted in a definite reduction compared with the composite containing only neat diatomaceous earth (II), in which surface discoloration occurred due to poor filler dispersion in the polymer matrix. The modification of the diatomaceous earth with silanes, especially GPTMOS silane, resulted in the formation of a free polymer layer on the sample surface. Considering the thickness of this layer, it can be concluded that natural (beeswax) wax causes this phenomenon to be inhibited, leading to the formation of a composite with a higher degree of dispersion. The composites filled with diatomaceous earth did not show the ability to transmit light, unlike the reference PLA.

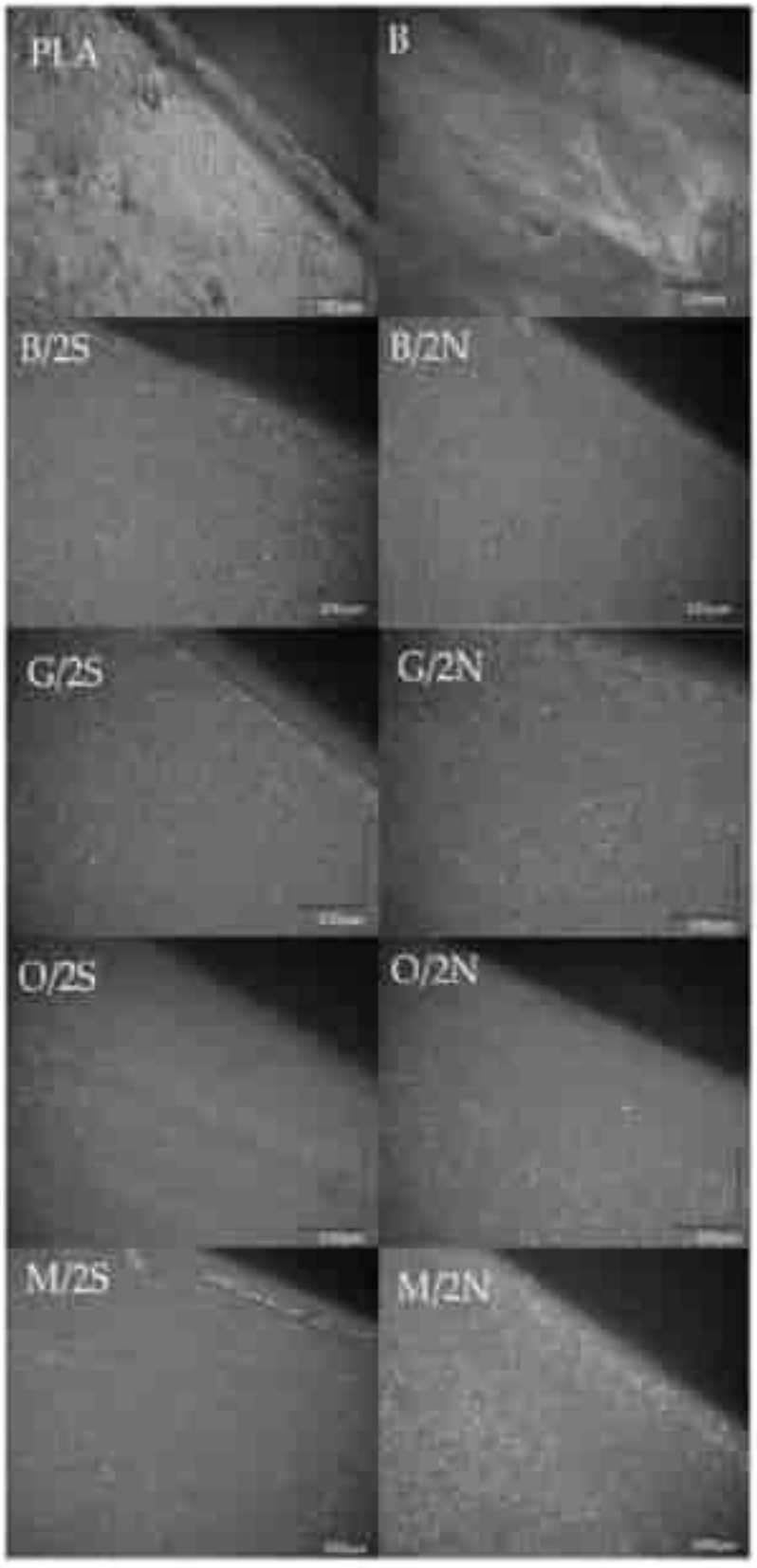

Figure 13. Light microscope images of the edges of PLA/DE composites.

4. Conclusions

A series of diatomite-filled, PLA-based composites was fabricated, and the effects of the filler silanization and the addition of either natural or synthetic wax as processing aids was studied. For most of the systems studied, silanization did not affect mechanical properties of the composites in a significant fashion, proving either the presence of wax on the matrix–filler interphase or weak matrix–filler interaction, depending on the silane–wax system studied. It was observed by means of capillary viscosity, MFR, and DSC that there is an interaction between the waxes and the silanized surface of the filler, which impacts the wax segregation either in the filler–matrix interphase, or in the polymer matrix, which causes differences in melt rheology and thermal behavior, especially cold crystallization and melting. From the point of view of the processing and mechanical properties of the diatomite-filled composites, it is more advantageous to modify the PLA with silanized filler and synthetic wax than with untreated filler and/or no wax as this affords better control over the material's processability. Synthetic wax has a positive effect on a number of composite properties, including mechanical properties, with a satisfactory level of tensile and flexural strength observed in particular, though this combination makes the produced composite less biodegradable and environmentally friendly than a composite containing beeswax. From the ecological point of view, natural waxes leave a smaller carbon footprint because of their production method. The selection of the appropriate wax to improve performance should be dictated by the desire to improve the specific properties of the composites, which vary depending on their type. Independently of the wax type used, satisfactory improvements in processing characteristics in terms of shear thinning rheology were obtained, and these are crucial for high throughput processing technologies, such as injection molding and extrusion. Synthetic wax, on the other hand, provided an increased melt flow index, making it a preferable choice for other processing methods, such as compression molding.

Author Contributions: Conceptualization, R.E.P.; methodology, R.E.P. and M.D.; formal analysis, R.E.P., M.D. and R.D.; investigation, R.E.P., M.D., P.K., M.P.-S. and D.B.; data curation, M.D., M.P.-S., E.G. and J.G.; writing—original draft preparation, M.D., R.E.P., R.D., D.B. and M.P.-S.; writing—review and editing, M.D., R.E.P., R.D. and D.B.; visualization, M.D., *J.G. and R.E.P.*; supervision, R.E.P., R.D. and K.J.K.; project administration, R.D. and K.J.K.; funding acquisition, R.D. and K.J.K. All authors have read and agreed to the published version of the manuscript.

Funding: This work was financially supported within the frame of the project "Advanced Biocomposites for Tomorrow's Economy BIOG-NET", FNP POIR.04.04.00-00-1792/18-00. The project was carried out within the TEAM-NET program of the Foundation for Polish Science, co-financed by the European Union under the European Regional Development Fund.

Institutional Review Board Statement: Not applicable.

Informed Consent Statement: Not applicable.

Data Availability Statement: Not applicable.

Conflicts of Interest: The authors declare no conflict of interest.

References

1. Aguero, A.; Quiles-Carrillo, L.; Jorda-Vilaplana, A.; Fenollar, O.; Montanes, N. Effect of different compatibilizers on environmentally friendly composites from poly (lactic acid) and diatomaceous earth. *Polym. Int.* **2019**, *68*, 895–903. [CrossRef]
2. Aggarwal, S.; Johnson, S.; Saloni, D.; Hakovirta, M. Novel 3D printing filament composite using diatomaceous earth and polylactic acid for materials properties and cost improvement. *Compos. Part B Eng.* **2019**, *177*, 107310. [CrossRef]
3. Dobrzeńska, M.; Przekop, R.E.; Sobczak, B.; Brząkalski, D.; Zgłobicka, I.; Łępicka, M.; Dołęga, R.; Kurzydłowski, K.J. Biogenic Composite Filaments Based on Polylactide and Diatomaceous Earth for 3D Printing. *Materials* **2020**, *13*, 4632. [CrossRef] [PubMed]
4. Mokhena, T.C.; Sefadi, J.S.; Sadiku, E.R.; John, M.J.; Mochane, M.J.; Mtibe, A. Thermoplastic Processing of PLA/Cellulose Nanomaterials Composites. *Polymers* **2018**, *10*, 1363. [CrossRef]
5. Qian, S.; Zheng, H.; Yao, W.; Sheng, K. Effects of bamboo cellulose nanowhisker content on the morphology, crystallization, mechanical, and thermal properties of PLA matrix biocomposites. *Compos. Part B Eng.* **2018**, *153*, 203–209. [CrossRef]

6. Lv, S.; Gu, J.; Tan, H.; Zhang, Y. Enhanced durability of sustainable poly (lactic acid)-based composites with renewable starch and wood flour. *J. Clean. Prod.* **2018**, 203, 328–339. [CrossRef]
7. Sun, C.; Huang, Z.; Liu, Y.; Li, C.; Tan, H.; Zhang, Y. The Effect of Carbodiimide on the Stability of Wood Fiber/Poly (lactic acid) Composites During Soil Degradation. *J. Polym. Environ.* **2020**, 28, 1315–1325. [CrossRef]
8. Ouchiar, S.; Stoclet, G.; Cabaret, C.; Georges, E.; Smith, A.; Martias, C.; Addad, A.; Gloaguen, V. Comparison of the influence of talc and kaolinite as inorganic fillers on morphology, structure and thermomechanical properties of polylactide based composites. *Appl. Clay Sci.* **2015**, 116, 231–240. [CrossRef]
9. Ramesh, P.; Durga Prasad, B.; Narayana, K.L. Influence of Montmorillonite Clay Content on Thermal, Mechanical, Water Absorption and Biodegradability Properties of Treated Kenaf Fiber/ PLA-Hybrid Biocomposites. *Silicon* **2021**, 13, 109–118. [CrossRef]
10. Bezerra Lima, E.M.; Middea, A.; Marconcini, J.M.; Corrêa, A.C.; Fernandes Pereira, J.; Vieira Guimarães, A.; Firmino de Lima, J.; Ramos dos Anjos, M.; de Castro, I.M.; Nunes Oliveira, R.; et al. Biodegradable PLA based nanocomposites for packaging applications: The effects of organo-modified bentonite concentration. *Appl. Polym.* **2021**, 138, 36. [CrossRef]
11. Ferri, J.M.; Jordá, J.; Montanes, N.; Fenollar, O.; Balart, R. Manufacturing and characterization of poly (lactic acid) composites with hydroxyapatite. *J. Thermoplast. Compos. Mater.* **2017**, 31, 865–881. [CrossRef]
12. Wang, W.; Zhang, B.; Li, M.; Li, J.; Zhang, C.; Han, Y.; Wang, L.; Wang, K.; Zhou, C.; Liu, L.; Fan, Y.; et al. 3D printing of PLA/n-HA composite scaffolds with customized mechanical properties and biological functions for bone tissue engineering. *Compos. Part B Eng.* **2021**, 224, 109192. [CrossRef]
13. Galikhanov, M.; Guzhova, A.; Zagidullina, I. Improvement of Electret Properties of Polylactide by Loading Mineral Fillers. *IEEE Trans. Dielectr. Electr. Insul.* **2022**, 29, 784–787. [CrossRef]
14. Pape, P.G. 29—Adhesion Promoters: Silane Coupling Agents. In *Applied Plastics Engineering Handbook, Processing and Materials*; Plastics Design Library; Elsevier: Amsterdam, The Netherlands, 2011; pp. 503–517.
15. Brochier Salon, M.C.; Abdelmouleh, M.; Boufi, S.; Naceur Belgacem, M.; Gandini, A. Silane adsorption onto cellulose fibers: Hydrolysis and condensation reactions. *J. Colloid Interface Sci.* **2005**, 289, 249–261. [CrossRef] [PubMed]
16. Kucuk, F.; Sismanoglu, S.; Kanbur, Y.; Tayfun, U. Effect of silane-modification of diatomite on its composites with thermoplastic polyurethane. *Mater. Chem. Phys.* **2020**, 256, 123683. [CrossRef]
17. Mustar, E.A.; Christiansen, J.D.C.; Sanporean, C.D. Investigation of jojoba oil-wax as a plasticizer for Poly (lactic acid). *J. Optoelectron. Adv. Mater.* **2014**, 8, 109–114.
18. Thomas, T.; Chengal, M.; Alkayarathil, S. Antioxidant activity of mango seed wax additive on the properties of poly (lactic acid) transparent films for food packaging application. *J. Vinyl Addit. Technol.* **2022**, 28, 305–320. [CrossRef]
19. Chen, Y.J.; Huang, A.; Ellingham, T.; Chung, C.; Turng, L.S. Mechanical properties and thermal characteristics of poly (lactic acid) and paraffin wax blends prepared by conventional melt compounding and sub-critical gas-assisted processing (SGAP). *Eur. Polym. J.* **2018**, 98, 262–272. [CrossRef]
20. Kamarudin, S.H.; Abdullah, L.C.; Aung, M.M.; Ratnam, C.T.; Jusoh Talib, E.R. A study of mechanical and morphological properties of PLA based biocomposites prepared with EJO vegetable oil based plasticiser and kenaf fibres. *Mater. Res. Express* **2018**, 5, 8. [CrossRef]
21. Zych, A.; Perotto, G.; Trojanowska, D.; Tedeschi, G.; Bertolacci, L.; Francini, N.; Athanassiou, A. Super Tough Polylactic Acid Plasticized with Epoxidized Soybean Oil Methyl Ester for Flexible Food Packaging. *ACS Appl. Polym. Mater.* **2021**, 3, 5087–5095. [CrossRef]
22. Pawlak, F.; Aldas, M.; Parres, F.; López-Martínez, J.; Arrieta, M.P. Silane-Functionalized Sheep Wool Fibers from Dairy Industry Waste for the Development of Plasticized PLA Composites with Maleinized Linseed Oil for Injection-Molded Parts. *Polymers* **2020**, 12, 2523. [CrossRef] [PubMed]
23. Dobrosielska, M.; Dobrucka, R.; Brząkalski, D.; Frydrych, M.; Kozera, P.; Wieczorek, M.; Jałbrzykowski, M.; Kurzydłowski, K.J.; Przekop, R.E. Influence of Diatomaceous Earth Particle Size on Mechanical Properties of PLA/Diatomaceous Earth Composites. *Materials* **2022**, 15, 3607. [CrossRef] [PubMed]
24. Olejnik, O.; Masek, A. Bio-based packaging materials containing substances derived from coffee and tea plants. *Materials* **2020**, 13, 5719. [CrossRef] [PubMed]
25. Tulloch, A.P. Beeswax—Composition and Analysis. *Bee World* **1980**, 61, 47–62. [CrossRef]
26. Lee, J.C.; Choi, M.C.; Choi, D.H.; Ha, C.S. Toughness enhancement of poly (lactic acid) through hybridization with epoxide-functionalized silane via reactive extrusion. *Polym. Degrad. Stab.* **2019**, 160, 195–202. [CrossRef]
27. Barczewski, M.; Hejna, A.; Aniśko, J.; Andrzejewski, J.; Piasecki, A.; Mysiukiewicz, O.; Bąk, M.; Gapiński, B.; Ortega, Z. Rotational molding of polylactide (PLA) composites filled with copper slag as a waste filler from metallurgical industry. *Polym. Test.* **2022**, 106, 107449. [CrossRef]
28. Mofokeng, J.P.; Luyt, A.S.; Tábi, T.; Kovács, J. Comparison of injection moulded, natural fibre-reinforced composites with PP and PLA as matrices. *J. Thermoplast. Compos. Mater.* **2011**, 25, 927–948. [CrossRef]

H9

Effect of wax type on selected properties of biocomposites

Dobrosielska M., Dobrucka R., Kurzydłowski K.J., Przekop R.E.. Przemysł Chemiczny, 103, 7, 2024

Marta Dobrosielska[a], Renata Dobrucka[b,c,*], Krzysztof J. Kurzydłowski[c], Robert E. Przekop[d,**]

[a]Politechnika Warszawska; [b]Uniwersytet Ekonomiczny w Poznaniu; [c]Politechnika Białostocka; [d]Uniwersytet im. Adama Mickiewicza w Poznaniu

Effect of wax type on selected properties of biocomposites

Wpływ rodzaju wosków na wybrane właściwości biokompozytów

DOI: 10.15199/62.2024.7.4

Polylactide (PLA) was modified by addn. of amorphous diatomaceous earth, synthetic wax and beeswax (2.5–15% by mass, 0.5% by mass and 0.5% or 1% by mass, resp.) and direct injection moulding to improve its rheol. properties and then studied for tensile strength, elongation at break, flexural stress and flexural modulus as well as for wetting angle optionally after conditioning the samples in a climate chamber for 20 days. The modification resulted in increasing of PLA elasticity as well as in changing hydrophobic-hydrophilic character of the PLA surface and in an increase of the wetting angle up to 27.4° when compared to the pure PLA.

Keywords: *diatomaceous earth, ageing, polylactide composites, beeswax*

W celu zbadania wpływu symulowanych niekorzystnych warunków atmosferycznych na właściwości mechaniczne i powierzchniowe kompozytów na osnowie polilaktydowej, wytworzono metodą wtrysku bezpośredniego kilka materiałów zawierających jako napełniacz amorficzną ziemię okrzemkową oraz różne rodzaje wosków, które zastosowano w celu poprawy właściwości reologicznych. Wytworzone kompozyty cechowały się zawartością ziemi okrzemkowej w zakresie 2,5–15% mas. oraz wosku pszczelego (zawartość 0,5% lub 1% mas.) lub wosku syntetycznego (zawartość 0,5% mas.). Na podstawie przeprowadzonych badań stwierdzono, że dodatek ziemi okrzemkowej w połączeniu z dodatkiem wosków korzystnie wpływa m.in. na hydrofobowo-hydrofilowy charakter powierzchni kompozytów, gdzie po 20 dniach kondycjonowania próbek w komorze klimatycznej dla największych stężeń ziemi okrzemkowej odnotowano wzrost kąta zwilżania do maksymalnie 27,4° w porównaniu z czystym polilaktydem.

Słowa kluczowe: *ziemia okrzemkowa, starzenie, kompozyty polilaktydowe, wosk pszczeli*

Polilaktyd (PLA) zaliczany jest do biopolimerów ze względu na jego zdolność do biodegradacji oraz pozyskiwanie ze źródeł naturalnych, głównie poprzez fermentację mikrobiologiczną produktów ubocznych rolnictwa[1]. Polilaktyd może występować w trzech odmianach stereochemicznych: jako PLLA (poli(L-laktyd), PDLA (poli(D-laktyd) oraz PDLLA (poli(DL-laktyd). Dzięki swoim właściwościom może z powodzeniem zastępować wiele innych polimerów ropopochodnych. Może być przetwarzany na tych samych liniach produkcyjnych co tworzywa PET (formowanie z rozdmuchem, termoformowanie), a w przypadku polilaktydu o wyższym wskaźniku szybkości płynięcia może zastępować polistyren (formowanie wtryskowe) lub polipropylen (wytłaczanie włókien). PLA w określonych, kontrolowanych warunkach (temp. min. 70°C, wilgotność min. 70%) może być poddawany kompostowaniu, gdzie ulega biodegradacji. Właściwości polilaktydu zależą od temperatury przetwarzania, od izomerów składowych, czasu wygrzewania oraz masy cząsteczkowej[2]. PLA cechuje się modułem Younga na poziomie ok. 3 GPa, wytrzymałością na rozciąganie 50–70 MPa i wydłużeniem przy zerwaniu 4–7% oraz udarnością ok. 2,5 kJ/m²[3]. W porównaniu z innymi polimerami (PS lub PET), PLA cechują lepsze właściwości mechaniczne, m.in. wytrzymałość na rozciąganie,

Mgr Marta DOBROSIELSKA (ORCID: [illegible]) ukończyła studia na Wydziale Chemii Uniwersytetu im. Adama Mickiewicza w Poznaniu. Obecnie jest doktorantką na Wydziale Inżynierii Materiałowej Politechniki Warszawskiej, gdzie realizuje badania do pracy doktorskiej [illegible]. Specjalność – materiały kompozytowe.

Dr hab. Renata DOBRUCKA, prof. UEP (ORCID: [illegible]) pracuje w Instytucie Nauk o Jakości Uniwersytetu Ekonomicznego w Poznaniu. [illegible]

* Adres do korespondencji:

Katedra Jakości Produktów Przemysłowych i Opakowań, Instytut Nauk o Jakości, Uniwersytet Ekonomiczny w Poznaniu, al. Niepodległości 10, 61-875 Poznań, tel.: [illegible], e-mail: renata.dobrucka@ue.poznan.pl

jednakże, podobnie jak PS, PLA jest materiałem kruchym o małej udarności[5].

Dodatek ziemi okrzemkowej (DE) do polilaktydu nie tylko wpływa na wzmocnienie kompozytu[6-8], ale też sprzyja zwiększonej szybkości degradacji kompozytu[7], co jest istotne ze względu na problem zagospodarowania odpadów. W odpowiednich warunkach i przy zastosowaniu odpowiednich dodatków kompozyt PLA/DE może ulegać całkowitej degradacji już w ciągu 42 dni[8], ale zbyt szybki rozkład takiego kompozytu również nie jest do końca pożądany, ze względu na chociażby zużycie energii potrzebnej do jego wyprodukowania. Zwiększona szybkość degradacji kompozytu oraz zwiększona odporność materiału na niekorzystne warunki atmosferyczne jest zależna od charakteru produktu końcowego i jego przeznaczenia.

W pracy przeprowadzono badania wytrzymałości mechanicznej oraz badania charakteru hydrofobowo-hydrofilowego powierzchni kompozytów, które poddano badaniom starzeniowym w komorze klimatycznej przez 5 i 20 dni. Układy referencyjne poddano jedynie kondycjonowaniu w warunkach standardowego ciśnienia atmosferycznego i temperatury pokojowej. Kompozyty na osnowie polilaktydowej poddane badaniom zawierały 2,5, 5, 10 i 15% dodatku napełniacza (amorficznej ziemi okrzemkowej) oraz 0,5 i 1% dodatku wosku pszczelego lub 0,5% wosku syntetycznego (WTH-B). Kompozyty wytworzono analogicznie jak w poprzedniej pracy[9].

Część doświadczalna

Surowce

Stosowano polilaktyd (PLA) typ Ingeo 4043D (NatureWorks), amorficzną ziemię okrzemkową (Perma-Guard), wosk syntetyczny WTH-B ($C_{22}H_{45}NO$, WTH GmbH) oraz wosk naturalny pszczeli (Spółdzielnia Pszczelarska APIS).

Metodyka badań

Przygotowanie granulatu

Czysty polimer wraz z napełniaczem i modyfikatorem homogenizowano, używając walcarki laboratoryjnej Zamak Mercator WG 150/280. Porcję 500 g PLA Ingeo™ 4043 D mieszano z ziemią okrzemkową i woskiem aż do uzyskania końcowej zawartości ziemi okrzemkowej 5%, 10%, 20% i 30% mas., zawartości wosku pszczelego 1% i 2% mas. lub zawartości wosku syntetycznego 1% mas. Mieszanie prowadzono w temp. 215°C przez 20 min do uzyskania pełnej homogeniczności. Przedmieszki granulowano za pomocą młyna do mielenia tworzyw Wanner C17.26 sv, a następnie suszono przez 24 h w temp. 60°C.

Formowanie wtryskowe

Przygotowane przedmieszki rozcieńczono 1:1 czystym PLA bezpośrednio we wtryskarce Engel e-victory 170/80, analogicznie jak w poprzedniej pracy[9]. Znormalizowane próbki do badań mechanicznych otrzymano zgodnie z normą[10]. Końcowy skład układu przedstawiono w tabeli 1.

Właściwości materiałów

W celu wykonania badań mechanicznych (udarność, wytrzymałość na rozciąganie statyczne oraz wytrzymałość na zginanie) otrzymane granulaty formowano wtryskowo zgodnie z normami[9, 10] w celu utworzenia wiosł pomiarowych. Badanie wytrzymałości na zginanie i rozciąganie przeprowadzono za pomocą uniwersalnej maszyny wytrzymałościowej Instron 5969. Zastosowano prędkość przesuwu trawersy 2 mm/min, zarówno dla badania wytrzymałości na rozciąganie, jak

Table 1. Final compositions of the samples, % by mass

Tabela 1. Końcowe składy próbek, % mas.

Próbka	Ziemia okrzemkowa	Wosk pszczeli	Wosk syntetyczny (WTH-B)
PLA	0	0	0
2,5DE	2,5	0	0
5DE	5	0	0
10DE	10	0	0
15DE	15	0	0
2,5DE/0,5BW	2,5	0,5	0
5DE/0,5BW	5	0,5	0
10DE/0,5BW	10	0,5	0
15DE/0,5BW	15	0,5	0
2,5DE/1BW	2,5	1	0
5DE/1BW	5	1	0
10DE/1BW	10	1	0
15DE/1BW	15	1	0
2,5DE/0,5SW	2,5	0	0,5
5DE/0,5SW	5	0	0,5
10DE/0,5SW	10	0	0,5
15DE/0,5SW	15	0	0,5

Prof. dr hab. inż. Krzysztof J. KURZYDŁOWSKI (ORCID: [illegible]) [illegible]

Dr hab. Robert PRZEKOP, prof. UAM (ORCID: [illegible]), [illegible] Wydziale Chemii Uniwersytetu im. Adama Mickiewicza w Poznaniu. [illegible]

** Adres do korespondencji:

Centrum Zaawansowanych Technologii, Uniwersytet im. Adama Mickiewicza w Poznaniu, ul. Uniwersytetu Poznańskiego 10, 61-614 Poznań, tel.: [illegible], e-mail: [illegible]

i na zginanie. Badanie udarności metodą Charpy'ego przeprowadzono, wykorzystując maszynę Instron Ceast 9050, zgodnie z normą[11]. Badanie kąta zwilżania powierzchni kompozytów przeprowadzono metodą wiszącej kropli w temperaturze pokojowej i pod ciśnieniem atmosferycznym, przy użyciu goniometru Krüss DSA100. Objętość dozowanej kropli wynosiła 5 µL. Badania starzeniowe kompozytów przeprowadzono w komorze klimatycznej ESPEC ARS-0220, stosując zakres temperatur od -10°C do -50°C oraz wilgotność na poziomie 85%. Badanie prowadzono przez 5 oraz 20 dni. Badania wytrzymałości mechanicznej oraz badanie kąta zwilżania powierzchni kompozytów przeprowadzono zarówno dla próbek referencyjnych (przed starzeniem), jak i po 5 oraz 20 dniach kondycjonowania w komorze klimatycznej.

Wyniki badań i ich omówienie

Właściwości mechaniczne

Udarność czystego poliaktydu po procesie wtrysku wynosiła ok. 19 kJ/m^2. Dodatek już 2,5% ziemi okrzemkowej powodował znaczący wzrost udarności, bo aż do wartości ok. 25 kJ/m^2. Dodatek 1% wosku pszczelego spowodował wzrost udarności do powyżej 25 kJ/m^2 dla 5% DE, a więc wyższej niż dla czystej ziemi okrzemkowej oraz próbek z zawartością 0,5% wosku. Umieszczenie badanych próbek w komorze klimatycznej na 5 i 20 dni, gdzie poddane zostały zmiennej temperaturze i wilgotności, spowodowało zmiany w udarności zarówno dla referencyjnego poliaktydu, jak i dla układów modyfikowanych, co obrazują dane zestawione w tabeli 2. Po 5 dniach przebywania w komorze klimatycznej każda próbka cechowała się wyższą wartością udarności, zależnie od modyfikacji. Największy wzrost odnotowano dla próbek z dodatkiem 0,5% wosku pszczelego oraz dla dodatku 1%, ale przy większych stężeniach diatomitu (10 i 15%). Dla próbek modyfikowanych woskiem syntetycznym początkowo (po 5 dniach) nie odnotowano zbyt dużego wzrostu udarności, ale po 20 dniach w komorze klimatycznej jako jedyne nadal cechowały się coraz wyższymi wartościami. Większość pozostałych układów po tak długim pobycie w niekorzystnych warunkach uległa osłabieniu i udarność zmniejszyła się. Duże odchylenia od wartości zmierzonej wynikały zarówno z faktu, że modyfikacja kompozytów miała wpływ na jednorodność struktury, ale i ze względu na samo narażenie próbek na niekorzystne warunki atmosferyczne, gdzie nierównomiernie ulegały degradacji.

Wytrzymałość na rozciąganie oraz wydłużenie przy zerwaniu uległy zmianom po kondycjonowaniu kompozytów w komorze klimatycznej przez 5 i 20 dni, co obrazują dane na rys. 1 i 2. Czysty poliaktyd nie wykazywał zbyt drastycznych zmian w obrębie tych dwóch parametrów, nawet obserwowano niewielki wzrost wytrzymałości na rozciąganie po 20 dniach w komorze klimatycznej. Kompozyty modyfikowane ziemią okrzemkową bez wosków, co było spodziewane ze względu na charakterystykę napełniacza, cechowały się spadkiem wytrzymałości mechanicznej, zwłaszcza po 5 dniach w komorze klimatycznej, a dalsze ich narażenie

Table 2. Impact strength for samples after conditioning in room temperature (RT), 5 days and 20 days in climatic chamber, kJ/m²

Tabela 2. Udarność dla próbek kondycjonowanych w temperaturze pokojowej (RT), 5 i 20 dni w komorze klimatycznej, kJ/m²

Próbka	RT	SD	5 dni KK	SD	20 dni KK	SD
PLA	19,54	0,90	24,77	1,91	25,8	1,97
2,5DE	20,76	2,29	21,35	2,21	22,6	2,21
5DE	18,76	2,3	19,47	1,98	22,4	1,98
10DE	16,4	0,77	18,21	1,43	21,1	1,47
15DE	15,51	1,41	19,23	2,06	19,9	2,06
2,5DE0,5BW	23,86	2,27	26,43	2,32	27,5	2,32
5DE0,5BW	17,93	1,73	27,12	2,89	25,1	2,89
10DE0,5BW	16,57	1,43	20,49	2,24	17,3	2,24
15DE0,5BW	16,21	2,71	23,84	1,02	16,2	1,04
2,5DE1BW	19,33	1,38	26,99	2,22	26,1	2,22
5DE1BW	17,78	1,61	24,65	1,88	24,8	1,88
10DE1BW	14,44	1,63	22,02	0,67	17,01	0,67
15DE1BW	12,91	1,96	13,87	2,63	14,1	2,63
2,5DE0,5SW	32,71	2,91	28,18	3,46	24,1	3,46
5DE0,5SW	25,57	1,54	26,94	3,4	22,6	3,41
10DE0,5SW	17,93	1,18	20,20	2,64	18,4	2,64
15DE0,5SW	16,18	2,58	25,29	4,39	11,9	4,39

KK – komora klimatyczna

na zmiany temperatury i wilgotności powodowała, w miarę wzrostu stężenia napełniacza, dotarcie próbek, a co za tym idzie poprawę wytrzymałości na rozciąganie. Wzrost napełnienia kompozytu powodował zwiększenie porowatości układu, a zarazem chłonności wody, szybkości hydrolizy i emisji, spowodowanej cyklami zamrażania i rozmrażania. Podobnymi właściwościami i podobnym trendem cechowały się układy z 0,5-proc. dodatkiem wosku pszczelego, jednak wraz ze wzrostem stężenia napełniacza i wzrostem czasu kondycjonowania w komorze klimatycznej można było zaobserwować, że wosk naturalny wywierał niemalże negatywny wpływ na wytrzymałość na rozciąganie, co odzwierciedliło się w tendencji spadkowej tego parametru w przypadku dużych stężeń ziemi okrzemkowej. Większy dodatek wosku naturalnego (1%) powodował dalsze pogorszenie właściwości mechanicznych (wytrzymałości na rozciąganie) kompozytów, ale pozytywny wpływ dodatku odnotowano dla układów zawierających wosk syntetyczny, dla których mimo zastosowania ziemi okrzemkowej jako napełniacza, wartości wytrzymałości na rozciąganie kształtowały się na bardzo dobrym poziomie, nawet dla układów wysoko napełnionych. Podobnie w przypadku wydłużenia przy zerwaniu, gdzie również pozytywny wpływ odnotowano dla wosku syntetycznego. Otrzymano poprawę tego parametru, zwłaszcza dla układów kondycjonowanych w komorze klimatycznej przez 20 dni, w porównaniu z czystym niezmodyfikowanym poliaktydem. Największym brakiem zależności pomiędzy stopniem napełnienia a wynikami wydłużenia przy zerwaniu charakteryzował się układ zawierający 0,5% wosku pszczelego, co mogło wskazywać na niedostateczną dyspersję modyfikatora i zbyt wczesną propagację pęknięcia lub też powstanie aglomeratów, na co potencjalnie mógł mieć wpływ dodatek wosku tego rodzaju. Mimo wysokiego stopnia napełnienia (15% ziemi okrzemkowej), w każdym analizowanym układzie odnotowano najwyższe wyniki po 20 dniach w komorze klimatycznej właśnie dla tych

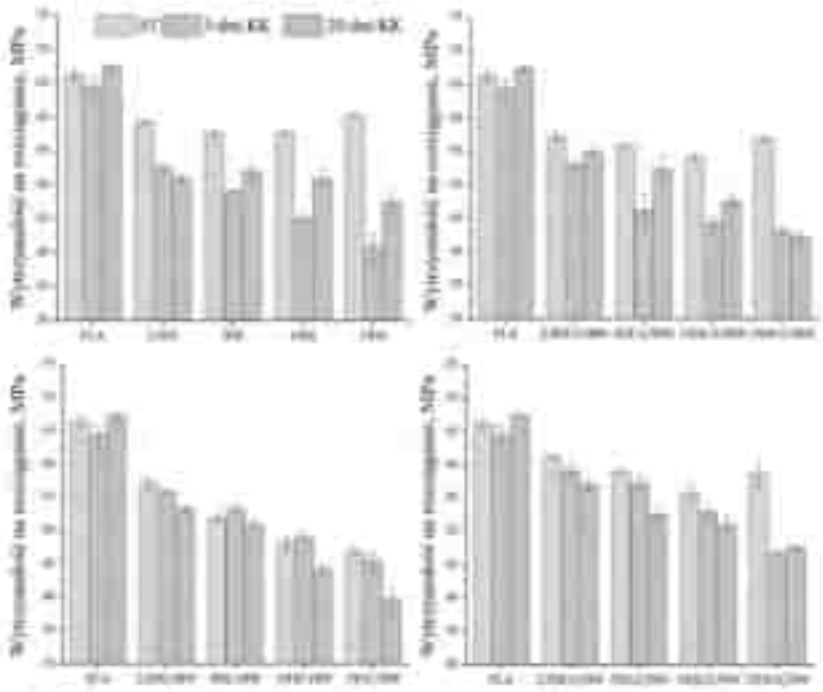

Fig. 2. Tensile strength for samples after conditioning in room temperature (RT), 5 and 20 days in climatic chamber (CC)

Rys. 3. Wytrzymałość na rozciąganie dla próbek kondycjonowanych w temperaturze pokojowej (RT), 5 i 20 dni w komorze klimatycznej (KK)

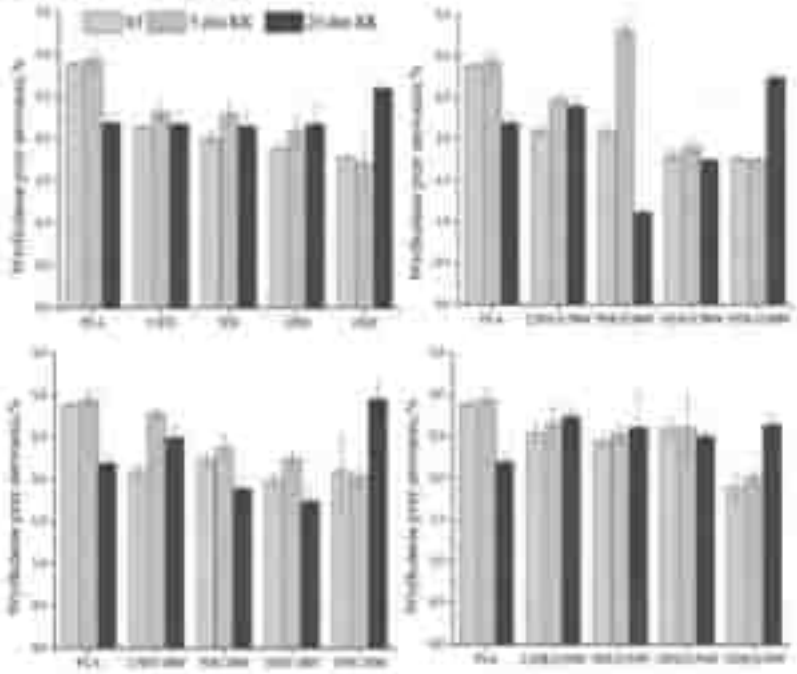

Fig. 3. Elongation for samples after conditioning in room temperature (RT), 5 and 20 days in climatic chamber (CC)

Rys. 4. Wydłużenie przy zerwaniu dla próbek kondycjonowanych w temperaturze pokojowej (RT), 5 i 20 dni w komorze klimatycznej (KK)

kompozytów. Oznacza to, że mimo zastosowania jako napełniacza ziemi okrzemkowej, która powodowała zwiększenie kruchości materiałów, narażenie próbek na potencjalnie niekorzystne warunki środowiskowe spowodowało zdecydowane polepszenie parametrów wytrzymałościowych (wydłużenie przy zerwaniu), co było związane z podwyższeniem elastyczności kompozytów. Przy zawartości 0,5% wosku syntetycznego efekt starzenia zmniejszał się z uwagi na jego hydrofobowość i brak podatności na hydrolizę.

Wytrzymałość na zginanie kompozytów również zbadano dla układów kondycjonowanych w temperaturze pokojowej (RT) oraz po 5 i 20 dniach w komorze klimatycznej (KK), co przedstawiono na rys. 3. Moduł elastyczności w każdym przypadku wzrastał wraz ze wzrostem stężenia napełniacza i był zdecydowanie wyższy niż dla czystego poliuretanu, nawet w zakresie małych zawartości. Ziemia okrzemkowa bez dodatku wosków osiągała wartość maks. 4,47 GPa, podczas gdy dla referencyjnego poliuretanu było to jedynie 3,8 GPa. Nie odnotowano znaczących różnic pomiędzy różnymi czasami kondycjonowania i próbką odniesienia (temperatura pokojowa), co oznaczało znikomy wpływ niekorzystnych warunków środowiskowych na wytrzymałość kompozytów. Najkorzystniejszy wpływ na moduł elastyczności, zwłaszcza w zakresie największych stężeń, odnotowano dla układów modyfikowanych woskiem naturalnym (pszczelim), w których zarówno dla 0,5-proc., jak i 1-proc. dodatku osiągnięto wyniki wyższe niż w pozostałych układach (odpowiednio 4,8 i 4,7 GPa), aczkolwiek dla największych stężeń odnotowano wpływ warunków środowiskowych w komorze klimatycznej, o czym świadczy niewielki spadek wartości modułu elastyczności w stanie upływu czasu. Wosk syntetyczny również pozytywnie wpływał na parametry wytrzymałościowe, jednak maksymalny uzyskany wynik dla największego stężenia wynosił 4,4 GPa. Zupełnie inaczej kształtowały się wyniki maksymalnego naprężenia zginającego przedstawione również na rys. 3. W miarę wzrostu zawartości napełniacza zauważalny był spadek tego parametru, również w porównaniu z czystym poliuretanem. Próbki bez dodatku

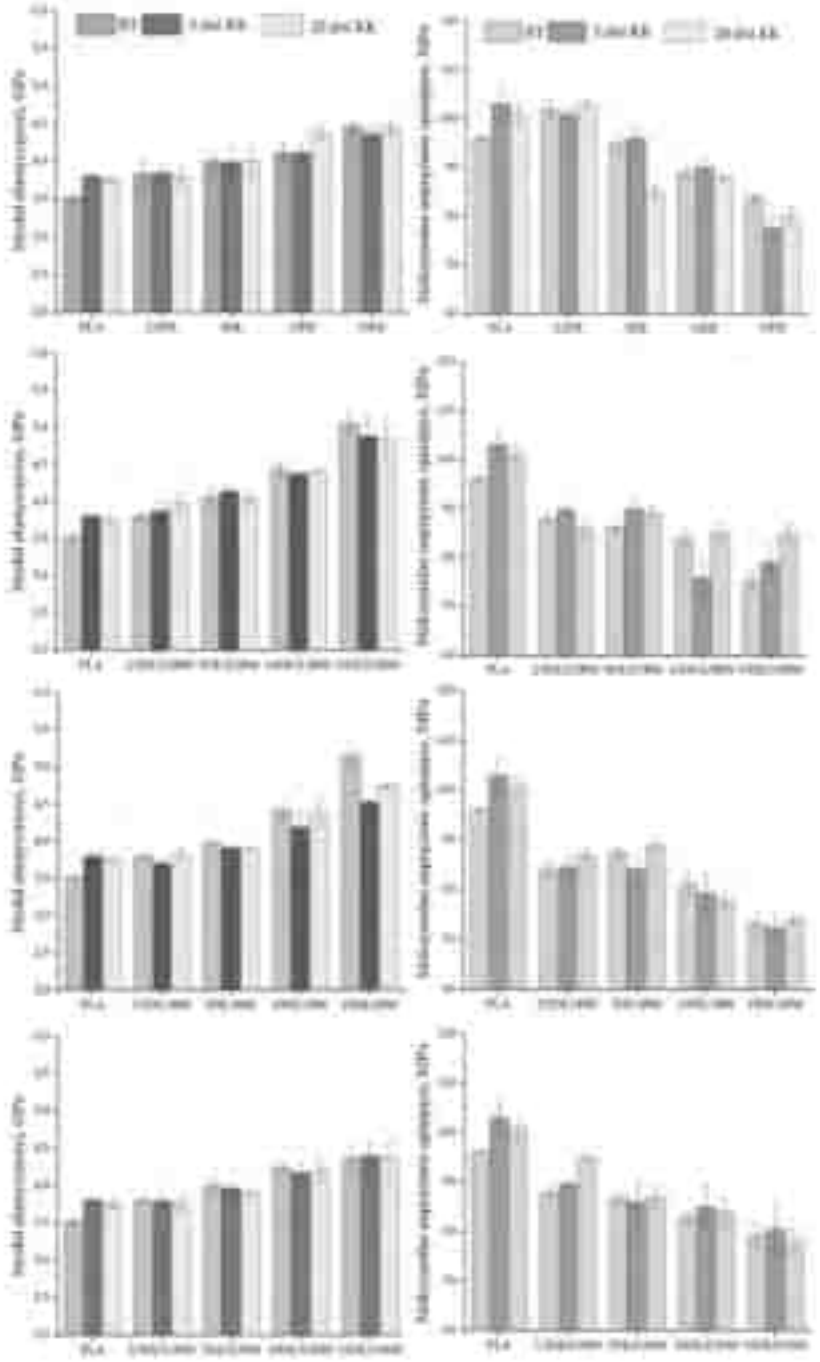

Fig. 3. Maximum flexural stress and flexural modulus for samples after conditioning in room temperature (RT), 5 and 20 days in climatic chamber (CC)

Rys. 3. Maksymalne naprężenie zginające i moduł elastyczności dla próbek kondycjonowanych w temperaturze pokojowej (RT), 5 i 20 dni w komorze klimatycznej (KK)

uzyskane wartości to 5%. Przy dalszym dodatku napełniacza wartość maksymalnego naprężenia zginającego, zwłaszcza dla 20 dni w komorze klimatycznej, odnotowano spadek wartości. Dla układów modyfikowanych 0,5-proc. dodatkiem wosku syntetycznego najwyższe wyniki odnotowano dla układów o najmniejszym stężeniu, ale w miarę wzrostu czasu spędzonego w komorze klimatycznej maksymalne naprężenie zginające przyjmowało coraz niższe wartości.

Kąt zwilżania powierzchni kompozytów

Kąt zwilżania został zmierzony dla układów kondycjonowanych w temperaturze pokojowej oraz w komorze klimatycznej przez 5 i 20 dni (tabele 3–5). Referencyjny polilaktyd cechował się hydrofilowym charakterem powierzchni przed komorą klimatyczną, ale po 5 dniach charakter ten ulegał zmianie w kierunku wartości hydrofobowych (kąt zwilżania ok. 90°), co było spowodowane zmianami mikrostrukturalnymi powierzchni tworzywa oraz wzrostem krystaliczności pod wpływem wody i zmian temperatury[10]. Dalsze narażenie próbek na zmienną temperaturę i wilgotność spowodowało spadek kąta zwilżania do ok. 70°, co wynikało z procesu hydrolizy polimeru, prowadzącej do spadku średniej masy cząsteczkowej i tworzenia oligomerów kwasu mlekowego na powierzchni tworzywa[11]. Próbki zawierające czystą ziemię okrzemkową niezależnie od zawartości i warunków kondycjonowania cechowały się kątem zwilżania w zakresie 86–104°, co wosków cechowały się zdecydowanie wyższą wartością maksymalnego naprężenia zginającego, zwłaszcza w zakresie małych zawartości napełniacza (2,5%), aczkolwiek dla tego układu oraz układu zawierającego 0,5% wosku pszczelego nie zauważono zależności pomiędzy wartościami maksymalnego naprężenia zginającego, stężeniem napełniacza oraz czasem spędzonym w komorze klimatycznej. Dla układów modyfikowanych 1-proc. dodatkiem wosku pszczelego najwyższe czyniło ich powierzchnię hydrofobową w większości przypadków. Było to spowodowane dodatkową mikrochropowatością wprowadzoną przez napełniacz. Tak jak w przypadku polilaktydu kondycjonowanie w komorze przez 5 dni również spowodowało niewielki wzrost hydrofobowości powierzchni kompozytów, ale po 20 dniach kąt zwilżania zmalał, jednak spadek ten był nieistotny ze względu na błąd pomiarowy. Kompozyty zawierające wosk pszczeli (przed komorą klima-

Table 3. Contact angle of composites and PLA after conditioning in room temperature (RT), deg

Tabela 3. Kąt zwilżania powierzchni kompozytów oraz PLA po kondycjonowaniu próbek w temperaturze pokojowej, deg

Kompozyt	Kąt zwilżania	Kompozyt	Kąt zwilżania	Kompozyt	Kąt zwilżania	Kompozyt	Kąt zwilżania
2,5DE	103,2	2,5DE/0,5BW	73,8	2,5DE/1BW	89,3	2,5DE/0,5SW	93,6
5DE	98,0	5DE/0,5BW	96,1	5DE/1BW	93,1	5DE/0,5SW	86,3
10DE	99,1	10DE/0,5BW	94,2	10DE/1BW	96,3	10DE/0,5SW	92,9
15DE	85,1	15DE/0,5BW	91,5	15DE/1BW	91,5	15DE/0,5SW	85,8
PLA	93,2						

Table 4. Contact angle of composites and PLA after conditioning in climate chamber (KK) for 5 days, deg

Tabela 4. Kąt zwilżania powierzchni kompozytów oraz PLA po kondycjonowaniu próbek przez 5 dni w komorze klimatycznej (KK), deg

Kompozyt	Kąt zwilżania	Kompozyt	Kąt zwilżania	Kompozyt	Kąt zwilżania	Kompozyt	Kąt zwilżania
2,5DE	103,1	2,5DE/0,5BW	85,4	2,5DE/1BW	99,9	2,5DE/0,5SW	94,2
5DE	98,6	5DE/0,5BW	93,7	5DE/1BW	73,7	5DE/0,5SW	91,7
10DE	99,7	10DE/0,5BW	91,6	10DE/1BW	95,7	10DE/0,5SW	91,1
15DE	90,3	15DE/0,5BW	80,9	15DE/1BW	92,7	15DE/0,5SW	92,1
PLA	93,9						

Table 5. Contact angle of composites and PLA after conditioning in climate chamber (KK) for 20 days, deg

Tabela 5. Kąt zwilżania powierzchni kompozytów oraz PLA po kondycjonowaniu próbek przez 20 dni w komorze klimatycznej (KK), deg

Kompozyt	Kąt zwilżania	Kompozyt	Kąt zwilżania	Kompozyt	Kąt zwilżania	Kompozyt	Kąt zwilżania
2,5DE	99,8	2,5DE/0,5BW	86,7	2,5DE/1BW	88,8	2,5DE/0,5SW	78,2
5DE	95,1	5DE/0,5BW	91,0	5DE/1BW	83,8	5DE/0,5SW	85,2
10DE	99,5	10DE/0,5BW	92,1	10DE/1BW	84,7	10DE/0,5SW	93,1
15DE	86,3	15DE/0,5BW	90,4	15DE/1BW	92,4	15DE/0,5SW	97,4
PLA	70,3						

tycznej) najwyższe wartości posiadały dla układów zawierających 5 i 10% ziemi okrzemkowej. Po komorze dla układów o najmniejszym stężeniu odnotowano znaczy wzrost wartości zarówno po 5, jak i po 20 dniach, a dla pozostałych układów spadek kąta zwilżania. Modyfikacja woskiem syntetycznym nie spowodowała znaczących różnic pomiędzy układami z woskiem pszczelim a syntetycznym przed komorą klimatyczną, a po kondycjonowaniu w nieprzyjaznych warunkach atmosferycznych, zwłaszcza po 20 dniach, trend ten uległ zmianie. Wraz ze wzrostem stężenia napełniacza liniowo wzrastał również kąt zwilżania i dla największego stężenia DE osiągnął wartość powyżej 95°.

Podsumowanie

Modyfikacja polilaktydu ziemią okrzemkową i dwoma rodzajami wosków (naturalny, syntetyczny) oraz narażenie tych kompozytów na niekorzystne warunki środowiskowe pozwoliły stwierdzić, że w przypadku badania charakteru hydrofilowo-hydrofobowego kompozytów ziemia okrzemkowa korzystnie wpływała na zachowanie wartości kąta zwilżania po kondycjonowaniu próbek w komorze klimatycznej. *Zaobserwowano również, że dodatek 0,5% wosku pszczelego i syntetycznego powodował wzrost stopnia hydrofobowości powierzchni. Zawartość 1% wosku pszczelego była korzystna z tego punktu widzenia, ale nie odnotowano tak dużego zwiększenia kąta zwilżania. Stąd można podejrzewać, że optymalny dodatek wosku to 0,5% mas. Zaobserwowano również zmiany we właściwościach mechanicznych kompozytów, w tym w elastyczności próbek. Kompozyty wysoko napełnione, bez względu na pochodzenie użytego wosku, cechowały się wzrostem tego parametru po 20-dniowym kondycjonowaniu w komorze klimatycznej, w przeciwieństwie do czystego polilaktydu, gdzie odnotowano zwiększenie sztywności, ale ma również odzwierciedlenie w wartościach wytrzymałości na rozciąganie.

Praca została wsparta finansowo w ramach projektu „Zaawansowane biokompozyty dla gospodarki jutra BIOG-NET", FNP POIR.04.04.00-00-1792/18-00. Projekt realizowany był w ramach programu TEAM-NET Fundacji na rzecz Nauki Polskiej współfinansowanego przez Unię Europejską w ramach Europejskiego Funduszu Rozwoju Regionalnego.

Artykuł jest finansowany przez Narodową Agencję Wymiany Akademickiej w ramach Programu Nowa Partnerstwa Strategiczne w ramach projektu pt. „Zintegrowany system badawczy i dydaktyczny dla wdrożeń technologii przyrodniczych" nr BPI/PST/2021/00092.

Otrzymano: 22-05-2024

LITERATURA

[1] R.P. John, K.M. Nampoothiri, A. Pandey, Proc. Biochem. 2006, **41**, 759.
[2] K.M. Nampoothiri, N.R. Nair, R.P. John, Biores. Technol. 2010, **101**, 8493.
[3] J.-M. Raquez, Y. Habibi, M. Murariu, P. Dubois, Progr. Polymer Sci. 2013, **38**, 1504.
[4] M. Dobrosielska, R. Dobrucka, D. Brząkalski, M. Frydrych, P. Kozera, M. Wieczorek, M. Jałbrzykowski, K.J. Kurzydłowski, R.E. Przekop, Materials 2022, **15**, 3021.
[5] T. Li, H. Sun, B. Wu, H. Han, D. Li, J.-K. Wang, J. Zhang, J. Huang, D. Sun, Mater. Design 2020, **190**, 108603.
[6] F. Carrasco, J. Gamez-Perez, O.O. Santana, M.L. Maspoch, Chem. Eng. J. 2011, **178**, 461.
[7] T. Li, H. Sun, H. Han, C. Zhang, B. Li, J. Huang, D. Sun, Compos. Sci. Technol. 2022, **223**, 109410.
[8] C. Zhang, J. Sun, S. Lyu, Z. Lu, T. Li, Y. Yang, B. Li, H. Han, B. Wu, H. Sun, D. Li, J. Huang, D. Sun, Adv. Compos. Hybrid Mater. 2022, **5**, 1221.
[9] M. Dobrosielska, R. Dobrucka, P. Kozera, D. Brząkalski, E. Gabriel, J. Głowacka, M. Jałbrzykowski, K.J. Kurzydłowski, R.E. Przekop, Sci. Rep. 2023, **13**, 1.
[10] PN-EN ISO 20753:2019-03, Tworzywa sztuczne. Kształtki do badań.
[11] PN-EN ISO 527-1:2020-01, Tworzywa sztuczne. Oznaczanie właściwości mechanicznych przy statycznym rozciąganiu. Cz. 1: Zasady ogólne.
[12] PN-EN ISO 178:2019-06, Tworzywa sztuczne. Oznaczanie właściwości przy zginaniu.
[13] PN-EN ISO 179-1:2023-11, Tworzywa sztuczne. Oznaczanie udarności metodą Charpy'ego. Cz. 1: Nieinstrumentalne badanie udarności.
[14] C. Kopeć, B. Sarl, Appl. Clay Sci. 2016, **121-122**, 36.
[15] B.D. Hirawasu, C. Kopeć, Mater. Today Comm. 2018, **15**, 346.

H10

The Influence of Environmental Factors on the Degradation of PLA/Diatomaceous Earth Composites

Dobrosielska M., Dobrucka R., Brząkalski D., Pajewska-Szmyt M., Kurzydłowski K.J., Przekop R.E.; Polymers, 16, 1450, 2024

polymers

MDPI

Article

The Influence of Environmental Factors on the Degradation of PLA/Diatomaceous Earth Composites

Marta Dobrosielska [1], Renata Dobrucka [2,*], Dariusz Brząkalski [3], Martyna Pajewska-Szmyt [2], Krzysztof J. Kurzydłowski [4] and Robert E. Przekop [3,*]

[1] Faculty of Materials Science and Engineering, Warsaw University of Technology, ul. Wołoska 141, 02-507 Warsaw, Poland; marta.dobrosielska@pw.edu.pl
[2] Department of Non-Food Products Quality and Packaging Development, Institute of Quality Science, Poznań University of Economics and Business, al. Niepodległości 10, 61-875 Poznań, Poland
[3] Centre for Advanced Technologies, Adam Mickiewicz University in Poznań, ul. Uniwersytetu Poznańskiego 10, 61-614 Poznań, Poland; dbrzakalski@gmail.com (D.B.); repszmy@amu.edu.pl (M.P.-S.)
[4] Faculty of Mechanical Engineering, Bialystok University of Technology, ul. Wiejska 45c, 15-351 Białystok, Poland; krzysztof.kurzydlowski@pb.edu.pl
* Correspondence: renata.dobrucka@ue.poznan.pl (R.D.); r.przekop@amu.edu.pl or r.przekop@gmail.com (R.E.P.)

Abstract: In the present study, tests were carried out on composite samples on a polylactide matrix containing 20% by weight of mineral filler in the form of diatomaceous earth, base, and silanized with GPTMOS (3-glycidoxypropyltrimethoxysilane), OTES (n-octyltriethoxysilane), and MTMOS (methyltrimethoxysilane) silanes. The addition of two types of waxes, synthetic polyamide wax and natural beeswax, were used as a factor to increase the rheological properties of the composites. The obtained samples were characterized in terms of the effect of filler silanization on the degradation rate of the composites. The tests were conducted under different conditioning conditions, i.e., after exposure to strong UV radiation for 250 and 500 h, and under natural sunlight for 21 days. The conditioning carried out under natural conditions showed that the modified samples exhibit up to twice the degradation rate of pure polylactide. The addition of synthetic wax to the composites increases the tendency to agglomerate diatomaceous earth, while natural wax has a positive effect on filler dispersion. For composites modified with GPTMOS and OTES silanes, it was noted that the addition of natural wax inhibited the degree of surface degradation, compared to the addition of synthetic wax, while the addition of MTMOS silane caused the opposite effect and samples with natural wax degraded more strongly. It was shown that, despite the high degree of surface degradation, the process does not occur significantly deep into the composite and stops at a certain depth.

Keywords: polylactide; diatomaceous earth; diatomite; silanes; chemical modification; degradation; mechanical properties

check for updates

Citation: Dobrosielska, M.; Dobrucka, R.; Brząkalski, D.; Pajewska-Szmyt, M.; Kurzydłowski, K.J.; Przekop, R.E. The Influence of Environmental Factors on the Degradation of PLA/Diatomaceous Earth Composites. Polymers 2024, 16, 1430. https://doi.org/10.3390/polym16101430

Academic Editor: Hong He

Received: 17 April 2024
Revised: 10 May 2024
Accepted: 18 May 2024
Published: 21 May 2024

Copyright: © 2024 by the authors. Licensee MDPI, Basel, Switzerland. This article is an open access article distributed under the terms and conditions of the Creative Commons Attribution (CC BY) license (https://creativecommons.org/licenses/by/4.0/).

1. Introduction

The weather resistance of composite materials is an important feature from the point of view of the consumer and various industries. The composite should be characterized, depending on the needs of the target group, by an appropriate mechanical strength, including impact resistance or flexibility, a hydrophobic or hydrophilic profile of the surface, or color stability under the influence of environmental factors or the passage of time. Commonly known and used polymers or composites for structural applications are usually petroleum-based, which, due to their production process, makes them harmful to the environment. A good alternative is polymers obtained from monomers synthesized from raw materials obtained from renewable sources, such as polyamide 11 or polylactide. In addition to the environmental aspect, they are also characterized by physicochemical or mechanical properties acceptable for selected applications, especially when combined with suitable

fillers, such as diatomaceous earth [1,2], wood flour [3] or various types of fibers (flax and jute [4], bamboo [5], and beech fibers [6]). Diatomaceous earth alone, as shown in previous works [7–9], can reinforce a composite based on polylactide [10] or polyamide 11, especially if it contains particles of the smallest size [9]. On the other hand, the elimination of these particles results in a composite that does not have adequate mechanical strength compared to the starting polymer [9].

According to the standard adopted by the EU, biodegradable plastic should be converted to carbon dioxide, water, and minerals by more than 90% in a maximum of six months. The biodegradation of polylactide itself takes place under biological conditions with the participation of fungal or algal bacteria, which use the polymer as a food source [11]. Biodegradable polymers should remain unchanged for the lifetime of the polymer, and then biodegrade. The degradation process of PLA itself begins at the surface of the polymer, and then occurs throughout the plastic. PLA can undergo photodegradation, thermal degradation, oxidative degradation, bacterial degradation, enzymatic degradation, and hydrolytic degradation, but, usually, scientific work focuses on the last two modes [12]. The process of hydrolytic degradation can occur under the influence of not only water, but also aqueous acetonitrile solutions, aqueous alcohol solutions, or alcohols (alcoholysis) [13–15]. During hydrolysis, the ester groups of the polymer chain are broken down, the polymer being converted into soluble oligomers and monomers, and the ester bonds are fragmented, leading to a decrease in the average molecular weight of the polymer [16].

In addition to atmospheric precipitation, which contributes to hydrolytic degradation, polylactide in structural applications is exposed to ultraviolet radiation, which is destructive to any organic material, which, in turn, starts the process of photolytic degradation, which, in turn, contributes to the cracking of the material or color change, which negatively affects the visual aspects [17,18]. Diatomaceous earth has been proven to increase the degradation rate of a polylactide-based composite [19]. Therefore, in the present work, we have attempted to develop a composite based on polylactide and silanized diatomaceous earth, resistant to both hydrolytic and photolytic degradation. From the point of view of ecology, the deliberate pursuit of a short life of the composite or polymer and rapid degradation under natural conditions is not beneficial due to the energy consumption in the production of the product or, despite the use of biocomposites, environmental pollution by the products of their decomposition, especially carbon dioxide. For this reason, attempts to produce a composite for structural applications appear to address the need to reduce the carbon footprint and pursue the concept of a circular economy, and could potentially contribute to reducing global warming by reducing CO_2 emissions into the atmosphere. To this end, polylactide-based composites filled with silanized diatomaceous earth were fabricated, and then aged under simulated (UV-aging chamber) and natural conditions for an appropriate period of time. After conditioning, among other things, the degree and depth of degradation of the composites were examined, and visual tests were carried out, including the study of color change under UV light. Various methods of degradation of composites, both laboratory and natural, are described in the literature. Polylactide matrix composites modified with mineral fillers have been conditioned under natural conditions in acidic soil [19], abiotic hydrolysis, biotic degradation, and composting conditions in a laboratory environment [20] or under conventional weathering conditions [21]. The degradation conditions we proposed combine both simulated and natural conditions, which allowed us to study the influence of photolytic and hydrolytic factors on the degradation of polylactide. As for the application in research on diatomaceous earth polylactic acid composites, they are in early development. The aim of our research was the impact of the weather conditions on the material. The aim of our research is to develop polylactide-based composites for use in products that do not come into contact with food. Most of the research focuses on the use of PLA in packaging. However, we see a problem related to plastic elements that are used as elements of, for example, textiles and clothes—buttons, clothes zippers, and other small elements used in home interiors, e.g., switches, and kitchen elements—which can be unintentionally or consciously transferred to the environment. The developed material

is, therefore, supposed to have good design features during its use and be characterized by rapid degradation when released into the environment. However, we believe that the development of a material that, if accidentally released into the environment, can degrade more quickly and harmlessly may be important. Moreover, we wanted to test whether polylactide could degrade faster under environmental conditions without the participation of bacteria or composting conditions.

2. Materials and Methods

2.1. Materials

Polylactide (PLA)-type Ingeo 4043D was purchased from NatureWorks (Minnetonka, Minneapolis, MN, USA). Diatomaceous earth (Perma-Guard, Bountiful, UT, USA) was derived from diatomite deposits. Synthetic wax WTH-B microbeads (behenamide, $CH_3(CH_2)_{19}CONH_2$) were bought from WTH GmbH (Hamburg, Germany). Beeswax was derived from Spółdzielnia Pszczelarska APIS (Lublin, Germany). Silanes GPTMOS (3-glycydoksypropylotrimetoksysilan) OTES (n-oktylotrietoksysilan) and MTMOS (metylotrimetoksysilan) were purchased from Sigma-Aldrich (Saint Louis, MO, USA).

2.2. Preparation of Modified Diatomaceous Earth

First, 1 kg of diatomaceous earth was placed in a 20 L glass reactor equipped with a mechanical stirrer. Then, 4 L of IPrOH, 10 mL of demineralized water and 1% w/w of the appropriate silane (GPTMOS, OTES, MTMOS) were added to the reactor and left for two hours with constant stirring (300 rpm). After 2 h, 10 mL of concentrated hydrochloric acid (HCl) was added in portions. After 24 h of continuous stirring, the mixture was transferred to a separate container and left to settle. After pouring off the liquid from the sediment, the diatomaceous earth was washed with demineralized water and placed in an oven at 60 °C for 24 h. The silanes used for modification were GPTMOS (3-glycodoxypropyltrimethoxysilane), OTES (n-octyltriethoxysilane), and MTMOS (methyltrimethoxysilane).

2.3. Preparation of Granulates

PLA-based composites were prepared using a ZAMAK MERCATOR WG 150/200 laboratory rolling mill (Skawina, Poland). For this purpose, 250 g of PLA 4043D Ingeo at 210 °C was mixed together with 250 g of modified or base diatomaceous earth and 2 or 4% by weight of natural (beeswax) or synthetic (WTH-B) wax, respectively. The process was carried out until homogeneous mixtures were obtained. The resulting systems were then ground using a WANNER C17.26 sr mill and dried for 24 h at 60 °C. Systems containing unmodified diatomaceous earth were also prepared.

2.4. Preparation of Samples for Measurements

The samples were diluted 1:1 with PLA directly in the injection molding machine. Table 1 shows the process parameters. A holding pressure of linear increment over 9 s time was applied. The mold temperature was maintained at 80 °C. Standardized molds for mechanical testing in accordance with PN-EN ISO 20753:2019-01 [22] were obtained. The final concentrations of the systems are shown in Table 2.

Table 1. Injection molding process parameters.

Temperature [°C]	Mold	Die	Zone 3	Zone 2	Zone 1	Feed
	80	190	195	200	185	40
Holding pressure			t [s]	0.0	9.0	
			P [bar]	500	1500	
Clamping force [kN]		Holding time [s]	Cooling time [s]	Screw diameter [mm]		
400		9.0	50.0	25.0		

Table 2. The prepared, injection-molded composite systems.

Full Name	*Short Name*
PLA	PLA
PLA/DE	B
PLA/DE + 1% wt. SW	B/1S
PLA/DE + 2% wt. SW	B/2S
PLA/DE + 1% wt. NW	B/1N
PLA/DE + 2% wt. NW	B/2N
PLA/DE + 1% wt. GPTMOS + 1% wt. SW	G/1S
PLA/DE + 1% wt. GPTMOS + 2% wt. SW	G/2S
PLA/DE + 1% wt. GPTMOS + 1% wt. NW	G/1N
PLA/DE + 1% wt. GPTMOS + 2% wt. NW	G/2N
PLA/DE + 1% wt. OTES + 1% wt. SW	O/1S
PLA/DE + 1% wt. OTES + 2% wt. SW	O/2S
PLA/DE + 1% wt. OTES + 1% wt. NW	O/1N
PLA/DE + 1% wt. OTES + 2% wt. NW	O/2N
PLA/DE + 1% wt. MTMOS + 1% wt. SW	M/1S
PLA/DE + 1% wt. MTMOS + 2% wt. SW	M/2S
PLA/DE + 1% wt. MTMOS + 1% wt. NW	M/1N
PLA/DE + 1% wt. MTMOS + 2% wt. NW	M/2N

DE—dolomite rare earth; PLA/DE—PLA + 25% wt. DE; SW—synthetic wax; NW—natural wax; GPTMOS—3-glycidoxypropyltrimethoxysilane; OTES—octyltriethoxysilane; MTMOS—methyltrimethoxysilane.

2.5. Characterization Methods

For tensile strength test, the materials obtained were injection-molded as type 1B dumbbell specimens in accordance with EN ISO 527:2012 [23] and EN ISO 178:2006 [24]. Tests of the obtained specimens were performed on a universal testing machine INSTRON 5969 (Norwood, MA, USA) with a maximum load force of 50 kN. The traverse speed for tensile strength measurements was set at 2 mm/min. Seven samples of each type were tested. Color change (ΔE) was measured using an NR60CP colorimeter in 8°/d geometry, SCI. The difference between two colors in CIELab space was calculated using the formula:

$$\Delta E = \sqrt{(\Delta L)^2 + (\Delta a)^2 + (\Delta b)^2}$$

where $\Delta L = L_1 - L_2$; $\Delta a = a_1 - a_2$; and $\Delta b = b_1 - b_2$.

Gel permeation chromatography was performed using an Agilent Technologies 1260 liquid chromatograph equipped with a refractive index detector. The mobile phase was tetrahydrofuran (THF), while the stationary phase was Phenogel 10 μ Linear(2) 300 × 7.8 mm (100–10,000,000 g/mol). A flow rate of 1 mL/min was used, the column was maintained at 35 °C, and a polystyrene standard (MW range—1310–3,640,000 g/mol) was used to prepare a standard curve. The sample for GPC testing was taken by scraping a layer of investigating material with a cutter and weighing 10–13 mg in glass vial. Next, the samples were suspended in tetrahydrofuran (THF), ultrasonicated at 35 °C until dissolved, and then filtered through a 0.2 μm-pore-size filter. The degradation degree was calculated from the changes in M_w parameter. Images of composite surfaces and fractures were taken using a KEYENCE VHX-7000 digital microscope (Keyence International NV/SA, Osaka, Japan) with a VH-Z100R wide-angle zoom lens with 100× and 1000× magnification. The images were taken using the depth composition and 3D image creation functions. Total coaxial illumination was used.

Composite conditioning was carried out in an Atlas UV Test aging chamber with 313 nm UV-B fluorescent lamps. The test was performed in accordance with ISO 4892-3 [25], test cycle 2 according to ASTM G154 [26], and PN-EN ISO 16474-3 [27]:

- UV irradiation—intensity of radiation 0.71 W/m^2, 60 °C—4 h (light segment);
- condensation 50 °C—4 h (dark segment).

Aging test was conducted for 250 and 500 h.

Samples for aging tests in the UV chamber were placed in custom-made holders, measuring 66 × 98 mm, printed from PET using FDM 3D printing. The holder has 12 spots measuring 20.0 × 23.0 × 6.4 mm. The wall thickness between the sample spots is 1.8 mm. A photo of the holder is shown in Figure 1. The composite samples were prepared in the form of cubes with dimensions corresponding to those of the spots available in the holder.

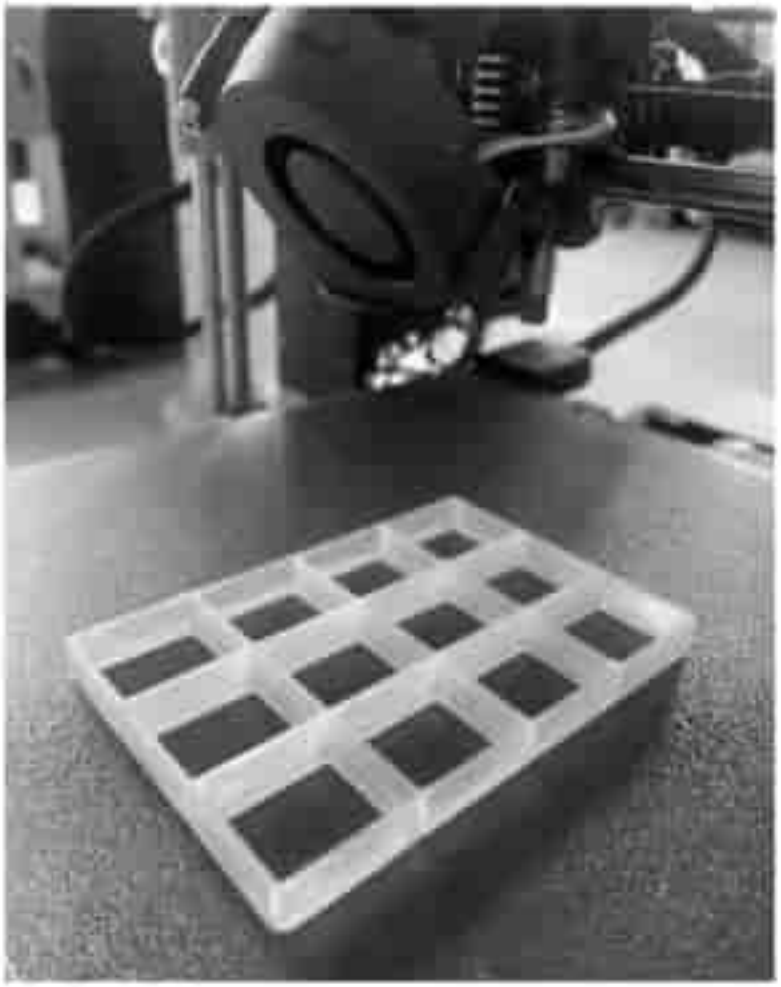

Figure 1. UV-aging sample holder.

Conditioning under natural sunlight was carried out from 15 June 2021 to 6 July 2021, for a total of 21 days (~500 h). The composite samples were placed in an unshaded location. Measurement data of weather conditions occurring during the conditioning of the samples were obtained from the meteorological station Poznań-Ławica with geographical co-ordinates 52°25′ 16°50′. Meteorological data are presented as follows: average daily air temperature, and maximum and minimum daily air temperature, are summarized in Figure 2A; average daily cloud cover, average daily wind speed, average daily rainfall, and number of hours of sunshine are summarized in Figure 2B; average UV index is summarized in Figure 2C; and average monthly humidity and average atmospheric pressure are presented in Figure 2D.

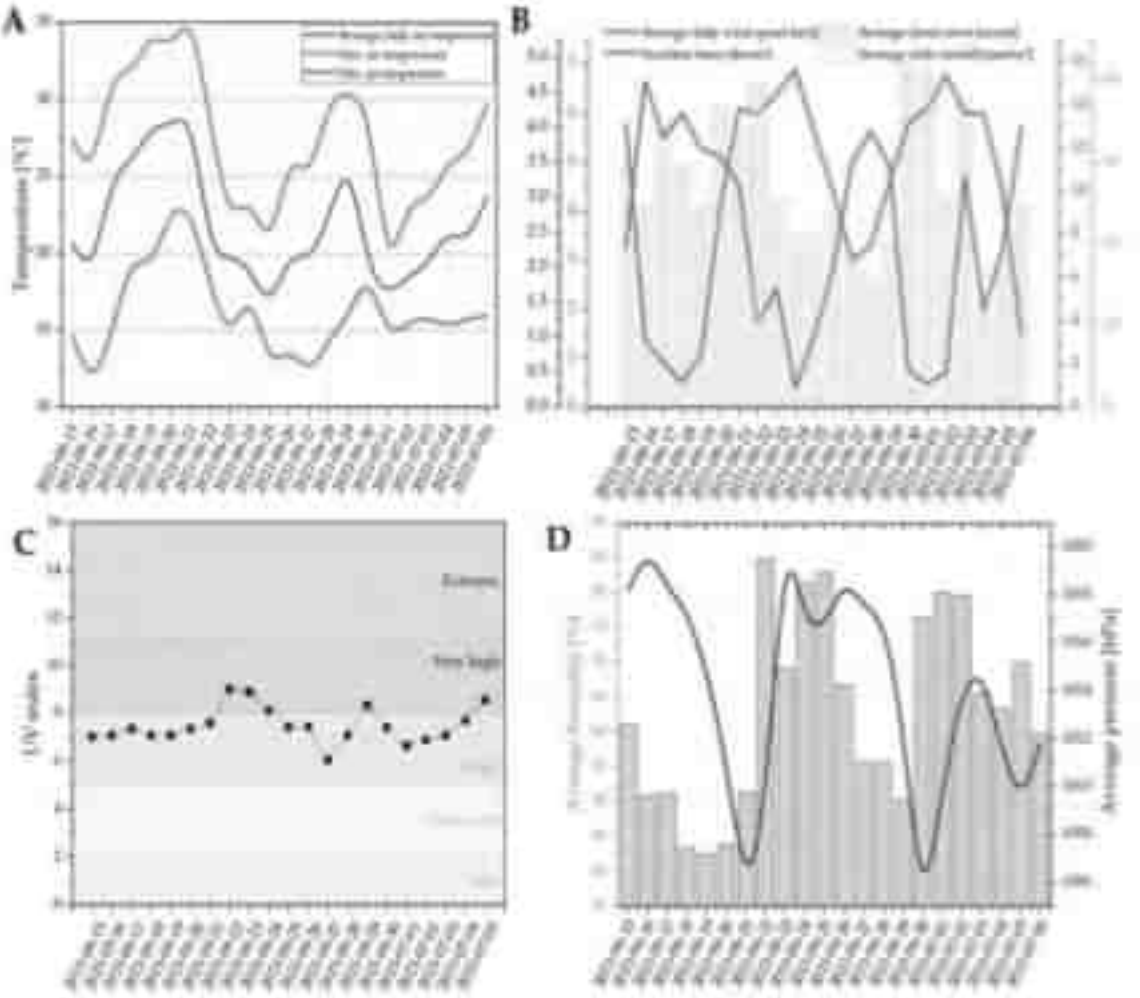

Figure 2. Average daily air temperature, and maximum air temperature and minimum air temperature (A); average daily wind speed, average cloud cover, sunshine hours, and average daily rainfall (B); UV index (C); and average humidity and average pressure (D) between 15 June 2023 and 6 July 2023.

3. Results

3.1. Mechanical Tests

Tensile strength tests were conducted on samples aged under natural conditions. After 21 days, the tests showed a slight decrease in both tensile strength and elongation at tension for all analyzed samples, including pure polylactide (Figure 3). The use of synthetic wax in composites with DE-silanized OTES and GPTES resulted in a decrease in the strength of the composites, indicating the limited compatibility of the filler prepared in this way with the wax. The effect of the compatibility of synthetic and natural waxes with diatomaceous earth subjected to surface modification with various silane coupling agents was discussed in detail in an earlier paper [26]. This work is a continuation of the previous paper. The decrease in mechanical strength is related to the degradation of neat PLA present in each analyzed system and comparable for most systems; however, the lowest is for composites with synthetic wax in combination with the silanized filler, indicating the greatest stability of the systems, probably due to the combined effects of the presence of a well-dispersed filler as a UV blocker and hydrophobic wax stopping the composite from moisture diffusion. On the other hand, the mentioned systems provided the poorest mechanical properties as received, showing the limited compatibility of synthetic wax with

the remaining components, especially the PLA matrix, as proven by the previous study [29]. Moreover, the polymer degradation occurs mostly in the near-surface region, which is further explained in the following sections (see Sections 3.2 and 3.4). The elongation at break was similar for most of the composites and was reduced in comparison to neat PLA due to the presence of the particulate filler.

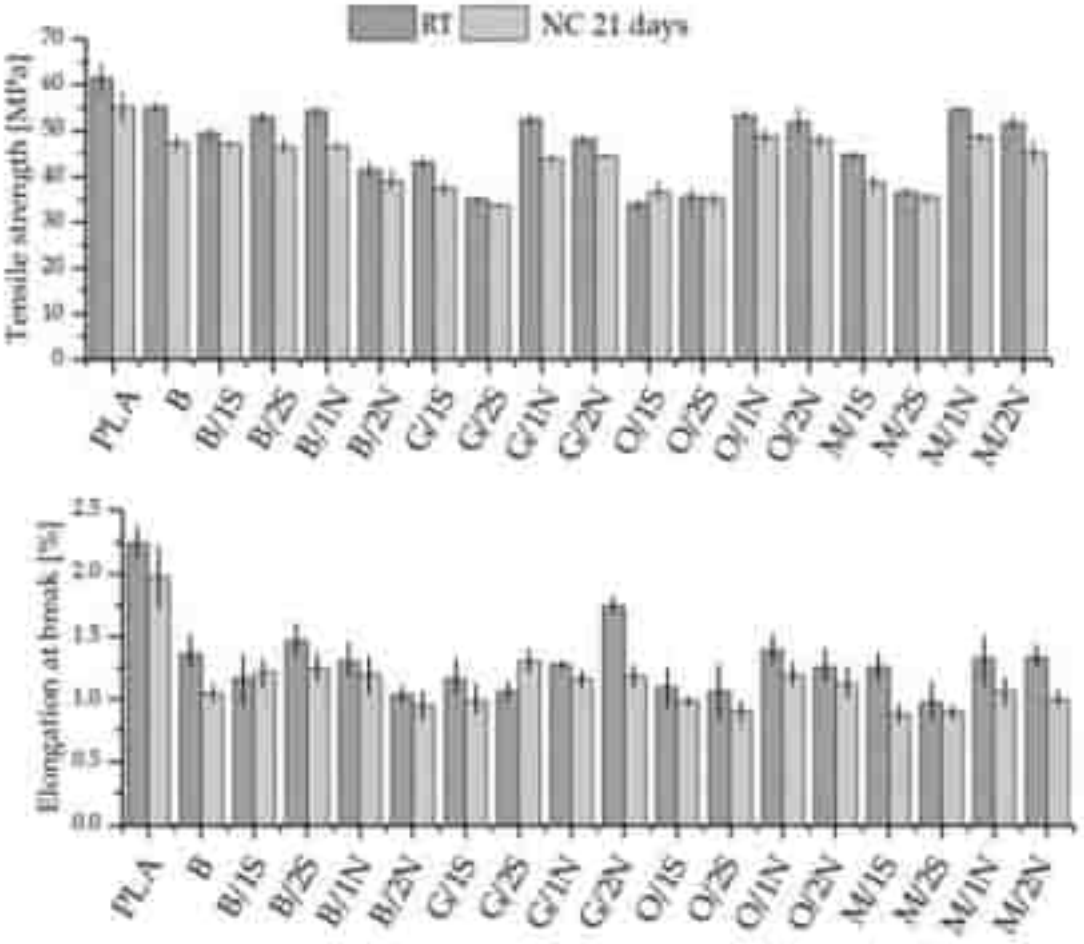

Figure 5. Tensile strength and elongation at break of the composites in as-received state and after aging under natural conditions.

3.2. Degradation of PLA Macromolecular Structure

Degradation tests were carried out for both the composite samples placed in the UV-aging chamber and the samples exposed to natural weathering for 21 days. The analysis was performed on the outer layer of the composite, as both a mechanical analysis (see Section 3.1) and a microscopy analysis (see Section 3.4) provided the evidence on the polymer degradation occurring mostly on the near-surface layer. The polymer degradation was studied on the basis of the number average (Mn) and weight average (Mw) molecular weight (Table 3). Samples for GPC were collected from the surface of the sample oriented toward sunlight. The addition of the filler, as well as the use of processing additives, increased the degradation of the polymer, as can be observed from the MWD mass distribution curves (Figure 6), where the individual curves shift to the left relative to the reference sample, as well as in the designated degradation degree (Figure 7). For the PLA sample without modifiers, the degradation was 20.7%, 35.9%, and 58.5% for samples subjected to accelerated aging after 250 h and 500 h and during natural exposure, respectively. Modifications of the polymer increased the degradation of the samples, however, without any correlation

between the exposure conditions. The highest percentage of chain degradation occurred for sample G/25, i.e., 79.8%, after UV-500h exposure.

Table 3. Summary of the molecular weights of the polymers tested and the calculated percentage of degradation.

Sample Name	Mn (250 h)	Mn (500 h)	Mn (NC)	Mw (250 h)	Mw (500 h)	Mw (NC)	%Degradation 250 h [M]	%Degradation 500 h [M]	%Degradation NC [M]
PLA	82,600	55,100	26,000	149,500	126,000	84,100	20.7	34.9	59.5
S	27,000	17,600	25,800	63,700	96,000	105,800	50.4	65.9	68.9
B/1S	71,400	46,900	33,600	134,400	109,900	109,400	37.8	45.3	66.5
B/2S	80,900	36,500	36,900	93,700	81,200	143,000	49.9	58.1	29.6
B/1N	85,100	36,400	38,500	94,800	82,800	9100	49.4	57.2	95.3
B/2N	43,100	36,300	31,300	95,600	82,860	116,300	46.8	57.2	42.6
G/1S	47,300	20,600	44,300	98,300	52,500	133,100	47.5	72.9	36.2
G/2S	35,100	36,400	45,700	90,500	30,200	119,000	31.6	79.8	41.3
G/1N	43,000	20,900	39,700	82,600	64,600	88,100	35.9	66.5	55.5
G/2N	33,300	31,000	19,400	70,300	74,000	56,600	45.8	62.5	72.1
O/1S	28,600	22,300	27,700	65,400	54,700	110,300	43.1	71.8	45.5
O/2S	35,000	25,100	17,500	74,600	54,900	103,800	40.1	71.6	66.7
O/1N	47,200	30,600	45,700	109,400	75,300	121,000	41.5	63.0	40.3
O/2N	61,100	27,300	75,000	90,800	74,000	146,100	33.5	62.3	27.9
M/1S	29,100	19,600	67,400	73,300	53,600	111,400	40.9	72.5	65.0
M/2S	24,500	17,600	42,000	58,600	32,500	143,900	68.6	72.7	29.6
M/1N	25,600	22,500	39,200	60,900	56,300	118,700	67.5	70.9	41.4
M/2N	44,300	24,500	43,100	103,300	72,600	120,400	65.9	62.5	40.2

NC—natural conditions; 250 h, 500 h—UV chamber; Mn—number average molecular weight; Mw—average molecular weight. [M]—degradation % calculated from Mw change.

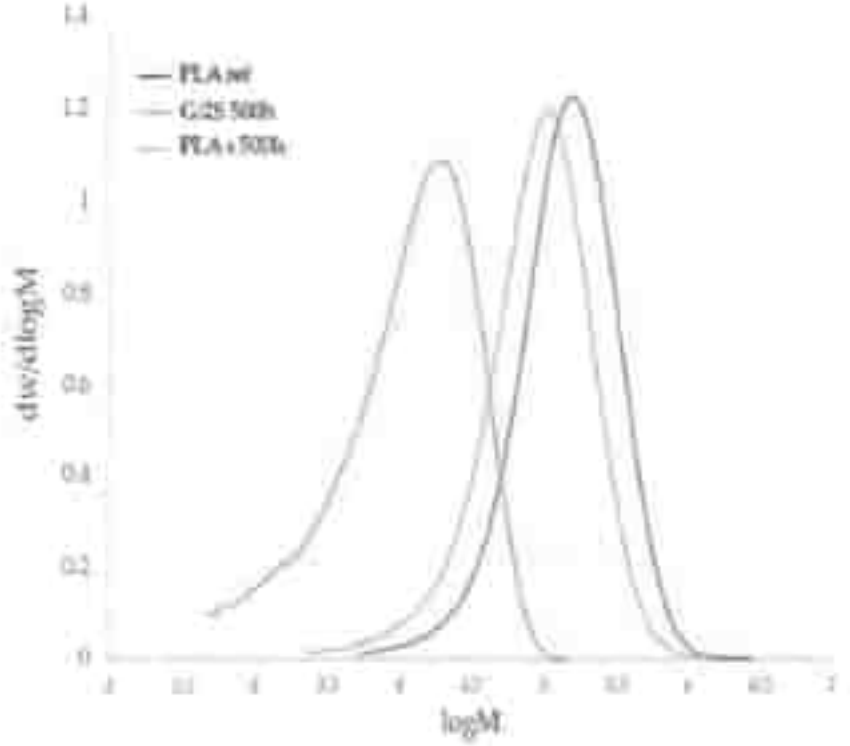

Figure 4. MWD curve of polylactide conditioned at room temperature and at 500 h in an aging chamber and G/2S-modified composite conditioned at 500 h in an aging chamber.

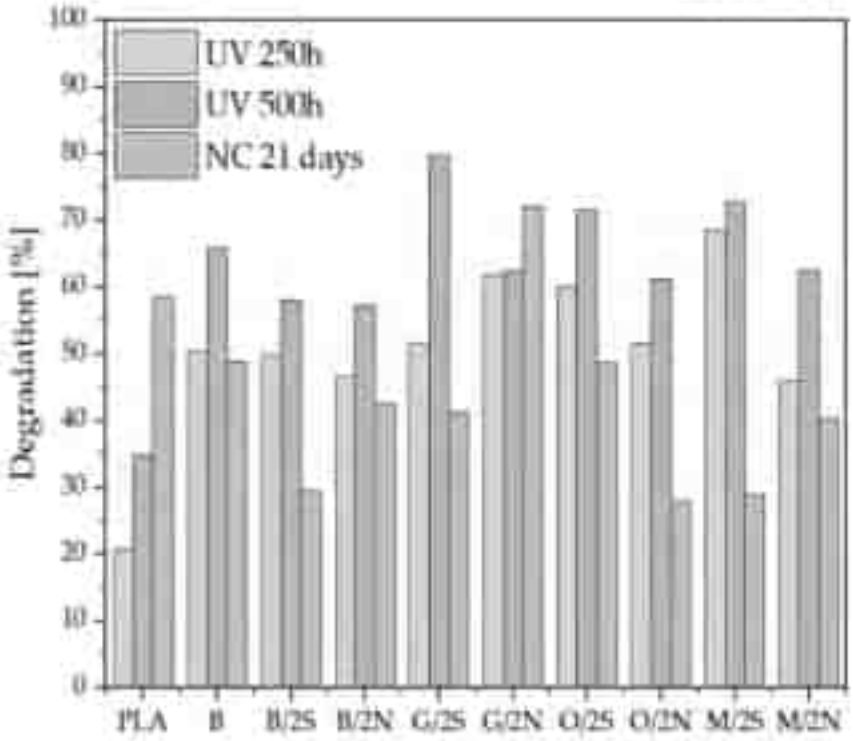

Figure 8. Determined chain degradation for the polymer samples tested.

Neat polylactide degraded progressively over time after aging in a UV chamber (20.7% and 34.9% after 250 h and 500 h, respectively), and degraded 58.5% after conditioning under natural conditions. The modified composites for each test time degraded more under controlled conditions than the reference PLA, both with the addition of neat diatomaceous earth and diatomaceous earth (base or silanized) in combination with waxes. Under natural conditions, the differences between the degradation of neat PLA and the composites, as well as between individual composites, were characterized by too much statistical scatter to show a significant effect of fillers and waxes on the stability of the materials under natural conditions. The factors influencing the observed differences are threefold: First, the samples in the UV chamber are subjected to aging under standardized radiation and humidity conditions. Secondly, in the UV chamber, the samples are subjected to moisture during the aging cycle, during the dark condensation segment. The contribution of moisture significantly accelerates the plastic degradation process [30]. Finally, under the natural aging conditions, the UV irradiation is of a wide range, while, under the simulated conditions, it is provided by UV-B 313 nm lamps. Under natural conditions, the UV index was oscillating around 8 for most of the experiment, as taken from the meteorological data provided, which is considered to be an equivalent of 0.2 W/m^2 of biologically effective UV irradiance; however, it depends on the calculation model and, therefore, cannot be simply compared to the total UV irradiance [31,32]. The last effect may also explain the significantly higher degradation of neat PLA under natural conditions when compared to the simulated ones. The above results suggest that the modification decreased the stability of the composites in an environment with a high proportion of moisture acting as a hydrolytic agent. This is related to the increased porosity of the material, introduced by the filler, which leads to the accelerated diffusion of water in the polymer and increases the contact area of water with the polymer phase. The addition of waxes, especially the synthetic one, slightly caused a decrease in the degradation of the polymer under natural conditions, which is related to the hydrophobicizing effect and the improved dispersion of the filler, translating into its effectiveness as a physical UV blocker. Under simulated conditions, on the other hand, it was noted for systems containing 2% wax that, each time,

the synthetic was caused a higher level of PLA degradation than the natural was in the corresponding system. This was due to the high proportion of moisture and radiation intensity, leading to the degradation and elimination of wax from the composite structure.

Based on the Mw/Mn ratio, the dispersity index (D, Figure 6), a measure of polymer chain length inhomogeneity, was determined. For the reference sample, it is about 1.95, while there is an increase in the index for samples subjected to UV and natural exposure, due to polymer chain breakage at statistically random locations. A significant increase in PDI for samples aged under natural conditions is noticeable. This is related to the occurrence of a less efficient mechanism of polymer degradation under environmental conditions. Under simulated conditions, the mechanism of polymer chain degradation involves water, which, in the form of water vapor and moisture, is able to penetrate the pores of the material and permeate the filler phase and diffuse through the amorphous phase of PLA [31], especially at an elevated test temperature (60 °C), resulting in the degradation of the composite in its depth and, thus, averaging the degree of degradation over the thickness of the sample, at a time when, under relatively dry conditions (natural conditions), the material is mainly exposed to UV radiation, which is retained by the filler acting as a UV blocker.

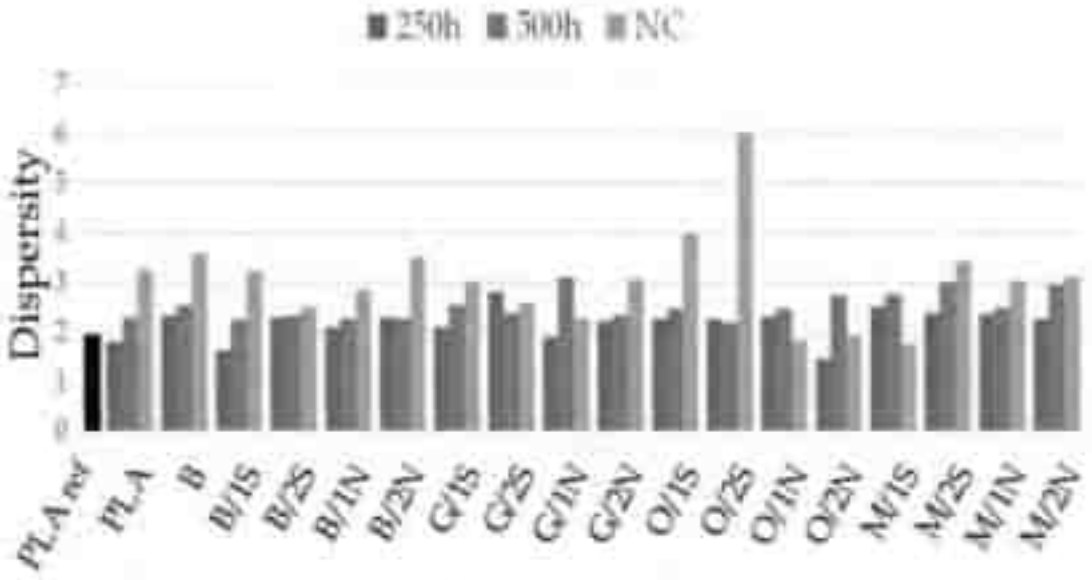

Figure 6. Determined dispersity index (D) for the tested samples, after different aging periods.

In the samples obtained from the aging of the composites, an additional peak (Figure 7) was observed at both 250 h and 500 h of degradation. It is suspected that its presence is related to the diatomaceous earth used for modification. Diatomaceous earth has particles in a wide size range, as illustrated in Figure 8. The DLS analysis of the filler used to prepare the PLA composites allowed the detection of particles with sizes whose lower size range was ~0.3 µm. The samples of aged composites were, after dissolution in THF, filtered through a membrane filter with a pore diameter of 0.2 µm. Considering the processing, which can lead to the crushing of filler particles, it can be suspected that the presence of the aforementioned peak is related to the content of particles with sizes below 0.2 µm. Magaletti and co-workers observed with GPC analyses of samples marine diatom *Cylindrotheca fusiformis* low-molecular-weight peaks (low-molecular-weight peaks) of exopolysaccharides, and it can also be suspected that the emerging peak (tR 11.7 min) may be related to compounds from the polysaccharide group released from diatoms [31].

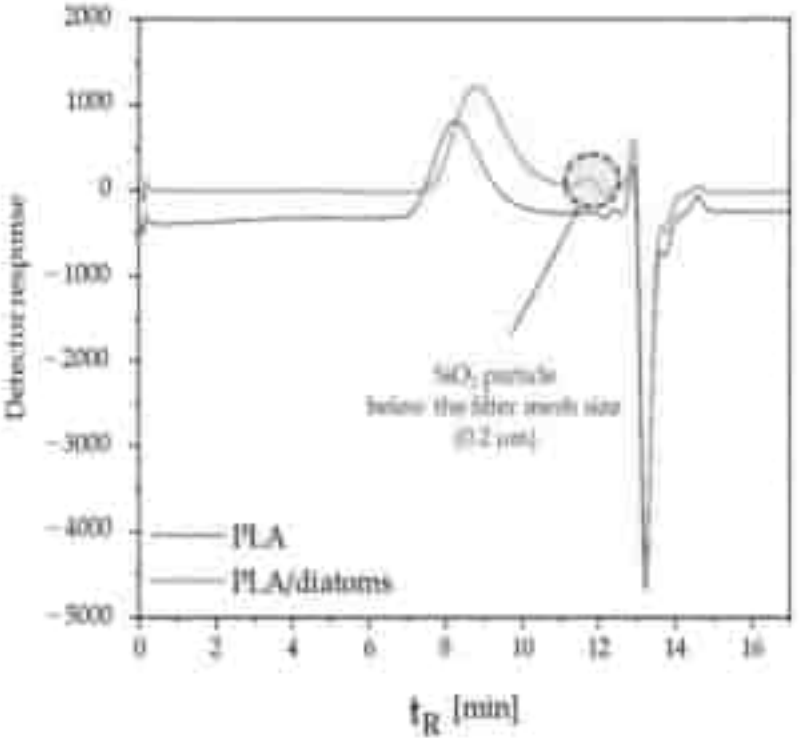

Figure 7. GPC-RI analysis for PLA sample without additive and with addition of diatomaceous earth.

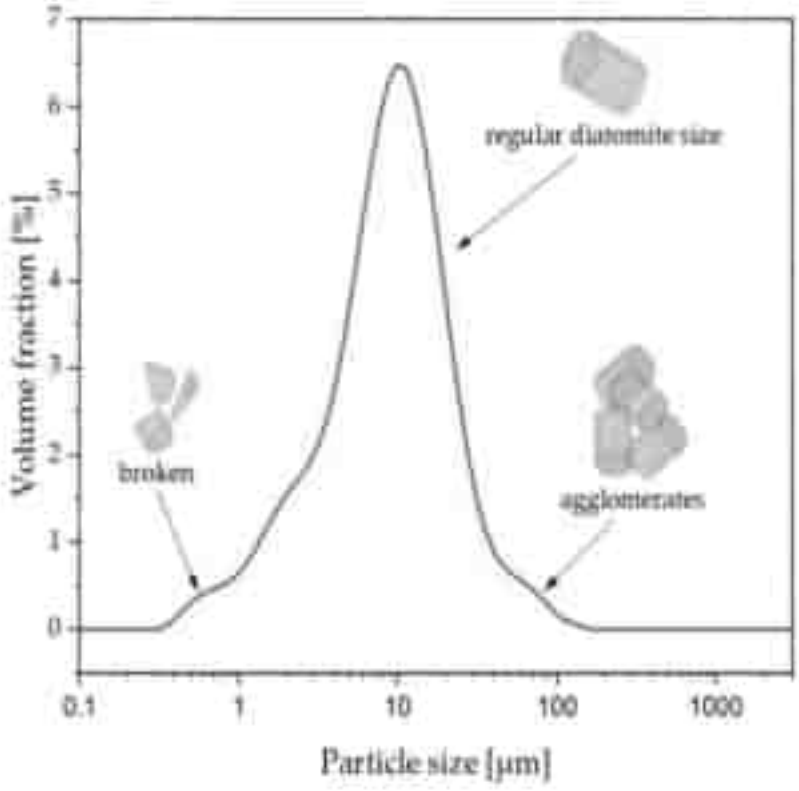

Figure 8. Particle size distribution of diatomaceous earth.

3.3. Color Testing after UV Irradiation

Figure 8 shows the differences in color (ΔE) of the different composites after exposure to both UV radiation and natural environmental conditions (NC). The color change was measured against baseline samples conditioned under room conditions. Significant and noticeable color changes were observed for all systems. Note that a color change according to the CIELAB color space scale, exceeding a value of 5, indicates a change that is significant and visible to the naked eye. The smallest color differences were observed for systems conditioned under natural sunlight, except for pure polylactide, for which ΔE was as high as ~25 (Figure 9). Compared to baseline PLA, systems filled with diatomaceous earth with the addition of synthetic wax showed improved color stability under natural conditions, while worse under simulated conditions. Natural wax caused a stronger color change with aging than synthetic wax, especially under natural conditions. Silanization of diatomaceous earth, especially OTES, led to an intensification of the color change effect, which may be explained by a reduction in wax concentration in the filler-polymer interphase and its easier migration to the plastic surface. An increase in the L parameter (CIELab method) indicates an increase in brightness of the material. In the case of the analyzed samples, the change in color each time consists in the discoloration of the sample under the influence of sunlight and a change to a whiter color. Considering the samples conditioned in the UV chamber for 250 h and 500 h, the color change for composites filled with diatomaceous earth is expected, i.e., the longer the time spent in sunlight, the greater the change in the L parameter (Figure 10). No significant differences were found between the systems, either due to the type of silane used or the type of wax and its concentration. The largest color change toward white was observed for the composites after 500 h in the UV chamber (L in the range of 80–90), while after 21 days under natural conditions, the swap is much smaller, as the L parameter is around 60.

Depending on the type of silane used or the type and concentration of the rheological agent (wax), the composites are characterized by differences in color (Figure 11), which was also found in colorimetric studies (Figures 9 and 10). After conditioning the composites for 250 h in a UV chamber, their surface became visually bleached. Conditioning for 500 h in a UV chamber the effect deepened, a stronger bleaching of the surface was visible, however visual inspection did not confirm the presence of cracks or other defects. The pure polylactide, initially transparent, became dull and slightly yellowed under UV irradiation. The energy transferred to the sample by means of heat and UV irradiation, as well as degradation-induced decrease in the average molecular weight may induce amorphous PLA phase crystallization and thus increase of crystalline phase content, especially near the sample surface, resulting in the sample opacity. The effects of PLA crystallinity during degradation have been discussed by others [34,35].

3.4. Microscopy Analysis of the Composites' Structure after UV Irradiation

An analysis of the composites before the exposure to degradation agents confirmed the homogeneous structure of their surfaces (Figures 12 and 13); no defects in the structure are noticeable. Placing the composites in the UV chamber for as short a time as 250 h caused both the transformation of the PLA matrix (most likely the crystallization mentioned earlier) and the migration of the wax on the surface of the samples, especially for all composites modified with natural wax, which is visible in the form of white, uneven discoloration on the surface of the composite. For samples containing synthetic wax, the effects of wax migration were negligible, with discoloration caused by changes in the PLA matrix. On the surface of pure PLA, after an identical time spent in the aging chamber, fine cracks are visible, which did not occur on the surface of the composites. Its further exposure to unfavorable conditions increased the cracks formed earlier and significant defects were observed in the structure. The synthetic wax-modified composites behaved similarly. The G/25, O/25, and M/25 systems are characterized by significant surface cracks, while, in the case of the silanized filler GPTMOS and OTES, analogous samples containing beeswax have no cracks and their surface is smooth with no visible defects. Regarding

the GPC analysis of the material from the surface of the composites, the aforementioned systems with synthetic wax were, each time, characterized by a higher degradation rate than those with natural wax, which indicates the differences in the degradation rate of these composites and the lack of effect of the synthetic wax protecting the composite surface from degradation.

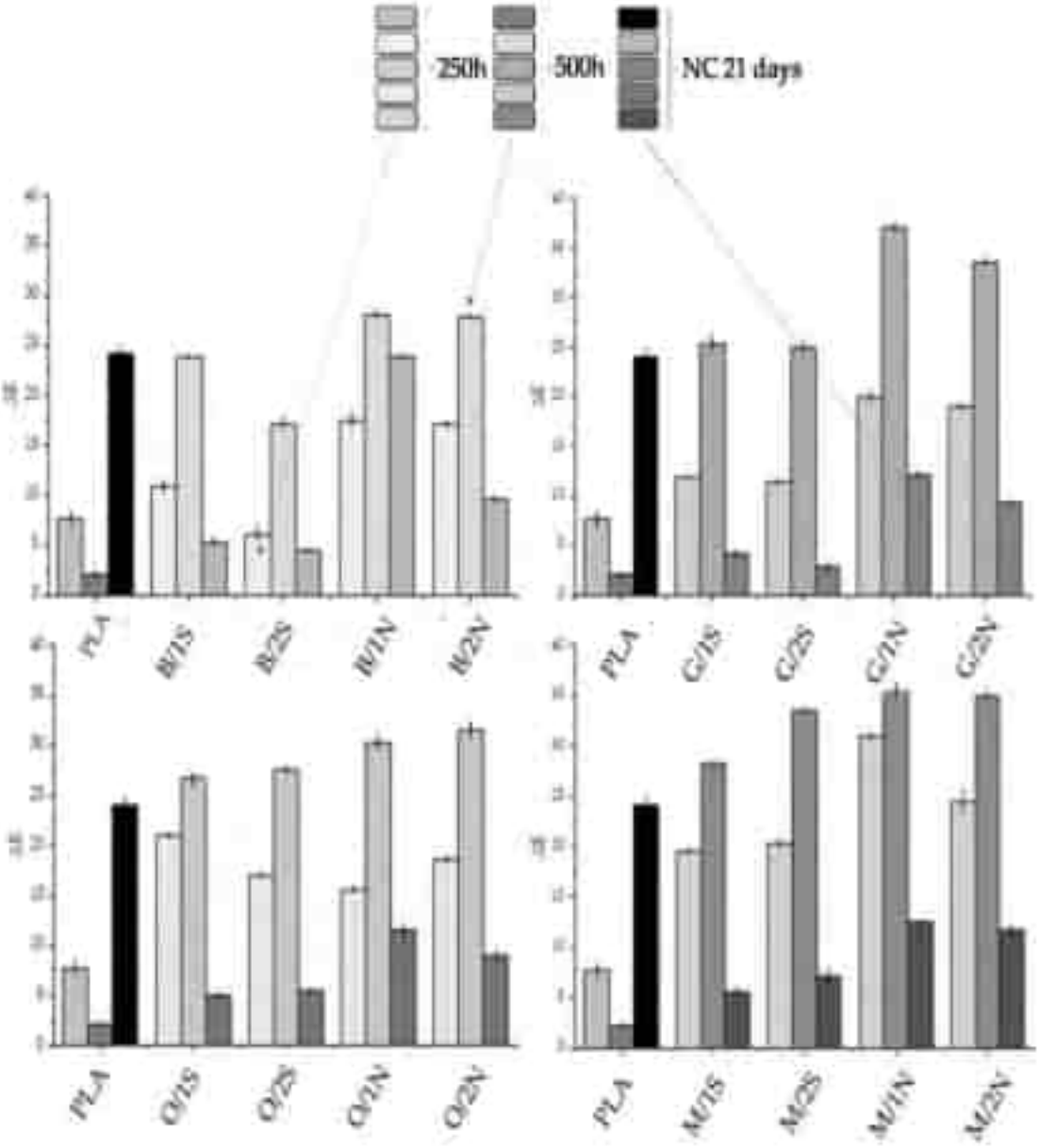

Figure 9. Differences in color of composites conditioned in an aging chamber for 250 and 500 h and under natural conditions.

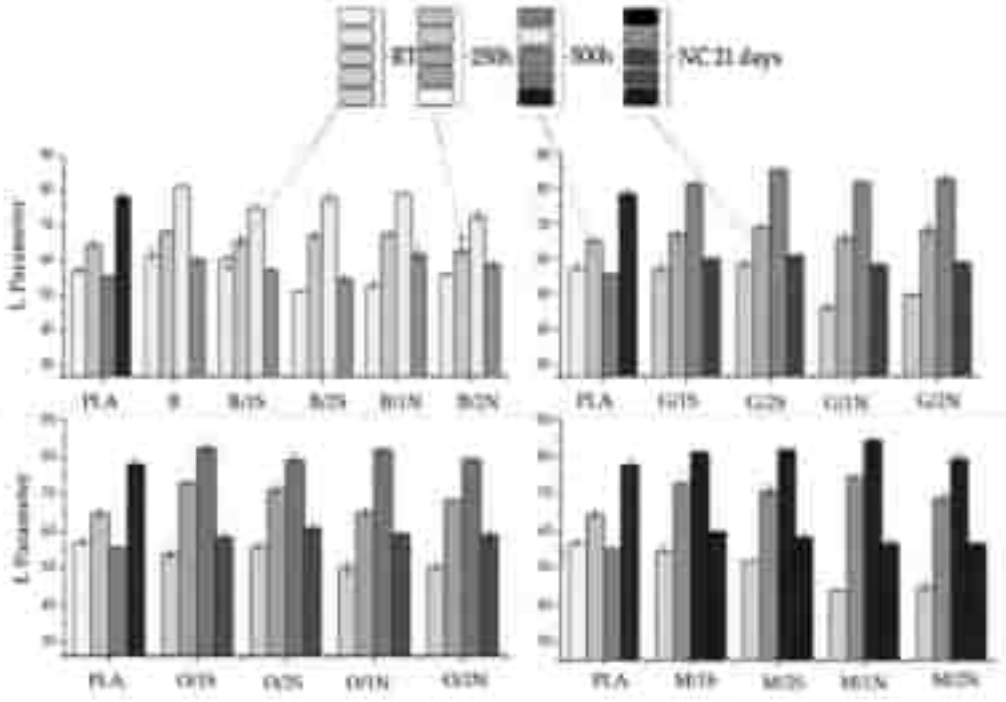

Figure 10. Luminance of composites conditioned in an aging chamber for 250 and 500 h and under natural conditions.

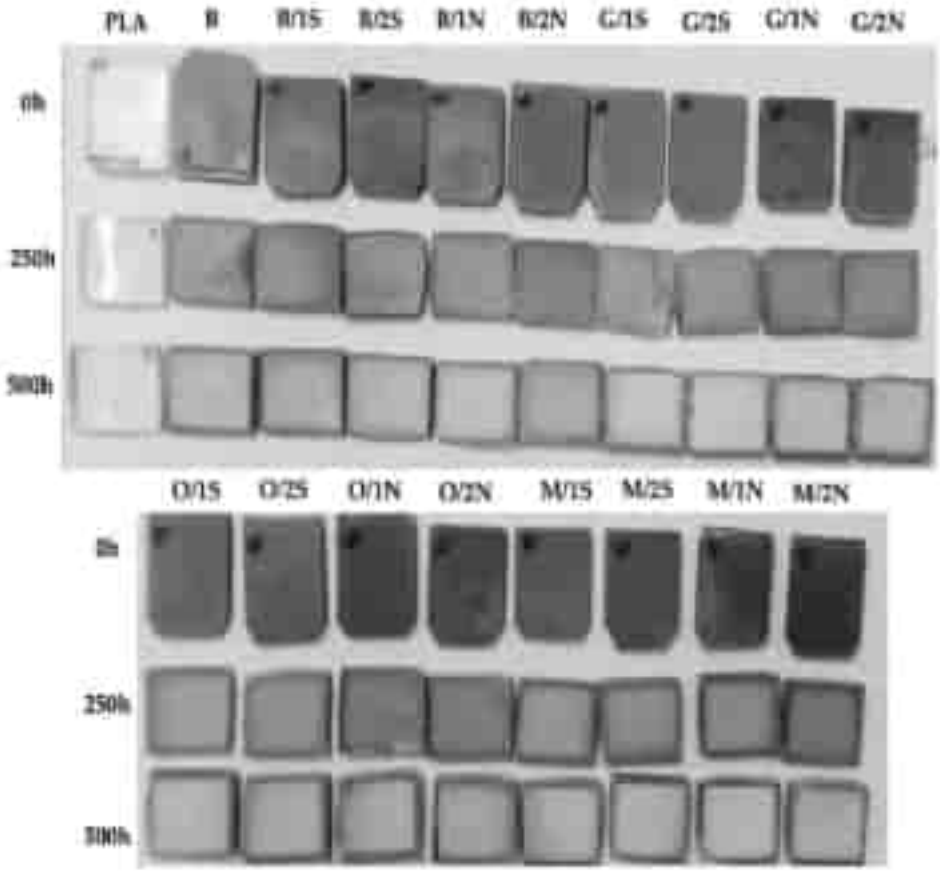

Figure 11. Composites before and after conditioning in a UV-aging chamber for 250 and 500 h.

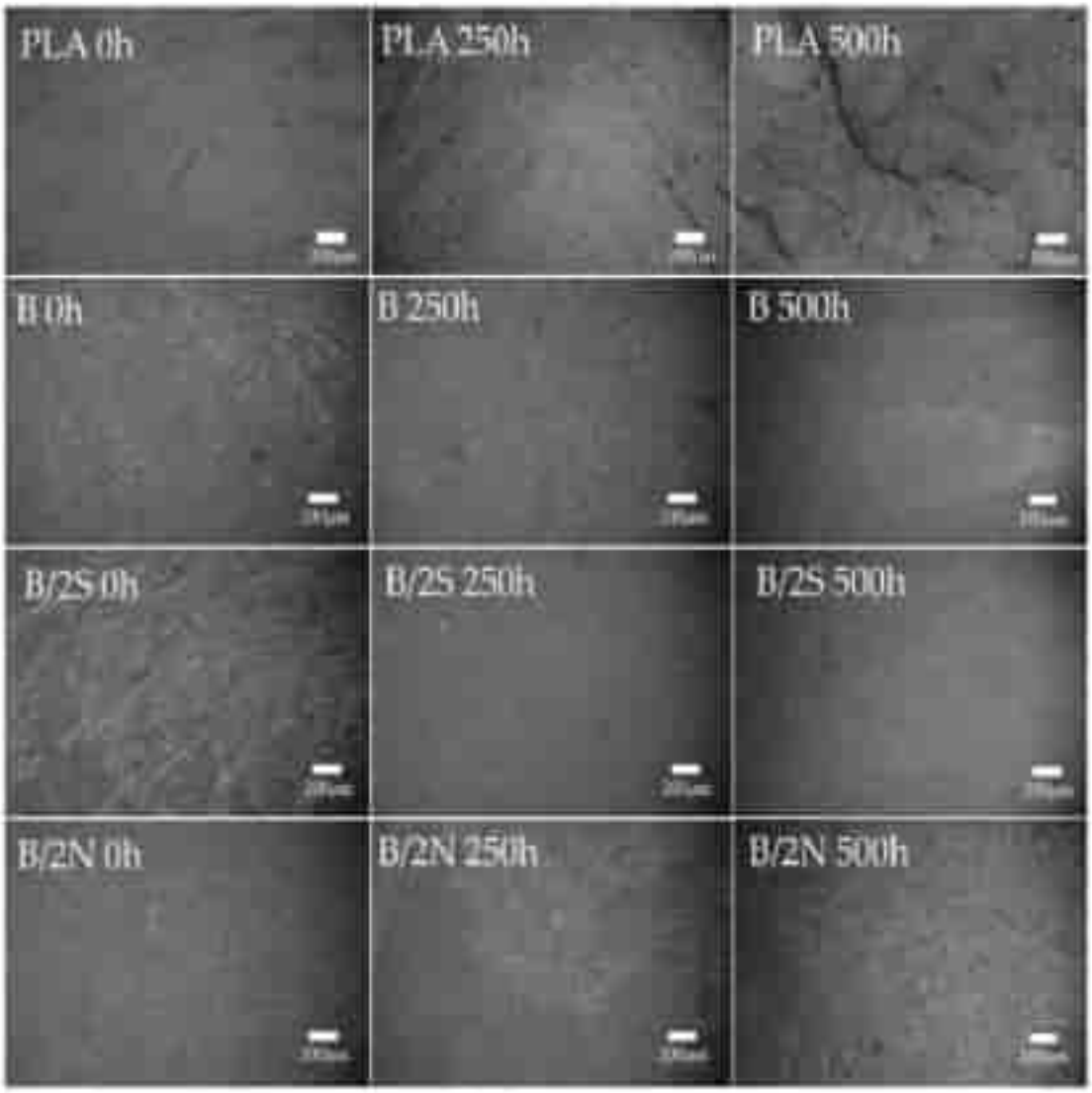

Figure 12. Surface of composites before and after placement in UV chamber (250 h and 500 h); systems without silanization.

It was also observed how deep the physicochemical changes (degradation-factoraffected zone) occurred in the composite sample under UV irradiation, as shown in Figures 14 and 15. The reference polylactide already shows changes throughout the volume after 250 h in the aging chamber, which is also evident in the sample conditioned for 500 h, and samples without added silanes (B, B/2S, B/2N) behaved similarly, which can be explained mostly by changes in the level of crystallinity and a decrease in the average molecular weight of PLA [34,35]. On the other hand, in composites filled with silanized diatomaceous earth and with the addition of waxes, the degree of surface degradation increases over time. For composites conditioned for 250 h, the physicochemical changes of the surface occurred no farther than at the 90 µm depth, while, for composites modified with GPTMOS and MTMOS silane, they occurredin the range of 50–60 µm. The system containing OTES silane was characterized by a slightly higher degree of degradation, because, depending on the type of wax used, the depth of changes was about 70 and 90 µm, for O/2S and O/2S, respectively. Only in this case was a slight effect of wax on the degradation rate of the composite observed. After conditioning for 500 h in a UV chamber, the differences became more pronounced. It was observed that the depth of transformation in the composite increased each time, and, for the G/2S and O/2S systems, the progressive depth of degradation and

its significantly higher proportion compared to the systems with the addition of natural wax coincides with the results of the microscopic surface analysis discussed above. The silanization of the filler may retard the water diffusion through the filler to the deeper layers of the material, which results in the visible depth of the physicochemical changes.

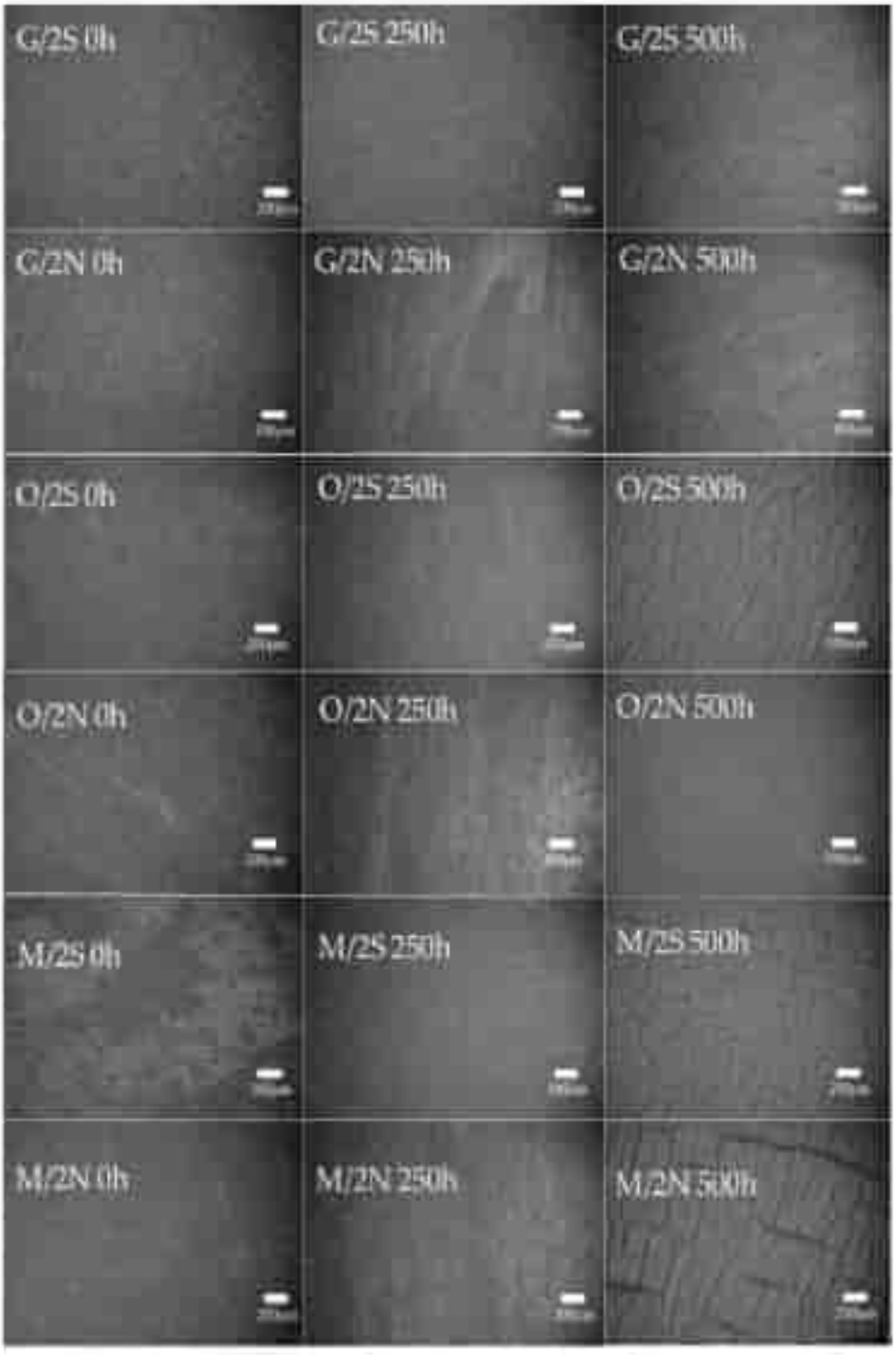

Figure 13. Surfaces of composites before and after placement in UV chamber for 250 and 500 h: silanized systems.

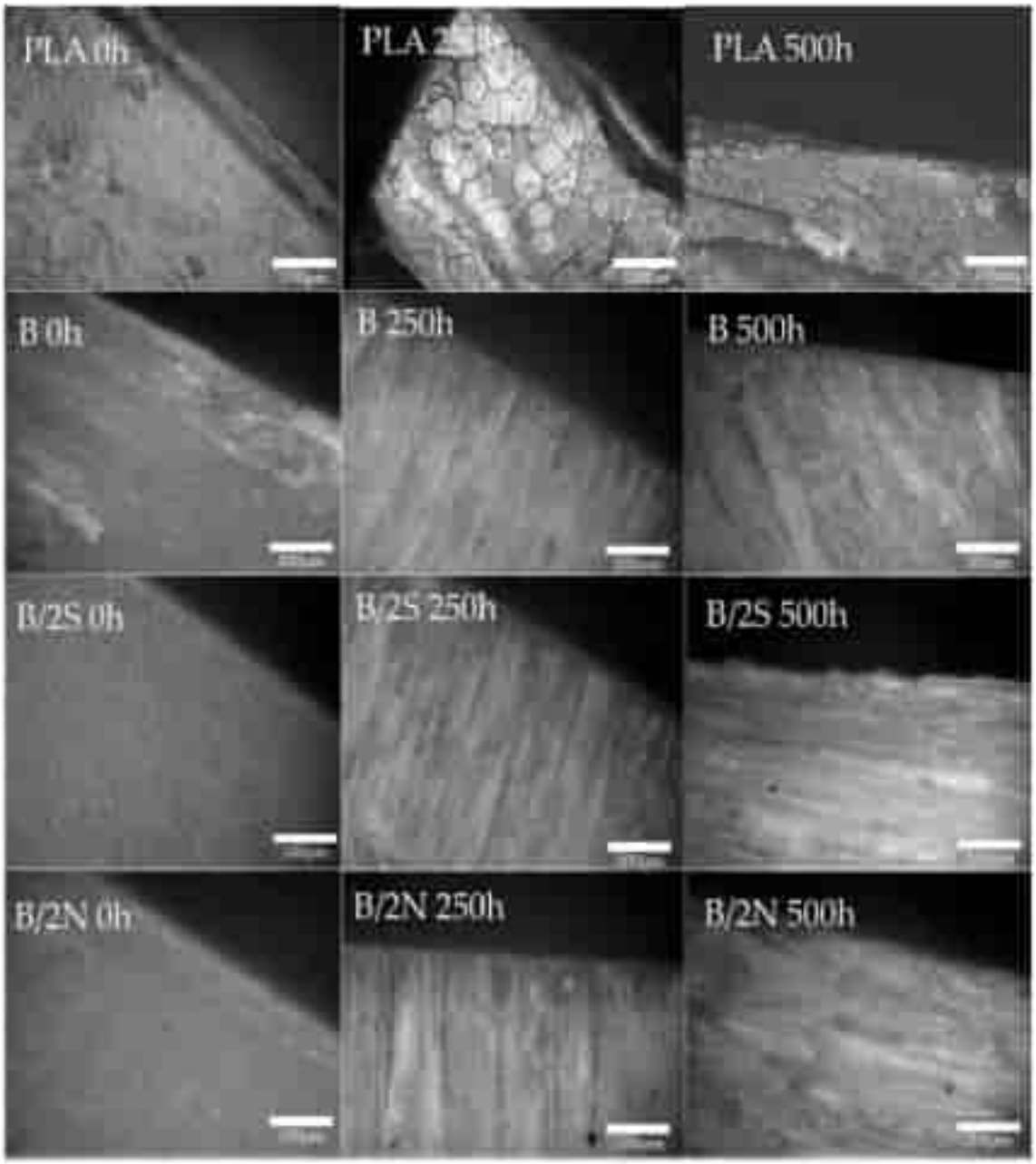

Figure 14. Edge structures of composite breakthroughs before and after placement in UV chamber (250 h and 500 h); systems without silanization.

For the system with the GPTMOS-modified filler and the addition of 2% natural wax, although it has a relatively high level of degradation (62%) after 500 h of aging in a UV chamber (Table 3), this degradation occurs only at a shallow depth, as confirmed by the results of a mechanical analysis of the composites. The results were similar in the case of the O/2N sample.

From the above correlations, it can be concluded that diatomaceous earth causes an increased degradation of polylactide, which is also confirmed by the work of Li T. et al. [36] and Zhang C. et al. [19], while silanization caused a reduction in the negative effect of DE on PLA degradation. The combination of the chemical modification of diatomaceous earth with silanes and the appropriate combination of waxes has the effect of reducing the depth of the degradation of composites.

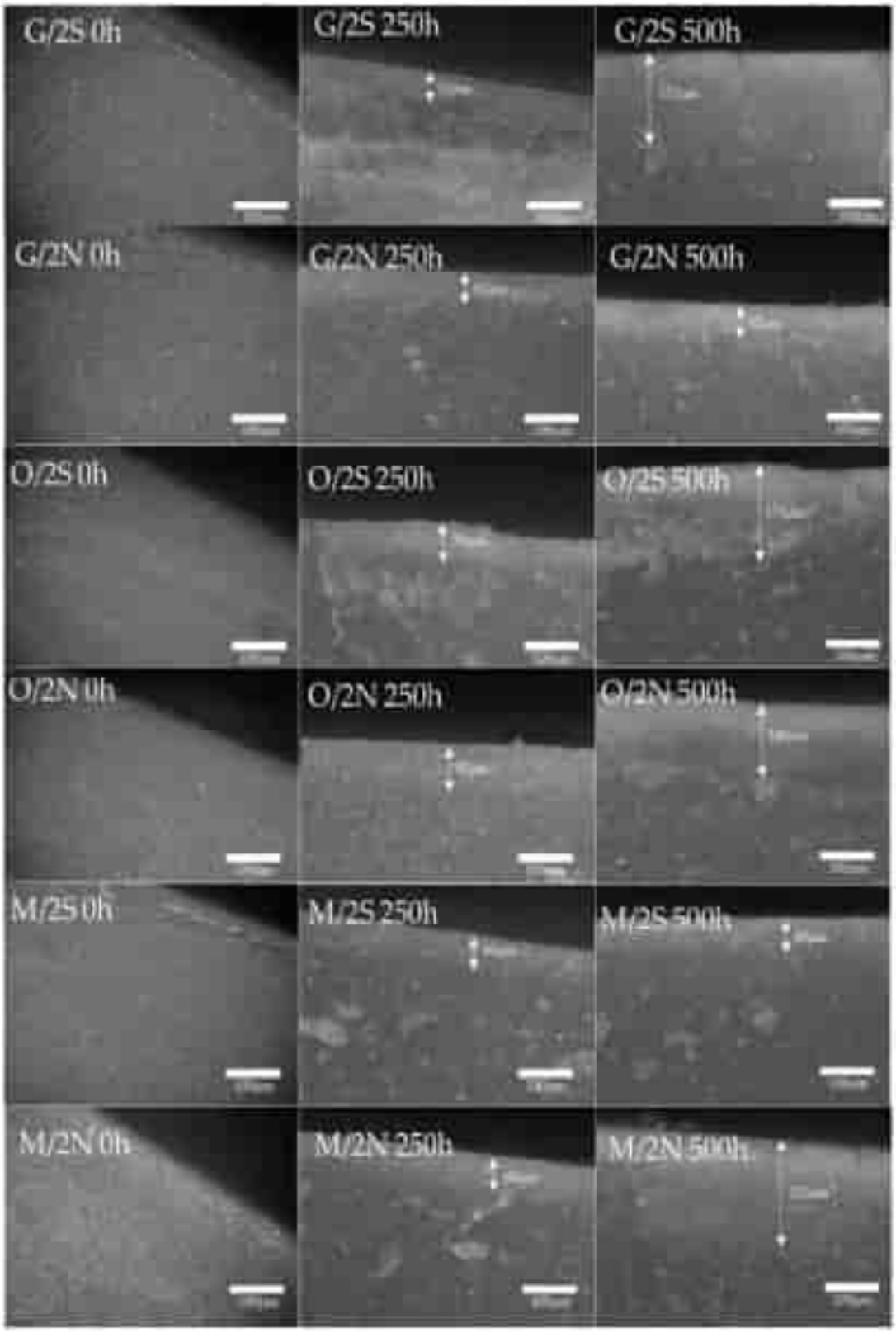

Figure 15. Edge structure of composite breakthroughs before and after placement in UV chamber for 250 and 500 h; silanized systems.

4. Conclusions

From the point of view of the mechanical properties of the filled composites, the modification of polylactide with silanized diatomaceous earth and synthetic wax is more favorable, not only for improving their processing properties. Both fillers and waxes contributed to an increase in the degradation rate of PLA on the surface of the composite, while limiting the depth of influence of the degradation factors, as proven by optical microscopy, which translated into a reduction in the effect of surface cracking and a decrease in mechanical parameters. The diatomite filler, although increasing the water diffusion through the composite and, therefore, accelerating the hydrolytic degradation of PLA, at the same time, works as a UV blocker, decreasing the negative effects of UV irradiation. This complements previous studies, where the positive effect of waxes on the mechanical and processing properties of PLA composites with diatomaceous earth was proven. In addition, it was observed that the physicochemical changes in the surface of composites with natural wax after 500 h in the aging chamber were smaller than with synthetic wax when GPTES- or OTES-modified filler was used. MTMOS caused the opposite effect and the samples with natural wax degraded more strongly. Ecologically, natural waxes leave a smaller carbon footprint because of their production method. The selection of an appropriate wax to improve performance should be dictated by the desire to improve the specific properties of the composites, which change depending on its type. Such a selection of modifiers for polylactide resulted in a significant improvement in the performance of this polymer, due to a reduction in the degree of degradation after conditioning the samples under sunlight. Under natural conditions, degradation was primarily affected by photolytic conditions due to the minimal precipitation during the test, while, under simulated conditions, the moisture level in the system was kept high.

Further research should focus on the further investigation of composites blends containing a different ratio of filler to natural wax for comparative purposes, as well as conducting studies, for example, on the release of components into the environment, while the degradation process occurs in selected composites tested in this study, especially on composites that showed extreme values of degradation depth.

Author Contributions: Conceptualization, R.E.P.; methodology, R.E.P. and M.D.; formal analysis, R.E.P., M.D. and R.D.; investigation, R.E.P., M.D., D.B. and M.P.-S.; data curation, M.D. and M.P.-S.; writing—original draft preparation, M.D., R.E.P., R.D., D.B. and M.P.-S.; writing—review and editing, M.D., R.E.P., D.B. and R.D.; visualization, M.D. and M.P.-S.; supervision, R.E.P., R.D. and K.J.K.; project administration, R.D. and K.J.K.; funding acquisition, R.D. and K.J.K. All authors have read and agreed to the published version of the manuscript.

Funding: This work was financially supported in the frame of the project "Advanced Biocomposites for Tomorrow's Economy BIOG-NET", FNP POIR.04.04.00-00-1792/18-00. The project is carried out within the TEAM-NET programme of the Foundation for Polish Science co-financed by the European Union under the European Regional Development Fund.

Institutional Review Board Statement: Not applicable.

Informed Consent Statement: Not applicable.

Data Availability Statement: Data are contained within the article.

Acknowledgments: Special acknowledgement goes to Kacper Wodarek for preparing the injection molding samples.

Conflicts of Interest: The authors declare no conflicts of interest.

References

1. Andrzejewski, L. Experimental Study of Reinforcing Mechanical Properties of Nylon-11 by Selective Laser Sintering. *Phys. Sci. Forum* **2022**, *4*, 22. [CrossRef]
2. Zgłobicka, I.; Jokiel-Yildiz, M.; Molak, R.; Kawalec, M.; Dobicki, A.; Wróblewski, J.; Dyjak, K.; Boczkowska, A.; Kurzydłowski, K.J. Poly(lactic acid) Matrix Reinforced with Diatomaceous Earth. *Materials* **2022**, *15*, 18. [CrossRef]

3. Pilla, S.; Gong, S.; O'Neill, E.; Rowell, R.M.; Krzysik, A.M. Polylactide-pine wood flour composites. *Polym. Eng. Sci.* **2008**, 48, 578–587. [CrossRef]
4. Samvada, U.K.; Marmol, G.; Brito, F.P.; Fangueiro, R. PLA Composites Reinforced with Flax and Jute Fibers—A Review of Recent Trends, Processing Parameters and Mechanical Properties. *Polymers* **2020**, 12, 237. [CrossRef]
5. Haddou, G.; Dandurand, J.; Dantras, E.; Maiduc, H.; Thai, H.; Vu Giang, N.; Trung, T.H.; Ponteins, P.; Lacabanne, C. Mechanical properties of continuous bamboo fiber-reinforced biobased polyamide 11 composites. *Int. J. Appl. Polym. Sci.* **2019**, 136, 4762. [CrossRef]
6. Zierdt, P.; Theumer, T.; Kulkarni, G.; Däumlich, V.; Klehm, J.; Hirsch, U.; Weber, A. Sustainable wood-plastic composites from bio-based polyamide 11 and chemically modified beech fibers. *Sustain. Mater. Technol.* **2015**, 6, 6–14. [CrossRef]
7. Dobrosielska, M.; Przekop, R.E.; Sztorch, B.; Brząkalski, D.; Zgłobicka, I.; Łępicka, M.; Dobosz, R.; Kurzydłowski, K.J. Biogenic Composite Filaments Based on Polylactide and Diatomaceous Earth for 3D Printing. *Materials* **2020**, 13, 4632. [CrossRef]
8. Dobrosielska, M.; Dobrucka, R.; Brząkalski, D.; Frydrych, M.; Kozera, P.; Jałbrzykowski, M.; Kurzydłowski, K.J.; Przekop, R.E. Influence of Diatomaceous Earth Particle Size on Mechanical Properties of PLA/Diatomaceous earth Composites. *Materials* **2022**, 15, 3607. [CrossRef]
9. Dobrosielska, M.; Dobrucka, R.; Kozera, P.; Kozera, R.; Kołodziejczak, M.; Gabriel, E.; Głowacka, J.; Jałbrzykowski, M.; Kurzydłowski, K.J.; Przekop, R.E. Biocomposites Based on Polyamide 11/Diatoms with Different Sized Frustules. *Polymers* **2022**, 14, 3153. [CrossRef]
10. Li, T.; Sun, H.; Wu, B.; Han, H.; Li, D.; Wang, J.-K.; Zhang, J.; Huang, J.; Sun, D. High-performance polylactic acid composites reinforced by artificially cultured diatom frustules. *Mater. Des.* **2020**, 195, 109003. [CrossRef]
11. Nair, N.R.; Sekhar, V.C.; Nampoothiri, K.M.; Pandey, A. 32-Biodegradation of Biopolymers. In *Current Developments in Biotechnology and Bioengineering*; Pandey, A., Negi, S., Soccol, C.R., Eds.; Elsevier: Amsterdam, The Netherlands, 2017; pp. 739–755.
12. Zaaba, N.F.; Jaafar, M. A review on degradation mechanisms of polylactic acid: Hydrolytic, photodegradative, microbial, and enzymatic degradation. *Polym. Eng. Sci.* **2020**, 60, 2061–2075. [CrossRef]
13. Siparsky, G.L.; Voorhees, K.J.; Miao, F. Hydrolysis of Polylactic Acid (PLA) and Polycaprolactone (PCL) in Aqueous Acetonitrile Solutions: Autocatalysis. *J. Polym. Environ.* **1998**, 6, 31–41. [CrossRef]
14. Hirao, K.; Nakatsuchi, Y.; Ohara, H. Alcoholysis of Poly(l-lactic acid) under microwave irradiation. *Polym. Degrad. Stab.* **2010**, 95, 925–928. [CrossRef]
15. Iñiguez-Franco, F.; Auras, R.; Burgess, G.; Holmes, D.; Fang, X.; Rubino, M.; Soto-Valdez, H. Concurrent solvent induced crystallization and hydrolytic degradation of PLA by water-ethanol solutions. *Polymer* **2016**, 99, 315–323. [CrossRef]
16. Castro-Aguirre, E.; Iñiguez-Franco, F.; Samsudin, H.; Fang, X.; Auras, R. Poly(lactic acid)—Mass production, processing, industrial applications, and end of life. *Adv. Drug Deliv. Rev.* **2016**, 107, 333–366. [CrossRef]
17. Qi, X.; Ren, Y.; Wang, X. New advances in the biodegradation of Poly(lactic) acid. *Int. Biodeterior. Biodegrad.* **2017**, 117, 215–223. [CrossRef]
18. Teixeira, S.; Morawa-Eblagon, K.; Miranda, F.; Pereira, M.F.R.; Figueiredo, J.L. Towards Controlled Degradation of Poly(lactic) Acid in Technical Applications. *C* **2021**, 7, 42. [CrossRef]
19. Zhang, C.; Sun, J.; Lyu, S.; Lu, Z.; Li, T.; Yang, Y.; Li, B.; Han, H.; Wu, B.; Sun, H.; et al. Poly(lactic acid)/artificially cultured diatom frustules nanofibrous membranes with fast and controllable degradation rates for air filtration. *Adv. Compos. Hybrid Mater.* **2022**, 5, 1221–1232. [CrossRef]
20. Drobnier, P.; Yuan, M.; Cruz, F.D.R.; Cruz, J.; Yaduliabi, Z.; Sedlarik, V. Comparative degradation study of a biodegradable composite based on polylactide with halloysite nanotubes and a polyacrylic acid copolymer. *Mater. Today Commun.* **2022**, 33, 104400. [CrossRef]
21. Qin, Q.; Yang, Y.; Yang, C.; Zhang, L.; Yin, H.; Yu, F.; Ma, J. Degradation and adsorption behavior of biodegradable plastic PLA under conventional weathering conditions. *Sci. Total Environ.* **2022**, 842(1), 156775. [CrossRef]
22. *PN-EN ISO 20753:2019-01*; Plastics—Test Specimens. ISO: Geneva, Switzerland, 2019.
23. *EN ISO 527:2012*; Standard—Plastics—Determination of Tensile Properties. ISO: Geneva, Switzerland, 2012.
24. *EN ISO 178:2006*; Plastics—Determination of Flexural Properties. ISO: Geneva, Switzerland, 2006.
25. *ISO 4892-3*; Methods of Exposure To Laboratory Light Sources—Part 3: Fluorescent UV Lamps. ISO: Geneva, Switzerland, 2006.
26. *ASTM G154*; Standard Practice for Operating Fluorescent Light Apparatus for UV Exposure of Nonmetallic Materials. American Society for Testing and Materials: West Conshohocken, PA, USA, 2016.
27. *PN-EN ISO 16474-3*; Paints and Varnishes—Methods of Exposure to Laboratory Light Sources—Part 3: UV Fluorescent Lamps. Polish Norm, International Organization for Standardization: Warsaw, Poland, 2014.
28. Dobrosielska, M.; Dobrucka, R.; Pajewska-Szmyt, M.; Kozera, P.; Gabriel, E.; Głowacka, J.; Brząkalski, D.; Kurzydłowski, K.J.; Przekop, R.E. Effect of Wax Additives and Silanization of Diatom Surfaces on Thermomechanical Properties of Polylactide Composites. *Polymers* **2022**, 14, 5511. [CrossRef]
29. Dobrosielska, M.; Dobrucka, R.; Kozera, P.; Brząkalski, D.; Gabriel, E.; Głowacka, J.; Jałbrzykowski, M.; Kurzydłowski, K.J.; Przekop, R.E. Beeswax as a natural alternative to synthetic waxes for fabrication of PLA/diatomaceous earth composites. *Sci. Rep.* **2023**, 13, 1161. [CrossRef]
30. Ho, K.L.G.; Pometto, A.L.; Hinz, P.N. Effects of Temperature and Relative Humidity on Polylactic Acid Plastic Degradation. *J. Environ. Polym. Degrad.* **1999**, 7, 83–92. [CrossRef]

31. Badarinath, K.V.S.; Kumar Kharol, S.; Krishna Prasad, V.; Rani Sharma, A.; Reddi, E.U.B.; Kambezidis, H.D.; Kaskaoutis, D.G. Influence of natural and anthropogenic activities on UV Index variations—A study over tropical urban region using ground based observations and satellite data. *J. Atmos. Chem.* **2008**, *59*, 219–236. [CrossRef]
32. Leccese, F.; Salvadori, G.; Lista, D.; Burattini, C. Outdoor Workers Exposed to UV Radiation: Comparison of UV Index Forecasting Methods. In Proceedings of the 2018 IEEE International Conference on Environment and Electrical Engineering and 2018 IEEE Industrial and Commercial Power Systems Europe (EEEIC/I&CPS Europe), Palermo, Italy, 12–15 June 2018. [CrossRef]
33. Trifol, J.; Plackett, D.; Szabo, P.; Daugaard, A.E.; Giacinti Baschetti, M. Effect of Crystallinity on Water Vapor Sorption, Diffusion, and Permeation of PLA-Based Nanocomposites. *ACS Omega* **2020**, *5*, 15362–15369. [CrossRef]
34. Copinet, A.; Bertrand, C.; Govindin, S.; Coma, V.; Couturier, Y. Effects of ultraviolet light (315 nm), temperature and relative humidity on the degradation of polylactic acid plastic films. *Chemosphere* **2004**, *55*, 763–773. [CrossRef]
35. Gallet, G.; Lempiäinen, R.; Karlsson, S. Characterisation by solid phase microextraction–gas chromatography–mass spectrometry of matrix changes of poly(l-lactide) exposed to outdoor soil environment. *Polym. Degrad. Stab.* **2000**, *71*, 147–151. [CrossRef]
36. Li, T.; Sun, H.; Han, H.; Zhang, C.; Li, B.; Huang, J.; Sun, D. Ultrafast bulk degradation of polylactic acid by artificially cultured diatom frustules. *Compos. Sci. Technol.* **2022**, *222*, 109410. [CrossRef]

Disclaimer/Publisher's Note: The statements, opinions and data contained in all publications are solely those of the individual author(s) and contributor(s) and not of MDPI and/or the editor(s). MDPI and/or the editor(s) disclaim responsibility for any injury to people or property resulting from any ideas, methods, instructions or products referred to in the content.